

Ben Leimkuhler
Charles Matthews

Molecular Dynamics

With Deterministic and Stochastic
Numerical Methods

Molecular Dynamics

Interdisciplinary Applied Mathematics

Editors

S.S. Antman P. Holmes

L. Greengard

Series Advisors

Leon Glass P.S. Krishnaprasad

Robert Kohn James D. Murray

James Sneyd Shankar Sastry

Problems in engineering, computational science, and the physical and biological sciences are using increasingly sophisticated mathematical techniques. Thus, the bridge between the mathematical sciences and other disciplines is heavily traveled. The correspondingly increased dialog between the disciplines has led to the establishment of the series: *Interdisciplinary Applied Mathematics*.

The purpose of this series is to meet the current and future needs for the interaction between various science and technology areas on the one hand and mathematics on the other. This is done, firstly, by encouraging the ways that mathematics may be applied in traditional areas, as well as point towards new and innovative areas of applications; and, secondly, by encouraging other scientific disciplines to engage in a dialog with mathematicians outlining their problems to both access new methods and suggest innovative developments within mathematics itself.

The series will consist of monographs and high-level texts from researchers working on the interplay between mathematics and other fields of science and technology.

More information about this series at

<http://www.springer.com/series/1390>

Ben Leimkuhler • Charles Matthews

Molecular Dynamics

With Deterministic and Stochastic
Numerical Methods



Springer

Ben Leimkuhler
University of Edinburgh
School of Mathematics
Edinburgh, United Kingdom

Charles Matthews
University of Chicago
Gordon Center for Integrative Science
Chicago, IL, USA

ISSN 0939-6047

ISSN 2196-9973 (electronic)

Interdisciplinary Applied Mathematics

ISBN 978-3-319-16374-1

ISBN 978-3-319-16375-8 (eBook)

DOI 10.1007/978-3-319-16375-8

Library of Congress Control Number: 2015938759

Springer Cham Heidelberg New York Dordrecht London

© Springer International Publishing Switzerland 2015

This work is subject to copyright. All rights are reserved by the Publisher, whether the whole or part of the material is concerned, specifically the rights of translation, reprinting, reuse of illustrations, recitation, broadcasting, reproduction on microfilms or in any other physical way, and transmission or information storage and retrieval, electronic adaptation, computer software, or by similar or dissimilar methodology now known or hereafter developed.

The use of general descriptive names, registered names, trademarks, service marks, etc. in this publication does not imply, even in the absence of a specific statement, that such names are exempt from the relevant protective laws and regulations and therefore free for general use.

The publisher, the authors and the editors are safe to assume that the advice and information in this book are believed to be true and accurate at the date of publication. Neither the publisher nor the authors or the editors give a warranty, express or implied, with respect to the material contained herein or for any errors or omissions that may have been made.

Printed on acid-free paper

Springer International Publishing AG Switzerland is part of Springer Science+Business Media
(www.springer.com)

Preface

For a number of years, we have been exploring the underpinnings of algorithms for simulating molecular dynamics from a mathematics perspective, i.e. as outsiders. We have learned the tricks of the trade through reading books written for practitioners, websites, documentation in software packages (yes, someone does really read that stuff!), Ph.D. theses (yes, someone does really read that stuff!), and a sometimes bewildering collection of research papers. As we have plumbed some of the deep recesses of the subject, and added our own contributions where we could, we have come to form a composite picture of the topic. Increasing numbers of scientists with an ever wider range of backgrounds are beginning to work within this area, therefore we feel that it is time to have a book that presents the topic at an introductory level and from a mathematical perspective.

Computational molecular dynamics is a field that has evolved in response to the needs of chemists, physicists and more recently biologists, materials engineers, drug designers, etc. The derivation of methods is often based on intuition or appeal to examples, but deeper insight into molecular dynamics methods can be obtained through a mathematical approach. Our book presents molecular dynamics methods from a mathematical perspective and describes numerical methods that form the basis for molecular simulation algorithms and, ultimately, software. Our treatment is far from comprehensive, in the sense that there are things that scientists investigate involving molecules and computers that we will say nothing about. We will largely avoid excessive detail in the formulation of models, and we will steer clear of some of the most recent developments in the field that are still unsettled. By placing the emphasis on foundations our intention is to provide a resource of lasting value for mathematicians and computational scientists, and a guide for those who must rely on molecular dynamics in their research, and for those who may need to develop new methods for complex applications.

The fact that molecular dynamics is sometimes seen as something of a black art is from our point of view the strongest motivation for us to take up the challenge of writing this book. We have sought to place each algorithm on a solid foundation, by introducing geometric integration and backward error analysis to explore the properties of methods for deterministic simulation, and then by

extending these concepts to provide foundations for studying Langevin dynamics integrators. Our presentation follows a simple pattern: give enough theory to describe the models and (deterministic or stochastic) differential equation systems, then discuss the design of numerical methods, and finally explain the performance of the methods using both analysis and numerical experiments. The approximation of averages was originally viewed as a by-product of computing trajectories of a Newtonian dynamical evolution. Our treatment emphasizes a recent change in perspective: numerical methods have their own effective global structures (perturbed Hamiltonians, invariant measures) and the design of methods can be enhanced by using this knowledge, thus providing better (more accurate, more robust) tools for thermodynamic calculation.

Our book emphasizes the construction of paths (deterministic or stochastic) for dynamics and for the computation of long-term properties for atomistic models. The numerical analysis for this has only just reached a state of maturity so that a book like this can be prepared. We aim to provide explicit and precise guidance on the properties of algorithms to aid in selection and implementation. A criticism that could be leveled at our book is that it is not a fully comprehensive treatment of modern work exploring the mathematical foundations of molecular modelling. Since the 1990s, researchers have begun to turn their attention to various topics arising in connection with molecular models, addressing a range of challenges including coarse-graining techniques, methods for computing free energies, metastable processes, rare event techniques, the relationship between quantum and classical models, parallel computing techniques, and the design of multiscale methods that interface molecular dynamics with solid mechanics models. While we make no effort to be complete in our coverage of the recent trends in the field of molecular modelling, the techniques described here are fundamental to most modern theories, and we therefore expect that they will play an important and enduring role in any broader frameworks of molecular simulation. (Below, we provide some references for advanced reading on timely themes.)

The best preparation for reading this book would consist of basic (undergraduate level) courses in elementary analysis, numerical analysis, differential equations and probability, and some knowledge of mechanics (Newton's laws, force balance, harmonic oscillators, the Kepler problem, etc.). The analysis of splitting methods by the Baker-Campbell-Hausdorff expansion can be explained in terms of the exponentials of sums of noncommuting matrices. Concepts such as generalized functions are introduced, but only the Dirac delta function needs really to be explained in this context. The discussion of stochastic differential equations and especially the Fokker-Planck equation (end of Chaps. 6, 7) necessarily gets a bit involved, but the essential results in Chap. 6 have been condensed into a few basic theorems which are stated without proof. For readers with limited exposure to analysis, one might stop in Sect. 6.4 after presenting the irreducibility of discrete Markov chains and then explain in general terms and by analogy the content of the remainder of the section, before continuing to the study of Langevin dynamics methods in Chap. 7. For advanced readers, it is recommended to consult a good book on stochastic processes; see references mentioned below (or other articles

referenced in Sect. 6.4). Results in Chaps. 7 and 8 are relatively new and are presented at a higher level, but still aimed at a broad audience. The book is bound to generate questions from students that cannot be answered entirely using methods and results presented in the book, but this is in many ways rather a strength than a weakness.

The assumption of limited background knowledge has some disadvantages—detailed and rigorous proofs are omitted, for example—but by the same token the book is hoped to be usable for interdisciplinary courses and for independent study by a broad audience. We put the emphasis here on making simple statements regarding algorithms. These statements could, in most cases, be made entirely rigorous with a more formal (but also much longer) presentation. In some cases, we impose more stringent assumptions of smoothness or boundedness than are actually needed in order to simplify the presentation. At the end of the day, it is not just theorems that define this subject. We are well aware that carefully crafted numerical experiments are often more informative than pages of analytical derivations and we therefore describe in detail quite a few simulations.

The appendices provide some notes on force evaluation, a brief review of some elements of basic probability theory that we rely on, and a brief discussion of Monte-Carlo methods.

A course in numerical methods for molecular dynamics could be taught entirely from this book. For a broader perspective on molecular simulation within a course setting, one should include readings on topics such as Monte-Carlo methods, and force calculation which could be found, for example, in [140, 328]. It would also be important to have some experience of using molecular simulation software to perform realistic calculations (see below).

Depending on the background of the reader, or to obtain a fuller picture of various issues, it may be useful to supplement our book with additional texts chosen from among the following:

- *for ordinary differential equations, and dynamical systems:* [51, 177, 216, 362, 386];
- *for classical mechanics:* [15, 16, 57, 151, 212, 249, 297];
- *for statistical mechanics:* [57, 70, 197, 264, 366, 372];
- *for molecular models and algorithms:* [7, 140, 159, 215, 307, 328, 372];
- *for numerical analysis, e.g. numerical ordinary differential equations, geometric integration and numerical methods for stochastic differential equations:* [164, 167, 227, 270];
- *for probability theory, stochastic processes and stochastic differential equations:* [18, 142, 269, 279, 298, 314].

Another excellent book we should mention here is that of Griebel et al. [155], which explores the computational aspects of molecular dynamics in the setting of high performance computing. This would provide an excellent complementary book for a course focussed more on the issues relevant to software, large scale simulation, and parallel computing.

For some readings taking in the modern span of molecular modelling, particularly the “multiscale” context, we propose articles on the string method [115–117, 384], the adaptive biasing force method [76, 91–93], metadynamics [23, 61, 207, 208], other methods of free energy calculation [83, 104, 231], Markov state modelling [282, 332], and atomistic-to-continuum coupling [243]. These articles can serve as starting points for advanced projects and help to put into practice ideas learned in the book. We also emphasize that an excellent follow-on book specialized to mathematical techniques in free energy calculation [233] is available and could help to guide study of this important topic.

Molecular Dynamics Software

It will be difficult to gain a full grasp of molecular dynamics without performing simulations. We have found that small systems (harmonic oscillators, double wells, Lennard-Jones trimers, etc.), suitably chosen, can often provide insight into the behavior of molecular dynamics methods. Experimentation with algorithm design using small toy models can in many cases be performed adequately using a system such as MATLAB.¹ To accompany the release of this book, we have prepared MATLAB code for many of the algorithms we present. These programs are released as the **MD.M** software package on the website linked from <http://MolecularDynamics.info>. This software (which interfaces to MATLAB as well as to the free alternative Octave²) allows easy experimentation with few-atom models (up to a dozen atoms, say). Using a C-language interface in combination with **MD.M** to compile the compute-intensive force field, the code can be accelerated to allow study of up to several hundred atoms.

Eventually, if one wishes to understand the more intricate nuances of numerical simulation, e.g., multiscale phenomena, or to treat larger systems with more realistic force fields, it will be necessary to have access to specialist software with which to try things out or for the purposes of modification. Fortunately, there are a handful of major “freeware” software packages in common use, each of which has a community of researchers and is maintained and developed by a substantial team with extensive funding by government agencies. We mention specifically the following: **AMBER** [393], **CHARMM** [246], **DL_Poly** [365], **GROMACS** [33, 236], **LAMMPS** [303], **NAMD** [302], **TINKER** (<http://dasher.wustl.edu/ffe/>). These codes are designed for different types of applications. For example, **NAMD**, **AMBER**, and **CHARMM** are very much oriented to biomolecular modelling, whereas **LAMMPS** and **DL_Poly** were originally designed more for materials applications. The **MOIL** code (<http://clsb.ices.utexas.edu/web/moil.html>) facilitates the study of rare events using molecular dynamics. The **DESMOND**

¹<http://www.mathworks.co.uk/products/matlab/>.

²GNU Octave is available from <http://www.gnu.org/software/octave/>

system (http://www.deshawresearch.com/resources_desmond.html) is produced by a commercial company, but provided free for non-commercial use. We also mention the commercial packages “Materials Studio” and “Discovery Studio” which are produced by Accelrys, Inc. The open software projects freely distribute the source code, so it is possible for a keen user to alter the algorithms. Unfortunately, it has to be mentioned that there is something of a trade-off between the efficiency of the codes (especially in the high performance computing setting) and the ease with which algorithms may be changed. **NAMD** and **GROMACS** are, in our experience, a little complicated to modify, whereas **TINKER** and **DL_Poly** are relatively easy. If one were to restrict oneself to a single code system in which all algorithms are to be tried out, then we highlight that **LAMMPS** offers a very convenient mechanism for code modification, making it particularly “developer-friendly”.

Acknowledgements

The authors would like to acknowledge some of the valuable materials obtained from colleagues and via the internet, in particular the miscellaneous unpublished lecture notes and lecture slides of Lawrence Evans (Berkeley), Jonathan Goodman (NYU), Martin Hairer (Warwick), Peter Olver (Minnesota), and Mark Tuckerman (NYU). In many cases, our reading of these has been inspirational.

We wish to thank the large number of people who have patiently assisted us in preparing this volume; our consultation was very broad, chosen to span researchers working in numerical analysis, in pure and applied analysis, in probability, and in theoretical chemistry, including Janis Bajars (Nottingham), Stephen Bond (Sandia), Ron Elber (Texas), Radek Erban (Oxford), Jason Frank (Utrecht), Alastair Gillespie (Edinburgh), Ben Goddard (Edinburgh), Martin Hairer (Warwick), Oliver Penrose (Heriot-Watt), Xiaocheng Shang (Edinburgh), Bob Skeel (Purdue), Gabriel Stoltz (Ecole des Ponts, Paris), Andrew Stuart (Warwick), and Mark Tuckerman (New York); their helpful contributions have been integrated into all chapters. Both Greg Pavliotis (Imperial College) and Michael Tretyakov (Nottingham), in addition to providing many helpful comments, were also generous in giving us advance access to their own books-in-progress on specific topics.

Edinburgh, UK
Chicago, Illinois, USA
October 2014

Benedict Leimkuhler
Charles Matthews

Notation

N	Number of atoms
N_d	Number of degrees of freedom
N_c	Number of configurational coordinates (dimension of position vector)
\mathbb{R}^m	m -dimensional Euclidean space
$\stackrel{\text{def}}{=}$	is defined to be
\coloneqq	Assignment operation (typically used in algorithms)
$\ \cdot\ $	Euclidean 2-norm, e.g., in two dimensions, $\ (u_1, u_2)\ = \sqrt{u_1^2 + u_2^2}$
C^k	$f \in C^k$ means that f is k -times continuously differentiable
\circ	Composition operation, i.e. if $(f \circ g)(x) = f(g(x))$
\mathbf{q}	Position vector, normally $\mathbf{q} \in \mathbb{R}^N$
q_j	Position vector of j th atom
$q_{i,x}$	x -coordinate of i th atom in an N-body system
$\dot{\mathbf{q}} = \frac{d\mathbf{q}}{dt}$	Derivative with respect to time of $\mathbf{q}(t)$.
\mathbf{p}	Momentum vector, normally $\mathbf{p} \in \mathbb{R}^{N_c}$
\mathbf{M}	Mass matrix, normally \mathbf{M} is an N_c by N_c matrix
\mathbf{I}	Identity matrix
$\mathbf{0}$	(Bold) a vector or matrix whose elements are all zero
\mathbf{F}	Force vector
E	(Italic) the energy function
E	(Roman) the value of energy
U	Potential energy function, normally U is a function of \mathbf{q} <i>Note: typically, $\mathbf{F} = -\nabla_{\mathbf{q}} U = -\partial U / \partial \mathbf{q}$</i>
φ	a pair or few-atom potential energy term
φ_{LJ}	Lennard-Jones pair potential
K	Kinetic energy, normally $K = \mathbf{p}^T \mathbf{M}^{-1} \mathbf{p} / 2$
L	Lagrangian, $L = K - U$
H	Hamiltonian function (energy)

τ	(Usually) length of time interval
ν	(Usually) number of timesteps
\mathcal{F}_t	Flow map
$\exp(A) = e^A$	Exponential of matrix A
$U''(\mathbf{q})$	Hessian matrix of potential energy function U
$f'(z)$	Jacobian matrix of vector function f
T	Temperature
P	Pressure
V	Volume (in three-dimensional space)
k_B	Boltzmann's constant
β	$(k_B T)^{-1}$
fcc	Face-centered cubic
bcc	Body-centered cubic
h	(Usually) time stepsize used for a numerical method
\mathcal{G}_h	Approximate flow map defined by a numerical method
$\nabla \cdot f$	Divergence of vector field f
$d\omega$	$= dq_1 dq_2 \dots dq_N dp_1 dp_2 \dots dp_N$
$\int_{\mathcal{D}} f(\mathbf{q}, \mathbf{p}) d\omega$	Lebesgue integral
$J = \begin{bmatrix} \mathbf{0} & \mathbf{I} \\ -\mathbf{I} & \mathbf{0} \end{bmatrix}$	Canonical symplectic structure matrix
\wedge	Wedge product of differentials
$\det(A)$	Determinant of matrix A
$\text{tr}(A)$	Trace of matrix A
\mathcal{G}_h^\dagger	"Adjoint" of method \mathcal{G}_h
\mathcal{L}_f	Lie derivative, $\mathcal{L}_f g = f \cdot \nabla g$
$C_{ab}(\tau)$	Correlation function
$\mathcal{D}, \mathcal{A}, \mathcal{S}, \dots$	Measurable sets
$\text{Av}_{H=E} g$	Microcanonical average on $H = E$ energy surface
$\text{Av}_\rho g$	Average with respect to density ρ
$\text{Av}_\beta g$	Average with respect to canonical probability measure ρ_β
$\mu_E(d\sigma) = \frac{1}{\ \nabla H\ } d\sigma$	Microcanonical probability measure
$\Pr(\mathcal{A})$	Probability measure of \mathcal{A}
$\bar{\phi}(\tau)$	Average of function $\phi(z(t))$ on interval $[0, \tau]$
ρ_∞	Invariant distribution
\mathcal{L}^\dagger	Adjoint with respect to L^2 inner product of operator \mathcal{L}
$L^2(\mathcal{D})$	Space of square integrable functions on \mathcal{D}
$\langle f, g \rangle$	L^2 inner product
$\langle f \rangle$	Used for various types of average, precise meaning from context

$W(t)$	Wiener process
dW	Infinitesimal increment of a Wiener process (Wiener measure)
$[A, B]$	Commutator of matrices A and B
$[\mathcal{L}, \mathcal{M}]$	Commutator of operators \mathcal{L} and \mathcal{M}
$\llbracket ABC \rrbracket$	Method obtained by composing maps associated with A, B, C
$S\{\mathbf{F}, \mathbf{G}\}$	Lie algebra generated by vector fields \mathbf{F}, \mathbf{G}
$\widehat{\lim}$	Limit in the sense of distribution
i.m.	Limit in the mean square sense
$\mathbf{1}_S$	Characteristic function for set S

Index of Formulations, Methods, and Algorithms

N-Body problem	18
Euler's method	54, 55
Verlet method (position and velocity versions)	67, 107
Symplectic Euler method (two variants)	140, 82
Runge-Kutta methods	89
Newmark methods	92
Takahashi-Imada method (and simplified form), also Rowlands' method	92, 138
Suzuki-Yoshida method for higher order	109
Implicit Midpoint method	142
Reversible RESPA algorithm	145
Constrained symplectic Euler method	156
SHAKE algorithm	161
RATTLE algorithm	161
Geodesic integrator	164
SHAKE for rigid body molecular dynamics	171
DLM method for rigid body molecular dynamics	174
Langevin dynamics	239
Leimkuhler-Matthews method	308
Brownian (overdamped Langevin) dynamics	240
Metropolis Monte-Carlo method	415
Euler-Maruyama method	264
ABO method for Langevin dynamics	270
ABOBA, BAOAB, OBABO, OABAO methods for Langevin dynamics	271
Stochastic position Verlet for Langevin dynamics	272
Brünger-Brooks-Karplus method for Langevin dynamics	273, 277
Exact Gibbs sampling method	281
Limit Method—high friction limit of BAOAB (alternative to Euler-Maruyama)	308
Constrained Langevin dynamics	317
Nosé-Hoover (NH) thermostat	331

Nosé-Poincaré (NP) thermostat	334
General stochastic-dynamical thermostat	343
Nosé-Hoover-Langevin (NHL) method	345
Stochastic velocity rescaling (VR) method	355
Gaussian isokinetic method	361
Stochastic line sampling (SLS) method	357
Stochastic isokinetic Nosé-Hoover (SIN) method	364
Stochastic isokinetic Nosé-Hoover RESPA (SIN(R)) algorithm.	371
Nosé-Hoover-Langevin piston method (constant pressure)	383
Dissipative particle dynamics (DPD)	390
Pairwise Nosé-Hoover-Langevin method (PNHL)	394
Hybrid Monte-Carlo method	417

Contents

1	Introduction	1
1.1	Classical Mechanics Models	5
1.1.1	Molecular Potentials	8
1.1.2	Other Potentials	11
1.2	The N-Body Problem	18
1.3	The Lagrangian and Generalized Coordinates	22
1.4	Hamiltonian Formulation	23
1.5	Existence and Uniqueness of Solutions	25
1.5.1	The Flow Map	26
1.5.2	Integrable Examples	28
1.5.3	Equilibrium Points, and the Linearization Theorem	31
1.6	Lattice Structures	33
1.6.1	Lattice Vibrations	36
1.7	Chaotic Trajectories of Nonlinear Systems	38
1.7.1	Global Solutions	41
1.7.2	Variational Equations and Lyapunov Exponents	44
	Exercises	46
2	Numerical Integrators	53
2.1	Error Growth in Numerical Integration of Differential Equations	55
2.1.1	Example: The Trimer	56
2.1.2	Higher Order Methods	58
2.2	The Verlet Method	60
2.2.1	Hamilton's Principle and Equations of Motion	60
2.2.2	Derivation of the Verlet Method	63
2.2.3	Convergence and the Order of Accuracy	66
2.2.4	First Integrals and Their Preservation Under Discretization	70

2.3	Geometric Integrators for Hamiltonian Systems	71
2.3.1	Volume Preserving Flows: Liouville's Theorem	72
2.3.2	Volume Preserving Numerical Methods	74
2.3.3	The Symplectic Property	76
2.3.4	Hamiltonian Flow Maps are Symplectic	79
2.3.5	The Symplectic Maps Form a Group	79
2.3.6	Symplectic Integrators	80
2.3.7	The Adjoint Method	81
2.4	Building Symplectic Integrators	82
2.4.1	Splitting Methods	83
2.4.2	General Composition Methods	85
2.4.3	Harmonic + Anharmonic Splitting	85
2.4.4	Explicit and Implicit Methods	86
2.4.5	"Processed" Methods and Conjugacy	88
2.5	Other Classes of Methods	89
2.5.1	Runge-Kutta Methods	89
2.5.2	Partitioned Runge-Kutta Methods	90
2.5.3	Newmark Methods	92
2.5.4	Multiderivative Methods	92
2.5.5	Other Methods	93
	Exercises	94
3	Analyzing Geometric Integrators	97
3.1	The Modified Hamiltonian	98
3.2	Lie Derivatives and Poisson Brackets	100
3.3	Backward Error Analysis for Hamiltonian Splitting Methods	103
3.3.1	Symplectic Euler	106
3.3.2	Verlet	107
3.3.3	Higher Order Symplectic Methods: The Suzuki-Yoshida Method	109
3.3.4	The Takahashi-Imada Method	112
3.4	Perturbative Expansion: Exponentially Small Errors	113
3.5	Energy Conserving Methods	122
3.6	On the Importance of Being Symplectic	127
3.6.1	Time-Reversal Symmetry	128
3.6.2	Time-Reversal Symmetry and Symmetric Numerical Methods	129
3.6.3	Comparing Symplectic and Time-Reversible Methods	130
3.7	Molecular Dynamics with Hard-Sphere Collisions	132
3.7.1	Splitting Methods for Hard Sphere Molecular Dynamics	133
3.7.2	Collisional Verlet Algorithm for Hard Spheres	135
3.7.3	Enhancements of the Collisional Verlet Method	136
	Exercises	136

4 The Stability Threshold	139
4.1 Implicit Schemes	142
4.2 Multiple Timestepping	144
4.2.1 The Reversible RESPA Scheme	145
4.2.2 The Mollified Impulse Method	148
4.3 Methods for Constrained Dynamics	149
4.3.1 Symplectic Structure with Holonomic Constraints	153
4.3.2 Numerical Methods with Holonomic Constraints	156
4.3.3 Iterative Component-Wise Solution of the Nonlinear Equations	158
4.3.4 Symplectic Constrained Dynamics Integrators	159
4.3.5 Higher Order Symplectic Methods: SHAKE and RATTLE	161
4.3.6 Algorithms for Molecular Simulation Using Constraints	164
4.3.7 Numerical Experiment with SHAKE	165
4.4 Rigid Body Systems	166
4.4.1 Euler Equations	171
4.4.2 Rigid Body Molecular Dynamics Algorithm	173
Exercises	175
5 Phase Space Distributions and Microcanonical Averages	179
5.1 The Solution Operator	180
5.2 Evolution of Probability Measure	182
5.2.1 Measure, Probability and Function Spaces	182
5.2.2 Liouville Equation	184
5.2.3 The Liouville Equation for Hamiltonian Systems	186
5.3 The Microcanonical Probability Measure	187
5.3.1 Generalized Functions	188
5.3.2 Steady States	189
5.3.3 The Microcanonical Probability Measure and Averages	194
5.4 Temporal Averages and Numerical Computations	195
5.4.1 The Concept of Ergodicity	197
5.5 Dynamical Averages	203
5.6 Numerical Methods and Invariant Distributions	206
Exercises	209
6 The Canonical Distribution and Stochastic Differential Equations	211
6.1 Ensembles for Molecular Simulation	213
6.1.1 The Microcanonical Ensemble	213
6.1.2 The Canonical Ensemble and the Boltzmann-Gibbs Distribution	214
6.1.3 The Gibbs-Boltzmann Probability Density	216
6.1.4 The Canonical Density and Thermodynamic Averages	219
6.1.5 Calculation of Temperature	220

6.2	Stochastic Differential Equations for Molecular Models	224
6.2.1	Random Walks and Wiener Processes	224
6.2.2	Stochastic Integration	228
6.3	Stochastic Differential Equations	231
6.3.1	The Itô Formula	233
6.3.2	Distributional Solution of the Ornstein-Uhlenbeck SDE	234
6.3.3	Models for Heat Baths and Langevin's Model for Brownian Motion	236
6.3.4	Overdamped Limit of Langevin Dynamics	240
6.3.5	Properties of SDEs	240
6.3.6	The Fokker-Planck Equation	241
6.3.7	Fokker-Planck Equation for Systems of SDEs	243
6.3.8	Fokker-Planck Equation for Langevin Dynamics	244
6.4	Ergodicity of Stochastic Differential Equations	244
6.4.1	Irreducibility of Finite Markov Chains	245
6.4.2	Ergodic Stochastic Differential Equations	247
6.4.3	Ergodicity of Brownian Dynamics	249
6.4.4	Ergodicity of Langevin Dynamics	251
6.4.5	Convergence of Averages	257
	Exercises	259
7	Numerical Methods for Stochastic Molecular Dynamics	261
7.1	Bias	263
7.2	Error in Methods for Stochastic Differential Equations	264
7.3	Sampling Iterations	267
7.3.1	Splitting Methods for Langevin Dynamics	268
7.3.2	Other Langevin Integrators	272
7.4	Error Results for Harmonic Problems	273
7.4.1	Invariant Averages for Schemes Using the A, B and O Splitting	275
7.4.2	More General Schemes	277
7.5	Errors in Configurational Quantities for the Perturbed Harmonic Oscillator	279
7.6	An Exact Gibbs Sampling Method	281
7.7	The Evolution of the Distribution Using a Numerical Method	283
7.7.1	Expansion of the Operator \hat{L}	285
7.7.2	First Order Operator Expansion	287
7.7.3	Perturbation Technique	289
7.8	First Order Schemes	291
7.8.1	Computing the Correction Functions $f_1(q, p)$	292
7.8.2	Numerical Experiment	295

7.9	Error Expansion for Symmetric Langevin Methods	297
7.9.1	Calculation of the Inhomogeneous Term	298
7.9.2	Expansion in Powers of γ^{-1}	301
7.9.3	Superconvergence of the BAOAB Scheme	305
7.10	The Limit Method	306
7.11	Applying the Schemes to a Biomolecule	308
7.11.1	Choosing the Friction Parameter	309
7.11.2	Results for Configurational Sampling	312
7.12	Constrained Langevin Dynamics	317
7.12.1	A “Geodesic Integrator”	319
7.13	Multiple Timestepping	323
	Exercises	326
8	Extended Variable Methods	329
8.1	Dynamics-Based Thermostat Techniques	330
8.1.1	Nosé Dynamics: A Deterministic Thermostat	331
8.1.2	Numerical Methods for Extended System Thermostats	333
8.2	More General Deterministic Thermostats	336
8.2.1	Continuity Equation	336
8.2.2	Nosé-Hoover Chains	339
8.2.3	Lack of Ergodicity of Deterministic Thermostats	340
8.3	Metropolis-Based Stochastic Sampling	341
8.4	Ergodic Stochastic-Dynamic Thermostats	342
8.4.1	Nosé-Hoover-Langevin: An Ergodic Weakly Coupled Thermostat	345
8.4.2	Numerical Integration of the Nosé-Hoover-Langevin Equations	349
8.4.3	Numerical Comparison of Dynamics	350
8.4.4	Velocity Rescaling	355
8.4.5	The Efficiency of a Thermostat and “Gentle” Thermostats	356
8.5	Non-Newtonian Dynamics-Based Iterations for Molecular Sampling	357
8.6	Isokinetic Methods and Integration with Very Large Timestep	361
8.6.1	A Stochastic, Isokinetic Method for Gibbs Sampling	363
8.6.2	Ergodicity	366
8.6.3	Multiple Timestepping Using the Stochastic Isokinetic Formulation	369
8.6.4	Numerical Example	373
8.7	Generalized Langevin Dynamics	373
8.7.1	Using an Extended Variable Representation	375
8.8	Constant Temperature and Pressure Molecular Dynamics	378
8.8.1	Equations of Motion for the NHL Piston	381
8.8.2	Discretization of the NHL Piston	382

8.8.3	Anisotropic Simulation Cell: The Method of Parrinello and Rahman.....	385
8.9	Momentum-Conserving Thermostats and the Dissipative Particle Dynamics (DPD) Method	386
8.9.1	Formulation of DPD	387
8.9.2	Numerical Treatment of the DPD System	390
8.9.3	Extended Variable Momentum-Conserving Thermostats: Pairwise Nosé-Hoover/Nosé-Hoover-Langevin Methods	393
8.9.4	Pairwise Nosé-Hoover-Langevin Thermostat	394
8.10	Numerical Experiments	396
	Exercises	399
A	Force Computation	403
A.1	Accumulation of Long-Ranged Forces	404
A.2	Particle Mesh Ewald (PME)	404
B	Concepts from Probability	407
C	Monte-Carlo Markov Chains	413
C.1	Metropolis Monte-Carlo.....	416
C.2	Metropolis Correction of Numerical Methods	416
C.3	Hybrid Monte-Carlo Methods.....	417
	References	419
	Index	437

Chapter 1

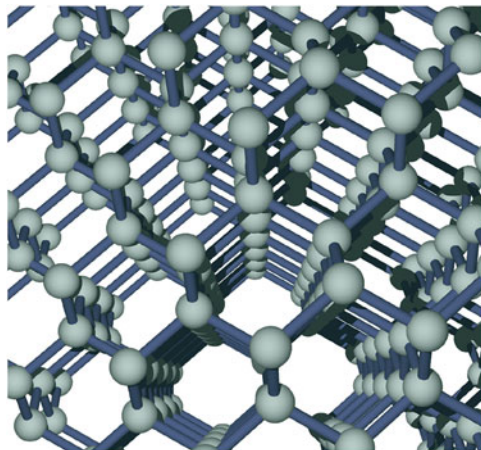
Introduction

Molecular dynamics is the study of how molecules move, deform and interact over time. Predicting or interpreting these changes is essential in chemistry, physics, biology, engineering and other fields. This book discusses the foundations of the numerical methods that are used for studying molecular dynamics.

Molecular dynamics, as a simulation technique, originated with the groundbreaking work of Alder and Wainwright [4, 5] which involved direct simulations of systems of interacting hard spheres and the extraction of thermodynamic data from simulation. During the 1960s, more sophisticated approaches were developed in famous papers of Rahman [306] and Verlet [387]. These techniques were refined and developed over many years with application to liquids, solids and gases. Molecular dynamics is now one of the most flexible and popular tools available for exploring molecular structure, thermodynamic properties and dynamics. For an account of some of the history of the subject, we refer the reader to [82]. The award of a Nobel Prize in 2013 to Martin Karplus, Michael Levitt and Arieh Warshel for their work involving molecular dynamics (specifically for the formulation of methods bridging classical and quantum approaches in molecular dynamics) is just the latest chapter in this great story.

Molecular dynamics is not primarily about making movies of molecules. More often it is about developing quantitative predictions of molecular size and shape, flexibilities, interactions with other molecules, behavior under pressure, and the relative frequency of one state or conformation compared to another. The complex nature of the force fields involved and the large size of typical molecular systems mean that molecular dynamics is almost always chaotic. The changes in a molecule that occur over time are important, but these should be understood in terms of changes in averaged quantities, structural forms, or families of “nearby” structures. Molecular dynamics relies on time-stepping to compute successive snapshots, but these are often used for sampling a probability distribution, or else a number of evolving paths are averaged to describe the likely sequence of changes that would be observed in a typical evolution of the molecule. A major theme of this book is

Fig. 1.1 Lattice of carbon in diamond



that the “sense” of molecular dynamics comes from its ability to allow systematic estimation of averaged quantities (and averaged dynamics), provided the methods and algorithms are constructed according to certain fundamental guiding principles.

In this chapter we consider some of the aspects that relate to understanding the dynamics of a molecular system. Subsequent chapters take up the numerical and statistical perspectives. Our treatment is primarily focussed on mathematical and computational issues, but the application context is important in the selection of methods and in developing a clear understanding of the relevant efficiency issues. For additional background on molecular dynamics the reader is referred to molecular modelling books such as that of Frenkel and Smit [140] or Schlick [328]. For understanding issues relevant for molecular dynamics simulation in relation to biological modelling, one should look to up to date review articles such as [169, 327]. Molecular dynamics is also in widespread use in materials science and engineering; an excellent introduction may be found in [234].

The first problem we run into when trying to talk about molecular dynamics in a sensible way is the choice of an appropriate scale. Familiar objects (such as paper, see Fig. 1.2) consist of a vast collection of atoms which are in constant motion. There are around 10^{23} atoms in a page of a book or 2×10^{25} in a glass of water. These quantities are far beyond what can be stored in a computer, so molecular dynamics relies on simulating a system of very small size compared to the familiar scales of everyday experience. When we discuss molecular systems with equations and computer programs, we typically work at the scale of a few nanometers or tens of nanometers. Diamond (see Fig. 1.1) has 176 atoms per cubic nanometer, aluminum about 60. There are about 33 water molecules in the same volume of liquid water (at standard atmospheric pressure). How many atoms we can handle will depend on how complicated the model is to work with, the extent of coupling between atoms, the available computer power, and the quality of the software available. It may be challenging in some cases to obtain the level of detail and accuracy needed to answer a given question due to the practical limitations of force fields or software

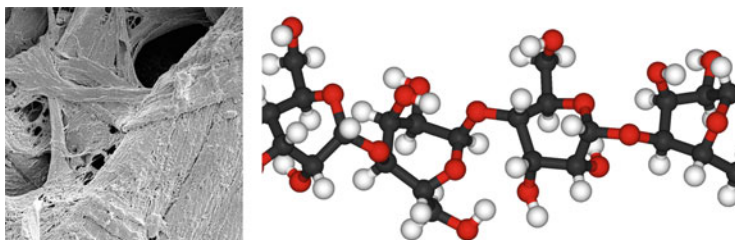


Fig. 1.2 *Left:* scanning electron microscope image of cotton rag paper showing interlocking cellulose fibers (magnification 800 \times , approximately; *source:* The Paper Project <http://paperproject.org/overview.html>); *right:* atomic structure of cellulose ($C_6H_{10}O_5$), *source:* wikipedia commons

or hardware. For other applications it may be possible to include millions of atoms because the interactions that it is essential to incorporate are relatively simple and short-ranged (they tend to weaken very rapidly with increasing distance). Measured by sheer numbers of atoms, the largest simulation to date involved over a trillion atoms interacting in short-ranged potentials and was performed on a computer with over 200,000 processors [145]. Simulations of small molecules with just a handful of atoms are also common, and in such cases attention may be paid to refining the approximation of forces or to including quantum mechanical interactions. The methods described in this book are relatively independent of the size of the system under study.

In organic substances, the computational costs rise more dramatically with the system size, since the atoms carry electronic charge and interact electrostatically even at fairly long range. A model for a protein surrounded by a box of water may involve 20,000 or 30,000 atoms. The terms in the force field lead to the need to use very small timesteps in simulation, therefore the challenge is often to provide a full sampling of the conformational states of the biomolecule on biologically relevant timescales.

Extremely large simulations of biological molecules are increasingly of interest, for example in drug design or the modelling of nucleic acids. Let us illustrate with one recent application. Therapies against human immunodeficiency virus type 1 (HIV-1) are always improving, but the virus continues to evolve and develop resistance to these treatments. HIV-1 virus particles contain conical cores formed by a protein shell composed of the viral capsid protein. This capsid protein plays critical roles in both late and early stages of the infection process and is thought to be a potential target for generating drugs that are active against all variants of HIV-1. Recent data suggest that disassembly (uncoating of the virus) occurs several hours after viral entry into the cell and that the capsid has a pivotal role in various stages of the infection process, namely for transport towards the nucleus, reverse transcription and nuclear import. Study of HIV-1 disassembly is difficult due to the vulnerability of the capsid assembly to experimental manipulation.

In 2013, all-atom simulations performed on the University of Illinois' massive “Blue Waters” computer system unlocked the detailed structure of the HIV-1 virus

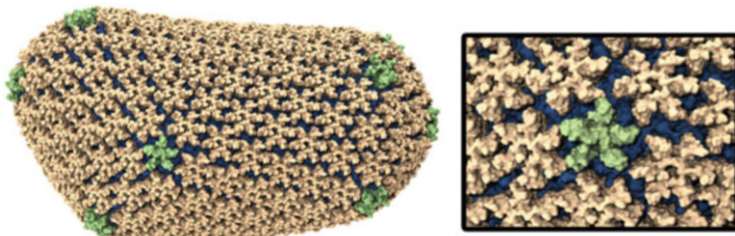


Fig. 1.3 Image of the HIV-1 virus capsid assembly, revealing the detailed structure obtained via all-atom molecular dynamics simulation [399]. This molecule consists of about 1,300 proteins. *Left:* full molecule; *right:* close up showing detail of hexamer/pentamer structure. This image courtesy of Juan Perilla and the Theoretical and Computational Biophysics Group at the University of Illinois Beckman Institute

capsid [399] (see Fig. 1.3).¹ The capsid assembly consists of over a thousand proteins, each of which contains thousands of atoms. The proteins are arranged across the cone-shaped surface to form hexamers and pentamers, in much the same way that a buckminsterfullerene includes both pentagonal and hexagonal faces. The structure was first obtained by cryo-electron-microscopy which then enabled modelling and refinement using large-scale molecular dynamics simulation. The resulting complete atomic HIV-1 capsid model provides a platform for further studies of capsid function and for targeted pharmacological intervention, specifically the development of drugs directly attacking the capsid.

Whether used in chemistry, engineering or medicine, molecular dynamics is an extremely powerful general purpose tool. It affords the prospect of easily changing the properties of the model system (by simply altering the model or adjusting a thermodynamic parameter), which might entail a great deal of preparation in experiment. It offers possibilities to understand the most probable structural forms of the molecule at given temperature and the stability of different conformers or the transitions between them, even where the environmental situation is difficult to achieve in a laboratory setting.

¹Building such a structure from microscopy data is complicated as one must first assemble the pentamer-hexamer frame and optimize the local hexamer and pentamer structural units (i.e. locate the atoms within the structure), using several levels of atomistic force fields (including also quantum-mechanical-molecular mechanical treatments). The last stage is a GPU-accelerated simulation involving 64M atoms for 200 ns using (a) r-RESPA multiple timestepping (See Chap. 4), and (b) constrained bonds to hydrogen atoms (Chap. 4), in (c) a constant temperature and pressure framework (see Chap. 8). (Details provided by one of the authors of the study, J. Perilla of the Theoretical and Computational Biophysics Group, University of Illinois.)

1.1 Classical Mechanics Models

Many of the models used for studying molecules with large numbers of atoms are said to be classical because they rely on assumptions that allow the use of Newton's equations for the motion of the nuclei. Coming to this subject for the first time, one may wonder why we don't use quantum mechanics, since that is a more modern and comprehensive theory of the behavior of matter. A system of N atoms can be described in a probabilistic way using the Schrödinger equation. For illustration, consider a water molecule which has 10 electrons and 3 nuclei, each of which is identified with a point in three dimensions, thus the basic object describing the probability distribution for an isolated water molecule is a complex-valued function of 39 variables. Denote a point in this space by the coordinates $q_{1,x}, q_{1,y}, q_{1,z}, q_{2,x}, q_{2,y}, q_{2,z}, \dots, q_{13,x}, q_{13,y}, q_{13,z}$. The Schrödinger equation itself is a partial differential equation of the following form:

$$i\hbar \frac{\partial \Phi}{\partial t} = -\hbar^2 \sum_{j=1}^{13} \frac{1}{2\mu_j} \left(\frac{\partial^2 \Phi}{\partial q_{j,x}^2} + \frac{\partial^2 \Phi}{\partial q_{j,y}^2} + \frac{\partial^2 \Phi}{\partial q_{j,z}^2} \right) + U_P(q_{1,x}, q_{1,y}, \dots, q_{13,z})\Phi. \quad (1.1)$$

i is the square root of minus 1, \hbar is Planck's constant, μ_j is the mass of the j th particle, Φ is the unknown "wave-function," and U_P is the primitive atomic potential energy function which includes formulas that model the repulsion of electrons due to their similar charge and the attraction of electrons to the positively charged nucleus of each atom. We cannot write down the solution of Schrödinger's equation in a simple form, so we would need eventually to solve the equation numerically, using a computer. Ultimately, the problem with the quantum mechanical approach is one of computational complexity. It is impossible (the "curse of dimensionality") to handle the numerical discretization of a partial differential equation in many variables, due to the rapid explosion in the number of grid points or basis functions that would be needed for approximation. Even the water molecule is beyond the reach of a full scale quantum mechanical treatment. In quantum mechanics we know the fundamental laws describing the system quite well, but the large number of independent spatial dimensions rules out any straightforward attack on the problem. In the words of Paul Dirac, "The underlying physical laws necessary for the mathematical theory of a large part of physics and the whole of chemistry are thus completely known, and the difficulty is only that the exact application of these laws leads to equations much too complicated to be soluble" [106].

An assumption that is often made in order to reduce the complexity of the problem is that the relatively light electrons of the system move instantaneously, entirely slaved to the motion of the heavier nuclei (this is called the *Born-Oppenheimer approximation*). It is then found under certain circumstances that the nuclear coordinates can be viewed as the approximate solutions of a system of ordinary differential equations involving a Born-Oppenheimer potential energy

function $U = U_{\text{BO}}$ depending only on their positions. The potential energy function U might be obtained by solving a time-independent version of Schrödinger's equation for just the electronic variables, but such *ab initio* methods can be very demanding (for the reasons mentioned above) and are only used in special cases. However, there is a lot of interest and great potential for *semi-classical* methods that vary the potential energy landscape ("surface-hopping" [378]) or model localized "wave packet" dynamics [240].

Using the Born-Oppenheimer approximation, it is possible to express the equations of motion of a system of nuclei, in some domain, by use of Newton's Second Law:

$$\text{mass} \times \text{acceleration} = \text{force},$$

where the forces are determined from the potential energy function U . Denoting the coordinates of the i th nucleus of an N -atom system by $q_{i,x}$, $q_{i,y}$, $q_{i,z}$, and the atomic mass by m_i , the equations of motion for the i th nucleus can be written out as

$$m_i \frac{d^2 q_{i,x}}{dt^2} = -\frac{\partial U}{\partial q_{i,x}}, \quad m_i \frac{d^2 q_{i,y}}{dt^2} = -\frac{\partial U}{\partial q_{i,y}}, \quad m_i \frac{d^2 q_{i,z}}{dt^2} = -\frac{\partial U}{\partial q_{i,z}}. \quad (1.2)$$

It is important to recognize that (1.2) does not, itself, give a complete description of the motion; it must be supplemented by initial conditions (positions and velocities given at some specified instant) for all atoms.

The potential U that appears here is much different than U_P that occurs in Schrödinger's equation (which governed the repulsive and attractive interactions of elementary particles). *Empirical force field methods* use assumptions about the form of the force field derived from first principles considerations for simplified systems. They represent a fairly dramatic simplification of the model. The pair interactions between isolated atoms may be well described by certain functional forms, but the empirical models go further in proposing that the potential energy U_{BO} can be replaced by an approximation constructed by summing up various contributions modelling the different interactions present; this approach is not quite consistent with the quantum mechanics of the system, but may allow sufficient accuracy for many practical purposes. A great deal of chemical insight, experimental data and simulation work goes into building the force fields used in molecular modelling, for examples see [9, 10, 53, 305, 394] and the references therein. U will be constructed from special functional forms to describe interactions of pairs, triples or quadruples of atomic nuclei, taking into account, at least to a limited extent, the interactions that would be predicted using quantum mechanics or which are observed in experiments. Some empirical potential models are described in the next section.

It is interesting that the passage from quantum mechanics to a classical model takes us from a linear partial differential equation (that of Schrödinger) to a nonlinear system of ordinary differential equations (those of Newton). Since linear problems are ones whose solutions (at least formally) can be written out, this might seem to be making the problem even more complex, or anyway just substituting

one kind of complexity for another, and indeed nonlinear equations are notoriously difficult to understand fully from a theoretical point of view. However, Newton's equations involve differentiating solutions only in time, and when we discretize the equations to put them on a computer we only have to introduce a grid in this one direction. The fact that there are many equations is not so serious, as the equations themselves are of a type that can easily be treated numerically. The total number of equations we need to solve only goes up linearly with N and the work involved in solving them numerically increases in a relatively modest "polynomial" way (i.e. as a polynomial function of N), compared to the exponential dependence of the computational work on the number of particles that is typically observed in the treatment of quantum mechanics. Even though there are simplified formulations of quantum mechanics and clever discretizations that make the complexity more manageable, the price is still much higher than that of the classical alternative.

The use of an empirical energy function limits the applicability of molecular dynamics, by ruling out certain behaviors that rely explicitly on chemical reactions; even when the assumption is appropriate, the derivation of an effective classical potential energy is nontrivial and may introduce modelling errors. The function U in (1.2) may thus be exceedingly complex in its structure, and the theoretical properties of the dynamical system are not easy to explain, yet, using Newton's equations, molecular simulations involving thousands or even millions of atoms become tractable. In this book we will work with the classical model since it has widespread significance and provides a very good starting point for numerical simulation. Most of the fundamental issues surrounding the theory of molecular dynamics and the construction of numerical methods are actually independent of the detailed features of the potential energy function—there is thus a remarkable generality to the molecular level models and methods used in chemistry, physics, engineering and biology.

Using a classical description based on a smooth, empirical force field is only one of several options available for molecular simulation. The simplest model for a molecular interaction potential is the hard-sphere model. We assume that each atom is an impenetrable sphere which interacts with other atoms via perfectly elastic collision with the atoms transferring, according to standard rules, momentum and energy to one another during the collisions. This was the first model treated in simulation [4] for understanding the statistical mechanics of liquids. Hard sphere simulations are sometimes referred to as "event-driven" since the steps in time are usually taken between the collision events (for recent examples, see [107]). We can think of hard sphere systems as being described by nonsmooth potentials ("infinite at short range"), and it is possible to model systems that include both hard core repulsion and smooth attractive potentials (we describe such methods in Sect. 3.7). Relying exclusively on hard spheres is very restrictive in terms of model accuracy and leads to less efficient propagation algorithms. Thus most modern simulations are based on smooth potentials.

1.1.1 Molecular Potentials

In practice, when designing a classical potential energy function in the empirical approach, the modeller simply works within a defined framework using parameters and prescribed functional forms to match the properties of the system to experimental data (or data obtained from quantum mechanical modelling of small systems). In this subsection, we briefly survey a few of the potential energy functions used in common molecular modelling applications.

In the most common situations, the potential energy function consists of a sum of 2-body, 3-body and/or 4-body terms,

$$U_{ij}(\mathbf{q}_i, \mathbf{q}_j), \quad U_{ijk}(\mathbf{q}_i, \mathbf{q}_j, \mathbf{q}_k), \quad U_{ijkl}(\mathbf{q}_i, \mathbf{q}_j, \mathbf{q}_k, \mathbf{q}_l),$$

where \mathbf{q}_i is the position vector of atom i such that $(q_{i,x}, q_{i,y}, q_{i,z}) = \mathbf{q}_i \in \mathbb{R}^3$. The 2-body terms describe repulsion due to the impenetrability of the outer valence shell of atoms (Pauli repulsion), bonds between atoms which “share” electrons, and the Coulombic attractive and repulsive forces due to net charges accumulating on the atoms of bound groups. Higher body terms model the asymmetry of the wave function for atoms in bound groups.

One of the simplest systems to study is H_2^+ , i.e. a system of two nuclei sharing a single electron. We suppose the two nuclei to be initially well separated with the electron density localized to one of the two and radially symmetric about it. As the internuclear separation is decreased, the charge cloud becomes elongated in the direction of the distant nucleus due to Coulombic attraction. The two nuclei will feel an effective attractive force. As the separation is reduced, the charge cloud will be shared equally by both nuclei. As the nuclei are brought still closer together, the repulsion of the nuclei due to their positive charges comes into play. The potential energy therefore initially decreases as the atoms are brought together from distance before increasing at short range. The situation is diagrammed in Fig. 1.4. The inherent quantum mechanical nature of the interaction is shown by indicating the first few discrete energy levels accessible to the H_2^+ system (source: [100]).

Similar potential energy curves can be found for other bonds. A simple potential energy function whose graph can be used to approximate the potential energy of bond dissociation is the *Morse potential*

$$\varphi_{\text{Morse}}(r) = D \left(1 - e^{-a(r-r_e)} \right)^2.$$

(See Fig. 1.5.) r_e is the location of the minimum, D gives the well depth, and a is a shape parameter that can be used to control the curvature at the minimum. In any given situation, the constants D, a, r_e can all be used to adjust the potential to approximate an effective energy graph from experiment or quantum mechanics. For example, Fig. 1.5 shows the approximation of the H_2 (not H_2^+) bond potential by a Morse curve (which has been shifted down to match the minimum energy).

Fig. 1.4 The H_2^+ interaction potential (charge cloud shown for illustration purposes only)

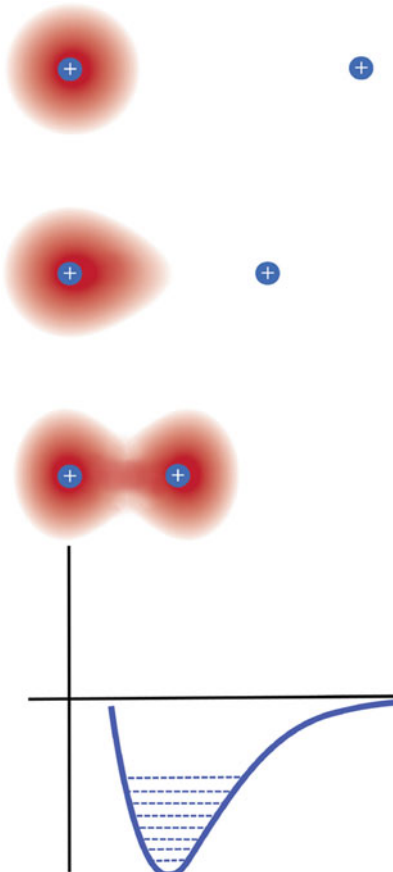
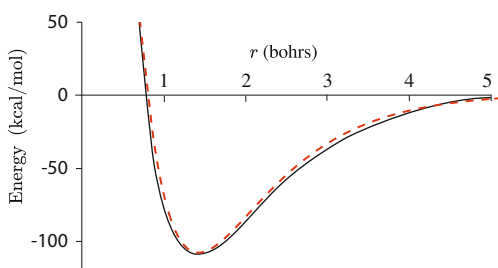


Fig. 1.5 The H_2 bond potential (solid) with a Morse potential fitted to it (dashed curve). Reference H_2 potential curve from [351]



Because they often do not need to be allowed to break during simulation and are very strong compared to other potential terms, *chemical bonds* such as the covalent H_2^+ bond described above are sometimes treated as springs with given rest-length:

$$\varphi_{ij}^{\text{len}}(r_{ij}) = \frac{k_{ij}^{\text{len}}}{2}(r_{ij} - r_{ij}^0)^2, \quad r_{ij} = \|\mathbf{q}_i - \mathbf{q}_j\|.$$

Such a potential can be fitted to the basin of a bond energy function. The molecular motion should be confined to the bottom of the basin for such a simplified harmonic model to be realistic. Of particular importance in models of organic matter are the bonds to hydrogen atoms CH, OH, NH, etc., which tend to have very large harmonic coefficients and therefore give rise to the highest frequency vibrations in the system. Other types of bonds include *ionic bonds* (in which one atom donates an electron to another atom creating a charge imbalance) and *hydrogen bonds*, which are relatively weak interactions that arise as polarization effects between hydrogens and other atoms.

Another type of force arises in multi-electron atoms due to the fluctuations of the charge fields around the atoms. This leads to an instantaneous polarization and an attractive interaction termed *London dispersion*; it is most often modelled using an inverse sixth power potential:

$$\varphi_{\text{disp}}(r) \sim -\frac{K}{r^6}, \quad K > 0.$$

On the other hand, as the atoms come together *Pauli repulsion* comes into play. As the nuclei approach one another, the wave-functions of the electrons in the outer shells of the two atoms will have significant overlap. Due to the Pauli exclusion principle, some of the electrons in these shells are forced into higher energy states and this leads to a higher overall energy (which grows as the internuclear distance is decreased); this is felt as a strong net repulsive force. There are many models for this repulsive wall. The tension between attraction and repulsion creates an energy well. This behavior is incorporated in most smooth short-ranged potential energy models. The combination of dispersive and repulsive forces are referred to as the *van der Waals forces*. Because no electrons are shared between the atoms, the van der Waals forces are much weaker than covalent bonds (in the sense that the potential energy well created due to van der Waals interaction is much more shallow than that associated to a bond).

Buckingham [56] suggested a combined potential of the form

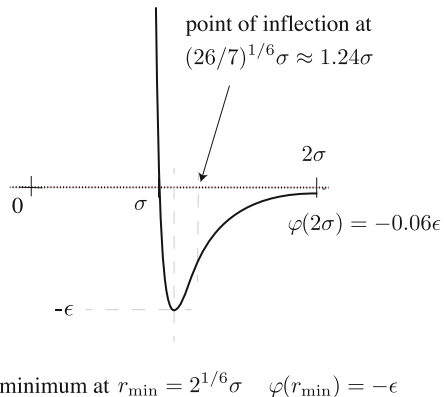
$$\varphi_B(r) = A e^{-Br} - \frac{C}{r^6}, \quad A > 0, B > 0, C > 0.$$

A more common choice in simulation is the Lennard-Jones (6–12) potential

$$\varphi_{\text{LJ}}(r) = 4\epsilon \left[\left(\frac{\sigma}{r}\right)^{12} - \left(\frac{\sigma}{r}\right)^6 \right].$$

The primary motivation for use of Lennard-Jones potentials in simulation is the fact that the 12th power can be obtained by a simple squaring of the 6th power, making the computation of the energy (and forces) relatively fast, however the efficiency obtained from this is not necessarily important, depending on the application and the type of computer hardware available. Because of the strongly repulsive character

Fig. 1.6 The Lennard-Jones pair potential
 $\varphi(r) = 4\epsilon[(\sigma/r)^{12} - (\sigma/r)^6]$
is shown



of short-ranged soft walls in molecular dynamics, i.e., the fact that φ_{LJ} tends rapidly to positive infinity as $r \rightarrow 0$, the atoms remain well separated in long simulations. The singularity at $r = 0$ is therefore rarely encountered in dynamics trajectories, however the presence of the singularity may nonetheless create problems for mathematical analysis, as many theoretical techniques rely on assumed smoothness. An alternative would be to replace the Lennard-Jones potential with a smooth fitted (e.g. piecewise polynomial) potential that captures, for a sufficiently large range of energies, both the attractive behavior and the strong repulsion, while mimicking the Lennard-Jones potential adequately on a sufficiently large interval, without introducing a singularity.

When there are many atoms of different types, the parameters of the potential will depend on this, so we obtain contributions to the total potential energy of the form

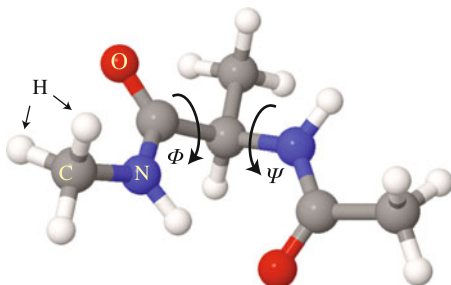
$$\varphi_{ij}^{\text{LJ}}(r_{ij}) = 4\epsilon_{ij} \left[\left(\frac{\sigma_{ij}}{r_{ij}} \right)^{12} - \left(\frac{\sigma_{ij}}{r_{ij}} \right)^6 \right],$$

where $r_{ij} = \|\mathbf{q}_i - \mathbf{q}_j\|$. The Lennard-Jones potential is graphed in Fig. 1.6.

1.1.2 Other Potentials

As we have already mentioned, an important and growing application area for molecular simulation methods lies in the modelling of biological molecules. For example, the alanine dipeptide is a very popular model for examining different simulation algorithms intended for use in biomolecular modelling. It consists of 22 atoms (carbon, oxygen, hydrogen, nitrogen) arranged as shown in the ball and stick diagram of Fig. 1.7.

Fig. 1.7 Illustration of the alanine dipeptide molecule. The central dihedral angles ϕ and ψ are shown which are relevant to describing the conformational states



When, as in the case of the alanine dipeptide, net charges are present on the atoms, one may model this by means of Coulomb potentials:

$$\varphi_{ij}^{\text{Coulomb}}(r_{ij}) = \frac{CQ_iQ_j}{\epsilon r_{ij}},$$

where $\epsilon > 0$ is the dielectric constant, and Q_i, Q_j are the charges on atoms i and j , respectively. C is a positive coefficient allowing the adjustment of units. Obviously the effect of the Coulombic potential depends strongly on whether the atoms have the same or oppositely signed charges.

In the simplest treatments, the Coulomb potential is simply cut off at distance r_{cut} , i.e., is taken to be zero for $r > r_{\text{cut}}$. This should be done in such a way that the potential remains at least continuously differentiable, preferably smoother (see Exercise 11).² However simply neglecting the potential energy after some distance r_{cut} (i.e. introducing a discontinuity in the potential energy function) can be catastrophic in larger systems where long potential energy tails play a significant role (see [242], for instance, where using a cut-off gives nearly an order-of-magnitude error in the computed electrostatic energy). More accurate treatments of the long range behavior include the use of an exponential term involving the Debye length κ which models screening due to the presence of a polar solvent, in which case the potential is modified to have the form of a *Yukawa potential*:

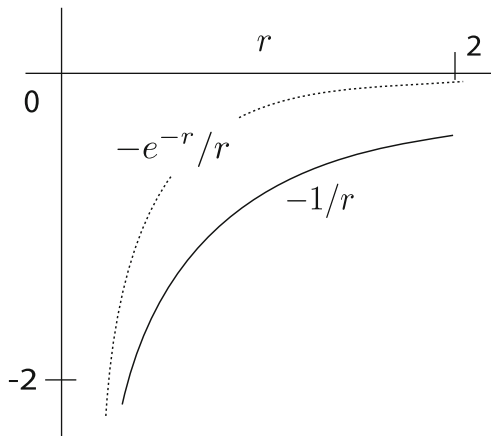
$$\varphi_{ij}^{\text{screened}}(r_{ij}) = \frac{CQ_iQ_j}{\epsilon r_{ij}} e^{-\kappa r_{ij}}.$$

The effect of screening is illustrated in Fig. 1.8. Further modifications substitute potential energies that smoothly go to a constant value (normally zero) at a finite distance, as, e.g. the damped, shifted force model [134].

In addition to length bonds, Lennard-Jones or other short range forces, and Coulomb potentials, it may also be necessary to incorporate *angle bonds* and

²In fact, many results and estimates given in this book technically require greater smoothness, but in practice discontinuity in second or higher derivatives of the potential at a single point does not usually cause great difficulty.

Fig. 1.8 Potentials for Coulombic attraction ($-1/r$, solid curve) and screened Coulomb ($-e^{-r}/r$, dotted curve) interaction are shown



dihedral angle bonds; these model various configurations defined by the chemical bonding of trios or quartets of atoms and are necessary to give correct structures (although 5-atom bond potentials could also, in principle, be introduced, they are generally found to be unnecessary in practice). When a trio of atoms with labels i, j , and k admits a pair of length bonds, say (i, j) and (j, k) , then an additional three-body term will need to be incorporated:

$$\varphi_{ijk}^{\text{ang}} = \frac{k_{ijk}^{\text{ang}}}{2} (\theta_{ijk} - \theta_{ijk}^0)^2,$$

where the angle θ_{ijk} is given in terms of the positions as

$$\theta_{ijk} = \arccos \frac{(\mathbf{q}_i - \mathbf{q}_j) \cdot (\mathbf{q}_j - \mathbf{q}_k)}{r_{ij} r_{jk}}.$$

The leading coefficients describe the energy of the bond in relation to the squared angle, with the rest lengths and angles appearing as parameters. Dihedral potentials typically are modelled using a trigonometric potential function, as

$$\varphi_{ijkl}^{\text{dih}} = k_{ijkl}^{\text{dih}} [1 + \cos(n_{ijkl}^{\text{dih}} \eta_{ijkl} - d_{ijkl}^{\text{dih}})].$$

The angle η_{ijkl} is calculated in the obvious way from the position coordinates, while k, n, d are coefficients appropriate to the local bond organization. In the alanine dipeptide, central dihedral angles Φ and Ψ shown in Fig. 1.7 are defined with reference to a particular bond via the two neighboring bonds along the carbon-nitrogen “backbone” of the chain, as indicated in the illustration. It is then discovered that the most common structures of the molecule can be described in terms of just these two angles, despite the fact that the individual atoms of the system vibrate substantially.

One of the crucial questions in dealing with a biomolecule is how to model the environment surrounding the molecule. It is possible and sometimes desirable to study such a molecule “in vacuum,” in which case only atoms of the molecule need to be treated (the 22 atoms indicated, in the case of the alanine dipeptide), but the real value of molecular dynamics typically comes through the inclusion of a solvent (water) bath which is representative of the living environment. For example, the protein may collapse to a compact, folded state in a different way if the solvent is present than if it is not. Because water is a complicated medium, its treatment requires care in modelling. Surrounding the small molecule by a box of waters (modelled using atomistic potentials) leads to the inclusion of additional degrees of freedom—far more than are associated to the biomolecule itself. The model needs to capture the bonds and non-bonded interactions within and forces between the water molecules and between water and solute. A charge distribution is typically described by point charges, but these need not be collocated with the nuclei.

In addition to the basic structural aspects captured by force fields for water, it may be necessary to model the polarizable nature of water (the tendency for molecules to line up, essentially instantaneously, in the direction of a prescribed or self-consistent electric field).

More discussion of biomolecular potential energy functions may be found in [54, 328]. For applications in materials modelling applications, different potential energy functions are typically used which are normally designed to provide specificity in modelling relevant crystalline structures [234]. Many of these can be viewed as pair potentials that attempt to capture some details of the local structure, such as the presence of a third nearby atom or changes in the local electronic structure.

Some of the most important materials modelling potentials are the following:

- *Stillinger-Weber potential* [344]. This is a model for semiconductors such as silicon. It incorporates two-body and three-body terms and is designed to favor tetrahedral atomic structures.
- *Embedded Atom potentials* [95]. These are designed for simulations of metals and incorporate a simplified approximation of the local electron cloud density due to the presence of neighboring atoms.
- *Bond Order potentials* [300, 361]. These are potentials based on local bond structure (single, double, triple bonding) that help to stabilize the structures of a wide range of materials. A particular family of potentials of this type are the Tersoff potentials which can be used to simulate carbon and other structures. For example, in [389] Tersoff-type potentials were used to model carbon nanotubules (see Fig. 1.9) and to simulate the effect of bending and buckling on thermal conductivity. Such simulations would be virtually impossible to perform using quantum mechanics (due to computational complexity) or using solid mechanics models which cannot resolve molecular-level details such as the sharp structural change at the bending point. These types of molecular potentials have also been used to model collisions of buckminsterfullerenes and the resulting formation of intermediate carbon states, e.g. peanut-like structures [120, 195].

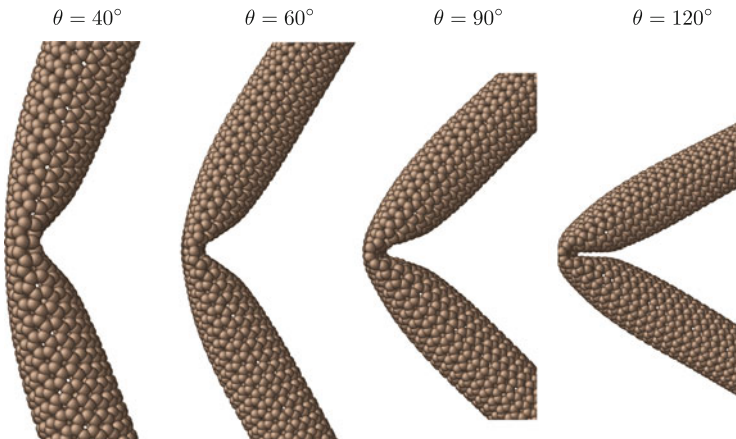


Fig. 1.9 Molecular models using Tersoff potentials allow for study of a wide range of static, dynamic and thermodynamics properties of carbon forms; here carbon nanotubules are shown in several phases of buckling [389]. Image courtesy Prof. Junichiro Shiomi and Dr. Takuma Shiga, Department of Mechanical Engineering, University of Tokyo

There are also ongoing efforts to design potentials that change “on-the-fly,” so to speak, via a range of adaptive techniques, see e.g. [27, 111]. This type of method is particularly important for treating systems that undergo dramatic changes in structure. For example, potentials derived from an adaptive neural network were recently used to simulate the nucleation mechanism by which graphite is converted to diamond under high temperature and extreme high pressure (20–60 GPa) [196].

We close this short survey of potentials in molecular modelling with a couple of simple examples of *coarse-grained* models, which are often used to reduce the number of atoms present in simulation.

Example 1.1 (n-Alkane Chains) In many cases the atomic description can be applied at a coarser level of structure, with several atoms combined and treated as “united atoms.” For example, in [250, 321, 371] this is done for alkane chains. For n-alkanes, the coarse-graining is based on the observation that the atoms of alkanes clump together tightly into four distinct units: two CH_3 groups at the ends of the chain, together with CH_2 groups in the middle. The groups are replaced by pseudoatoms and potentials are constructed to represent the average interaction energy between the different groups. We illustrate the structure of an isolated butane molecule ($\text{CH}_3\text{CH}_2\text{CH}_2\text{CH}_3$) in Fig. 1.10 in terms of the structural diagram which gives the bond connectivities among the different atoms in a two-dimensional layout. The length bonds between united atoms may be modelled using stiff springs but they are often replaced by rigid rods resulting in a constrained dynamics model. (Such models are discussed in Chap. 4.) The torsion potential incorporated into the model for butane has a global minimum for the *trans* (extended) conformer and a

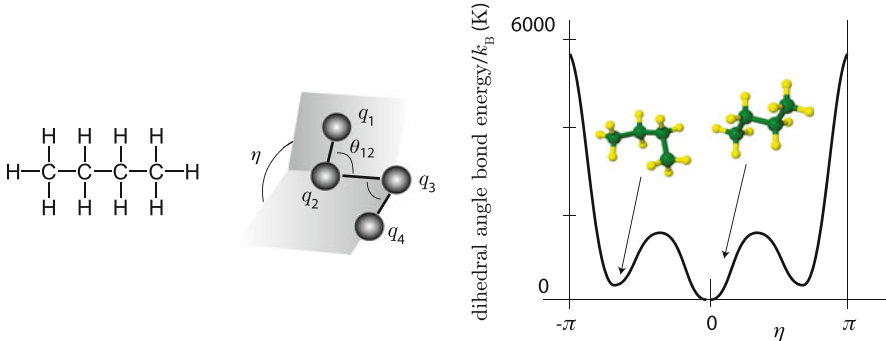


Fig. 1.10 *Left:* structural diagram of butane. *Center:* coarse-grained model of butane using CH_3 and CH_2 groups. *Right:* torsion (or dihedral) potential energy showing locations of local minimum corresponding to trans (global minimum) and gauche (secondary local minimum) states

secondary local minimum for the *gauche* (compact) state (see Fig. 1.10). The same approach can be used to treat many types of large flexible chain molecules.

When a liquid or gaseous alkane system is simulated, the potential energy will include all those intra-molecular terms as well as non-bonded interactions between the atoms of different butane molecules, which might be modelled by Lennard-Jones or, more commonly in recent treatments of alkanes, Buckingham potentials. The potential energy function for an alkane then consists of sums over all the potential energy terms. There are many choices for the detailed specification of parameters. See [340] for a well described model for n-alkane chains.

Example 1.2 (Gay-Berne Potential) In simulations of liquid crystals and other systems with a coarse-grained molecular dynamics model, it is common to replace groups of atoms by ellipsoidal rigid bodies. To correctly model the short ranged interactions of such objects, one needs to introduce an anisotropic intermolecular pair potential to model the short-ranged interactions Fig. 1.11a. A common choice for this purpose is the *Gay-Berne* potential [143] (and various generalizations) which takes into consideration the separation between ellipsoids as well as their orientations relative to the vector linking their centers of mass. The situation is diagrammed in Fig. 1.11b, where the centers of mass of two molecules are \mathbf{q}_1 and \mathbf{q}_2 , $\mathbf{q}_{12} = \mathbf{q}_2 - \mathbf{q}_1$ being the separation vector. $\hat{\mathbf{u}}_1$ and $\hat{\mathbf{u}}_2$ are unit vectors representing the orientations of the molecules. The potential energy may be written as

$$\varphi_{\text{GB}}(\mathbf{q}_1, \mathbf{q}_2, \hat{\mathbf{u}}_1, \hat{\mathbf{u}}_2) = 4\epsilon_{\text{GB}} \left[\left(\frac{\sigma_0}{\Delta} \right)^{12} - \left(\frac{\sigma_0}{\Delta} \right)^6 \right],$$

$$\epsilon_{\text{GB}}(\hat{\mathbf{r}}, \hat{\mathbf{u}}_1, \hat{\mathbf{u}}_2) = \epsilon_1(\hat{\mathbf{u}}_1, \hat{\mathbf{u}}_2)\epsilon_2(\hat{\mathbf{r}}, \hat{\mathbf{u}}_1, \hat{\mathbf{u}}_2),$$

with

$$\Delta(\mathbf{r}, \hat{\mathbf{u}}_1, \hat{\mathbf{u}}_2) = \|\mathbf{r}\| - \sigma_0 / \sqrt{W(\hat{\mathbf{r}}, \hat{\mathbf{u}}_1, \hat{\mathbf{u}}_2, \chi)},$$

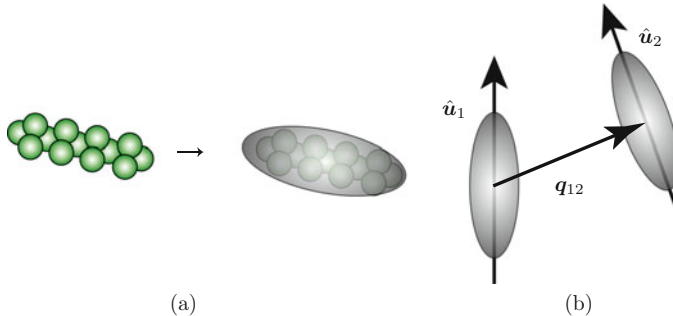


Fig. 1.11 (a) A typical coarse-graining method replaces groups of atoms by ellipsoidal rigid bodies. (b) The Gay-Berne potential models the anisotropic interaction between nonspherical coarse-grained molecules; potentials are described by the orientation of the molecules with respect to a fixed frame and the separation between their centers of mass

$$\epsilon_1(\hat{\mathbf{u}}_1, \hat{\mathbf{u}}_2) = \epsilon_0 [1 - \chi^2 (\hat{\mathbf{u}}_1 \cdot \hat{\mathbf{u}}_2)^2]^{-1/2},$$

$$\epsilon_2(\hat{\mathbf{r}}, \hat{\mathbf{u}}_1, \hat{\mathbf{u}}_2) = W(\hat{\mathbf{r}}, \hat{\mathbf{u}}_1, \hat{\mathbf{u}}_2, \chi'),$$

and

$$W(\hat{\mathbf{r}}, \hat{\mathbf{u}}_1, \hat{\mathbf{u}}_2, \chi) \stackrel{\text{def}}{=} 1 - \frac{\chi}{2} \left[\frac{(\hat{\mathbf{r}} \cdot (\hat{\mathbf{u}}_1 + \hat{\mathbf{u}}_2))^2}{1 + \chi \hat{\mathbf{u}}_1 \cdot \hat{\mathbf{u}}_2} + \frac{(\hat{\mathbf{r}} \cdot (\hat{\mathbf{u}}_1 - \hat{\mathbf{u}}_2))^2}{1 - \chi \hat{\mathbf{u}}_1 \cdot \hat{\mathbf{u}}_2} \right].$$

Finally

$$\chi = \frac{[\sigma_e/\sigma_s]^2 - 1}{[\sigma_e/\sigma_s]^2 + 1}, \quad \chi' = \frac{1 - [\epsilon_e/\epsilon_s]^{1/\mu}}{1 + [\epsilon_e/\epsilon_s]^{1/\mu}}.$$

In the original paper, the parameters were taken to be

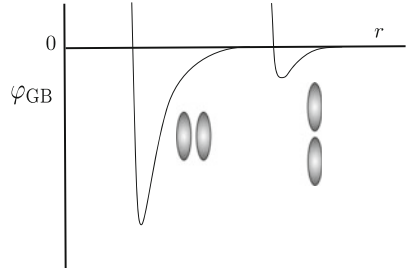
$$\sigma_e/\sigma_s = 3, \quad \epsilon_e/\epsilon_s = 0.2, \quad \mu = 2,$$

yielding $\chi = 4/5$, $\chi' = 0.38$.

The Gay-Berne potential is similar to a Lennard-Jones interaction, but the well depth and its location are adjusted according the orientations of the molecules relative to the vector q_{12} . Figure 1.12 shows the appearance of the Gay-Berne potential energy for two different alignments of the rigid bodies.

Let us emphasize that the design and parameterization of force fields for complicated molecular systems is a difficult task as the properties of the system may only be realized via extensive simulation. In particular, where molecular models are used to make predictions in thermodynamic regimes that are far from available experimental data, the results can occasionally be unpredictable. For example, a NAMD [302] case study simulating the melting of ice demonstrates the care needed

Fig. 1.12 The Gay-Berne potential depends strongly on the relative orientations of the rigid bodies, after a figure in [143]



in providing a precise parameterization [187]: using a general model for water (one not optimized for their specific experiment) the melting point of ice was underestimated by approximately 20 °K.

1.2 The N-Body Problem

In this book, we shall frequently use a compact, vectorial notation, where \mathbf{q} and $\dot{\mathbf{q}}$ represent vectors of the positions and velocities, and \mathbf{M} is a diagonal mass matrix, so the equations of motion (1.2) become

$$\mathbf{M} \frac{d^2}{dt^2} \mathbf{q} = \mathbf{F}(\mathbf{q}) = -\nabla U(\mathbf{q}). \quad (1.3)$$

If the N particles are confined to the real line, then $\mathbf{q} = (q_1, q_2, \dots, q_N)$ and the components of the force \mathbf{F} are $F_i = -\partial U / \partial q_i$. For motion in \mathbb{R}^3 , we write $\mathbf{q}_i = (q_{i,x}, q_{i,y}, q_{i,z})$ for the position vector of the i th particle, and the force acting on this particle is $\mathbf{F}_i = -\nabla_{\mathbf{q}_i} U = -\partial U / \partial \mathbf{q}_i$, that is, the vector with components $F_{i,x} = -\partial U / \partial q_{i,x}, F_{i,y} = -\partial U / \partial q_{i,y}, F_{i,z} = -\partial U / \partial q_{i,z}$. We may also write x_k, y_k, z_k for the x, y and z components of the position of particle k . We let N_c represent the total number of position coordinates of our system, thus for a system of N atoms in three space dimensions there are $N_c = 3N$ coordinates. In the typical case of 3-dimensional space, we view \mathbf{q} as a $N_c = 3N$ -dimensional vector and write $\mathbf{M} = \text{diag}(m_1, m_1, m_1, m_2, m_2, m_2, \dots, m_N, m_N, m_N)$.

The number of local directions in which the configurational (position) state can be varied is called the number of *degrees of freedom* N_d . For the N-body system in \mathbb{R}^3 without additional constraints there are $N_d = N_c = 3N$ degrees of freedom. If r independent constraints are present the number of degrees of freedom is $N_d = N_c - r$.

The total energy of the N-body system is a function of positions and velocities,

$$E(\mathbf{q}_1, \mathbf{q}_2, \dots, \mathbf{q}_N, \dot{\mathbf{q}}_1, \dot{\mathbf{q}}_2, \dots, \dot{\mathbf{q}}_N) = \sum_{j=1}^N \frac{m_j \|\dot{\mathbf{q}}_j\|^2}{2} + U(\mathbf{q}_1, \mathbf{q}_2, \dots, \mathbf{q}_N). \quad (1.4)$$

Along the solutions of (1.3), the energy is conserved, since its derivative vanishes:

$$\frac{d}{dt}E = \sum_{j=1}^N m_j \dot{\mathbf{q}}_j \cdot \ddot{\mathbf{q}}_j + \sum_{j=1}^N \frac{\partial U}{\partial \mathbf{q}_j} \cdot \dot{\mathbf{q}}_j = \sum_{j=1}^N \left(m_j \ddot{\mathbf{q}}_j + \frac{\partial U}{\partial \mathbf{q}_j} \right) \cdot \dot{\mathbf{q}}_j = 0.$$

As will become apparent in later chapters, it is sometimes necessary to introduce additional terms into the model to account for environmental conditions; these may destroy or alter the conservation of energy.

When we refer to the *value* of energy in a conservative system we typically write E instead of \dot{E} (which represents the energy function).³ Thus the positions and velocities of system evolving under Newtonian dynamics satisfy the equation

$$E(\mathbf{q}_1, \mathbf{q}_2, \dots, \mathbf{q}_N, \dot{\mathbf{q}}_1, \dot{\mathbf{q}}_2, \dots, \dot{\mathbf{q}}_N) = E.$$

In addition to the energy, there may be other constants of motion which arise from the structure of the equations of motion. For example, if the full set of particles of an N-body system is included in the model, then the instantaneous force acting on particle i due to the presence of particle j will be the exact negative of the force acting on particle j due to particle i ; this is a direct consequence of Newton's third law (every action has an equal and opposite reaction). This means that the sum of all the forces will vanish. Since

$$\frac{d\mathbf{p}_i}{dt} = \mathbf{F}_i,$$

we have

$$\sum_{i=1}^N \frac{d\mathbf{p}_i}{dt} = \sum_{i=1}^N \mathbf{F}_i = 0$$

and thus the three components of the *total momentum vector* $\mathbf{p}_{\text{tot}} := \sum_{i=1}^N \mathbf{p}_i$ will be conserved quantities. Additional first integrals sometimes arise in specific situations, depending on the form of the potential energy function.

For a few very special N-body systems, analytical solution is possible.

Example 1.3 (Harmonic Oscillator) Consider the system

$$\dot{x} = v, \quad \dot{v} = -\Omega^2 x.$$

³We use roman (non-italic) letters for parameters that describe the thermodynamic state, e.g. number of degrees of freedom, the volume, the energy, the temperature or the pressure.

This system describes the behavior of a particle with unit mass in one dimension, with energy function $E(x, \dot{x}) = \dot{x}^2/2 + \Omega^2 x^2/2$, where its motion is governed by a linear 2nd order equation $\ddot{x} + \Omega^2 x = 0$. The solution, for given $x(0) = \xi$, $\dot{x}(0) = v(0) = \eta$, is

$$x(t) = \xi \cos(\Omega t) + \frac{\eta}{\Omega} \sin(\Omega t).$$

This system, despite its simplicity, is an important test case for many schemes in molecular dynamics and will appear in many forms throughout this book (we generally refer to any system where the energy has quadratic position dependence as harmonic and any one degree of freedom harmonic system as a harmonic oscillator).

Example 1.4 (Single Degree of Freedom) Consider a simple system with a single degree of freedom (with unit mass $m = 1$ for simplicity) and energy function $E(x, \dot{x}) = \dot{x}^2/2 + U(x)$ (which includes the harmonic oscillator as a special case). The equations of motion are

$$\dot{x} = v, \quad \dot{v} = -\frac{\partial U}{\partial x}.$$

Solutions are smooth functions $(x(t), v(t))$ that evolve on curves that are defined by $E(x, v) \equiv E$, where E is the energy calculated at the initial point $(x(0), v(0)) = (\xi, \eta)$. Near this point, provided $\eta \neq 0$, let us solve the equation $E(x, v) = E(\xi, \eta)$ for v as a unique smooth function of x , ξ , η using the implicit function theorem: $v = V(x, \xi, \eta)$. Inserting this into the differential equations we then find

$$\frac{dx}{dt} = v = V(x, \xi, \eta).$$

This is a separable differential equation; it is therefore easily integrated from any provided initial value, $x(0) = \xi$, as a function of t , resulting in a relation $x = X(t, \xi, \eta)$. Then $v = V(X(t, \xi, \eta), \dot{x}, \eta)$ and we see that it is possible to derive the formula for the solution (x, v) as a function of t and the initial conditions. This representation provides a complete characterization of the *local* behavior of solutions, i.e., within a small interval of our starting point. To describe the *global* solutions, we would need to piece together several such local representations. For example if we used this approach to solve the harmonic oscillator, the equation for x would be $\dot{x} = \pm \sqrt{2E - \Omega^2 x^2}$, and the sign that appears would define different parts of the solution which may be concatenated together to describe a global solution. “Degenerate” points, where $\partial E / \partial v = 0$, lead to difficulties that must be resolved on a case by case basis.

In more complicated systems, it is usually impossible to write down a formula for the solution in an explicit form; so approximation (typically using numerical methods) becomes essential to being able to predict dynamics.

Example 1.5 (Simple N-Body Molecular System) We can now describe a molecular system consisting of N neutral atoms with pairwise Lennard-Jones potentials; this could be used to model liquid argon or a similar inert system; it is one of the first important simulations performed using a smooth classical potential [306, 387]. The Lennard-Jones potential is

$$\varphi_{\text{LJ}}(r) = 4\epsilon \left[\left(\frac{\sigma}{r}\right)^{12} - \left(\frac{\sigma}{r}\right)^6 \right],$$

with typical parameters (for argon) $\epsilon = 1.65 \times 10^{-21}$ J and $\sigma = 3.4 \times 10^{-10}$ m. The energy of the system is

$$E = \frac{1}{2} \sum_{i=1}^N m\dot{\mathbf{q}}_i^2 + \sum_{i=1}^{N-1} \sum_{j=i+1}^N \varphi_{\text{LJ}}(r_{ij}),$$

where $r_{ij} = \|\mathbf{q}_i - \mathbf{q}_j\|$ and the mass m of an argon atom is 6.69×10^{-26} kg. The equations of motion are, for $i = 1, 2, \dots, N$, using the chain rule,

$$\begin{aligned} m\ddot{\mathbf{q}}_i &= \sum_{\substack{j=1 \\ j \neq i}}^N \frac{\varphi'_{\text{LJ}}(r_{ij})}{r_{ij}} (\mathbf{q}_i - \mathbf{q}_j) \\ &= -24 \frac{\epsilon}{\sigma} \sum_{\substack{j=1 \\ j \neq i}}^N r_{ij}^{-1} \left[2 \left(\frac{\sigma}{r_{ij}}\right)^{13} - \left(\frac{\sigma}{r_{ij}}\right)^7 \right] (\mathbf{q}_i - \mathbf{q}_j). \end{aligned}$$

Now introduce the change of variables

$$\mathbf{Q}_i = \sigma^{-1} \mathbf{q}_i, \quad i = 1, 2, \dots, N,$$

then $\dot{\mathbf{q}}_i = \sigma \dot{\mathbf{Q}}_i$, $\ddot{\mathbf{q}}_i = \sigma \ddot{\mathbf{Q}}_i$, and $\|\mathbf{q}_i - \mathbf{q}_j\| = \sigma \|\mathbf{Q}_i - \mathbf{Q}_j\|$. The equations of motion in these normalized coordinates may be written

$$\frac{m\sigma^2}{\epsilon} \frac{d^2 \mathbf{Q}_i}{dt^2} = - \sum_{\substack{j=1 \\ j \neq i}}^N \frac{\hat{\varphi}'_{\text{LJ}}(R_{ij})}{R_{ij}} (\mathbf{Q}_i - \mathbf{Q}_j),$$

where $R_{ij} = \|\mathbf{Q}_i - \mathbf{Q}_j\|$ and $\hat{\varphi}_{\text{LJ}}(R) = 4[R^{-12} - R^{-6}]$. Thus we see that if we make the additional time transformation

$$\tau = \alpha t, \quad \alpha^2 = \frac{\epsilon}{m\sigma^2},$$

Fig. 1.13 Table of units and their values for a model of argon (Ar)

Quantity	Unit	Typical value (Ar)
length	σ	3.4×10^{-10} m
mass	m	6.69×10^{-26} Kg
energy	ϵ	1.65×10^{-21} J
time	$\sigma\sqrt{m/\epsilon}$	2.17×10^{-12} s
velocity	$\sqrt{\epsilon/m}$	1.57×10^2 m/s
force	ϵ/σ	4.85×10^{-12} Newtons
temperature	ϵ/k_B	120K
pressure	ϵ/σ^3	4.20×10^7 Newtons/m ²

then the equations become

$$\frac{d^2\mathbf{Q}_i}{d\tau^2} = - \sum_{\substack{j=1 \\ j \neq i}}^N \frac{\hat{\phi}'_{\text{LJ}}(R_{ij})}{R_{ij}} (\mathbf{Q}_i - \mathbf{Q}_j).$$

This means that a natural choice for the unit of time is

$$\alpha^{-1} = \sigma \sqrt{\frac{m}{\epsilon}} \approx 2.17 \times 10^{-12} \text{ s}.$$

By using the units given here, we may work with a simplified form of the Lennard-Jones system involving unit masses and a parameter-independent potential energy function.

In Fig. 1.13 we summarize the typical units relevant for studies of argon. The role of temperature and pressure will be discussed in Chaps. 6–8. \square

1.3 The Lagrangian and Generalized Coordinates

An N-body system is often formulated in terms of its *Lagrangian* $L = L(\mathbf{q}, \dot{\mathbf{q}})$: the difference between kinetic and potential energies. The somewhat mysterious Lagrangian function was introduced by Joseph Louis Lagrange. Its relevance becomes clear in formulating the *principle of least action*, a variational principle which gives an abstract formulation of the equations of motion. We defer introducing this derivation of the equations of motion until Chap. 2, where it is also used as a means of deriving a numerical method for molecular simulation.

For the system (1.3) with N atoms and $N_c = 3N$ configuration coordinates, the Lagrangian is

$$L \stackrel{\text{def}}{=} \frac{\dot{\mathbf{q}}^T M \dot{\mathbf{q}}}{2} - U(\mathbf{q}).$$

The equations of motion may be expressed in terms of the Lagrangian as:

$$\frac{d}{dt} \frac{\partial L}{\partial \dot{q}} = \frac{\partial L}{\partial q}.$$

(Note that this must be interpreted in general as a set of $N_c = 3N$ equations, one for each atomic coordinate.) The real usefulness of the Lagrangian perspective comes when we introduce different types of coordinates to express the equations of motion; examples of this are given below.

When we introduce a smooth change of variables $\mathbf{q} = \Phi(\mathbf{Q})$, where $\Phi : \mathbb{R}^{N_c} \rightarrow \mathbb{R}^{N_c}$, this induces a corresponding transformation of the velocity vector by

$$\dot{\mathbf{q}} = \Phi'(\mathbf{Q})\dot{\mathbf{Q}},$$

where Φ' is the $N_c \times N_c$ Jacobian matrix of Φ . Then the Lagrangian of the system is transformed to

$$\tilde{L} = \frac{\dot{\mathbf{Q}}^T \Phi'(\mathbf{Q})^T M \Phi'(\mathbf{Q}) \dot{\mathbf{Q}}}{2} - U(\Phi(\mathbf{Q})),$$

It is not essential for the change of variables to be a map from \mathbb{R}^{N_c} to \mathbb{R}^{N_c} . For example, in a system with constraints, the change of variables might represent a parameterization of the manifold defined by the constraints. Then the mapping Φ might be from \mathbb{R}^{N_d} to \mathbb{R}^{N_c} , where $N_c \geq N_d$. An abstract set of configuration variables is referred to as a set of *generalized coordinates*. The introduction of generalized coordinates in an N -body system typically leads to a Lagrangian which can be viewed as quadratic in the velocities but with a “configuration-dependent mass matrix.” We will assume that any such changes of variables are regular transformations in the sense that Φ' is of full rank and the resulting generalized mass matrix is invertible.

Although generalized coordinates are often useful for understanding molecular systems, as we shall learn in later chapters, it is desirable to avoid the use of formulations with a configuration-dependent mass matrix since it complicates the design of numerical methods with good conservation properties. This is one reason that molecular simulation methods are typically described in a Cartesian coordinate framework.

1.4 Hamiltonian Formulation

In this section, we introduce the Hamiltonian description of the motion which is useful for discussing the underlying geometric structure associated to classical mechanics. We can understand the Hamiltonian formulation as a natural description of classical mechanics from several perspectives. First, it is based directly on the

most basic conservation law associated to a closed system (the conservation of energy) as it is formulated in terms of the energy function. Second, it is the starting point for the quantum mechanical treatment of a system of particles, since the Schrödinger equation is written in terms of the quantum analogue of the energy function. Third, we may view the Hamiltonian as the *Legendre transformation* of the Lagrangian viewed as a function of the velocities. This is a *conjugacy* relationship which ensures that the properties of the two systems are, under typical conditions, equivalent.

Abstractly, a Legendre transformation of a given convex function $g = g(\xi) : \mathbb{R}^m \rightarrow \mathbb{R}$ is a new function $\tilde{g} = \tilde{g}(\eta) : \mathbb{R}^m \rightarrow \mathbb{R}$ defined by

$$\tilde{g}(\eta) = \sup_{\xi} (\eta^T \xi - g(\xi)),$$

where the symbol \sup_{ξ} means to find the supremum of the given expression with respect to variation of the vector ξ . In the case of the Lagrangian $L(q, v) = v^T M(q)v/2 - U(q)$ (which we have seen is the formulation of a mechanical system in generalized coordinates) we find

$$\sup_v (p^T v - (v^T M(q)v/2 - U(q))) = \sup_v (p^T v - v^T M(q)v/2) + U(q).$$

If $M(q)$ is invertible, the supremum is achieved precisely when

$$v = M^{-1}(q)p,$$

which gives the standard definition of the momentum vector p in terms of velocities,

$$p = \frac{\partial L}{\partial \dot{q}} = M(q)\dot{q},$$

and, with $v = M^{-1}(q)p$, the Legendre transformation results in a new function

$$H(q, p) \stackrel{\text{def}}{=} p^T M(q)^{-1} p / 2 + U(q).$$

This is precisely the energy function, written in terms of positions and momenta. In this form it is termed the *Hamiltonian* and it provides an alternative description of the system. The equations of motion can be written

$$\dot{q} = \frac{\partial H}{\partial p}, \quad \dot{p} = -\frac{\partial H}{\partial q}.$$

For constant M we obtain the dynamical equations,

$$\dot{q} = M^{-1}p, \quad \dot{p} = F = -\partial U / \partial q.$$

This is not a big step from the Newtonian form of the equations of motion $\dot{\mathbf{q}} = \mathbf{v}; \mathbf{M}\dot{\mathbf{v}} = \mathbf{F}$. More generally, for molecular models, the Hamiltonian and Lagrangian formulations are interchangeable, but the use of the Hamiltonian form is preferred for allowing simplified description of the geometric character of the solutions of the system as we discuss in Chaps. 2–4.

The set of all positions and momenta for which the energy is finite is termed the *phase space*. The instantaneous state of a molecular system involving many, say N , particles moving in \mathbb{R}^3 is described by coordinates and positions, i.e., by a point in \mathbb{R}^{6N} . The “points” defining atomic positions (generally taken to be located in \mathbb{R}^3) should be clearly distinguished from the “points,” in \mathbb{R}^{6N} , of the phase space, which represent the collection of all position and momenta vectors of the atoms. One may speak of a “phase space point” or simply “phase point” to describe the latter. We are ultimately going to be interested in how sets of phase points are carried forward by solution of the differential equations. It is crucial to observe that when we discuss such sets the individual points therein are understood to be completely independent of one another, and their motion is governed only by the laws of mechanics as described by the equations of motion.

1.5 Existence and Uniqueness of Solutions

One of the most important properties of a typical classical molecular Hamiltonian system is the existence and uniqueness of solutions started from a generic initial condition. The traditional study of existence and uniqueness for systems of nonlinear ordinary differential equations gives local results only, but for Hamiltonian systems considered in molecular dynamics the solutions are typically globally defined. The uniqueness of solutions is easily verified in the usual way (as for the local result for uniqueness of solutions). The key point is that, with the energy constraint, solutions typically remain bounded for all time.

Assume that U is a potential energy function which is bounded below, $U \geq U_{\min}$. For given $E_0 \geq U_{\min}$ define $\Sigma_{E_0} = \{(\mathbf{q}, \mathbf{p}) | H(\mathbf{q}, \mathbf{p}) = E_0\}$. Then, for $(\mathbf{q}, \mathbf{p}) \in \Sigma_{E_0}$ we have

$$\frac{\mathbf{p}^T \mathbf{M}^{-1} \mathbf{p}}{2} + U(\mathbf{q}) = E_0 \Rightarrow \frac{\mathbf{p}^T \mathbf{M}^{-1} \mathbf{p}}{2} = E_0 - U(\mathbf{q}) \leq E_0 - U_{\min}.$$

\mathbf{M}^{-1} is a positive definite matrix (assumed here to be constant), so we can infer that the momenta are bounded at fixed total energy. We would like to say something similar for positions. We have, at energy E_0 ,

$$U_{\min} \leq U(\mathbf{q}) \leq E_0.$$

What is needed is an assumption that the level sets $\hat{\Sigma}_\alpha = \{\mathbf{q} | U(\mathbf{q}) = \alpha\}$ are bounded uniformly for $\alpha \in [U_{\min}, E_0]$. Then it follows that solutions satisfying the energy constraint remain confined to a compact (closed and bounded) set.

The assumption on U is not satisfied by some simple potentials. For example consider $U(x, y) = x^2$ which is completely independent of y and so places no restriction on that variable for constant energy. The condition on U means that it has a *confining* property. To ensure bounded solutions in systems that do not have a confining potential, we should add other assumptions, for example the assumption that the position vectors of each atom are restricted by periodic boundary conditions to lie on a three-dimensional torus (see Section 1.6).

1.5.1 The Flow Map

Consider now the initial value problem

$$\dot{z} = f(z), \quad z(0) = \xi, \quad (1.5)$$

in a m -dimensional space. If we assume that f corresponds to a molecular Hamiltonian system satisfying the assumptions of the existence and uniqueness result of the previous subsection, then we may define a mapping from a point in phase space to the point t units later along the time-evolution starting from the initial point. We refer to this map as the *flow map* and denote it by \mathcal{F}_t . $\mathcal{F}_t(\xi) = z(t)$ solves the initial value problem (1.5). It may equally describe the evolution of a point with time, or the evolution of a set of points with time.

The classical systems treated here can be solved forward or backward in time. Observe that $\mathcal{F}_{-t}\mathcal{F}_t = \text{Id}$ (the identity map), thus the flow map is invertible and, indeed, the family of flow maps defined for different values of t form an Abelian group under the operation of composition ($\mathcal{F}_t\mathcal{F}_s = \mathcal{F}_s\mathcal{F}_t = \mathcal{F}_{t+s}$). The flow map of a Hamiltonian system conserves its Hamiltonian, thus

$$H(\mathcal{F}_t(\xi)) \equiv H(\xi).$$

(This equation just expresses the conservation of energy.)

The flow map provides an easy notation for describing solutions (even in cases where it is difficult or impossible to compute it exactly). When we speak of numerical methods for solving differential equations, we generally mean methods that approximate the flow map in a suitable sense.

Despite the existence of a well-defined flow map, we cannot solve most systems of differential equations analytically (even Hamiltonian ones) so we cannot usually write out a formula for the flow map. An exception is the harmonic oscillator,

$$\dot{q} = p, \quad \dot{p} = -\Omega^2 q,$$

for which the solution subject to initial values $q(0) = q_0, p(0) = p_0$ is

$$\begin{pmatrix} q(t) \\ p(t) \end{pmatrix} = \mathcal{F}_t \begin{pmatrix} q_0 \\ p_0 \end{pmatrix} \equiv \begin{pmatrix} q_0 \cos(\Omega t) + p_0 \sin(\Omega t)/\Omega \\ -q_0 \Omega \sin(\Omega t) + p_0 \cos(\Omega t) \end{pmatrix}.$$

In somewhat more generality, suppose we are given an initial value problem for a linear system of ordinary differential equations,

$$\frac{dz}{dt} = Az, \quad z(t_0) = \zeta,$$

where $A = (a_{ij})$ is a constant $m \times m$ matrix. The solution of this linear system may be described in several ways. If A has a basis of eigenvectors $\eta_i, i = 1, \dots, m$, with corresponding eigenvalues $\lambda_1, \lambda_2, \dots, \lambda_m$, then we may write the solution at time t as

$$z(t) = \sum_{i=1}^m c_i e^{\lambda_i(t-t_0)} \eta_i$$

where the coefficients c_i are obtained by solving the equation

$$z(t_0) \equiv \zeta = \sum_{i=1}^m c_i \eta_i.$$

Observations: (i) eigenvectors, eigenvalues, and coefficients c_i may be complex, but if A and ζ have real coefficients, it is nonetheless possible to obtain a real solution, and (ii) with our assumption that the $\{\eta_i\}$ form a basis, the calculation of the coefficients is always possible, since the matrix X whose columns are the eigenvectors will be invertible, that is, the coefficients c_i can be enumerated as the components of a vector c which satisfies the square linear system

$$\zeta = Xc.$$

An alternative expression for the solution is in terms of the exponential of the matrix A scaled by time,

$$z(t) = e^{A(t-t_0)} \zeta.$$

The exponential of a matrix can be defined, in the case of a matrix with a full set of eigenvectors, in terms of the eigenvector expansion. Alternatively, one may think of $\exp(A)$ as the sum of the exponential series

$$e^A \equiv I + A + \frac{1}{2!}A^2 + \frac{1}{3!}A^3 + \dots$$

although this is seldom the most efficient method to compute it (this series converges for all matrices A , and so in fact the exponential expression for the solution of the linear system is well defined even in the absence of a full set of eigenvectors). Typically one favours diagonalization of the matrix A in order to exponentiate (for more details see for instance [52, 273, 275]).

Noting that the origin of time is arbitrary in an autonomous system such as this one, we may think of the exponential as a representation of the flow map,

$$\mathcal{F}_t(z) \equiv e^{At}z.$$

1.5.2 Integrable Examples

Given a differential equation system, the first instinct is to try to solve the equations. Being able to do this relies on having enough constants of motion available to “pin down” the solution. Systems whose solutions are constrained in this way are examples of *integrable systems*.

As mentioned previously, for the N-body system, energy and total momentum are constants of motion—they do not change even as the bodies of the system move along their natural paths (defined by the equations of motion). Another term for constant of motion is *first integral*. In general, if we have a dynamical system $\dot{z} = f(z)$, a *first integral* is a smooth function $I(z)$ which is constant along solutions, for all values of the initial condition. Let $z(t) : t \in \mathbb{R}$ be a solution, then

$$I(z(t)) \equiv I(z(0)) \Rightarrow 0 \equiv \frac{d}{dt}I(z(t)) = \nabla I(z(t)) \cdot \dot{z}(t) = \nabla I(z(t)) \cdot f(z(t)).$$

Since this should hold everywhere, the condition for I to be a first integral is that $\nabla I \cdot f \equiv 0$.

The existence of a first integral of a two-dimensional system of ordinary differential equations $\dot{x} = g(x, y), \dot{y} = h(x, y)$ allows the description of all the solutions of the equation in terms of the level curves of a scalar-valued function I : $I(x, y) \equiv I_0$.

In principle such an equation can be solved (locally at least) for y as a function of x due to the implicit function theorem. Hence one may write $y = \psi(x)$. Reinsert this into the first differential equation to get a reduced equation in just one dependent variable:

$$\frac{dx}{dt} = g(x, \psi(x)).$$

Such an ordinary differential equation is said to be *separable*, and theoretically can be solved, given an initial condition, for x as a function of t .

Example 1.6 The single degree of freedom model of Example 1.4 has the energy as a first integral. The system is therefore integrable.

Example 1.7 The Kepler problem describes the motion of a body in the plane moving under gravitational force exerted by a second, fixed body (located at the origin); it has the energy $E(x, y, \dot{x}, \dot{y}) = \dot{x}^2/2 + \dot{y}^2/2 - \frac{1}{\sqrt{x^2+y^2}}$. Note that a consequence of fixing one of the bodies in the Kepler problem is that the two components of the total momentum vector, i.e. $(m\dot{x}, m\dot{y})$, are obviously no longer conserved; however, due to the fact that the potential energy is rotationally invariant (dependent only on the distance of the moving particle from the origin), the *angular momentum* of the system is conserved. The two conserved quantities, energy and angular momentum, mean that the Kepler problem is an integrable system.

In polar coordinates $(x, y) = (r \cos \theta, r \sin \theta)$, the Lagrangian L for the Kepler problem is

$$\begin{aligned} L &= K - U \\ &= \frac{1}{2}(\dot{r} \cos \theta - r \dot{\theta} \sin \theta)^2 + \frac{1}{2}(\dot{r} \sin \theta + r \dot{\theta} \cos \theta)^2 + \frac{1}{r} \\ &= \frac{\dot{r}^2}{2} + \frac{r^2 \dot{\theta}^2}{2} + \frac{1}{r}. \end{aligned}$$

The form of Hamilton's equations is the same no matter what variables we work in (as long as the change of variables is regular, i.e., it can be inverted). Thus, in polar coordinates,

$$\frac{d}{dt} \frac{\partial L}{\partial \dot{r}} = \frac{\partial L}{\partial r}, \quad \frac{d}{dt} \frac{\partial L}{\partial \dot{\theta}} = \frac{\partial L}{\partial \theta}.$$

Working these out directly, one gets

$$\begin{aligned} \ddot{r} &= -\frac{1}{r^2} + r \dot{\theta}^2, \\ 0 &= \frac{d}{dt}(r^2 \dot{\theta}). \end{aligned}$$

In terms of the original variables, $l_z = x\dot{y} - y\dot{x}$ is the coordinate of the angular momentum which points out of the plane of motion. Expressed in polar coordinates this is

$$\begin{aligned} l_z &= (r \cos \theta)(\dot{r} \sin \theta + r \dot{\theta} \cos \theta) - (r \sin \theta)(\dot{r} \cos \theta - r \dot{\theta} \sin \theta) \\ &= r^2 \dot{\theta}(\cos^2 \theta + \sin^2 \theta) = r^2 \dot{\theta}, \end{aligned}$$

so the second equation of motion in polar coordinates just expresses the constancy of angular momentum. Taking this quantity as fixed, we may write the remaining equation as $\ddot{r} = -\frac{1}{r^2} + \frac{l_z^2}{r^3}$. The equation for r is that of a one degree-of-freedom

system with energy

$$\hat{E}(r, \dot{r}) = \frac{\dot{r}^2}{2} - \frac{1}{r} + \frac{l_z^2}{2r^2}.$$

From our previous work, we know that this system (a single degree of freedom system) can be solved for r as a function of t and the initial conditions. Once $r = r(t)$ is known, we may obtain θ by integration:

$$\theta = \theta(0) + \int_0^t \frac{l_z}{r^2(s)} ds.$$

The example shows that the full solution of the Kepler problem can be worked out given the initial conditions, as long as we are happy to express the solution in terms of antiderivatives of simple functions (and their inverses). Obviously the practical aspects may complicate things, but the idea that the solution can be expressed in this way is already important.

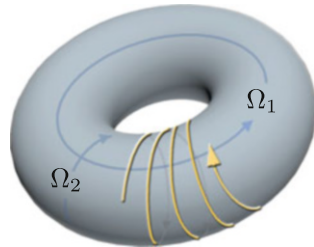
The harmonic oscillator and Kepler problem are both examples of *integrable* systems. In each case there are as many first integrals as there are degrees of freedom. For integrable systems, it is possible, at least locally, to rewrite the equations in new variables that greatly simplify the presentation of the solutions. “Writing a system in new variables” means introducing a change of coordinates. For the harmonic oscillator, recall that the energy is $E(x, v) = v^2/2 + \Omega^2 x^2/2$ and the equations of motion are $\dot{x} = v$, $\dot{v} = -\Omega^2 x$. Define new variables

$$x = \sqrt{2I/\Omega} \cos \theta, \quad v = \sqrt{2I\Omega} \sin \theta.$$

In these variables, the energy is $E = I\Omega$. Introducing these formulas into the equations of motion and simplifying leads to $\dot{I} = 0$, $\dot{\theta} = -\Omega$. The first equation expresses the constancy of energy; the second describes a rotation with frequency Ω , i.e., the solution is $\theta(t) = \theta(0) - \Omega t$. The variables (I, Ω) are referred to as “action-angle” variables.

A slightly more complicated integrable system would consist of d decoupled harmonic oscillators, each of which has equations of motion $\dot{x}_j = v_j$, $\dot{v}_j = -\Omega_j^2 x_j$. The simple change of variables $((x_j, v_j) \rightarrow (I_j, \theta_j))$, applied to each oscillator, would yield equations of motion $\dot{I}_j = 0$, $\dot{\theta}_j = -\Omega_j$. This describes a point winding about a d -dimensional torus defined by angular rotation frequencies Ω_j and radii $|I_j|$ (Fig. 1.14). Depending on the ratio of frequencies such motions may be periodic or quasi-periodic; in the latter case the paths do not “close up” but instead we the curve gradually fills in the surface of the torus. This type of regular motion is sometimes referred to as “tori motion.” More generally, one finds occasional examples of nonlinear systems which possesses as many independent first integrals as degrees of freedom (satisfying a certain “involution” condition); such systems may be reduced via coordinate transformation to action-angle variables, i.e. they exhibit tori motion.

Fig. 1.14 Integrable dynamics may be viewed as periodic or quasi-periodic motion on the surface of a torus (illustrated for a system with two degrees of freedom)



1.5.3 Equilibrium Points, and the Linearization Theorem

Molecular systems can be written in the form

$$\frac{dz}{dt} = f(z). \quad (1.6)$$

An *equilibrium point* of such a system is a solution of $f(z) = 0$.⁴ An equilibrium point z^* corresponds to an equilibrium solution, since if we define a constant function $z(t) \equiv z^*$ then we have $\dot{z}(t) \equiv f(z^*) = 0$. In some cases, it is possible to discuss the motion of solutions close to equilibrium points by means of *linearization*: the technique of replacing a nonlinear system by a linear one which approximates it locally.

We assume that f is continuously differentiable in the vicinity of the equilibrium point z^* and make use of the fact that $f(z) \approx f(z^*) + f'(z^*)(z - z^*)$ for $\|z - z^*\|$ sufficiently small. Since $f(z^*) = 0$ we have, defining $\delta z := z - z^*$,

$$\frac{d\delta z}{dt} \approx A\delta z, \quad A = f'(z^*).$$

The symbol \approx is not very precise. In general, the approximation of solutions is only local in time meaning that solutions of the nonlinear system and the linear approximation may diverge. We refer to the system

$$\frac{d\delta z}{dt} = f'(z^*)\delta z$$

as the *linearization* of the system (1.6) around z^* .

In case the equilibrium point is *hyperbolic*, meaning that the real parts of the eigenvalues of $A = f'(z^*)$ are nonzero, then one can infer that the solutions of the

⁴For readers conversant with concepts of statistical mechanics and in preparation for later discussions, we emphasize that the concept of *mechanical equilibrium* given in relation to the system of ordinary differential equation (1.6) is entirely different from the notion of *statistical* or *thermal equilibrium* of Chap. 6.

nonlinear and linear systems are in fact *topologically conjugate*: if z is the solution of the nonlinear system and δz is the solution of the linear system, then there is a smooth, invertible map Φ of \mathbb{R}^m defined in a neighborhood of the origin such that

$$z(t) = z^* + \Phi(\delta z(t)).$$

This is referred to as the Hartman-Grobman theorem (for more discussion, see [177], where this result is referred to as the ‘‘Linearization Theorem’’; a proof may be found in [362]).

Let z^* be an equilibrium point. We say that z^* is stable (‘‘in the sense of Lyapunov’’) if, for all ε , there exists δ such that, for all z_0 such that $\|z_0 - z^*\| < \delta$,

$$\sup_{t \geq 0} \|\mathcal{F}_t(z_0) - z^*\| < \varepsilon.$$

That is, the solution started near to z^* stays near z^* for all time. The Hartman-Grobman theorem clearly implies that the stability of a given hyperbolic equilibrium point z^* of a nonlinear system can be inferred from the stability of the origin for the linearization of the system around z^* .

In the case of Hamiltonian systems, the eigenvalues are, very often, on the imaginary axis, and the Hartman-Grobman theorem is not of much use. However, there is another result which is relevant in this case. Observe that an equilibrium point $z^* = (\mathbf{q}^*, \mathbf{p}^*)$ of a Hamiltonian system in ‘‘kinetic plus potential’’ form

$$H(\mathbf{q}, \mathbf{p}) = \mathbf{p}^T \mathbf{M}^{-1} \mathbf{p} / 2 + U(\mathbf{q})$$

will always have $\mathbf{p}^* = 0$ and $\nabla U(\mathbf{q}^*) = 0$. We say that \mathbf{q}^* is a *strong local minimum* of the potential if there exists $\varepsilon > 0$ such that

$$0 < \|\mathbf{q} - \mathbf{q}^*\| < \varepsilon \Rightarrow U(\mathbf{q}) > U(\mathbf{q}^*).$$

Then we have

Theorem 1.1 *If \mathbf{q}^* is a strong local minimum of smooth potential U then $z^* = (\mathbf{q}^*, \mathbf{0})$ is stable.*

The proof of this theorem relies on showing that if trajectories are started from a point sufficiently close to z^* they cannot wander away to infinity. Although the result holds in greater generality, it is easy to show under assumptions of local smoothness of U (which we are normally happy to make in molecular dynamics). For more discussion see the text [216]. If the potential is C^2 , the linearized version of this system has ‘‘kinetic plus potential’’ form with Hamiltonian

$$\bar{H} = \frac{\delta \mathbf{p}^T \mathbf{M}^{-1} \delta \mathbf{p}}{2} + \frac{\delta \mathbf{q}^T U''(\mathbf{q}^*) \delta \mathbf{q}}{2}.$$

A condition for this system to have a strong local minimum at $\delta\mathbf{p} = \mathbf{0}, \delta\mathbf{q} = 0$ is that the Hessian matrix $U''(\mathbf{q}^*)$ be positive definite. In case the eigenvalues of $U''(\mathbf{q}^*)$ are all distinct and positive, then the strong local minimum property will also follow for \mathbf{q}^* in relation to the original potential.

1.6 Lattice Structures

Let us suppose we have a uniform pair potential φ and define the total potential energy of a system of N atoms by

$$U(x_1, x_2, \dots, x_N) = \sum_{i=1}^{N-1} \sum_{j=i+1}^N \varphi(|x_i - x_j|).$$

The computation of the energy requires $N(N - 1)/2$ separate calculations, which could be very expensive if N is large. We can reduce this by assuming only *nearest neighbor* forces, which means the energy becomes

$$U(x_1, x_2, \dots, x_N) = \sum_{i=1}^{N-1} \varphi(|x_{i+1} - x_i|).$$

While a Lennard-Jones interaction will maintain the particle ordering, a nearest neighbor system may otherwise require some care in the implementation, for example a mechanism for relabelling the particles when they cross. If the system is simulated without boundary conditions using short-ranged potentials like Lennard-Jones or Morse, then some atoms are likely to be ejected from the ends during simulation. In order to keep such a system bounded we might think to introduce walls at the ends of the chain, e.g. by adding confining potentials to U :

$$U(x_1, x_2, \dots, x_N) = \varphi_c(|x_1|) + \varphi_c(|L - x_N|) + \sum_{i=1}^{N-1} \varphi(|x_{i+1} - x_i|). \quad (1.7)$$

For example, one could assume $\varphi_c = \varphi$ in which case we have effectively placed fixed particles at the ends of the interval, or one might use a different potential, e.g. a “soft wall” potential ($x^{-\alpha}$, e.g. $\alpha = 10$) or a spring (Cx^2). Alternatively one could restrict to a bounded domain by use of periodic boundary conditions, introducing the potential energy:

$$U(x_1, x_2, \dots, x_N) = \sum_{i=1}^{N-1} \varphi(|x_{i+1} - x_i|) + \varphi(|L + x_1 - x_N|). \quad (1.8)$$

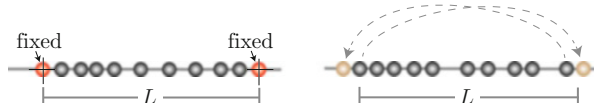


Fig. 1.15 Typical methods for modelling a fixed length domain. *Left*: particles are introduced at fixed locations $x = 0$ and $x = L$; *right*: in periodic boundary conditions, potentials are introduced to model the effect of an atom just outside the domain (on either end)

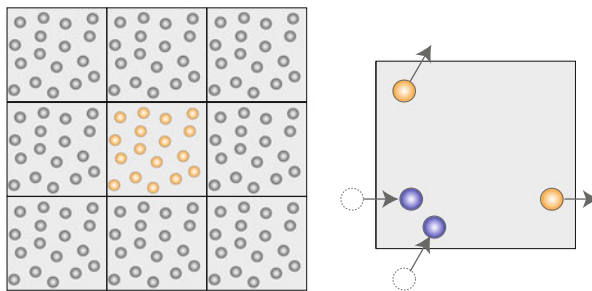


Fig. 1.16 Periodic boundary conditions illustrated in two dimensions. *Left*: the atom locations of the central simulation cell are repeated in each neighboring cell; potential energy contributions must be included not only for atom-atom interactions within the simulation cell but also for interactions between atoms of the central cell and those in the neighbors. *Right*: as an atom leaves the central region, it reenters via the opposite boundary

If a particle moves to the right of $x = L$ we simply shift its position to $x - L$; likewise any particle exiting to the left of $x = 0$ has its position shifted to $x + L$ (see Fig. 1.15). This type of boundary condition is a common choice and considered more relevant in simulations of realistic systems than confining boundary conditions. Periodic boundary conditions allow us to preserve Newton's third law, the translational symmetry, and thus the conservation of momentum.

When dealing with crystalline materials, or for initializing more general systems, the atoms are typically confined for most of their evolution to small neighborhoods of a collection of periodic points called a lattice. On the line, we think of a (finite) lattice as a sequence of discrete points separated by a fixed distance Δx . An obvious benefit of using periodic boundary conditions is that, with a uniform pair potential, the energy minimizers are points of a regular lattice; with confining potentials this is unlikely to be the case.

The technique of periodic boundary conditions can be extended to 2D or 3D (Fig. 1.16). We assume our simulation box is surrounded not by a large number of particles moving on completely independent paths, but, rather, that our box is bordered on each face by a box of particles whose positions are exact shifted images of those of the resolved system. Atoms moving out of the central box are not reflected back into the central domain, but enter the box at a corresponding point on the opposite face. For purposes of illustration we have diagrammed the situation for a planar region. If φ_{ij} is the potential energy function for interactions between

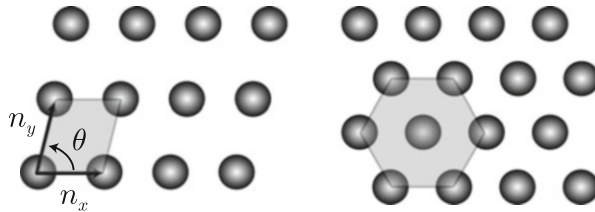


Fig. 1.17 The standard rhombic lattice in the plane is shown at *left*; at *right* is a regular hexagonal lattice which can be viewed as a rhombic lattice with $n_x = n_y$ and $\theta = 120^\circ$; it can also be viewed as a rhombic lattice with $\theta = 60^\circ$

atoms i and j , and we wish to confine these to the cube $[0, L] \times [0, L] \times [0, L]$, then periodic boundary conditions involve an extended potential energy of the form

$$U^{\text{pbc}}(\mathbf{q}) = \sum_{klm} \sum_{i=1}^{N-1} \sum_{j=i+1}^N \varphi_{ij}(\mathbf{q}_i, \mathbf{q}_j + k\mathbf{v}_1 + l\mathbf{v}_2 + m\mathbf{v}_3),$$

where k, l, m run over $-1, 0, 1$ (in case interactions are restricted to the simulation cell and its immediate neighboring copies), and $\mathbf{v}_i^T = (\mathbf{L}\mathbf{e}_i^T, \mathbf{L}\mathbf{e}_i^T, \dots, \mathbf{L}\mathbf{e}_i^T)$, $i = 1, 2, 3$, where \mathbf{e}_i is the i th Euclidean basis vector in \mathbb{R}^3 . During simulation, the coordinates of each atom must be checked and possibly shifted after each positional step. The use of periodic boundary conditions may be likened to placing the molecular system (the configurational coordinates) on the surface of a torus. It may seem that periodic boundary conditions greatly increase the number of interactions that must be tracked in simulation, but this is not normally the case. First, for short-ranged interactions, such as those defined by the Lennard-Jones potential, the distant force terms will be negligible and can simply be taken to be zero. A *cut-off* is usually employed based on the interatomic distance. (See Exercise 11 for an illustration.) With or without periodic boundary conditions there will be only a finite number of close neighbors that actually contribute to the energy or force sum. The *minimum image convention* states that, in computing the force, a given atom interacts only with the nearest replica of any other atom.

The low potential energy configurations are natural starting points for simulation, and these normally correspond to a lattice structure. In 2D, the typical geometry observed at low temperature is defined by a rhombic lattice with sides of fixed length n_x, n_y and the angle between them (θ), see Fig. 1.17. For a system of uniform molecular pair potentials (such as Lennard-Jones), without boundary conditions, the equilibrium state will typically be close to the hexagonal lattice.

3D systems, particularly crystalline materials, favor lattice structures which can be viewed as stackings of planar layers. The *unit cell* is a description of the arrangement of atoms within a box; unit cells may be stacked in each direction to describe an atomic lattice. Three of the most common unit cells are the body-centered cubic (bcc), face-centered cubic (fcc) and hexagonal close-packed

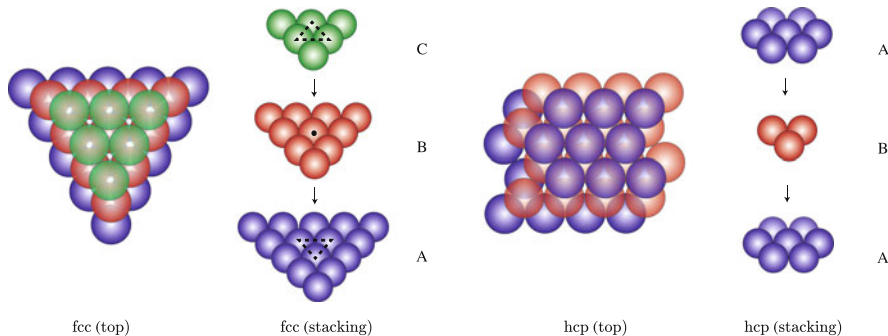


Fig. 1.18 The face centered cubic and hexagonally close packed lattice are associated to two different stacking arrangements of hexagonally structured planar lattices. The *dashed triangles* indicated in the upper and lower layers of the fcc lattice are centered on the atom indicated by a *dot* in the middle layer

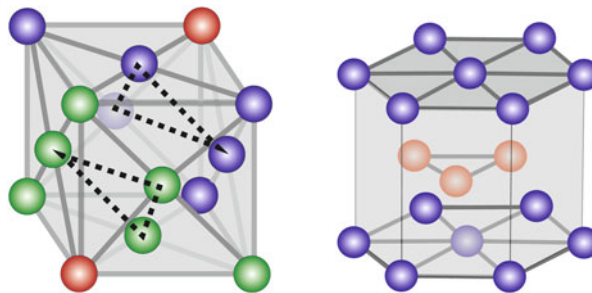


Fig. 1.19 Unit cells for fcc (*center*), and hcp (*right*) geometries. The coloring of atoms and *dashed triangles* are indicated to match the stacking of layers in Fig. 1.18

(hcp) lattices. The fcc lattice corresponds to the common arrangement by which cannonballs are stacked into pyramidal structures; it can be viewed as a periodic stacking (ABCABC...) of three hexagonally structured planar layers, as illustrated in Fig. 1.18. Also shown in Fig. 1.18 is the hcp lattice, which, on the other hand, alternates two distinct planar lattices. Layer stackings then define a certain unit cell as shown in Fig. 1.19.

1.6.1 Lattice Vibrations

Regardless of the choice of boundary and/or the inclusion of non-pairwise potentials, the minimum of the potential energy occurs where

$$\nabla U = \mathbf{0},$$

which gives in general a nonlinear system of N_c equations in N_c unknowns to be solved for the position vector \mathbf{q}^* associated to mechanical equilibrium.

At the equilibrium point, we can linearize the system of differential equations by computing the Hessian matrix, then we find

$$\nabla U(\mathbf{q}) \approx U''(\mathbf{q}^*)(\mathbf{q} - \mathbf{q}^*).$$

Then, letting $\delta\mathbf{q} = \mathbf{q} - \mathbf{q}^*$, $\delta\mathbf{p}$ represent small deviations from the equilibrium point at $(\mathbf{q}, \mathbf{p}) = (\mathbf{q}^*, \mathbf{0})$, we have

$$\begin{aligned}\frac{d\delta\mathbf{q}}{dt} &= \mathbf{M}^{-1}\delta\mathbf{p}, \\ \frac{d\delta\mathbf{p}}{dt} &= -U''(\mathbf{q}^*)\delta\mathbf{q}.\end{aligned}$$

At the minimum of the potential energy, U'' is a positive definite symmetric matrix. The eigenvalues of the matrix

$$\mathbf{A} := \begin{bmatrix} \mathbf{0} & \mathbf{M}^{-1} \\ -U''(\mathbf{q}^*) & \mathbf{0} \end{bmatrix}$$

are therefore all purely imaginary ($\pm i\Omega$, $\Omega \in \mathbb{R}$). Associated to each eigenvalue pair we have a pair of complex conjugate eigenvectors $\xi, \bar{\xi}$ and also a pair of solutions which can be written in the complex form

$$\mathbf{z}(t) = ae^{i\Omega t}\xi + be^{-i\Omega t}\bar{\xi},$$

(a, b complex coefficients), or recast in real form as (α, β real coefficients):

$$\mathbf{z}(t) = \alpha[\sin(\Omega t)\text{Re}(\xi) + \cos(\Omega t)\text{Im}(\xi)] + \beta[\cos(\Omega t)\text{Re}(\xi) - \sin(\Omega t)\text{Im}(\xi)].$$

These are referred to as the “normal modes” of oscillation of the system (Fig. 1.20 illustrates the normal modes for a linear molecule).

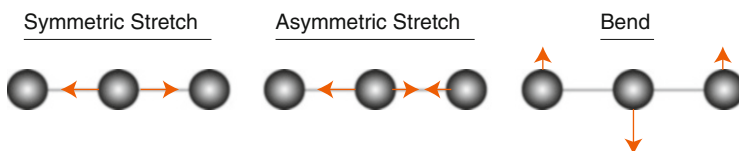


Fig. 1.20 Three normal modes of a linear molecule (i.e., a molecule in which the atoms, at minimum energy, are arranged on a line)

1.7 Chaotic Trajectories of Nonlinear Systems

Restricting our study to the curves defined by a system of first integrals and/or the consideration of small oscillations near equilibrium points would greatly limit the range of accessible dynamical phenomena. If we construct a molecular system describing many bodies interacting in nonlinear force laws, there would be no obvious reason to expect that there are many first integrals present to constrain the motion. Indeed, experience indicates that the situation is quite the opposite: typically only the energy and the total momentum of a molecular system are conserved quantities. Thus we are in general left with a complicated dynamical system whose solutions cannot be analytically determined.

Example 1.8⁵(Planar Lennard-Jones Trimer) One of the simplest illustrations of the chaotic nature of molecular systems is given by the Lennard-Jones model consisting of just three atoms with motion restricted to the plane. The energy is

$$E = K + U = \frac{\|\dot{\mathbf{q}}_1\|^2}{2} + \frac{\|\dot{\mathbf{q}}_2\|^2}{2} + \frac{\|\dot{\mathbf{q}}_3\|^2}{2} + \hat{\varphi}_{\text{LJ}}(\|\mathbf{q}_1 - \mathbf{q}_2\|) + \hat{\varphi}_{\text{LJ}}(\|\mathbf{q}_2 - \mathbf{q}_3\|) + \hat{\varphi}_{\text{LJ}}(\|\mathbf{q}_1 - \mathbf{q}_3\|),$$

with the interatomic interaction given by $\hat{\varphi}_{\text{LJ}}(r) = 4[r^{-12} - r^{-6}]$.

The global minimum of this simple system must be radially symmetric. Placing the atoms at the vertices of an equilateral triangle, we have

$$U = 3\hat{\varphi}_{\text{LJ}}(r),$$

where r is the length of a side. This is minimized when $r = 2^{1/6} \approx 1.1225$.

In general, when the total potential is a sum of distance potentials

$$U = \frac{1}{2} \sum_{i \neq j} U_{ij},$$

where $U_{ij}(\mathbf{q}_i, \mathbf{q}_j) = \varphi_{ij}(\|\mathbf{q}_i - \mathbf{q}_j\|)$, we say that the system has *central forces*. In this case,

$$\frac{\partial}{\partial \mathbf{q}_i} U_{ij}(\mathbf{q}_i, \mathbf{q}_j) = -\frac{\partial}{\partial \mathbf{q}_j} U_{ij}(\mathbf{q}_i, \mathbf{q}_j),$$

⁵The Lennard-Jones Trimer is included as an example in the **MD.M** package, see <http://MolecularDynamics.info>

and so, for central forces,

$$\sum_{i=1}^N m_i \ddot{\mathbf{q}}_i = \mathbf{0},$$

which expresses the constancy of the momentum. Moreover, viewing the \mathbf{q}_i as vectors in \mathbb{R}^3 (with 0 as their third component),

$$\mathbf{q}_i \times \frac{\partial}{\partial \mathbf{q}_i} U_{ij}(\mathbf{q}_i, \mathbf{q}_j) = -\mathbf{q}_j \times \frac{\partial}{\partial \mathbf{q}_j} U_{ij}(\mathbf{q}_i, \mathbf{q}_j),$$

which implies

$$\frac{d}{dt} \sum_{i=1}^N \mathbf{q}_i \times (m_i \dot{\mathbf{q}}_i) = \mathbf{0},$$

and tells us that the total *angular momentum* is also conserved. This means that the system will translate and rotate at a constant rate in time.⁶ By a judicious choice of initial conditions, the center of mass can be kept at the origin and the net rotation removed. This corresponds to a symmetric configuration which is termed the *isosceles* three body problem (i.e., at all times the atoms are the vertices of an isosceles triangle). The original system had six positional degrees of freedom, but four have now been removed by imposing the momentum constraints. Therefore we would expect a model with just two degrees of freedom. While the conservation of angular and total momentum allow us to remove some of the degrees of freedom of the problem, reducing it to a smaller system, this problem is not integrable.

Let us introduce new coordinates in the Lennard-Jones trimer as illustrated in Fig. 1.21, so that the center of mass is fixed at the origin: that is,

$$\mathbf{q}_1 = \begin{bmatrix} x \\ -y/3 \\ 0 \end{bmatrix}, \quad \mathbf{q}_2 = \begin{bmatrix} -x \\ -y/3 \\ 0 \end{bmatrix}, \quad \mathbf{q}_3 = \begin{bmatrix} 0 \\ 2y/3 \\ 0 \end{bmatrix},$$

reducing the energy to

$$E = \dot{x}^2 + \frac{\dot{y}^2}{3} + 2\hat{\varphi}_{\text{LJ}}(\sqrt{x^2 + y^2}) + \hat{\varphi}_{\text{LJ}}(2x),$$

which describes the vibrational motion. Over time the positions will vary within some region in the xy plane, whose boundary is dependent on the energy E of the initial condition. What is this boundary? Since the energy is conserved, and the

⁶Note that in periodic boundary conditions the linear momentum would also be preserved, but the angular momentum is not.

Fig. 1.21 Coordinates in the isosceles 3-body problem

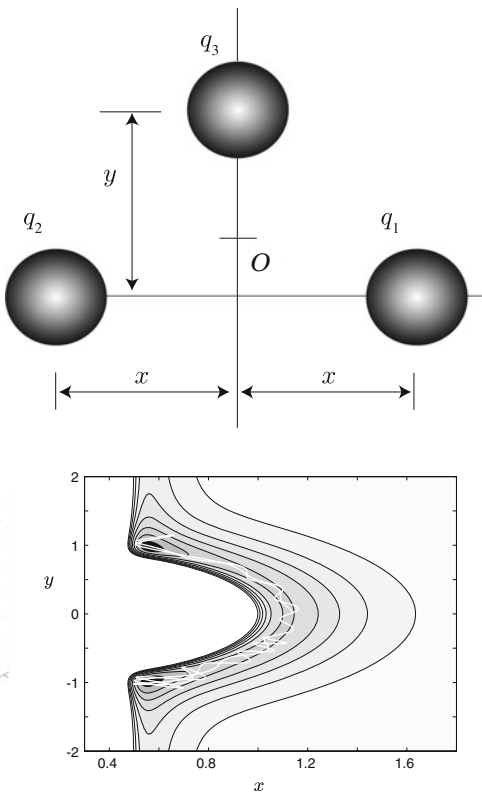


Fig. 1.22 Left: surface plot of the negative potential energy for the isosceles 3-body problem showing iso-potential curves. Right: the level sets of the potential energy function are shown for the isosceles 3-body problem, together with a snapshot of a constant energy trajectory (light curve)

kinetic energy is non-negative, we must have

$$2\hat{\varphi}_{\text{LJ}}(\sqrt{x^2 + y^2}) + \hat{\varphi}_{\text{LJ}}(2x) \leq E.$$

On the left side of Fig. 1.22 are shown the level curves of the potential energy function, with color gradations indicating the energy level between -3 and 0 . (When $E > 0$, the bodies eventually escape to infinity; $E < -3$ is not attainable.) Superimposed on the level curves we have shown a short time trajectory (the wiggly white curve).

A surface plot of the **negative of** potential energy is shown on the left in Fig. 1.22. Arranging the three atoms in a collinear configuration ($y = 0$) the potential energy becomes $\hat{U} = \hat{U}(x) = 2\hat{\varphi}_{\text{LJ}}(x) + \hat{\varphi}_{\text{LJ}}(2x)$. Minimizing the potential in the collinear configuration allows us to determine the *saddle point* ($x_*, 0$). Near this point, U decreases if we move in the $\pm y$ direction and increases if we move in the $\pm x$

direction. (For further discussion of the Lennard-Jones few-body problem from a dynamical systems perspective, the reader is referred to [87].) \square

1.7.1 Global Solutions

Looking at the trajectories of a molecular dynamics simulation involving even a few atoms (such as the restricted trimer model, above) suggests their erratic, irregular aspect. Individual paths will not be expected to be predictable in any practical sense—every time one atom collides with another it will exchange a small amount of energy and momentum with the other atom, the precise amounts depending in an intricate way on the motions of all the atoms of the system, and the atoms then move on in perturbed directions. In a very short time, the state of the system is well stirred by the molecular interactions. This is one of the elements of the common view of what constitutes a chaotic dynamical system.

In the words of H. Poincaré, writing over a century ago [304],

A very small, unnoticeable cause can determine a visible very large effect; in this case we claim that this effect is the product of random chance. However, even if the natural laws were perfectly known, we would only be able to know the initial conditions with some approximation. If this allows us to know the future with the same approximation that is all we need. We will say that the phenomenon is foreseeable, that it is governed by laws. However this is not always the case, it is possible that a very small initial difference leads to a very large change in the final state...

Poincaré's comments probably derived from his understanding of the three-body gravitational problem, but they would apply as well to a typical molecular system.

Typical definitions of a “chaotic dynamical system” [103] require at least the following conditions to be satisfied on the phase space \mathcal{D} :

- The solutions depend sensitively on the initial data taken from \mathcal{D} ;
- The flow is topologically transitive in \mathcal{D} .

Let us address these in turn, without being entirely formal. The sensitive dependence on initial conditions can be taken to mean that if a pair of initial points of phase space is given which are separated by any finite amount, no matter how small, then the gap between these solutions grows rapidly (typically exponentially fast) in time. A problem with this concept is that we often think of molecular systems as having an evolution that is bounded by some sort of domain restriction or a property of the energy function: the exponential growth for a finite perturbation can therefore only be valid until the separation approaches the limits of the accessible region of phase space. In order to be able to make sense of the calculation of an exponential rate in the asymptotic ($t \rightarrow \infty$) sense, we need to consider infinitesimal perturbations of the initial conditions, and this can be made precise by consideration of the Lyapunov characteristic exponents mentioned at the end of this chapter.

The second condition states that given arbitrarily small neighborhoods \mathcal{D}_1 and \mathcal{D}_2 of two different points in \mathcal{D} then it is possible to find a trajectory that goes

from some point of \mathcal{D}_1 to some point of \mathcal{D}_2 . This condition roughly says that the trajectories starting from some arbitrarily small open set in \mathcal{D} will eventually fill the interior of \mathcal{D} densely. We will see later that this concept, which is essentially equivalent to *ergodicity*, is a crucial component of molecular theories. Below, we will demonstrate, using numerical experiments, that even a simple nonlinear system reminiscent of molecular dynamics can exhibit the hallmarks of a chaotic system. After a short time, small perturbations of the initial conditions will become large, of order of the dimension of the system, and the “memory” of the initial conditions is lost. In this sense the arrangement of atoms rapidly becomes disordered in a similar way to the playing cards of a deck as they are shuffled. The idea of a chaotic dynamical system and its interpretation as a randomizing process is further developed in later chapters. For an informal but valuable introduction to this topic the reader is referred to the short book of Ruelle [318].

*Example 1.9*⁷ (*Anisotropic Oscillator*) A perturbation of the central force problem illustrates the consequences of a breakdown of integrability. Consider the system with energy

$$E(x, y, \dot{x}, \dot{y}) = \frac{1}{2}(\dot{x}^2 + \dot{y}^2) + \frac{\kappa(c_3)}{2}(r - l(c_3))^2, \quad r = \sqrt{x^2 + y^2}, \quad (1.9)$$

where

$$c_3 = \cos(3\theta)$$

is defined in terms of the angular coordinate of the position (x, y) with respect to the $(1, 0)$ -direction,

$$\cos \theta = c = \frac{x}{r}, \quad c_3 = 4c^3 - 3c,$$

and we have defined

$$\kappa(c_3) = \kappa_0(1 - \frac{1}{2}\varepsilon c_3), \quad l(c_3) = l_0(1 + \frac{1}{2}\varepsilon c_3).$$

Effectively this models the mythical behavior of an atom that binds more tightly to a molecule in certain configurations than in others. In our experiments we took, for simplicity, $l_0 = \kappa_0 = 1$, and considered the effect of varying ε . For $\varepsilon \neq 0$, the angular momentum is not preserved, and the only invariant is the energy.

When ε is small one finds trajectories have a regular appearance for many values of the initial conditions, typically either a periodic orbit or one which repeatedly and *quasiperiodically* traverses a portion of the domain. As ε is increased, the orbits

⁷The Anisotropic Oscillator is included as an example in the **MD.M** package, see <http://MolecularDynamics.info>

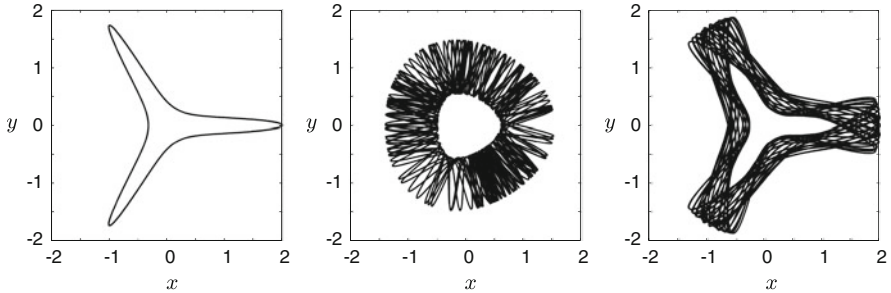


Fig. 1.23 Trajectories of the perturbed central force problem. *Left diagram*: $\varepsilon = 0.1$ on time interval $[0, 10^3]$, initial position $q_0 = (2, 0)$, $p_0 = (0, 0.1)$; *center*: same as above but with initial position $q_0 = (1, 1)$; *right*: $\varepsilon = 0.2$, and $q_0 = (2, 0)$

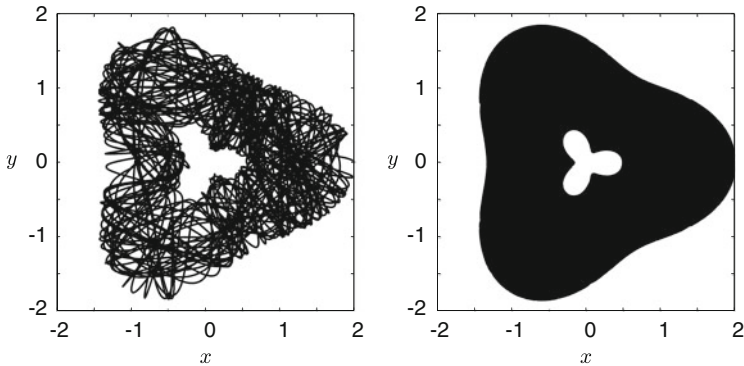


Fig. 1.24 Trajectories of the perturbed central force problem for $\varepsilon = 0.5$, $q_0 = (1, 1)$. *Left diagram*: on time interval $[0, 10^3]$; *right*: time interval $[0, 10^5]$

quickly lose this regular appearance. Several orbits are shown for $\varepsilon = 0.1$ or $\varepsilon = 0.2$ in Fig. 1.23. In Fig. 1.24, a modest length orbit for $\varepsilon = 0.5$ is shown at left; at longer times, Fig. 1.24 (right), the orbit appears to completely fill in a two-dimensional set in the plane, illustrating the topological transitivity property.

To appreciate the sensitive dependence on initial condition when $\varepsilon = 0.5$, superimpose as in Fig. 1.25 (left) a pair of trajectories, computed from two initial conditions differing only by a perturbation of size 10^{-10} in one component. Even in this relatively short simulation, the trajectories become completely distinct from one another, with the difference growing until it is of order the size of the accessible phase space at the given energy. In the right panel of the same figure, the norm of the position displacement is plotted against time-step number for the same simulation in a logarithmic scale. The diagram suggests a rapid growth of their separation with time, consistent with an approximate exponential increase on a moderate time interval.

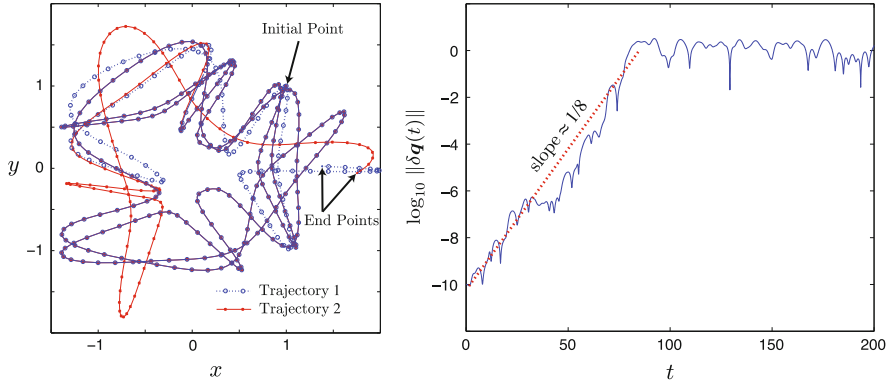


Fig. 1.25 Rapid separation of trajectories in the perturbed central force problem. The trajectories in the *left panel* are started from initial conditions differing only in the 10th digit. They are then found to separate rapidly and end up following entirely different paths. The *right panel* shows that the trajectories separate exponentially fast in the early going; eventually, once the difference is of the same order as the size of the domain, the norm of the difference stabilizes

1.7.2 Variational Equations and Lyapunov Exponents

One way of quantifying the sensitive dependence on initial conditions in a nonlinear dynamics model is via *Lyapunov exponents*. Usually this is done by introducing the *variational equations* which describe the time-dependent variation of perturbations of a solution of a dynamical system. Besides giving us a means to verify the chaotic nature of given system, the variational equations prove useful in describing the *symplectic structure* (taken up in the next chapter) which is essential to the design of effective numerical methods for molecular dynamics.

Let a dynamical system $\dot{z} = f(z)$ be given in \mathbb{R}^m with flow map $\mathcal{F}_t : \mathbb{R}^m \rightarrow \mathbb{R}^m$ which we assume to be continuously differentiable. Let $z(t, \xi)$ represent the solution of initial value problem

$$\dot{z} = f(z), \quad z(0) = \xi.$$

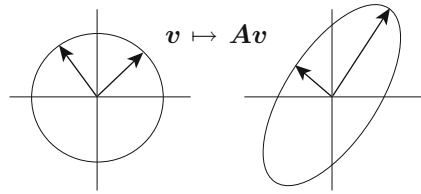
We then compute the $m \times m$ Jacobian matrix of $\mathcal{F}_t(z(t, \xi))$:

$$W(t) = \mathcal{F}'_t(z(t, \xi)) = \frac{\partial \mathcal{F}_t}{\partial z}(z(t, \xi)).$$

Differentiating $W(t)$ with respect to t and using the differential equation and the chain rule, we have

$$\frac{d}{dt} W(t) = f'(z(t, \xi)) W(t). \quad (1.10)$$

Fig. 1.26 A regular linear map takes an $m - 1$ -dimensional sphere to an $m - 1$ -dimensional ellipsoid



\mathbf{W} satisfies a system of linear (time-dependent) differential equations involving the matrix f' (the Jacobian matrix of vector field) evaluated along the solution $\mathbf{z}(t)$. \mathbf{W} may be seen as a fundamental matrix solution of the indicated linear system.

The system of Eq. (1.10) is referred to as the system of *variational equations* corresponding to the dynamical system $d\mathbf{z}/dt = \mathbf{f}(\mathbf{z})$.

If we have two solutions started from nearby initial conditions $\xi, \hat{\xi}$, then their difference is approximated by the solution of the variational equations

$$\mathbf{z}(t, \hat{\xi}) - \mathbf{z}(t, \xi) \approx \mathbf{W}(t)(\hat{\xi} - \xi).$$

The usefulness of the variational equations lies, however, in the fact that they are scale independent, one may view them as defining the relative variation induced over time of an infinitesimal perturbation of the initial condition.

We may view a regular linear mapping $\mathbf{v} \mapsto \mathbf{A}\mathbf{v}$, where $\mathbf{A} \in \mathbb{R}^{m \times m}$, as a mapping of an $m - 1$ -dimensional sphere (embedded in the m -dimensional Euclidean space) to an ellipsoid in the same space (Fig. 1.26). The square roots of the eigenvalues of $\mathbf{A}^T \mathbf{A}$, also called the singular values of \mathbf{A} , then give the axes of the image ellipsoid.

In the case of the transformation $\mathbf{v} \mapsto \mathbf{W}(t)\mathbf{v}$, the singular values of the transformation give insight into how much the ellipse is expanded or contracted in different directions over time. The Lyapunov exponents $\lambda_1, \lambda_2, \dots, \lambda_m$ are defined by

$$\lambda_i = \limsup_{t \rightarrow \infty} \frac{1}{t} \log \sigma_i(\mathbf{W}),$$

where σ_i represents the i th singular value of the given matrix (to maintain continuity, these should be ordered in some way, say largest to smallest). The \limsup is needed as we wish to ignore any initial fluctuations and are only interested in the long-term behavior. The presence of a positive Lyapunov exponent implies exponential growth of perturbations, which, as we have seen, is one of the hallmarks of chaos.

This is not a very easy computation to carry out in the general case. The difficulty lies in the fact that the limit taken in the definition may require a very long simulation, typically millions or billions of time-steps, and the eigenvalues must be computed at each step. Even for modest-sized systems a sophisticated approach is needed [146, 343]. We have used special purpose software [105], resulting in an estimate of the largest Lyapunov exponent of approximately 0.28. Observe that in the right hand panel of Fig. 1.25, the growth of the logarithm of the trajectory

separation is approximately linear in the initial phase, with a slope of $1/8$. This means that the perturbation multiplier is about 10 in each 8 units of time. From examination of discussion above, we expect that, for the leading Lyapunov exponent λ , we have

$$\exp(8\lambda) \approx 10,$$

which gives $\lambda \approx 0.29$. Thus the calculated Lyapunov exponent is very close to that which would be predicted by examination of the actually growth of perturbations. Although it is not a “smoking gun”, the positive Lyapunov exponent provides convincing evidence for the chaotic nature of this problem.

Exercises

1. Solve the linear systems $d\mathbf{z}/dt = A\mathbf{z}$ in the following special cases of 2×2 matrices A by directly computing the exponential of the matrix At :

- a. $A = D = \begin{bmatrix} d_1 & 0 \\ 0 & d_2 \end{bmatrix}$, where d_1 and d_2 are given constants.
- b. $A = \begin{bmatrix} 1 & \alpha \\ 0 & 1 \end{bmatrix}$, where α is a given constant.
- c. $A = XDX^{-1}$, where D is as in part a.

2. It is worth noting several properties of the matrix exponential which are all easily proven:

- a. $\exp(\mathbf{0}) = I$, where $\mathbf{0}$ indicates the $N \times N$ matrix of zeros.
- b. Suppose A and B commute (i.e., $AB = BA$). Then

$$\exp(A + B) = \exp(A) \exp(B).$$

(This is not true for general matrices A and B !)

- c. The identity

$$(e^A)^{-1} = e^{-A}.$$

- d. Let A be $N \times N$, nonsingular and have a basis of eigenvectors $\eta_1, \eta_2, \dots, \eta_N$, with corresponding eigenvalues $\lambda_1, \lambda_2, \dots, \lambda_N$. Then e^A has the same set of eigenvectors and the corresponding eigenvalues $e^{\lambda_1}, e^{\lambda_2}, \dots, e^{\lambda_N}$.
- e. For any square matrix A with a basis of eigenvectors,

$$\ln \det \exp(A) = \text{tr}(A),$$

where $\text{Tr}(\mathbf{A})$ is the trace of the matrix \mathbf{A} which can be taken to be the sum of the eigenvalues or the sum of the diagonal elements. Note: to show this, use part (d) and the fact that the determinant of a matrix can be taken to be the product of its eigenvalues.

- 3.** Consider the 2-body problem consisting of a pair of point particles in the plane with identical masses m , interacting in a potential field $\varphi(r)$ dependent on their separation distance r .

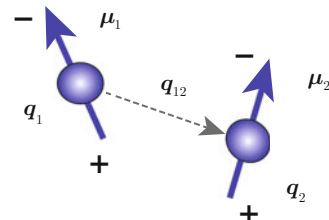
- Let \mathbf{q}_1 and \mathbf{q}_2 be the position vectors of the two particles at any time. Write the Lagrangian for this system, and the equations of motion.
- The center of mass of the system is $\mathbf{q}_{cm} = (\mathbf{q}_1 + \mathbf{q}_2)/2$. Let $\Delta = \mathbf{q}_2 - \mathbf{q}_1$. Express the physical variables (and hence the Lagrangian) in terms of the vectors \mathbf{q}_{cm} and Δ , and show that the equations of motion reduce to linear motion of the center of mass coupled with vibrational-rotational motion in the separation Δ :

$$\ddot{\mathbf{q}}_{cm} = 0, \quad m\ddot{\Delta} = -\frac{1}{r}\varphi'(r)\Delta.$$

- Show that this system can be integrated by rewriting the equations of motion for Δ using polar coordinates. [That is, let $\Delta = (r \cos \theta, r \sin \theta)$, differentiate twice, and insert this into the differential equation for Δ . This should result in an equation that can be reduced to one involving r only.]

- 4.** An angle bond potential can be defined for a trio of atoms.
- Write the formula for an angle bond potential for the angle $\angle \mathbf{q}_1 \mathbf{q}_2 \mathbf{q}_3$ for atoms with positions $\mathbf{q}_1, \mathbf{q}_2, \mathbf{q}_3$.
 - Show that forces arising from the angle bond preserve linear and angular momentum.
- 5.** A dipole is created when oppositely charged particles are held at a fixed distance from each other. It generates a directional charge distribution defined by its orientation, i.e. by a unit vector μ . Stockmayer [345] proposed a potential for the interaction of a pair of bodies at positions \mathbf{q}_1 and \mathbf{q}_2 , with associated dipoles, μ_1, μ_2 (see Fig. 1.27). It can be shown that the potential energy of interaction

Fig. 1.27 Dipole-dipole interactions



at sufficiently long range takes the form

$$\varphi_{\text{dip}}(\mathbf{q}_1, \boldsymbol{\mu}_1, \mathbf{q}_2, \boldsymbol{\mu}_2) = \alpha \left[\frac{\boldsymbol{\mu}_1 \cdot \boldsymbol{\mu}_2}{r_{12}^3} - 3 \frac{(\boldsymbol{\mu}_1 \cdot \mathbf{q}_{12})(\boldsymbol{\mu}_2 \cdot \mathbf{q}_{12})}{r_{12}^5} \right],$$

where $\mathbf{q}_{12} = \mathbf{q}_2 - \mathbf{q}_1$, and $r_{12} = \|\mathbf{q}_{12}\|$. (Normally, an additional pair-wise Lennard-Jones potential is included.) A polar fluid can be modelled in this way.

- a. Assuming the dipoles have constant and uniform strength $\mu = \|\boldsymbol{\mu}_{12}\|$, show that the dipole-dipole interaction potential can be written as

$$\tilde{\varphi}_{\text{dip}}(r, \theta_1, \phi_1, \theta_2, \phi_2) = \frac{\mu^2}{r^3} f(\theta_1, \phi_1, \theta_2, \phi_2),$$

where

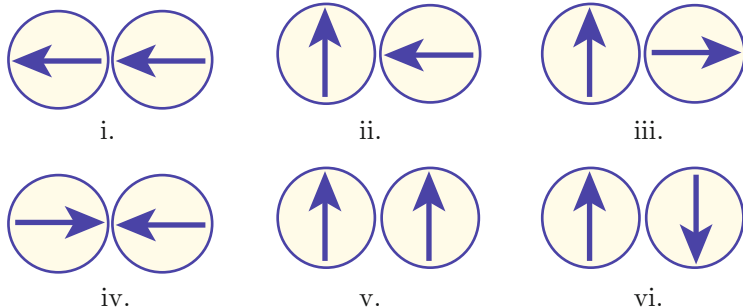
$$f(\theta_1, \phi_1, \theta_2, \phi_2) = [\sin \phi_1 \sin \phi_2 \cos(\theta_1 - \theta_2) - 2 \cos \phi_1 \cos \phi_2],$$

where the dipoles have been expressed in spherical coordinates,

$$\boldsymbol{\mu}_i = \mu [\cos \theta_i \sin \phi_i, \sin \theta_i \sin \phi_i, \cos \phi_i],$$

with respect to an alignment that places the z -axis in the \mathbf{q}_{12} direction. The angles can all be taken in $[0, \pi]$.

- b. Calculate the values of f from part (a) for each of the six configurations shown below.



6. Sketch the level sets of energy for a single degree of freedom model with energy $E(q, \dot{q}) = \dot{q}^2/2 + \varphi_{LJ}(q)$, where φ_{LJ} is the Lennard-Jones potential.
7. In Example 1.8 what is the exact location of the saddle point?
8. The planar motion of a pair of particles in central forces can be described by a Lagrangian of the form

$$L(\mathbf{q}, \mathbf{p}) = \frac{\|\dot{\mathbf{q}}\|^2}{2} - \varphi(\|\mathbf{q}\|), \quad \mathbf{q} \in \mathbb{R}^2, \quad (1.11)$$

where \mathbf{q} represents the vector separating the two bodies, and φ is a potential giving the strength of attraction or repulsion in terms of interatomic distance. Show that in polar coordinates the energy may be written as

$$E(r, \dot{r}) = \frac{1}{2}\dot{r}^2 + \tilde{\varphi}(r), \quad \tilde{\varphi}(r) = \varphi(r) + \frac{l_z^2}{2r^2},$$

with l_z a constant of motion (the angular momentum).

9. Show that for a system in \mathbb{R}^3 subject to pair potentials $U = \sum_{i=1}^{N-1} \sum_{j=i+1}^N \varphi(\|\mathbf{q}_i - \mathbf{q}_j\|)$, the Hessian matrix is given by

$$U'' = \sum_{i=1}^{N-1} \sum_{j=i+1}^N \mathbf{D}_{ij}^{ij},$$

where \mathbf{D}_{ij}^{ij} is an $N \times N$ symmetric matrix which has four nonzero 3×3 blocks corresponding to the i and j components. That is, the matrix \mathbf{D}_{ij}^{ij} is an $N \times N$ block matrix of 3×3 blocks. Denoting by \mathbf{D}_{kl}^{ij} the kl block, then we have

$$\mathbf{D}_{ii}^{ij} = \mathbf{D}_{jj}^{ij} = \mathbf{B}, \quad \mathbf{D}_{ij}^{ij} = \mathbf{D}_{ji}^{ij} = -\mathbf{B},$$

where

$$\mathbf{B} = \frac{\varphi'(r)}{r} (\mathbf{I} - \mathbf{P}_{12}) + \varphi''(r) \mathbf{P}_{12}, \quad \mathbf{P}_{12} = r^{-2} \mathbf{q}_{12} \mathbf{q}_{12}^T,$$

and $\mathbf{q}_{12} = \mathbf{q}_1 - \mathbf{q}_2$, $r = \|\mathbf{q}_{12}\|$.

10. Consider the planar pendulum model with potential energy function

$$U = k(r - L)^2/2, \quad r = \sqrt{q_x^2 + q_y^2},$$

where $k > 0$ is a given constant. (This is a central force problem and so could be simplified using the conservation of angular momentum, but ignore this fact for the purposes of this exercise.)

- a. Assuming a unit mass, show that the equations of motion for the pendulum are given by

$$\begin{aligned} \dot{q}_x &= v_x, \\ \dot{q}_y &= v_y, \\ \dot{v}_x &= -k(1 - L/r)q_x, \\ \dot{v}_y &= -k(1 - L/r)q_y. \end{aligned}$$

- b. Show that any point on the circle $q_x^2 + q_y^2 = L^2$ is an equilibrium point.

- c. Suppose $k \gg 0$ and describe (in words) the motion from $q_x = L, q_y = 0, p_x = 0, p_y = \alpha > 0$.
- d. Suppose $k \gg 0$ and describe (in words) the motion from $q_x = L, q_y = 0, p_x = \alpha, p_y = 0$.
- e. Derive the system of variational equations and show that these may be written as

$$\dot{\mathbf{W}} = \begin{bmatrix} \mathbf{0} & \mathbf{I} \\ \mathbf{A}(t) & \mathbf{0} \end{bmatrix} \mathbf{W},$$

where the blocks are 2×2 and \mathbf{A} takes the form

$$\mathbf{A} = -k(1 - L/r)\mathbf{I} - kLr^{-3}\mathbf{q}\mathbf{q}^T.$$

- f. Find the four eigenvectors and eigenvalues of the variational equations at a point on the circle ($r = L$). Discuss the variational equations in relation to the motions described in (c) and (d), above.
- 11 Smooth Cut-Off.** In molecular dynamics simulations it is convenient to have a pair potential with compact support for efficiency reasons. While it is possible to simply use a split function (setting the potential—or force—to zero outside some finite range), this has undesirable consequences for energy conservation if the function is not sufficiently smooth. Consider the alternative [346]:

$$\varphi_{\text{LJ}}^{\text{cut-off}}(r) = 4\epsilon \left[\left(\frac{\sigma}{r}\right)^{12} - \left(\frac{\sigma}{r}\right)^6 + \left(6\left(\frac{\sigma}{r_c}\right)^{12} - 3\left(\frac{\sigma}{r_c}\right)^6\right) \left(\frac{r}{r_c}\right)^2 - 7\left(\frac{\sigma}{r_c}\right)^{12} + 4\left(\frac{\sigma}{r_c}\right)^6 \right].$$

Defining the pair potential as a split function

$$\hat{\varphi}_{\text{LJ}}(r) = \begin{cases} \varphi_{\text{LJ}}^{\text{cut-off}}(r) & r < r_c \\ 0 & r \geq r_c \end{cases},$$

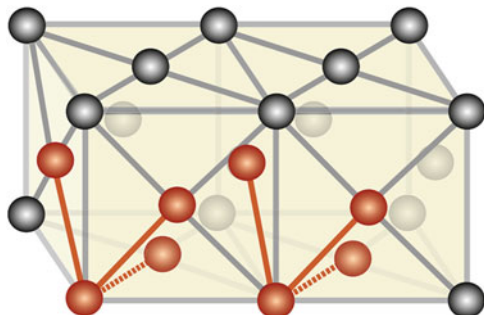
show that $\hat{\varphi}_{\text{LJ}}(r)$ is C' smooth, that is, it is continuously differentiable at r_c . In typical practice, cut-off radii of around 2.5σ to 5σ are used.

- 12 Initialization of an fcc System.** The density ϱ of an N-body system in a cubic box of side L is given by

$$\varrho = \frac{N}{L^3}.$$

For a prescribed density ϱ we first compute the side length $L = (N/\varrho)^{1/3}$, then assign the positions to sites of the fcc lattice. Assume for simplicity that $N/4$ is

Fig. 1.28 Tiling by unit cells allows placement of all atoms on an fcc lattice



a perfect cube, i.e. that there is an integer η such that $\eta^3 = (N/4)$. The idea is to tile a cube with η^3 subcubes, each defining the positions of 4 atoms. This basic cell is replicated, shifted (in three directions) and concatenated to produce the full collection of atoms, as shown in Fig. 1.28. Write an algorithm to perform the initialization of an fcc system as described above.

Chapter 2

Numerical Integrators

At its most basic level, molecular dynamics is about mapping out complicated point sets using trajectories of a system of ordinary differential equations (or, in Chaps. 6–8, a stochastic-differential equation system). The sets are typically defined as the collection of probable states for a certain system. In the case of Hamiltonian dynamics, they are directly associated to a region of the energy landscape. The trajectories are the means by which we efficiently explore the energy surface. In this chapter we address the design of numerical methods to calculate trajectories.

When we use the equations of motion for an atomic system and compute a trajectory, we are producing what we hope to be a representative path of the system. For the moment, we discount any external interactions (such as due to heating at a boundary or other driving forces), so we can think of the system as a closed, Hamiltonian dynamics model. This introduces the *microscopic* perspective which concerns the detailed description of the instantaneous atomic positions and velocities as time is varied. These microscopic paths are the cornerstone of statistical mechanical theory, which is the tool that we will eventually develop for understanding molecular systems at a more abstract level, thus it is essential in developing a computational methodology that we have an understanding of how to generate trajectories reliably and efficiently.

The challenge before us is to compute solutions of

$$\dot{\mathbf{q}} = \mathbf{M}^{-1}\mathbf{p}, \quad \dot{\mathbf{p}} = \mathbf{F}(\mathbf{q}) = -\nabla U(\mathbf{q}),$$

or, more compactly, with \mathbf{z} representing the collection of all positions and momenta,

$$\dot{\mathbf{z}} = \mathbf{f}(\mathbf{z}), \quad \mathbf{f}(\mathbf{z}) = \mathbf{J}\nabla H, \tag{2.1}$$

where $\mathbf{J} = \begin{bmatrix} \mathbf{0} & \mathbf{I} \\ -\mathbf{I} & \mathbf{0} \end{bmatrix}$, and $H = \mathbf{p}^T \mathbf{M}^{-1} \mathbf{p} / 2 + U(\mathbf{q})$ is the Hamiltonian.

In order to correctly model the different possible states of the system, it will be necessary to cover a large part of the accessible phase space, so either trajectories must be very long or we must use many initial conditions. There are many ways to solve initial value problems such as (2.1) combined with an initial condition $\mathbf{z}(0) = \boldsymbol{\zeta}$. The methods introduced here all rely on the idea of a discretization with a finite stepsize h , and an iterative procedure that computes, starting from $\mathbf{z}_0 = \boldsymbol{\zeta}$, a sequence $\mathbf{z}_1, \mathbf{z}_2, \dots$, where $\mathbf{z}_n \approx \mathbf{z}(nh)$. The simplest scheme is certainly Euler's method which advances the solution from timestep to timestep by the formula¹

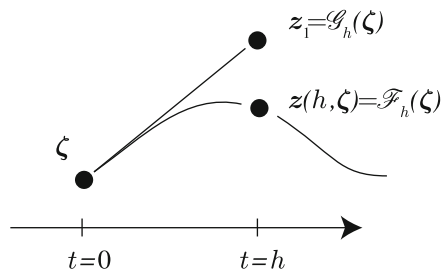
$$\mathbf{z}_{n+1} = \mathbf{z}_n + h\mathbf{f}(\mathbf{z}_n).$$

The method is based on the observation that $\mathbf{z}(t+h) \approx \mathbf{z}(t) + h\dot{\mathbf{z}}(t)$, i.e. the beginning of a Taylor series expansion in powers of h , and the further observation that the solution satisfies the differential equation, hence $\dot{\mathbf{z}}(t)$ may be replaced by $\mathbf{f}(\mathbf{z}(t))$.

In order to be able to easily compare the properties of different methods in a unified way, we focus in this chapter primarily on a particular class of schemes, generalized *one-step methods*. Suppose that the system under study has a well defined flow map \mathcal{F}_t defined on the phase space (which is assumed to exclude any singular points of the potential energy function). The solution of the initial value problem, $\dot{\mathbf{z}} = \mathbf{f}(\mathbf{z})$, $\mathbf{z}(0) = \boldsymbol{\zeta}$, may be written $\mathbf{z}(t, \boldsymbol{\zeta})$ (with $\mathbf{z}(0, \boldsymbol{\zeta}) = \boldsymbol{\zeta}$), and the flow-map \mathcal{F}_t satisfies $\mathcal{F}_t(\boldsymbol{\zeta}) = \mathbf{z}(t, \boldsymbol{\zeta})$. A *one-step method*, starting from a given point, approximates a point on the solution trajectory at a given time h units later. Such a method defines a map \mathcal{G}_h of the phase space as illustrated in Fig. 2.1.

We assume here a basic understanding of ordinary differential equations; some good references for review of this topic are [16, 51, 177, 362]. For basic concepts in the numerical analysis of ordinary differential equations the definitive reference is [167].

Fig. 2.1 A step with the flow map approximation \mathcal{G}_h is illustrated in comparison to the corresponding step along the solution curve defined by the flow map \mathcal{F}_h



¹Subscripts were used previously to indicate the components of vectors and here they are used to indicate the indexing of timesteps. Although in theory this could lead to some confusion, it normally does not in practice, since we index components in descriptions of details of models and we discuss timesteps in context of defining numerical methods for general classes of systems. Moreover, we use boldface for vectors, so a subscript on a boldface vector indicates a timestep index. When we wish to refer to both the timestep and the component index, we may write $z_{n,i}$ to denote the i th component at timestep n .

Let us emphasize that the issues arising in the design and analysis of numerical methods for molecular dynamics are slightly different than those confronted in other application areas. For one thing the systems involved are highly structured having conservation properties such as first integrals and Hamiltonian structure. We address the issues related to the inherent structure of the molecular N-body problem in both this and the next chapter; wherein we shall learn that *symplectic* discretizations are typically the most appropriate methods.

Another special aspect of the molecular system is that normally it is sensible to use a fixed stepsize, that is each timestep corresponds to a fixed interval of real time. This is in contrast to other applications where it is found to be important to vary the step during simulation. The reason that a uniform stepsize is used is because, in a simulation of many particles, the complexity of the system ensures that if a strong local force is encountered in some corner of the system, a force of similar magnitude will be found somewhere else at the next instant. Even if, occasionally, an instantaneous event is observed that could be controlled by reducing the stepsize, the necessary adaptive machinery can impair the geometric properties and reduce the efficiency of the numerical procedure.² There is no trivial way of selecting the stepsize *a priori*. In typical practice, one performs several trial runs, examining the fluctuations in energy or other easily computable quantities and makes the choice of stepsize in order to keep these within a tolerable range. The molecular dynamics timesteps are typically quite small, measured in femtoseconds, in order to capture the rapid fluctuations of the atoms (in Chap. 4, we discuss ways of increasing the timestep).

2.1 Error Growth in Numerical Integration of Differential Equations

In this section we discuss the issues of convergence and accuracy in numerical integration methods for solving ordinary differential equations.

Let us begin by considering Euler's method in a bit more detail to understand its convergence order. The *convergence* of a numerical method refers to the ability of the method to provide an arbitrary level of accuracy by using small enough timesteps. The *order of accuracy* is the exponent in the power law by which the error in the method is related to the stepsize. For example, when we say that a method is third order accurate, we mean that the global error (on a fixed finite time interval) can be bounded by Kh^3 , where h is a sufficiently small timestep and K is a number which depends on the length of the time interval and the features of the problem, but which is independent of h .

The flow map approximation in the case of Euler's method is

²A variable stepsize is only used where one expects extreme changes in particle velocities over the course of a simulation (see e.g. [75, 390] for examples arising in radiation damage cascades).

$$\mathcal{G}_h(z) = z + hf(z),$$

and we have

$$z_{n+1} = \mathcal{G}_h(z_n), \quad n = 0, 1, 2, \dots \quad (2.2)$$

with $z_0 = \zeta$. The points $\{z_n\}$ are intended to be approximations to the values of the solution. The obvious question is this: how good an approximation is z_n of $z(nh)$?

Let the approximate solution vectors at successive timesteps be z_0, z_1, \dots, z_v where $v h = \tau$. We assume that τ , the length of the time interval, is fixed, and v is an integer parameter representing the total number of timesteps. In order to improve the quality of the approximation, the parameter v may be increased, as the stepsize is proportionately decreased. The error at step n is defined by $e_n = \|z_n - z(t_n)\|$, where $t_n = nh$; it clearly depends on h . With these definitions one can prove the following result, which is typical of the sorts of results that are available for numerical methods for initial value problems:

Theorem 2.1 *Let \mathcal{D} be a bounded, open region in \mathbb{R}^m such that $f : \mathcal{D} \rightarrow \mathbb{R}^m$ is continuously differentiable. Let ζ be an interior point of \mathcal{D} and suppose the initial value problem (2.1) has a unique solution that remains in \mathcal{D} for $t \in [0, \tau]$. Then there exists a constant $C(\tau) > 0$ such that for sufficiently large $v \in \mathbb{N}$ the numerical solution z_n remains in \mathcal{D} for $n = 0, 1, \dots, v$, where $hv = \tau$, and, moreover, the maximum global error in Euler's method satisfies*

$$\bar{e} := \max_{0 \leq n \leq v} e_n \leq C(\tau)h.$$

In short, the error in the approximation obtained on $[0, \tau]$ is reduced in direct proportion to the number of steps taken to cover this interval. Another way to say this is that $\bar{e} \propto h$, or, using the order notation, $\bar{e} = \mathcal{O}(h)$. Because the global error is of order h^r , where $r = 1$, we say that Euler's method is a *first order* method, or that it *converges with order r = 1*.

2.1.1 Example: The Trimer

Let us test Euler's method on the trimer model (formulated as a system in \mathbb{R}^4). Fixing initial values ($q_0 = (0.5, 1.0); p_0 = (0.1, 0.1)$) we solve the trimer on $[0, 4]$ using the Euler method first with 40 time-steps of length 0.1, next using 80 time-steps of length 0.05 and then with 160 steps of size 0.025, etc. Each calculation results in a different “discrete trajectory.” The solutions are graphed in the xy projection in the left panel of Fig. 2.2 with line segments connecting the points; these piecewise linear paths take on the appearance of smooth curves as the stepsize is reduced.

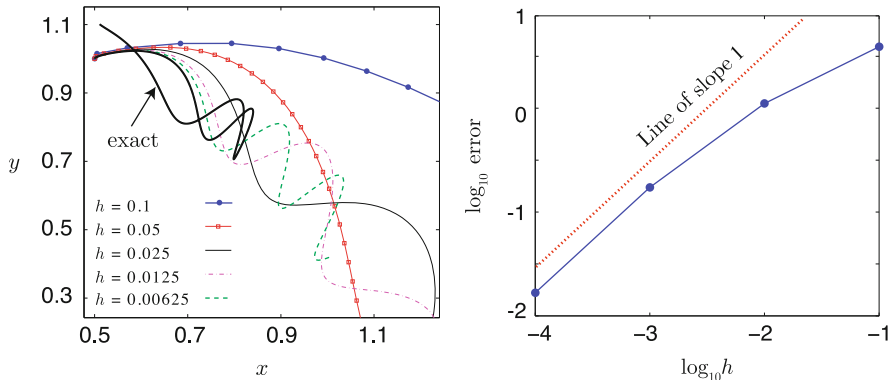


Fig. 2.2 Euler’s method applied to the trimer. *Left*, the solution trajectories for different step-sizes; *right*: the maximum global errors in position projections of solutions computed using four different time-steps appear to show an asymptotic linear relationship to step-size, when plotted in log-log scale

A natural question is how can one measure the error in the discrete approximations, since for the trimer, no exact analytical solution is available? Although it is not possible to compute this error exactly, if it is assumed that the process is convergent (as certainly appears to be the case from our experiment) we may use the accurate solution computed with very small steps as a reference and compute the differences between iterates along the trajectories and corresponding points on the reference trajectory. The maximum of the differences between positions of corresponding points is then used as a measure of the global error in the solution for a given step-size h . For the reference solution in the case of the trimer, we have used a simulation with a superior numerical method (the Verlet method) and very small steps of size 10^{-7} . This is the “exact” solution that has been plotted in the left panel of Fig. 2.2. In the right hand panel of Fig. 2.2, the global error $\bar{e}(h)$ is calculated in this way and plotted against the stepsize, using a logarithmic scale. Studying this figure, we see that in log-log scale, the observed relationship between \bar{e} and h is linear, with slope 1 (for h sufficiently small):

$$\ln \bar{e} \approx \ln h + \alpha,$$

where α is a constant. Hence, by exponentiating both sides we obtain

$$\bar{e} \approx Ch,$$

where $C = e^\alpha$, confirming the first order relationship between the global error and the step-size.

In the simulations of the example above, it is apparent that the errors are larger at the end of the interval than at earlier times. We know that molecular dynamics trajectories need to be very long compared to the time-step used in

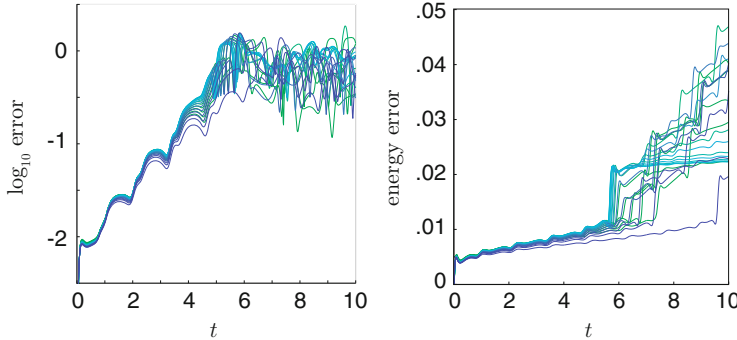


Fig. 2.3 These graphs show the way in which the error grows in relation to time in simulations of the trimer using Euler’s method. *Left:* the growth of the logarithm of the trajectory error; *right:* the energy error growth as a function of time

order for them to be useful, so how the error grows in long simulations is quite important. Convergence theorems for numerical methods like that mentioned above are normally formulated for computations on a finite interval, and often do not tell us much about how the error depends on time (i.e. on the length of the interval, τ).

To examine the issue of error growth we perform a simulation using a particular timestep ($h = 0.001$) on the time interval $[0, 10]$ and compare against the reference solution on this interval. The logarithm of the error at each time-step, e_n , is then computed and the result plotted against n . We repeated this for 20 separate initial conditions having the same initial energy. In the left panel of Fig. 2.3, the error graphs are shown, for each of these numerical trajectories, demonstrating that the error in each case grows very rapidly in the early going. Eventually the error growth tapers off, but only when the error is around the same size as the diameter of the system, thus there is little meaningful information remaining regarding a particular trajectory after $t \approx 5$. The right panel shows the errors in energies seen in the same set of simulations, showing that the energy errors initially grow only linearly while the global error is rising exponentially.

To summarize, in this example, with the time interval fixed, the error in Euler’s method increases in proportion to the stepsize. On the other hand, the global error grows with the length of the time interval, and at a rapid rate, until it is clear that the numerical trajectory is entirely unrelated to the exact trajectory. Moreover, we observe that the energy errors grow much more slowly than the trajectory errors.

2.1.2 Higher Order Methods

One approach to higher accuracy is to decrease the step-size while continuing to use Euler’s method. Since we know that the error on a given fixed interval is proportional to h , using a smaller stepsize should decrease the error in proportion, albeit at the

cost of requiring more timesteps to cover the given time interval. A more efficient means to get better accuracy is to use a higher order method. Higher order methods are ones that satisfy a global error estimate (for finite time intervals) of the form

$$\bar{e} \approx C(\tau)h^r,$$

where $r > 1$.

Example 2.1 The Taylor series expansion of the solution may be written $z(t+h) = z(t) + h\dot{z}(t) + (h^2/2)\ddot{z}(t) + \dots$. Whereas a first order truncation of this series leads to Euler's method, retaining terms through second order leads to

$$z_{n+1} = z_n + h\dot{z}_n + \frac{h^2}{2}\ddot{z}_n,$$

which is referred to as the 2nd order Taylor series method. In this formula $\dot{z}_n = f(z_n)$, and the second derivative is obtained by differentiating the differential equation itself:

$$\ddot{z}(t) = \frac{d}{dt}\dot{z}(t) = \frac{d}{dt}f(z(t)) = f'(z(t))\dot{z}(t) = f'(z(t))f(z(t)),$$

so one may write the 2nd order Taylor series method as

$$z_{n+1} = z_n + hf(z_n) + \frac{h^2}{2}f'(z_n)f(z_n).$$

This method generates the flow map approximation

$$\mathcal{G}_h(z) = z + hf(z) + \frac{h^2}{2}f'(z)f(z).$$

Note that by the notation $f'(z)$ where $z \in \mathbb{R}^m$ and $f : \mathbb{R}^m \rightarrow \mathbb{R}^m$, is meant the $m \times m$ Jacobian matrix whose ij -component is $(f'(z))_{ij} = \partial f_i / \partial z_j$. An alternative notation for f' is $\partial f / \partial z$.

Methods like the Taylor series method offer the prospect of better accuracy in the local approximation, and smaller global error in a given simulation, but they do not necessarily resolve the more important issue relevant for very long time integrations (which we will need in molecular dynamics): the unlimited growth of perturbations from the energy surface. In molecular dynamics, we have already seen that the Euler method has growing energy error which suggests that it will be a poor scheme where the goal is to approximate the behavior of a constant energy trajectory. This same qualitative behavior is seen in other numerical methods, such as the Taylor series method. However, there are alternatives that give both higher order of accuracy and, typically, improved energy accuracy. We discuss one of the most popular schemes of this type in the next section.

2.2 The Verlet Method

The Verlet method (also known as leapfrog or Störmer-Verlet) is a second order method that is popular for molecular simulation. It is specialized to problems that can be expressed in the form $\dot{\mathbf{q}} = \mathbf{v}$, $M\dot{\mathbf{v}} = \mathbf{F}(\mathbf{q})$, with even dimensional phase space \mathbb{R}^{2N_c} , which includes constant energy molecular dynamics. Some generalizations exist for other classes of Hamiltonian systems.

The Verlet method is a numerical method that respects certain conservation principles associated to the continuous time ordinary differential equations, i.e. it is a geometric integrator. Maintaining these conservation properties is essential in molecular simulation as they play a key role in maintaining the physical environment. As a prelude to a more general discussion of this topic, we demonstrate here that it is possible to derive the Verlet method from the variational principle. This is not the case for every convergent numerical method. The Verlet method is thus a special type of numerical method that provides a discrete model for classical mechanics.

2.2.1 Hamilton's Principle and Equations of Motion

Hamilton's principle of least action provides a mechanism for deriving equations of motion from a Lagrangian. Recall from Chap. 1 that the Lagrangian for the N-body system is defined by

$$L(\mathbf{q}, \mathbf{v}) \stackrel{\text{def}}{=} \frac{\mathbf{v}^T \mathbf{M} \mathbf{v}}{2} - U(\mathbf{q}),$$

where \mathbf{M} is the mass matrix and the potential energy function U is, for simplicity, taken to be smooth (C^2). We consider the collection of all twice continuously differentiable curves in the configuration space which start from a certain point \mathbf{Q} and end at another given point \mathbf{Q}' . We may think of any such curve as being represented by a parameterization $\mathbf{q}(t)$, $t \in [\alpha, \beta]$ with $\mathbf{q}(\alpha) = \mathbf{Q}$ and $\mathbf{q}(\beta) = \mathbf{Q}'$, where the components of $\mathbf{q}(t)$ are C^∞ functions. Denote by $G = G(\mathbf{Q}, \mathbf{Q}', \alpha, \beta)$ the class of smooth parameterized curves such that $\mathbf{q}(\alpha) = \mathbf{Q}$, $\mathbf{q}(\beta) = \mathbf{Q}'$. Then the *classical action* (or, simply, *action*) of the Lagrangian L is defined for any $\Gamma \in G$ by

$$\mathcal{A}_L(\Gamma) \stackrel{\text{def}}{=} \int_{\alpha}^{\beta} L(\mathbf{q}(t), \dot{\mathbf{q}}(t)) dt.$$

The variational calculus approach to classical mechanics is based on minimizing the action \mathcal{A}_L over the class G of parameterized curves. This is normally referred to as the “principle of least action”. It is difficult to provide a physical motivation for this concept, but it is normally taken as a foundation stone for classical mechanics.

Given Γ in G with parameterization $\mathbf{q}(t)$, $t \in [\alpha, \beta]$, we consider the curve Γ^ε with parameterization \mathbf{q}^ε defined by

$$\mathbf{q}^\varepsilon(t) = \mathbf{q}(t) + \varepsilon \boldsymbol{\eta}(t), \quad t \in [\alpha, \beta], \quad (2.3)$$

where $\boldsymbol{\eta}(t)$ satisfies $\boldsymbol{\eta}(\alpha) = \boldsymbol{\eta}(\beta) = 0$. Thus $\boldsymbol{\eta}$ is a C^∞ parameterized curve linking $\mathbf{0}$ to $\mathbf{0}$. In defining variations in this way, we are using, implicitly, the fact that we can add together functions in C^∞ and multiply them by scalars (e.g. ε) and remain in C^∞ . We also make use of the intuitive concept that (2.3) defines \mathbf{q}^ε in such a way that it is “close” to \mathbf{q} when ε is small. This can be made precise by a little more elaboration, but we forego this here. Effectively, we are using our understanding of C^∞ as a *normed function space* to restrict attention to variations of the base curve Γ in a particular “direction.”

Using a Taylor series expansion of the Lagrangian,³ we have

$$\begin{aligned} \mathcal{A}_L(\Gamma^\varepsilon) - \mathcal{A}_L(\Gamma) &= \int_{\alpha}^{\beta} [L(\mathbf{q}(t) + \varepsilon \boldsymbol{\eta}(t), \dot{\mathbf{q}}(t) + \varepsilon \dot{\boldsymbol{\eta}}(t)) - L(\mathbf{q}(t), \dot{\mathbf{q}}(t))] dt, \\ &= \int_{\alpha}^{\beta} \left[\varepsilon \left(\frac{\partial L}{\partial \mathbf{q}}(\mathbf{q}(t), \dot{\mathbf{q}}(t)) \boldsymbol{\eta}(t) + \frac{\partial L}{\partial \dot{\mathbf{q}}}(\mathbf{q}(t), \dot{\mathbf{q}}(t)) \dot{\boldsymbol{\eta}}(t) \right) + \mathcal{O}(\varepsilon^2) \right] dt. \end{aligned}$$

Hamilton’s principle states that the natural motion of the system described by the Lagrangian L is a stationary point of the classical action which implies that the $\mathcal{O}(\varepsilon)$ term above should vanish for any smooth variation $\boldsymbol{\eta}(t)$ with $\boldsymbol{\eta}(\alpha) = \boldsymbol{\eta}(\beta) = 0$, i.e.,

³In the multidimensional setting, Taylor’s theorem states that given a C^{k+1} function $f : \mathbb{R}^m \rightarrow \mathbb{R}$ and a point \mathbf{z}_0 , we have

$$\begin{aligned} f(\mathbf{z}) - f(\mathbf{z}_0) &= \nabla f(\mathbf{z}_0) \cdot (\mathbf{z} - \mathbf{z}_0) + f^{(2)}(\mathbf{z} - \mathbf{z}_0, \mathbf{z} - \mathbf{z}_0) + f^{(3)}(\mathbf{z} - \mathbf{z}_0, \mathbf{z} - \mathbf{z}_0, \mathbf{z} - \mathbf{z}_0) \\ &\quad + \dots f^{(k)}(\mathbf{z} - \mathbf{z}_0, \mathbf{z} - \mathbf{z}_0, \dots, \mathbf{z} - \mathbf{z}_0) + \mathcal{O}(\|\mathbf{z} - \mathbf{z}_0\|^{k+1}) \end{aligned}$$

where $\nabla f = \partial f / \partial \mathbf{z}$ is the gradient, i.e. a vector with m components, $f^{(2)}$ is the $m \times m$ Hessian matrix of f (the matrix whose ij component is $\partial^2 f / \partial z_i \partial z_j$), and $f^{(2)}(\mathbf{u}, \mathbf{v})$, $\mathbf{u}, \mathbf{v} \in \mathbb{R}^m$, represents the quadratic form $\mathbf{u}^T f^{(2)} \mathbf{v}$. In a similar way we interpret $f^{(3)}$ as a tensor which we can think of as a $m \times m \times m$ triply-indexed array, the ijk element being $\partial^3 f / \partial z_i \partial z_j \partial z_k$ and

$$f^{(3)}(\mathbf{u}, \mathbf{v}, \mathbf{w}) = \sum_{i=1}^m \sum_{j=1}^m \sum_{k=1}^m (\partial^3 f / \partial z_i \partial z_j \partial z_k) u_i v_j w_k.$$

$$I = \int_{\alpha}^{\beta} \left[\frac{\partial L}{\partial \mathbf{q}}(\mathbf{q}(t), \dot{\mathbf{q}}(t)) \boldsymbol{\eta}(t) + \frac{\partial L}{\partial \dot{\mathbf{q}}}(\mathbf{q}(t), \dot{\mathbf{q}}(t)) \dot{\boldsymbol{\eta}}(t) \right] dt = 0.$$

We use integration by parts to remove the differentiation of $\boldsymbol{\eta}$, thus (in light of the boundary conditions on $\boldsymbol{\eta}(t)$),

$$I = \int_{\alpha}^{\beta} \left[\frac{\partial L}{\partial \mathbf{q}}(\mathbf{q}(t), \dot{\mathbf{q}}(t)) - \frac{d}{dt} \frac{\partial L}{\partial \dot{\mathbf{q}}}(\mathbf{q}(t), \dot{\mathbf{q}}(t)) \right] \boldsymbol{\eta}(t) dt = 0.$$

Since the variation $\boldsymbol{\eta}$ is meant to be arbitrary, it requires

$$\frac{d}{dt} \frac{\partial L}{\partial \dot{\mathbf{q}}}(\mathbf{q}(t), \dot{\mathbf{q}}(t)) = \frac{\partial L}{\partial \mathbf{q}}(\mathbf{q}(t), \dot{\mathbf{q}}(t)),$$

which is precisely the Lagrangian formulation of the equations of motion.

The method of derivation described here may be formulated in direct analogy to the traditional method of minimizing a function of several variables based on finding critical points. Define the *variational derivative* of a functional \mathcal{F} , $\delta \mathcal{F}/\delta \mathbf{q}$ so that

$$\mathcal{F}(\mathbf{q} + \varepsilon \boldsymbol{\eta}) = \varepsilon \frac{\delta \mathcal{F}}{\delta \mathbf{q}} \boldsymbol{\eta} + O(\varepsilon^2),$$

for all suitable (say, C^∞) functions $\boldsymbol{\eta}$. Viewing the action $\mathcal{A}_L(\Gamma)$ as the functional \mathcal{F} , the stationarity condition (the Euler-Lagrange equations) may be written

$$\frac{\delta \mathcal{F}}{\delta \mathbf{q}} = 0.$$

Thus the calculus of variations becomes a generalization of the traditional method of minimizing smooth functions by finding critical points.⁴

⁴This discussion is a great simplification. Any curve which satisfies this equation will represent a “stationary point” (actually, “stationary curve” would be more accurate) of the classical action. Such curves could include smooth local action minimizers, local action maximizers, or “saddle points” of the actional functional in a generalized sense. Deciding whether a given stationary curve is an actual minimizer of the action would require analysis of the second variation (the coefficient of ε^2 in the expansion above), which introduces additional complexity. For a more comprehensive treatment, see e.g. [210].

2.2.2 Derivation of the Verlet Method

Now let us consider the discrete version of “minimizing the action”. We work on the time interval $[0, \tau]$. Consider the $v + 1$ points \mathbf{q}_0 to \mathbf{q}_v in configuration space

$$\hat{\Gamma} = (\mathbf{q}_0, \mathbf{q}_1, \dots, \mathbf{q}_v).$$

We must first define the action for such a discrete path. One perspective is that we first formulate a discrete version of the Lagrangian in terms of only the point set $\mathbf{q}_0, \mathbf{q}_1, \dots, \mathbf{q}_v$, but this somehow requires that we define velocities. Noting that

$$\dot{\mathbf{q}}(t) \approx \frac{\mathbf{q}(t+h) - \mathbf{q}(t)}{h},$$

we are led to consider the approximation at time level n

$$\mathbf{v}_n \stackrel{\text{def}}{=} \frac{\mathbf{q}_{n+1} - \mathbf{q}_n}{h},$$

and thus, by Riemann summation

$$\mathcal{A}_L \approx \hat{\mathcal{A}} \stackrel{\text{def}}{=} \sum_{n=0}^{v-1} L\left(\mathbf{q}_n, \frac{\mathbf{q}_{n+1} - \mathbf{q}_n}{h}\right) h.$$

At first glance, it looks like this is a crude approximation, since we have employed a one-sided difference, however, let us proceed anyway to see the implications of this choice. In the case of a mechanical system with Lagrangian $L(\mathbf{q}, \mathbf{v}) = \dot{\mathbf{v}}^T \mathbf{M} \mathbf{v} / 2 + U(\mathbf{q})$, we then have

$$\hat{\mathcal{A}} = \sum_{n=0}^{v-1} \left[\frac{(\mathbf{q}_{n+1} - \mathbf{q}_n)^T \mathbf{M} (\mathbf{q}_{n+1} - \mathbf{q}_n)}{2h^2} - U(\mathbf{q}_n) \right] h.$$

We should think of $\hat{\mathcal{A}}$ as a function of all the positions $\mathbf{q}_0, \mathbf{q}_1, \dots, \mathbf{q}_v$ defining the discrete path. Critical points of this function satisfy

$$\nabla \hat{\mathcal{A}} = 0,$$

where the gradient must be taken with respect to all configurational points on the path (and all coordinates). This condition leads to the equations

$$\frac{\partial \hat{\mathcal{A}}}{\partial \mathbf{q}_n} = 0, \quad n = 1, \dots, v,$$

since we think of the starting point \mathbf{q}_0 as fixed. To calculate the derivative of $\hat{\mathcal{A}}$ with respect to \mathbf{q}_n , $n = 1, 2, \dots, v - 1$, note that only a few terms of the discrete action involve this configurational point, thus

$$\begin{aligned}\frac{\partial \hat{\mathcal{A}}}{\partial \mathbf{q}_n} &= \frac{\partial}{\partial \mathbf{q}_n} \left[\frac{1}{2h} ((\mathbf{q}_n - \mathbf{q}_{n-1})^T \mathbf{M} (\mathbf{q}_n - \mathbf{q}_{n-1}) + (\mathbf{q}_{n+1} - \mathbf{q}_n)^T \right. \\ &\quad \times \left. \mathbf{M} (\mathbf{q}_{n+1} - \mathbf{q}_n)) - U(\mathbf{q}_n)h \right] \\ &= \frac{1}{h} [\mathbf{M}(\mathbf{q}_n - \mathbf{q}_{n-1}) - \mathbf{M}(\mathbf{q}_{n+1} - \mathbf{q}_n)] - \nabla U(\mathbf{q}_n)h,\end{aligned}$$

which yields the equations

$$\mathbf{M}(\mathbf{q}_{n+1} - 2\mathbf{q}_n + \mathbf{q}_{n-1}) = -h^2 \nabla U(\mathbf{q}_n), \quad n = 1, 2, \dots, v - 1. \quad (2.4)$$

We can think of

$$\frac{1}{h^2} (\mathbf{q}_{n+1} - 2\mathbf{q}_n + \mathbf{q}_{n-1})$$

as a centered finite difference approximation of the acceleration (the second derivative of position), thus the Eq.(2.4) is a direct discretization of Newton's equations.

Somewhat surprisingly, the one-sided approximation of velocities in the discrete Lagrangian has led to a symmetric discretization of the equations of motion. There is a slight issue of what to do at the endpoints. In the variational formulation we think of the endpoints of the curve as fixed points which means that we are effectively solving a boundary value problem and Eq.(2.4) tells us how to compute all the interior points along the path. In the case of an initial value problem (the usual issue in molecular dynamics) we do not know in advance the right endpoint value, but we assume that we can, in some way, calculate \mathbf{q}_1 (by a *starting procedure*) and so Eq.(2.4) defines $\mathbf{q}_2, \mathbf{q}_3, \dots, \mathbf{q}_v$.

The method (2.4) is commonly referred to as *Störmer's rule*. It was used by the mathematician Störmer for calculations in the first decade of the 1900s. In molecular dynamics this method is referred to as the Verlet method since it was used by Verlet in his important 1967 paper [387].

The scheme is usually given in an alternative “velocity Verlet” form that takes a step from a given vector $\mathbf{q}_n, \mathbf{v}_n$ to $\mathbf{q}_{n+1}, \mathbf{v}_{n+1}$ by the sequence of operations

$$\mathbf{v}_{n+1/2} = \mathbf{v}_n + (h/2)\mathbf{M}^{-1}\mathbf{F}_n, \quad (2.5)$$

$$\mathbf{q}_{n+1} = \mathbf{q}_n + h\mathbf{v}_{n+1/2}, \quad (2.6)$$

$$\mathbf{v}_{n+1} = \mathbf{v}_{n+1/2} + (h/2)\mathbf{M}^{-1}\mathbf{F}_{n+1}, \quad (2.7)$$

where $\mathbf{F}_n = \mathbf{F}(\mathbf{q}_n) = -\nabla U(\mathbf{q}_n)$. The force computed at the end of a given step may be reused at the start of the following step, thus effectively a single force evaluation is needed at each timestep (the method has a similar “cost” to the Euler method, if we measure cost in terms of force evaluations). The derivation of the Störmer form from the velocity Verlet form is straightforward: write down two consecutive steps of (2.5)–(2.7) then eliminate velocities.

The method is widely used but is often stated in other forms, so let us consider these here.

The most straightforward rewriting of the Verlet method is to put the equations and the discretization in Hamiltonian form, i.e. introducing momenta $\mathbf{p} = \mathbf{M}\mathbf{v}$, and thus $\mathbf{p}_n = \mathbf{M}\mathbf{v}_n$, which results in the flow map approximation (taking us from any point in phase space (\mathbf{q}, \mathbf{p}) to a new point (\mathbf{Q}, \mathbf{P})):

$$\mathbf{Q} = \mathbf{q} + h\mathbf{M}^{-1}\mathbf{p} + \frac{h^2}{2}\mathbf{M}^{-1}\mathbf{F}(\mathbf{q}), \quad \mathbf{P} = \mathbf{p} + \frac{h}{2}[\mathbf{F}(\mathbf{q}) + \mathbf{F}(\mathbf{Q})]. \quad (2.8)$$

Alternatively,

$$\mathbf{p}_{n+1/2} = \mathbf{p}_n + (h/2)\mathbf{F}_n, \quad \mathbf{q}_{n+1} = \mathbf{q}_n + h\mathbf{M}^{-1}\mathbf{p}_{n+1/2}, \quad \mathbf{p}_{n+1} = \mathbf{p}_{n+1/2} + (h/2)\mathbf{F}_{n+1}.$$

Returning to (2.5)–(2.7), write out the formulas for two successive steps $((q_{n-1}, v_{n-1}) \mapsto (q_n, v_n)$ and $(q_n, v_n) \mapsto (q_{n+1}, v_{n+1})$) and note that, from

$$\mathbf{v}_n = \mathbf{v}_{n-1/2} + (h/2)\mathbf{M}^{-1}\mathbf{F}_n,$$

one has

$$\mathbf{v}_{n+1/2} = \mathbf{v}_{n-1/2} + h\mathbf{M}^{-1}\mathbf{F}_n,$$

$$\mathbf{q}_{n+1} = \mathbf{q}_n + h\mathbf{v}_{n+1/2}.$$

How do we use this if, as is typical, initial conditions of the form $\mathbf{q}(0) = \mathbf{q}_0, \mathbf{v}(0) = \mathbf{v}_0$ are specified? It is necessary to define an initialization procedure for $\mathbf{v}_{-1/2}$:

$$\mathbf{v}_{-1/2} = \mathbf{v}_0 - (h/2)\mathbf{M}^{-1}\mathbf{F}(\mathbf{q}_0).$$

And it is also necessary to use, at any subsequent step,

$$\mathbf{v}_n = \mathbf{v}_{n-1/2} + (h/2)\mathbf{M}^{-1}\mathbf{F}_n,$$

if $\mathbf{q}_n, \mathbf{v}_n$ are both needed, e.g. for the evaluation of the energy or other velocity-dependent observable.

The difference between formulations is typically subtle, and largely influence the details of computer software design. For many applications the difference can

be safely ignored, but it can have implications when used as part of a more complex algorithm (see [29] and the discussion therein). The use of different formulations can result in differences in the accumulation of rounding error [167].⁵

2.2.3 Convergence and the Order of Accuracy

A typical integrator computes successive steps from the formulas

$$z_{n+1} = \mathcal{G}_h(z_n), \quad z_0 = \xi.$$

Assume that \mathcal{G}_h is a smooth map for all $h > 0$. The exact solution satisfies

$$z(t_{n+1}) = \mathcal{F}_h(z(t_n)).$$

To each $h > 0$ we may associate a finite set of phase space points $z_0, z_1, z_2, \dots, z_v$; these represent the numerical solution at $t_0 = 0, t_1 = h, t_2 = 2h, \dots, t_v = vh = \tau$.

Taking the difference of the numerical and exact solutions, we have

$$z_{n+1} - z(t_{n+1}) = \mathcal{G}_h(z_n) - \mathcal{F}_h(z(t_n)). \quad (2.9)$$

The first assumption is that \mathcal{G}_h is an $\mathcal{O}(h^{p+1})$ approximation of \mathcal{F}_h in the sense that there is a constant $K \geq 0$ and a constant $\Delta > 0$ such that, for $t \in [0, \tau]$, we have

$$\|\mathcal{F}_h(z(t)) - \mathcal{G}_h(z(t))\| \leq \tilde{K}h^{p+1}, \quad h < \Delta. \quad (2.10)$$

This assumption is usually verified by expanding the numerical and exact solutions in powers of h , using Taylor series expansions.

To tackle the question of the growth of local error, we still must make an important assumption on \mathcal{G}_h , namely that it satisfies a *Lipschitz condition* of the form

$$\|\mathcal{G}_h(\mathbf{u}) - \mathcal{G}_h(\mathbf{w})\| \leq (1 + hL)\|\mathbf{u} - \mathbf{w}\|, \quad \mathbf{u}, \mathbf{w} \in D, h \leq \Delta. \quad (2.11)$$

The set D should be a domain containing the exact solution for $[0, \tau]$, and it is assumed that, for all $h \leq \Delta$ the numerical solution is also contained in D for $n =$

⁵Rounding error is the error introduced when numbers are forced into the finite word length representation in a typical digital computer. Adding together two “computer numbers,” then rounding, results in another computer number. Rounding errors may accumulate in long computations, but in molecular dynamics they are normally dominated by the much larger “truncation errors” introduced in the process of discretization, that is, due to replacing the differential equation by a difference equation such as the Euler or Verlet method. For an example of the role of rounding error in the context of constrained molecular dynamics, see [237].

$0, 1, \dots, v$. (This is a simplifying assumption the removal of which would require somewhat more intricate assumptions regarding the differential equations.)

With these assumptions in hand, begin from (2.9) and write

$$z_{n+1} - z(t_{n+1}) = \mathcal{G}_h(z_n) - \mathcal{G}_h(z(t_n)) + \mathcal{G}_h(z(t_n)) - \mathcal{F}_h(z(t_n)),$$

then take norms and use the triangle inequality and (2.10), (2.11) to get the following recurrent inequality for the error $\varepsilon_n = \|z_n - z(t_n)\|$:

$$\varepsilon_{n+1} \leq (1 + Lh)\varepsilon_n + \bar{K}h^{p+1}.$$

From this, the bound

$$\varepsilon_n \leq \frac{\bar{K}}{L} e^{Lnh} h^p, \quad n = 0, 1, \dots, v, \quad (2.12)$$

follows by a straightforward calculation, for $h \leq \Delta$.

The assumption (2.10) that the local error is of order $p + 1$, $p > 0$, is termed the *consistency* of the numerical method. We say the method is *consistent of order p*.

The assumption (2.11) that the method does not increase the separation between two nearby trajectories by more than a factor of the form $1 + hL$ in each step is referred to as the *stability* of the method.

This result shows that a method which is consistent of order p and stable is convergent of order p .

Example 2.2 (The Verlet Method is 2nd Order) In this example, assume a single degree of freedom system, i.e. $q, p \in \mathbb{R}$, and take $M = 1$. The Verlet method can be written in the form of a map, as in (2.8), or, in slightly more detail, as

$$Q = q + hp + \frac{h^2}{2} F(q), \quad (2.13)$$

$$P = p + \frac{h}{2} \left[F(q) + F(q + hp + \frac{h^2}{2} F(q)) \right]. \quad (2.14)$$

The first equation is already a polynomial, i.e. it is in the form of a series expansion in powers of h where the coefficients are functions of the starting point (q, p) . The second equation may be written as a series expansion in powers of h as well:

$$\begin{aligned} P = p + \frac{h}{2} F(q) + \frac{h}{2} \left[F(q) + hF'(q)(p + \frac{h}{2} F(q)) \right. \\ \left. + \frac{h^2}{2} F''(q)(p + \frac{h}{2} F(q))^2 + \dots \right]. \end{aligned}$$

Note that the neglected terms will involve 4th (and higher) powers of h .

Combining terms of like powers of h , we have

$$P = p + hF + \frac{h^2}{2}pF' + \frac{h^3}{4}[F'F + p^2F''] + \mathcal{O}(h^4).$$

We carry these terms to compare against the expansion of the exact solution. Since $\dot{q} = p$, we have $\ddot{q} = \dot{p} = F(q)$, and the third derivative is $q^{(3)} = F'(q)p$. On the other hand $\dot{p} = F(q)$ implies that $\ddot{p} = F'(q)\dot{q} = pF'$, and thus

$$p^{(3)} = p^2F'' + F'F.$$

The Taylor expansion of the solution is (taking $q(t) = q, p(t) = p$):

$$\begin{aligned} q(t+h) &= q + hp + \frac{h^2}{2}F + \frac{h^3}{6}F'p + \mathcal{O}(h^4), \\ p(t+h) &= p + hF + \frac{h^2}{2}pF' + \frac{h^3}{6}[p^2F'' + F'F] + \mathcal{O}(h^4). \end{aligned}$$

We now examine the series expansions for the exact and Verlet solutions and find that these differ in the third (and higher) order terms.

$$Q - q(t+h) = \frac{h^3}{6}F'p + \mathcal{O}(h^4),$$

and

$$P - p(t+h) = \frac{h^3}{12}[p^2F'' + F'F] + \mathcal{O}(h^4).$$

These relations can be summarized as telling us that

$$\|\mathcal{G}_h(z) - \mathcal{F}_h(z)\| = \kappa(z)h^3 + \mathcal{O}(h^4),$$

where $\kappa(z) = \kappa(q, p)$ is a function of the position and momentum.

We may then define

$$\bar{K} = \max_{t \in [0, \tau]} \kappa(z(t))$$

bounding the local error by (with neglect of the fourth order terms) $\bar{K}h^3$. Thus the Verlet method is consistent of order two.

To complete the convergence proof for Verlet's method, we would still need to verify the second assumption. This requires the assumption that the force field \mathbf{F} satisfy a Lipschitz condition:

$$\|\mathbf{F}(\mathbf{u}) - \mathbf{F}(\mathbf{w})\| \leq \hat{L}\|\mathbf{u} - \mathbf{w}\| \quad (2.15)$$

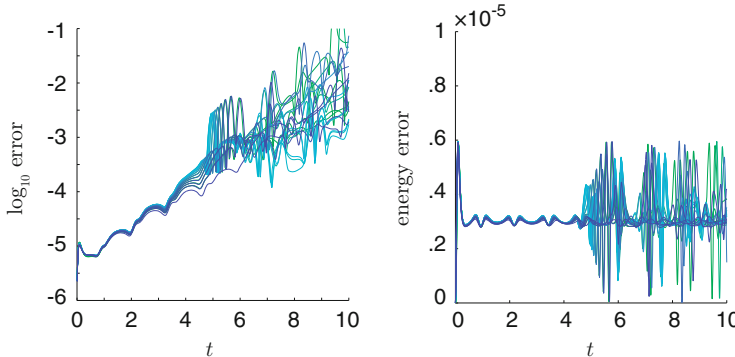


Fig. 2.4 The performance of the Verlet method is demonstrated by repeating the tests of error growth discussed for Euler’s method (compare Fig. 2.3). *Left panel:* In the case of the Verlet method, the error is much smaller in an absolute sense than that for the Euler method with the same step-size, but the growth still appears to be exponential. *Right:* the energy error growth as a function of time, very remarkably, compared to the equivalent figure for Euler’s method the energy error appears not to grow at all beyond some reasonably small limiting value, suggesting that the Verlet numerical approximation will remain near the desired energy surface

for all \mathbf{u}, \mathbf{w} . Generally speaking this could be taken to hold in a neighborhood of the solution where all approximate solutions for $h < \bar{h}$ are assumed to lie. With a bit of effort, it is then possible to demonstrate the stability condition for the numerical method (see Exercise 4).

In the left-hand panel of Fig. 2.4 we report the Verlet error growth as a function of time for the Lennard-Jones trimer. Verlet is substantially more accurate in this simulation, although the error still appears to grow exponentially.

Due to the chaotic nature of molecular dynamics, which implies a sensitivity to perturbations of the initial condition or the differential equations themselves, it is to be expected that the global error due to using a numerical method will always grow rapidly (exponentially) in time. As we shall see in later chapters, this does not necessarily mean that a long trajectory is entirely without value. In molecular dynamics it turns out that the real importance of the trajectory is that it provides a mechanism for calculating averages that maintain physical parameters. The simplest example of such a parameter is the energy.

What is more relevant for using Verlet to simulate molecular dynamics is the remarkable stability of energy shown in the right-hand panel of Fig. 2.4. Notice that the energy error does not appear to exhibit a steady accumulation in time (unlike for Euler’s method, where it exhibited a linear-in-time growth). The explanation for this unexpected behavior lies in the structural properties of the method, a topic we explore in this and the next chapter.

As another illustration of the performance of the Verlet method, we mention that the dynamical trajectories given in the previous chapter (in particular those given Examples 1.8 and 1.9) were computed using this method (with stepsize $h = 0.00001$). In the case of the calculation of the exponential separation of

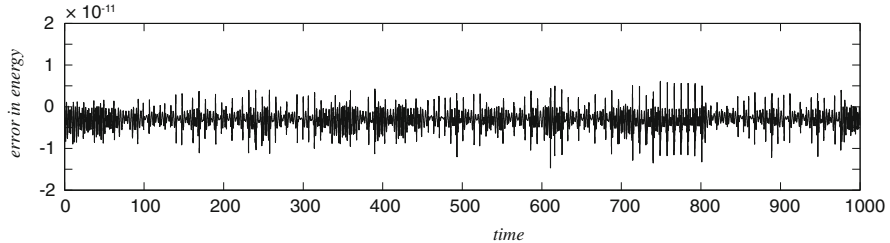


Fig. 2.5 The error in energy in a numerically computed trajectory (Verlet method) with stepsize $h = 0.00001$, for the anisotropic oscillator, showing that it remains bounded by 1.5×10^{-11} in very long runs

trajectories for the anisotropic oscillator shown in Fig. 1.25, the energy errors (see Fig. 2.5) remain bounded and small, suggesting that we may have some confidence in the numerical results presented. This example also provides additional evidence for the lack of “secular growth”⁶ of the energy error in Verlet simulations even in a relatively large number (10^8) of timesteps.

2.2.4 First Integrals and Their Preservation Under Discretization

Recall that the condition for a given function $I : \mathbb{R}^m \rightarrow \mathbb{R}$ to be a first integral is that

$$\nabla I(z) \cdot f(z) = \sum_{j=1}^m \frac{\partial I}{\partial z_j}(z) f_j(z) \equiv 0.$$

It is important in this definition that this is an equivalence that holds *everywhere* (or at least in some open set in \mathbb{R}^m), so the statement is not just that $I(z(t)) = I(z(0))$ for some particular trajectory, but, moreover, I is conserved for all nearby initial conditions. The flow map preserves the first integral, thus $I(\mathcal{F}_t(z)) \equiv I(z)$. For example, in a Hamiltonian system, the flow map conserves the energy:

$$H \circ \mathcal{F}_t = H.$$

⁶The term “secular growth” in this context is a reference to the long-term growth of perturbations in celestial mechanics. For example, the precession of the Earth’s polar axis occurs on a long period relative to its orbital motion and much longer period than its rotation, and so may be classed as a secular motion. In the context of molecular simulations, we use this to refer to accumulation of drift that takes the system steadily away from the energy surface.

There may, in specific instances, be additional first integrals present. For example, in a planar 2-body system in central forces, the angular momentum $xp_y - yp_x = l$ is a conserved quantity, thus $l \circ \mathcal{F}_t = l$.

Now if $I : \mathbb{R}^m \rightarrow \mathbb{R}$ has continuous partial derivatives, we may conclude directly that

$$I(\mathbf{a}) = I(\mathbf{b}) + \nabla I(\mathbf{z}_*) \cdot (\mathbf{a} - \mathbf{b}),$$

where \mathbf{z}_* is a point on the line in \mathbb{R}^m connecting \mathbf{a} to \mathbf{b} . Hence

$$|I(\mathbf{a}) - I(\mathbf{b})| \leq \|\nabla I(\mathbf{z}_*)\| \|\mathbf{a} - \mathbf{b}\|.$$

This means if we know that $\|\nabla I(\mathbf{z})\|$ remains bounded, say less than B , in an open domain containing the solution, we could conclude that the error in I -values computed along a numerical trajectory is of order h^p ,

$$|I(\mathbf{z}(t_n)) - I(\mathbf{z}_n)| \leq \frac{\bar{K}B}{2L} e^{nLh} h^p, \quad h < \bar{h}, \quad (2.16)$$

with the same assumptions as are needed to characterize the convergence of the method. This also means that we can see a ready means of improving the error in a first integral: simply reduce the timestep. If we have identified a time interval of interest, $[0, \tau]$, then we will automatically have $nh < \tau$ and we need only to choose a stepsize h which brings the error within a target tolerance.

In many cases we will be satisfied with this level of control of the error in the first integrals, but there are a number of limitations of this approach. First, we may find that the constants involved, \bar{K} and, more often, L , are simply so large that it is impossible to conclude anything useful from the bound given above. The stepsize would need to be so preposterously small to make the bound of practical interest that it is better to ignore the bound entirely.

Another limitation may arise when the time interval (the maximum of $\tau = vh$) is very long, as when we use trajectories to sample an energy landscape (the most common use of molecular dynamics). As this enters in the exponent in (2.16) it means that errors may continue to accumulate as we collect more samples and we would eventually leave the acceptable level of deviation in the first integral.

2.3 Geometric Integrators for Hamiltonian Systems

The discussion of the previous section suggests the need for methods with reliable conservation properties. We shall develop methods which, although their errors grow exponentially in time, nonetheless provide excellent energy conservation for very long times. These methods obtain their energy preservation properties indirectly: we design the methods to exactly conserve a certain geometric property

(*symplecticness*) of the phase flow. We will later show (in Chap. 3) that such symplectic methods preserve a perturbed energy-like invariant (to very high accuracy); the preservation of this modified energy then ensures that the original energy is nearly conserved.

The methods considered in this chapter are for the most part very simple in terms of their composition and are based on principles of classical mechanics. The reader may be aware of methods for using variable stepsize, extrapolation, etc. For reasons discussed in the next chapter, these methods and the concerns that motivated their development, which are undoubtedly essential in many applications of ordinary differential equations, are less relevant in the setting of molecular dynamics. The basic issue is that the dynamics of a Hamiltonian system are highly restricted by conservation laws or volume preservation; violation of these principles by naive schemes (which normally do not take advantage of underlying structure) leads to a gradual corruption of the solution. In particular, the errors may accumulate in such a way that the error in energy is severe. It should be stressed that these issues of instability due to violation of structural features of Hamiltonian systems are not always important in small models or for short time computations (where we can just use very small timesteps); historically, they only became apparent as larger, longer simulations began to be performed, as the appetite for numerical data grew.

The framework of geometric integration builds on an understanding of the properties of Hamiltonian mechanics which are well explained in the book of Arnold [15] or in the monograph of Landau and Lifshitz [212].

2.3.1 Volume Preserving Flows: Liouville's Theorem

Consider a set of points $\mathcal{S}(t)$ in phase space with evolution associated to a differential equation $\dot{\mathbf{z}} = \mathbf{f}(\mathbf{z})$ described by the flow map $\mathcal{F}_t(\mathcal{S}(0)) = \mathcal{S}(t)$. Liouville's theorem [16] states that the volume of such a set is invariant with respect to t if the divergence of \mathbf{f} vanishes, i.e.

$$\nabla \cdot \mathbf{f} = \sum_{i=1}^m \frac{\partial f_i}{\partial z_i} = 0.$$

It is a simple exercise to show that for a Hamiltonian system the divergence vanishes, since

$$\nabla \cdot \mathbf{f} = \sum_{i=1}^{N_c} \frac{\partial^2 H}{\partial q_i \partial p_i} - \sum_{i=1}^{N_c} \frac{\partial^2 H}{\partial p_i \partial q_i} = 0,$$

by equality of mixed partials. Thus Hamiltonian systems always have volume preserving flows.

If we view the map \mathcal{F}_t as a change of variables, we have

$$\text{Vol}(\mathcal{S}(t)) = \int_{\mathcal{S}} |D| d\omega,$$

where $D = \det\left(\frac{\partial \mathcal{F}_t}{\partial z}\right)$.

To understand where Liouville's theorem comes from, recall that the variational equations of the last chapter are a system of ordinary differential equations for $\mathbf{W}(t) = \mathcal{F}'_t(z(t))$:

$$\frac{d\mathbf{W}}{dt} = f'(z(t))\mathbf{W}.$$

Thus

$$\dot{\mathbf{W}}\mathbf{W}^{-1} = f'(z(t)).$$

Now let $D = \det(\mathbf{W})$. One can show (see Exercise 5) that

$$\frac{\dot{D}}{D} = \text{tr}(\dot{\mathbf{W}}\mathbf{W}^{-1}).$$

This implies that

$$\dot{D} = \text{div}(f(z(t)))D,$$

and thus

$$D(t) = D(0)e^{\int_0^t \text{div}(f(z(s))) ds}.$$

In particular, if $\text{div } f \equiv 0$, we see that $D \equiv D(0) = 1$ and it follows that the volume is constant.

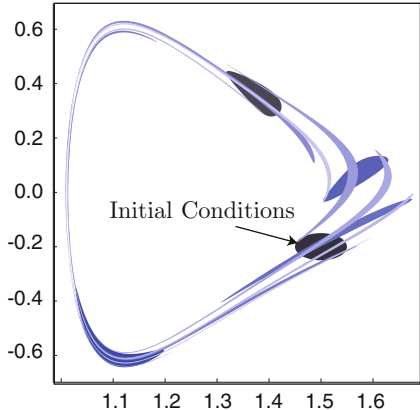
Liouville's theorem may be summarized compactly as:

$$\nabla \cdot f = 0 \Rightarrow \det \mathcal{F}'_t = 1.$$

Example 2.3 A 1-d oscillator with Lennard-Jones potential is described by the equations

$$\begin{aligned}\dot{q} &= p, \\ \dot{p} &= -\varphi'_{\text{LJ}}(q).\end{aligned}$$

Fig. 2.6 Filamentation of an evolving disk under the flow map of the Lennard-Jones oscillator. Lighter regions represent later images. Despite the increasing complexity of the shapes, each snapshot has the same area



As a consequence of energy conservation, any bounded individual trajectory of this system will be a periodic orbit. Consider the propagation of a small disk of initial conditions,

$$\mathcal{R} = \{(q_0, p_0) | \| (q_0, p_0) - (1.5, -0.2) \| \leq 0.5\}.$$

In Fig. 2.6, we have plotted the sets $\mathcal{F}_t(\mathcal{R})$, for $t = 0, 1, 2, \dots, 10$, using lighter tones to represent later snapshots. The sets become extremely elongated along the orbital direction.

At all times the energies stay bounded within the interval

$$-0.0960 \leq H(q, p) \leq -0.0669,$$

which is defined by the range of energies in the initial conditions.

Even as the sets become more and more elongated, they always maintain the same total area. This is the direct consequence of Liouville's theorem.

2.3.2 Volume Preserving Numerical Methods

The next question is what happens to the volume of a set of points in phase space, which would be conserved by the dynamical system, when we use a numerical method to approximate its evolution.

Consider a linear differential equation system in \mathbb{R}^m ,

$$\dot{\mathbf{z}} = S\mathbf{z},$$

for some matrix $S \in \mathbb{R}^{m \times m}$. The condition for the flow of this system to conserve volume is just that the trace of S (which is the divergence of the vector field

$f(z) = Sz$ be zero. Applying Euler's method to the same system results in

$$z_{n+1} = z_n + hSz_n = (\mathbf{I} + hS)z_n,$$

and the condition for Euler's method to conserve volume is that $\det(\mathbf{I} + hS) = 1$. The conditions for volume preservation by the flow map and its Euler approximation are essentially unrelated. Thus Euler's method does not in general conserve phase space volume (it conserves volume only in very special cases—see Exercise 6).

Yet it turns out that there are some numerical methods that always conserve the volume when this is conserved by the flow of the differential equations, or for some particular classes of differential equations. For example, consider the planar system

$$\dot{u} = f(u, v),$$

$$\dot{v} = g(u, v),$$

satisfying the condition $\frac{\partial f}{\partial u} + \frac{\partial g}{\partial v} = 0$, and the asymmetrical variant of Euler's method defined by

$$u_{n+1} = u_n + hf(u_{n+1}, v_n),$$

$$v_{n+1} = v_n + hg(u_{n+1}, v_n).$$

The components of the Jacobian matrix can be obtained using implicit differentiation, they are:

$$a_{11} = \frac{\partial u_{n+1}}{\partial u_n}, \quad a_{12} = \frac{\partial u_{n+1}}{\partial v_n}, \quad a_{21} = \frac{\partial v_{n+1}}{\partial u_n}, \quad a_{22} = \frac{\partial v_{n+1}}{\partial v_n}.$$

So

$$a_{11} = 1 + hf_u a_{11}, \quad a_{12} = hf_u a_{12} + hf_v, \quad a_{21} = hg_u a_{21}, \quad a_{22} = 1 + hg_u a_{22} + hg_v.$$

Solving for the various entries we have

$$\mathcal{G}'_h = \begin{bmatrix} 1/(1 - hf_u) & hf_v/(1 - hf_u) \\ hg_u/(1 - hf_u) & 1 + hg_v + h^2 g_u f_v / (1 - hf_u) \end{bmatrix},$$

and calculating the determinant of the Jacobian results in

$$\det \mathcal{G}'_h = \frac{1 + hg_v}{1 - hf_u}.$$

In the event that the vector field is divergence free, we have $f_u + g_v = 0$ which implies that the numerator and denominator are identical, and it follows that

$\det \mathcal{G}'_h = 1$. Thus the asymmetric variant of the Euler method is area preserving, even though the standard Euler method is not.

It would be valuable to have a general method for deriving volume conserving methods. It turns out that volume conservation is, itself, most readily obtained as a consequence of a more fundamental property of Hamiltonian flows, the conservation of the symplectic form.

2.3.3 The Symplectic Property

Let $m = 2N_c$. A symplectic map $\Phi : \mathbb{R}^m \rightarrow \mathbb{R}^m$ is one that preserves the symplectic differential 2-form. The simplest way to write this is as the following algebraic condition on the Jacobian matrix of Φ :

$$\Phi'^T J \Phi' = J.$$

Recall that the Jacobian matrix is the $m \times m$ matrix of partial derivatives of the components of Φ , $(\Phi')_{ij} = \frac{\partial \Phi_i}{\partial z_j}$, while

$$J = \begin{bmatrix} \mathbf{0} & \mathbf{I} \\ -\mathbf{I} & \mathbf{0} \end{bmatrix}.$$

So the equation $\Phi'^T J \Phi' = J$ represents a large number ($4N_c^2$) of equations.

To explain the origin of this formula, we need a brief diversion into the world of differential forms. This language will also be useful in Chap. 4, where we consider constrained systems.

A *1-form* α defined on \mathbb{R}^m is a family of linear mappings from \mathbb{R}^m to \mathbb{R} , defined for each point of \mathbb{R}^m . Let $a : \mathbb{R}^m \rightarrow \mathbb{R}^m$, then we may define a one-form associated to this vector by $\alpha(x)(\xi) = a(x)^T \xi$.

The *differential* of a function $g : \mathbb{R}^m \rightarrow \mathbb{R}$, denoted dg , is a family of linear mappings (one for each point in phase space) from vectors $\xi \in \mathbb{R}^m$ into the reals defined by

$$dg(q, p)(\xi) = \nabla g(q, p)^T \xi.$$

So, denoting the i th position coordinate by q_i , we have $dq_i(\xi) = \xi_i$; the differential is thus an example of a 1-form.

On the other hand the so called *wedge product* of 1-forms α, β , is an example of a *2-form*, at any point in phase space it can be viewed as a quadratic form, i.e. a scalar valued function of two vectors which is linear in each argument. It is written $\alpha \wedge \beta$ and is defined, for vectors $\xi, \eta \in \mathbb{R}^m$ by

$$\alpha \wedge \beta(\xi, \eta) = \alpha(\xi)\beta(\eta) - \alpha(\eta)\beta(\xi).$$

The wedge product of the coordinate differentials $\mathrm{d}q_i, \mathrm{d}p_i$ may be written

$$\mathrm{d}q_i \wedge \mathrm{d}p_i(\xi, \eta) = \xi_i \eta_{i+N_c} - \xi_{i+N_c} \eta_i = \xi^T J^{(i)} \eta,$$

where $J^{(i)}$ is the matrix which has zeros everywhere except for $(J^{(i)})_{i,i+N_c} = 1$, $(J^{(i)})_{i+N_c,i} = -1$. Summing these terms results in the *symplectic 2-form*, denoted ψ_S :

$$\psi_S = \sum_{i=1}^{N_c} \mathrm{d}q_i \wedge \mathrm{d}p_i(\xi, \eta) = \xi^T \left(\sum_{i=1}^{N_c} J^{(i)} \right) \eta = \xi^T J \eta.$$

Thus the matrix

$$J = \begin{bmatrix} \mathbf{0} & I \\ -I & \mathbf{0} \end{bmatrix}$$

defines a representation for the 2-form ψ_S . It is easy to verify that

$$\psi_S = \sum_{i < j} \mathrm{d}z_i \wedge J_{ij} \mathrm{d}z_j.$$

In general, a differential 2-form ψ is represented in coordinates by

$$\psi_z = \sum_{i,j} a_{ij}(z) \mathrm{d}z_i \wedge \mathrm{d}z_j,$$

with matrix of coefficients $A(z) = (a_{ij}(z))$.

The *pull-back* of a differential 1-form ψ under a phase space mapping Φ is defined as the action of ψ after transformation by the Jacobian matrix of the mapping. It is written $\Phi^* \psi$, so

$$(\Phi^* \psi_z)(\xi) = \psi_{\Phi(z)}(\Phi'(z)\xi).$$

The pull-back of a differential 2-form $\psi_1 \wedge \psi_2$ is consequently defined as

$$\Phi^*(\psi_1 \wedge \psi_2) = (\Phi^*\psi_1) \wedge (\Phi^*\psi_2).$$

Given a differential 2-form ψ_z represented by the matrix $A(z) = (a_{ij}(z))$, the *pull-back* of ψ_z under Φ is defined by

$$\Phi^* \psi_z = \sum_{ij} b_{ij}(z) \mathrm{d}z_i \wedge \mathrm{d}z_j,$$

where the matrix $\mathbf{B}(z) = (b_{ij}(z))$ is related to $\mathbf{A}(z)$ by

$$\mathbf{B}(z) = \boldsymbol{\Phi}'^T(z)\mathbf{A}(\boldsymbol{\Phi}(z))\boldsymbol{\Phi}'(z).$$

We say that a 2-form ψ is *conserved under mapping $\boldsymbol{\Phi}$* if

$$\boldsymbol{\Phi}^*\psi = \psi.$$

In coordinates, the conservation of the 2-form represented by matrix \mathbf{A} under a mapping $\boldsymbol{\Phi}$ means that

$$\boldsymbol{\Phi}'^T\mathbf{A}\boldsymbol{\Phi}' = \mathbf{A}.$$

In the particular case of the symplectic 2-form ψ_S , we have $\mathbf{A} = \mathbf{J}$, and the following condition for conservation under the mapping $\boldsymbol{\Phi}$

$$\boldsymbol{\Phi}'^T\mathbf{J}\boldsymbol{\Phi}' = \mathbf{J}. \quad (2.17)$$

A map that conserves the symplectic 2-form, or, in coordinates, satisfies (2.17), is termed a *symplectic map*.

Taking the determinant of both sides of (2.17), we have

$$\det(\boldsymbol{\Phi}'^T\mathbf{J}\boldsymbol{\Phi}') = \det(\mathbf{J}) \Rightarrow \det(\boldsymbol{\Phi}'^T)\det(\mathbf{J})\det(\boldsymbol{\Phi}') = \det(\mathbf{J}),$$

hence

$$\det(\boldsymbol{\Phi}')^2 = 1,$$

so $|\det(\boldsymbol{\Phi}')| = 1$. This raises a curious issue since we could conceivably have $\det(\boldsymbol{\Phi}') = -1$.

In the case of a flow map $\boldsymbol{\Phi} = \mathcal{F}_t$, we know that for $t \rightarrow 0$, the map reduces to the identity map (the same has to happen for a consistent numerical method). This means that we would have to have

$$\lim_{t \rightarrow 0} \det(\mathcal{F}'_t) = 1.$$

If the system is Hamiltonian, the map is symplectic for all t , and the determinant will be a continuous function of t , so the cases of interest have $\det(\mathcal{F}'_t) = +1$. The flow map of a Hamiltonian system is volume preserving.

2.3.4 Hamiltonian Flow Maps are Symplectic

As we saw at the end of the last chapter, the variational equations describe the change in an infinitesimal perturbation of a solution of a dynamical system. For the Hamiltonian system $\dot{z} = J\nabla H(z)$, these take the form:

$$\dot{W} = JS(t)W,$$

where $S(t) = H_{zz}(z(t, \xi))$ is a symmetric matrix. Computing

$$W^T JW = W^T J^2 SW = -W^T SW,$$

whereas

$$\dot{W}^T JW = W^T S^T J^T JW = W^T SW,$$

hence

$$\frac{d}{dt} W^T JW = W^T J\dot{W} + \dot{W}^T JW = 0.$$

This means that $W^T JW$ is a constant matrix. Observe that $W(t) = \mathcal{F}_t'(z(t, \xi))$ and that $W(0) = \mathcal{F}_t'(z(t, \xi))|_{t=0} = I$, hence

$$W^T JW \equiv W(0)^T JW(0) = J.$$

This proves that the flow map of a Hamiltonian system is a symplectic map.

2.3.5 The Symplectic Maps Form a Group

Let Φ_1 and Φ_2 be any pair of symplectic maps. Then

$$(\Phi_1 \circ \Phi_2)' = \Phi'_1 \Phi'_2,$$

by the chain rule, hence

$$[(\Phi_1 \circ \Phi_2)']^T J (\Phi_1 \circ \Phi_2)' = [\Phi'_1 \Phi'_2]^T J \Phi'_1 \Phi'_2 = \Phi'^T_2 \Phi'^T_1 J \Phi'_1 \Phi'_2 = \Phi'^T_2 J \Phi'_2 = J.$$

Thus the composition of any pair of symplectic maps is a symplectic map. The determinant of a symplectic map is ± 1 , hence these maps are always invertible, and the inverse of a symplectic map is symplectic since $\Phi'^T J \Phi' = J$ implies $J = \Phi'^{-T} J \Phi'^{-1}$. Thus the symplectic maps form a group under composition.

2.3.6 Symplectic Integrators

A symplectic integrator is an approximation of the flow map that conserves the symplectic 2-form. Some first steps in the theory of symplectic integration, i.e. numerical methods explicitly designed to mimic the symplectic property of the flow map, were made by Vogalaere [98] (in 1956!) but this work went unnoticed. The first practical methods conserving the symplectic property were suggested by Ruth in 1983 [320] and followed by a number of works on a similar theme [71, 72, 129–131, 267, 353]. Later works, e.g. [132, 139, 214, 325, 398] were aimed at developing methods with higher order of accuracy or better understanding of the meaning of the symplectic property (we will discuss this aspect in the next chapter). Some symplectic integrators are found within existing families (like Runge-Kutta methods), but the most useful are typically obtained using a splitting and composition framework that allows us to build families of such methods.

In the sequel we will write $\mathbf{Z} = \mathcal{G}_h(z)$ to specify the starting point z and ending point \mathbf{Z} of a step.

Alternatively, if we wish to emphasize the decomposition into positions and momenta, we write

$$\begin{bmatrix} \mathbf{Q} \\ \mathbf{P} \end{bmatrix} = \mathcal{G}_h \left(\begin{bmatrix} \mathbf{q} \\ \mathbf{p} \end{bmatrix} \right).$$

Recall that, in terms of \mathbf{q} and \mathbf{p} , the differential equations take the form

$$\dot{\mathbf{q}} = \nabla_{\mathbf{p}} H, \quad \dot{\mathbf{p}} = -\nabla_{\mathbf{q}} H.$$

In molecular dynamics, the Hamiltonian is usually of the form

$$H = \mathbf{p}^T \mathbf{M}^{-1} \mathbf{p} / 2 + U(\mathbf{q}),$$

with \mathbf{M} a diagonal mass matrix, and we will concentrate on this case for the moment. In this case,

$$\dot{\mathbf{q}} = \mathbf{M}^{-1} \mathbf{p}, \quad \dot{\mathbf{p}} = -\nabla_{\mathbf{q}} U(\mathbf{q}) \equiv \mathbf{F}(\mathbf{q}).$$

The following scheme is a slight modification of the Euler method.

$$\mathbf{Q} = \mathbf{q} + h \mathbf{M}^{-1} \mathbf{P}, \tag{2.18}$$

$$\mathbf{P} = \mathbf{p} + h \mathbf{F}(\mathbf{q}). \tag{2.19}$$

The method is explicit: to advance the timestep, we use the second equation to compute \mathbf{P} and then insert this in the first to get \mathbf{q} . Let the vectors $\mathbf{q}, \mathbf{p}, \mathbf{Q}, \mathbf{P}$ have i th

components q_i, p_i, Q_i, P_i , respectively; we may think of Q_i and P_i as functions of \mathbf{q} and \mathbf{p} , then

$$dQ_i = dq_i + hm_i^{-1}dP_i, \quad (2.20)$$

$$dP_i = dp_i - h \sum_{j=1}^{N_c} \frac{\partial^2 U}{\partial q_j \partial q_i} dq_j. \quad (2.21)$$

Computing the 2-form,

$$dQ_i \wedge dP_i = dq_i \wedge dP_i + hm_i^{-1}dP_i \wedge dP_i,$$

but $du \wedge du \equiv 0$ for any u , hence

$$dQ_i \wedge dP_i = dq_i \wedge dP_i,$$

and (2.21) implies

$$dQ_i \wedge dP_i = dq_i \wedge dp_i - h \sum_{j=1}^{N_c} dq_i \wedge \frac{\partial^2 U}{\partial q_j \partial q_i} dq_j.$$

It is then a simple exercise to show that

$$\sum_{i=1}^{N_c} \sum_{j=1}^{N_c} dq_i \wedge \frac{\partial^2 U}{\partial q_j \partial q_i} dq_j = 0,$$

using the skew-symmetry of the wedge product and the fact that the Hessian matrix is symmetric. This implies that

$$\sum_{i=1}^{N_c} dQ_i \wedge dP_i = \sum_{i=1}^{N_c} dq_i \wedge dp_i,$$

which means that the method is symplectic.

2.3.7 The Adjoint Method

Given any numerical integrator \mathcal{G}_h , consider the map

$$\mathcal{G}_h^\dagger = \mathcal{G}_{-h}^{-1}.$$

This is popularly referred to as the *adjoint* of \mathcal{G}_h , although it seems something of an abuse of mathematical language to refer to it in this way. For the flow map \mathcal{F}_h , we know that the inverse map is precisely \mathcal{F}_{-h} , so $\mathcal{F}_h^\dagger = \mathcal{F}_h$, i.e. the flow map is in the normal sense “self-adjoint,” i.e. *symmetric*. However, such a property does not hold in the general case. In particular, consider Euler’s method

$$\mathbf{Z} = \mathbf{z} + hf(\mathbf{z}).$$

The adjoint method is defined by

$$\mathbf{Z} = \mathbf{z} + hf(\mathbf{Z}),$$

and where the first was explicit, the second is implicit (it is the so-called *backward Euler* method).

The method (2.18)–(2.19) is called the Symplectic Euler method. Its adjoint method has a similar structure:

$$\mathbf{Q} = \mathbf{q} + h\mathbf{M}^{-1}\mathbf{p}, \quad (2.22)$$

$$\mathbf{P} = \mathbf{p} + h\mathbf{F}(\mathbf{Q}). \quad (2.23)$$

Comparing with (2.18)–(2.19), we see that (2.22)–(2.23) is also explicit.

Given a method \mathcal{G}_h with adjoint method \mathcal{G}_h^\dagger , it is possible to obtain the adjoint of the adjoint method $\mathcal{G}_h^{\ddagger\dagger}$, but, as we might expect, the adjoint of the adjoint is the original method:

$$\mathcal{G}_h^{\ddagger\dagger} = [\mathcal{G}_{-h}^\dagger]^{-1} = [\mathcal{G}_h^{-1}]^{-1} = \mathcal{G}_h.$$

2.4 Building Symplectic Integrators

Symplectic integrators may be constructed in several ways. First, we may look within standard classes of methods such as the family of Runge-Kutta schemes to see if there are choices of coefficients which make the methods automatically conserve the symplectic 2-form. A second, more direct approach is based on *splitting*. The idea of splitting methods, often referred to in the literature as *Lie-Trotter methods*, is that we divide the Hamiltonian into parts, and determine the flow maps (or, in some cases, approximate flow maps) for the parts, then compose the maps to define numerical methods for the whole system.

2.4.1 Splitting Methods

Let $H(\mathbf{q}, \mathbf{p}) = H_1(\mathbf{q}, \mathbf{p}) + H_2(\mathbf{q}, \mathbf{p})$ have flow map \mathcal{F}_h , and indicate by $\mathcal{F}_h^1, \mathcal{F}_h^2$ the flow maps for the systems with Hamiltonians H_1, H_2 , respectively. The proposal is that the map

$$\mathcal{G}_h = \mathcal{F}_h^1 \circ \mathcal{F}_h^2$$

is an approximation of \mathcal{F}_h . For this to be a first order method, we need at least

$$\|\mathcal{G}_h(\mathbf{u}) - \mathcal{F}_h(\mathbf{u})\| \leq C(\mathbf{u})h^2.$$

Expand $\mathcal{F}_h(\mathbf{u})$ in a Taylor series:

$$\mathcal{F}_h(\mathbf{u}) = \mathbf{u} + h\mathbf{J}\nabla H + \mathcal{O}(h^2) = \mathbf{u} + h(\mathbf{J}\nabla H_1 + \mathbf{J}\nabla H_2) + \mathcal{O}(h^2). \quad (2.24)$$

On the other hand,

$$\mathcal{F}_h^1(\mathbf{u}) = \mathbf{u} + h\mathbf{J}\nabla H_1(\mathbf{u}) + \mathcal{O}(h^2), \quad \mathcal{F}_h^2(\mathbf{u}) = \mathbf{u} + h\mathbf{J}\nabla H_2(\mathbf{u}) + \mathcal{O}(h^2).$$

Composing the maps we have

$$\mathcal{F}_h^1 \circ \mathcal{F}_h^2(\mathbf{u}) = \mathbf{u} + h\mathbf{J}\nabla H_2(\mathbf{u}) + h\mathbf{J}\nabla H_1(\mathbf{u} + h\mathbf{J}\nabla H_2(\mathbf{u})) + \mathcal{O}(h^2).$$

Assuming H_1 is C^2 , we have

$$\mathcal{F}_h^1 \circ \mathcal{F}_h^2(\mathbf{u}) = \mathbf{u} + h(\mathbf{J}\nabla H_2(\mathbf{u}) + \mathbf{J}\nabla H_1(\mathbf{u})) + \mathcal{O}(h^2),$$

which agrees with the expansion (2.24) of the flow map through the terms of first order. Thus the splitting method does indeed provide a second order local approximation of the flow map.

Example 2.4 Let

$$H_1(\mathbf{q}, \mathbf{p}) = \mathbf{p}^T \mathbf{M}^{-1} \mathbf{p} / 2, \quad H_2(\mathbf{q}, \mathbf{p}) = U(\mathbf{q}),$$

then a splitting method for $H = H_1 + H_2$ may be obtained by determining the flow maps for each of the two parts. For H_1 we have the differential equations

$$\dot{\mathbf{q}} = \mathbf{M}^{-1} \mathbf{p}, \quad \dot{\mathbf{p}} = \mathbf{0}.$$

The second equation tells us that \mathbf{p} is constant, so it is fixed at its initial value, whereas the first equation says that \mathbf{q} evolves on a linear path, hence its flow map is

$$\begin{aligned} \mathbf{Q} &= \mathbf{q} + h\mathbf{M}^{-1} \mathbf{p}, \\ \mathbf{P} &= \mathbf{p}. \end{aligned}$$

Similarly, the flow map of the system with Hamiltonian $H_2 = U$ is

$$\begin{aligned} \mathbf{Q} &= \mathbf{q}, \\ \mathbf{P} &= \mathbf{p} - h\nabla U(\mathbf{q}). \end{aligned}$$

The composition of these maps simplifies to

$$\begin{aligned} \mathbf{Q} &= \mathbf{q} + h\mathbf{M}^{-1}\mathbf{P}, \\ \mathbf{P} &= \mathbf{p} - h\nabla U(\mathbf{q}), \end{aligned}$$

which is precisely the Symplectic Euler method. Similarly, composing the same two maps in the opposite order gives the adjoint Symplectic Euler method.

Example 2.5 (Verlet is Symplectic) For the Symplectic Euler method \mathcal{G}_h and its adjoint method \mathcal{G}_h^\dagger , consider the composition

$$\mathcal{K}_h := \mathcal{G}_{h/2}^\dagger \circ \mathcal{G}_{h/2}.$$

Let

$$\begin{bmatrix} \bar{\mathbf{q}} \\ \bar{\mathbf{p}} \end{bmatrix} = \mathcal{G}_{h/2} \begin{bmatrix} \mathbf{q} \\ \mathbf{p} \end{bmatrix},$$

i.e.,

$$\bar{\mathbf{q}} = \mathbf{q} + (h/2)\mathbf{M}^{-1}\bar{\mathbf{p}}, \quad \bar{\mathbf{p}} = \mathbf{p} - (h/2)\nabla U(\mathbf{q}).$$

and set

$$\begin{bmatrix} \mathbf{Q} \\ \mathbf{P} \end{bmatrix} = \mathcal{G}_{h/2}^\dagger \begin{bmatrix} \bar{\mathbf{q}} \\ \bar{\mathbf{p}} \end{bmatrix},$$

i.e.,

$$\mathbf{Q} = \bar{\mathbf{q}} + (h/2)\mathbf{M}^{-1}\bar{\mathbf{p}}, \quad \mathbf{P} = \bar{\mathbf{p}} - (h/2)\nabla U(\mathbf{Q}).$$

The composition simplifies to

$$\begin{aligned} \bar{\mathbf{p}} &= \mathbf{p} - \frac{h}{2}\nabla U(\mathbf{q}), \\ \mathbf{Q} &= \mathbf{q} + h\mathbf{M}^{-1}\bar{\mathbf{p}}, \\ \mathbf{P} &= \bar{\mathbf{p}} - \frac{h}{2}\nabla U(\mathbf{Q}). \end{aligned}$$

This is just the leapfrog/Verlet method in its Hamiltonian form. Since we have obtained the method as the composition of two symplectic maps, and the symplectic maps form a group, we know that this method will also be symplectic.

When we construct a composition of a method with its adjoint method, we see readily that it is symmetric, i.e. self-adjoint, since

$$\mathcal{K}_h^\dagger := [\mathcal{G}_{h/2}^\dagger \circ \mathcal{G}_{h/2}]^\dagger = \mathcal{G}_{h/2}^\dagger \circ \mathcal{G}_{h/2} = \mathcal{K}_h.$$

Self-adjoint, or *symmetric* schemes have unique features; in particular they have even order [164, 227].

As we shall see in the next chapter, it is possible to construct methods of arbitrary order by employing more sophisticated multi-stage compositions of mappings.

2.4.2 General Composition Methods

When using splittings, it is not necessary to solve each Hamiltonian of a splitting using the exact flow. Instead, we may replace the flow maps of any part by an approximation. More generally, if we have any two symplectic numerical methods, say \mathcal{G}_h^1 and \mathcal{G}_h^2 , then the composition

$$\mathcal{G}_h := \mathcal{G}_{h/2}^1 \circ \mathcal{G}_{h/2}^2$$

is another symplectic numerical method. The order of this method is typically the minimum of the orders of the two methods involved, but it can be higher, as the example of the Verlet method (constructed by composing symplectic Euler and its adjoint) shows.

2.4.3 Harmonic + Anharmonic Splitting

Some systems can be decomposed into a harmonic (quadratic) part $H_0(\mathbf{q}, \mathbf{p}) = \mathbf{p}^T \mathbf{M}^{-1} \mathbf{p}/2 + \mathbf{q}^T \mathbf{A} \mathbf{q}/2$ and an anharmonic part $H_1(\mathbf{q}, \mathbf{p}) = \hat{U}(\mathbf{q})$. Then a splitting method can be formulated based on exact solution of the linear system together with “kicks” representing impulses defined by the anharmonic part. For a simple system consisting of a harmonic oscillator $H_0(\mathbf{q}, \mathbf{p}) = \mathbf{p}^2/2 + \Omega^2 \mathbf{q}^2/2$, such a method can be written

$$\begin{bmatrix} Q \\ \hat{p} \end{bmatrix} = \begin{bmatrix} \cos h\Omega & \frac{1}{\Omega} \sin h\Omega \\ -\Omega \sin h\Omega & \cos h\Omega \end{bmatrix} \begin{bmatrix} q \\ p \end{bmatrix},$$

$$P = \hat{p} - h\hat{U}'(Q).$$

2.4.4 Explicit and Implicit Methods

All of the methods mentioned so far are said to be *explicit* discretizations, since producing the next approximation point on a trajectory does not require solving any implicit equations defined in terms of the previous one. The Verlet method is not implicit even though Q appears on the right in the second equation, since it is given in an explicit way in terms of \mathbf{q} and \mathbf{p} . Implicitness adds another layer in both analysis and numerical implementation, which, however, in certain applications, is readily justified.

Example 2.6 The *Backward Euler* method,

$$\mathbf{z}_{n+1} = \mathbf{z}_n + h\mathbf{f}(\mathbf{z}_{n+1}),$$

is an example of an implicit method. The calculation of a timestep involves solving a system of equations of the form

$$\mathbf{g}(\mathbf{w}) \equiv \mathbf{w} - \mathbf{z}_n - h\mathbf{f}(\mathbf{w}) = 0.$$

The map \mathcal{G}_t is defined implicitly by the equation

$$\mathcal{G}_h(\mathbf{z}) = \mathbf{z} + h\mathbf{f}(\mathcal{G}_h(\mathbf{z})).$$

An implicit method will typically result in a system of nonlinear equations of the form

$$\mathbf{g}(\mathbf{z}_{n+1}) = \boldsymbol{\tau}_n, \tag{2.25}$$

which will need to be solved at each timestep. The right hand side $\boldsymbol{\tau}_n$ is a vector that depends on the previous time-step \mathbf{z}_n , perhaps in a complicated way. We may assume the number of equations represented by (2.25) is equal to the dimension of the space where \mathbf{z} is defined, so we have a square nonlinear system. Typically \mathbf{g} will depend on the stepsize and coefficients of the method and will have the property that for h sufficiently small, the solution is uniquely defined and is continuously defined in terms of $\boldsymbol{\tau}_n$, that is the mapping \mathbf{g} has a bounded and smooth inverse.

Solving the system may then proceed, from an initial guess $\mathbf{z}_{n+1}^{(0)}$ by use of Newton's method:

$$\mathbf{z}_{n+1}^{(k+1)} = \mathbf{z}_{n+1}^{(k)} - [\mathbf{J}^{(k)}]^{-1} (\mathbf{g}(\mathbf{z}_n^{(k)}) - \boldsymbol{\tau}_n),$$

where $\mathbf{J}^{(k)}$ is the Jacobian matrix of the mapping \mathbf{g} evaluated at $\mathbf{z}_n^{(k)}$, or else an approximation of this Jacobian (assumed to be nonsingular due to the invertibility

of the mapping). The iteration may be recast in the form

$$\mathbf{b}_k = -(\mathbf{g}(z_n^{(k)}) - \boldsymbol{\tau}_n), \quad \mathbf{J}^{(k)} \Delta z_k = \mathbf{b}_k, \quad z_{n+1}^{(k+1)} = z_{n+1}^{(k)} + \Delta z_k.$$

The potentially demanding steps here are the calculation of the Jacobian matrix and the solution of the linear system.

One way to save computational work is to recycle the Jacobian from a previous timestep. Alternatively, it may be possible to approximate the Jacobian crudely in such a way that the iteration still converges. For example, if the Jacobian matrix is large and can be written in the form

$$\mathbf{J}(z) = \mathbf{D} + \mathbf{E}(z),$$

where \mathbf{E} is small in norm and \mathbf{D} is a constant sparse matrix, then, in many cases, the Jacobian matrix may be replaced by the constant matrix \mathbf{D} and the iteration will still converge. Newton's method (without approximation of the Jacobian matrix) has a remarkable *quadratic* convergence property, meaning that, when the initial guess is close to the solution, the errors e_k, e_{k+1} at the k th and $k + 1$ st iterations satisfy the relation

$$e_{k+1} \leq K e_k^2.$$

This rapid convergence is typically lost when the Jacobian matrix is approximated in some way, and one finds instead

$$e_{k+1} \leq \rho e_k,$$

where $0 < \rho < 1$, i.e., quadratic convergence is replaced by geometric convergence.

In some cases *semi-implicit* methods can be developed which may only require the solution of a low-dimensional nonlinear system at each step. In Chap. 4, we discuss constrained systems for which implicit methods are needed and, in the case of the SHAKE method, for which the nonlinear system that must be solved at each step is of dimension equal to the number of constraints imposed. This is an example of a semi-implicit method.

In other cases, the special structure of the underlying problem may lead to certain efficiencies in the implementation, as when a sparse matrix is obtained in the linear equations that must be solved at each timestep.

Other methods may be substituted for Newton's method for the purpose of solving the nonlinear equations [292] of an implicit method.

2.4.5 “Processed” Methods and Conjugacy

One of the intriguing ideas that can be exploited to improve numerical integrators is that of *conjugacy*. In general, we say that two maps \mathbf{A} and \mathbf{B} are conjugate if there is a homeomorphism⁷ χ such that

$$\mathbf{A} = \chi^{-1} \circ \mathbf{B} \circ \chi.$$

That is, we may evaluate one map by first transforming the input, then applying the other map, then transforming the output by the inverse of the first transformation. Conjugate maps have the property that their iterates are also conjugate, since

$$\begin{aligned}\mathbf{A}^n &= (\chi^{-1} \circ \mathbf{B} \circ \chi)^n \\ &= (\chi^{-1} \circ \mathbf{B} \circ \chi) \circ (\chi^{-1} \circ \mathbf{B} \circ \chi) \cdots (\chi^{-1} \circ \mathbf{B} \circ \chi) \\ &= \chi^{-1} \circ \mathbf{B}^n \circ \chi.\end{aligned}$$

If \mathbf{A} and \mathbf{B} are maps of phase space, then the conjugacy implies that they have equivalent stability properties under iteration, since if $\mathbf{B}^n(z_0) \rightarrow z^*$, as $n \rightarrow \infty$, for all initial points z_0 , then also $\mathbf{A}^n(z_0) \rightarrow \chi^{-1}(z^*)$.

A common use made of conjugacy in the setting of numerical integration is to increase the order of accuracy. Numerical integrators are dependent on the stepsize h . The idea is to introduce a conjugacy via a map χ_h which also depends on the stepsize and by judicious design of the map, to eliminate leading terms in the expansion of the local error of the method. As an illustration, the Symplectic Euler method turns out to be conjugate to the Verlet method (see Exercise 12). One sometimes refers to the “effective order” of a numerical method as the order attainable via processing, thus the effective order of the Symplectic Euler method would be two.

Let us suppose that we have such a conjugacy between two numerical methods \mathcal{G}_h and $\tilde{\mathcal{G}}_h$, that is

$$\mathcal{G}_h = \chi_h^{-1} \circ \tilde{\mathcal{G}}_h \circ \chi_h,$$

defined in such a way that \mathcal{G}_h has order r and $\tilde{\mathcal{G}}_h$ has order s where $s < r$. Then, given an initial condition z_0 , we first modify (“pre-process”) this to $\tilde{z}_0 = \chi_h(z_0)$, then take multiple steps with the method $\tilde{\mathcal{G}}_h$, and finally transform (“post-process”) the end result by χ_h^{-1} . The resulting approximation will be of order r even though all timestepping was performed using a lower order method. The situation is diagrammed in Fig. 2.7.

⁷A homeomorphism is a continuous bijection which has a continuous inverse.

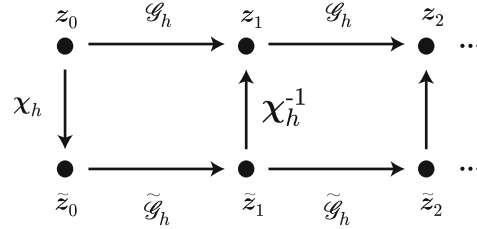


Fig. 2.7 In a “processed method” the inputs are first transformed before repeated application of a given method; after post-processing, the output may have higher order of accuracy than would be obtained using a straightforward application of the scheme

The use of conjugacy as a method to develop enhanced numerical methods was introduced in [397] under the name *symplectic correctors*.

2.5 Other Classes of Methods

2.5.1 Runge-Kutta Methods

The family of Runge-Kutta methods for solving $\dot{\mathbf{z}} = \mathbf{f}(\mathbf{z})$ is defined by

$$\mathbf{Z} = \mathbf{z} + h \sum_{i=1}^s b_i \mathbf{F}_i,$$

where the vectors \mathbf{F}_i , $i = 1, \dots, s$, are computed by solving the system

$$\mathbf{F}_i = \mathbf{f}\left(\mathbf{z} + h \sum_{j=1}^s a_{ij} \mathbf{F}_j\right), \quad i = 1, \dots, s.$$

The parameters s , b_1, b_2, \dots, b_s , and the $s \times s$ matrix of coefficients $\mathbf{A} = (a_{ij})$ describe the method. In some cases the determination of the vectors \mathbf{F}_i requires the solution of a nonlinear system, i.e. the method is *implicit*; in other cases the method can be explicit. An example of a popular 4th order explicit method is the choice of matrix \mathbf{A} with coefficients $a_{ij} \equiv 0$ except $a_{21} = 1/2$, $a_{32} = 1/2$ and $a_{43} = 1$, and $b_1 = 1/6$, $b_2 = 1/3$, $b_3 = 1/3$, $b_4 = 1/6$. This method is not symplectic, and it is in fact impossible to find symplectic explicit methods within the Runge-Kutta family.

Let us emphasize that, while a typical RK method is not symplectic, **some** implicit Runge-Kutta methods **are** symplectic. The precise condition that must be

satisfied [325] is

$$b_i a_{ij} + b_j a_{ji} = b_i b_j, \quad i = 1, \dots, s, \quad j = 1, \dots, s.$$

The implicitness reduces the usefulness of Runge-Kutta methods for applications like molecular dynamics, because the complexity and cost of the molecular force laws usually means that implicit methods are inefficient (this is certainly not *prima facie* obvious, but the issue has been examined by several researchers without much positive result; see, e.g. [308]).

Example 2.7 The Gauss-Legendre family of Runge-Kutta (GLRK) methods correspond to approximating the vector field at the Gauss points, i.e. the zeros of the orthogonal polynomials that arise in Gaussian quadrature. As these points are symmetrically distributed the GLRK schemes are symmetric, hence have even order. The simplest such method is the *implicit midpoint rule*:

$$\mathbf{Z} = \mathbf{z} + h\mathbf{F}_1, \quad \mathbf{F}_1 = f(\mathbf{z} + \frac{h}{2}\mathbf{F}_1),$$

which has order 2. The 4th order method ($s = 2$) has coefficients

$$b_1 = b_2 = \frac{1}{2}, \quad A = (a_{ij}) = \begin{bmatrix} \frac{1}{4} & \frac{1}{4} - \frac{\sqrt{3}}{6} \\ \frac{1}{4} + \frac{\sqrt{3}}{6} & \frac{1}{4} \end{bmatrix}.$$

2.5.2 Partitioned Runge-Kutta Methods

It can be seen that Runge-Kutta methods treat all components of the differential equation identically. On the other hand, in molecular dynamics the equations of motion often have a special structure: for example the differential equation system is typically linear in \mathbf{p} , and, moreover, the equations have a special coupling structure so that the differential equation for \mathbf{q} depends only on \mathbf{p} and that for \mathbf{p} depends only on \mathbf{q} . So-called partitioned Runge-Kutta methods allow us to exploit this structure. As an illustration, consider the method:

$$\hat{\mathbf{P}} = \mathbf{p} - \frac{h}{2} \nabla_{\mathbf{q}} H(\mathbf{q}, \hat{\mathbf{P}}), \tag{2.26}$$

$$\mathbf{Q} = \mathbf{q} + \frac{h}{2} (\nabla_{\mathbf{p}} H(\mathbf{q}, \hat{\mathbf{P}}) + \nabla_{\mathbf{p}} H(\mathbf{Q}, \hat{\mathbf{P}})), \tag{2.27}$$

$$\mathbf{P} = \hat{\mathbf{P}} - \frac{h}{2} \nabla_{\mathbf{q}} H(\mathbf{Q}, \hat{\mathbf{P}}). \tag{2.28}$$

When $H = \mathbf{p}^T \mathbf{M}^{-1} \mathbf{p}/2 + U(\mathbf{q})$ this is just the leapfrog/Verlet method, but it can be used also for more general systems. In the more general setting it is implicit (a nonlinear set of equations must be solved to advance from time level to time level). To see that it is symplectic, we first note that this is a symmetric composition of the form

$$\mathcal{K}_h = \mathcal{G}_{h/2}^\dagger \circ \mathcal{G}_{h/2},$$

where \mathcal{G}_h is defined by

$$\mathbf{P} = \mathbf{p} - h \nabla_{\mathbf{q}} H(\mathbf{q}, \mathbf{P}), \quad (2.29)$$

$$\mathbf{Q} = \mathbf{q} + h \nabla_{\mathbf{p}} H(\mathbf{q}, \mathbf{P}), \quad (2.30)$$

so it is enough to show that this basic method is symplectic. Taking differentials of (2.30) defining \mathcal{G}_h and then wedge products and summing, we have

$$\begin{aligned} \sum_i dQ_i \wedge dP_i &= \sum_i dq_i \wedge dP_i + h \sum_i \sum_j H_{p_i q_j} dq_j \wedge dP_i \\ &\quad + h \sum_i \sum_j H_{p_i p_j} dP_j \wedge dP_i. \end{aligned}$$

The last term on the right vanishes by equality of mixed partials and the antisymmetry of the wedge product. On the other hand, using (2.29), we obtain, by similar means,

$$\sum_i dq_i \wedge dP_i = \sum_i dq_i \wedge dp_i - h \sum_i \sum_j H_{q_i p_j} dq_i \wedge dP_j.$$

Relabelling the indices in this sum and using our previous work results in

$$\sum_i dQ_i \wedge dP_i = \sum_i dq_i \wedge dp_i,$$

implying that the method is symplectic.

The more general family of Partitioned Runge-Kutta methods is defined by making use of a partitioning of the system and introducing combinations of a set of internal stages. This more general family of schemes is discussed in some detail in [326] (see also discussions of [164, 227]).

2.5.3 Newmark Methods

As a special case of a partitioned Runge-Kutta method, consider the Newmark family of methods [280] defined for two parameters σ and η by the formulas

$$\begin{aligned}\mathbf{P} &= \mathbf{p} - h(1 - \sigma)\nabla U(\mathbf{q}) - h\sigma\nabla U(\mathbf{Q}), \\ \mathbf{Q} &= \mathbf{q} + h\mathbf{M}^{-1}\mathbf{p} - h^2 \left(\frac{1}{2} - \eta \right) \nabla U(\mathbf{q}) - h^2\eta\nabla U(\mathbf{Q}).\end{aligned}$$

This is an exact transcription of the formulas in Newmark's original paper, only substituting $\mathbf{M}^{-1}\mathbf{p}$ for the velocity \mathbf{v} wherever it appears. In practice the choice $\sigma = 1/2$ is used to avoid spurious damping (it can be demonstrated for a simple model problem); this certainly would appear to be desirable in the setting of molecular dynamics. For $\eta = 0$ we then arrive at the Verlet method. For other values of η the scheme is clearly implicit, which likely is the reason it is rarely used in molecular simulation, although it is popular in structural mechanics. The implicit Newmark methods are not symplectic, but a related family of symplectic methods can be constructed by replacing interpolated forces by forces evaluated at interpolated positions [395].

2.5.4 Multiderivative Methods

All of the methods discussed above rely on computing values of the vector field (i.e. momenta and forces) only. However, as we saw earlier in this chapter, in the setting of a Taylor series method, we may approximate a single step by

$$\mathbf{z}_{n+1} = \mathbf{z}_n + h\dot{\mathbf{z}}_n + \frac{h^2}{2}\ddot{\mathbf{z}}_n + \dots + \frac{h^k}{k!}\mathbf{z}_n^{(k)},$$

where it is possible to make use of higher order derivatives of the solution in formulating the method. Then using the differential equation, the time derivatives may be replaced by elementary differentials of the vector field. This same idea can be used in a more sophisticated way to improve the accuracy of molecular dynamics methods. Letting $H(\mathbf{q}, \mathbf{p}) = \mathbf{p}^T \mathbf{M}^{-1} \mathbf{p} / 2 + U(\mathbf{q})$, the Takahashi-Imada method [355] (also known as Rowlands' method [316]) has the same form as the Verlet method

$$\begin{aligned}\hat{\mathbf{P}} &= \mathbf{p} - (h/2)\nabla \tilde{U}(\mathbf{q}), \\ \mathbf{Q} &= \mathbf{q} + h\mathbf{M}^{-1}\hat{\mathbf{P}}, \\ \mathbf{P} &= \hat{\mathbf{P}} - (h/2)\nabla \tilde{U}(\mathbf{Q}),\end{aligned}$$

where the corresponding potential energy function is

$$\tilde{U}(\mathbf{q}) = U(\mathbf{q}) - \frac{h^2}{24} \nabla U(\mathbf{q})^T \mathbf{M}^{-1} \nabla U(\mathbf{q}).$$

The forces arising from such a modified potential can be worked out:

$$\tilde{\mathbf{F}} = -\nabla \tilde{U} = -\left[\mathbf{I} + \frac{h^2}{12} \mathbf{U}'' \mathbf{M}^{-1} \right] \nabla U,$$

where \mathbf{U}'' is the Hessian matrix of the potential. It may in some cases be a daunting task to compute the Hessian matrix as would be required in the Takahashi-Imada method, but this is not always the case. Advantage can be made of the fact that for systems with short-ranged potentials, the Hessian matrix is likely to be very sparse, in which case this computation can be effected with little additional overhead, although this will depend on the underlying computer architecture, the size of the system, etc.

This method can be shown to have effective order four, meaning that there is a change of variables χ_h which can be used to transform the Takahashi-Imada method into one of order four using the processing technique of Sect. 2.4.5. The potential energy modification has been specifically chosen to annihilate terms in the local error expansion (after coordinate transformation).

A discussion and comparison of several multiderivative methods for molecular applications may be found in [239].

2.5.5 *Other Methods*

We have mentioned previously that it is possible to reduce the Verlet method to a scheme involving positions only:

$$\mathbf{q}_{n+1} - 2\mathbf{q}_n + \mathbf{q}_{n-1} = h^2 \mathbf{M}^{-1} \mathbf{F}(\mathbf{q}_n).$$

This is a type of a *multipstep* method. Such methods may be studied using a generalization of the techniques used to understand one-step methods [167]. There are a variety of multipstep methods which could in principle be used for molecular dynamics, however, we regard the benefits as unproven; in particular, such methods neglect the phase space structure such as the symplectic property.

Another scheme which is sometimes used in molecular dynamics is Beeman's Algorithm [30, 331].

Example 2.8 (Beeman’s Algorithm) The method treats the positions and momenta differently, updating these from the formulas

$$\mathbf{q}_{n+1} = \mathbf{q}_n + h\dot{\mathbf{q}}_n + \frac{h^2}{6}[4\ddot{\mathbf{q}}_n - \ddot{\mathbf{q}}_{n-1}]. \quad (2.31)$$

$$\mathbf{p}_{n+1} = \mathbf{p}_n + \frac{h}{6}\mathbf{M}[2\ddot{\mathbf{q}}_{n+1} + 5\ddot{\mathbf{q}}_n - \ddot{\mathbf{q}}_{n-1}]. \quad (2.32)$$

The shorthand $\dot{\mathbf{q}}_n \equiv \mathbf{M}^{-1}\mathbf{p}_n$, $\ddot{\mathbf{q}}_n \equiv \mathbf{M}^{-1}\mathbf{F}(\mathbf{q}_n)$ has been used.

This method requires that the positions (and forces) be known at two successive points h apart in time in order to initialize the iteration. These might be generated by using the Verlet method or some other self-starting scheme. Beeman’s algorithm is explicit since, given \mathbf{q}_n , \mathbf{q}_{n-1} and \mathbf{p}_n , one directly obtains \mathbf{q}_{n+1} and then, $\dot{\mathbf{q}}_{n+1}$, and thus \mathbf{p}_{n+1} , with only one new force evaluation. Because it is a “partitioned multistep method,” its analysis is more involved than for the one-step methods, and, in particular its qualitative features are difficult to relate to those of the flow map. The order of accuracy of the scheme above can be shown to be three.

Exercises

1. The Morse potential is often encountered in molecular modelling and takes the form

$$\varphi_{\text{Morse}}(r) = D \left(1 - e^{-a(r-r_e)}\right)^2.$$

Consider a one-particle oscillator in the Morse potential (Hamiltonian $H = p^2/2 + \varphi_{\text{Morse}}(q)$). Explain why the trajectory of a particle will be bound for all time if the initial energy $H(q_0, p_0) < D$. Implement the 4th order Runge-Kutta and Verlet methods and explore the problem for $a = 1$, $D = 1$, $r_e = 1$. You should observe that all trajectories of the Runge-Kutta method eventually diverge. Study the dissociation time (the time until the particle is ejected to some fixed large distance, say $r = 3$) as a function of the stepsize and the initial energy.

2. Demonstrate the bound (2.12). [Hint: use $e^{Lh} > 1 + hL$.]
 3. Let f satisfy the Lipschitz condition $|f(u) - f(v)| \leq L|u - v|$. Let \mathcal{G}_h represent the flow map approximation associated to Euler’s method. Show that

$$|\mathcal{G}_h(u) - \mathcal{G}_h(v)| \leq (1 + hL)|f(u) - f(v)|.$$

Next prove (2.10) holds by finding Δ , \bar{K} and p . This can be used to prove Theorem 2.1.

4. Let \mathcal{G}_t denote the Verlet approximation of the flow map defined by (2.13)–(2.14). Using the Lipschitz condition on F (2.15), show that, for h sufficiently small,

$$\|\mathcal{G}_h(\mathbf{u}) - \mathcal{G}_h(\mathbf{v})\| \leq (1 + hR)\|\mathbf{u} - \mathbf{v}\|,$$

and find R .

5. Let $\mathbf{W} = \mathcal{F}'_t$ and let $D = \det(\mathbf{W})$. We will aim to show that

$$\frac{\dot{D}}{D} = \text{tr}(\dot{\mathbf{W}}\mathbf{W}^{-1}), \quad (2.33)$$

which is the key step in the proof of Liouville's theorem. To prove this, recall that the determinant of a matrix can be defined in terms of a co-factor expansion (expansion by minors). If $\mathbf{A} = (a_{ij})$ is a given $m \times m$ matrix, then for any $i \in \{1, 2, \dots, m\}$ we have

$$\det \mathbf{A} = \sum_{j=1}^m a_{ij} \hat{A}_{ij},$$

where \hat{A}_{ij} is $(-1)^{i+j}$ times the determinant of the $(m-1) \times (m-1)$ dimensional matrix obtained from \mathbf{A} by crossing out the i th row and j th column of \mathbf{A} . Using the cofactor expansion we can easily carry out a proof of the desired relation as follows:

- a. Let $\mathbf{W} = (w_{ij})$. Show that

$$\frac{\partial \det(\mathbf{W})}{\partial w_{ij}} = \hat{W}_{ij},$$

where \hat{W}_{ij} is the ij -co-factor of \mathbf{W} .

- b. Show that

$$\dot{D} = \sum_{i=1}^m \sum_{j=1}^m \hat{W}_{ij} \dot{w}_{ij}.$$

- c. On the other hand, the inverse matrix of \mathbf{W} can also be defined in terms of cofactors (the adjugate). If $\mathbf{W}^{-1} = (\eta_{ij})$, then

$$\eta_{ij} = \frac{\hat{W}_{ji}}{\det(\mathbf{W})}.$$

Demonstrate that this implies (2.33).

6. Euler's method is not symplectic for a general Hamiltonian system. Similarly for a general divergence free vector field, Euler's method is not volume preserving. Find conditions on the vector field that imply that Euler's method is volume preserving. Are there special Hamiltonian systems for which Euler's method is a symplectic method?
7. Let U be a C^2 potential energy function in N_c variables. Show that

$$\sum_{i=1}^{N_c} \sum_{j=1}^{N_c} dq_i \wedge \frac{\partial^2 U}{\partial q_j \partial q_i} dq_j = 0,$$

using the skew-symmetry of the wedge product and the fact that the Hessian matrix is symmetric.

8. Is it true that any symplectic method will have a symplectic adjoint method? Either give a proof or find a counterexample.
9. Consider the linear map defined by

$$\Phi(z) = Rz, \quad R = \begin{bmatrix} a_{11} & a_{12} \\ a_{21} & a_{22} \end{bmatrix}.$$

Show that, for this to be symplectic, we must have:

$$\begin{bmatrix} a_{11}(a_{21} - a_{12}) & a_{11}a_{22} - a_{12}^2 \\ a_{21}^2 - a_{22}a_{11} & a_{21}a_{22} - a_{22}a_{12} \end{bmatrix} = J.$$

10. Show that the implicit midpoint method

$$z_{n+1} = z_n + hf\left(\frac{z_n + z_{n+1}}{2}\right)$$

is symplectic. Hint: let $\bar{z} = \frac{z_n + z_{n+1}}{2}$ and use the properties of the wedge product to show that

$$dz_{n+1} \wedge J dz_{n+1} = dz_n \wedge J dz_n.$$

11. Considering a simple model for a bound pair of atoms with positions q_1 and q_2 , moving in a position dependent potential field φ , with Hamiltonian

$$H(q, p) = \frac{\|p_1\|^2}{2m_1} + \frac{\|p_2\|^2}{2m_2} + \varphi(q_1) + \varphi(q_2) + \frac{\kappa_b}{2}(\|q_1 - q_2\| - l_b)^2,$$

where κ_b and l_b are the bond vibration coefficient and bond length, respectively. Explain how to treat this problem using a splitting method which involves an exact solution of the isolated problem in the absence of the potential field φ .

12. Show that the Symplectic Euler method is conjugate to the Verlet method.

Chapter 3

Analyzing Geometric Integrators

In the previous chapter, we discussed the growth of error in numerical methods for differential equations. We saw that if the time interval is fixed, the error obeys the power law relationship with stepsize that is predicted by the convergence theory. We also saw that this did not contradict the exponential growth in the error with time (when the stepsize is fixed). The latter issue casts doubt on the reliance on the convergence order as a means for assessing the suitability of an integrator for molecular dynamics.

At the same time, tantalizingly, the Verlet method appears to exhibit a remarkable energy conservation property that was not predicted by the standard convergence theorem, even as the error itself grows exponentially fast. This is particularly surprising as the Verlet method does not seem to be constructed in a fundamentally different way to the Euler method or other schemes such as explicit Runge-Kutta methods (which do not exhibit a similar conservation property). That is, they use force evaluations at a few points in the step to approximate the solution at the next step. What is it that Verlet has that many other methods lack? A strong hint has been given in the previous section, where we learned that the Verlet method is a symplectic method, but it is still not obvious why this should lead to a qualitatively different energy conservation behavior.

In this chapter, we show that a symplectic integrator can be viewed as being effectively equivalent to the flow map of a certain Hamiltonian system. The starting point is that symplectic integrators are symplectic maps that are “near to the identity” since they depend on a parameter (the stepsize h) which can be chosen as small as needed, and, if consistent, in the limit $h \rightarrow 0$, such a map must tend to the identity map. We can express the fundamental consequence as follows: *not only are Hamiltonian flow maps symplectic, but also near-identity symplectic maps are (in an approximate sense) Hamiltonian flow maps [31]*. The fact leads to the existence of a modified (perturbed) Hamiltonian from which the discrete trajectory may be derived (as snapshots of continuous trajectories). In some cases we may derive this perturbed Hamiltonian as an expansion in powers of the stepsize.

Besides the symplectic structure there are other possible choices which could underpin the design of numerical methods. For example, symplectic methods are volume preserving, but it is possible to construct volume preserving methods that are not symplectic. Similarly time-reversibility is a fundamental property of molecular dynamics models (due to the quadratic kinetic energy function) and could be used as a starting point for developing numerical schemes. We discuss these alternatives in this chapter. We also look at the performance of methods which are specifically designed to preserve the energy using a projection technique. The conclusion of this chapter is that symplectic methods are to be preferred in most cases; this observation is in agreement with current practice in molecular dynamics simulation. In molecular dynamics we typically have a restricted class of systems which are purely Hamiltonian, so geometric integration seems the natural starting point. A related concept to geometric integration is that of *variational integration* [395] which is in some ways more general (including some mechanical systems that are not in Hamiltonian form) but does not provide a useful backward error analysis (except in the same cases as geometric integration).

Geometric integration has been developed as a subject from around 1985 to the present. There remain many interesting open questions in this area. The discussion presented here is necessarily highly compressed and focussed to the issues directly relevant for molecular dynamics. For starting points to more comprehensive understanding of the topic, one may study the books [164, 227] or articles [121, 369].

3.1 The Modified Hamiltonian

We begin by asking the following question which takes us right to the heart of what is needed in molecular dynamics: how is the energy affected by numerical discretization?

Let us begin with an illustrative example. Consider the harmonic oscillator with frequency Ω which has Hamiltonian $H(q, p) = p^2/2 + \Omega^2 q^2/2$, and consider the adjoint symplectic Euler method

$$Q = q + hp, \quad P = p - h\Omega^2 Q,$$

If $H(q, p) = E$ then, for typical steps, we cannot expect $H(Q, P) = E$. (Just insert the formulas for Q and P into the Hamiltonian and check that the value is not the same as $H(q, p)$.)

However, if we modify the Hamiltonian from $H(q, p) = p^2/2 + \Omega^2 q^2/2$ to

$$\tilde{H}(q, p) = \frac{p^2 + h\Omega^2 pq + \Omega^2 q^2}{2}, \quad (3.1)$$

then we find that,

$$\begin{aligned}\tilde{H}(Q, P) &= \frac{P^2}{2} + \frac{h\Omega^2 PQ}{2} + \frac{\Omega^2 Q^2}{2} \\ &= \frac{1}{2}p^2 - \frac{h\Omega^2}{2}pQ + \frac{\Omega^2 Q^2}{2} \\ &= \tilde{H}(q, p)\end{aligned}$$

This means that \tilde{H} is a conserved quantity of the numerical method.

Recall that the graph of

$$\frac{x^2}{a^2} + \frac{y^2}{b^2} = 1$$

is an ellipse with major and minor axes aligned to the coordinate axes. If ε is a small value, then

$$\frac{x^2}{a^2} + \frac{y^2}{b^2} + \varepsilon xy = 1$$

will be a slightly rotated ellipse (with slightly different major and minor axes). Thus we can think of the energy surface of the numerical method as being a small perturbation of the ellipse which represents the ‘energy surface’ (energy curve, in this case) of the harmonic oscillator itself.

For some values of the stepsize, it is possible that the points generated by the numerical method will constitute a finite periodic sequence. For example let $\Omega = 1$ and use the large stepsize of $h = 1$. Then from the initial point $(q_0, p_0) = (1, 0)$ we have $q_1 = q_0 + p_0 = 1$, and $p_1 = p_0 - q_1 = -1$, so we visit $(1, -1)$, then $(0, -1)$, then $(-1, 0)$, $(-1, 1)$, $(0, 1)$ and finally return to $(1, 0)$ (diagrammed in the left panel of Fig. 3.1). For a different choice of the stepsize, the point sequence may

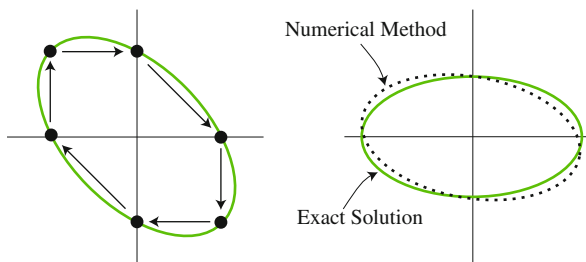


Fig. 3.1 Numerical solutions of the harmonic oscillator may cycle through a finite number of discrete points (*left*) or may gradually fill in an ellipse that is just a slight perturbation of the correct energy level set (*right*)

not be periodic and the numerical method then computes a discrete sequence of points which gradually fill in the ellipse (see the right panel of Fig. 3.1).

Obviously this conservation property (the existence of a perturbed energy surface) is a special feature of the method we have considered. If we used Euler's method to solve the harmonic oscillator we would find that energy grows without bound.

Now consider the more general Hamiltonian setting. Let \mathcal{G}_h be a r th order symplectic integrator, $r \geq 1$. Suppose that it is the flow map of a certain Hamiltonian system, with Hamiltonian \tilde{H}_h . If the method order is r , we may expect this Hamiltonian to be a $\mathcal{O}(h^r)$ approximation of H , thus we posit an expansion of the form

$$\tilde{H}_h = H + h^r H^{(r)} + h^{r+1} H^{(r+1)} + \dots$$

To determine the terms $H^{(r)}, H^{(r+1)}, \dots$, we write the differential equations on \tilde{H}_h :

$$\dot{z} = J \nabla H + h^r J \nabla H^{(r)} + h^{r+1} J \nabla H^{(r+1)} + \dots$$

The solution of this system can be expanded in powers of h and equated term-by-term with the expansion of \mathcal{G}_h in powers of h . In this way, successive terms may be computed. Although mechanical, this procedure is tedious. For splitting methods, a more elegant approach is available using the *Lie derivative*, which we next introduce.

3.2 Lie Derivatives and Poisson Brackets

Let $\phi(z)$ be an arbitrary smooth, scalar-valued function of the phase variables (assumed to lie in \mathbb{R}^m). At any point $z = \xi$ in phase space assume that there is a unique solution $z(t, \xi)$ such that $\dot{z}(t) = f(z(t))$, $z(0) = \xi$ that is globally defined for all t . Now differentiate $\hat{\phi}(t) = \phi(z(t))$ with respect to time, using the chain rule, to see how $\phi(z(t))$ is changing as t is varied:

$$\frac{d}{dt} \hat{\phi} \Big|_{t=0} = \left[\sum_{i=1}^m \frac{\partial \phi}{\partial z_i} \dot{z}_i \right] \Big|_{z=\xi} = \nabla \phi(\xi) \cdot f(\xi).$$

The right hand side suggests a shorthand notation. If we define the Lie derivative \mathcal{L}_f by

$$\mathcal{L}_f \phi = f \cdot \nabla \phi,$$

and note that the origin of time is irrelevant, then the equation for the evolution of ϕ could be written

$$\frac{d}{dt}\hat{\phi} = (\mathcal{L}_f\phi)(z). \quad (3.2)$$

Similarly,

$$\frac{d^2}{dt^2}\phi(z(t)) = (\mathcal{L}_f^2\phi)(z(t)).$$

The Taylor series expansion of $\phi(z(t))$ along a solution of the differential equation can therefore be written as

$$\begin{aligned} \phi(z(t)) &= \phi(z(0)) + t \left. \frac{d}{dt}\phi(z(t)) \right|_{t=0} + \frac{t^2}{2} \left. \frac{d^2}{dt^2}\phi(z(t)) \right|_{t=0} + \dots \\ &= \phi(z(0)) + t(\mathcal{L}_f\phi)(z(0)) + \frac{t^2}{2}(\mathcal{L}_f^2\phi)(z(0)) + \dots \\ &= (e^{t\mathcal{L}_f}\phi)(z(0)). \end{aligned}$$

This gives a concise formula for the evolution of any function of the phase variables, including, in particular, any solution component z_i . Thus the flow map of the system can be represented by $\exp(t\mathcal{L}_f)$. When one writes $\mathcal{F}_t = \exp(t\mathcal{L}_f)$, what is actually meant is that the individual components satisfy

$$z_i(t, \xi) = [\mathcal{F}_t(\xi)]_i = (\exp(t\mathcal{L}_f)z_i)|_{z=\xi}.$$

By analogy with the derivation of the matrix exponential, it is tempting to express the exponential as a series expansion in powers of t :

$$e^{t\mathcal{L}_f} = \text{Id} + t\mathcal{L}_f + \frac{t^2}{2}\mathcal{L}_f^2 + \dots$$

However, as \mathcal{L}_f is a first order operator, this series involves high order mixed partial derivatives, and the convergence of the expansion has to be considered in connection with its application to given initial data, that is, we should consider the expansion

$$e^{t\mathcal{L}_f}\phi = \phi + t\mathcal{L}_f\phi + \frac{t^2}{2}\mathcal{L}_f^2\phi + \dots$$

then the primary issue is the boundedness of the terms with respect to functions ϕ of a certain space of functions; we ignore the convergence issue here and treat the operator exponential as a formal series expansion. Methods derived using the formal expansion technique should be subject to further investigation (either numerical or analytical) to establish their validity.

Another common notation for performing computations involving Hamiltonian systems is the *Poisson bracket* which is defined for two smooth scalar-valued functions g_1 and g_2 of the phase variables (\mathbf{q}, \mathbf{p}) of a Hamiltonian system in \mathbb{R}^m by

$$\{g_1, g_2\} = \sum_{i=1}^{N_c} \left(\frac{\partial g_1}{\partial q_i} \frac{\partial g_2}{\partial p_i} - \frac{\partial g_2}{\partial q_i} \frac{\partial g_1}{\partial p_i} \right) = \nabla g_1^T \mathbf{J} \nabla g_2,$$

where \mathbf{J} is the skew symmetric symplectic structure matrix:

$$\mathbf{J} = \begin{bmatrix} 0 & \mathbf{I} \\ -\mathbf{I} & 0 \end{bmatrix},$$

and \mathbf{I} represents the $N_c \times N_c$ identity matrix. The Poisson bracket has the following properties, which are easily verified from the definition (for g_1, g_2, g_3 being three arbitrary functions of the phase variables):

Bilinearity $\{g_1, \alpha g_2 + \beta g_3\} = \alpha \{g_1, g_2\} + \beta \{g_1, g_3\}.$

Skew symmetry $\{g_1, g_2\} = -\{g_2, g_1\}$ and this implies $\{g_1, g_1\} = 0.$

Jacobi identity $\{g_1, \{g_2, g_3\}\} + \{g_3, \{g_1, g_2\}\} + \{g_2, \{g_3, g_1\}\} = 0.$

In terms of the Poisson bracket, it is possible to write the differential equation corresponding to a coordinate q_i , say, as

$$\dot{q}_i = \{q_i, H\}.$$

More generally, if $F(\mathbf{q}, \mathbf{p})$ is any smooth, scalar-valued function of the phase variables, we may write

$$\dot{F} = \frac{d}{dt} F(\mathbf{q}(t), \mathbf{p}(t)) = \{F, H\}.$$

As a consequence, we have the following relation between the Lie derivative and the Poisson bracket:

$$\mathcal{L}_{J\nabla H} F \equiv \{F, H\}.$$

For a Hamiltonian flow, we typically simplify notation by writing \mathcal{L}_H in place of $\mathcal{L}_{J\nabla H}$.

3.3 Backward Error Analysis for Hamiltonian Splitting Methods

As the relation

$$\mathcal{L}_H \phi = \{\phi, H\}$$

is linear in H , we may write, for Hamiltonians H_1, H_2 ,

$$\mathcal{L}_{H_1+H_2} = \mathcal{L}_{H_1} + \mathcal{L}_{H_2}.$$

The flow map of the system with Hamiltonian $H = H_1 + H_2$ is

$$\mathcal{F}_t = e^{t(\mathcal{L}_{H_1} + \mathcal{L}_{H_2})}.$$

On the other hand, the splitting method based on a composition of flows on H_1 and H_2 is

$$\mathcal{G}_h = e^{h\mathcal{L}_{H_1}} e^{h\mathcal{L}_{H_2}}.$$

The issue then becomes the comparison of the exponential series

$$e^{h(A+B)}$$

with

$$e^{hA} e^{hB},$$

for noncommuting operators A, B . Expanding these out using the exponential series we have

$$\begin{aligned} e^{h(A+B)} &= \text{Id} + h(A+B) + \frac{h^2}{2}(A+B)^2 + \frac{h^3}{6}(A+B)^3 + \mathcal{O}(h^4) \\ &= \text{Id} + h(A+B) + \frac{h^2}{2}(AB + BA + A^2 + B^2) \\ &\quad + \frac{h^3}{6}(A^3 + A^2B + AB^2 + ABA + B^2A + BA^2 + BAB + B^3) \\ &\quad + \mathcal{O}(h^4), \end{aligned}$$

whereas,

$$\begin{aligned}
e^{hA} e^{hB} &= (\text{Id} + hA + \frac{h^2 A^2}{2} + \frac{h^3 A^3}{6} + \mathcal{O}(h^4)) \\
&\quad \times (\text{Id} + hB + \frac{h^2 B^2}{2} + \frac{h^3 B^3}{6} + \mathcal{O}(h^4)) \\
&= \text{Id} + h(A + B) + \frac{h^2}{2}(2AB + A^2 + B^2) \\
&\quad + \frac{h^3}{6}(A^3 + B^3 + 3AB^2 + 3A^2B) + \mathcal{O}(h^4).
\end{aligned}$$

So the difference is

$$\begin{aligned}
e^{hA} e^{hB} - e^{h(A+B)} &= \frac{h^2}{2}(AB - BA) \\
&\quad + \frac{h^3}{6}(2AB^2 + 2A^2B - BA^2 - BAB - B^2A - ABA) + \mathcal{O}(h^4) \\
&= \frac{h^2}{2}[A, B] + \mathcal{O}(h^3),
\end{aligned}$$

where $[A, B] = AB - BA$ is the commutator of A and B .

For a splitting method, we have, replacing A by \mathcal{L}_{H_1} and B by \mathcal{L}_{H_2} ,

$$e^{h\mathcal{L}_{H_1}} e^{h\mathcal{L}_{H_2}} - e^{h\mathcal{L}_H} = \frac{h^2}{2}[\mathcal{L}_{H_1}, \mathcal{L}_{H_2}] + \mathcal{O}(h^3).$$

Observe that, for any real-valued functions f and H of phase space,

$$\mathcal{L}_H f = \nabla f^T J \nabla H = \{f, H\}.$$

Hence

$$\mathcal{L}_{H_1} \mathcal{L}_{H_2} f = \{\{f, H_2\}, H_1\},$$

and, using this and skew-symmetry of the Poisson bracket,

$$[\mathcal{L}_{H_1}, \mathcal{L}_{H_2}]f = \{\{f, H_2\}, H_1\} - \{\{f, H_1\}, H_2\} = \{\{f, H_2\}, H_1\} + \{\{H_1, f\}, H_2\}.$$

By the Jacobi identity,

$$\{\{f, H_2\}, H_1\} + \{\{H_2, H_1\}, f\} + \{\{H_1, f\}, H_2\} = 0.$$

Therefore

$$[\mathcal{L}_{H_1}, \mathcal{L}_{H_2}]f = -\{\{H_2, H_1\}, f\} = \{f, \{H_2, H_1\}\}.$$

This means that it is possible to relate the commutator of Lie derivatives of Hamiltonian vector fields to the Lie derivative of the Poisson bracket of the corresponding Hamiltonians, i.e.,

$$[\mathcal{L}_{H_1}, \mathcal{L}_{H_2}]f = \mathcal{L}_{\{H_1, H_2\}}f.$$

Because of this, we may interpret the first term in the expansion of the error as itself being derived from a Hamiltonian. This is a crucial observation which suggests an alternative perspective on the error expansion in splitting. The idea is to view the product of exponentials as an exponential:

$$e^{hA} e^{hB} = e^{h(A+B+hR)},$$

for some operator R . Expanding out the right hand side gives

$$\begin{aligned} e^{h(A+B+hR)} &= \text{Id} + h(A + B + hR) \\ &\quad + \frac{h^2}{2}(A + B + hR)^2 + \dots \\ &= \text{Id} + hA + hB + h^2R \\ &\quad + \frac{h^2}{2}(A^2 + AB + BA + B^2 \\ &\quad \quad + h^2R^2 + h(A + B)R + hR(A + B)) + \dots \end{aligned}$$

Comparing this to our expansion for $e^{hA} e^{hB}$, for agreement to $\mathcal{O}(h^2)$ we must have

$$\frac{1}{2}(2AB + A^2 + B^2) = R + \frac{1}{2}(A^2 + AB + BA + B^2) = \mathcal{O}(h),$$

or

$$R = AB - \frac{1}{2}(AB + BA) = \frac{1}{2}[A, B] + \mathcal{O}(h),$$

and from this it follows that

$$e^{h\mathcal{L}_{H_1}} e^{h\mathcal{L}_{H_2}} = e^{h\mathcal{L}_G},$$

where

$$G = H_1 + H_2 + \frac{h}{2}\{H_1, H_2\} + \mathcal{O}(h^2).$$

This is the start of the celebrated Baker-Campbell-Hausdorff series [21] (often referred to as the BCH Lemma for short) which gives an explicit formula for the product of exponentials of non-commuting operators.

Higher order terms can also be worked out, for example,

$$\begin{aligned} e^A e^B = \exp(A + B + \frac{1}{2}[A, B] + \frac{1}{12}([A, [A, B]] - [B, [A, B]]) \\ - \frac{1}{24}[B, [A, [A, B]]] + \dots) \end{aligned}$$

and, using the correspondence between Lie and Poisson brackets,

$$e^{h\mathcal{L}_{H_1}} e^{h\mathcal{L}_{H_2}} = e^{h\mathcal{L}_{\tilde{H}_h}},$$

where

$$\begin{aligned} \tilde{H}_h = H_1 + H_2 + \frac{h}{2}\{H_1, H_2\} + \frac{h^2}{12}(\{H_1, \{H_1, H_2\}\} - \{H_2, \{H_1, H_2\}\}) \\ - \frac{h^3}{24}\{H_2, \{H_1, \{H_1, H_2\}\}\} + \dots \end{aligned}$$

We refer to this series as the *modified* (also *perturbed*, *shadow*) Hamiltonian corresponding to the splitting method. The implication of the series is that the numerical method may be viewed as being equivalent to the exact solution of a nearby Hamiltonian system, although we have not addressed the convergence of the expansion.

If H_1 and H_2 Poisson-commute, i.e.

$$\{H_1, H_2\} = 0,$$

then there is no error in splitting. This is an extreme example, but there are a number of special cases of splittings such that some of the terms vanish from the expansion, for example where H_1 or H_2 is quadratic, or where there are restricted dependencies.

3.3.1 Symplectic Euler

Splitting our Hamiltonian using $H_1 = T(\mathbf{p}) = \mathbf{p}^T \mathbf{M}^{-1} \mathbf{p}/2$ and $H_2 = U(\mathbf{q})$ gives the symplectic Euler method. The BCH expansion gives the perturbed Hamiltonian

$$\begin{aligned} \tilde{H}_h = H - \frac{h}{2}\mathbf{p}^T \mathbf{M}^{-1} \nabla U(\mathbf{q}) + \frac{h^2}{12}(\mathbf{p}^T \mathbf{M}^{-1} U''(\mathbf{q}) \mathbf{M}^{-1} \mathbf{p} + \nabla U(\mathbf{q})^T \mathbf{M}^{-1} \nabla U(\mathbf{q})) \\ - \frac{h^3}{12}\nabla U(\mathbf{q})^T \mathbf{M}^{-1} U''(\mathbf{q}) \mathbf{M}^{-1} \mathbf{p} + \mathcal{O}(h^4). \end{aligned}$$

3.3.2 Verlet

Recall the position and velocity Verlet methods:

Position Verlet:	Velocity Verlet:
$\hat{\mathbf{Q}} := \mathbf{q} + (h/2) \mathbf{M}^{-1} \mathbf{p},$	$\hat{\mathbf{P}} := \mathbf{p} - (h/2) \nabla U(\mathbf{q}),$
$\mathbf{P} := \mathbf{p} - h \nabla U(\hat{\mathbf{Q}}),$	$\mathbf{Q} := \mathbf{q} + h \mathbf{M}^{-1} \hat{\mathbf{P}},$
$\mathbf{Q} := \hat{\mathbf{Q}} + (h/2) \mathbf{M}^{-1} \mathbf{P}.$	$\mathbf{P} := \hat{\mathbf{P}} - (h/2) \nabla U(\mathbf{Q}).$

(3.3)

We can think of the velocity Verlet method as being defined by a splitting into three parts:

$$\begin{aligned} H(\mathbf{q}, \mathbf{p}) &= H_1 + H_2 + H_3, \\ H_1 &= \frac{1}{2} U(\mathbf{q}), \\ H_2 &= \frac{1}{2} \mathbf{p}^T \mathbf{M}^{-1} \mathbf{p}, \\ H_3 &= \frac{1}{2} U(\mathbf{q}). \end{aligned}$$

This is a sequence of two types of operations: it consists of a “kick” exhibited by a jump in the momentum, linear “drift” with the resulting momentum, followed by a final kick. The symmetry of the method is one of its important features. Switching the order of the operations, i.e. drift-kick-drift, gives the position Verlet method.

In general for the Verlet method applied to Hamiltonians of the form $H(\mathbf{q}, \mathbf{p}) = T(\mathbf{p}) + U(\mathbf{q})$, the BCH lemma gives

$$\begin{aligned} \tilde{H}_h &= T + U + \frac{h^2}{12} \left(\{T, \{T, U\}\} - \frac{1}{2} \{U, \{U, T\}\} \right) \\ &\quad + \frac{h^4}{120} \left(-\frac{1}{6} \{T, \{T, \{T, \{T, U\}\}\}\} + \frac{1}{3} \{U, \{T, \{T, \{T, U\}\}\}\} \right. \\ &\quad \left. - \frac{1}{4} \{U, \{U, \{T, \{T, U\}\}\}\} + \{T, \{T, \{U, \{U, T\}\}\}\} \right) + \mathcal{O}(h^6) \end{aligned}$$

The extra power of h in the leading perturbation reflects the fact that this method is 2nd order accurate, rather than first order, as Symplectic Euler. Note that only even order terms (h^2, h^4, \dots) appear in the perturbative expansion; this is a consequence of the symmetry of the method.

We can exploit certain features of the BCH series to obtain more general second order symplectic methods. For Hamiltonians X and Y , consider symmetrizing a composition of exponentials (a Strang splitting), such that

$$\begin{aligned}\exp\left(\frac{t}{2}X\right)\exp(tY)\exp\left(\frac{t}{2}X\right) &= \exp(tZ_t) \\ &= \exp(t\tilde{Z}_{[1]} + t^2\tilde{Z}_{[2]} + t^3\tilde{Z}_{[3]} + t^4\tilde{Z}_{[4]} + \dots).\end{aligned}$$

Multiplying by the same expansion using a different time step s , we have

$$\begin{aligned}\exp\left(\frac{s}{2}X\right)\exp(sY)\exp\left(\frac{s}{2}X\right)\exp\left(\frac{t}{2}X\right)\exp(tY)\exp\left(\frac{t}{2}X\right) \\ &= \exp(sZ_s)\exp(tZ_t).\end{aligned}\tag{3.4}$$

But we know that Z_t commutes with Z_s , giving

$$\begin{aligned}\exp(sZ_s)\exp(tZ_t) &= \exp(sZ_s + tZ_t) \\ &= \exp((s+t)\tilde{Z}_{[1]} + (s^2 + t^2)\tilde{Z}_{[2]} + (s^3 + t^3)\tilde{Z}_{[3]} \\ &\quad + (s^4 + t^4)\tilde{Z}_{[4]} + \dots).\end{aligned}\tag{3.5}$$

Setting $s = -t$, the left hand side of (3.4) collapses to the identity. Hence the surviving even-powered terms in the expansion on the right hand side of (3.5) must be zero. If the even order terms vanish, then the effect of composing linear operators symmetrically is to keep only odd order terms in the exponent, giving the symmetric BCH formula

$$\exp\left(\frac{t}{2}X\right)\exp(tY)\exp\left(\frac{t}{2}X\right) = \exp(t(X + Y) + t^3\tilde{Z}_{[3]} + \dots),\tag{3.6}$$

where

$$\tilde{Z}_{[3]} = \frac{1}{12}[Y, [Y, X]] - \frac{1}{24}[X, [X, Y]].\tag{3.7}$$

More complicated symmetric second-order schemes can be devised by proceeding almost arbitrarily and maintaining a symmetric composition, but it is not found that alternative approaches improve on the two Verlet schemes, at least for molecular applications. The Verlet methods are seen as the gold-standard for molecular dynamics computations: both require only one evaluation of $\nabla U(\mathbf{q})$ per iteration (where the velocity Verlet scheme can reuse $\nabla U(\mathbf{Q})$ for the next iteration), and offer a second-order symplectic evolution.

3.3.3 Higher Order Symplectic Methods: The Suzuki-Yoshida Method

Yoshida [398] gives an elegant method for creating a symplectic scheme of arbitrarily high order, using Trotter's results for compositions of linear operators [370]. This work is related to methods suggested by Suzuki [354] in the context of Trotter factorization of quantum operators. Consider a scheme with order $2s$ (for $s \geq 1$) and where the evolution of the system under the method is given by $\exp(h \tilde{\mathcal{L}}_h)$, where

$$\hat{\mathcal{L}}_h \stackrel{\text{def}}{=} \mathcal{L}_{\tilde{H}_h} = \mathcal{L}_H + h^{2s} \tilde{\mathcal{L}}_{[2s]} + h^{2s+2} \tilde{\mathcal{L}}_{[2s+2]} + h^{2s+4} \tilde{\mathcal{L}}_{[2s+4]} + \mathcal{O}(h^{2s+6})$$

is the method's characteristic operator (with corresponding shadow Hamiltonian \tilde{H}_h). The linear operators $\tilde{\mathcal{L}}_{[2i]}$ are compositions of Lie derivatives, and can be computed using the symmetric BCH formula. We now consider iterating this scheme three times, first using a step of $\tau_0 h$, followed by a step of $\tau_1 h$, and finally another step with stepsize $\tau_0 h$ (where $\tau_0 h + \tau_1 h + \tau_0 h = h$). The overall effect on the system is given by a product of exponentials, as

$$\exp(\tau_0 h \hat{\mathcal{L}}_{\tau_0 h}) \exp(\tau_1 h \hat{\mathcal{L}}_{\tau_1 h}) \exp(\tau_0 h \hat{\mathcal{L}}_{\tau_0 h}) = \exp(h Z_h),$$

where, using repeated application of the BCH formula, we find

$$\begin{aligned} Z_h &= 2\tau_0 \hat{\mathcal{L}}_{\tau_0 h} + \tau_1 \hat{\mathcal{L}}_{\tau_1 h} + \mathcal{O}(h^{2s+2}), \\ &= (2\tau_0 + \tau_1) \mathcal{L}_H + (2\tau_0^{2s+1} + \tau_1^{2s+1}) h^{2s} \tilde{\mathcal{L}}_{[2s]} + \mathcal{O}(h^{2s+2}). \end{aligned}$$

We have free reign over constants τ_0 and τ_1 as long as $2\tau_0 + \tau_1 = 1$. Hence we have an opportunity to annihilate the perturbation operator at order h^{2s} by choosing $2\tau_0^{2s+1} + \tau_1^{2s+1} = 0$ as well. Solving simultaneously, there exists a unique real solution

$$\tau_0 = \frac{1}{2 - \kappa}, \quad \tau_1 = -\frac{\kappa}{2 - \kappa}, \quad \kappa^{2s+1} = 2,$$

giving us a scheme of order $2s + 2$. We can then proceed recursively, as this new order $2s + 2$ scheme can be composed similarly to wipe out successive higher order terms.

Though the fourth-order version of the scheme was given first by Forest and Ruth [139] (and discovered independently by Yoshida [398] and Candy and Rozmus [66]), we shall simply refer to these higher-order schemes as Yoshida methods, owing to the elegant derivation of schemes of arbitrary order.

Example 3.1 Consider using velocity Verlet as the base second-order method to build a Yoshida fourth-order method from. As the scheme is second-order, we have

$s = 1$, and hence

$$\tau_0 = \frac{1}{2 - \sqrt[3]{2}}, \quad \tau_1 = -\frac{\sqrt[3]{2}}{2 - \sqrt[3]{2}}.$$

The overall scheme is then three iterations of velocity Verlet, using stepsizes $\tau_0 h$, $\tau_1 h$ and $\tau_0 h$ respectively. We write this with subindices α , β to indicate the intermediate stages.

Yoshida fourth-order scheme (velocity Verlet):

$$\begin{aligned} \mathbf{P}_\alpha &:= \mathbf{p} - (\tau_0 h/2) \nabla U(\mathbf{q}), \\ \mathbf{Q}_\alpha &:= \mathbf{q} + (\tau_0 h) \mathbf{M}^{-1} \mathbf{P}_\alpha, \\ \mathbf{P}_\alpha &:= \mathbf{P}_\alpha - (\tau_0 h/2) \nabla U(\mathbf{Q}_\alpha), \\ \mathbf{P}_\beta &:= \mathbf{P}_\alpha - (\tau_1 h/2) \nabla U(\mathbf{Q}_\alpha), \\ \mathbf{Q}_\beta &:= \mathbf{Q}_\alpha + (\tau_1 h) \mathbf{M}^{-1} \mathbf{P}_\beta, \\ \mathbf{P}_\beta &:= \mathbf{P}_\beta - (\tau_1 h/2) \nabla U(\mathbf{Q}_\beta), \\ \mathbf{P} &:= \mathbf{P}_\beta - (\tau_0 h/2) \nabla U(\mathbf{Q}_\beta), \\ \mathbf{Q} &:= \mathbf{Q}_\beta + (\tau_0 h) \mathbf{M}^{-1} \mathbf{P}, \\ \mathbf{P} &:= \mathbf{P} - (\tau_0 h/2) \nabla U(\mathbf{Q}). \end{aligned} \tag{3.8}$$

The equations could easily be written in a simplified form, combining several of the steps. This scheme requires three new evaluations of the force ∇U per iteration, making it significantly more expensive than the vanilla second-order Verlet method. We may use this fourth-order scheme (now $s = 2$) to then find a scheme of order $2s + 2 = 6$.

We compare the symplectic methods developed so far in Fig. 3.2, for $t \in [0, 100]$ using planar phase space and the Lennard-Jones oscillator (the one degree-of-freedom problem with Hamiltonian $H(q, p) = p^2/2 + \varphi_{\text{LJ}}(q)$). As anticipated, there is no visible drift in the Hamiltonian as the simulation time increases. In each case, we observe an oscillation in the fluctuation of the total energy. Additionally we compute trajectories propagated at different stepsizes, and plot the maximum deviation

$$\max |H(q_k, p_k) - H(q_0, p_0)|$$

over the entire trajectory. We can see that for an order s method, the maximum deviation in the Hamiltonian is of order s , as is expected from the analysis. Yoshida fourth-order schemes are tested using both the position and velocity Verlet schemes

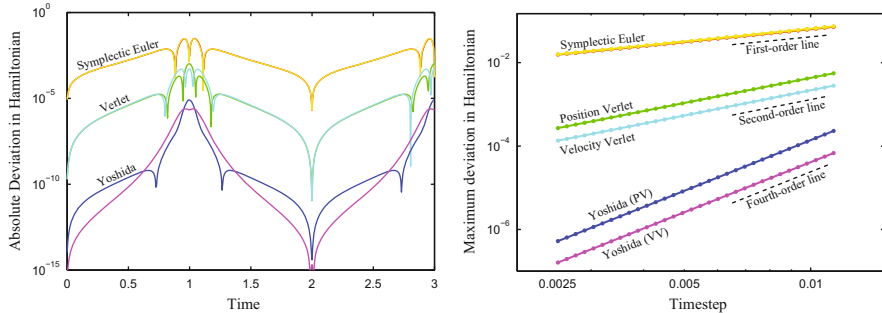


Fig. 3.2 We compare the symplectic Euler, Verlet and Yoshida schemes in application to a Lennard-Jones oscillator. The plot shows the absolute deviation in the computed Hamiltonian (*left*) as a function of time, for each scheme at a fixed timestep $h = 0.005$. Moreover we simulate the system using different stepsizes and compute for each stepsize the maximum deviation in the Hamiltonian (*right*), comparing the results with guide lines associated to various powers of the step size. The scheme used as the “base” method for the Yoshida composition methods is denoted in the parenthesis (either position or velocity Verlet)

as their base second-order methods (the base method is denoted in parenthesis in Fig. 3.2), giving similar results.

Of course we need not stop at a fourth-order scheme: we can use the constructed method to target any higher order terms we wish by composing the new scheme in a symmetric form and proceeding identically to the above.

These methods are not the best possible choices among schemes that alternate solving the terms of the splitting [260, 277], either in the sense of having the greatest stability or in the sense of having the smallest leading error coefficients. We can view the Suzuki-Yoshida methods as one type of general composition scheme [260, 277, 326]:

$$\begin{aligned} \mathcal{F}_h = & \exp(\alpha_1 h \mathcal{L}_T) \circ \exp(\beta_1 h \mathcal{L}_U) \circ \exp(\alpha_2 h \mathcal{L}_T) \circ \exp(\beta_2 h \mathcal{L}_U) \circ \cdots \circ \\ & \exp(\alpha_k h \mathcal{L}_T) \circ \exp(\beta_k h \mathcal{L}_U). \end{aligned}$$

The coefficients of these methods can be optimized according to many criteria, for example to reduce the coefficients associated to certain types of elementary differentials appearing in the leading error term [260], or to have maximal performance for particular families of applications, such as celestial mechanics [37, 127]. For many applications, for example celestial mechanics, such high order methods, and improved variants, are extremely useful, but in the setting of molecular dynamics, it is often found that second-order methods provide a ‘good enough’ option for numerical integration, the computational price-tag of higher order methods outweighing potential numerical gains. After all, the potential energy functions used in the ODEs are not perfect reflections of the laws of physics, and past a certain point using a high order method merely finds a better solution to an approximate model. Furthermore, most molecular simulations are performed at large timestep,

where the asymptotic error analysis (for $h \rightarrow 0$) may be less relevant. Nevertheless there are applications in molecular modelling where higher accuracy is needed in certain parts of a calculation in order to provide optimal sampling. An example will be found in the isokinetic stochastic integrator of Chap. 8.

For more discussion of higher order integrators, refer to [139, 164, 227, 259, 260, 262, 277, 290]. Of particular relevance for molecular dynamics is the excellent numerical study of [153].

3.3.4 The Takahashi-Imada Method

Recall the Takahashi-Imada method introduced in the last chapter,

$$\begin{aligned}\hat{\mathbf{P}} &:= \mathbf{p} - (h/2)\nabla\tilde{U}(\mathbf{q}), \\ \mathbf{Q} &:= \mathbf{q} + h\mathbf{M}^{-1}\hat{\mathbf{P}}, \\ \mathbf{P} &:= \hat{\mathbf{P}} - (h/2)\nabla\tilde{U}(\mathbf{Q}),\end{aligned}$$

with modified potential energy function

$$\tilde{U}(\mathbf{q}) = U(\mathbf{q}) - \frac{h^2}{24}\nabla U(\mathbf{q})^T\mathbf{M}^{-1}\nabla U(\mathbf{q}).$$

One might recognize the modification as being proportional to one part of the commutator expansion in the Verlet method, in fact

$$\nabla U(\mathbf{q})^T\mathbf{M}^{-1}\nabla U(\mathbf{q}) = \{U, \{U, T\}\}.$$

This is certainly not a coincidence. If we replace the potential U by \tilde{U} in the Verlet expansion, we have

$$\begin{aligned}\tilde{H}_h &= T + \tilde{U} + \frac{h^2}{12}\left(\{T, \{T, \tilde{U}\}\} - \frac{1}{2}\{\tilde{U}, \{\tilde{U}, T\}\}\right) + \mathcal{O}(h^4) \\ &= T + U - \frac{h^2}{24}\{U, \{U, T\}\} + \frac{h^2}{12}\left(\{T, \{T, \tilde{U}\}\} - \frac{1}{2}\{\tilde{U}, \{\tilde{U}, T\}\}\right) + \mathcal{O}(h^4) \\ &= H + \frac{h^2}{12}(\{T, \{T, \tilde{U}\}\} - \{\tilde{U}, \{\tilde{U}, T\}\}) + \mathcal{O}(h^4) \\ &= H + \frac{h^2}{12}(\mathbf{p}^T\mathbf{M}^{-1}U''\mathbf{M}^{-1}\mathbf{p} - \nabla U^T\mathbf{M}^{-1}\nabla U) + \mathcal{O}(h^4).\end{aligned}$$

Introducing coordinate transformations

$$\tilde{\mathbf{q}} = \mathbf{q} - \frac{h^2}{12} \mathbf{M}^{-1} \nabla U(\mathbf{q}), \quad \tilde{\mathbf{p}} = \mathbf{p} + \frac{h^2}{12} U''(\mathbf{q}) \mathbf{M}^{-1} \mathbf{p} \quad (3.9)$$

and inserting these into H yields, after expanding in a Taylor series:

$$\begin{aligned} H(\tilde{\mathbf{q}}, \tilde{\mathbf{p}}) &= T + \frac{h^2}{12} (\mathbf{p}^T \mathbf{M}^{-1} U'' \mathbf{M}^{-1} \mathbf{p} - \nabla U^T \mathbf{M}^{-1} \nabla U) + \mathcal{O}(h^4) \\ &= \tilde{H}_h(\mathbf{q}, \mathbf{p}) + \mathcal{O}(h^4). \end{aligned}$$

Since \tilde{H}_h is assumed to be constant along the numerical solution, the coordinate transformations have the result of giving an effective order of four for the energy. It turns out that the Takahashi-Imada method is, more generally, an effective 4th order scheme, i.e. for arbitrary quantities, not just the energy [166].

3.4 Perturbative Expansion: Exponentially Small Errors

Let us summarize the general situation with regard to backward error analysis.

Assume a smooth differential equation system

$$\frac{dz}{dt} = f(z)$$

with flow map \mathcal{F}_t , and a one-step method \mathcal{G}_h . We obtain, typically by matching of terms from Taylor expansion, a “modified differential equation” as a series expansion

$$\frac{dz}{dt} = \tilde{f}_h(z) = f(z) + h^r f_r(z) + h^{r+1} f_{r+1}(z) + \dots,$$

where r is the classical order of accuracy of the method. In fact, it is straightforward to show that if numerical method satisfies

$$\mathcal{G}_h(z) - \mathcal{F}_h(z) = h^{r+1} \Gamma_{r+1}(z) + \mathcal{O}(h^{r+2}),$$

i.e. $h^{r+1} \Gamma_{r+1}$ is the leading term in the local error expansion, then we have

$$f_r(z) = \Gamma_{r+1}(z).$$

Now in the case of a Hamiltonian system (with Hamiltonian H) solved using a symplectic numerical method, the above construction can generally be carried out to any desired order by matching of terms in Taylor expansions, assuming sufficient differentiability. In this case it will turn out that

$$\tilde{f}_h = J \nabla \tilde{H}_h,$$

where \mathbf{J} is the skew symmetric symplectic structure matrix and

$$\tilde{H}_h = H + h^r H_r + h^{r+1} H_{r+1} + \dots \quad (3.10)$$

We have worked out formulas above for the first terms in the expansion in the case of several splitting methods. We can thus view (at least locally) our numerical trajectory as the stroboscopic map (snapshots) of the evolution of a continuous Hamiltonian system.

Ideally, we would like to be able write that the solution to the modified equations is equivalent to mapping via the specified one-step method:

$$\mathcal{G}_h = e^{h\mathcal{L}_{\tilde{f}_h}}.$$

Unfortunately, this statement is elusive. The series expansion in question rarely converges. It is easy to show that for the harmonic oscillator, the series does indeed converge, but it turns out that this is an anomaly. The reason for the lack of convergence of the series is, precisely, its global nature (which is also its chief benefit). In order to proceed, one normally has to truncate the series at some finite number of terms. A natural question is where should we terminate the series? If we include only the $\mathcal{O}(h^r)$ term, then we have not really gained much. For example we would not be able to say that \tilde{H}_h is essentially a conserved quantity along the numerical solutions.

The analysis of the expansion was first treated systematically in [31, 359], where it was shown that a *finite* truncation to terms of order h^k can be achieved in such a way that the error is “exponentially small” in the stepsize. (See also [163, 310].) Define

$$\bar{H}_k \stackrel{\text{def}}{=} H + h^r H_r + h^{r+1} H_{r+1} + \dots + h^k H_k. \quad (3.11)$$

Let us state and prove the following basic result (see [162, 164, 227]):

Theorem 3.1 Suppose the Hamiltonian H and modified Hamiltonian \tilde{H}_k are smooth functions globally defined on a convex, compact subset \mathcal{B} of \mathbb{R}^{2N} and suppose that the exact solution and numerical approximations (for h sufficiently small) are confined to \mathcal{B} . Then, we have asymptotically for $h \rightarrow 0$ that

$$H(\mathbf{z}_n) = H(\mathbf{z}_0) + \mathcal{O}(h^r),$$

for $n = 0, 1, \dots, v$ where $\tau = vh = \mathcal{O}(h^{-k+r})$.

Proof First observe that due to smoothness and the assumptions on \mathcal{B} , we have a global Lipschitz constant

$$|H(\mathbf{u}) - H(\mathbf{v})| \leq L\|\mathbf{u} - \mathbf{v}\|$$

for all $\mathbf{u}, \mathbf{v} \in \mathcal{B}$.

Denote by $\mathcal{F}_h^{(k)}$ the flow map of the truncated Hamiltonian expansion \bar{H}_k ,

$$\mathcal{F}_h^{(k)} \stackrel{\text{def}}{=} \exp(h\mathcal{L}_{\bar{H}_k}).$$

By construction, we have

$$\mathbf{z}_{n+1} = \mathcal{F}_h^{(k)}(\mathbf{z}_n) + \boldsymbol{\eta}_n$$

where $\|\boldsymbol{\eta}_n\| \leq Ch^{k+1}$.

Since $\mathcal{F}_h^{(k)}$ preserves its Hamiltonian (3.11), we have

$$\bar{H}_k(\mathcal{F}_h^{(k)}(\mathbf{z}_n)) = \tilde{H}_k(\mathbf{z}_n).$$

Now

$$\begin{aligned} \bar{H}_k(\mathbf{z}_v) - \bar{H}_k(\mathbf{z}_0) &= \sum_{n=0}^{v-1} \bar{H}_k(\mathbf{z}_{n+1}) - \bar{H}_k(\mathbf{z}_n) \\ &= \sum_{n=0}^{v-1} \bar{H}_k(\mathbf{z}_{n+1}) - \tilde{H}_k(\mathcal{F}_h^{(k)}(\mathbf{z}_n)) \\ &= \sum_{n=0}^{v-1} \bar{H}_k(\mathcal{F}_h^{(k)}(\mathbf{z}_n) + \boldsymbol{\eta}_n) - \tilde{H}_k(\mathcal{F}_h^{(k)}(\mathbf{z}_n)). \end{aligned}$$

Hence

$$|\bar{H}_k(\mathbf{z}_v) - \bar{H}_k(\mathbf{z}_0)| \leq L \sum_{n=0}^{v-1} \|\boldsymbol{\eta}_n\| \leq Lv h^{k+1}.$$

We have $v = \tau/h$, thus

$$|\bar{H}_k(\mathbf{z}_v) - \bar{H}_k(\mathbf{z}_0)| \leq L\tau h^k.$$

Next observe that

$$H = \bar{H}_k - h^r H_{(r)} - h^{r+1} H_{(r+1)} - \dots - h^k H_{(k)} = \bar{H}_k + \mathcal{O}(h^r).$$

Therefore

$$|H(\mathbf{z}_v) - H(\mathbf{z}_0)| \leq Lv h^{k+1} + \mathcal{O}(h^r),$$

so that, as long as $v \leq C_2 h^{-k+r-1}$, we have

$$|H(z_v) - H(z_0)| \leq \mathcal{O}(h^r).$$

□

If the differential equations are infinitely differentiable, we may take the truncation index k as large as we like, but the constants appearing in the above theorem will depend on the truncation index in a complicated way. It is possible to prove (see discussions in [164, 227] for more detail), that for many standard classes of numerical methods, there are real, positive constants C, D such that

$$\|\mathcal{G}_h(\xi) - \mathcal{F}_h^{(k)}(\xi)\| \leq Ch [D(k+1)h]^{k+1},$$

giving a precise bound on the magnitude of the difference between the time h evolution under the truncated perturbed Hamiltonian and the numerical method.

If h is small, then for k sufficiently small the quantity in brackets is less than one and the difference from the truncated approximation decreases in magnitude with increasing k . As soon as k satisfies

$$k+1 > \frac{1}{Dh}$$

the power grows monotonically without bound. We can minimize the difference between \mathcal{G}_h and $\mathcal{F}_h^{(k)}$ by choosing

$$k = \frac{1}{hDe} - 1,$$

in which case,

$$\|\mathcal{G}_h(\xi) - \mathcal{F}_h^{(k)}(\xi)\| < \tilde{C}he^{-\frac{1}{\gamma h}}, \quad \gamma = \frac{1}{De}.$$

This bound tends to zero extremely rapidly (more rapidly than any power of h) as $h \rightarrow 0$. The assumption is that if this error in the approximation of the numerical map by the flow of a truncated perturbed Hamiltonian flow map is much smaller than the other errors present in our model, any drift due to lack of convergence would be minor, perhaps even invisible, on the timescale of simulation.

It is not recommended to take these estimates too literally, i.e. to try to compute the constants C and D (which might be quite difficult). Instead, we simply use the estimates to guide our intuition that the energy will be expected to fluctuate on very long time intervals with a magnitude bounded by $\mathcal{O}(h^r)$. To gain a full understanding of the issue of energy drift in the setting of molecular dynamics, the article [121] is highly relevant.

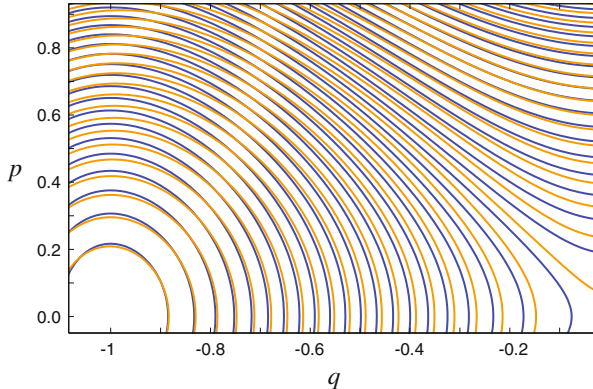


Fig. 3.3 The isoenergy contours are shown for the double well model (dark curves) together with the corresponding curves for the Verlet modified Hamiltonian (light curves)

The implication of backward error analysis is that the convergence order is still directly relevant in molecular simulations, even when the accuracy of trajectories (described by the convergence theorem) cannot be verified. We can think of the modified energy surface as a rippled version of the original. The order determining the allowed magnitude of the fluctuation.

To illustrate this idea, we have plotted, in Fig. 3.3 the contours of the energy and the Verlet modified energy (including terms through h^4) for the double well example (potential $U(q) = (q^2 - 1)^2/2$) in part of phase space. The figure shows that the contours of the two energy functions are interleaved. If we are confined to the contours of the modified energy the physical energy will be seen to fluctuate along it.¹

Suppose that, somehow, H were exactly conserved along the numerical solution, so

$$\dot{H} = 0 \Rightarrow \{H, \tilde{H}_h\} = 0.$$

¹The modified energy for the Verlet method for a single degree of freedom system with energy $H = p^2/2 + U(q)$ is

$$\begin{aligned} \tilde{H}_h &= H + \frac{h^2}{24}(2p^T U'' p - (U')^2) \\ &\quad + h^4 \left(\frac{1}{720} p^4 U''' - \frac{1}{120} p^2 U' U''' - \frac{1}{240} (U')^2 U'' - \frac{1}{60} p^2 ((U'')^2 + U' U''') \right) \\ &\quad + \mathcal{O}(h^6) \end{aligned}$$

Since $\{g_1, g_2\} = -\{g_2, g_1\}$, we have

$$\{\tilde{H}_h, H\} = 0.$$

This would imply that \tilde{H}_h is actually, itself, a first integral of the molecular system. This certainly seems unlikely to hold except in very special cases indeed, unless the numerical method happens to coincide with the exact solution (up to a time rescaling). Thus the properties of symplecticness and energy conservation for numerical methods are essentially mutually exclusive from a practical point of view. A more precise formulation of this result was first given by Ge and Marsden [400].

Example 3.2 (7-Atom Lennard-Jones System) To test some of the methods presented in this chapter, let us see how they fare when we apply them to a system of $N = 7$ unit-mass particles moving in a pairwise potential $\varphi(r) = r^{-12} - 2r^{-6}$. This modified Lennard-Jones potential has stronger attraction (due to the factor of 2 multiplying r^{-6}) which tends to keep the system bound and makes testing a little easier (without worrying about boundary conditions or particle ejections). The Hamiltonian for our model is

$$H = \frac{1}{2} \sum_{i=1}^N \|\mathbf{p}_i\|^2 + U(\mathbf{q}), \quad U(\mathbf{q}) = \sum_{i=1}^{N-1} \sum_{j=i+1}^N \varphi(\|\mathbf{q}_i - \mathbf{q}_j\|).$$

In our simulations we fixed the total momentum to be zero, so, although there may be net rotation, there is no translation of the atoms. It is easy to understand the minimum energy states for this system. At the global minimum potential energy configuration $U = E_0 = -12.5292$, the atoms are clustered in the compact arrangement with one at the center and the other six at the vertices of a regular hexagon. The positions of the outer atoms may be rotated without affecting the energy. At low total energy $E \approx E_0$, meaning that the system is started near the minimizing configuration, the particles remain in the hexagonal state, up to rotation and small vibrations. In order for two of the atoms to switch locations, it is necessary for the radial symmetry to be broken which requires crossing an energy “barrier.” For moderate energies, the atoms remain near the conformational states (local minima of potential) shown in Fig. 3.4 which are likewise separated by energy barriers.

A natural goal of simulation would be the computation of the relative probabilities of these various states. A more elementary task is to compute the radial distribution which gives the distribution of distance between atom pairs observed. The radial density function may be approximated from a histogram of all pair distances observed in a long simulation. (There are 21 at each step, so the amount of data is helpfully increased, reducing the “sampling error”.) This distribution is displayed in Fig. 3.5. The peaks of the radial distribution function are correlated with the various interatomic distances that appear in the cluster configurations shown in Fig. 3.4.

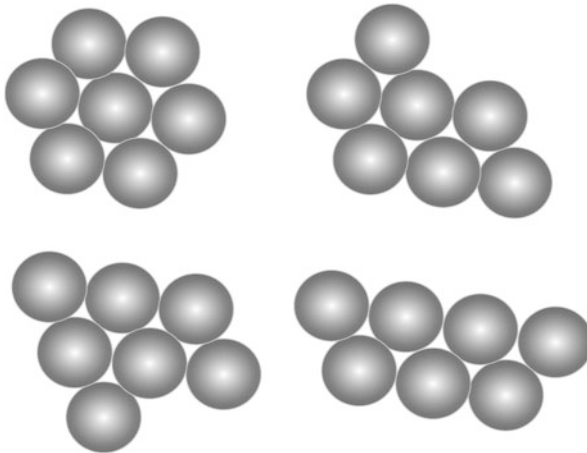


Fig. 3.4 The four local minima of the potential energy of the 7-atom system are shown (other local minima are either rotations of these with respect to the center of mass or else symmetric reflections)

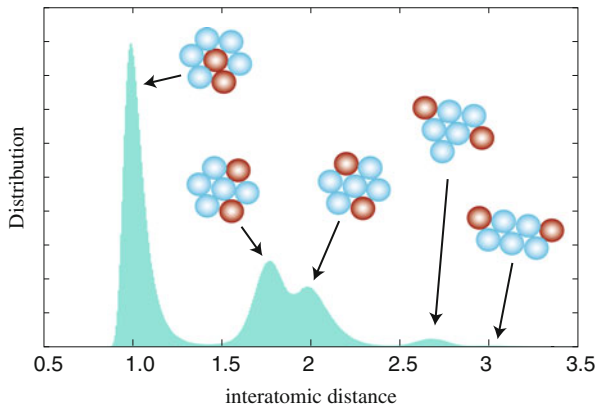


Fig. 3.5 The radial distribution function is shown for the Lennard-Jones 7-atom system at constant energy. The peaks in the radial distribution function correspond to common separations observed among the atoms at the potential energy minima. *Shaded pairs* in the diagrams illustrate the locations within the atomic arrangements where these probable distances are found

We now set about comparing various methods. With the Verlet method, it was found that one million timesteps of length about $h = 0.01$ gave reasonable accuracy for the radial distribution function (see Fig. 3.6).

Taking the stepsize of $h = 0.01$, one quickly dispatches Euler's method. In fact it was not possible to simulate the system at such a stepsize using Euler's method due to instability. The energy error grows dramatically even with smaller timesteps (Fig. 3.7). The drift can be seen to exhibit a linear growth rate of the form

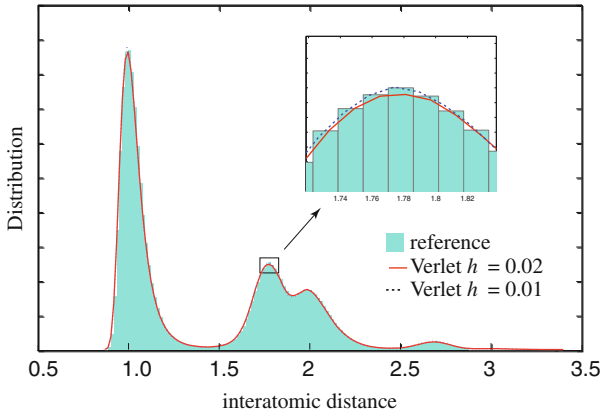


Fig. 3.6 The radial distribution computed using the Verlet method is well resolved with a stepsize of $h = 0.01$ (even the $h = 0.02$ is a reasonable approximation)

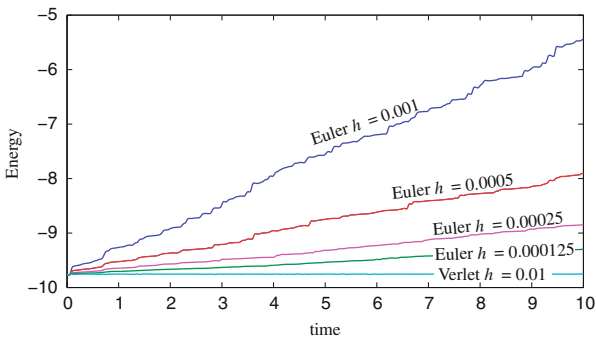


Fig. 3.7 The energy for Euler's method applied to the 7-atom Lennard-Jones cluster is seen to exhibit a secular drift with the energy error growing approximately linearly in time

$\Delta E(\tau) \propto h \times \tau$. The linear drift can likely be related to the effect of an almost-periodic error connected to interatomic vibrational motions; an error is introduced at each oscillation of the atom pairs. These errors, which accumulate on the vibrational period to $\mathcal{O}(h)$ (as Euler's method is first order), build at each oscillation, effectively heating the molecule (it would eventually burst apart).

The popular explicit (and nonsymplectic) 4th order Runge-Kutta method was tested next. The energy errors (Fig. 3.8) still grow in time, but the rate is much lower. Comparing with the drift in Euler's method, the drift in energy can be examined more closely and is found to behave like $\Delta E(\tau) \propto h^4 \tau$, where τ is the length of the time interval. In a curious development, we see that the fluctuations in energy are now much smaller than those for the Verlet method at the same stepsize, which is consistent with the higher order of accuracy. However, the drift means that in a long simulation the results are comparatively poor. This may be seen in

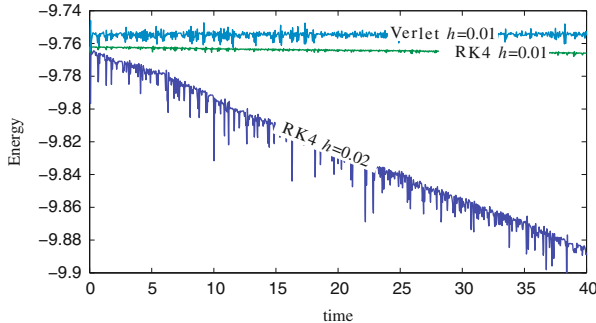


Fig. 3.8 The energy for the explicit 4th order Runge-Kutta method applied to the 7-atom Lennard-Jones cluster is seen to exhibit a secular drift

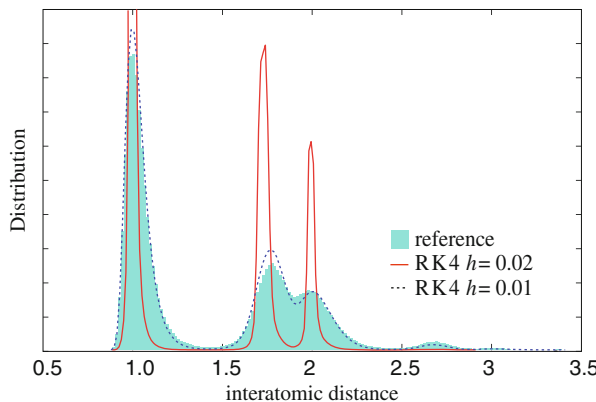


Fig. 3.9 The radial distribution computed using the explicit 4th order Runge-Kutta method with stepsizes of $h = 0.01$ and $h = 0.02$. Due to energy drift, the $h = 0.02$ solution is completely inaccurate, whereas even the $h = 0.01$ curve is much worse than that obtained using Verlet with $h = 0.02$, despite the fact that the Runge-Kutta method uses four times the number of force evaluations per timestep. These calculations were performed using 1M timesteps; if a longer simulation were used, the RK4 errors in distribution would be expected to increase (due to the increasing energy drift) whereas the errors reported in Figure 3.6 for the Verlet method would not be expected to depend appreciably on the time interval

the radial distribution function which is computed in Fig. 3.9. This method requires four evaluations of the force for each timestep, yet the results are poor even when the stepsize is the same as that used in Verlet which only requires one force evaluation per step. A more natural comparison would need to be with $h = 0.04$ in the Runge-Kutta method, but at such a stepsize, the performance would be disastrous. Note that at a slightly larger stepsize than that considered here, $h = 0.03$, the Verlet method would show a large error in distribution. To gain some insight into what is happening for this stepsize, see Fig. 3.10, where energy is graphed vs. time for stepsizes of $h = 0.025$ and $h = 0.03$. Evidently, at the largest stepsize, energy

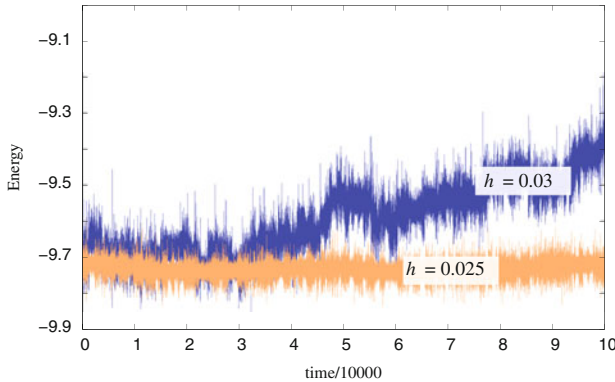


Fig. 3.10 Energy as a function of time for the Verlet method with two different stepsizes. The drift is controlled for $h = 0.025$ but much more dramatic at $h = 0.03$

is not well conserved by the Verlet method. The explanation is that the backward error analysis presented previously, and therefore the assumption that the numerical method is described by a Hamiltonian flow map, is invalid. This is a consequence of the mentioned fact that construction of the modified Hamiltonian depends on an optimal truncation at high order. For $h = 0.03$ in this example, the truncation would introduce a substantial error, or, alternatively, the “Hamiltonian flow” interpretation for the numerical method is poor. Either the stepsize must be reduced in such cases (already $h = 0.025$ shows much less drift) or some other method must be used.

3.5 Energy Conserving Methods

It is possible to derive numerical methods that exactly (i.e. to within rounding error) conserve the energy at each step and this may seem a more natural approach to molecular dynamics than symplectic integration since we have discussed and evaluated methods in terms of their energy conservation.

Consider the following 2D example of a differential equation system

$$\dot{u} = f(u, v), \quad \dot{v} = g(u, v).$$

Notice that this system has a first integral

$$I(u, v) = u - v,$$

and consider the application of Euler’s method:

$$u_{n+1} = u_n + hf(u_n, v_n), \quad v_{n+1} = v_n + hg(u_n, v_n).$$

We see that

$$I(u_{n+1}, v_{n+1}) = u_{n+1} - v_{n+1} = u_n - v_n = I(u_n, v_n),$$

which means that Euler's method conserves this first integral. We say that this conservation property is *exact*, even though, in practice, there could be fluctuations in the result depending on how the computations are carried out on a computer (normally, if the relevant algebraic equations are solved numerically, there will be small residual errors which are similar in magnitude to the computer rounding error).

Generalizing this slightly, we could imagine a system of ODEs of the form

$$\dot{z} = f(z),$$

such that, for some vector \mathbf{b} ,

$$\mathbf{b} \cdot f(z) \equiv 0,$$

then $I(z) = \mathbf{b} \cdot z$ is a first integral. It is straightforward to see that Euler's method conserves such a *linear* first integral exactly, as is true of many other popular numerical methods. Thus momentum conservation is rarely violated by (sensible) numerical methods.

The interest is usually in conserving some more complicated first integrals, for example the energy of the system. None of the schemes we have considered so far (Euler's method, Störmer-Verlet, etc.) conserves this quantity exactly, even in the case of a harmonic oscillator. In the case of Euler's method applied to the harmonic oscillator, the error in energy grows with time and without bound. In the case of Störmer-Verlet, the energy fluctuates but remains bounded for all time and at its worst is of size proportional to h^2 , a numerical observation that is supported by the existence of the modified Hamiltonian.

It is tempting to consider energy-conserving methods by which the energy is corrected at each step back to the initial value. This is easy to do in general, and there are in fact many choices of the method used. Let us consider one particular approach. We start by taking a timestep with any arbitrary (nonconserving) numerical method, say to an intermediate phase point $\bar{\mathbf{Q}}, \bar{\mathbf{P}}$, then we “fix it up” by scaling the momentum by an adjustment factor, defining

$$\mathbf{Q} = \bar{\mathbf{Q}}, \quad \mathbf{P} = \gamma \bar{\mathbf{P}},$$

selecting γ so that the energy in the result is a prescribed value E . The energy fluctuation in our pre-correction scheme would typically be small in a single timestep, so the correction γ should also be close to one. This method is easy to implement: the equation that must be solved is

$$\frac{\gamma^2 \bar{\mathbf{P}}^T \mathbf{M}^{-1} \bar{\mathbf{P}}}{2} + U(\bar{\mathbf{Q}}) = E, \tag{3.12}$$

and, since $\bar{\mathbf{Q}}$ is known, this gives

$$\gamma = \left(\frac{E - \bar{U}}{\bar{K}} \right)^{1/2}, \quad (3.13)$$

where $\bar{U} = U(\bar{\mathbf{Q}})$ and $\bar{K} = \bar{\mathbf{P}}^T \mathbf{M}^{-1} \bar{\mathbf{P}} / 2$ are the potential and kinetic energies after a step of the original non-conserving scheme. As long as the steps are small enough we could hope that the resulting method is sensible. This is, however, not quite true. If, in the harmonic oscillator, \bar{p}_{n+1} happens to vanish, then γ is not defined. We could work around this obstacle by assuming a large number of degrees of freedom, in which case \bar{K} is only zero if all the momenta simultaneously vanish and this situation is, in a realistic model of a molecule, extremely unlikely. We also must assume that $E - \bar{U} \geq 0$, which, for a large system, seems the likely situation, since we may suppose $\bar{K} + \bar{U} = \bar{E} \approx E$, thus $E - \bar{U} \approx \bar{K} \geq 0$. Thus we assume a system with many degrees of freedom so that all the conditions for the method to be well defined are satisfied. Although it may appear that the method requires two evaluations of the energy at each timestep (which may seem a high cost, since Euler's method and even the 2nd order Verlet method only require one), the evaluation of the energy needed to compute γ is at the end point of the combined step, and this is the starting point for the next step—essentially the same work would be needed anyway to compute the forces at the next step. In practice, some care must be exercised in implementing this method. In particular the kinetic energy needs to be monitored for approach to zero; when this occurs the projections must be disabled or replaced by an alternate scheme.

When we adjust the momenta by scaling in order to satisfy the energy constraint, we are, in effect, projecting the preliminary numerical approximation onto an energy surface, using one particular type of projection. There are many alternative projection methods which we could use for this purpose, which might alter both the positions and momenta. Modifying the positions means that we will somehow need to solve the equation

$$H(\mathbf{Q}, \mathbf{P}) = E,$$

where \mathbf{Q} depends on a parameter or parameters (typically a Lagrange multiplier that is used to maintain the constraint). These methods are necessarily implicit and require solving nonlinear equations involving the potential energy U [308]. In an iterative strategy such as Newton's method, we will need to compute the potential energy several times at each timestep. This is a very high price to pay in practice and is one reason why complicated energy projection methods are not popular.

Another reason why energy conserving methods are rarely used in molecular simulation is that they may lead to behavior that is not consistent with the properties of our original model. If we think of the procedure that we use to define the step as defining a map of phase space, the map does not necessarily have qualitative properties that mimic those of the original system. Note that, as we have mentioned

earlier in this chapter, it is in general impossible to simultaneously preserve the energy and the symplectic structure in a numerical method for Hamiltonian systems. There is nothing that tells us that the map constructed by energy projection may not exhibit artificial behavior (uncharacteristic of Hamiltonian systems). These artificial dynamical artifacts are particularly prevalent in low-dimensional models and at large stepsizes, although they may be manifest in any system.

We examine here the application of energy conserving methods in connection with the Lennard-Jones example discussed previously. The projection method may be used with any integrator. With respect to both Euler's method and the 4th order Runge-Kutta method, for large stepsizes, nonphysical effects are noticeable. However, for small enough stepsize, it is possible to improve the accuracy of averages obtained using the Runge-Kutta method by incorporating the projection (Fig. 3.11 shows the radial distribution for $h = 0.01$ with and without projection.) The lesson of this example is that one of the most important features of a method for molecular dynamics is its conservation of energy. However, already at $h = 0.02$ the results were poor with the projected Runge-Kutta method. Thus the energy conservation seems only to offer a benefit as a fine-tuning. The addition of energy projection does not make the Runge-Kutta scheme competitive with Verlet for molecular simulation.

As a second example, we consider a simple model of an atom bonded to a pair of fixed neighbors by (nonlinear) springs, as depicted in Fig. 3.12. The coefficients k_1 and k_2 determine the potential energy function U of the system (a function of the position of the moving body $\mathbf{q} = (x, y)$, which we assume to lie in a plane). The

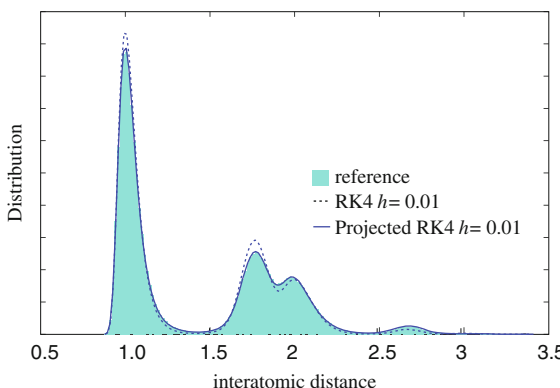
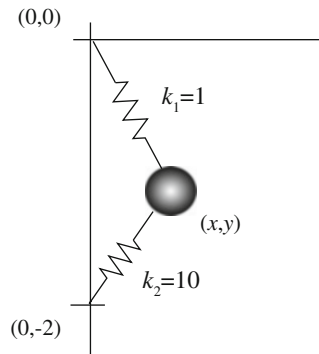


Fig. 3.11 The radial distribution computed using the projected Runge-Kutta method (3.12)–(3.13) with 1M steps of stepsize $h = 0.01$, in comparison to that obtained using the unprojected RK4 method with the same number of steps. This result demonstrates improving energy conservation can have an important effect on the accuracy of computed averages

Fig. 3.12 Pendulum model with two different natural frequencies



springs are assumed to have rest lengths of ℓ_1 , ℓ_2 , respectively. The potential energy function is

$$U(x, y) = \frac{k_1}{2}(r_1 - \ell_1)^2 + \frac{k_2}{2}(r_2 - \ell_2)^2,$$

where $r_1 = \sqrt{x^2 + y^2}$, $r_2 = \sqrt{x^2 + (y + 2)^2}$.

We take $k_1 = 1$, $k_2 = 10$ (each spring has a rest length of 1) and the initial conditions $\mathbf{q}_0 = (0, -2.9)$; $\mathbf{p}_0 = (.8718, 0)$ with energy $E \approx 2.235$. The pendulum positions fill in a region which is approximately a disk with a hole cut out. A correct result is obtained using the Verlet method with a stepsize of $h = 0.04$. Yet, for exactly the same stepsize, using the energy projection method, the results are completely different.

In Fig. 3.13, the position of the point x, y is shown for three successive series of timesteps: (i) $0 \leq n < 25,000$, (ii) $25,000 \leq n < 30,000$, and (iii) $30,000 \leq n \leq 500,000$. In the first phase, the discrete trajectory appears to be filling in the correct region and without any evidence of nonphysical behavior. The performance is very similar to a Verlet method without projection during this period. In the second phase the system begins to move toward a limit cycle, i.e. an attractive periodic orbit. The presence of such limit cycles is impossible in a Hamiltonian system, thus it is evident that a nonphysical artefact has been introduced by the projection method. Finally, in the third phase, the trajectory is increasingly confined. In Fig. 3.14, the trajectory is shown for timesteps $n = 50,000$ to $500,000$ and this is contrasted with the correct image of the configurational region. Because of the use of energy as a constraint, we have also given up this means of assessing the quality of the solution; the projected numerical method makes errors in the energy of relative size 10^{-14} or less. However, the observation here is that the energy conserving projection would be utterly useless at this stepsize, although, if we were to judge the quality of the method from the first 25,000 steps, we would see nothing amiss.

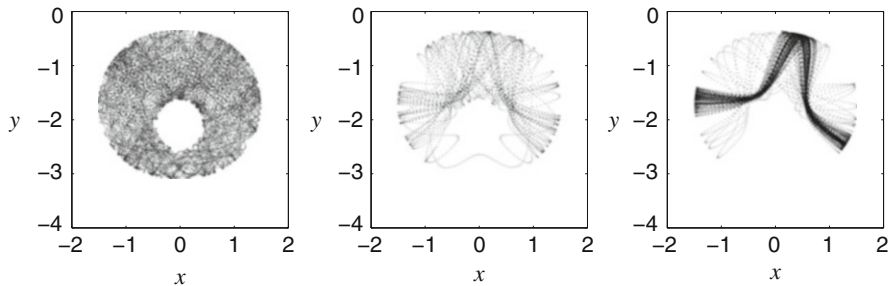


Fig. 3.13 A projected Verlet trajectory for the pendulum model is shown in its xy projection for three successive intervals of timesteps (see text for discussion). The graphs show the transition from correct sampling behavior to motion confined to a limit cycle

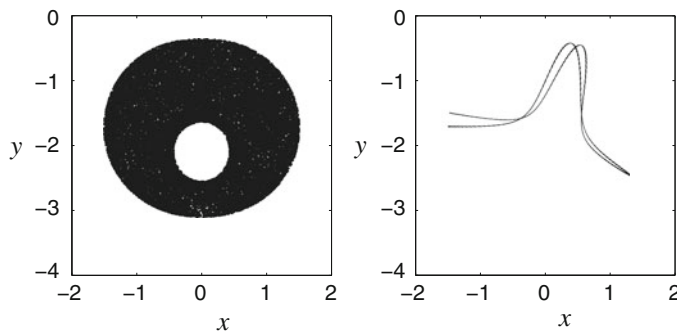


Fig. 3.14 The steady state behavior obtained in the pendulum example using Verlet (left) and the projected Verlet method (right). The graphs show the final 450,000 steps of simulation in a 500,000 step trajectory

3.6 On the Importance of Being Symplectic

Symplecticness is a strong condition and we have seen, in the construction of the perturbed Hamiltonian the last section, that it implies a constraint on the growth of errors in energy. This does not, however, automatically mean that there are no other suitable principles that could underpin the design of good numerical methods for molecular dynamics. The flow of a Hamiltonian system of the form $H = \mathbf{p}^T \mathbf{M}^{-1} \mathbf{p} / 2 + U(\mathbf{q})$ will preserve all of the following²:

²Other conserved quantities may be present in specific situations, but this is the exception rather than the rule. For example the conservation of angular momentum, which we would expect in the case of celestial mechanics, is destroyed by the use of various boundary conditions in molecular simulation.

1. The symplectic two-form $d\mathbf{q} \wedge d\mathbf{p}$.
2. The Hamiltonian (i.e., the energy) H .
3. The volume in phase space (as the vector field is divergence free).
4. The time-reversal symmetry.

A natural question is which of these properties should underpin the design of a numerical method for molecular dynamics? In this section we address this through illustrative examples.

The phase volume conservation can be seen as a consequence of the symplectic property, but it is a weaker condition. It is possible to construct methods that preserve volume but which are not symplectic, and we can build methods that exactly conserve the energy (as we shall show below). Until now we have said little about the time-reversal symmetry of molecular dynamics.

3.6.1 Time-Reversal Symmetry

The term *time-reversal symmetry* or *time-reversibility* is used in two ways in connection with molecular dynamics. In this chapter, we use the term to refer to a property that can be expressed in terms of the individual trajectories of the system. (A somewhat different reversibility property is related to the evolution of probability distributions, see Chap. 8.)

Let $\dot{\mathbf{z}} = \mathbf{f}(\mathbf{z})$ be a dynamical system. By an *involution* we mean a linear mapping $\mathbf{z} \mapsto \mathbf{R}\mathbf{z}$ where $\mathbf{R}^2 = \mathbf{I}$, i.e. \mathbf{R} is its own inverse. Given the involution \mathbf{R} we define the *time reversal* of the vector field \mathbf{f} with respect to \mathbf{R} by

$$\tilde{\mathbf{f}}(\mathbf{z}) = -\mathbf{R}^T \mathbf{f}(\mathbf{R}\mathbf{z}).$$

When a vector field is its own reversal we say that it is a time-reversible vector field.

Let $H(\mathbf{q}, \mathbf{p}) = \mathbf{p}^T \mathbf{M}^{-1} \mathbf{p} / 2 + U(\mathbf{q})$ be the Hamiltonian for a system of N_c configuration variables. Define the $2N_c \times 2N_c$ matrix \mathbf{R} by

$$\mathbf{R} = \begin{bmatrix} \mathbf{I} & \mathbf{0} \\ \mathbf{0} & -\mathbf{I} \end{bmatrix}.$$

The vector fields involved are

$$\mathbf{f} = \begin{bmatrix} \mathbf{M}^{-1} \mathbf{p} \\ -\nabla U(\mathbf{q}) \end{bmatrix}, \quad \tilde{\mathbf{f}} = -\mathbf{R}\mathbf{f}(\mathbf{R}\mathbf{z}) = -\begin{bmatrix} -\mathbf{M}^{-1} \mathbf{p} \\ \nabla U(\mathbf{q}) \end{bmatrix},$$

which are clearly equal. Therefore the molecular dynamics Hamiltonian system is time-reversible.

The time-reversal symmetry may be understood as a property of the vector field. This engenders a symmetry at the level of the trajectories of the system.

For the system $\frac{dz}{dt} = f(z)$, a coordinate transformation $z \mapsto \tilde{z} = Rz$ results in

$$\frac{d\tilde{z}}{dt} = R \frac{dz}{dt} = Rf(R^{-1}\tilde{z}) = Rf(R\tilde{z}),$$

since $R^{-1} = R$.

A change of time $t \mapsto \tau = -t$ results in

$$\frac{dz}{d\tau} = \frac{dt}{d\tau} \frac{dz}{dt} = -f(z).$$

In other words, for a reversible vector field, the coordinate transformation $z \mapsto Rz$ is equivalent to the change of time $t \mapsto -t$.

3.6.2 Time-Reversal Symmetry and Symmetric Numerical Methods

The flow map $\mathcal{F}_t(z_0)$ gives a solution of the differential equation, thus for a time-reversible system, we have, with $z(t) = \mathcal{F}_t(z_0)$,

$$\frac{d}{dt} \mathcal{F}_t(z_0) = \frac{dz}{dt} = -Rf(R\mathcal{F}_t(z_0)).$$

Hence

$$\frac{d}{dt} R\mathcal{F}_t(z_0) = -f(R\mathcal{F}_t(z_0)),$$

and if we define $\tilde{z}(t) = R\mathcal{F}_t(z_0)$ then $\tilde{z}(t)$ satisfies the differential equation

$$\frac{d\tilde{z}}{dt} = -f(\tilde{z}).$$

From this we see that if we start from a point z_0 and integrate forward in time (i.e apply \mathcal{F}_t) then apply the involution R , we get the exact same result as if we start from $\tilde{z}(0) = Rz_0$ and integrate *backward* in time (i.e apply \mathcal{F}_{-t}). In sum, since z_0 is an arbitrary point,

$$\mathcal{F}_{-t}(Rz) = R\mathcal{F}_t(z).$$

For the flow map, $\mathcal{F}_{-t} = \mathcal{F}_t^{-1}$ so we can recast the identity as

$$R \circ \mathcal{F}_t \circ R \circ \mathcal{F}_t = \text{Id}, \quad (3.14)$$

where we have slightly abused notation by allowing the symbol \mathbf{R} to refer to both the involution matrix and the corresponding mapping $z \mapsto \mathbf{R}z$.

We may seek numerical methods that mimic this property, which we refer to time-reversible numerical methods. Recall from the previous chapter that a numerical method \mathcal{G}_h was said to be symmetric if it satisfied

$$\mathcal{G}_{-h} = \mathcal{G}_h^{-1}.$$

It does not automatically follow that a symmetric numerical method is time-reversible, i.e. satisfies a relation inspired by (3.14), namely

$$\mathbf{R} \circ \mathcal{G}_h \circ \mathbf{R} \circ \mathcal{G}_h = \text{Id}. \quad (3.15)$$

The additional condition needed to ensure (3.15) is the *affine invariance* property (or invariance with respect to the specific affine transformation $z \mapsto \mathbf{R}z$).

Definition 3.1 (Affine Invariance) Let

$$\frac{dz}{dt} = f(z) \quad (3.16)$$

be a given ordinary differential equation. The transformation $\tilde{z} = Az$, where A is a non-singular square matrix, results in the modified differential equation

$$\frac{d\tilde{z}}{dt} = Af(A^{-1}\tilde{z}). \quad (3.17)$$

Let z_0, z_1, \dots be a sequence of points obtained by application of the numerical method \mathcal{G}_h to (3.16). If the same method, when applied to (3.17) produces the set of points Az_0, Az_1, \dots , then we say that the numerical method is invariant with respect to the transformation $\tilde{z} = Az$. An affine invariant method is one which is invariant under any such transformation.

If a differential equation is time-reversible with respect to the involution \mathbf{R} , and we apply a method which is affine invariant and symmetric, then the method will be time-reversible (3.15).

All Runge-Kutta methods and Partitioned Runge-Kutta methods are affine invariant, thus, if they are also symmetric, then they preserve time-reversal symmetry.

3.6.3 Comparing Symplectic and Time-Reversible Methods

The symplectic property

$$\mathcal{F}'_t^T J \mathcal{F}'_t = J$$

and the time-reversal symmetry

$$\mathcal{F}_t \circ \mathbf{R} \circ \mathcal{F}_t = \mathbf{R}$$

have a formal similarity, but they are essentially unrelated. A method can be symplectic but not time-reversible (e.g. Symplectic Euler) or it can be time-reversible and not symplectic (e.g. Trapezoidal Rule). However there are intriguing relationships between these properties which we discuss here.

Interestingly the time-reversal symmetry provides analogous properties in some respects to the properties of Hamiltonian systems. For example, consider a linear Hamiltonian system $dz/dt = \mathbf{J}\mathbf{A}z$, with \mathbf{A} a symmetric matrix. If λ is an eigenvalue of $\mathbf{J}\mathbf{A}$ then $\mathbf{J}\mathbf{A}\mathbf{u} = \lambda\mathbf{u}$ for some eigenvector $\mathbf{u} \neq 0$. Because the matrix $\mathbf{J}\mathbf{A}$ is real, we know that $\bar{\lambda}$ will also be an eigenvalue. At the same time, we know that since λ is an eigenvalue of $\mathbf{J}\mathbf{A}$ it is also an eigenvalue of its transpose $(\mathbf{J}\mathbf{A})^T = \mathbf{A}^T\mathbf{J}^T = -\mathbf{A}\mathbf{J}$, thus

$$-\mathbf{A}\mathbf{J}\mathbf{u} = \lambda\mathbf{u}$$

multiplying by \mathbf{J} and setting $\mathbf{v} = \mathbf{J}\mathbf{u}$ we have

$$-\mathbf{J}\mathbf{A}\mathbf{v} = \lambda\mathbf{v}$$

implying that $-\lambda$ (and hence also $-\bar{\lambda}$) is an eigenvalue of $\mathbf{J}\mathbf{A}$. Real eigenvalues of $\mathbf{J}\mathbf{A}$ are paired with their negatives. If the imaginary part is nonzero, the eigenvalues occur in quadruplets $\{\pm\lambda, \pm\bar{\lambda}\}$. The flow map is

$$\mathcal{F}_t(z) = e^{t\mathbf{J}\mathbf{A}}z$$

and the exponential matrix will inherit a related structure within the spectrum: λ an eigenvalue of $\exp(t\mathbf{J}\mathbf{A})$ implies that $\bar{\lambda}$, $1/\lambda$ and $1/\bar{\lambda}$ are all eigenvalues of $\exp(t\mathbf{J}\mathbf{A})$. This eigenvalue structure is generic for linear symplectic maps in general.

Suppose now we have a linear time-reversible map $\Phi(z) = \mathbf{T}z$, then

$$\mathbf{T}^{-1} = \mathbf{R}\mathbf{T}\mathbf{R}.$$

Given an eigenvalue, eigenvector pair (λ, \mathbf{u}) of \mathbf{T} , let $\mathbf{u} = \mathbf{R}\mathbf{v}$, so that $\mathbf{R}\mathbf{u} = \mathbf{R}^2\mathbf{v} = \mathbf{v}$, then

$$\mathbf{T}^{-1}\mathbf{v} = \mathbf{R}\mathbf{T}\mathbf{R}\mathbf{v} = \mathbf{R}\mathbf{T}\mathbf{u} = \lambda\mathbf{R}\mathbf{u} = \lambda\mathbf{v}.$$

Thus λ is an eigenvalue of \mathbf{T}^{-1} which, in turn, implies that $1/\lambda$ is an eigenvalue of \mathbf{T} . The matrix being real implies that the conjugates of λ and $1/\lambda$ are also eigenvalues, thus we have the same eigenvalue quadruplets as for a linear symplectic map.

Recall that a pair of maps Φ and Ψ are said to be conjugate if there is a homomorphism χ such that

$$\Phi = \chi^{-1} \Psi \chi.$$

In such a case the iterates of the two maps will also be conjugate and, if they are numerical methods, they will have similar stability properties and performance (e.g. the same effective order). It is difficult to separate the relevance of the two properties in cases where symplectic and reversible maps are conjugate. This is however rarely the case and certainly does not hold generically for discrete maps in many dimensions [209]. There is no direct correspondence between reversible and symplectic maps, however each class of maps admits certain theorems of dynamical systems which are in many ways analogous (for example, the Kolmogorov-Arnold-Moser, or KAM, theory for symplectic maps near elliptic fixed points [386] has an analogue for reversible maps [97]).

Of particular importance for molecular dynamics are the following properties: a symplectic map will preserve volume, whereas a time-reversible map need not do so, and a symplectic integrator will approximately conserve energy due to the existence of the perturbed Hamiltonian, whereas a time-reversible integrator may give rise to a drift in energy [166].

3.7 Molecular Dynamics with Hard-Sphere Collisions

We close this chapter with a discussion of molecular dynamics with hard-core repulsion. This is a system which is not, properly speaking, Hamiltonian, but which has dynamics that are largely defined by a Hamiltonian system. The added complication is the nonsmooth character of the motion as impulses are applied at points of collision. The discussion below is a summary of work in [40, 184].

We assume, as usual a Hamiltonian $H = \mathbf{p}^T \mathbf{M}^{-1} \mathbf{p} / 2 + U(\mathbf{q})$ but we add the inequality constraint $\|\mathbf{q}_i - \mathbf{q}_j\| \geq \sigma_i + \sigma_j$ where $\sigma_i, i = 1, \dots, N$ is a core radius. The condition $\|\mathbf{q}_i - \mathbf{q}_j\| = \sigma_i + \sigma_j$, some i, j defines the constraint surface. When the particles are not touching, they move along Newtonian paths defined by the standard equations of motion. At impact, they exchange momentum and energy according to the rules of elastic collision. Specifically, at the point of contact, the momentum vectors of the two spheres are adjusted according to the rule:

$$\mathbf{p} := \mathbf{p} + \alpha \mathbf{u}_{\perp}$$

where \mathbf{u}_{\perp} is normal to the constraint surface and α is a parameter chosen to maintain the conservation of energy. Let \mathcal{R}_c denote the action of the collision operator on the vector of positions and momenta. Then we can write the evolution formally as

$$\mathcal{F}_\tau^{\text{h.s.}}(\mathbf{q}, \mathbf{p}) = \mathcal{G}_{\Delta\tau_r} \circ \mathcal{R}_c \circ \mathcal{G}_{\Delta\tau_{r-1}} \dots \circ \mathcal{R}_c \circ \mathcal{G}_{\Delta\tau_0}$$

where $\Delta\tau_1, \Delta\tau_2, \dots, \Delta\tau_{r-1}$ are the times between collisions, $\Delta\tau_0$ is the time until the first collision, and $\Delta\tau_r$ is the time between the last collision and τ . Here \mathcal{G}_t is the flow map of the smooth system (Hamiltonian H). The trajectory is thus piecewise smooth with continuous configurational path and momenta exhibiting finite jump discontinuities.

Various numerical methods have been proposed for collisional Hamiltonian systems [136, 176, 184, 263, 348, 352]. Typically, these schemes rely on the Verlet method to propagate the system between collisions, with collisions detected either (i) by checking for overlap at the end of the step, (ii) checking for overlap during the step, or (iii) approximating the time to collision before the step. Collisions lead to momentum exchange between particles according the principle outlined above.

3.7.1 Splitting Methods for Hard Sphere Molecular Dynamics

Splitting methods are suggested by considering a formal hard-sphere Hamiltonian

$$H_{\text{h.s.}} = \mathbf{p}^T \mathbf{M}^{-1} \mathbf{p} / 2 + U(\mathbf{q}) + U_{\text{h.s.}},$$

where $U_{\text{h.s.}}$ is assumed to be infinite for overlapping configurations (some $\|\mathbf{q}_i - \mathbf{q}_j\| \leq \sigma_i + \sigma_j$) and zero otherwise. The hard sphere system described by

$$H_{\text{free}} = \mathbf{p}^T \mathbf{M}^{-1} \mathbf{p} / 2 + U_{\text{h.s.}}$$

consists of purely ballistic (straight line) motion punctuated by momentum jumps. This system is formally integrable, i.e. we may write down its exact solution for any given initial conditions. (In practice, for large systems solved in parallel, this computation may be highly nontrivial [108, 336].) One approach is to consider the splitting $H = H_{\text{free}} + U$, evolving H_{free} for fixed intervals punctuated by impulses derived from the smooth potential U . In [40, 184] this algorithm is termed the “Primitive Splitting Algorithm” and can be described by the three steps:

$$\mathbf{P} := \mathbf{p} - \frac{h}{2} \nabla U(\mathbf{q}), \quad (\mathbf{Q}, \mathbf{P}) := \mathcal{G}_h^{\text{free}}(\mathbf{q}, \mathbf{P}), \quad \mathbf{P} := \mathbf{P} - \frac{h}{2} \nabla U(\mathbf{Q}).$$

Even with this symmetric form (“kick”, “drift”, “kick”) where “drift” now involves the solution of the system H_{free} , it was shown in [184] that energy accumulates rapidly. Assuming a finite number of collisions on a fixed interval, the error behaves as $\mathcal{O}(h)$. In long simulations the energy error grows without bound.

To understand why this is the case, we consider a step of the primitive splitting algorithm applied to a simple system consisting of a fixed body at the origin and a single body (mass=1) moving under an external potential and in occasional contact with the fixed body, both bodies having radius 0.5. Let us consider three possibilities: (i) there is no collision in the timestep, (ii) there is a collision only at

the end of the timestep, and (iii) there is a single collision within the timestep. [The case of additional collisions within the step could be handled as in (iii).] In cases (i) and (ii) it is clear that the error accumulating in a single step will be third order in the stepsize, since the Verlet method has local error of order three (since it is a second order method).

Now consider case (iii). The contact happens when the particles are separated by a distance 1, at which point $\mathbf{u}_\perp = \mathbf{q}$. We assume the time of contact is τ_c .

$$\begin{aligned}\bar{\mathbf{P}} &:= \mathbf{p} - \frac{h}{2} \nabla U(\mathbf{q}), \quad \mathbf{q}_c := \mathbf{q} + \tau_c \bar{\mathbf{P}}, \\ \mathbf{u}_\perp &:= \mathbf{q}_c, \quad \hat{\mathbf{P}} := \bar{\mathbf{P}} + \alpha \mathbf{u}_\perp, \\ \mathbf{Q} &:= \mathbf{q}_c + (h - \tau_c) \hat{\mathbf{P}}, \quad \mathbf{P} := \hat{\mathbf{P}} - \frac{h}{2} \nabla U(\mathbf{Q}),\end{aligned}$$

The coefficient α is chosen so that the kinetic energy is conserved through collision, thus

$$\alpha = -2 \frac{\mathbf{u}_\perp \cdot \bar{\mathbf{P}}}{\mathbf{u}_\perp \cdot \mathbf{u}_\perp}.$$

We next calculate the change in energy in a single step by inserting \mathbf{Q} and \mathbf{P} into the Hamiltonian and expanding around the point of collision \mathbf{q}_c , obtaining

$$\begin{aligned}\Delta H &\stackrel{\text{def}}{=} H(\mathbf{Q}, \mathbf{P}) - H(\mathbf{q}, \mathbf{p}) \\ &= -(h - 2\tau_c) \frac{\mathbf{q}_c^T \bar{\mathbf{P}}}{\mathbf{q}_c^T \mathbf{q}_c} \mathbf{q}_c^T \nabla U(\mathbf{q}_c) + O(h^2)\end{aligned}$$

Energy is therefore conserved only to first order through the collision unless one of the following conditions holds:

- there is no collision
- the collision occurs at the end of a timestep
- the collision occurs at the middle of the timestep, $\tau_c = h/2$,
- the directional derivative of U along the collision vector ($\mathbf{u}_\perp = \mathbf{q}_c$) vanishes, or
- the momentum vector is orthogonal to the collision vector at the point of contact.

In general, because an error of size $\mathcal{O}(h)$ occurs in each collision and there are a finite number of collisions in a fixed time interval, the total error is also $\mathcal{O}(h)$, i.e. first order.

3.7.2 Collisional Verlet Algorithm for Hard Spheres

A method was given in [184] based on a modified collision procedure which greatly reduces the error growth.

The idea is to make use of the quadratic

$$\mathbf{Q}(t) = \mathbf{q} + t\mathbf{M}^{-1}\mathbf{p} - \frac{t^2}{2}\mathbf{M}^{-1}\nabla U(\mathbf{q}) \quad (3.18)$$

which represents the position vector obtained from a Verlet step of size t . Note that this defines quadratic paths for all particles in the system. It is then possible to calculate the collision times by solving equations

$$\|\mathbf{Q}_i(t) - \mathbf{Q}_j(t)\| = \sigma_i + \sigma_j, \quad i \neq j. \quad (3.19)$$

A step can then be taken to the first point of subsequent collision, with positions updated using the quadratic and momenta adjusted according to the Verlet map combined with \mathcal{R}_c . In this way, all steps taken are Verlet steps so the order of accuracy is two. Effectively, this is a Verlet method with variable timestep chosen to match collision times. A maximum outer stepsize h_{\max} is incorporated to prevent too-large steps from being taken (in case collisions are infrequent). We write the method here in a slightly different form than in [184]: both the stepsize taken and the coordinates are viewed as variables.

Collisional Verlet Algorithm (CVA) [Single Step]

[computes h (the timestep) and (\mathbf{Q}, \mathbf{P}) given a starting point (\mathbf{q}, \mathbf{p})]

Calculate τ_c the time of next collision from the Verlet paths (quadratics) of (3.18) using collision conditions (3.19).

If $\tau_c < h_{\max}$, then

$$\begin{aligned} h &:= \tau_c \\ (\mathbf{Q}, \mathbf{P}) &:= \mathcal{R}_c \mathcal{G}_h^{\text{Verlet}}(\mathbf{q}, \mathbf{p}) \end{aligned}$$

else

$$\begin{aligned} h &:= h_{\max} \\ (\mathbf{Q}, \mathbf{P}) &:= \mathcal{G}_h^{\text{Verlet}}(\mathbf{q}, \mathbf{p}) \end{aligned}$$

An alternative to Verlet could be used for propagation between collisions, but it is likely that the collision computations would then become more costly.

If the Verlet method is used, then it turns out that the insertion of (3.18) into (3.19) results in a quartic polynomial that must be solved for each particle pair. Care must be taken in solving these quartics to ensure that roots are not missed. Using hash tables, neighbor lists and similar methods (like those used to compute non-bonded forces), the number of computations can be greatly reduced. Importantly, the calculations needed are all explicit and finite (no iteration is needed).

Timestepping then proceeds as usual, with the slight modification that the time between steps will vary throughout integration. Numerical results with this method reported in [184] are very favorable.

3.7.3 Enhancements of the Collisional Verlet Method

A further idea introduced in [184] was to use a force decoupling strategy to reduce the cost of computations. The idea is to exploit the observation that impulsive forces (“kicks”) can be supplied without reducing the order of accuracy as long as these have a vanishing component in the direction of the collision vector \mathbf{u}_\perp , that is if $\mathbf{F}_\perp = -\nabla U(\mathbf{q}_c) \cdot \mathbf{u}_\perp = 0$. This can be achieved in systems of spheres with pair potentials φ_{ij} only by writing $\varphi_{ij} = \alpha_{ij} + \beta_{ij}$ where the derivative of the second term is chosen to vanish at the point of contact between the spheres, i.e. $\alpha'_{ij}(\sigma_i + \sigma_j) = 0$. If this decomposition is used, then it is possible to build a 2nd order accurate hybrid method that uses only the first part α to define the quadratic Verlet paths for the collision detection scheme, whereas β is introduced as a standard “kick” at collision points.

In Collisional Verlet, the momenta are adjusted at the collision point to preserve the kinetic energy (and hence the total energy). It is possible to project to some other manifold using projection techniques like those mentioned previously, as discussed in [40]. In particular, one may use the backward error analysis to obtain a modified Hamiltonian \tilde{H}_h corresponding to the Verlet method with stepsize h , then to project during collisions not onto the energy surface, but onto the modified energy surface, so that

$$\tilde{H}_h \equiv \text{const.}$$

(In practice, a low order approximation of \tilde{H}_h is used, such as the truncation to terms of order four or six in the stepsize.) The resulting method substantially exhibits higher accuracy than the standard Collisional Verlet method in long term simulations, including accurate recovery of statistical properties (for example velocity autocorrelation functions). Additional cost is, however, involved in the handling of the collisions.

Other methods for hard sphere molecular dynamics and polymer modelling based on variational integration strategies, as well as comparative discussion, are provided in [235].

Exercises

1. Consider the solutions of

$$a^2x^2 + \varepsilon xy + b^2y^2 = 1$$

for a, b, ε real coefficients.

- a. Show that for ε sufficiently small the equation describes an ellipse.
 - b. Determine the angle of rotation and major and minor axes as a function of ε .
 - c. Apply this result to the example of Sect. 3.1.
2. The Verlet method applied to the harmonic oscillator $H = p^2/2 + \Omega^2q^2/2$ results in a linear transformation of the form

$$Q = q + hp - \frac{h^2\Omega^2}{2}q, \quad P = p - \frac{h\Omega^2}{2}[q + Q].$$

- a. By solving the equations, rewrite this as an explicit mapping, i.e. determine the matrix \mathbf{T} such that

$$\begin{bmatrix} Q \\ P \end{bmatrix} = \mathbf{T} \begin{bmatrix} q \\ p \end{bmatrix}.$$

- b. Show that $\det \mathbf{T} = 1$.
c. Show that \mathbf{T} is a symplectic matrix, i.e.,

$$\mathbf{T}^T \mathbf{J} \mathbf{T} = \mathbf{J}, \quad \mathbf{J} = \begin{bmatrix} 0 & 1 \\ -1 & 0 \end{bmatrix}.$$

- d. Introducing the rescaling $\tilde{Q} = \Omega Q$, $\tilde{q} = \Omega q$, show that one Verlet step may be written in the form

$$\begin{bmatrix} \tilde{Q} \\ P \end{bmatrix} = \tilde{\mathbf{T}} \begin{bmatrix} \tilde{q} \\ p \end{bmatrix},$$

where $\tilde{\mathbf{T}} = \mathbf{D}\mathbf{R}\mathbf{D}^{-1}$ where

$$\mathbf{D} = \begin{bmatrix} 1 & 0 \\ 0 & \cos(\theta/2) \end{bmatrix}, \quad \mathbf{R} = \begin{bmatrix} \cos(\theta) & \sin(\theta) \\ -\sin(\theta) & \cos(\theta) \end{bmatrix},$$

and $\theta = 2 \arcsin(\Omega h/2)$, for $h\Omega \leq 2$. Explain how this observation relates to the backward error analysis. Compare with the exact solution of the harmonic oscillator through a time interval of size h . [Note that \mathbf{D} may be viewed as a stretch, while \mathbf{R} is a planar rotation through angle θ .]

3. Verify the Jacobi identity

$$\{\{F, G\}, H\} + \{\{H, F\}, G\} + \{\{G, H\}, F\} = 0,$$

where $\{F, G\}$ is the Poisson bracket of the functions F and G .

4. Write out the update schemes Yoshida high-order methods of order 6 and 8. How many force evaluations are required per iteration?
5. Show that, for A and B two noncommuting operators,

$$e^{\frac{h}{2}A} e^{hB} e^{\frac{h}{2}A} = e^{h(A+B)} + \mathcal{O}(h^3).$$

6. Show that any Runge-Kutta method is affine invariant, thus the Trapezoidal Rule is time-reversible.
7. Show that any splitting method for Hamiltonian systems is affine invariant, thus the Verlet method is time-reversible.
- 8 **Shear Transformations.** A shear transformation is one of the form $(q, p) \mapsto (q + a(p), p)$. Show that any such transformation is area preserving.
- 9 **Simplified Takahashi-Imada Method.** The following method was first given by Wisdom, Holman and Touma [397]:

$$\begin{aligned}\hat{\mathbf{P}} &:= \mathbf{p} - \frac{h}{2} \nabla U(\mathbf{q} + \frac{1}{12} h^2 \mathbf{M}^{-1} \nabla U(\mathbf{q})), \\ \mathbf{Q} &:= \mathbf{q} + h \mathbf{M}^{-1} \hat{\mathbf{P}}, \\ \mathbf{P} &:= \hat{\mathbf{P}} - \frac{h}{2} \nabla U(\mathbf{Q} + \frac{1}{12} h^2 \mathbf{M}^{-1} \nabla U(\mathbf{Q})).\end{aligned}$$

Show that this method is time-reversible, volume-preserving (see Exercise 8), and is a (locally) $\mathcal{O}(h^5)$ perturbation of the Takahashi-Imada method. Hint: the order can be determined by Taylor-expanding the force evaluations.

Chapter 4

The Stability Threshold

Let us recall the method of studying the asymptotic numerical stability of a linear system

$$\dot{\mathbf{z}} = \mathbf{A}\mathbf{z}, \quad (4.1)$$

where $\mathbf{z} \in \mathbb{R}^m$, $\mathbf{A} \in \mathbb{R}^{m \times m}$, when solved by a numerical method. Typically one shows that under generic conditions analyzing the asymptotic behavior of the numerical method for solving the system can be related to analyzing scalar equations defined via an eigendecomposition of \mathbf{A} , that is, for the purposes of stability analysis, we may replace the system (4.1) by m scalar equations of the form $\dot{u} = \lambda u$ where λ is an eigenvalue of \mathbf{A} . Here λ , hence u may in general be complex. Then one applies the numerical method directly to the scalar equation. For example Euler's method yields

$$u_{n+1} = (1 + h\lambda)u_n.$$

The iteration is stable if $|u_n|$ remains bounded as $n \rightarrow \infty$, implying the following condition for asymptotic stability:

$$|1 + h\lambda| \leq 1.$$

This defines the “stability region” for Euler's method as a disk in the complex $h\lambda$ -plane centered around -1 of radius 1. This region is shown in Fig. 4.1. If $h\lambda$, where λ is an eigenvalue of \mathbf{A} lies in the indicated stability region, then Euler's method will be stable for the linear system $\dot{\mathbf{z}} = \mathbf{A}\mathbf{z}$.

If we consider applying this technique to the harmonic oscillator $\dot{q} = p; \dot{p} = -\Omega^2 q$, then the matrix \mathbf{A} is

$$\mathbf{A} = \begin{bmatrix} 0 & I \\ -\Omega^2 & 0 \end{bmatrix}.$$

The eigenvalues are $\pm i\omega$. The reason a method like Euler's method can never perform well for molecular dynamics is that molecular dynamics is a Hamiltonian system and at the bottoms of basins on the energy surface, which correspond to stable centers, we expect all the eigenvalues of a local linearization of the problem to be purely imaginary. The stability condition always fails to hold and, for Euler's method, z_n grows exponentially rapidly away from the equilibrium point.

Let us perform a similar analysis for the Symplectic Euler method. Because Symplectic Euler cannot be applied to scalar equations (due to its partitioned structure) we must work directly with the second order system, but this is straightforward for the harmonic oscillator. The timestep map is defined by

$$\begin{aligned} Q &= q + hP, \\ P &= p - h\Omega^2 q. \end{aligned}$$

Solving for Q, P this yields

$$\begin{bmatrix} Q \\ P \end{bmatrix} = \begin{bmatrix} 1 - h^2\Omega^2 & h \\ -h\Omega^2 & 1 \end{bmatrix} \begin{bmatrix} q \\ p \end{bmatrix}.$$

The eigenvalues of the matrix are easily found, they are

$$\lambda_{1,2} = 1 - \frac{h^2\Omega^2}{2} \pm \frac{1}{2}\sqrt{h^4\Omega^4 - 4h^2\Omega^2}.$$

Then we observe that for $h^2\Omega^2 \leq 4$, they are complex and their squared magnitude is

$$|\lambda_{1,2}|^2 = \left(1 - \frac{h^2\Omega^2}{2}\right)^2 + \frac{1}{4}(4h^2\Omega^2 - h^4\Omega^4) = 1,$$

thus both eigenvalues lie on the unit circle in the complex plane as long as

$$h\Omega \leq 2.$$

This is the so-called linear stability condition of the Symplectic Euler method: if $h\Omega \leq 2$ the integrator is stable. When $h\Omega > 2$, the eigenvalues of the discretization method are both real, with one strictly inside and one strictly outside the unit circle. This implies that the method will exhibit exponentially growing solutions. We say that the *stability threshold* of the Symplectic Euler method is $2/\Omega$.

Among explicit symplectic Partitioned Runge-Kutta methods this is the maximum stability threshold [74]. In a similar way one can analyze the stability of the Verlet and other methods and one thus obtains conditions on the stepsize that must hold for the equilibrium points to be stable in the linearization. Analyzing the stability of both continuous and discrete iteration is much more complicated for

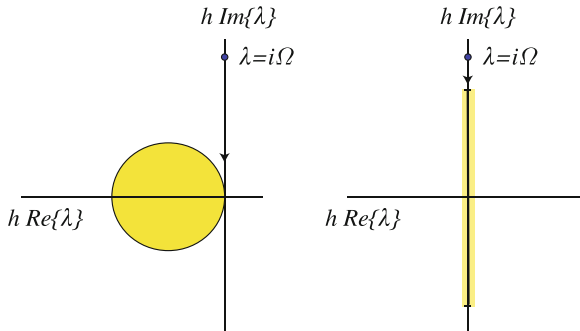


Fig. 4.1 Stability regions for Euler's method (left) and Symplectic Euler/Verlet (right). When a harmonic oscillator is treated using these methods, the origin is unstable for Euler's method, regardless of stepsize—this means that there is no choice of scaling h which will allow us to ensure that $|1 + h\lambda| \leq 1$. On the other hand, the Verlet method has an interval of stability on the imaginary axis, and it is always possible to find a value of h which guarantees that $|h\Omega| \leq 2$

general nonlinear systems. It is possible for the linearized system to be stable and for the equilibrium point nonetheless to be unstable, since, with Hamiltonian systems, we typically encounter the purely imaginary eigenvalue case, but the linearized analysis is nonetheless helpful. For example, applying the Verlet method to the harmonic oscillator with frequency Ω we find that the origin is stable (and the numerical solution stays bounded for all time) provided $h\Omega \leq 2$ (the same condition as for stability of Symplectic Euler). The situation with regard to Euler and Verlet (or Symplectic Euler) methods for the harmonic oscillator is illustrated in Fig. 4.1.

In the context of molecular dynamics involving chemical bonds, the linear stability condition $h\Omega \leq 2$ is often quoted as the stepsize limiting condition where Ω is assumed to be the frequency of the fastest (highest energy) bond stretch, Ω_F , present in the molecular dynamics model. This is realistic because the bond stretches are the highest frequency components in general in these models, and the potential energy function used for the bond stretch is typically quadratic in the separation distance:

$$U_{\text{bond}}(\mathbf{q}_i, \mathbf{q}_j) = \frac{\kappa}{2} (\|\mathbf{q}_i - \mathbf{q}_j\| - l_{ij})^2,$$

for positive parameters κ and l_{ij} . It should be noted that even this term leads to a nonlinear differential equation system and so the relation to the harmonic model should be understood as being of a heuristic nature; it is only through numerical experiment that the correspondence is ultimately established.

More generally, even without the presence of bonds, the “stepsize threshold” in the simulation of molecular models by an explicit method like Verlet arises because of the shape of the energy surface. The understanding of this for a nonlinear system like the Lennard-Jones cluster requires examining the linearization of the problem near equilibrium points and even then the discussion is always quite technical

(and, in a certain sense, incomplete, since anharmonicity can produce an unstable dynamic from a stable linearized problem). Nevertheless such a stability threshold can be found by numerical experiment and it can be verified that this is not too far from the stability threshold that would correspond to a model linearized at equilibrium points.

The only way to increase the stability threshold is by introducing implicitness or by changing in some fundamental way the timestepping framework. We consider some alternatives below.

4.1 Implicit Schemes

By introducing a coordinate transformation, we may reduce the harmonic oscillator system to a pair of decoupled complex scalar ODEs of the form

$$\dot{z} = \pm i\Omega z.$$

Applying a Runge-Kutta method to such a linear system allows direct determination of the stability condition. For example, Euler's method would yield

$$z_{n+1} = (1 \pm ih\Omega)z_n,$$

which exhibits a growing solution $|z_{n+1}| = (1 + h^2\Omega^2)^{n/2} |z_0|$.

The Implicit Midpoint method which, for the ODE $\dot{z} = f(z)$ takes the form

$$z_{n+1} = z_n + h \frac{f(z_n) + f(z_{n+1})}{2},$$

can be applied to $\dot{z} = i\Omega z$ and yields

$$z_{n+1} = \frac{1 + ih\Omega/2}{1 - ih\Omega/2} z_n.$$

For all real Ω , we find

$$\left| \frac{1 + ih\Omega/2}{1 - ih\Omega/2} \right| = 1.$$

This indicates that the Implicit Midpoint method has no stability threshold for the stepsize when solving a linear system! This remarkable property may inspire some optimism that Implicit Midpoint would allow much larger stepsize in molecular dynamics simulation than does Verlet.

In actual practice, this does not work out quite as expected. To understand why not, we need to recognize that the linear stability condition only describes the

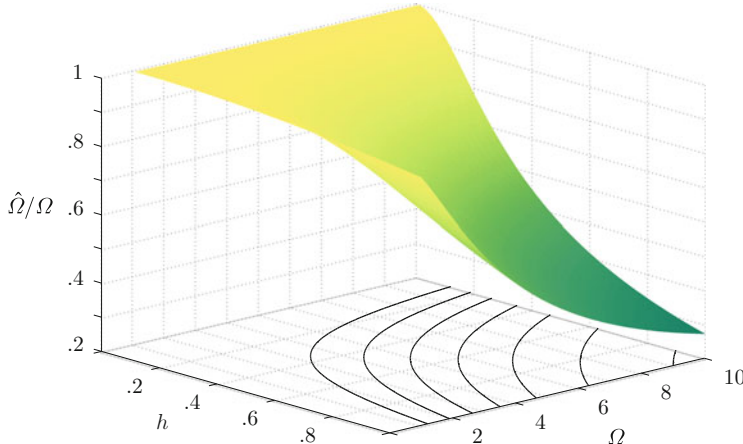


Fig. 4.2 The frequency ratio $\hat{\Omega}/\Omega$ for the Implicit Midpoint method. A frequency ratio of 1 indicates that the phase of the harmonic oscillator is accurate

boundedness of the timestepping iteration, and then only at the point of linearization. Other issues are often in play.

If the Implicit Midpoint method is viewed as the exact solution of a perturbed harmonic oscillator, then the frequency of this oscillator is

$$\hat{\Omega} = \frac{1}{ih} \ln \frac{1 + ih\Omega/2}{1 - ih\Omega/2}.$$

In the diagram below (Fig. 4.2), we plot the ratio $\hat{\Omega}/\Omega$ against h and Ω . If this ratio is 1, the frequency is accurately represented. The figure shows that the frequency is only well approximated in case $h\Omega$ is sufficiently small. For $h\Omega \gg 1$ the frequency is highly modified. From this we might infer that a molecular dynamics simulation performed using the Implicit Midpoint method is only likely to be accurate in terms of resolution of temporally correlated quantities in case $h\Omega$ is relatively small.

The inaccuracy of phase contributions computed using an implicit method with large stepsize (much larger than the Verlet stability threshold, i.e. $h \gg 2/\Omega$) may, in complicated systems, have additional consequences for error growth. For example, consider a large harmonic system with slow and fast dynamical components. The frequency ratio shown in Fig. 4.2 suggests that, when using larger timesteps, the most severe errors will be introduced in approximating the fast variables. The modification of frequencies will mean that these components will resonate (in a nonphysical way) with the low frequency components, thus we would anticipate a rapid propagation of errors from fast components into slow variables (in practice an error in the bond stretch may lead, on a rapid timescale, to propagation into a dihedral bend). We refer the interested reader to more in-depth treatments of these issues [17, 152] for more details.

When we apply a method such as Implicit Midpoint to a nonlinear molecular dynamics problem, we may reduce the equations to determining midpoint values $\hat{\mathbf{q}}$, $\hat{\mathbf{p}}$ such that

$$\hat{\mathbf{q}} = \mathbf{q}_n + \frac{h}{2} \mathbf{M}^{-1} \hat{\mathbf{p}}, \quad \hat{\mathbf{p}} = \mathbf{p}_n - \frac{h}{2} \nabla U(\hat{\mathbf{q}}),$$

where, then,

$$\mathbf{q}_{n+1} = \hat{\mathbf{q}} + \frac{h}{2} \mathbf{M}^{-1} \hat{\mathbf{p}}, \quad \mathbf{p}_{n+1} = \hat{\mathbf{p}} - \frac{h}{2} \nabla U(\hat{\mathbf{q}}).$$

We may therefore view the step as a composition of Implicit Euler and Explicit Euler half-steps. Eliminating $\hat{\mathbf{p}}$, we find

$$\hat{\mathbf{q}} = \mathbf{q}_n + \frac{h}{2} \mathbf{M}^{-1} \mathbf{p}_n - \frac{h^2}{4} \mathbf{M}^{-1} \nabla U(\hat{\mathbf{q}}).$$

This is a nonlinear system of equations for $\hat{\mathbf{q}}$. There is no avoiding the substantial challenge of solving this system. In principle this can be achieved using various iterative methods, such as the Gauss-Newton method. In case the forces are long-ranged (e.g. due to Coulombic terms) the cost of a single iteration will include the cost of a force evaluation, although we must also cope with numerically solving a system of linear equations for the update. In order to benefit from the symplectic property of the Implicit Midpoint method, the iteration must be performed to high accuracy (i.e. several iterations will typically be needed), otherwise one will observe growing errors in energy and trajectory accuracy. Given the accuracy issue associated to using large stepsizes due to the corruption of the phase, the possible gain from using an implicit method is found to be limited and methods like this are rarely encountered in molecular modelling applications. An exception are the methods used in handling constrained systems (see Section 4.3, below).

4.2 Multiple Timestepping

The stringency of the timestep threshold and the failure of implicit methods to address the issue have led to alternative proposals for ameliorating the instability in molecular dynamics, in particular the method of “multiple timestepping” which we next describe. Variants of this method were described in a series of papers in the early 1990s by Tuckerman and Berne [374] and Tuckerman et al. [375, 377]. A simultaneous development by Grubmüller et al. [158] most closely matches the presentation given here. The first resonance analysis is due to Biesiadecki and Skeel [35].

4.2.1 The Reversible RESPA Scheme

In many molecular dynamics applications, the system may be decomposed as $H(\mathbf{q}, \mathbf{p}) = \mathbf{p}^T \mathbf{M}^{-1} \mathbf{p}/2 + U_S(\mathbf{q}) + U_F(\mathbf{q})$ where U_S is a “soft” potential, in which the natural motion would be relatively slow, whereas U_F is a much stronger term which would give rise to relatively rapid motion. We further suppose U_S (with its gradient) is expensive to compute, perhaps because it involves many terms, whereas U_F is relatively simple. Because U_F requires small timesteps, we think of separating the calculation of a timestep, typically in a symmetric form. Let \mathcal{G}_h^F denote the map associated to the Verlet method for the system without U_S , using a stepsize h :

$$\mathcal{G}_h^F = e^{\frac{h}{2}\mathcal{L}_{U_F}} e^{h\mathcal{L}_K} e^{\frac{h}{2}\mathcal{L}_{U_F}},$$

where \mathcal{L}_K is the Lie-derivative corresponding to the kinetic energy component of the Hamiltonian ($K = \mathbf{p}^T \mathbf{M}^{-1} \mathbf{p}/2$). Now consider the map constructed by taking r steps using $\mathcal{G}_{F,h/r}$ and composing this with kicks from the soft force:

$$\mathcal{G}_h^{\text{MTS}} = e^{\frac{h}{2}\mathcal{L}_{U_S}} [\mathcal{G}_{F,h/r}^F]^r e^{\frac{h}{2}\mathcal{L}_{U_S}}.$$

One step of the multiple timestepping algorithm is then implemented as follows:

Reversible RESPA Algorithm

$$\mathbf{P} := \mathbf{p} - (h/2)\nabla U_S(\mathbf{q}),$$

$$\mathbf{Q} := \mathbf{q},$$

Repeat r times:

$$\left| \begin{array}{l} \mathbf{P} := \mathbf{P} - (h/2)\nabla U_F(\mathbf{Q})/r, \\ \mathbf{Q} := \mathbf{Q} + h\mathbf{M}^{-1}\mathbf{P}/r, \\ \mathbf{P} := \mathbf{P} - (h/2)\nabla U_F(\mathbf{Q})/r, \end{array} \right. \quad (4.2)$$

$$\mathbf{P} := \mathbf{P} - (h/2)\nabla U_S(\mathbf{Q}).$$

Multiple timestepping is widely used for efficiency purposes in systems with expensive force computations, but it should be used cautiously. To illustrate the potential dangers of multiple timestepping, one need only consider its application to a linear one-DOF model problem

$$H(q, p) = p^2/2 + U_S(q) + U_F(q), \quad U_S(q) = q^2/2, \quad U_F(q) = \Omega^2 q^2/2,$$

where it is assumed that $\Omega \gg 1$. The differential equations describing this system are

$$\begin{aligned}\dot{q} &= p, \\ \dot{p} &= -(1 + \Omega^2)q.\end{aligned}$$

The frequency is therefore $\bar{\Omega} = \sqrt{1 + \Omega^2}$. In the limit of small inner step, we solve the system with Hamiltonian $H_F = p^2/2 + \Omega^2 q^2/2$ exactly, meanwhile punctuating with impulses from U_S , thus the MTS flow map approximation, which is linear in this case, can be written in the form of a matrix-vector multiply

$$\begin{bmatrix} \mathcal{Q} \\ P \end{bmatrix} = \mathbf{W}_h \begin{bmatrix} q \\ p \end{bmatrix},$$

where

$$\mathbf{W}_h = \mathbf{S}_{h/2} \mathbf{F}_h \mathbf{S}_{h/2},$$

with

$$\mathbf{S}_h = \begin{bmatrix} 1 & 0 \\ -h & 1 \end{bmatrix}, \quad \mathbf{F}_h = \begin{bmatrix} \cos(\Omega h) & \Omega^{-1} \sin(\Omega h) \\ -\Omega \sin(\Omega h) & \cos(\Omega h) \end{bmatrix}.$$

Both of these matrices have unit determinant for any h , so the product of the eigenvalues of \mathbf{W}_h is 1. On the other hand, a short calculation shows that

$$\lambda_1 + \lambda_2 = \text{Tr}(\mathbf{W}_h) = 2 \cos(h\Omega) - \frac{h}{\Omega} \sin(h\Omega).$$

For a given h , the eigenvalues of \mathbf{W}_h are either complex conjugates or they are real and reciprocal to one another. If they are complex conjugates with nonzero imaginary part, then we have $\lambda_1 \lambda_2 = \lambda_1 \bar{\lambda}_1 = 1$, so $|\lambda_1| = 1$ and the two eigenvalues are clearly distinct and on the unit circle in the complex plane.

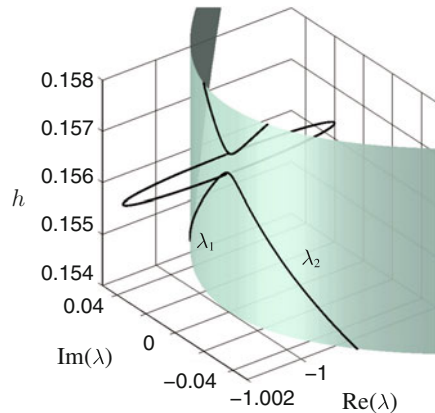
If we consider a relatively small step of size $h\Omega = k\pi$ we find that the eigenvalues cross, and the system is unstable. For example, at $h = \pi/\Omega$, we have

$$\mathbf{F}_h = -\mathbf{I} \Rightarrow \mathbf{W}_h = -\mathbf{S}_{h/2}^2 = -\begin{bmatrix} 1 & 0 \\ -h & 1 \end{bmatrix},$$

so that

$$\mathbf{W}_h^n = (-1)^n \begin{bmatrix} 1 & 0 \\ -nh & 1 \end{bmatrix},$$

Fig. 4.3 Eigenvalues of the simple multiple timestepping method. The eigenvalues coil around the surface of the cylinder $|\lambda| = 1$ except at exceptional points near $k\pi/\Omega$, where $k \in \mathbb{Z}$. Near these points of resonance, exponential instabilities are present



and the norm of the solution will oscillate and grow linearly with n as $n \rightarrow \infty$. This is the simplest type of *linear resonance* present in multiple timestepping. The resonance at $h = \pi/\Omega$ only gives rise to a relatively weak ‘linear’ instability, but what is more serious is that in the vicinity of $h = \pi/\Omega$ the eigenvalues actually leave the unit circle. We can see this by expanding $\mu(h) = 2 \cos(h\Omega) - \frac{h}{\Omega} \sin(h\Omega)$ in a Taylor expansion around $h = \pi/\Omega$:

$$\mu(h) = -2 + \varepsilon, \quad \varepsilon = \frac{\pi}{\Omega}(h - \pi/\Omega).$$

Both eigenvalues satisfy

$$\lambda + \lambda^{-1} = -2 + \varepsilon + \mathcal{O}(\varepsilon^2).$$

In case $\varepsilon > 0$, i.e. *after* $h = \pi/\Omega$, we have complex eigenvalues and we already know this case to be stable. For $\varepsilon < 0$, however, we have

$$\lambda = -1 \pm (|\varepsilon|/2)^{1/2} + \mathcal{O}(\varepsilon).$$

Here both eigenvalues are real and one is outside the unit circle. There is thus a small interval of *exponential* instability directly below $h = \pi/\Omega$.

We can easily solve for the two eigenvalues as functions of h and graph them as points in three dimensions: $x = \text{Re}(\lambda)$, $y = \text{Im}(\lambda)$, $z = h$ (Fig. 4.3). Such resonances will also occur at integer multiples of π/Ω , and we can therefore expect many small intervals in the stepsize where the multiple timestepping method is unstable. When a large system involves a combination of many different interactions, the intervals of instability would expect to proliferate from all the different natural frequencies.

A linear resonance is a rational relationship between the period of the harmonic oscillator and the timestep used in simulation. If we substitute a nonlinear oscillator

for the harmonic one, then we encounter more complicated *nonlinear resonances*. It is challenging (perhaps impossible) to analyze the destabilizing effect of such resonances in a general molecular dynamics setting, but it is possible to do so in some cases for low-dimensional model problems [247, 329, 339].

In practice the presence of resonances may or may not render the multiple timestepping technique ineffective. One would be concerned if the only gain were from the Verlet stability threshold at $\bar{h}_{\text{Verlet}} = 2/\Omega$ to the location of the first resonance peak at $\bar{h}_{\text{MTS}} = \pi/\Omega$, since the multiple timestepping method introduces additional complexity. However, the picture is complicated by the observation that the strength of the leading resonance is often modest, so the growth observed in practice may be slow and, depending on the nature of the coupling of the variables of the system (which depends on details of the potential energy functions, natural coupling of the modes of the system, and the presence of solvent molecules which may introduce a stochastic effect) the growth of error due to resonance may be masked by other factors of a strongly system-dependent nature. Moreover, molecular systems are often subject to a stochastic thermostat (a topic to be addressed in later chapters) which may further alter the role of the resonances. Thus the study of the effect of linear and nonlinear resonance peaks on the error in molecular dynamics simulation becomes quickly a numerical issue which must be investigated using carefully crafted experiments. The analysis of [245] clearly raises some concerns regarding the use of multiple timestepping in molecular simulation, in particular they suggest that the usable gain from RESPA simulations in systems with detailed solvent (water) is only around a factor of $\pi/2$ compared what can be achieved using a standard integrator such as Verlet (similar what would be suggested by resonance analysis). Nevertheless there are practical examples where multiple timestepping is used, especially in schemes incorporating stochastic perturbation and with relatively strong scale separation, as when multiple timestepping is combined with the particle-mesh Ewald summation long-ranged force computation technique. In Sect. 7.13 we discuss the use of multiple timestepping in connection with Langevin dynamics. In Sect. 8.6, we describe the combination of multiple timestepping with isokinetic constraints and stochastic perturbation, where very substantial increases in outer timestep are found to be possible.

4.2.2 *The Mollified Impulse Method*

The onset of instability of multiple timestepping is a consequence of introducing periodic impulses (via slow force updates) in resonance with a natural frequency of the system. As a means of avoiding or at least ameliorating the effect of resonances, it has been proposed to modify the points at which the slow forces in multiple timestepping are evaluated. The *mollified impulse method* (MOLLY) [141] is a form of multiple timestepping in which the potential energy function is modified based on an averaging of the position variable (over fast dynamics) in such a way as to filter out destabilizing excitations. Effectively, one replaces $U_S(\mathbf{q})$ wherever it appears

within the MTS method by a modified potential function $\bar{U}(\mathbf{q}) \stackrel{\text{def}}{=} U_S(\mathcal{A}(\mathbf{q}))$. The mapping $\mathcal{A}(\mathbf{q})$ is defined by reference to the fast dynamics, e.g. by the weighted average

$$\mathcal{A}(\mathbf{q}) = \frac{1}{K+1} \sum_{i=0}^K \phi_i \boldsymbol{\theta}_i(\mathbf{q}),$$

where the $\boldsymbol{\theta}_i$ are defined recursively by solving the system with Hamiltonian

$$H^{\text{fast}}(\mathbf{q}, \mathbf{p}) = \mathbf{p}^T \mathbf{M}^{-1} \mathbf{p} / 2 + U_F(\mathbf{q})$$

starting from initial position \mathbf{q} and zero initial momentum \mathbf{p} , for K timesteps using a small stepsize τ_f . This small step does not have to be directly related to the timestep used for integrating the fast dynamics within the MTS scheme; it is only used for the averaging procedure. The resulting sequence of $\boldsymbol{\theta}_i$ clearly are functions of \mathbf{q} only and so \mathcal{A} is well defined. The weights ϕ_i appearing in the average may be selected in various ways. The initialization of the calculation of the $\boldsymbol{\theta}_i$ can, moreover, be modified by various alternative \mathbf{q} -dependent proposals, or may be randomized.

An alternative, simpler, and probably more robust, procedure is simply to fix the value of $\mathcal{A}(\mathbf{q})$ by constraining \mathbf{q} to its mechanical equilibrium value [189] in which case no fast averaging whatsoever needs to be performed. This approach relies on the use of the SHAKE method of constrained molecular dynamics (see the following section).

In each of the mollified multiple timestepping methods, since only the potential energy is modified, and by a smooth mapping of positions, the forces derived by differentiating \bar{U} are still conservative, and, just as with the MTS method, the scheme remains symplectic.

The mollification is only applied for the purpose of modifying the slow impulse and the mollified methods are in other ways identical to multiple timestepping. These schemes appear to confer some distinct advantage in the large stepsize in molecular dynamics. For example where a detailed and fully flexible molecular model of a solvated biomolecule might require stepsizes of 2 fs in a Verlet simulation, mollified impulse methods may allow increases to 6 fs [189] in the ‘large’ timestep, i.e. the period between reevaluations of the slow forces. This benefit may be substantial in simulations of large systems.

4.3 Methods for Constrained Dynamics

Constraints are used frequently in molecular modelling. By a constraint, we mean a modification of a dynamical system to maintain the constancy of a given function of coordinates (or coordinates and momenta). In this section we consider *holonomic* constraints which may be expressed in terms of positions only, and perhaps time,

i.e.

$$g(\mathbf{q}, t) = 0. \quad (4.3)$$

Note that by differentiating (4.3) with respect to time, we obtain $\nabla_{\mathbf{q}} g(\mathbf{q}, t) \cdot \dot{\mathbf{q}} + \partial g / \partial t = 0$ which involves velocities. The definition of holonomic constraints thus includes equations which relate positions and momenta, but only where these are, through the differential equations, equivalent to equations involving positions only (4.3). For more details on constrained dynamics, see for example [67, 79, 83, 164, 227, 249].

An important type of holonomic constraint arising in molecular dynamics relates to bond vibration. Recall that the stretch of a chemical bond between two atoms gives rise to a potential energy contribution of the form

$$\varphi(r) = \frac{k}{2}(r - r_0)^2,$$

where r would typically represent the distance between a pair of atoms, say atoms i and j , $r = \|\mathbf{q}_i - \mathbf{q}_j\|$. The strong chemical bond stretches involving hydrogens and various heavier atoms such as nitrogen and carbon give rise to the most rapid modes present in the atomic motion. As we have seen, a harmonic oscillator with frequency Ω , when solved using the Verlet method, has a stability restriction of the form

$$h < \frac{2}{\Omega}.$$

One approach to addressing these stiff terms is to use a multiple timestepping method. A more direct approach is to introduce constraints to simply remove the stiff bond stretches. This makes sense if (a) the motion of the constrained system can be simulated using larger timesteps and (b) the rigidification of certain vibrational terms does not significantly alter the thermodynamic or dynamic properties of interest to the modeller.

To illustrate the progression from vibrational model to constrained model, one may consider a single particle subject to a potential $U(\mathbf{q})$ as well as an additional stiff restraint. We suppose the restraint to have an associated coefficient $k = \varepsilon^{-1}$, where ε is a small parameter. Then we have a generalized flexible pendulum with Hamiltonian $H = \|\mathbf{p}\|^2/(2m) + U(\mathbf{q}) + \varepsilon^{-1}(\|\mathbf{q}\| - r_0)^2/2$ (see the left panel of Fig. 4.4). The differential equations describing this model are

$$\begin{aligned} \dot{\mathbf{q}} &= m^{-1}\mathbf{p}, \\ \dot{\mathbf{p}} &= -\nabla U(\mathbf{q}) - \nabla\varphi_\varepsilon(\mathbf{q}), \end{aligned}$$

where the restraint potential $\varphi_\varepsilon(\mathbf{q}) = \varepsilon^{-1}(\|\mathbf{q}\| - r_0)^2/2$ has associated restoring force

$$\mathbf{F}_\varepsilon = -\nabla\varphi_\varepsilon(\mathbf{q}) = \varphi_\varepsilon(\mathbf{q}).$$

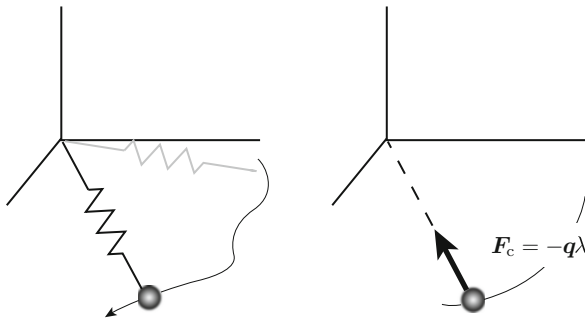


Fig. 4.4 *Left:* a flexible pendulum model; the bob moves on a path under some applied force defined by the potential U and the stiff spring holding the bob near a fixed distance from the origin. *Right:* a constrained version of the same model, where the spring has been replaced with a rod; the tension in the rod acts on the bob so as to maintain a precise fixed distance from the origin

To formulate a constrained model we use Gauss's principle of least constraint which says that the force \mathbf{F}_c needed to compensate for the presence of a constraint of the form

$$g(\mathbf{q}) \stackrel{\text{def}}{=} \|\mathbf{q}\|^2 - r_0^2 = 0$$

will be transverse to the tangent space of the manifold $\{\mathbf{q} | g(\mathbf{q}) = 0\}$, that is, it must point in the normal direction

$$\mathbf{F}_c = -\mathbf{q}\lambda,$$

where $\lambda \in \mathbb{R}$ will vary over time so that the force \mathbf{F}_c represents the tension in the stiff rod holding the pendulum bob to the origin (right panel of Fig. 4.4) The equations of motion for the constrained system take the form

$$\begin{aligned} \dot{\mathbf{q}} &= \mathbf{v}, \\ \dot{\mathbf{v}} &= -\nabla U(\mathbf{q}) - \mathbf{q}\lambda, \\ 0 &= \|\mathbf{q}\|^2 - r_0^2. \end{aligned}$$

These are called the Euler-Lagrange equations, and they may be derived formally by use of the calculus of variations. We refer to λ , which is a function of time, as a Lagrange multiplier.

More generally, if we have a system with N_c configurational coordinates¹ and l constraints $g_1(\mathbf{q}) = 0, g_2(\mathbf{q}) = 0, \dots, g_l(\mathbf{q}) = 0$, the tension forces due to the

¹Note that with l constraints the actual number of degrees of freedom, which is needed for things like the computation of temperature, is $N_d = N_c - l$.

k th constraint will act in the transverse direction to that constraint, i.e. along the direction of the gradient ∇g_k , and the equations of motion may be written

$$\dot{\mathbf{q}} = \mathbf{M}^{-1}\mathbf{p}, \quad (4.4)$$

$$\dot{\mathbf{p}} = -\nabla U(\mathbf{q}) - \sum_{k=1}^l \lambda_k \nabla g_k(\mathbf{q}), \quad (4.5)$$

$$0 = g_j(\mathbf{q}), \quad j = 1, 2, \dots, l, \quad (4.6)$$

where $\lambda_1, \lambda_2, \dots, \lambda_l$ are the Lagrange multipliers. It is often convenient to combine all the constraints and to describe them by a single vector-valued function $\mathbf{g} : \mathbb{R}^{N_c} \rightarrow \mathbb{R}^l$, then we may write the constrained equations of motion in the form

$$\dot{\mathbf{q}} = \mathbf{M}^{-1}\mathbf{p}, \quad (4.7)$$

$$\dot{\mathbf{p}} = -\nabla U(\mathbf{q}) - \mathbf{g}'(\mathbf{q})^T \boldsymbol{\lambda}, \quad (4.8)$$

$$\mathbf{0} = \mathbf{g}(\mathbf{q}). \quad (4.9)$$

Here $\boldsymbol{\lambda}$ is an l -dimensional vector of Lagrange multipliers.

Constraints such as those described above define a manifold in the configuration space $\mathcal{M} = \{\mathbf{q} | \mathbf{g}(\mathbf{q}) = \mathbf{0}\}$. Given a motion $(\mathbf{q}(t), \mathbf{p}(t), \boldsymbol{\lambda}(t))$ of (4.7)–(4.9) we note that $\mathbf{g}(\mathbf{q}(t)) \equiv \mathbf{0}$ at all times t , hence, by differentiation

$$\mathbf{g}'(\mathbf{q}(t))\dot{\mathbf{q}}(t) \equiv \mathbf{0},$$

which we may rephrase as

$$\mathbf{g}'(\mathbf{q}(t))\mathbf{M}^{-1}\mathbf{p}(t) \equiv \mathbf{0}.$$

Thus while $\mathbf{q} \in \mathcal{M}$, \mathbf{q} and \mathbf{p} together satisfy a separate constraint relationship $\mathbf{g}'(\mathbf{q})\mathbf{M}^{-1}\mathbf{p} = \mathbf{0}$. This is sometimes referred to as a *co-tangency condition* or the *hidden constraint*. The set of pairs (\mathbf{q}, \mathbf{p}) satisfying, simultaneously, the equations

$$\mathbf{g}(\mathbf{q}) = \mathbf{0}, \quad \mathbf{g}'(\mathbf{q})\mathbf{M}^{-1}\mathbf{p} = \mathbf{0},$$

is called the *co-tangent bundle* associated to the manifold \mathcal{M} , and we refer to it as $T^*\mathcal{M}$. The co-tangent bundle is the collection of valid positions and momenta for a holonomically constrained mechanical system; it is the constrained analog of the phase space. The word “co-tangent” refers to the fact that velocities $\mathbf{v} = \dot{\mathbf{q}}$ lie in the tangent space $\mathbf{g}'(\mathbf{q})\mathbf{v} = \mathbf{0}$, whereas the momenta are viewed as “co-vectors,” that is one-forms or linear mappings taking tangent vectors to scalars (through the Euclidean inner product).

The solution of (4.7)–(4.9) evolves on the co-tangent bundle. Along a solution we have $\mathbf{g}'(\mathbf{q}(t))\mathbf{M}^{-1}\mathbf{p}(t) \equiv \mathbf{0}$. If we differentiate this again, we obtain

$$\mathbf{g}'(\mathbf{q}(t))\mathbf{M}^{-1}\dot{\mathbf{p}}(t) + \boldsymbol{\varphi} \equiv \mathbf{0}, \quad (4.10)$$

where φ is an l -dimensional vector whose k th component is

$$\varphi_k = \mathbf{p}(t)^T \mathbf{M}^{-1} \nabla^2 g_k(\mathbf{q}(t)) \mathbf{M}^{-1} \mathbf{p}(t).$$

Using (4.8) in (4.10) we obtain

$$\mathbf{g}'(\mathbf{q}) \mathbf{M}^{-1} [\mathbf{F} - \mathbf{g}'(\mathbf{q})^T \boldsymbol{\lambda}] + \varphi \equiv \mathbf{0},$$

This is a system of linear equations for $\boldsymbol{\lambda}$. Assuming $\mathbf{g}'(\mathbf{q}) \mathbf{M}^{-1} \mathbf{g}'(\mathbf{q})^T$ is invertible, we may solve for $\boldsymbol{\lambda}$. Reinserting this expression for $\boldsymbol{\lambda}$ into (4.8) then gives a system of ordinary differential equations whose solutions, starting from a point on $T^*\mathcal{M}$, will remain on $T^*\mathcal{M}$ for all time. The co-tangent bundle becomes an invariant manifold of this ODE system. $\boldsymbol{\lambda}$ is defined at any time by the physical variables \mathbf{q} and \mathbf{p} .

The presence of such an underlying ordinary differential equation is very useful for conceptual purposes, but in practice it is usually found to be preferable to work directly with the constrained formulation (4.7)–(4.9) for numerical discretization and for describing statistical mechanical properties.

The formulation of Hamiltonian systems with constraints is discussed from various perspectives in [15, 151, 249]. Here, we take a practical perspective on these systems, addressing ourselves only to the issues that are directly relevant for the extension of numerical methods derived in previous chapters to the constrained setting. More detailed treatment of numerical methods for constrained mechanical systems may be found in [164, 227].

4.3.1 Symplectic Structure with Holonomic Constraints

Describing the Hamiltonian structure for a constrained system is a little complicated to do formally. The simplifying concept that we exploit is that the symplectic 2-form in the ambient space can be projected to the co-tangent bundle to define an associated symplectic form on the manifold.

One way to understand the symplecticness of the Hamiltonian flow in the unconstrained case is as follows. Think of the flow map as defining $\mathbf{Z}(t, z) = \mathcal{F}_t(z)$, where we can write the vector $\mathbf{Z}(t, z) = [Z_1(t, z), \dots, Z_{2N_c}(t, z)]$. Then the symplecticness condition is

$$d\mathbf{Z} \wedge \mathbf{J} d\mathbf{Z} = dz \wedge \mathbf{J} dz.$$

Taking the time derivative, as the right hand side is constant we have

$$d\mathbf{Z} \wedge \mathbf{J} \frac{d}{dt}(d\mathbf{Z}) + \frac{d}{dt}(d\mathbf{Z}) \wedge \mathbf{J} d\mathbf{Z} = 0,$$

where

$$dZ_i = \sum_{j=1}^{2N_c} \frac{\partial Z_i}{\partial z_j} dz_j.$$

Taking the derivative with respect to t and defining $\dot{Z}_i = f_i(\mathbf{Z}(t, \mathbf{z}))$, we can see that

$$\begin{aligned} \frac{d}{dt} dZ_i &= \sum_{j=1}^{2N_c} \frac{\partial \dot{Z}_i}{\partial z_j} dz_j \\ &= d\dot{Z}_i. \end{aligned}$$

The symplecticness condition therefore becomes

$$d\mathbf{Z} \wedge \mathbf{J} d\dot{\mathbf{Z}} + d\dot{\mathbf{Z}} \wedge \mathbf{J} d\mathbf{Z} = 0,$$

or, in canonical coordinates,

$$\sum_{j=1}^{N_c} d\dot{q}_j \wedge dp_j + dq_j \wedge d\dot{p}_j = 0,$$

which is essentially a Leibniz differentiation rule for wedge products. The functions \dot{q}_j, \dot{p}_j that appear here are just the components of the vector field.

We next demonstrate that a similar property holds for the constrained equations. Taking differentials, we have

$$\begin{aligned} d\dot{\mathbf{q}} &= dM^{-1}\mathbf{p}, \\ d\dot{\mathbf{p}} &= -d\nabla U(\mathbf{q}) - \sum_{k=1}^l d(\lambda_k \nabla g_k(\mathbf{q})), \\ 0 &= dg_j(\mathbf{q}), \quad j = 1, 2, \dots, l, \end{aligned}$$

Next, we interchange time derivatives and differentials, and use the chain rule to write

$$\frac{d}{dt} d\mathbf{q} = M^{-1} d\mathbf{p}, \tag{4.11}$$

$$\frac{d}{dt} d\mathbf{p} = -U''(\mathbf{q}) d\mathbf{q} - \sum_{k=1}^l [(d\lambda_k) \nabla g_k(\mathbf{q}) + \lambda_k g_k'' d\mathbf{q}], \tag{4.12}$$

$$0 = g'_j(\mathbf{q}) d\mathbf{q}, \quad j = 1, 2, \dots, l, \tag{4.13}$$

where we have written U'' for the Hessian matrix of U and g_k'' for the Hessian matrix of g_k .

For simplicity, we will assume the mass matrix is diagonal with i th diagonal element m_i . Now we write a formula for the time rate of change of the wedge product

$$\frac{d}{dt} \sum_{i=1}^{N_c} dq_i \wedge dp_i = \sum_{i=1}^{N_c} \frac{d}{dt} dq_i \wedge dp_i + dq_i \wedge \frac{d}{dt} dp_i,$$

then use formulas (4.11)–(4.13) to simplify, obtaining

$$\sum_{i=1}^{N_c} \frac{d}{dt} dq_i \wedge dp_i = \sum_{i=1}^{N_c} m_i^{-1} dp_i \wedge dp_i = 0,$$

and, writing $U''_{ij} = \partial^2 U / \partial q_i \partial q_j$,

$$\begin{aligned} \sum_{i=1}^{N_c} dq_i \wedge \frac{d}{dt} dp_i &= - \sum_{i=1}^{N_c} \sum_{j=1}^{N_c} dq_i \wedge U''_{ij} dq_j \\ &\quad - \sum_{i=1}^{N_c} \sum_{k=1}^l [dq_i \wedge (d\lambda_k) g'_{ki} + dq_i \wedge \lambda_k \sum_{j=1}^{N_c} (g_k'')_{ij} dq_j]. \end{aligned}$$

Treating each term in turn, first observe that

$$\sum_{i=1}^{N_c} \sum_{j=1}^{N_c} dq_i \wedge U''_{ij} dq_j = 0.$$

This follows from the antisymmetry of the wedge product ($dx \wedge dy = -dy \wedge dx$), and the fact that the Hessian matrix of U is symmetric. Next, note that

$$\sum_{i=1}^{N_c} \sum_{k=1}^l dq_i \wedge \lambda_k \sum_{j=1}^{N_c} (g_k'')_{ij} dq_j = \sum_{k=1}^l \lambda_k \sum_{i=1}^{N_c} dq_i \wedge \sum_{j=1}^{N_c} (g_k'')_{ij} dq_j = 0,$$

by the same reasoning, since each of g_k'' is a symmetric matrix. Finally

$$\sum_{i=1}^{N_c} \sum_{k=1}^l [dq_i \wedge (d\lambda_k) g'_{ki}] = \sum_{k=1}^l \left(\sum_{i=1}^{N_c} g'_{ki} dq_i \right) \wedge d\lambda_k = \sum_{k=1}^l dg_k \wedge d\lambda_k = 0,$$

since we know that $dg_k = 0$ from (4.13). Therefore

$$\frac{d}{dt} \sum_{i=1}^{N_c} dq_i \wedge dp_i = 0.$$

Thus we see that the projected version of the symplectic form in the ambient space is conserved by the differential equation system (4.7)–(4.9). This is what is meant by saying that the constrained system is analogous to a Hamiltonian system. We may also think of its flow map as being a symplectic map of the co-tangent bundle.

4.3.2 Numerical Methods with Holonomic Constraints

In what follows, we discuss the development of constrained integration methods, with a focus on the symplectic structure. Although we do this in a different way here, our presentation is based on the article [229].

From a mathematical point of view, the natural concept of a numerical method for the holonomic system (4.7)–(4.9) is that of a mapping from $T^*\mathcal{M}$ to itself which approximates the dynamical evolution on a step of length h .

Actually, many methods in common use for molecular dynamics cannot be seen as maps of $T^*\mathcal{M}$ since the hidden constraint is allowed to be violated. A simple example of such a method is the constrained Symplectic Euler-like method

$$\mathbf{q}_{n+1} = \mathbf{q}_n + h\mathbf{M}^{-1}\mathbf{p}_{n+1}, \quad (4.14)$$

$$\mathbf{p}_{n+1} = \mathbf{p}_n - h\mathbf{F}_n - hg'(\mathbf{q}_n)^T\boldsymbol{\lambda}_n, \quad (4.15)$$

$$\mathbf{0} = \mathbf{g}(\mathbf{q}_{n+1}). \quad (4.16)$$

Here $\boldsymbol{\lambda}_n$ is a vector which needs to be computed to define the projection onto \mathcal{M} . We would typically assume that \mathbf{q}_0 lies on \mathcal{M} so that (4.14)–(4.16) defines a map on \mathcal{M} . The hidden constraint $\mathbf{g}'(\mathbf{q}_0)\mathbf{M}^{-1}\mathbf{p}_0 = 0$ will be violated, but one hopes it remains approximately satisfied. The justification for the latter assumption is that if we expand \mathbf{g} in a Taylor series, we may write

$$\mathbf{g}(\mathbf{q}_n) \approx \mathbf{g}(\mathbf{q}_{n+1}) + \mathbf{g}'(\mathbf{q}_{n+1})(\mathbf{q}_n - \mathbf{q}_{n+1}).$$

Then since we maintain $\mathbf{g}(\mathbf{q}_n) = 0$ for all n , we have

$$\mathbf{g}'(\mathbf{q}_{n+1})\mathbf{M}^{-1}\mathbf{p}_{n+1} \approx 0.$$

To solve the Eqs. (4.14)–(4.16), insert the second in the first and the first then in the third to obtain the simplified equation

$$\mathbf{g}(\mathbf{Q}_n - \mathbf{M}^{-1}\mathbf{G}_n^T\boldsymbol{\Lambda}) = 0, \quad (4.17)$$

where

$$\mathbf{Q}_n = \mathbf{q}_n + h\mathbf{M}^{-1}\mathbf{p}_n - h^2\mathbf{M}^{-1}\mathbf{F}_n,$$

$$\mathbf{G}_n = \mathbf{g}'(\mathbf{q}_n),$$

$$\boldsymbol{\Lambda} = h^2\boldsymbol{\lambda}_n.$$

Once Λ is known, then this gives λ_n which in turn gives, after using (4.15), p_{n+1} and finally (4.14) yields q_{n+1} .

Since Q_n and G_n are known at step n , Eq.(4.17) is an equation for the m components of Λ . This may be solved by various iterative strategies. The simplest is Gauss-Newton iteration, which may be written

$$\Lambda^{(l+1)} = \Lambda^{(l)} + [g'(Q^{(l)})M^{-1}G_n^T]^{-1}g(Q^{(l)}), \quad (4.18)$$

$$Q^{(l)} := Q_n - M^{-1}G_n^T\Lambda^{(l)}, \quad (4.19)$$

which might be initialized with $\Lambda^{(0)} = \mathbf{0}$. A more sensible way to write this is

$$R^{(l)} \Delta \Lambda^{(l)} = g(Q^{(l)}), \quad R^{(l)} \stackrel{\text{def}}{=} g'(Q^{(l)})M^{-1}G_n^T,$$

with $\Delta \Lambda^{(l)} = \Lambda^{(l+1)} - \Lambda^{(l)}$. The usual way of solving such equations is by Gaussian elimination, which will require re-evaluation of R and refactorization at each iteration. However, assuming that the steps are sufficiently small and that g' is sufficiently smooth, we may be able to fix R at the beginning of the timestep, factor it once only, and then solve at each iteration with the same factors. Moreover, in case we have chosen $\Lambda^{(0)} = 0$, we have

$$R^{(0)} = G_n M^{-1} G_n^T,$$

which is a symmetric matrix, and it is well known that in such a case, where a Cholesky factorization is available, both efficiency and reliability of the elimination process are favorably improved.

When the solution is unique, the constraints sufficiently smooth, and the determinant of R is bounded well away from zero, Newton's method has a very rapid asymptotic convergence property. It is possible to show that, if Λ_* is the solution of (4.17), then sufficiently near the zero we have

$$\|\Lambda^{(l+1)} - \Lambda_*\| \leq C \|\Lambda^{(l)} - \Lambda_*\|^2.$$

Thus, if C is of moderate size, then two digits of accuracy becomes four, four becomes eight, etc. This rapid rate of convergence is only seen sufficiently near the root and only if R is re-evaluated at each stage of iteration. When R is evaluated only once per step, the asymptotic convergence of Newton's method is linear, i.e. we have instead

$$\|\Lambda^{(l+1)} - \Lambda_*\| \leq \hat{C} \|\Lambda^{(l)} - \Lambda_*\|,$$

sufficiently near to the solution. To stop the Newton iteration, we may check the stopping condition

$$\|\Lambda^{(l+1)} - \Lambda^{(l)}\| < \text{tol},$$

or else check the constraint residuals, or do both.

It is worth noting that $\Lambda(h) = \mathcal{O}(h^2)$, i.e. for small steps Λ will also be small. This justifies the initial guess $\Lambda^{(0)} = 0$, and it also suggests that if convergence of the Newton iteration is poor, this might be improved by taking a smaller timestep, since this effectively places $\Lambda^{(0)}$ closer to the solution of the equation.

In the context of large systems with large numbers of constraints it makes sense to invest significant effort to ensure that the algebraic equations are solved in the most efficient way possible. In [25], this topic was studied in depth, and a variety of iterative Newton-based numerical algorithms were proposed and compared.

4.3.3 Iterative Component-Wise Solution of the Nonlinear Equations

An alternative method for solving (4.17) is based on solving for Λ component-wise [322]. To describe this algorithm let us enumerate the equations as

$$g_j(\mathbf{Q}_n - \mathbf{M}^{-1}\mathbf{G}_n^k\Lambda_k) = 0, \quad \mathbf{G}_n^k = \nabla g_k(\mathbf{q}_n),$$

i.e. \mathbf{G}_n^k is the k th column of \mathbf{G}_n^T .

We begin with the initializations $\Lambda = \mathbf{0}$ and $\mathbf{Q} = \mathbf{Q}_n$, and solve for $\Delta\Lambda_1$ from

$$g_1(\mathbf{Q} - \mathbf{M}^{-1}\mathbf{G}_n^1\Delta\Lambda_1) = 0.$$

This is scalar nonlinear equation for $\Delta\Lambda_1$. We approximate its solution using a linear approximation at \mathbf{Q} thus we have

$$\Delta\Lambda_1 = [\nabla g_1(\mathbf{Q})^T \mathbf{M}^{-1} \mathbf{G}_n^1]^{-1} g_1(\mathbf{Q}).$$

We then update \mathbf{Q} by

$$\mathbf{Q} := \mathbf{Q} - \mathbf{M}^{-1}\mathbf{G}_n^1\Delta\Lambda_1,$$

and continue to update Λ_2 in the same manner (using the second constraint). In general, we perform a sequence of updates

$$\begin{aligned} \Delta\Lambda_j &= [\nabla g_j(\mathbf{Q})^T \mathbf{M}^{-1} \mathbf{G}_n^j]^{-1} g_j(\mathbf{Q}), \\ \mathbf{Q} &:= \mathbf{Q} - \mathbf{M}^{-1}\mathbf{G}_n^j\Delta\Lambda_j, \end{aligned}$$

as j cycles repeatedly from 1 to m . We halt the iteration when an appropriate stopping criterion is satisfied, which might be

$$\|\Delta\Lambda_j\| \leq \text{tol}, \quad j = 1, 2, \dots, m.$$

As is the case for Newton iteration, one may use the constraint residuals as an additional test. It is certainly unsafe to check only the latest difference of iterates (of a single component), and one should instead check that these are small for an entire cycle. The iteration described above is an example of a Gauss-Seidel-Newton iteration and it and many other iterative nonlinear solvers are discussed in [292].

4.3.4 Symplectic Constrained Dynamics Integrators

Is (4.14)–(4.16) symplectic (in the sense outlined above for holonomic systems)?

It is difficult to make sense of this question, since (4.14)–(4.16) does not even constitute a map of the co-tangent bundle. On the other hand it is not too difficult to correct this defect by incorporating an additional projection onto the cotangent space:

$$\mathbf{q}_{n+1} = \mathbf{q}_n + h\mathbf{M}^{-1}\bar{\mathbf{p}}_{n+1}, \quad (4.20)$$

$$\bar{\mathbf{p}}_{n+1} = \mathbf{p}_n - h\mathbf{F}_n - hg'(\mathbf{q}_n)^T\boldsymbol{\lambda}_n, \quad (4.21)$$

$$\mathbf{0} = \mathbf{g}(\mathbf{q}_{n+1}), \quad (4.22)$$

$$\mathbf{p}_{n+1} = \bar{\mathbf{p}}_{n+1} - g'(\mathbf{q}_{n+1})^T\boldsymbol{\mu}_{n+1}, \quad (4.23)$$

$$\mathbf{0} = g'(\mathbf{q}_{n+1})\mathbf{M}^{-1}\mathbf{p}_{n+1}. \quad (4.24)$$

The demonstration that the method is symplectic can be seen as a consequence of the following lemma.

Lemma 4.1 *Let $\gamma : \mathbb{R}^{N_c} \rightarrow \mathbb{R}$ be C^2 . Let $\mathbf{q}, \mathbf{p} \in \mathbb{R}^{N_c}$ be constrained to the manifold defined by*

$$\gamma(\mathbf{q}) = 0, \quad \mathbf{p} \cdot \nabla \gamma(\mathbf{q}) = 0,$$

and suppose $\mathbf{P}, \boldsymbol{\mu}$ satisfy

$$\mathbf{P} = \mathbf{p} - \boldsymbol{\mu} \nabla \gamma(\mathbf{q}).$$

Then

$$\sum_{j=1}^{N_c} dq_j \wedge dP_j = \sum_{j=1}^{N_c} dq_j \wedge dp_j.$$

Proof Clearly the result follows provided

$$\sum_{j=1}^{N_c} dq_j \wedge d[\mu \nabla \gamma(\mathbf{q})]_j = 0,$$

where $[\dots]_j$ indicates the j th component of the term in brackets. We have

$$\sum_{j=1}^{N_c} dq_j \wedge d[\mu \nabla \gamma(\mathbf{q})]_j = \sum_{j=1}^{N_c} dq_j \wedge \left(\frac{\partial \gamma}{\partial q_j} d\mu + \mu \sum_{i=1}^{N_c} \gamma''_{ij} dq_j \right).$$

Then we note

$$\sum_{j=1}^{N_c} dq_j \wedge \frac{\partial \gamma}{\partial q_j} d\mu = \sum_{j=1}^{N_c} \frac{\partial \gamma}{\partial q_j} dq_j \wedge d\mu = 0,$$

since $\gamma(q) \equiv 0$ implies $d\gamma(q) = \sum_{j=1}^{N_c} \frac{\partial \gamma}{\partial q_j} dq_j \equiv 0$. Moreover

$$\sum_{j=1}^{N_c} dq_j \wedge \sum_{i=1}^{N_c} \gamma''_{ij} dq_j = 0,$$

since the Hessian matrix γ'' is symmetric. \square

Observe that

$$\mathbf{g}'(\mathbf{q}_{n+1})^T \boldsymbol{\mu}_{n+1} = \sum_{k=1}^l \mu_{n+1,k} \nabla g_k(\mathbf{q}_{n+1}).$$

Thus we may apply Lemma 4.1 with γ replaced by each g_k to demonstrate

$$\sum_{j=1}^{N_c} dq_{n+1,j} \wedge dp_{n+1,j} = \sum_{j=1}^{N_c} dq_{n+1,j} \wedge d\bar{p}_{n+1,j}.$$

Using similar argumentation based on the properties of the wedge product, we next show

$$\sum_{j=1}^{N_c} dq_{n+1,j} \wedge d\bar{p}_{n+1,j} = \sum_{j=1}^{N_c} dq_{n,j} \wedge d\bar{p}_{n+1,j},$$

and, finally, invoking Lemma 4.1 again,

$$\sum_{j=1}^{N_c} dq_{n,j} \wedge d\bar{p}_{n+1,j} = \sum_{j=1}^{N_c} dq_{n,j} \wedge dp_{n,j}.$$

4.3.5 Higher Order Symplectic Methods: SHAKE and RATTLE

The projected symplectic constrained method (4.20)–(4.24) is only first order accurate. We forego providing a detailed proof of this fact, but note that it could be demonstrated using standard methods [164]. Note that (4.20)–(4.24) reduces to the symplectic Euler method in the absence of constraints, and the projection of the momenta would not alter this fact. There are several constraint-preserving, second-order alternatives which generalize the Störmer-Verlet scheme. One of these is the SHAKE method [322]. The original derivation of the SHAKE method began from the position-only, two-step form of the Störmer rule for $\dot{\mathbf{q}} = \mathbf{F}(\mathbf{q})$

$$\mathbf{q}_{n+1} - 2\mathbf{q}_n + \mathbf{q}_{n-1} = h^2 \mathbf{M}^{-1} \mathbf{F}(\mathbf{q}_n).$$

In the presence of the constraint, we consider the scheme

$$\mathbf{q}_{n+1} - 2\mathbf{q}_n + \mathbf{q}_{n-1} = h^2 \mathbf{M}^{-1} \mathbf{F}(\mathbf{q}_n) - h^2 \mathbf{g}'(\mathbf{q}_n)^T \boldsymbol{\lambda}_n, \quad (4.25)$$

$$\mathbf{g}(\mathbf{q}_{n+1}) = 0. \quad (4.26)$$

The symmetry suggests that this will be second order. In order to understand the symplectic property associated to this method, we need to define the updates for both positions and momenta. A natural choice is to consider the phase space formulation of the Störmer-Verlet method for $\dot{\mathbf{q}} = \mathbf{M}^{-1} \mathbf{p}, \dot{\mathbf{p}} = \mathbf{F}(\mathbf{q})$, then replace \mathbf{F} by $\mathbf{F} - \mathbf{g}'(\mathbf{q})^T \boldsymbol{\lambda}$, resulting in

$$\mathbf{q}_{n+1} = \mathbf{q}_n + h \mathbf{M}^{-1} \mathbf{p}_{n+1/2}, \quad (4.27)$$

$$\mathbf{p}_{n+1/2} = \mathbf{p}_n + (h/2) \mathbf{F}(\mathbf{q}_n) - (h/2) \mathbf{g}'(\mathbf{q}_n)^T \boldsymbol{\lambda}_n, \quad (4.28)$$

$$\mathbf{p}_{n+1} = \mathbf{p}_{n+1/2} + (h/2) \mathbf{F}(\mathbf{q}_{n+1}) - (h/2) \mathbf{g}'(\mathbf{q}_{n+1})^T \boldsymbol{\lambda}_{n+1}. \quad (4.29)$$

It is possible to demonstrate (see exercises) that this method reduces to (4.25)–(4.26) by eliminating the momenta. However (4.27)–(4.29) does not give a map of the cotangent bundle, since $\mathbf{g}'(\mathbf{q}_{n+1}) \mathbf{p}_{n+1} = 0$ will not be preserved, even if both the constraint and hidden constraint hold at step n .

A method that automatically preserves both the constraint and hidden constraint is the RATTLE method [12] which consists of the following steps:

$$\mathbf{q}_{n+1} = \mathbf{q}_n + h \mathbf{M}^{-1} \mathbf{p}_{n+1/2}, \quad (4.30)$$

$$\mathbf{p}_{n+1/2} = \mathbf{p}_n + (h/2) \mathbf{F}_n - (h/2) \mathbf{g}'(\mathbf{q}_n)^T \boldsymbol{\lambda}_n, \quad (4.31)$$

$$\mathbf{0} = \mathbf{g}(\mathbf{q}_{n+1}), \quad (4.32)$$

$$\mathbf{p}_{n+1} = \mathbf{p}_{n+1/2} + (h/2) \mathbf{F}_{n+1} - \mathbf{g}'(\mathbf{q}_{n+1})^T \boldsymbol{\mu}_{n+1}, \quad (4.33)$$

$$\mathbf{0} = \mathbf{g}'(\mathbf{q}_{n+1}) \mathbf{M}^{-1} \mathbf{p}_{n+1}. \quad (4.34)$$

In practice, the implementation of this method is essentially the same as that of the constrained Symplectic Euler method (including the cotangency projection). Moreover, the symplecticness of (4.30)–(4.34) may be demonstrated using a very similar approach to that used to demonstrate the symplectic condition for (4.20)–(4.24).

What is not perhaps immediately obvious is that RATTLE and SHAKE are in fact equivalent methods in a certain, precisely defined sense. The SHAKE method defines a mapping \mathcal{G}_h^S of $\mathcal{M} = \{(\mathbf{q}, \mathbf{p}) | \mathbf{g}(\mathbf{q}) = 0\}$. That is, starting from $\mathbf{z}_0 = (\mathbf{q}_0, \mathbf{p}_0) \in \mathcal{M}$, it generates a set of points $\mathbf{z}_1, \mathbf{z}_2, \dots \in \mathcal{M}$ such that $\mathbf{z}_{n+1} = \mathcal{G}_h^S(\mathbf{z}_n)$. In a similar way, RATTLE defines a mapping of the lower dimensional cotangent bundle, $\mathcal{G}_h^R : T^*\mathcal{M} \rightarrow T^*\mathcal{M}$. Even though these methods are maps defined on sets of different dimensionalities, the iterations generated by them can be related to the following staggered iteration

$$\mathbf{q}_{n+1} = \mathbf{q}_n + h\mathbf{M}^{-1}\mathbf{p}_{n+1/2}, \quad (4.35)$$

$$\mathbf{p}_{n+1/2} = \mathbf{p}_{n-1/2} + h\mathbf{F}_n - h\mathbf{g}'(\mathbf{q}_n)^T \tilde{\boldsymbol{\lambda}}_n, \quad (4.36)$$

$$\mathbf{0} = \mathbf{g}(\mathbf{q}_{n+1}), \quad (4.37)$$

where, for SHAKE, $\tilde{\boldsymbol{\lambda}}_n = \boldsymbol{\lambda}_n$, while, in case of RATTLE, we must define $\tilde{\boldsymbol{\lambda}}_n = (\boldsymbol{\lambda}_n + \boldsymbol{\mu}_n)/2$. The proof of this is contained in one of the exercises. Given an initial condition $(\mathbf{q}_0^S, \mathbf{p}_0^S)$ for the SHAKE discretization, we easily determine $\boldsymbol{\lambda}_0^S$ by taking a step. Then it follows that

$$\mathbf{p}_{-1/2} = \mathbf{p}_0 - (h/2)\mathbf{F}(\mathbf{q}_0^S) - (h/2)\mathbf{g}'(\mathbf{q}_0^S)^T \boldsymbol{\lambda}_0^S,$$

by solving (4.29). Next we obtain \mathbf{p}_0^R by solving (4.33)–(4.34) with $n = -1$. Then the sequences generated using $(\mathbf{q}_0^S, \mathbf{p}_0^S)$ as the initial point for SHAKE and that generated using $(\mathbf{q}_0^S, \mathbf{p}_0^R)$ in RATTLE will have identical positions (the momenta can be made compatible by simply projecting the SHAKE momenta onto the constraints).

Given the above discussion and derivation, the proof of symplecticness of the RATTLE method (4.30)–(4.34) is now a formality. For details refer to [229].

4.3.5.1 Symmetric Composition Methods with Constraints

Recall that the Störmer-Verlet method could be constructed by composing steps using Symplectic Euler and its adjoint method. Using more complicated methods it is possible to build higher order schemes. It seems natural that a similar procedure should be possible in the constrained setting. But what, precisely, is the adjoint method in the case of (4.20)–(4.24)?

Recall that, for a given method \mathcal{G}_h the definition of the adjoint method \mathcal{G}_h^* is given by

$$\mathcal{G}_h^* = \mathcal{G}_{-h}^{-1}.$$

For Symplectic Euler with constraints, we view \mathcal{G}_h as a mapping of the co-tangent bundle and write $(\mathbf{Q}, \mathbf{P}) := \mathcal{G}_h(\mathbf{q}, \mathbf{p})$ where

$$\begin{aligned}\hat{\mathbf{P}} &= \mathbf{p} + hF(\mathbf{q}) - hg'(\mathbf{q})^T \boldsymbol{\lambda}, \\ \mathbf{Q} &= \mathbf{q} + hM^{-1}\hat{\mathbf{P}}, \\ \mathbf{P} &= \hat{\mathbf{P}} - hg'(\mathbf{Q})^T \boldsymbol{\mu},\end{aligned}$$

and the multipliers $\boldsymbol{\lambda}, \boldsymbol{\mu}$ are defined by the conditions $\mathbf{g}(\mathbf{Q}) = 0, \mathbf{g}'(\mathbf{Q})M^{-1}\mathbf{P} = 0$.

Now replace h by $-h$ and then swap \mathbf{Q} with \mathbf{q} and \mathbf{P} with \mathbf{p} , resulting in

$$\begin{aligned}\hat{\mathbf{P}} &= \mathbf{p} - hg'(\mathbf{q})^T \boldsymbol{\lambda}, \\ \mathbf{Q} &= \mathbf{q} + hM^{-1}\hat{\mathbf{P}}, \\ \mathbf{P} &= \hat{\mathbf{P}} + hF(\mathbf{Q}) - hg'(\mathbf{Q})^T \boldsymbol{\mu},\end{aligned}$$

where $\boldsymbol{\lambda}, \boldsymbol{\mu}$ are again defined by the constraint conditions. This defines the adjoint method, another first order method for the constrained system. By composing the maps $\mathcal{G}_{h/2}$ and $\mathcal{G}_{h/2}^*$ we get a second order symplectic method. In the sense that it is defined by first order maps which reduce to the Symplectic Euler method and its adjoint, this is an analogous scheme to the Störmer-Verlet method. Interestingly, this method is not equivalent to SHAKE or RATTLE.

Yet this is not the only constrained composition method we could have designed in analogy with Störmer-Verlet. Recall that Störmer-Verlet is also the symmetric composition of the flow maps of the two Hamiltonians $K = \mathbf{p}^T M^{-1} \mathbf{p} / 2$ and $U = U(\mathbf{q})$. It would be natural to consider a composition of steps resolving the constrained flows on K and U separately. For the potential energy term, an exact solution is given by

$$\begin{aligned}\mathbf{Q} &= \mathbf{q}, \\ \mathbf{P} &= \mathbf{p} - h\boldsymbol{\Pi}(\mathbf{q})\nabla U(\mathbf{q}),\end{aligned}$$

where $\boldsymbol{\Pi}$ is a mass-weighted projector onto the tangent space of the constraints at the point \mathbf{q} defined by

$$\boldsymbol{\Pi} = I - \mathbf{g}'(\mathbf{q})^T [\mathbf{g}'(\mathbf{q})M^{-1}\mathbf{g}'(\mathbf{q})^T]^{-1} \mathbf{g}'(\mathbf{q})M^{-1}.$$

The constrained flow on the kinetic energy term, on the other hand, is generated by the equations of motion

$$\begin{aligned}\frac{dq}{dt} &= M^{-1} p, \\ \frac{dp}{dt} &= -g'(q)^T \lambda, \\ 0 &= g(q).\end{aligned}$$

This is nothing other than the mass-weighted geodesic flow on the given constraint surface. In most cases, the complication of solving the geodesic flow would lead to a need for additional approximations, however it is worth noting that in many applications, by far the most important cost is the calculation of the force $-\nabla U$, hence a further approximation of the geodesic flow could be justified if this method conferred additional stability or other benefits. We do not consider this further here, but take up the construction as part of our treatment of constrained stochastic dynamics in Section 7.12.

For an alternative approach to the construction of higher-order composition methods for constrained systems see [309].

4.3.6 Algorithms for Molecular Simulation Using Constraints

Because of their importance in the molecular simulation process, a wide variety of methods for handling holonomic constraints have been proposed in the past few decades. We summarize a few of these here.

The term “SHAKE” normally refers to both the discretization mentioned above and the component-wise solution of the nonlinear equations (these methods were suggested together in the paper [322]). Using the traditional SHAKE approach we solve the Eqs. (4.27)–(4.29) using the iterative procedure of Sect. 4.3.3. If RATTLE is used for discretization, the iterative method of Sect. 4.3.3 can again be used to solve (4.30)–(4.32), followed by a subsequent solve of Eqs. (4.33)–(4.34).

While SHAKE/RATTLE is a robust procedure the sequential, iterative character of nonlinear solvers needed for its implementation can lead inefficiencies when it is implemented on a parallel computer. Therefore, a number of the alternative methods avoid iteration. We briefly summarize a few of the popular alternative schemes here.

M-Shake This is Newton-iteration-based implementation of SHAKE, using (4.18)–(4.19) to solve Eqs. (4.27)–(4.29). Methods like this were first proposed by Ciccotti and Ryckaert [84] in the context of rigid body molecular dynamics. An extended discussion of such methods with reference to their convergence, implementation, in particular linear system solvers, and variants such as SHAKE-SOR (which uses the “successive over-relaxation” method) can be found in [25]. A conjugate gradient method can also be used [392].

SETTLE The SETTLE method [274] is just the SHAKE approach applied to a small system combined with an exact solve of the nonlinear equations. It is usually applied to treat rigid bodies (as discussed in the following section).

LINCS In solving the Eqs. (4.27)–(4.29) by Newton iteration, the largest cost and the most significant barrier to parallelization is the linear solve. The LINCS method [119, 175] uses a series expansion to approximate the inverse matrix (which is valid only under certain conditions). The method gives substantial speedups in large, weakly-coupled systems.

It is also possible to use internal coordinate representations to treat constraints, i.e. parameterization schemes, which are typically based on partitioning the coordinates of the system into a set of independent variables and a complementary collection of dependent variables (which are expressed in terms of the first set). These approaches result in systems of slightly smaller dimension, but typically greater complexity. Moreover, the parameterization is typically local which leads to additional implementation issues. For some details on such schemes and discussion of their use in molecular simulation, the reader is referred to [20, 190, 255].

4.3.7 Numerical Experiment with SHAKE

We demonstrate the numerical stability benefit of using constraints in simulation by considering a periodic box of 116 TIP3P water molecules in a periodic box with side length 16Å (for computational convenience the simulated particle density is slightly below that of liquid water). We simulate the system using the NAMD package [302], with the CHARMM22 forcefield [246] parameterizing the potential energy functions. After an initial equilibration of 1ns, we look at the stability and conservation of energy in this system, when using either the constrained or unconstrained version of the model. The deviation in the total energy over a further 1ns simulation is plotted in Fig. 4.5. In the unconstrained version of the model, the internal angle and the bond lengths of each molecule are free to change, governed by a restraining force from the corresponding potential energy terms. This model proves to be unstable for stepsizes chosen at 3 fs and over, while the simulation at $h = 2$ fs showed a large variance in the energy error (as well as exhibiting energy drift in longer simulations). For accurate results, we would expect the stepsize to be restricted to around $h = 1$ fs, where there is significantly smaller average energy fluctuation.

By contrast, when using constraints to keep the angle and bond lengths fixed, we observe that the energy fluctuations are dramatically reduced and we are able to use considerably higher stepsizes than in the unconstrained case. Although the use of constraints slightly increases the required computational workload (relative to the flexible model), the non-bonded force calculation (especially the Coulombic component) is typically still the dominant cost in each step of the simulation. As the SHAKE method does not require extra force evaluations, the ability to increase

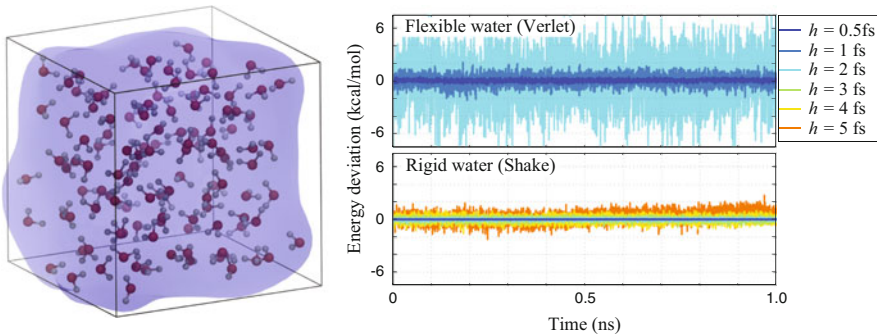


Fig. 4.5 We simulate a cubic box of TIP3P water (*left*) with box side length 16Å using periodic boundary conditions. The deviation in the total energy is shown for simulations using different timesteps (*right*), when using either the flexible or rigid (constrained) model. Note that the flexible model could not be stably simulated at the larger timesteps

the timestep makes constrained simulation typical more efficient than unconstrained dynamics. In general, a doubling of the timestep is often possible.

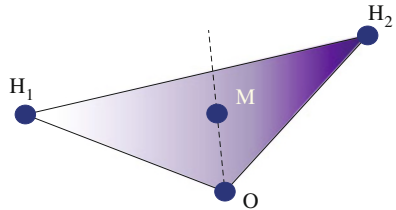
A concern might be that the change of the model from unconstrained to constrained could alter the properties of the system in a way that would affect the overall simulation results. In practice, it is normally found that the other model and sampling errors present mean that the errors due to using constraints are relatively minor, particularly if the constraints are limited to bond lengths only, and even less of a factor if the constraints are limited to the bonds between hydrogen atoms and heavier atoms in biomolecules.

4.4 Rigid Body Systems

In some cases the effect of introducing constraints may be to rigidify completely certain molecular groups. Constraints are also used as part of coarse-graining procedures in which large collections of atoms may have their relative motions eliminated. In this case it is often useful to replace the rigid groups by ideal rigid bodies and to model these using rigid body dynamics. There is an extensive research literature on numerical methods for rigid body molecular dynamics, our discussion here of this topic is limited to a few schemes that we feel offer a reasonable combination of efficiency and geometric fidelity. For a more complete introduction to the topic, we recommend [80, 84] and the references therein.

As an example, in the TIP4P model for water, one of the most popular, the waters are assumed to be rigid bodies and there are 3 charge sites associated to each: the locations of the hydrogen nuclei and an additional “ghost” site located in the plane created by the three nuclei and along the perpendicular bisector of the HOH angle (Fig. 4.6). The potential energy for the interaction of a pair of such molecules, the

Fig. 4.6 Rigid representation of a water molecule used in TIP4P, indicating the “ghost” charge site



sets of whose charge sites are denoted by A and B, takes the form

$$\varphi^{\text{water-water}} = \sum_{i \in A} \sum_{j \in B} k_1 \frac{Q_i Q_j}{r_{ij}} + \frac{k_2}{r_{OO}^{12}} - \frac{k_3}{r_{OO}^6},$$

where r_{OO} represents the distance between the oxygen atoms of the two molecules, and k_1, k_2, k_3 are positive constants. Similar potentials are needed for interactions between the atoms of the solute and the atoms of the water molecules.

More generally, consider a collection of N atoms (masses m_i , positions \mathbf{q}_i , $i = 1, 2, \dots, N$) subject to an external potential U . The kinetic energy is

$$K = \frac{1}{2} \sum_{i=1}^N m_i \|\dot{\mathbf{q}}_i\|^2.$$

The atomic positions may be referred to a coordinate system placed at the center of mass of the collection

$$\mathbf{q}_{\text{cm}} = \frac{\sum_{i=1}^N m_i \mathbf{q}_i}{M},$$

where $M = \sum_{i=1}^N m_i$ is the total mass. We write $\mathbf{q}_i = \mathbf{q}_{\text{cm}} + \boldsymbol{\delta}_i$, where $\sum_{i=1}^N m_i \boldsymbol{\delta}_i = 0$. Thus the kinetic energy becomes

$$\begin{aligned} K &= \frac{1}{2} \sum_{i=1}^N m_i \|\dot{\mathbf{q}}_{\text{cm}}\|^2 + \sum_{i=1}^N m_i \dot{\mathbf{q}}_{\text{cm}} \cdot \dot{\boldsymbol{\delta}}_i + \frac{1}{2} \sum_{i=1}^N m_i \|\dot{\boldsymbol{\delta}}_i\|^2 \\ &= \underbrace{\frac{M}{2} \|\dot{\mathbf{q}}_{\text{cm}}\|^2}_{\equiv K_{\text{trans}}} + \underbrace{\frac{1}{2} \sum_{i=1}^N m_i \|\dot{\boldsymbol{\delta}}_i\|^2}_{\equiv K_{\text{rot}}}, \end{aligned}$$

where we have used the fact that $\sum_{i=1}^N m_i \dot{\boldsymbol{\delta}}_i \equiv 0$, hence that the time derivative also vanishes, in order to remove the middle term. At time t , each vector $\boldsymbol{\delta}_i$ can be related to its initial value by a certain orthogonal 3×3 rotation matrix $\boldsymbol{\Theta}(t)$:

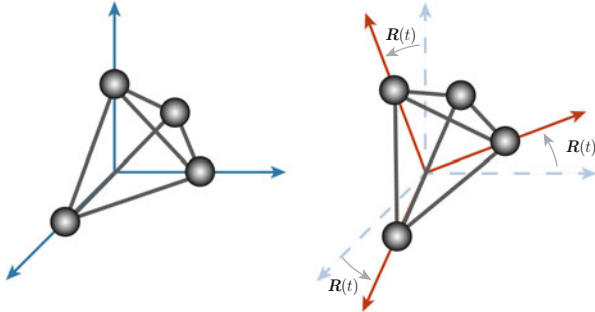


Fig. 4.7 A rigid rotation can be viewed as premultiplication by an orthogonal matrix Θ . In this way the orientation of the position vectors of points in the rigid body at any time t are described by a trajectory in the space of 3×3 orthogonal matrices, $\Theta(t), t \in \mathbb{R}$

$\delta_i(t) = \Theta(t)\delta_i(0)$, see Fig. 4.7, thus we have

$$K_{\text{rot}} = \frac{1}{2} \sum_{i=1}^N m_i \delta_i(0)^T \dot{\Theta}^T \dot{\Theta} \delta_i(0).$$

This expression may be rewritten as

$$K_{\text{rot}} = \frac{1}{2} \text{Tr}(\dot{\Theta} R \dot{\Theta}^T),$$

where the fixed matrix R is given by

$$R = \sum_{i=1}^N m_i \delta_i(0) \delta_i(0)^T.$$

By choosing an appropriate coordinate frame, it is possible to insure that the symmetric matrix R is a diagonal matrix.

An alternative form for the rotational kinetic energy may be obtained by writing

$$\begin{aligned} \dot{\delta}_i &= \dot{\Theta} \delta_i(0) \\ &= \dot{\Theta} \Theta^T \Theta \delta_i(0) = \dot{\Theta} \Theta^T \dot{\delta}_i, \end{aligned}$$

where we have used the fact that Θ is orthogonal. Moreover, since $\Theta \Theta^T = I$, we have

$$\dot{\Theta} \Theta^T + \Theta \dot{\Theta}^T = 0,$$

which indicates that $\dot{\Theta}\Theta^T$ is a skew symmetric matrix. Any 3×3 skew matrix may be written as

$$\dot{\Theta}\Theta^T = \text{skew}(\omega) \equiv \begin{bmatrix} 0 & -\omega_3 & \omega_2 \\ \omega_3 & 0 & -\omega_1 \\ -\omega_2 & \omega_1 & 0 \end{bmatrix}. \quad (4.38)$$

ω is referred to as the *spatial angular velocity* of the rigid body. It follows that

$$\frac{d}{dt}\delta_i = \text{skew}(\omega)\delta_i = \omega \times \delta_i = -\text{skew}(\delta_i)\omega, \quad (4.39)$$

which is the usual definition.

We now insert the expression for $\dot{\delta}_i$ into the rotational kinetic energy, to obtain

$$K_{\text{rot}} = \frac{1}{2} \sum_{i=1}^N m_i \|\dot{\delta}_i\|^2 = -\frac{1}{2} \sum_{i=1}^N m_i \omega^T \text{skew}(\delta_i)^2 \omega.$$

It is convenient to express this in terms of the so-called *body angular velocity* $\omega_b = \Theta^T \omega$ in which case it becomes

$$K_{\text{rot}} = \frac{1}{2} \omega_b^T T \omega_b,$$

where the matrix $T = -\sum_{i=1}^N m_i \text{skew}(\delta_i(0))^2$ is referred to as the *moment of inertia tensor* or simply the *inertia tensor* and can be written as

$$T = \sum_{i=1}^N m_i [\|\delta_i(0)\|^2 I - \delta_i(0)\delta_i(0)^T].$$

This matrix is closely related to the matrix R :

$$R = \sum_{i=1}^N m_i \delta_i \delta_i^T = \sum_{i=1}^N m_i \|\delta_i\|^2 I - T = (T_{11} + T_{22} + T_{33})I - T. \quad (4.40)$$

Example 4.1 (Dipolar Molecular Liquid) The Stockmayer model for a molecular liquid with permanent dipoles [388] treats this as a system of rigid bodies (spheres) with dipole-dipole interaction potential; we already encountered this in the exercises of Chap. 1. From a computational and modelling perspective, there is no real reason to use spheres (and perhaps good reasons not to); for example they might be taken to be ellipsoidal. Let us assume that they are identical ellipsoids. The Hamiltonian for a more general dipolar system can be written

$$H = K_{\text{rot}}(\boldsymbol{\pi}_1, \boldsymbol{\pi}_2, \dots, \boldsymbol{\pi}_N) + K_{\text{trans}}(\boldsymbol{p}_1, \boldsymbol{p}_2, \dots, \boldsymbol{p}_N) + U(\boldsymbol{q}_1, \boldsymbol{q}_2, \dots, \boldsymbol{q}_N, \boldsymbol{\mu}_1, \boldsymbol{\mu}_2, \dots, \boldsymbol{\mu}_N),$$

Where K_{rot} represents the rotational kinetic energy expressed in terms of the body-fixed angular momentum vectors, K_{trans} is the translational kinetic energy, U is the potential energy which is a function of all the positions and dipole orientations. The vectors $\boldsymbol{\mu}_k$ can be taken to be unit vectors reflecting the dipole orientation, so they are subject to the constraint $\|\boldsymbol{\mu}_k\| \equiv 1$. The total dipole-dipole interaction potential then takes the form

$$\varphi_{ij}^{\text{dip}} = \varphi_{\text{LJ}}(r_{ij}) + \boldsymbol{\mu}_i^T \mathbf{L}(\mathbf{q}_{ij}) \boldsymbol{\mu}_j,$$

with U given as the sum of these over pairs. The 3×3 matrix \mathbf{L} is given by

$$\mathbf{L}(\mathbf{q}_{ij}) = \frac{1}{r_{ij}^3} - \frac{3}{r_{ij}^5} \mathbf{q}_{ij} \mathbf{q}_{ij}^T, \quad \mathbf{q}_{ij} = \mathbf{q}_i - \mathbf{q}_j.$$

The rotational kinetic energy may be written

$$K_{\text{rot}}(\boldsymbol{\pi}_1, \boldsymbol{\pi}_2, \dots, \boldsymbol{\pi}_N) = \frac{1}{2} \sum_{i=1}^N \frac{\boldsymbol{\pi}_{i,1}^2}{I_1} + \frac{\boldsymbol{\pi}_{i,2}^2}{I_2} + \frac{\boldsymbol{\pi}_{i,3}^2}{I_3},$$

with I_1, I_2, I_3 the moments of inertia, taken to be diagonal with respect to a suitable coordinate system. Introducing a rotation matrix $\boldsymbol{\Theta}_k$ for the k th dipole, we have $\boldsymbol{\mu}_k(t) = \boldsymbol{\Theta}_k \boldsymbol{\mu}_k(0)$, where $\boldsymbol{\mu}_k(0)$ is a reference configuration of the dipole (its initial state). Then

$$K_{\text{rot}} = \sum_{i=1}^N \text{Tr} \left(\dot{\boldsymbol{\Theta}}_i \mathbf{R} \dot{\boldsymbol{\Theta}}_i^T \right),$$

with \mathbf{R} defined in terms of $\mathbf{T} = \text{diag}(I_1, I_2, I_3)$ by (4.40).

We now have two alternatives for representing the rotational motion. In the first, the rotation matrix describing the rigid body's orientation is the dynamical quantity (and we need to enforce the orthogonality of this matrix as a constraint). This leads to a constrained integration method, which makes use of SHAKE (in a somewhat different way from the method [84] which constrains the relative positions of particles). In the second formulation, the orthogonality is used to perform a reduction to an angular velocity (or momentum) representation with respect to the body frame of reference.

A Hamiltonian description of the motion may be formulated in either system of notation. The Hamiltonian formulation with rotation matrices involves variables $\mathbf{q}_{\text{cm}}, \mathbf{p}_{\text{cm}}$ (phase space variables describing the center of mass motion) and $\boldsymbol{\Theta}, \boldsymbol{\Pi}$, which are 3×3 matrices. The Hamiltonian is (for a single rigid body):

$$H_{\text{RB}} = \frac{\|\mathbf{p}_{\text{cm}}\|^2}{2M} + \frac{\text{Tr} (\boldsymbol{\Pi} \mathbf{R}^{-1} \boldsymbol{\Pi}^T)}{2} + U(\mathbf{q}_{\text{cm}}, \boldsymbol{\Theta}),$$

subject to the orthogonality constraint $\boldsymbol{\Theta}^T \boldsymbol{\Theta} = \mathbf{I}$. Here the potential energy has been expressed in terms of \mathbf{q}_{cm} and the orientation of the body. The constraint may be enforced using Lagrange multipliers with the following equations

$$\begin{aligned}\frac{d}{dt} \mathbf{q}_{\text{cm}} &= \mathbf{p}_{\text{cm}}/M, \quad \frac{d}{dt} \boldsymbol{\Theta} = \boldsymbol{\Pi} \mathbf{R}^{-1}, \\ \frac{d}{dt} \mathbf{p}_{\text{cm}} &= -\nabla_{\mathbf{q}_{\text{cm}}} U, \quad \frac{d}{dt} \boldsymbol{\Pi} = -\nabla_{\boldsymbol{\Theta}} U - \boldsymbol{\Theta} \boldsymbol{\Lambda}, \\ \mathbf{I} &= \boldsymbol{\Theta}^T \boldsymbol{\Theta}.\end{aligned}$$

These equations may be solved using a SHAKE or RATTLE algorithm [84, 201]. However, we will present an alternative which is both conceptually simpler and easier to implement.

4.4.1 Euler Equations

An elegant form of the equations of motion for the free rigid body is expressed in terms of the angular momentum vector referred to the body frame.

The angular momentum vector in the reference frame is given by

$$\mathbf{l} = \sum_{i=1}^N m_i \boldsymbol{\delta}_i \times \dot{\boldsymbol{\delta}}_i.$$

From Eq. (4.39) we may write this as

$$\mathbf{l} = \sum_{i=1}^N m_i \boldsymbol{\delta}_i \times \boldsymbol{\omega} \times \boldsymbol{\delta}_i,$$

from which, using the vector triple product identity $\mathbf{a} \times \mathbf{b} \times \mathbf{c} = (\mathbf{a} \cdot \mathbf{c})\mathbf{b} - (\mathbf{a} \cdot \mathbf{b})\mathbf{c}$, we obtain

$$\mathbf{l} = \sum_{i=1}^N m_i [\|\boldsymbol{\delta}_i\|^2 \mathbf{I} - \boldsymbol{\delta}_i \boldsymbol{\delta}_i^T] \boldsymbol{\omega}.$$

Define $\boldsymbol{\pi} = \boldsymbol{\Theta}^T \mathbf{l}$, the angular momentum vector referred to the body frame of reference, then we have (using $\boldsymbol{\delta}_i = \boldsymbol{\Theta} \boldsymbol{\delta}_i(0)$):

$$\boldsymbol{\pi} = \mathbf{T} \boldsymbol{\omega}_b.$$

Thus the inertia tensor relates the angular momentum vector in the body frame to the angular velocity vector in the body frame.

In the absence of external forces,

$$\mathbf{0} = \frac{d}{dt} \mathbf{l} = \dot{\boldsymbol{\Theta}} \boldsymbol{\pi} + \boldsymbol{\Theta} \dot{\boldsymbol{\pi}}.$$

Therefore

$$\dot{\boldsymbol{\pi}} = -\boldsymbol{\Theta}^T \dot{\boldsymbol{\Theta}} \boldsymbol{\pi}.$$

Next observe that

$$\boldsymbol{\Theta}^T \dot{\boldsymbol{\Theta}} = \text{skew}(\boldsymbol{\omega}_b).$$

This follows from the definition of the angular velocity and properties of the cross product (see exercises). Thus

$$\dot{\boldsymbol{\pi}} = -\boldsymbol{\omega}_b \times \boldsymbol{\pi} = \boldsymbol{\pi} \times \boldsymbol{\omega}_b,$$

but since $\boldsymbol{\omega}_b = \mathbf{T}^{-1} \boldsymbol{\pi}$, we may conclude

$$\dot{\boldsymbol{\pi}} = \boldsymbol{\pi} \times \mathbf{T}^{-1} \boldsymbol{\pi}. \quad (4.41)$$

These are the so-called *Euler equations* for the free rigid body.

Let us observe that (4.41) is in the form

$$\dot{\boldsymbol{\pi}} = \tilde{\mathbf{J}}(\boldsymbol{\pi}) \nabla \tilde{H},$$

where $\tilde{\mathbf{J}}(\boldsymbol{\pi}) = \text{skew}(\boldsymbol{\pi})$ is obviously skew symmetric, and $\tilde{H} = \boldsymbol{\pi}^T \mathbf{T}^{-1} \boldsymbol{\pi} / 2$ is the energy function. Thus the Euler equations are in the form of a Hamiltonian system on a three-dimensional phase space. The symplectic structure matrix is dependent on the phase variables, and it is degenerate: $\tilde{\mathbf{J}}\boldsymbol{\pi} = \boldsymbol{\pi} \times \boldsymbol{\pi} = \mathbf{0}$, signifying that total angular momentum is conserved: $\|\boldsymbol{\pi}\| = \text{constant}$. This is a generalization of our previous concept of *Hamiltonian system*. Much of the previously developed theory of Hamiltonian systems can be adapted to the setting of the free rigid body with analogous definitions of splitting method and symplectic integrators obtained by additive decomposition of the Hamiltonian.

It is possible to solve the Euler equations using an exact solution and to use this to design efficient integrators [68, 249, 382], but in the most common setting of molecular dynamics, where additional approximations will be needed, we are usually justified in treating these equations using a more elementary procedure [258]. If \mathbf{T} is a diagonal matrix, $\mathbf{T} = \text{diag}(I_1, I_2, I_3)$, then we split the Euler equations and approximate the solution by successive rotations around the three axes of inertia,

i.e. we compose the flows of

$$\dot{\pi} = \pi \times \begin{bmatrix} T_1^{-1}\pi_1 \\ 0 \\ 0 \end{bmatrix}, \quad \dot{\pi} = \pi \times \begin{bmatrix} 0 \\ T_2^{-1}\pi \\ 0 \end{bmatrix}, \quad \dot{\pi} = \pi \times \begin{bmatrix} 0 \\ 0 \\ T_3^{-1}\pi \end{bmatrix},$$

Each of these is, it turns out, easily integrated as a planar rotation (see Exercise 7). This yields a simple, efficient algorithm for the free rigid body which is symplectic in a generalized sense.

4.4.2 Rigid Body Molecular Dynamics Algorithm

To develop an integrator for the complete system (including external forces), we invoke the splitting technique,² solving successively for the translational motion from the center of mass equations, integrating the torques due to the rotational interactions, then solving the Euler equations, and recovering the rotation matrix from the linear system

$$\dot{\Theta} = \Theta \operatorname{skew}(T^{-1}\pi).$$

This is the approach described in [112] and is implemented in several software packages.

The reliability of these methods is supported by the fact that the combined scheme is a symplectic method in the generalized sense of constrained dynamics.

The specific steps of the algorithm proposed in [112] are given here. In what follows, we denote the variables associated to the k th rigid body by \mathbf{q}^k (position of center of mass), Θ^k (3×3 rotation matrix), \mathbf{p}^k (linear momentum vector), and π^k (angular momentum vector). Individual components are defined by double subscripts: the 2nd component of π^k is π_2^k . Procedures given below for rigid body k are meant to be performed for all rigid bodies in the system.

The algorithm is initialized by computing the forces \mathbf{F}^k and torques $\boldsymbol{\tau}^k$ acting on the k th rigid body, evaluated at the initial point. The relevant expressions are:

$$\mathbf{F}^k = -\frac{\partial U}{\partial \mathbf{q}^k}, \quad \boldsymbol{\tau}^k = -\operatorname{rot}\left(\left[\Theta^k\right]^T \frac{\partial U}{\partial \Theta^k}\right).$$

²We note the seminal role of the work in astronomy of Touma and Wisdom [368] in elucidating the “divide and conquer” approach for deriving such schemes for rigid bodies.

The notation $\partial U / \partial \Theta^k$ refers to a 3×3 matrix of partial derivatives of the potential with respect to the corresponding elements of the rotation matrix Θ^k , and, for a 3×3 matrix A ,

$$\text{rot}(A) = \text{skew}^{-1}(A - A^T).$$

Then the algorithm proceeds by iteration of timesteps, as shown below.

DLM Rigid Body Molecular Dynamics Step

1. “Kick”: update the momenta and angular momentum vectors with known forces and torques for a half step:

$$\mathbf{p}^k := \mathbf{p}^k + \frac{h}{2} \mathbf{F}^k, \quad \boldsymbol{\pi}^k := \boldsymbol{\pi}^k + \frac{h}{2} \boldsymbol{\tau}^k.$$

2. “Drift”: step forward a whole step in positions

$$\mathbf{q}^k := \mathbf{q}^k + h\mathbf{p}^k.$$

3. “Spin”: update the rotational state of the k th rigid body by the sequence of steps

$$\begin{aligned} \Theta &:= \Theta^x \left(\frac{h}{2} \boldsymbol{\pi}_1^k / I_1 \right); \boldsymbol{\pi}^k := \Theta \boldsymbol{\pi}^k; \Theta^k := \Theta^k \Theta^T \\ \Theta &:= \Theta^y \left(\frac{h}{2} \boldsymbol{\pi}_2^k / I_2 \right); \boldsymbol{\pi}^k := \Theta \boldsymbol{\pi}^k; \Theta^k := \Theta^k \Theta^T \\ \Theta &:= \Theta^z \left(h \boldsymbol{\pi}_3^k / I_3 \right); \boldsymbol{\pi}^k := \Theta \boldsymbol{\pi}^k; \Theta^k := \Theta^k \Theta^T \\ \Theta &:= \Theta^y \left(\frac{h}{2} \boldsymbol{\pi}_2^k / I_2 \right); \boldsymbol{\pi}^k := \Theta \boldsymbol{\pi}^k; \Theta^k := \Theta^k \Theta^T \\ \Theta &:= \Theta^x \left(\frac{h}{2} \boldsymbol{\pi}_1^k / I_1 \right); \boldsymbol{\pi}^k := \Theta \boldsymbol{\pi}^k; \Theta^k := \Theta^k \Theta^T \end{aligned}$$

The notation $\Theta^x(\phi)$ refers to a rotation around the x -axis by an angle ϕ , that is

$$\Theta^x(\phi) = \begin{bmatrix} 1 & 0 & 0 \\ 0 & \cos(\phi) & -\sin(\phi) \\ 0 & \sin(\phi) & \cos(\phi) \end{bmatrix},$$

with corresponding formulae for Θ^y and Θ^z .

4. “Kick”: update the momenta and angular momentum vectors (as in Step 1) with a half step using new forces \mathbf{F}^k and torques $\boldsymbol{\tau}^k$ evaluated at the current \mathbf{q} , Θ .

Note that the symmetric character of the algorithm could be revealed more clearly by dividing the “Drift” step into two half steps sandwiched around the Spin step (Kick, Drift, Spin, Drift, Kick), but as the updates Drift/Spin are decoupled, the order they are performed is not important.

Exercises

- 1 Implicit Midpoint Preserves First Integrals.** Show that the implicit midpoint method exactly preserves quadratic first integrals. That is, if we have a matrix $\mathbf{A} \in \mathbb{R}^{m \times m}$, a vector $\mathbf{b} \in \mathbb{R}^m$ and a scalar c , such that the function $I(\mathbf{z}) = \mathbf{z}^T \mathbf{A} \mathbf{z} + \mathbf{b}^T \mathbf{z} + c$ is a first integral of the differential equation system

$$\frac{d\mathbf{z}}{dt} = \mathbf{f}(\mathbf{z}),$$

then it follows that $I(\mathbf{z}_{n+1}) \equiv I(\mathbf{z}_n)$, where

$$\mathbf{z}_{n+1} = \mathbf{z}_n + h\mathbf{f}((\mathbf{z}_n + \mathbf{z}_{n+1})/2).$$

(The same property holds for all symplectic Runge-Kutta methods.)

- 2 Fermi-Pasta-Ulam Problem.** Consider the Fermi-Pasta-Ulam (FPU) problem, with Hamiltonian

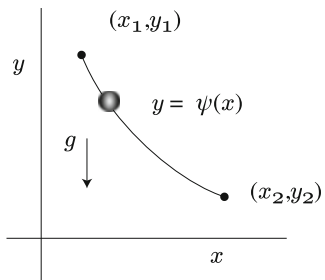
$$H = \frac{1}{2}\mathbf{p}^T \mathbf{M}^{-1} \mathbf{p} + \frac{\kappa}{2} \sum_{i=0}^N (q_{i+1} - q_i)^2 + \frac{\mu}{4} \sum_{i=0}^N (q_{i+1} - q_i)^4, \quad q_0 = q_{N+1} = 0,$$

where \mathbf{q} and \mathbf{p} give the respective positions and momenta of $N+1$ -many particles on a line. We shall consider $N = 10$ moving atoms with $\mathbf{M} = \mathbf{I}$, $\kappa = 10$ and $\mu = 1/10$.

- a. Implement the Symplectic Euler scheme and numerically estimate the maximum stepsize where the scheme is stable.
 - b. Implement the multiple time-stepping r-RESPA scheme (4.2) by splitting the potential energy into the fast term and slow term. Investigate how the maximum stable stepsize changes as the number of fast steps r is varied.
 - c. In the r-RESPA scheme, we approximated the flow map of the fast motion using r small steps. Instead, as the fast motion is the result of a linear force term, we can solve exactly rather than approximating. Implement a version of the scheme (4.2) which replaces the r -step approximation of the fast motion with an exact solve.
- 3 Bead-on-Wire.** We model a bead sliding along a curved wire ($y = \psi(x)$) in the plane and moving under an external force $-[\varphi_x(x, y), \varphi_y(x, y)]$ generated by potential φ . Show that the equations of motion for this system can be written

$$\begin{aligned} \frac{dx}{dt} &= p_x \\ \frac{dy}{dt} &= p_y \end{aligned}$$

Fig. 4.8 Brachistochrone problem



$$\frac{dp_x}{dt} = -\varphi_x(x, y) + \lambda \psi'(x)$$

$$\frac{dp_y}{dt} = -\varphi_y(x, y) - \lambda$$

$$0 = y - \psi(x)$$

- a. Apply SHAKE to this system and write out the resulting discrete equations.
 - b. Implement the method and use it to find the solution of the *Brachistochrone problem*: to minimize the passage time for a bead moving on a curved section of wire between two points, under a constant external force (gravity), see Fig. 4.8. You may wish to compare your solution with the classical solution obtained using the calculus of variations [206].
4. By eliminating the momenta, show that (4.27)–(4.29) reduce to (4.25)–(4.26).
5. Refer to the Eqs. (4.35)–(4.37).
- a. Show that it is possible write the equations of SHAKE (4.27)–(4.29) in the form (4.35)–(4.37) by defining
- $$\tilde{\lambda}_n = \lambda_n.$$
- b. Show that it is possible to write the equations of RATTLE (4.30)–(4.34) in the form (4.35)–(4.37) by defining
- $$\tilde{\lambda}_n = (\lambda_n + \mu_n)/2.$$

6. Prove that

$$\boldsymbol{\Theta}^T \dot{\boldsymbol{\Theta}} = \text{skew}(\boldsymbol{\omega}_b).$$

Note that this follows if we have $\boldsymbol{\Theta}^T \dot{\boldsymbol{\Theta}} \delta_0 = \text{skew}(\boldsymbol{\omega}_b) \delta_0$ for any vector δ_0 .

- a. Let A be a 3×3 matrix and let \mathbf{u}, \mathbf{v} be vectors in \mathbb{R}^3 . Prove the identity $A(\mathbf{u} \times \mathbf{v}) = (A\mathbf{u}) \times (A\mathbf{v})$.

- b. Premultiply Eq. (4.39) by $\boldsymbol{\Theta}^T$, using $\boldsymbol{\delta}_i = \boldsymbol{\Theta}(t)\boldsymbol{\delta}_i(0)$, and use part (a), then the definition of $\boldsymbol{\omega}_b$ to obtain

$$\boldsymbol{\Theta}^T \dot{\boldsymbol{\Theta}} \boldsymbol{\delta}_i(0) = \boldsymbol{\omega}_b \times \boldsymbol{\delta}_i(0).$$

Thus

$$\text{skew}(\boldsymbol{\omega}_b) = \boldsymbol{\Theta}^T \dot{\boldsymbol{\Theta}}.$$

7. Determine the exact solution of the differential equation system

$$\dot{\boldsymbol{\pi}} = \boldsymbol{\pi} \times \begin{bmatrix} T_1^{-1}\pi_1 \\ 0 \\ 0 \end{bmatrix}$$

and thus obtain, by splitting, a second order symplectic integrator for the Euler equations of a rigid body (4.41).

Chapter 5

Phase Space Distributions and Microcanonical Averages

In the previous chapters, we considered the approximation of Hamiltonian trajectories. In this chapter we study the paths emanating from the collection of all initial conditions within a given set. This is the starting point for statistical mechanics which allows the calculation of averages.

Making sense of molecular dynamics requires that we understand and quantify the uncertainty due to its chaotic nature. Ultimately we will see that it is useful to think of the visited positions and velocities of the atoms as being spread out over the phase space with a certain density. Trajectories of a molecular system then trace out random paths which effectively sample the underlying distribution. In this picture, individual movements of the atoms have no relevance, but what is interesting and relevant is their average motions, or the likelihood of finding an atom at a given location relative to its neighbors. The use of averages and a statistical mechanical interpretation is therefore intimately connected with the nonlinear and chaotic nature of molecular dynamics.

Consider a set of points in phase space, viewing each point as an initial condition for a trajectory of a dynamical system. The set is mapped forward in time by solving some differential equations. At any given instant in time we may examine the snapshot of all the trajectories. The points of the initial set (or any later image of it) do not have to be (and indeed are unlikely to be) uniformly distributed throughout the phase space. For example the collection may favour certain energies (or they may all have the same energy), or, due to some arbitrariness in their selection, they may be concentrated in one small, localized region of the phase space. As the trajectories are evolved, the way the points are dispersed would also be expected to vary in time. One may observe that the paths spread out and eventually cover an extended region, or they may remain clumped together for all time.

To discuss the changes in the relative concentrations of phase points in one or another region, we introduce the concept of a *probability measure* for the distribution of phase space points. Normally this is represented by a *density*, a non-negative function of the phase space variables that can be used to characterize sets

in terms of the relative concentration of phase points. The density may be viewed as depending both on time and space. When discussing the changes in the density over time, we are taking a *macroscopic* perspective. The density itself can be viewed as another type of state, a *macroscopic state* or *macrostate*. In the case of Hamiltonian dynamics, the evolution of the density is governed by Liouville's equation. We discuss this equation below. The behavior of the evolving point set is slightly complicated by the fact that each trajectory is confined to a particular level set of energy. The corresponding points of two trajectories evolving on different level sets would be expected to differ for all time in a way that reflects the geometry of the energy function. To simplify the discussion we initially consider the dependencies within a particular energy level set only, however, at the end of the chapter we discuss the situation which commonly arises when using a symplectic integrator: the energy surface sampled by the discretization method is different from the desired energy surface.

Our treatment of statistical mechanics is abbreviated and specialized as our focus is ultimately on certain types of systems frequently arising in molecular dynamics and their numerical treatment. We refer the interested reader to more detailed treatments including [57, 70, 168, 197, 264, 297, 372].

5.1 The Solution Operator

In Chap. 3, we introduced the Lie derivative of a function g of the phase variables with respect to a dynamical system $\dot{z} = f(z)$:

$$\mathcal{L}_f g = \mathbf{f} \cdot \nabla g.$$

This is obtained by differentiating a composite function $g(z(t))$ with respect to t , along a solution trajectory. That is, describing a trajectory in terms of the flow map by $z(t) = \mathcal{F}_t(\xi)$, $t \in \mathbb{R}$, we have

$$\frac{d}{dt} g(\mathcal{F}_t(\xi)) = (\mathcal{L}_f g)(\mathcal{F}_t(\xi)).$$

Replacing ξ by z (it is an arbitrary point), define a function $\tilde{g}(z, t) \stackrel{\text{def}}{=} g(\mathcal{F}_t(z))$. The partial derivative of $\tilde{g}(z, t)$ with respect to t is

$$\frac{\partial \tilde{g}}{\partial t}(t, z) = \nabla g(\mathcal{F}_t(z)) \cdot \frac{d}{dt} \mathcal{F}_t(z) = \nabla g(\mathcal{F}_t(z)) \cdot \mathbf{f}(\mathcal{F}_t(z)) = (\mathcal{L}_f g)(\mathcal{F}_t(z)). \quad (5.1)$$

On the other hand, viewing \mathcal{L}_f as an operator on the phase variables only, we have

$$\begin{aligned} (\mathcal{L}_f \tilde{g})(z) &= f(z) \cdot \nabla_z [g(\mathcal{F}_t(z))] \\ &= f(z) \cdot [\mathcal{F}'_t(z)^T \nabla g(\mathcal{F}_t(z))] \\ &= [\mathcal{F}'_t(z) f(z)] \cdot \nabla g(\mathcal{F}_t(z)) \\ &= f(\mathcal{F}_t(z)) \cdot \nabla g(\mathcal{F}_t(z)) \\ &= (\mathcal{L}_f g)(\mathcal{F}_t(z)). \end{aligned}$$

This is the same as the right hand side of (5.1). This means that \tilde{g} satisfies the equation

$$\frac{\partial \tilde{g}}{\partial t} = \mathcal{L}_f \tilde{g}. \quad (5.2)$$

This is a time-dependent, linear (hyperbolic) partial differential equation. The steady state solutions of this equation (defined by $\partial \tilde{g} / \partial t = 0$) are of the form $\tilde{g}(z, t) = \varphi(z)$ where φ satisfies $\mathcal{L}_f \varphi(z) \equiv 0$. These are just the first integrals of the ordinary differential equation system $\dot{z} = f(z)$.

It is intuitively appealing to define the solution of (5.2) by

$$\tilde{g}(z, t) = G_t \tilde{g}(z, 0), \quad \text{where } G_t = e^{t\mathcal{L}_f}.$$

Let us refer to G_t as the *solution operator* associated to the differential equation $\dot{z} = f(z)$. Calculating the exponential operator $e^{t\mathcal{L}_f}$ can be thought of as tantamount to solving a linear partial differential equation for given (Cauchy) initial data.

The projection onto the i th coordinate, denoted ∂_i , is itself a scalar valued function of z ($\partial_i(z) = z_i$). Calculating directly we have $\mathcal{L}_f z_i = f_i$. The interpretation of the solution of the initial value problem in terms of the solution operator G_t is given by

$$(e^{t\mathcal{L}_f} \partial_i)(z(0)) = z_i(t).$$

The notion of the solution operator and the concept of flow map are essentially equivalent descriptions of the dynamics of the system.

In physics treatments, the Liouvillian is often denoted $i\mathcal{L}$. This may seem natural since (a) it allows a formal correspondence with the Schrödinger equation and between the propagators of quantum mechanics and classical mechanics, and (b) for Hamiltonian dynamics, as we shall see, the Liouvillian is skew-adjoint (in a certain sense skew symmetric) and the inclusion of i explicitly calls attention to this fact. However, we feel it is more natural to omit the i in a treatment that includes study of both stochastic and deterministic models.

5.2 Evolution of Probability Measure

The solution operator describes how a function of the phase variables is mapped forward in time under the flow of the differential equation. An alternative (“dual”) perspective is in terms of the evolution of the measure (or density) of points in phase space. We begin by summarizing a few basic principles needed to provide a foundation for working with probability measures.

5.2.1 Measure, Probability and Function Spaces

A probability distribution is assumed to be characterized by a *measure* on the state space of the problem which is the integral of a probability density function defined on the phase space of the problem that assigns nonnegative real numbers to each state. We outline the technical setting here. To gain a fuller understanding of the mathematical issues involved in this chapter, it may be helpful to refer to an introductory text on analysis such as [26, 317].

Assume, as usual, a system of N atoms with phase space having dimension m (typically $m = 2N_c = 2N_d = 6N$). Let $\mathcal{D} \subset \mathbb{R}^m$ be a suitable set comprising the collection of admissible phase space points z .¹ A *density* on \mathcal{D} is a function $\rho : \mathcal{D} \rightarrow \mathbb{R}$ such that (i) $\rho(z) \geq 0$, $z \in \mathcal{D}$, and (ii) $\int_{\mathcal{D}} \rho d\omega < \infty$, where $d\omega = dz_1 dz_2 \dots dz_m$ (i.e. $\int_{\mathcal{D}} \rho d\omega$ is the integral of the measurable function ρ in the Lebesgue sense). A *probability density function* (or *p.d.f.*) on \mathcal{D} is a density which is normalized so that

$$\int_{\mathcal{D}} \rho d\omega = 1.$$

Any density (with positive total integral) can be normalized by dividing by $\int_{\mathcal{D}} \rho d\omega$.

For any measurable subset \mathcal{A} of \mathcal{D} , and probability density ρ , we define

$$\Pr(\mathcal{A}) \stackrel{\text{def}}{=} \int_{\mathcal{A}} \rho d\omega.$$

¹The technical requirement is that \mathcal{D} be Lebesgue-measurable. There are some pathological sets for which this condition fails, but we will always assume the sets we are interested in are measurable. Open and closed sets in \mathbb{R}^m are Lebesgue-measurable, for example a rectangular box. Sets which are constructed by taking countable unions or intersections of measurable sets are measurable. A suitable family of sets on which Lebesgue measure can be defined is the so-called Borel σ -algebra obtained by countable unions, intersections, or relative complements of open balls in \mathbb{R}^m .

It is automatic that $0 \leq \Pr(\mathcal{A}) \leq 1$. Certain properties need to be assumed regarding ρ and the way that this is formalized in mathematics is by description of the vector space of functions to which ρ belongs.

A useful class of functions from a domain $\mathcal{D} \subset \mathbb{R}^m$ to \mathbb{R} are those that satisfy the following boundedness condition:

$$\int_{\mathcal{D}} \phi^2(z) d\omega < \infty. \quad (5.3)$$

The set of functions from $\mathcal{D} \subset \mathbb{R}^m$ to \mathbb{R} which satisfy (5.3) is referred to as the space $L^2(\mathcal{D})$ and we define the $L^2(\mathcal{D})$ norm by

$$\|\phi\|_{L^2(\mathcal{D})} \stackrel{\text{def}}{=} \left[\int_{\mathcal{D}} \phi^2(z) d\omega \right]^{1/2}.$$

This is a real *Hilbert space* or *complete inner product space* in which, for any $\phi, \psi \in L^2(\mathcal{D})$, the inner product is defined by

$$\langle \phi, \psi \rangle_{L^2(\mathcal{D})} \stackrel{\text{def}}{=} \int_{\mathcal{D}} \phi(z) \psi(z) d\omega.$$

Thus $\|\phi\|_{L^2(\mathcal{D})}^2 = \langle \phi, \phi \rangle_{L^2(\mathcal{D})}$.

The inner product is a symmetric, bilinear operation: if α, β are real scalars and $f, g, h \in L^2(\mathcal{D})$, then

$$\langle \alpha f + \beta g, h \rangle = \alpha \langle f, h \rangle + \beta \langle g, h \rangle,$$

and

$$\langle f, g \rangle = \langle g, f \rangle.$$

The space $L^2(\mathbb{R}^m)$ includes for example the continuous functions with compact (closed, bounded) support, where the *support* of a function f is the closure of the set of arguments for which the function is nonzero and is denoted $\text{supp } f$.²

² $L^2(\mathbb{R}^m)$ also includes many other types of functions important in molecular modelling, for example the multivariate Gaussian $\exp(-\sum_{i=1}^m \alpha_i x_i^2)$, where $\alpha_i > 0$, $i = 1, 2, \dots, m$ are coefficients; such a function goes rapidly to zero as any $x_i \rightarrow \infty$, so the improper integral converges. $L^2(\mathbb{R}^m)$ also includes the compactly supported functions with finite “jump discontinuities” at a finite number of locations.

Given a density ρ , we may identify a collection of functions g for which the integral with respect to ρ is bounded, i.e. for which we can define the inner product $\langle g, \rho \rangle = \int_{\mathcal{D}} g(z)\rho(z)d\omega$, and thus we can define

$$\text{Av}_\rho(g) \stackrel{\text{def}}{=} \frac{1}{\int_{\mathcal{D}} \rho(z)d\omega} \langle g, \rho \rangle = \int_{\mathcal{D}} g \hat{\rho} d\omega.$$

We term this the *spatial average* of the function g with respect to the probability measure associated to ρ .

5.2.2 Liouville Equation

We now use the concept of a smooth probability density to discuss the change in concentration of points present in a given small volume in phase space.

Let $\rho(z, t)$ be the probability density associated to a collection of phase points moving under a vector field f on the phase space \mathbb{R}^m . Let \mathcal{A} be a suitable region of volume V within the phase space (say a rectangular m -dimensional box). The fraction v of phase points present in \mathcal{A} at time t is the integral of ρ over \mathcal{A} :

$$v(t) = \int_{\mathcal{A}} \rho(z, t)d\omega,$$

which may be viewed as a smooth function of time. On the one hand

$$\frac{d}{dt} v = \int_{\mathcal{A}} \frac{\partial \rho(z, t)}{\partial t} d\omega,$$

while, on the other hand, this same rate of change may be written as the negative of the particle flux over the boundary of \mathcal{A} :

$$\frac{d}{dt} v = - \int_{\partial \mathcal{A}} f \cdot n \rho(z, t) d\sigma,$$

where $n(z)$ is the unit outward normal to the surface $\partial \mathcal{A}$ at the point z and $d\sigma$ is the surface element. Using the divergence theorem, we may rewrite the latter quantity as a volume integral:

$$\frac{d}{dt} v = - \int_{\mathcal{A}} \nabla \cdot (f(z)\rho(z, t)) d\omega.$$

Therefore, since this should hold for an arbitrary domain \mathcal{A} , we must have

$$\frac{\partial \rho}{\partial t} = -\nabla \cdot (\rho f).$$

This is called the Liouville equation or continuity equation. It tells us how the distribution of phase points varies in time and space.

An alternative form for the continuity equation is:

$$\frac{\partial \rho}{\partial t} = - \sum_i \left[\rho \frac{\partial f_i}{\partial z_i} + f_i \frac{\partial \rho}{\partial z_i} \right].$$

The operator \mathcal{M}_f , defined for a scalar valued function w by $\mathcal{M}_f w = -\nabla \cdot (wf)$, is called the Liouvillian operator.

There is a close relationship between \mathcal{M}_f and the Lie derivative discussed earlier. Let u, v be two scalar valued functions in \mathbb{R}^m which tend to zero sufficiently rapidly at infinity. We truncate the domain to a large box \mathcal{A}_ℓ with edge of length 2ℓ centered at the origin, approximating the inner product by:

$$\langle u, \mathcal{L}_f v \rangle \approx \int_{\mathcal{A}_\ell} u \mathcal{L}_f v d\omega = \int_{\mathcal{A}_\ell} u \sum_i f_i \frac{\partial v}{\partial z_i} d\omega.$$

Splitting this sum up, we treat each term by integration by parts

$$\int_{\mathcal{A}_\ell} u \sum_i f_i \frac{\partial v}{\partial z_i} d\omega = \sum_i \int_{\mathcal{A}_\ell} u f_i \frac{\partial v}{\partial z_i} d\omega \quad (5.4)$$

$$= B - \sum_i \int_{\mathcal{A}_\ell} v \frac{\partial}{\partial z_i} (u f_i) d\omega, \quad (5.5)$$

where the term $B = \sum_i \int_{\partial \mathcal{A}_\ell} u f_i v v_i d\sigma$, is a surface integral over the boundary of \mathcal{A}_ℓ , where v_i is the i 'th component of the unit outward normal to the surface $\partial \mathcal{A}_\ell$ bounding the region \mathcal{A}_ℓ . By our assumptions that u and v are rapidly decaying we know that $B \rightarrow 0$, as $\ell \rightarrow \infty$. Taking the limit, we are thus left with the equation

$$\langle u, \mathcal{L}_f v \rangle = - \sum_i \int_{\mathbb{R}^m} v \frac{\partial}{\partial z_i} (u f_i) d\omega = \langle \mathcal{M}_f u, v \rangle.$$

We refer to \mathcal{M}_f as the *adjoint operator*³ of \mathcal{L}_f and we write $\mathcal{M}_f = \mathcal{L}_f^\dagger$, where

$$\langle u, \mathcal{L}_f v \rangle = \langle \mathcal{L}_f^\dagger u, v \rangle$$

and

$$\mathcal{L}_f^\dagger u = -\nabla \cdot (uf).$$

The density ρ evolves as the solution of the partial differential equation

$$\frac{\partial \rho}{\partial t} = \mathcal{L}_f^\dagger \rho,$$

where we interpret ρ as a function of both z and t and view \mathcal{L}_f^\dagger as only operating on the spatial components. This means, formally, $\rho(z, t) = e^{t\mathcal{L}_f^\dagger} \rho(z, 0)$. We can think of $\exp(t\mathcal{L}_f^\dagger)$ as defining the *propagator* of measure.

5.2.3 The Liouville Equation for Hamiltonian Systems

Until now we have considered a general system $\dot{z} = f(z)$. What happens when f is derived from a Hamiltonian?

From the above we know that for a smooth scalar function $u = u(z)$,

$$\mathcal{L}_f^\dagger u = -\nabla \cdot (uf) = -f \cdot \nabla u - u \nabla \cdot f.$$

The term $\nabla \cdot f$ vanishes for $f = J\nabla H$. Thus we have

$$\mathcal{L}_f^\dagger u = -f \cdot \nabla u = -\mathcal{L}_f u.$$

If this holds for all smooth u , we write

$$\mathcal{L}_f^\dagger = -\mathcal{L}_f.$$

³The adjoint operator (acting on functions) is not to be confused with the adjoint of a map (which acts on points in phase space) encountered in Chap. 2.

In this case we say that the operator \mathcal{L}_f is *skew-adjoint*. The equations

$$\frac{\partial g}{\partial t} = \mathcal{L}_f g,$$

for the solution operator, and

$$\frac{\partial \rho}{\partial t} = \mathcal{L}_f^\dagger \rho = -\mathcal{L}_f \rho,$$

for the propagation of measure, are obviously closely related. Simply changing the direction of time in one ($t \rightarrow -t$) results in the other. In common parlance, $e^{t\mathcal{L}_f^\dagger}$ is referred to as the *forward* propagator and $e^{t\mathcal{L}_f}$ the *backward* propagator.

An important consequence of the skew symmetry of \mathcal{L}_f for a divergence-free system is that the propagator $e^{t\mathcal{L}_f^\dagger}$ preserves the integral over the whole phase space, i.e.

$$\begin{aligned} \int_{\mathcal{D}} e^{t\mathcal{L}_f^\dagger} \rho(z) d\omega &= \int_{\mathcal{D}} e^{-t\mathcal{L}_f} \rho(z) d\omega \\ &= \int_{\mathcal{D}} \rho(\mathcal{F}_{-t}(z)) d\omega \\ &= \int_{\mathcal{D}} \rho(z) d\omega, \end{aligned}$$

since we can view $\mathcal{F}_{-t}(z)$ as a change of variables by a volume-preserving map.

The Liouvillian of a Hamiltonian system with N_c degrees of freedom and a Hamiltonian of the form $H = \sum_{i=1}^{N_c} p_i^2/(2m_i) + U(q_1, \dots, q_{N_c})$ can be written

$$\mathcal{L}_H^\dagger = - \sum_{i=1}^{N_c} m_i^{-1} p_i \frac{\partial}{\partial q_i} - \sum_{i=1}^{N_c} F_i \frac{\partial}{\partial p_i},$$

where $F_i = -\partial U / \partial q_i$.

5.3 The Microcanonical Probability Measure

In this section, we continue the discussion of the Hamiltonian case by introducing the microcanonical probability measure, the natural measure associated to a surface of fixed energy. The framework we have discussed so far is useful when the density is known to be a C^∞ function of phase space, but this is not always the case.

A simple example which we would wish to include in our framework is the point distribution which concentrates all measure at a single point. This type of object cannot be directly represented by a smooth function (or even by one in L^2), but it is nonetheless possible to extend our framework in a way that makes sense in such cases.

5.3.1 Generalized Functions

In order to address the need to describe the evolution of a broader class of distributions, we introduce the concept of “generalized function” as a mathematical framework incorporating, for example, Dirac delta functions.⁴ Formally, we define a *generalized function* as a real-valued linear operation (a *linear functional*) defined on a suitable space of functions. The functions on which the generalized function acts are called *test functions*. Some choices for the space of test functions \mathcal{T}^m defined on \mathbb{R}^m include:

- the C^∞ functions with compact support in \mathbb{R}^m , denoted $C_0^\infty(\mathbb{R}^m)$,
- the space $S(\mathbb{R}^m)$ of C^∞ functions on \mathbb{R}^m whose derivatives decay rapidly at infinity (the so-called *Schwartz space*)⁵

If f is a bounded, smooth function on \mathbb{R}^m , we may define a generalized function T_f by reference to its *action* on a test function $\phi \in \mathcal{T}$ via integration:

$$T_f(\phi) = \int_{\mathbb{R}^m} f(z)\phi(z)d\omega.$$

This is very like the L^2 inner product, but the functions involved do not both need to lie in L^2 . Nevertheless, we write

$$T_f(\phi) = \langle f, \phi \rangle,$$

⁴The alternate term for “generalized function” is “distribution” which is suggestive of “probability distribution,” but “distribution” is a more general concept.

⁵The formal definition of S is

$$S(\mathbb{R}^m) \stackrel{\text{def}}{=} \{f \in C^\infty(\mathbb{R}^m) \mid \|f\|_{\alpha,\beta} < \infty\},$$

where α and β are arbitrary *multi-indices*, i.e. vectors of non-negative integers, and

$$\|f\|_{\alpha,\beta} \stackrel{\text{def}}{=} \sup_{z \in \mathbb{R}^m} \left| z_1^{\alpha_1} z_2^{\alpha_2} \cdots z_m^{\alpha_m} \frac{\partial^{\beta_1+\beta_2+\dots+\beta_m} f}{\partial z_1^{\beta_1} \partial z_2^{\beta_2} \cdots \partial z_m^{\beta_m}} \right|.$$

as a helpful shorthand. For the Dirac delta δ , its action on a function $\phi \in \mathcal{T}$ is $\delta[\phi] = \phi(0)$. We write this also as

$$\langle \delta, \phi \rangle = \int \delta(z)\phi(z)d\omega = \phi(0).$$

This concept of the delta function (that appears in the integral) may be motivated by introducing a sequence of continuous functions d_ε having the properties (i) $\int d_\varepsilon d\omega = 1$, (ii) $\text{supp}(d_\varepsilon) \rightarrow 0$, as $\varepsilon \rightarrow 0$. Then the action of the delta function can be seen as the limit of the actions of the functions d_ε . Alternatively, one may use a sequence of smooth functions $\{d_\varepsilon\}$, such as, in one dimension,

$$d_\varepsilon = \frac{1}{\sqrt{2\varepsilon\pi}} \exp\left(-\frac{z^2}{2\varepsilon}\right).$$

An example where the smooth probability density in Euclidean space is not quite the right one is in the setting of conservative (Hamiltonian) systems such as our N-body molecular system, since the evolution is restricted by invariants. The most obvious of these is the energy which we know to be a constant of motion. Therefore we need to work not on open subsets of the phase space \mathbb{R}^m of our differential equations, but on lower dimensional submanifolds embedded within the phase space, e.g. the energy surface. It will be necessary to assume a density that is defined over the submanifold of constant energy. If other invariants are present, such as fixed total momentum, the discussion would need to be modified to reflect this fact.

5.3.2 Steady States

We are inclined to view the steady states (equilibrium solutions) of the Liouville equation as solutions of

$$\mathcal{L}_f^\dagger \rho = 0.$$

However, this requires a little care. In general, we would like to be able to apply \mathcal{L}_f^\dagger to nonsmooth distributions such as Dirac delta functions for which the application of the Liouville operator does not make obvious sense (as we have not mentioned how to differentiate delta functions). Instead we will define the stationary solution in terms of integrals against test functions.

The idea of defining a distribution in terms of an integral against another function is very appropriate in the setting of molecular dynamics. We are, after all, interested in the convergence of averages of smooth functions with respect to the evolving

probability distribution. Let ϕ be a C^∞ function of the phase variables with compact support and define the time t average by

$$\bar{\phi}(t) = \frac{\int_{\mathcal{D}} \phi(\mathbf{q}, \mathbf{p}) \rho(\mathbf{q}, \mathbf{p}, t) d\omega}{\int_{\mathcal{D}} \rho(\mathbf{q}, \mathbf{p}, t) d\omega}. \quad (5.6)$$

As the flow is Hamiltonian, $\int_{\mathcal{D}} \rho(\mathbf{q}, \mathbf{p}, t) d\omega \equiv \int_{\mathcal{D}} \rho(\mathbf{q}, \mathbf{p}, 0) d\omega$. Thus the condition for $\bar{\phi}$ to converge is just that

$$\int_{\mathcal{D}} \phi(\mathbf{q}, \mathbf{p}) \frac{\partial \rho}{\partial t}(\mathbf{q}, \mathbf{p}, t) d\omega \rightarrow 0.$$

Since

$$\frac{\partial \rho}{\partial t} = \mathcal{L}_f^\dagger \rho,$$

this suggests that the condition for the invariant probability density function ρ_∞ should be

$$\int_{\mathcal{D}} \phi \mathcal{L}_f^\dagger \rho_\infty d\omega = 0,$$

for all suitable functions $\phi \in C_0^\infty(\mathbb{R}^m)$. We say that ρ_∞ satisfies

$$\mathcal{L}_f^\dagger \rho_\infty = 0,$$

in the *weak* or *variational* sense. When such a density exists, we refer to the associated probability distribution as an *invariant distribution*. Such invariant distributions are essential tools in molecular modelling. In the case of a Hamiltonian system, we know that $\mathcal{L}_f^\dagger = -\mathcal{L}_f$, and, moreover,

$$\mathcal{L}_f H = 0,$$

so that H is a first integral. Any probability distribution whose density is a smooth function of H will also be an invariant distribution.

In particular, consider the density

$$\rho_\varepsilon(\mathbf{q}, \mathbf{p}) = Z_\varepsilon^{-1} e^{-(H(\mathbf{q}, \mathbf{p}) - E)^2/2\varepsilon},$$

where ε is an arbitrary small positive constant and E is an accessible energy level. We assume that H tends to infinity sufficiently rapidly as $\|\mathbf{z}\| \rightarrow \infty$ so that the exponential decays sufficiently rapidly (and thus the total integral exists) and take

Z_ε to be a normalization factor that insures that we have, for each ε , a well defined probability density function.

As we decrease ε , the density remains invariant under Liouville's equation. The prefactor means that we can think of a sequence of smooth densities taken with successively smaller values of ε as approaching the limiting distribution defined in terms of the delta function by

$$\rho_0(\mathbf{q}, \mathbf{p}) = Z_{H=E}^{-1} \delta[H(\mathbf{q}, \mathbf{p}) - E], \quad (5.7)$$

where $Z_{H=E}$ is the appropriate limiting value of the normalization constant. To make this statement precise, the definition of the limit must be taken here in the weak sense, that is, we need to study the limit

$$\lim_{\varepsilon \rightarrow 0} Z_\varepsilon^{-1} \int_{\mathcal{D}} \phi(\mathbf{q}, \mathbf{p}) \rho_\varepsilon d\omega, \quad (5.8)$$

taken in relation to a test function $\phi \in \mathcal{T}$. The proof that (5.8) can be taken and that

$$\lim_{\varepsilon \rightarrow 0} Z_\varepsilon^{-1} \int_{\mathcal{D}} \phi(\mathbf{q}, \mathbf{p}) \rho_\varepsilon d\omega = \rho_0(\mathbf{q}, \mathbf{p}) = Z_{H=E}^{-1} \int_{\mathcal{D}} \phi(\mathbf{q}, \mathbf{p}) \delta[H(\mathbf{q}, \mathbf{p}) - E] d\omega$$

may be found in the PhD thesis of Hartmann [171, Appendix D].

From a mathematical perspective, we may prefer to have a concept of the microcanonical probability measure that does not involve delta functions. It is possible to understand computations of averages with respect to a Dirac-type generalized function like ρ_0 as integrals on a set in a space of dimension one less than that of the ambient phase space (which is typically an even dimensional Euclidean space). We assume the level sets $\Sigma_E = \{(\mathbf{q}, \mathbf{p}) | H(\mathbf{q}, \mathbf{p}) = E\}$ to be bounded and define the invariant measure of a set $\mathcal{M} \subset \Sigma_E$ by

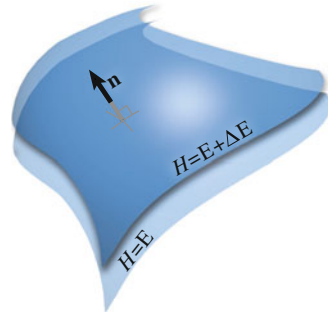
$$\mu(\mathcal{M}) = \int_{\mathcal{M}} \frac{1}{\|\nabla H\|} d\sigma,$$

where $d\sigma$ is the “area element” of the energy surface. (The term “area” in this context might be replaced by “hyperarea” or “volume” since we are in many dimensions.) If we can represent the $m - 1$ -dimensional set \mathcal{M} as the image of an open set $\mathcal{U} \in \mathbb{R}^{m-1}$ under a smooth mapping $\mathbf{g} : \mathbb{R}^{m-1} \rightarrow \Sigma_E$, then we have

$$\text{Vol}(\mathcal{M}) = \int_{\mathcal{U}} \sqrt{\det[(\mathbf{g}'(\xi))^T \mathbf{g}'(\xi)]} d\xi_1 d\xi_2 \dots d\xi_{m-1}.$$

Thus the invariant measure of interest to us is a rescaling of the indicated metric by the factor $1/\|\nabla H\|$.

Fig. 5.1 A thickened shell between energy levels E and $E + \Delta E$



Let us attempt to motivate the definition of the invariant measure. Consider a subset M of the level set Σ_E . We suppose $\|\nabla H\|$ to be bounded away from zero on Σ_E . At each point of M we let $\mathbf{n} = \nabla H / \|\nabla H\|$ be the unit normal to the energy surface and define a local coordinate ξ measuring distance along the direction of the unit normal, so that for a small offset ΔE of the energy, $z + \xi \mathbf{n}$ is the point of intersection with the level set $\Sigma_{E+\Delta E}$. We thus obtain a thickened shell of points around the patch M with energy between E and $E + \Delta E$ (Fig. 5.1).

The volume of this thickened shell is clearly

$$\Delta V = \int_{\mathcal{M}} \xi d\sigma,$$

but since

$$\Delta E = H(z + \mathbf{n}\xi) - H(z) = \nabla H \cdot \mathbf{n}\xi + \mathcal{O}(\Delta E^2),$$

and $\mathbf{n} = \nabla H / \|\nabla H\|$, we have

$$\xi = \frac{\Delta E}{\|\nabla H\|} + \mathcal{O}(\Delta E^2),$$

and

$$\Delta V = \int_{\mathcal{M}} \frac{\Delta E}{\|\nabla H\|} d\sigma + \mathcal{O}(\Delta E^2).$$

Taking the ratio of ΔV to ΔE we find

$$\frac{\Delta V}{\Delta E} = \int_{\mathcal{M}} \frac{1}{\|\nabla H\|} d\sigma + \mathcal{O}(\Delta E).$$

The limit of this as $\Delta E \rightarrow 0$ defines a quantity

$$\mu(\mathcal{M}) = \int_{\mathcal{M}} \frac{1}{\|\nabla H\|} d\sigma.$$

As both volume and energy are invariant under the Hamiltonian flow, $\mu(\mathcal{M})$ must be invariant under the flow, thus

$$\mu(\mathcal{F}_t(\mathcal{M})) = \mu(\mathcal{M}).$$

The invariant measure of the whole level set Σ_E is defined as the *microcanonical partition function*

$$Z_E = \mu(\Sigma_E).$$

Example 5.1 Consider the harmonic oscillator $H(q, p) = p^2/2 + \Omega^2 q^2/2$. The energy surface $H = E > 0$ is an ellipse. The partition function is obtained by integrating in the standard way. Parameterizing the surface by q , we have $p = \sqrt{2E - \Omega^2 q^2}$, then

$$\begin{aligned} \mu(\Sigma_E) &= 4 \int_0^{\sqrt{2E}} \frac{\sqrt{1 + p_q^2}}{\sqrt{H_p^2 + H_q^2}} dq \\ &= 4 \int_0^{\sqrt{2E}/\Omega} \frac{\sqrt{1 + \frac{\Omega^4 q^2}{2E - \Omega^2 q^2}}}{\sqrt{p^2 + \Omega^4 q^2}} dq \\ &= 4 \int_0^{\sqrt{2E}/\Omega} \frac{1}{\sqrt{2E - \Omega^2 q^2}} dq \\ &= 2\pi/\Omega. \end{aligned}$$

Example 5.2 Consider a system of N non-interacting particles of mass m moving in periodic boundary conditions within a box of volume V . The Hamiltonian is

$$H = \frac{1}{2m} \sum_{i=1}^N \|\mathbf{p}_i\|^2$$

so

$$Z_E = V^N \int_S \frac{m}{r} d\sigma$$

where \mathcal{S} is the $3N - 1$ dimensional sphere in $3N$ dimensions of radius $r = \sqrt{2mE}$, and $d\sigma$ is the surface area element on this sphere. V^N is the contribution due to integration over positions. Thus we have

$$\begin{aligned} Z_E &= V^N \frac{m}{\sqrt{2mE}} A(\mathcal{S}) = V^N \frac{\sqrt{m}}{\sqrt{2E}} 3N\pi^{3N/2} \frac{(2mE)^{(3N-1)/2}}{\Gamma(3N/2 + 1)}, \\ &= V^N \frac{(2\pi mE)^{3N/2}}{E\Gamma(3N/2)}, \end{aligned}$$

where Γ is the gamma function, and we have used the standard formula for the surface area of the $3N - 1$ dimensional sphere.

It should be clear that, despite these simple examples, the invariant measure of a subset of phase space is rarely obtainable in an analytic form.

Note that in typical treatments of systems involving identical particles, the partition function is normally multiplied by a factor $\hbar^{-3N}/N!$ that measures the number of distinct quantum states available. The $N!$ quantifies the number of possible arrangements of N identical objects, since, in quantum mechanics, identical particles are formally indistinguishable. It would become complicated to incorporate such factors for a system with many different species of atoms. When computing probabilities, we would need to incorporate a corresponding counting factor which would, in typical cases, cancel with the prefactor. Our interest in this book is in classical systems of particles, and the number of particles is fixed in discussion of any particular system, so we may simply ignore this factor in our discussion.

5.3.3 The Microcanonical Probability Measure and Averages

Let

$$d\mu_E = Z_E^{-1} \frac{1}{\|\nabla H\|} d\sigma.$$

We refer to this as the microcanonical probability density and write, for an “appropriate” set \mathcal{A} ,

$$\Pr(\mathcal{A}) = \mu_E(\mathcal{A}) = \int_{\mathcal{A}} d\mu_E.$$

The only requirement for this to make sense is that the set \mathcal{A} be a measurable subset of the $H = E$ energy surface, i.e. that it be possible to compute its surface area.

We have the standard properties of a probability function:

- $0 \leq \Pr(\mathcal{A}) \leq 1$ for all measurable sets \mathcal{A} .
- $\Pr(\Sigma_E) = 1$.

We also note that lower order objects such as a point or a curve in \mathbb{R}^2 , or a surface in \mathbb{R}^3 , have zero measure with respect to Lebesgue measure for the ambient space. Similarly, for a Hamiltonian system with N_d degrees of freedom, the energy surface is of dimension $2N_d - 1$ and the probability measure of sets of lower dimension than this will vanish.

As we mentioned in motivating the microcanonical distribution, we could alternatively view microcanonical averages as integrals with respect to the singular measure on the ambient space \mathcal{D} defined by

$$\rho'_E d\omega = Z_E^{-1} \delta[H - E] d\omega,$$

where δ represents the Dirac delta function. The notation $d\omega$ represents the volume element in the Euclidean space defined by all coordinates and momenta. This is the more common definition of the microcanonical distribution encountered in physics treatments.

Regardless of which formulation is adopted, we may use the probability measure to compute expectations (averages) of (suitable) functions defined on the phase space. We write such an expectation as

$$\text{Av}_{H=E}(g) = \int_{\Sigma_E} g(z) d\mu_E = \int_{\mathcal{D}} g(z) \rho'_E d\omega.$$

Incidentally, any such function is referred to as an *observable function* (or, simply, an *observable*) of the system in this context.

As shorthand, where the underlying space and probability density are assumed, one may write such an average more simply as

$$\text{Av}_{H=E}(g) = \langle g \rangle.$$

5.4 Temporal Averages and Numerical Computations

Given an autonomous system of differential equations $\dot{z} = f(z)$ in \mathbb{R}^m , and a trajectory $\Gamma = \{z(t) | t \in [0, \infty]\}$, let $g = g(z)$ be any smooth scalar valued function of z (an observable) and define (assuming it exists) the infinite time average of g along Γ by

$$\bar{g}_\Gamma = \lim_{\tau \rightarrow \infty} \tau^{-1} \int_0^\tau g(z(t)) dt. \quad (5.9)$$

A natural question that arises in the context of chaotic systems is whether such a trajectory average in fact makes sense. Considering any conservative system, we know that the energy itself is a conserved quantity along trajectories, and its average is therefore a function of the initial condition. On the other hand, imagine trajectories emanating from different points on a single energy level set Σ_E , can we necessarily conclude that all such trajectories will yield the same average value for any observable? This question is obviously important as the initial conditions of a molecular system are typically generated through approximations and estimations—it would be disturbing if the choice of these (at uniform energy) were to greatly impact the computation of an average.

One situation in which we would expect different initial conditions to yield different trajectory averages is if the energy surface has several connected components.

Example 5.3 Consider the *double well potential*

$$\phi(q) = (1 - q^2)^2.$$

The energy $H(q, p) = p^2/2 + \phi(q)$ will tend to $+\infty$ as $q \rightarrow \infty$ or $p \rightarrow \infty$, but is obviously bounded below (by zero). The graph of the energy, along with some level curves, is shown in Fig. 5.2. From the graph it is clear that the energy surface $H(q, p) = E$ has more than one component if $0 < E < 1$. If an initial condition is taken from one of the two basins, say with energy E_0 , then the trajectory through that point will remain forever in the one basin, thus the averages of many quantities, if computed using the trajectory values, would not be a good approximation of the overall average at constant energy E_0 .

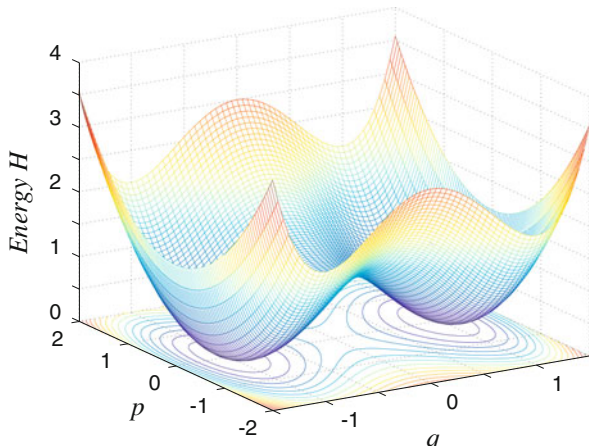


Fig. 5.2 Energy function for the double well. The energy surface corresponding to a value of energy $E \in (0, 1)$ is not connected

More generally, if a given system has a first integral (conserved quantity) $I = I(z)$, different from the energy, which is preserved along trajectories, then the average of this conserved quantity (and any other quantity that depends upon it) will be dependent on the choice of initial condition.

5.4.1 The Concept of Ergodicity

While being mindful of the examples given above, there are many systems which, at least for a useful range of energy, appear to have the property that averages are independent of initial condition. Systems for which the trajectory averages are the same as phase space averages on the energy surface are said to be *ergodic*.⁶ The concept of ergodicity can be introduced in the setting of general dynamical systems, but it is very challenging to analyze this property for realistic systems. An analogous concept for stochastic differential equations will be introduced in the next chapter; in this setting of randomized models ergodicity is much more amenable to mathematical study. Nonetheless, we motivate the concept in this section using deterministic systems and numerical examples.

The formal definition of ergodicity takes one of several forms. For our current purposes, we opt for a definition that is close to our intended goal (the computation of averages).

Definition 5.1 A Hamiltonian system is said to be ergodic on an energy surface Σ_E (microcanonically ergodic) if, for almost all trajectories Γ emanating from initial conditions on Σ_E , and for any observable g , the following holds

$$\bar{g}_\Gamma = \text{Av}_{H=E}(g),$$

where \bar{g}_Γ is defined in (5.9). By “almost all” we mean that there could be a low-dimensional subset for which the trajectory averages fail to equal the space averages. The term “almost all” thus allows for the existence of some fixed points and periodic orbits, which are almost certain to be present in a deterministic system.

Alternatively, we may say that a dynamical system is ergodic if the probability measure of any invariant set \mathcal{A} of the flow is either 0 or 1. An invariant set \mathcal{A} of the flow is one such that

$$\mathcal{F}_t(\mathcal{A}) = \mathcal{A},$$

for all $t \neq 0$. To see that this is the same concept of ergodicity as defined above, let χ be the “indicator function” of the complement of \mathcal{A} whose values is zero if $z \in \mathcal{A}$

⁶The term “ergodic” was coined by Boltzmann in 1887. He joined the Greek term *ergon* (“action,” “work”) with *hodos* (“path”) to refer to an energy-path. An ergodic path one that traverses the entire energy surface eventually touching all points thereof.

and one if $z \in \Sigma_E \setminus \mathcal{A}$ (the symbol \setminus means the removal of the second set from the first). Then for any trajectory starting in \mathcal{A} , we have that the average of χ along Γ vanishes, i.e.

$$\bar{\chi}_\Gamma = \lim_{\tau \rightarrow \infty} \tau^{-1} \int_0^\tau \chi(z(t)) dt = 0,$$

since \mathcal{A} is an invariant set.

On the other hand, the average of χ on Σ_E is just the probability measure of $\Sigma_E \setminus \mathcal{A}$. If we assume the system is ergodic, we must have $\text{Pr}(\Sigma_E \setminus \mathcal{A}) = 0$, thus $\text{Pr}(\mathcal{A}) = 1$. Since, according to the definition, equality of time and space averages is allowed to fail only on a set of probability measure zero, we have that either $\text{Pr}(\mathcal{A}) = 0$ or $\text{Pr}(\mathcal{A}) = 1$.

If a system is not ergodic, then there will be an invariant set \mathcal{A} whose probability measure is strictly between zero and one. The trajectories emanating from this set are unable to explore the entire energy surface and the corresponding trajectory averages will, at least for some observables, be different than the spatial average of that observable. A system which is not microcanonically ergodic has an energy surface that can be partitioned into subdomains of nonzero measure in which trajectories are forever trapped.

Often, the strict definition of ergodicity must be relaxed to accommodate the realistic modelling setting; for example only some portion of the energy surface may be accessible by trajectories in the time-interval available, due to the cost of computing steps with a numerical method. For a more detailed discussion of these and other ergodicity issues in the context of deterministic molecular dynamics, see the articles of Tupper [379, 381].

Given a system with energy of the form $H(\mathbf{q}, \mathbf{p}) = \mathbf{p}^T \mathbf{M}^{-1} \mathbf{p} / 2 + U(\mathbf{q})$, what can be said about the ergodicity of the system on the energy surface $H = E$? Coverage of the set may follow in certain cases from periodic or quasiperiodic motion in which the trajectories wrap around the surface filling in space.

As a very simple example, the harmonic oscillator is always ergodic on its energy surfaces (i.e. energy curves, in this case). Some examples of two-dimensional systems are shown in Fig. 5.3.

Ergodicity is a concept that often becomes more relevant in systems with many degrees of freedom. For example if one thinks of having not just one but many double well oscillators connected together in some way so that they can exchange energy, then it is likely that the energy can accumulate, given enough time, in one of the oscillators, enabling it to overcome the barrier.

Example 5.4 (2D Harmonic System) Consider a two-dimensional harmonic system, i.e. the system with Hamiltonian

$$H = p_1^2/2 + p_2^2/2 + \Omega_1^2 q_1^2/2 + \Omega_2^2 q_2^2/2,$$

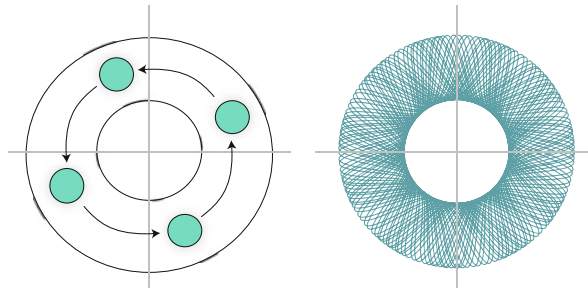


Fig. 5.3 Two examples in which we suppose the accessible domain at given energy is the annulus. On the *left*, periodic transport of a collection of points with positive area is evidence of non-ergodic motion (the union of the four disks shown would constitute an invariant region of positive measure). In the figure at *right* a quasi-periodic space-filling trajectory is shown. The oscillatory motion, although quite regular in appearance, gradually fills in the whole domain

where Ω_1, Ω_2 are two nonzero parameters. Because the two systems involving q_1, p_1 and q_2, p_2 are not coupled in the equations of motion, this system has two invariants $H_1 = p_1^2/2 + \Omega_1^2 q_1^2/2$ and $H_2 = p_2^2/2 + \Omega_2^2 q_2^2/2$. For any $E_1, E_2 > 0$, the set of points satisfying $H_1 = E_1, H_2 = E_2$ is a two-dimensional torus. If the frequencies Ω_1 and Ω_2 are not rationally related (i.e. Ω_1/Ω_2 is an irrational number), then for any E_1, E_2 the torus will eventually be filled in by any trajectory. On the other hand, the energy surface $H = E$ is the union of all such 2-tori with $E_1 + E_2 = E$. There is no mechanism for the system to move from one torus to the other, so the system is not ergodic.

In typical molecular dynamics applications with multiple bodies and complicated force laws, the motion is assumed to be chaotic. Ergodic coverage of Ω_E would then have to arise from the global properties of a chaotic system (sensitivity to initial conditions and transitivity). Liouville's equation,

$$\frac{\partial \rho}{\partial t} = \mathcal{L}_f^\dagger \rho,$$

describes how a distribution of initial conditions is carried forward under the time evolution of a dynamical system. That is, starting from the initial distribution of phase space points described by $\rho(z, 0)$, we arrive at a new distribution $\rho(z, t)$. We will see in an example to be presented below that various sets of initial conditions with uniform energy E may appear to spread out to cover (become dense in) a particular region, the accessible energy surface at energy level E .

An even stronger property than the ergodic property is the concept of a *mixing* system. For a mixing system, the finite time density $\rho(z, t)$ converges, in the weak sense, to the invariant distribution $\rho_\infty(z)$, as $t \rightarrow \infty$. That is, we have, for all test functions ϕ in some chosen space

$$\lim_{t \rightarrow \infty} \langle \phi, \rho(\cdot, t) \rangle = \langle \phi, \rho_\infty \rangle.$$

Rigorous proof that a given Hamiltonian dynamical system is ergodic (or mixing) is extremely difficult for even simple cases, and is likely to be dependent on the choice of the potentials, themselves.

In practical simulation, as we cannot consider an infinite t with finite computational resources, experimenters often must choose between estimating $\langle \phi, \rho_\infty \rangle$ using a single long trajectory, or multiple shorter trajectories. Both techniques have their merits, although the correct procedure will be largely system-dependent. For example, let us consider a system with a large number of deep wells (consider an eggbox-like landscape), where our initial condition resides at a peak in-between wells. We may find that when using one single trajectory we only sample the space inside a small number of basins, as the trajectory takes a long time to escape any one well during the simulation. Using multiple trajectories will increase our chance of a thorough sampling of the space, as we are likely to visit more wells in general from our initial condition.

On the other hand, if our initial condition is inside the basin itself, our chances of escaping the well over the course of our simulation is maximized in general by using one long trajectory (simply observe that one trajectory of 100 steps travels further than 100 trajectories of only one step).⁷

It is important to note that a system may be chaotic without being ergodic on a particular level set of energy. For additional discussion of chaotic Hamiltonian systems and their trajectories, see [64, 174, 386].

Example 5.5 (Double Pendulum) To explore some of the issues related to ergodicity, let us return to the double pendulum considered in Chap. 3. For given positive values of the coefficients, the region swept out in the plane by trajectories can be seen to be a union of intersections of pairs of disks centered at the origin and $(0, -2)$, with radii r_1, r_2 respectively, which themselves represent a point on an ellipse in the first quadrant. Determining the boundary of this region analytically is difficult but it is easy to find it numerically. For the special case $k_1 = k_2 = 2$, $\ell_1 = \ell_2 = 1$, and $E = 4$ that the projected region covered by positions at this energy is the interior of the level set $U = E$ shown as a dark oval curve in the three panels of Fig. 5.4. If the system were ergodic, we would expect that initial conditions with energy $E = 4$ would result in trajectories which traverse the outlined region. Instead, we find that the trajectories are generally confined to only an isolated subset of the accessible set. The trajectories starting from different initial conditions would therefore automatically result in different averages of functions that depend on position. The energy surface is three-dimensional (represented as the zero-set of a single constraint in four-dimensional space), but apparently it bifurcates into a collection of isolated components (bounded by two-dimensional closed surfaces). These are none other than the tori predicted by the KAM theory [386]. An illustration of the presence of these tori is obtained by plotting the

⁷Generally, optimizing the molecular dynamics computational cost between “one long” or “many short” is a nontrivial problem which depends on, for example, the availability of parallel computing power, for some discussion see [7, 140, 233].

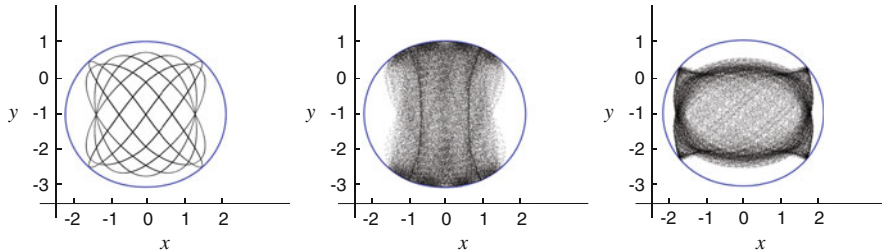


Fig. 5.4 Graphs of trajectories obtained by choosing three different initial conditions on the energy surface $H = 4$. The initial conditions are as follows: (left) $\mathbf{q}_0 = (1.75, 0); \mathbf{p}_0 = (0, 1.1748)$, (center) $\mathbf{q}_0 = (0, -2.9); \mathbf{p}_0 = (0.8718, 0)$, (right) $\mathbf{q}_0 = (0, -2.7), \mathbf{p}_0 = (0, 1.4283)$. The numerical method (the Verlet method) used 100 million steps with stepsize $\Delta t = 0.0001$

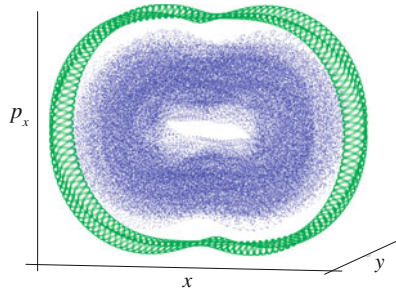


Fig. 5.5 Projecting the data from two of the initial conditions on the $H = 4$ energy surface onto the x, y, p_x subspace reveals the accessible set to be fragmented by 2-tori; the system clearly fails to be ergodic on the energy surface

projection of one of the orbits in the x, y, p_x coordinates and is shown in Fig. 5.5.

Example 5.6 (Anisotropic Oscillator) The anisotropic oscillator was used in Chap. 1 to illustrate the concept of a chaotic dynamical system. Fix, arbitrarily, a small set of initial conditions for the anisotropic pendulum at energy E_0 , with positions in a small interval on the positive x axis, $1.05 \leq x \leq 1.15$ and $y = 0$. For each point $(x, 0)$ taken from this set select the initial velocities as $\dot{x} = 0$, $\dot{y} = [2(E_0 - U(x, 0))]^{1/2}$. The set $y = 0, \dot{y} = 0$ is invariant under the differential equations of the perturbed central force problem, since the force acts in the radial direction; our choice of initial conditions ensures that trajectories explore the larger $H = E_0$ energy surface.

The set of initial conditions forms a line segment in the four-dimensional phase space. These points are then integrated forward in time by solving the differential equations (using a numerical method), and the resulting image sets are shown in Fig. 5.6. The first panel of Fig. 5.6 shows, in one set of axes, the image of the initial set at times $t = 4, 8, 12, 16$. Successive figures show the images of the initial set after times $t = 20, 28, 36$. The line segment becomes curved, and spreads out,

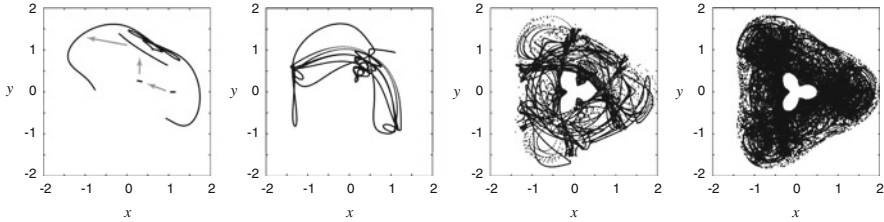


Fig. 5.6 Evolution of the line segment of initial conditions, for $t = 4, 8, 20, 28, 36$; the first four images are recorded in the *leftmost panel* and successive images are ordered *left to right*

becoming extended, and folding back on itself in an increasingly complex manner. Eventually the points fill in a region in the plane which is to all appearances identical to that obtained as the limit of a single long trajectory shown in the right panel of Fig. 1.24. (In these figures we chose $\varepsilon = 0.5$ and $E_0 = 0.21048$, which matches the energy observed in our earlier simulations.)

The segment of initial conditions, a one-dimensional object, when transformed by the smooth map defined by solving initial value problems, should result, again, in a one-dimensional object, i.e. a curve. Yet it appears also to provide a dense covering of a two-dimensional region in the position projection. Given the presence of the momenta, the energy surface $H = E_0$ is generically three-dimensional, since it is the level set of a function defined on \mathbb{R}^4 . A more detailed numerical investigation would reveal that the trajectories of the differential equations themselves appear to generate, in the limit, three-dimensional space-filling curves.

Now consider an alternative initial set. Begin, as before, with a line segment on the x -axis, but now choose the initial momenta from the uniform distribution on the circle $p_x^2 + p_y^2 = 2(E_0 - U(x, 0))$. In this way we again get initial conditions on the $H = E_0$ energy surface, but this time the points are not close to one another in phase space, since the momenta of successive points may differ greatly. Integrate the set forward in time by solving the differential equations, and examine the image sets at successive instants in time. The leftmost panel in Fig. 5.7 shows the evolution of the initial interval at times $t = 0, 0.2, 0.4, \dots, 1.8$. In the projection onto positions, the set now spreads out in a series of uneven concentric bands. The structure of these bands becomes increasingly complex and filamented and eventually spreads around the accessible region at the given energy. Snapshots at $t = 8, 16, 24$ are shown in Fig. 5.7.

A small set of initial conditions is eventually mapped forward by solving the differential equation into what appears to be a dense covering of the same region seen already in the right panel of Fig. 1.24 (which arose from the very long term evolution of a single initial condition).

As we see in the above example, the early evolution of the set is strongly dependent on the initialization, but in the long term, a similar region is ultimately covered (at least to visual inspection). However, also note that the approach to equilibrium is very different for the two choices of initialization, as we can see from

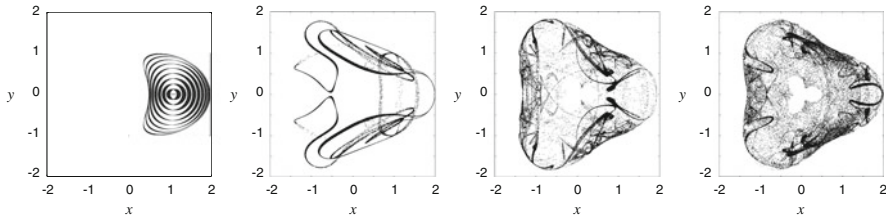


Fig. 5.7 The early evolution of the discrete set of initial conditions in their projection onto positions, for $t = 0, 0.2, \dots, 1.8$, is shown in the *left-most panel*. The subsequent panels show the positions of trajectories at $t = 8, 16, 24$

the nonuniform covering of the area traced out by the pendulum, thus we would not necessarily obtain similar averages until a very long time had passed. Behavior like this is observed in typical molecular models.

5.5 Dynamical Averages

Although the computation of stationary averages is one of the most common uses of molecular dynamics, there is also a need for methods that allow exploration of dynamical processes. We have already seen that the chaotic nature of molecular dynamics means that trajectories are highly sensitive to initial conditions; in the terminology of numerical analysis, such a calculation is *ill-conditioned*. On the other hand it is well known that many molecular systems evolve along sequential *pathways* that can be viewed as the bundles of trajectories emanating from a collection of initial conditions. An example of a dynamical calculation is a transition time, another is the rate of phase space exploration (as measured by the average distance travelled in a given time). These are quite different; the first relies on a spatial localization of the initial and final states; the second is more likely a global average across many states.

In order to define dynamical averages and to describe methods to calculate such quantities, we introduce a straightforward approach based on replacing dynamical averages with stationary averages of an observable that incorporates the action of the flow map. Let \mathbf{a} and \mathbf{b} be mappings from the phase space to the same Euclidean space, and define the temporal correlation of \mathbf{a} and \mathbf{b} (on the surface of energy E) by

$$\begin{aligned} C_{ab}(\tau) &\stackrel{\text{def}}{=} k \text{Av}_{H=E} (\mathbf{a}(\mathcal{F}_t(z)) \cdot \mathbf{b}(z)) \\ &= k Z_E^{-1} \int_{\Sigma_E} \mathbf{a}(\mathcal{F}_t(z)) \cdot \mathbf{b}(z) \delta[H - E] d\omega, \end{aligned}$$

where k is a normalization constant that is often incorporated to ensure that $C_{ab}(0) = 1$.

Using the notation developed earlier for the propagator, this has the alternative formulation

$$C_{ab}(t) = k \text{Av}_{H=E} (\mathbf{b}(z) \cdot (e^{t\mathcal{L}}\mathbf{a})(z)).$$

If the system is ergodic, we could write this as a temporal average with respect to any trajectory initiated on the $H = E$ energy surface:

$$C_{a,b}(t) = k \lim_{\tau \rightarrow \infty} \frac{1}{\tau} \int_0^\tau \mathbf{a}(z(s+t)) \cdot \mathbf{b}(z(s)) ds.$$

The *velocity autocorrelation function* is often written in the shorthand notation

$$C_{v,v}(t) \stackrel{\text{def}}{=} \frac{\langle \mathbf{v}(t) \cdot \mathbf{v}(0) \rangle}{\langle \mathbf{v}(0) \cdot \mathbf{v}(0) \rangle},$$

where the averaging may be assumed to be against the microcanonical measure, if otherwise unspecified.

Now let \mathcal{A} and \mathcal{B} be subsets of configuration space (i.e. subsets in the position space) of nonzero measure, and define

$$T_{\mathcal{A}\mathcal{B}}(\tau) \stackrel{\text{def}}{=} C_{\mathbf{1}_{\mathcal{B}}, \mathbf{1}_{\mathcal{A}}}(\tau),$$

where χ_S is the *characteristic* or *indicator* function of the set S defined by

$$\mathbf{1}_S(z) = \begin{cases} 1, & z \in S \\ 0, & z \notin S \end{cases}.$$

We may understand $T_{\mathcal{A}\mathcal{B}}$ as quantifying the number of trajectories which, started from set \mathcal{A} at time $t = 0$, transition to set \mathcal{B} at time τ . Dividing $T_{\mathcal{A}\mathcal{B}}$ by the measure of the set \mathcal{A} , we obtain the probability for a trajectory to make this transition in the given time, which we may write as

$$\Pr(\mathcal{A} \rightarrow_\tau \mathcal{B}) = \frac{\langle \mathbf{1}_{\mathcal{B}}(z(\tau)) \mathbf{1}_{\mathcal{A}}(z(0)) \rangle}{\langle \mathbf{1}_{\mathcal{A}}(z(0)) \rangle},$$

where the averaging is assumed to be with respect to the microcanonical distribution at given energy E .

An important aspect of a mixing system is the *decay of autocorrelation* [338]. Note that

$$\begin{aligned}
\int_{\Sigma_E} \phi(z) \rho(z, t) d\omega &= \int_{\Sigma_E} \phi(z) e^{t\mathcal{L}^\dagger} \rho(z, 0) d\omega \\
&= \int_{\Sigma_E} [e^{t\mathcal{L}} \phi(z)] \rho(z, 0) d\omega \\
&= \int_{\Sigma_E} \phi(\mathcal{F}_t(z)) \rho(z, 0) d\omega \\
&= \int_{\Sigma_E} \phi(\mathcal{F}_t(z)) \frac{\rho(z, 0)}{\rho_E(z)} \rho_E(z) d\omega. \tag{5.10}
\end{aligned}$$

We assume $\psi(z) \stackrel{\text{def}}{=} \frac{\rho(z, 0)}{\rho_E(z)}$ is bounded on Σ_E , and moreover

$$\text{Av}_{H=E}(\psi) = \int_{\Sigma_E} \frac{\rho(z, 0)}{\rho_E(z)} \rho_E(z) d\omega = 1$$

(i.e., the initial density is a probability density on the energy surface), and that the system is mixing. Then the integral (5.10) is well defined and we may view it as a two-point correlation function of ϕ and ψ . By the mixing property it must converge to $\int_{\Sigma_E} \phi(z) \rho_E d\omega$, thus the average value of ϕ is ultimately independent of the initial conditions. We have

$$\lim_{t \rightarrow \infty} \int_{\Sigma_E} \phi(\mathcal{F}_t(z)) (\psi(z) - 1) \rho_E d\omega = 0$$

We say that the system loses memory of its initial state. More generally, in a mixing system, if \mathbf{a} and \mathbf{b} are two arbitrary functions of the phase variables, then

$$\lim_{t \rightarrow \infty} C_{ab}(t) = \text{Av}_{H=E}(\mathbf{a}) \cdot \text{Av}_{H=E}(\mathbf{b}).$$

So if either property has mean zero, then the absolute value of the autocorrelation function decays with time to zero. In practice, it may take the system a very long time to decorrelate from its initial state [135].

5.6 Numerical Methods and Invariant Distributions

In the previous section, we introduced the temporal average of a function along a solution of a differential equation (as a means of computing the microcanonical ensemble average). Since we cannot compute an exact trajectory, we would hope that such an average could be computed in an analogous way using a numerical method. If z_n represents the approximation to $z(t_n)$, then we might attempt to estimate \bar{g}_T by

$$\bar{g}_T \approx \lim_{n \rightarrow \infty} n^{-1} \sum_{k=0}^n g(z_k).$$

However, as is well known, numerical methods may introduce growing errors so an infinite average might not make sense, even if the time average does! Still we might hope that trajectory averages could be approximated by discrete averages of moderately long length. In the several examples in this chapter, we have used numerical methods to simulate Hamiltonian dynamics in order to gain intuition about their ergodic properties, but we have not discussed the effect of the choice of the discretization method itself on this issue.

We have seen that the Liouville equation defines the propagation of the distribution associated to system of differential equations. In a similar way, a numerical method $z_{n+1} = \mathcal{F}_h(z_n)$ induces an effective distributional propagator. One way to understand this propagator is to interpret the numerical method as being approximately equivalent to the solution of a perturbed differential equation

$$\frac{dz}{dt} = f(z) + h^r f_{(r)}(z) \equiv \tilde{f}_h(z).$$

The perturbation term may be viewed as the finite truncation of the perturbative expansion obtained from the backward error analysis using the methods of the previous chapter. (r is the order of the numerical method.) Let us assume that the perturbed equation is a realistic model for the numerical solutions, then define the evolving density by

$$\frac{\partial \rho}{\partial t} = \mathcal{L}_{\tilde{f}}^\dagger \rho \stackrel{\text{def}}{=} \mathcal{L}_f^\dagger \rho + h^r \mathcal{L}_{f_{(r)}}^\dagger \rho.$$

Under suitable boundedness assumptions on the remainder, we could expect that the distributional error remains bounded by a quantity of order h^r . Unfortunately, it is not always true that ρ remains bounded.

As a simple illustration, consider the harmonic oscillator with Hamiltonian $H(q, p) = p^2/2 + q^2/2$ and the invariant distributions obtained using several numerical methods. Applying Forward Euler to the harmonic oscillator, we have

$$q_{n+1} = q_n + hp_n, \quad p_{n+1} = p_n - hq_n,$$

or

$$\begin{bmatrix} q_{n+1} \\ p_{n+1} \end{bmatrix} = \begin{bmatrix} 1 & h \\ -h & 1 \end{bmatrix} \begin{bmatrix} q_n \\ p_n \end{bmatrix}$$

and we see that the eigenvalues of the propagation matrix are outside the unit disk. Thus both solution components tend to infinity unless $(q_0, p_0) = (0, 0)$. This means that with the single exception $\rho(q, p, 0) = \delta[q]\delta[p]$ there is no limiting (invariant) distribution for Forward Euler. To put it another way, the only solution, in the weak sense, of $\mathcal{L}_f^\dagger \rho = 0$ is the point distribution $\delta[q]\delta[p]$, and this solution is not “asymptotically stable.”

As an alternative, consider the Backward Euler method: $q_{n+1} = q_n + hp_{n+1}$, $p_{n+1} = p_n - hq_{n+1}$. Then it is easily shown that both eigenvalues of the matrix lie in the interior of the unit disk, and hence all solutions of the recurrence relation tend to the origin with increasing n (the origin is an attractive equilibrium point). In this case, all densities evolve toward the Dirac distribution centered at the origin: $\delta[q]\delta[p]$. The only (distributional) solution of $\mathcal{L}_{\tilde{f}} \rho = 0$ is again $\delta[q]\delta[p]$, which in this case is attractive.

Now consider the application of the Symplectic Euler method, $q_{n+1} = q_n + hp_{n+1}$, $p_{n+1} = p_n - hq_n$. As we know, the solution through any given initial point remains confined to an ellipse for all n defined by $\tilde{H}_h(q, p) = \tilde{H}_h(q_0, p_0)$, where \tilde{H}_h is the perturbed Hamiltonian defined by the backward error analysis. This implies that a density which is a function of \tilde{H}_h will remain invariant under the associated Liouville equation. There are many solutions of $\mathcal{L}_{\tilde{f}}^\dagger \rho = 0$, none of which is attractive.

The harmonic oscillator is of course an integrable system. When the underlying system is a chaotic Hamiltonian system, the trajectories from any collection of initial conditions become disordered (even while preserving the energetic constraints defined by their initial states). The hope (in some cases, naive) is that typical trajectories computed using a symplectic method applied to such a chaotic system provide space filling curves on the $\tilde{H}_h = E$ perturbed energy surface.

Example 5.7 (Ergodicity in the Trimer) At positive energies, the trimer is unstable and the atoms separate, into a bound pair and a single atom. At very low (but admissible) energies, the timer has an insurmountable energy barrier between the two basins. At moderate energies, the trimer will visit both basins, however, the mean passage time between basins may be greatly extended depending on the energy level.

Consider the level set of potential corresponding to $U = -0.5$. Note that the kinetic energy is everywhere positive, so that a trajectory with total energy $E = -0.5$ will have to be bounded within the $U = -0.5$ level set. Would the dynamics (started from an initial condition with total energy $E = -0.5$) completely fill in this level set over time? Because this system is chaotic, we cannot write down a formula for the exact solution, or find exact trajectories of the system, but we can use numerical methods to attempt to shed some light on the question. In Fig. 5.8 we

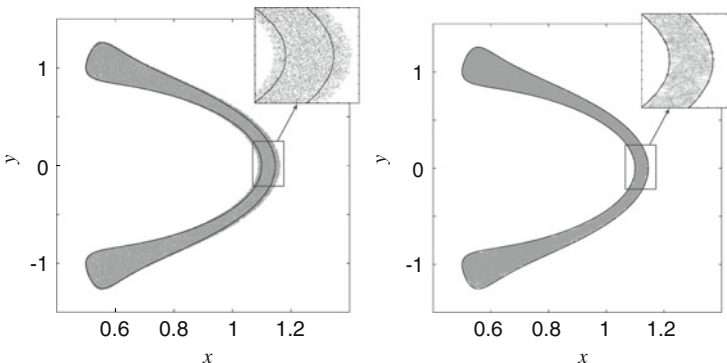


Fig. 5.8 Long trajectories of the isosceles 3-body problem computed using two different timesteps, $h = 0.07$ (left) and $h = 0.01$ (right). The discrete values have been used to draw small dots which appear to fill in a region bounded by a level curve of the potential energy, with some error at the boundary that decreases with stepsize h

have plotted two long numerical solutions (100,000 timesteps) in their xy projection for two different stepsizes $h = 0.07$ and $h = 0.01$, started from a point with energy $E = -0.5$ which is (a) admissible and (b) connected and (c) bounded. The dark curve represents the level curve of the potential energy for $U = -0.5$ while the numerical steps are shown in gray. As we can see in this figure, the points appear to shade the region completely, however spilling over a bit from the interior of the curve. This overspill is due to the numerical error, as it is decreased by a decrease in the stepsize.

As we have seen in the Chap. 3, when a symplectic method is applied to a molecular dynamics problem it induces a perturbed Hamiltonian (energy) function. For the Verlet scheme the modified Hamiltonian is

$$\tilde{H}_h = H + \frac{h^2}{24} (2\mathbf{p}^T \mathbf{M}^{-1} \mathbf{U}''(\mathbf{q}) \mathbf{M}^{-1} \mathbf{p} - \nabla \mathbf{U}(\mathbf{q}) \mathbf{M}^{-1} \nabla \mathbf{U}(\mathbf{q})) + \mathcal{O}(h^4).$$

Actually, as explained previously, we must interpret this carefully: a finite truncation of this expansion may characterize the discrete trajectories observed in practice, but the series expansion itself does not typically converge. Assuming such a perturbative expansion is valid, the issue of ergodicity of the numerical method can be related to the corresponding issue for the dynamical system characterized by \tilde{H}_h .

A result in [338] provides a formula to calculate the perturbation of the microcanonical average induced by the Hamiltonian perturbation. This result has been recast in the more convenient form in [14]:

Theorem 5.1 *Let $H(\mathbf{q}, \mathbf{p})$ and $\tilde{H}(\mathbf{q}, \mathbf{p}) = H(\mathbf{q}, \mathbf{p}) + \varepsilon \eta(\mathbf{q}, \mathbf{p})$ be two Hamiltonian functions. Suppose the energy surface $\Sigma_E = \{(\mathbf{q}, \mathbf{p}) | H(\mathbf{q}, \mathbf{p}) = E\}$ to be compact and define the perturbed energy surface by $\tilde{\Sigma}_E = \{(\mathbf{q}, \mathbf{p}) | \tilde{H}(\mathbf{q}, \mathbf{p}) = E\}$, also assumed compact.*

Suppose that \mathbf{w} is an arbitrary smooth vector field such that $\mathbf{w} \cdot \nabla H \neq 0$ on Σ_E . Then the perturbation of the microcanonical average of a smooth function g is given by

$$\text{Av}_{H=E}(g) - \text{Av}_{\tilde{H}=E}(g) = \text{Av}_{\tilde{H}=E}(\nabla \cdot g\mathbf{u}) - \text{Av}_{\tilde{H}=E}(g)\text{Av}_{\tilde{H}=E}(\nabla \cdot \mathbf{u}) + \mathcal{O}(\varepsilon^2),$$

where

$$\mathbf{u} = \varepsilon \frac{\eta}{\mathbf{w} \cdot \nabla H} \mathbf{w}.$$

The point of this result is that it allows all computations to be done in the terms of \tilde{H}_h which is the system we can study using the numerical trajectories (assuming, of course, ergodicity). In other words we can correct an average computed using a symplectic numerical method for the effect of its truncation error. A natural choice of the function \mathbf{w} that appears in the theorem is $\mathbf{w} = \nabla H$. In [14] this result is applied to the Verlet method, providing an accurate calculation of the averaging error along a numerical trajectory.

The interpretation of a dynamical average (e.g. an autocorrelation function) as a stationary average means that we can apply the perturbation result to such computations as well. For more discussion of numerical averages and computation of correlation functions, see [338].

Exercises

- For the harmonic oscillator, calculate, for any function $g = g(q, p)$, the action of the Liouvillian $\mathcal{L}_f g$. Also calculate $\exp(t\mathcal{L}_f)g$.
- Recall from Chap. 3 that a splitting method defines a mapping via a composition of the flow maps associated to additive decomposition of a vector field, i.e. for $f = f_1 + f_2$, then

$$\exp(h\mathcal{L}_f) \approx \exp(h\mathcal{L}_{f_1}) \exp(h\mathcal{L}_{f_2}).$$

Let ρ be a phase space density. How is the density evolved under such a splitting method?

- Let $H = \mathbf{p}^T \mathbf{M}^{-1} \mathbf{p}/2 + U(\mathbf{q})$ be a Hamiltonian for N particles, where U is a sum of distance potentials only.

- Show by direct calculation that $\mathcal{L}_{J\nabla H} P_x = 0$ where $P_x = \sum_{i=1}^N p_{i,x}$ is the first component of the total momentum.
- Show that $\mathcal{L}_{J\nabla H} H = 0$.
- Calculate $\mathcal{L}_{J\nabla H} U$.
- Calculate $\mathcal{L}_{J\nabla H}^2 U$.

4. The planar pendulum can be written as a Hamiltonian system,

$$\dot{\theta} = p_\theta, \quad \dot{p}_\theta = -\alpha \sin \theta,$$

where $\alpha = g/\ell > 0$, where g is the gravitational constant and ℓ is the length. Assume that the pendulum bob is released without initial velocity from a position at angle θ_0 .

- a. Write a formula for the Hamiltonian (energy) in terms of θ and p_θ .
 - b. Explain why the motion of the pendulum is periodic.
 - c. Show that for small angles θ_0 the period of the motion will be $\tau \approx \tau_0 = 2\pi/\sqrt{\alpha}$.
 - d. Explain why, as the initial angle approaches $\theta_0 = \pi$ the period will tend to infinity.
 - e. Consider the set S of initial conditions satisfying $p_\theta(0) = 0$ and $0 < \theta_0 < \pi$. Sketch the sets S and $\mathcal{F}_{\tau_0}(S)$, where \mathcal{F}_t is the flow map of the pendulum system. Try to sketch $\mathcal{F}_{\tau_0}^2(S)$, i.e. the result of propagating the set of initial conditions through two periods of the harmonic approximation.
 - f. Use Verlet's method to approximate the images of S described in part (e) and graph $\mathcal{F}_{\tau_0}^m$ for various values of m .
5. Using the definition of ergodicity given in this chapter, is the single degree of freedom Lennard-Jones oscillator ergodic? Justify your answer.
6. Volume preserving systems $\dot{z} = f(z)$ in \mathbb{R}^m are defined by the condition $\operatorname{div}f = 0$, where

$$\operatorname{div}f = \nabla \cdot f = \sum_{i=1}^m \frac{\partial f_i}{\partial z_i}$$

is the *divergence* of the vector field f .

- a. Show that any Hamiltonian system is divergence free.
- b. Show that if the two systems $\dot{z} = f(z)$ and $\dot{z} = g(z)$ are volume preserving, then also the system $\dot{z} = \alpha f(z) + \beta g(z)$ is volume preserving.
- c. Define a system in k -dimensions with vector field f having components

$$f = Dz + g(z).$$

Assuming g is divergence free, find a condition on the matrix D so that f is divergence free.

- d. Consider the system with variables (q, p, ξ) , where $q, p \in \mathbb{R}^k$ and $\xi \in \mathbb{R}$ defined by

$$\frac{dq}{dt} = p, \quad \frac{dp}{dt} = g(q) + \xi A(q)p, \quad \frac{d\xi}{dt} = h(q),$$

here A is a $k \times k$ matrix that depends on the vector q . Under what circumstances is this system volume preserving?

Chapter 6

The Canonical Distribution and Stochastic Differential Equations

Until now, we have considered molecular models for isolated collections of atoms. We have seen how to derive equations of motion, and studied the properties of the relevant dynamical systems. We have also observed that the chaotic nature of a typical system imparts a random aspect which suggests that the dynamics defines, at least in some approximate sense, a limiting probability distribution.

This random aspect is an essential component of a molecular model which parallels the interaction between a real system studied in a laboratory setting and the environment. Unless extraordinary measures are taken to produce a perfect isolate, any experimental study will depend on the vessel, substrate or surrounding atmosphere. Any of these will consist of atoms and they will respond directly to changes in the system of interest. Thus when a reaction contained in a flask generates heat, the glass itself becomes hot to the touch, signalling the transfer of energy to the walls of the vessel; in a similar way a change in the environment in which it is conducted will affect the results of an experiment. One could take the extreme view that there is only one vast system and any restriction would then be artificial, but even if this philosophical perspective is valid, it does not mean that an experiment which is limited in extent (or a simulation of a finite molecular model) cannot have predictive power.

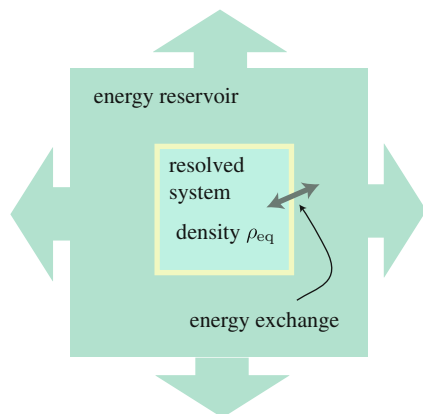
The first assumption in constructing the models considered throughout this book is that we may work with a fixed number of atoms; this allows us to model the motions as paths in a finite-dimensional Euclidean space. In addition we usually incorporate a mechanism to confine the system to a finite volume, with the ratio of the number of particles N to the volume V defining the average particle density. In this chapter we describe techniques used in molecular modelling to produce finite models which can be related, in terms of the invariant distribution, to the behavior of an “extended” or “bulk” system, that may be regarded as much larger than that which we actually model in detail. The extended system might even be regarded as infinite, the ratio in spatial scales (or number of atoms) between the large and small systems being so great. Thus we have two systems, one small and one large,

which interact in a complicated way defined by the microscopic interactions. In order to separate the two, we make the assumption that, in relation to the invariant measure, the detailed motions of the bulk system do not need to be known. A useful approximation may be obtained by modelling the exchange of only one or several quantities, for example the net energy and perhaps the momentum flux. The framework for discussing relationships among the properties of a system in contact with a reservoir is referred to as thermodynamics.

From the point of view of defining molecular models, we would like to be able to specify the macroscopic properties, in particular the temperature and pressure which are easily measured in the laboratory setting. The energy (and, in the case of pressure control, also the volume) may then fluctuate over time.¹

With various assumptions on the thermodynamic parameters, we obtain different *molecular ensembles* to which we associate a stationary probability distribution. An obvious practical challenge is then to calculate averages with respect to this probability distribution. Although this can sometimes be achieved (in an approximate sense) using deterministic molecular dynamics, it is normally better to employ stochastic differential equations. Using stochastic paths it is possible to obtain more reliable results with less effort—the computational difficulty of implementing methods is reduced, and the molecular models become easier to parameterize. The use of random paths is entirely natural in molecular simulation, since finite Hamiltonian models suppress microscopic interactions between the resolved system and the reservoir, as well as some internal modes of transfer of energy due to simplifications used to make simulation more practical; we may suppose that stochastic forces are simply restoring some of these lost interactions (Fig. 6.1).

Fig. 6.1 Concept of a thermodynamic reservoir. The thermodynamic state of the large system (resolved system plus reservoir) is defined by various macroscopic parameters that are assumed to be constant. This results in an equilibrium probability distribution for the small system, i.e. a thermodynamic state



¹The number of particles N considered in our model could also be allowed to vary but in practice it is usually simpler, from a simulation perspective, to fix N , which implies a restriction on the types of ensembles that we work with.

There are two distinct perspectives that may be chosen in discussing the statistical properties of a molecular system. On the one hand we may consider the evolution of a particular set of state variables over time. On the other hand we may consider a snapshot in time of a whole collection of evolving systems started from various initial states. Our emphasis in this chapter (and in much of the book) will be on the “ensemble” perspective and the fundamental tool for approximating the distribution is a system of stochastic differential equations (SDEs); in practice we compute this ensemble using one or several stochastic paths. In discussing the collection of paths defined by SDEs, we can separate the short term changes in the distribution initialized in some starting state from the long term (equilibrium) properties. We typically speak of the *transient* and *steady-state* regimes. The transient regime is defined with reference to both an initial distribution of states and a timescale. For a well behaved stochastic system, the steady-state regime is independent both of time and initial conditions and is characterized by the molecular ensemble. It should be emphasized that steady here does not refer to the motion of the atoms themselves; they will be constantly moving. It is the density which describes the phase space distribution of the particles of our system which converges in the long term. Thus the SDEs are constructed so as to provide, in the weak sense, an approximation of a realistic system, at least in the long term.

6.1 Ensembles for Molecular Simulation

We next discuss the formulation of statistical mechanics from the ensemble perspective, following references [147, 264, 364]. It is crucial to decide on the target ensemble before any experimentation (or simulation) begins. The dynamics we will compute is essentially just a tool to sample a particular density, and so choosing the correct sampling measure is tantamount to deciding on the problem we wish to solve. The ensemble is characterized by the constraints placed on the system and the interaction between systems of the ensemble. In this section we describe two of the most common statistical mechanical ensembles: the constant-energy or *microcanonical* ensemble and the constant-temperature or *canonical* ensemble. The key assumption made in statistical mechanics is that each system satisfying the given constraints is *equally probable*.

6.1.1 The Microcanonical Ensemble

The microcanonical ensemble, which we have already gently introduced in a simplified setting in the previous chapter, is defined by constant number of particles N , volume V and total energy E . We assume that all systems of the ensemble evolve independently and are isolated from each other. If a Hamiltonian description is used, the first and third invariances are automatically maintained in a molecular

simulation. Periodic boundary conditions can be used to ensure constant volume. The density function may then be represented by a Dirac delta function as follows:

$$\rho_{mc} = Z^{-1} \delta[H - E], \quad Z = \int_{\mathcal{D}} \delta[H - E] d\omega.$$

The partition function Z , which normalizes the density, is effectively a function of N , V and E ; it represents the number of microstates available under given conditions. As this ensemble is associated to constant particle number N , volume V and energy E , it is often referred to as the NVE-ensemble, and when we speak of NVE simulation, we mean simulation that is meant to preserve the microcanonical distribution; this, most often, would be based on approximating Hamiltonian dynamics, e.g. using the Verlet method or another of the methods introduced in Chaps. 2 and 3, and assuming the ergodic property. For a discussion of alternative stochastic microcanonical methods see [126].

6.1.2 The Canonical Ensemble and the Boltzmann-Gibbs Distribution

Next, we consider the formulation of an ensemble model that will better capture the realistic environment of a molecular system. Let the system of interest embedded in a much larger system, which acts as a “heat bath.” The two systems are assumed to be weakly coupled, so energy is continuously exchanged between them. This energy is assumed to be in the form of heat, with equilibrium naturally associated to the systems having matching temperature. The sole mechanism of interaction between the two systems is in the form of energy exchange, they do not exchange particles (or momentum).

The cornerstone of statistical mechanical theory is the concept of entropy, which may be taken as the number of states available to a discrete system (e.g. a quantum mechanical system), or, in the case of a classical system, the volume of the accessible phase space. In terms of a microcanonical system, the entropy is enshrined in the famous formula that appears on Boltzmann’s tombstone:²

$$S \equiv k_B \ln Z, \tag{6.1}$$

where k_B is Boltzmann’s constant $k_B \approx 1.38 \times 10^{-23} \text{ J/K}$. The second law of thermodynamics states that the entropy in a closed system naturally tends to increase to a maximum (a critical point).

²Despite Boltzmann being the first to formulate the concept, it was Planck who first wrote this equation.

We refer to the system of interest as the *active* system, or part A. The heat bath, or the bulk, is labelled B. Let us denote the total energy of the combined system AB by E. If the active system has energy E_A then the energy of the heat bath is $E_B = E - E_A$. We suppose that the number of states accessible to a given system A or B depends on its energy, writing this as $Z_i(E_i)$ where $i = A$ or B . (For an idealized classical system, we may take Z_α to be the volume of the relevant energy surface.) As the size (number of particles) of the system is increased, the energy, being an *extensive* quantity, is expected to increase in proportion. We denote by $Z(E_A, E_B)$ the total number of states the system can occupy with systems A and B having energies E_A and E_B , respectively. We make use of our assumption that the two systems do not exchange particles so that the total number of states the combined system can be found in depends solely on the energies of the two independent systems, i.e.,

$$Z(E_A, E_B) = Z_A(E_A) \times Z_B(E_B).$$

Taking logarithms and replacing the value for E_B by $E - E_A$, we have

$$\ln Z(E_A, E - E_A) = \ln Z_A(E_A) + \ln Z_B(E - E_A).$$

The crucial assumption is that each of the states in $Z(E)$ is equally probable, and hence we can find the most likely energy distribution between the systems by maximizing the value of $Z(E_A, E_B)$, or equivalently maximizing $\ln Z(E_A, E - E_A)$. This value of E_A occurs where

$$\frac{d}{dE_A} \ln Z(E_A, E - E_A) = 0,$$

or equivalently where

$$\frac{d}{dE_A} S_A = \frac{d}{dE_B} S_B,$$

where we have used Boltzmann's relation to express this in terms of the entropy.

We have assumed that our systems are in thermal equilibrium, but if we had not, and instead invested the heat bath with the total system energy, we would expect that the energy would transfer back into system A until the point where the stationarity relation is satisfied. This assumption is the same as saying that the system obeys the second law of thermodynamics; furthermore this equilibrium occurs when the entropy of the system is at its maximum.

The temperature of a system T, is defined as

$$\frac{1}{T} := \frac{\partial S}{\partial E},$$

giving, when the system is in thermal equilibrium,

$$\frac{d}{dE_A} \ln Z_A(E_A) = \frac{d}{dE_B} \ln Z_B(E_B) = \frac{1}{k_B T} =: \beta. \quad (6.2)$$

We shall refer to the quantity β as the system's inverse or reciprocal temperature.

The volume of states of the active system with energy α is $Z_A(\alpha)$. On the other hand the probability for the active system to have energy $\leq \alpha$ is the same as the probability of the bath having energy $\geq E - \alpha$, this must be

$$P(\alpha) = \Pr\{E_B \geq E - \alpha\} \propto \int_0^\alpha Z_B(E - s) ds.$$

Since $Z_B(E - s) = \exp(S_B(E - s)/k_B)$, and $s \ll E$, we (naively³) apply the mean value theorem to S_B to obtain

$$S_B(E - s) = S_B(E) - S'_B(\xi)s,$$

and from $S'_B(\xi) = 1/T$, we obtain

$$Z_B(E - s) \propto \exp(-\beta s),$$

where $\beta = (k_B T)^{-1}$. Thus we have

$$P(\alpha) \propto \int_0^\alpha \exp(-\beta s) ds.$$

This is the probability of finding any given active system of our ensemble having energy $\leq \alpha$. The volume (or number, in the case of discrete systems) of states available at energy α is $Z_A(\alpha)$. Thus the energy density of the canonical ensemble at energy level α is proportional to $Z_A(\alpha)\exp(-\beta\alpha)$.

6.1.3 The Gibbs-Boltzmann Probability Density

Observe that the previous discussion does not quite tell us the form of the phase space density associated to the canonical ensemble. An elegant way to derive this

³This is one of several imprecisions in this discussion whose correction would entail significant additional labor; since our ultimate aim is to use the framework and not to provide its rigorous derivation, we prefer to retain the intuitive continuity of presentation, in keeping with popular treatments.

density is as a stationary point of the Gibbs-Boltzmann entropy⁴

$$S = -k_B \int \rho \ln \rho d\omega,$$

subject to the constraints

$$\int \rho(z) d\omega = 1, \quad \int H(z) \rho(z) d\omega = \bar{E},$$

where the first constraint amounts to a normalization to make ρ a probability density, whereas the second fixes the average energy of the system to a predefined value. It does not matter what this value is at this point.

This can be seen as a variational principle. Using the method of Lagrange multipliers, we seek stationary solutions of

$$V = S/k_B - \lambda \left[\int \rho(z) d\omega - 1 \right] - \beta \left[\int H(z) \rho(z) d\omega - \bar{E} \right]$$

with respect to the choice of density ρ and coefficients λ and β . The resulting equations for the maximizing density are obtained by variational differentiation (see Sect. 2.2.1):

$$\begin{aligned} \frac{\delta V}{\delta \rho} &= 0 \\ \int \rho(z) d\omega &= 1 \\ \int H(z) \rho(z) d\omega &= \bar{E}. \end{aligned}$$

The first equation reduces to

$$-(1 + \ln \rho) - \lambda - \beta H = 0$$

yielding

$$\rho = e^{-1-\lambda} e^{-\beta H}.$$

⁴This form of the entropy is more general than the ‘‘Boltzmann’’ form (6.1); it was introduced in Gibbs’ treatise [147].

The normalization condition determines the parameter λ , whereas β and hence the temperature arises from the choice of average energy, i.e. from solving the equation

$$\frac{\int H(z)e^{-\beta H(z)}d\omega}{\int e^{-\beta H(z)}d\omega} = \bar{E}$$

Alternatively, we may take the position that the temperature is specified and the mean energy is a direct consequence of this choice.

This defines the phase space density of the canonical ensemble which we refer to as the Gibbs-Boltzmann density:

$$\rho_\beta = Z_{\text{can}}^{-1}e^{-\beta H(\mathbf{q}, \mathbf{p})}. \quad (6.3)$$

where the parameter $\beta = 1/(k_B T)$. The quantity Z_{can} is a normalizing constant so that this is a probability density. The canonical ensemble is referred to as the NVT ensemble, due to the a constancy of the number of particles, volume, and temperature.

Now let us see the consequences of assuming that the states of a given system are canonically distributed. In order for the density in (6.3) to be normalizable, it is necessary that the quantity Z_{can} defined by

$$Z_{\text{can}} = \int e^{-\beta H(\mathbf{q}, \mathbf{p})}d\omega$$

be finite, i.e., that the integral converge. Here the form of the system and the assumptions regarding boundaries come into play. If we have a standard molecular Hamiltonian $H(\mathbf{q}, \mathbf{p}) = \mathbf{p}^T \mathbf{M}^{-1} \mathbf{p}/2 + U(\mathbf{q})$ with $N_c = N_d$ degrees of freedom, then the integral separates

$$Z_{\text{can}} = \int_{\mathcal{D}} e^{-\beta H(\mathbf{q}, \mathbf{p})}d\omega = \int_{\mathbb{R}^{N_c}} e^{-\beta \mathbf{p}^T \mathbf{M}^{-1} \mathbf{p}/2}d\omega_p \times \int_{\mathcal{Q}} e^{-\beta U(\mathbf{q})}d\omega_q,$$

where \mathcal{Q} is the accessible position domain, $d\omega_p = dp_1 dp_2 \dots dp_{N_c}$ and $d\omega_q = dq_1 dq_2 \dots dq_{N_c}$. If U is smooth and the domain \mathcal{Q} is finite, then clearly both integrals are well defined, so the normalization is sensible. When U has singularities, it is important that at these points $U \rightarrow +\infty$ instead of $-\infty$. Moreover, if no boundary conditions are employed to restrict the particles, we would need to introduce an additional restriction on the potential U in order to ensure that the configurational integral converges.

Typically one assumes that (i) U is smooth except on a low-dimensional set of singular points, (ii) U is bounded below (which is normally the case if a potential such as Lennard-Jones, steeply repulsive at short range, is incorporated between all pairs of atoms), and (iii) U grows sufficiently rapidly as $\mathbf{q} \rightarrow \infty$, in the case of an infinite domain.

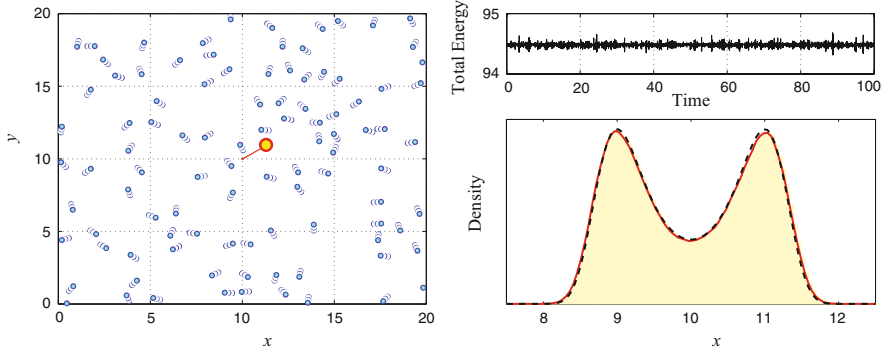


Fig. 6.2 We simulate 100 particles in the plane (*left*) using a periodic box of length $L = 20$, with the Lennard-Jones potential governing all pairwise interactions. One of these particles, marked in red, also feels a double-well potential in both coordinates. The total system energy (*plotted in the top right*) is conserved (with some variance due to numerical error). The distribution for the x -coordinate of the red particle (*plotted in the bottom right*), averaged over a single long trajectory (*solid red*) shows good agreement with the expected canonically distributed result (*dashed black*)

For example a collection of atoms on the infinite domain interacting in Lennard-Jones potentials does not satisfy the third condition, and it does not have a well defined canonical partition function. We can understand this by considering what happens over time in such a system. For simplicity, just take the case of a one degree-of-freedom system with $H = p^2/2 + q^{-12} - q^{-6}$, $q > 0$. If the temperature is low, the particle will remain for a long time in the vicinity of the well bottom. At any given time there is a positive probability of finding the particle essentially any distance from the origin, although the probability of being found very near the origin is extremely small due to the repulsive steep wall. Due to the presence of the thermal bath, eventually the particle will receive enough energy to overcome the attractive force and will be ejected and tend to infinity. The restriction to a bounded domain thus eliminates this problem which otherwise would complicate the technical treatment.

In order to use a one degree-of-freedom model on an infinite domain in the canonical setting, we would need to incorporate a restraining potential, slightly modifying for example the Lennard-Jones potential to $U(q) = q^{-12} - q^{-6} + \varepsilon q^2$ (Fig. 6.2).

6.1.4 The Canonical Density and Thermodynamic Averages

The distributional approach described above and in the previous chapter and used to define microcanonical averages on a bounded energy surface must be modified to make it applicable to the canonical ensemble. Recall that in the microcanonical setting we assumed ρ was a smooth density defined on the bounded energy surface

Σ_E or, more generally, a distribution. For a canonical system there is no longer a constraint of the form $H = E$ and thus we must allow the phase space to include essentially all points for which the position coordinates lie in the defined configurational domain (a 3-torus, if periodic boundary conditions are used). In general the momenta are unbounded. It thus becomes necessary to restrict the set of functions on which the functional $\langle \cdot, \rho \rangle$ acts. In the case of periodic boundary conditions we will assume that, for any observable of interest,

$$|\phi(\mathbf{q}, \mathbf{p})| = \mathcal{O}(\|\mathbf{p}\|^\alpha), \quad \mathbf{p} \rightarrow \infty,$$

for some positive constant α .

If the position domain \mathcal{Q} is unbounded (for example choosing $\mathcal{Q} = \mathbb{R}^N$) then some other restriction is needed on the potential energy function U (and on the observables) in order that averages are well defined. Typical assumptions for potentials on the unbounded domain are that (i) U is bounded below, and (ii) U grows sufficiently rapidly as $\mathbf{q} \rightarrow \infty$. This ensures that

$$\int_{\mathcal{Q}} \exp(-\beta U(\mathbf{q})) d\omega_q < \infty.$$

Under assumptions on the potential energy as discussed above, and with ϕ continuous and allowed to grow at most polynomially fast at infinity, we may proceed to define averages with respect to the canonical density ρ_β , namely

$$\text{Av}_\beta(\phi) = Z_{\text{can}}^{-1} \int_{\mathcal{D}} \phi(\mathbf{q}, \mathbf{p}) \rho_\beta(\mathbf{q}, \mathbf{p}) d\omega. \quad (6.4)$$

6.1.5 Calculation of Temperature

Consider the one degree-of-freedom model $H(q, p) = \frac{p^2}{2m} + U(q)$ on the unbounded domain, with U bounded below and growing sufficiently rapidly as $|q| \rightarrow \infty$. The associated canonical density is

$$\rho_\beta = Z_{\text{can}}^{-1} \exp\left(-\beta \left[\frac{p^2}{2m} + U(q)\right]\right),$$

where

$$Z_{\text{can}}^{-1} = \int_{-\infty}^{\infty} \int_{-\infty}^{\infty} \exp\left(-\beta \left[\frac{p^2}{2m} + U(q)\right]\right) dp dq.$$

We will denote the average with respect to the canonical probability density by Av_β . Using (6.4), we can compute the average of the function p^2 as

$$\begin{aligned}\text{Av}_\beta(p^2) &= \int_{-\infty}^{\infty} \int_{-\infty}^{\infty} p^2 \rho_\beta dq dp \\ &= \frac{\int_{-\infty}^{\infty} p^2 \exp(-\beta m^{-1} p^2/2) dp}{\int_{-\infty}^{\infty} \exp(-\beta m^{-1} p^2/2) dp},\end{aligned}$$

where we have used the fact that the exponential of H separates into a product of p and q dependent factors. We then integrate by parts to obtain

$$\text{Av}_\beta(p^2) = m\beta^{-1},$$

which means that

$$T = \text{Av}_\beta \left(\frac{p^2}{mk_B} \right).$$

Thus the temperature can be related to the canonical average of the kinetic energy.

If we consider a $N_d = N_c$ degree of freedom system with kinetic energy $K = \sum_{i=1}^{N_c} p_i^2 / (2m_i)$ and potential energy $U(q_1, q_2, \dots, q_{N_c})$, then we may decompose the unnormalized canonical distribution as

$$\begin{aligned}\exp(-\beta[K(\mathbf{p}) + U(\mathbf{q})]) &= \exp(-\beta K(\mathbf{p})) \exp(-\beta U(\mathbf{q})) \\ &= \exp(-\beta U(\mathbf{q})) \prod_{i=1}^{N_c} \exp\left(-\beta \frac{p_i^2}{2m_i}\right).\end{aligned}$$

Then we again find, by the integration argument given above, that

$$\text{Av}_\beta(m_i^{-1}k_B^{-1}p_i^2) = T.$$

Thus the average kinetic energy of any individual particle is directly related to the temperature, and thus also

$$\text{Av}_\beta(2K) = N_c k_B T.$$

Very often, this is taken to be the definition of temperature in practical settings. However, since the temperature relation is derived by integration with respect to

the canonical measure, we can find many functions that have the same average. For example, Rugh [319] suggested the formula

$$\frac{\text{Av}_\beta(\|\nabla U\|^2)}{\text{Av}_\beta(\Delta U)} = k_B T. \quad (6.5)$$

We can see this as a consequence of the following proposition (see [193, 211]).

Proposition 6.1 *Let H be a Hamiltonian defined on the phase space \mathbb{R}^{2N_c} and suppose $\mathbf{G} : \mathbb{R}^{2N_c} \rightarrow \mathbb{R}^{2N_c}$ is a smooth (C^1) vector field with the following properties:*

- $0 < |\text{Av}_\beta(\mathbf{G} \cdot \nabla H)| < \infty$,
- $0 < \text{Av}_\beta(\nabla \cdot \mathbf{G}) < \infty$,
- $|\mathbf{G} e^{-\beta H}| < \infty$

Then

$$k_B T = \frac{\text{Av}_\beta(\mathbf{G} \cdot \nabla H)}{\text{Av}_\beta(\nabla \cdot \mathbf{G})}.$$

Proof The proof relies on a $2N_c$ -dimensional version of integration by parts. Let \mathcal{B}_R be the $2N_c$ -dimensional ball centered at the origin, of radius R , and let Γ_R be its boundary, the $2N_c - 1$ -dimensional sphere. Then, for any smooth scalar field g defined on \mathcal{B}_R , we have

$$\int_{\mathcal{B}_R} \mathbf{G} \cdot \nabla g d\omega = \int_{\Gamma_R} (\mathbf{G} g) \cdot \hat{\mathbf{n}} d\Gamma - \int_{\mathcal{B}_R} (\nabla \cdot \mathbf{G}) g d\omega, \quad (6.6)$$

where $d\omega = dq_1 \dots dp_{N_c}$ is the standard measure of Lebesgue integration in \mathbb{R}^{2N_c} and $d\Gamma$ is the surface area element of the hypersphere, and $\hat{\mathbf{n}}$ represents the unit outward normal to the sphere. Replace g by $\rho_\beta = \exp(-\beta H)$, then it follows that

$$\left| \int_{\Gamma_R} (\mathbf{G} \rho_\beta) \cdot \hat{\mathbf{n}} d\Gamma \right| \leq \max_{\Gamma_R} |\mathbf{G} \rho_\beta| \sigma_R,$$

where σ_R is the surface area of the hypersphere. Divide (6.6) by the volume v_R of \mathcal{B}_R . Then, for large R , since the ratio of surface area to volume is proportional to R^{-1} , we have

$$\frac{\int_{\mathcal{B}_R} \mathbf{G} \cdot \nabla \rho_\beta d\omega}{v_R} \approx - \frac{\int_{\mathcal{B}_R} (\nabla \cdot \mathbf{G}) \rho_\beta d\omega}{v_R}.$$

Since $\nabla \rho_\beta = -\beta \nabla H \rho_\beta$, we obtain, in the limit $R \rightarrow \infty$, the desired result. \square

Observe that, defining

$$\mathbf{G} = \begin{bmatrix} 0 \\ \mathbf{p} \end{bmatrix}$$

yields the kinetic temperature observable $k_B T = \text{Av}_\beta(\mathbf{p}^T \mathbf{M}^{-1} \mathbf{p}) / N_c$, whereas

$$\mathbf{G} = \begin{bmatrix} \nabla U(\mathbf{q}) \\ 0 \end{bmatrix}$$

gives the *configurational* temperature observable (6.5).

An even simpler configuration-dependent choice is derived from

$$\mathbf{G} = \begin{bmatrix} \mathbf{q} \\ 0 \end{bmatrix},$$

corresponding to

$$k_B T = \frac{\text{Av}_\beta(\mathbf{q} \cdot \nabla U)}{N_c}.$$

An important point is that the formula of Rugh may not be robust from a computational perspective in cases where the denominator may be close to zero. The simple choice of the kinetic temperature is often desirable since it works for both the infinite domain and for periodic boundary conditions and is such that the denominator is a nonzero constant.

Rugh's principle gives generalized temperature indicators on an infinite domain, but as we have already pointed out, typical molecular dynamics models are confined by periodic boundary conditions to a torus in configuration space (or a toric-cylinder in phase space). Similar results may be obtained in this case. The key point in the proof above is the vanishing contribution from the boundary as $R \rightarrow \infty$; in the case of periodic boundary conditions, the boundary terms from opposite sides of the domain can be seen to cancel out, leaving the desired relation. In general one should ensure that the formula for temperature is invariant under translations of the periodic domain along coordinate directions in the configurational domain. If \mathbf{G} and H are both periodic in \mathbf{q} and \mathbf{G} is smooth, then everything works since the outward pointing normal will be in opposite directions on each side of the simulation cell, and the boundary term will cancel.

Thus for periodic boundary conditions we may choose

$$\mathbf{G}(z) = \begin{bmatrix} \mathbf{0} \\ \mathbf{p} \end{bmatrix},$$

or

$$\mathbf{G}(\mathbf{z}) = \begin{bmatrix} \nabla U(\mathbf{q}) \\ \mathbf{0} \end{bmatrix}.$$

However $\mathbf{G}(\mathbf{z}) = \begin{bmatrix} \mathbf{q} \\ \mathbf{0} \end{bmatrix}$ is problematic for periodic boundary conditions.

6.2 Stochastic Differential Equations for Molecular Models

We now have established a framework for the thermodynamic properties of a model system. What would be desirable is that we could approximate the force terms arising in the bulk, without the need to simulate them directly. It should be apparent that constant-energy dynamics (designed to sample the microcanonical ensemble with constant energy E) will not sample the canonical distribution in the absence of the heat bath: such Newtonian trajectories cannot access regions of the phase space where $H(\mathbf{z}) \neq H(\mathbf{z}_0)$, where \mathbf{z}_0 is the initial condition.

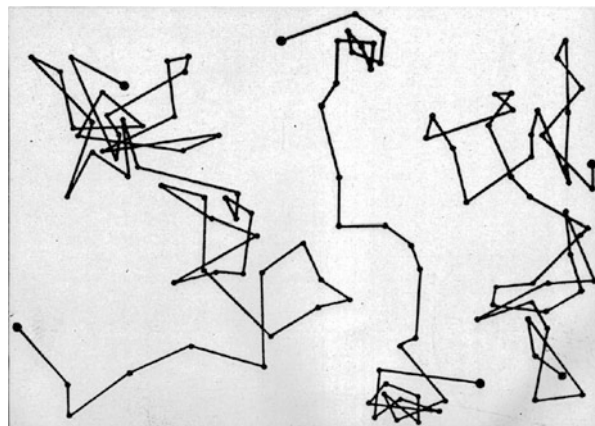
On the other hand, changing our perspective to think of trajectories as general tools for sampling a defined distribution, we may consider an alternative dynamics designed specifically to sample the canonical distribution. We refer to a dynamical system that samples ρ_β as a “thermostat,” or “thermostatted molecular dynamics” since the canonical ensemble is characterized by a fixed temperature. In principle, even grossly non-physical dynamics would be permissible, if the goal is only to compute stationary (equilibrium) averages. (In Chap. 8, we take up the issue of comparison of dynamics computed using different thermostat methods.) We might also think of a thermostat as a “governor” in the tradition of the governors used in steam engines to regulate the engine temperature. (It is interesting to note that J.W. Gibbs, one of the fathers of modern statistical mechanics, had himself designed a governor for steam engines.) Because it is very difficult (in some sense, probably impossible) to build ergodic thermostats using deterministic dynamical systems, which are, until now, the only tool available to us, we need to develop the theory of stochastic differential equations and, in particular, the application of that theory in the setting of molecular dynamics. This is a fairly tall order and to achieve it in a compact presentation, we assume that the reader is familiar with basic concepts from probability theory (see Appendix B for a quick summary of the main principles).

6.2.1 Random Walks and Wiener Processes

In 1827 Robert Brown noticed that small particles in a fluid were in constant motion, following irregular paths.⁵ The essential properties of Brownian motion

⁵Brown was not in fact the only—or even the first—to observe this: Jan Ingenhouz had observed a similar property of coal dust particles on the surface of alcohol already in 1785.

Fig. 6.3 Perrin's plot of the motion of small particles formed from resin of the tree *garcinia xanthochymus* buffeted by interactions with a bath of water molecules. Perrin's careful observations were consistent with those of earlier observers, beginning with Brown's study of pollen grains in 1827



were worked out in the late 1800s by Thorvald Thiele and Louis Bachelier, although the complete picture was only obtained in the early 1900s in celebrated works by Albert Einstein and Marian Smoluchowski. Brownian motion describes the process by which particles placed in a fluid bath move about subject to collisions with the molecules of the fluid. These collisions, which for all practical purposes may be viewed as random, introduce a jerky character to motion such as that shown in Fig. 6.3.

To model the randomized motion of the Brownian particle, the concept of a random walk is typically used. A random walk is an example of a stochastic process, a collection of random variables parameterized by either a discrete or continuous index parameter [269, 314]. A random walk is a discrete stochastic process in which the state X_n at a given instant (defined by the index n) is related to the state X_{n-1} , at step $n - 1$ by an offset that may be viewed as a random variable. That is, we have

$$X_{n+1} = X_n + \delta x J_n.$$

We initiate the random walk with $X_0 = 0$. The quantity J_n is a random variable drawn from a certain probability distribution. In the classic model of a random walk the jump takes values ± 1 with equal probability. The *increments* of the random walk are the differences $\Delta X_n = X_n - X_{n-1} = \delta x J_{n-1}$, thus (X_n) is a random process with independent increments.

The solution X_n of the random walk may be written

$$X_n = \delta x \sum_{k=0}^{n-1} J_k,$$

hence the variance is

$$\mathbb{E} X_n^2 = \delta x^2 \mathbb{E} \left(\sum_{k=0}^{n-1} J_k \right)^2.$$

Expanding the squared sum we see that there are (i) n squares J_k^2 plus (ii) products of the form $J_k J_l$, $k \neq l$. Clearly the former are always one and the latter have zero expectation, thus

$$\mathbb{E}X_n^2 = n\delta x^2.$$

The variance therefore grows linearly with the number of steps taken.

Now let us take a slightly different perspective. We start with a time interval $[0, \tau]$ and subdivide this into v steps of size $\delta t = \tau/v$. Let $t_n = n\delta t$, $n = 0, 1, \dots, v$ and define

$$Y(t_{k+1}) = Y(t_k) + \sqrt{\delta t} J_k, \quad k = 0, 1, \dots, v-1,$$

where $Y(0) = 0$. Effectively we are making the size of the jump δx taken at each step of the random walk equal to $\sqrt{\delta t}$.

We will use the shorthand $Y_k = Y(t_k)$ and $\Delta Y_k = Y_{k+1} - Y_k = \sqrt{\delta t} J_k$.

The increments are clearly independent. Let us observe the following facts, for $0 \leq k \leq l \leq v$

- (i) $\mathbb{E}(Y_l - Y_k) = 0$,
- (ii) $\text{Var}(Y_l - Y_k) = t_l - t_k$.

For points between t_k and t_{k+1} we define the value of $Y(t)$ by linear interpolation:

$$Y(t) = Y_k + \frac{(t - t_k)}{\delta t} \Delta Y_k$$

Then, for $0 \leq t \leq s \leq \tau$, we have

$$\mathbb{E}(Y(s) - Y(t)) = 0.$$

This is easy to demonstrate. However, the intuitive corresponding statement $\text{Var}(Y(s) - Y(t)) = (s - t)$ does not quite hold due to the reliance on interpolation. Nevertheless, such a relation holds in an approximate sense and in the limit of small step.

The relation $\delta t = \delta x^2$ defines a scaling of time in relation to distance. When we take limits as these two quantities go to zero in such a way that $\delta t = \delta x^2$ we refer to it as a *diffusion limit*. It is this type of random diffusion model that has the greatest relevance for experiments like those of Brown and Perrin.

In the diffusion limit the motion of the random walk can be viewed as an everywhere continuous (but almost nowhere smooth) path which is called a *Wiener process* (after Norbert Wiener).

$$W(t) = \widehat{\lim}_{\delta t \rightarrow 0} \sqrt{\delta t} \sum_{k=0}^{\lfloor t/\delta t \rfloor} J_k.$$

The convergence here, signified by the symbol $\widehat{\lim}$ is in the sense of distributions (see Appendix B).

As $W(t)$ is the limit of a sum of independent, identically distributed random variables, it makes sense to use the Central Limit Theorem to determine its distribution. Recall (see Appendix B) that the Central Limit Theorem tells us that the sum of a set of independent, identically distributed random variables has an approximately normal distribution with mean and variance determined from the underlying parameters of the distribution. Let δt be a small finite value and $n = t/\delta t$, then, using the Central Limit Theorem, and the fact that $\mathbb{E}J_k = 0$, we have, for a large number n of random steps, the approximate relation

$$\sum_{k=0}^{n-1} \sqrt{\delta t} J_k \sim \mathcal{N}(0, n\delta t).$$

As we take n to infinity, δt to zero, in such a way that $n\delta t \equiv t$, we obtain the random variable $W(t)$ such that

$$W(t) \sim \mathcal{N}(0, t).$$

Moreover, we may easily demonstrate that

$$\mathbb{E}(W(t) - W(s))^2 = |t - s|. \quad (6.7)$$

For the Wiener process, we know that $W(t) - W(s)$ is normally distributed with mean zero and variance $|t - s|$; this does not depend on whether there is additional information available regarding its value prior to $\min(t, s)$, that is to say, the Wiener process is a *Markov process*. More generally, when we say that a stochastic process is Markovian, we mean that the probability of a future event conditioned on the current state of the process and the past history of the process is the same as the probability conditioned on the current state of the process. Let $\mathcal{A}(x)$, $\mathcal{B}(x)$ and $\mathcal{C}(x)$ be three events dependent on state variable x , and let $t_+ > t_0 > t_-$ be three times, then, for a Markov process $X(t)$ we have (using the notation for conditional probability):

$$\Pr[\mathcal{A}(X(t_+)) | \mathcal{B}(X(t_0)), \mathcal{C}(X(t_-))] = \Pr[\mathcal{A}(X(t_+)) | \mathcal{B}(X(t_0))].$$

The Markov property greatly simplifies the task of finding the joint probability distribution of the values of the stochastic process at two times.

6.2.2 Stochastic Integration

In order to develop good sampling paths for the Gibbs-Boltzmann distribution, we need to introduce a method of adding random perturbations into a differential equation. Let us first consider the definition of the integral *with respect to Wiener measure*.

Recall that the Riemann integral of a continuous function g on $[0, \tau]$ is the limit of Riemann sums constructed as follows: partition the interval $[0, \tau]$ into K subintervals each of width $\delta t = \tau/v$, choose an arbitrary t_k from the k th subinterval, $1 \leq k \leq v$, and evaluate the integral as a limit of the sum of products:

$$\int_0^\tau g(t)dt = \lim_{v \rightarrow \infty} \sum_{k=0}^{v-1} g(t_k)\delta t.$$

We know that this limit does not depend on where the t_k are chosen within the subintervals. For example we can take the left or right endpoint of each subinterval or the midpoint.

By analogy, we would like to write the stochastic integral of a function g , where g may, itself, be defined in terms of a stochastic process, as the limit of a sum:

$$\sum_{k=0}^{v-1} g(t_k)[W((k+1)\delta t) - W(k\delta t)], \quad v \rightarrow \infty,$$

where the increments $W((k+1)\delta t) - W(k\delta t)$ identified here are the increments of a Wiener process whose properties are given above. (In particular they are normally distributed with mean zero and variance δt .) First, we should be careful regarding the sense in which we expect convergence, since sequences of random variables may converge in various ways.

Next, unlike in the case of the Riemann sums, it turns out that the result depends on where we place the points t_k . Using the properties of the Wiener process we may easily show that the choice $t_k = k\delta t$ (left endpoint) and the choice $t_k = (k + 1/2)\delta t$ yield different formulas for the integral. The first choice is commonly referred to as *Itô integration*, and the second as *Stratonovich integration*. As an example, consider the case where $g(t) = W(t)$. We suppose this to be approximated by a sum

$$\begin{aligned} \int_0^\tau W(t)dW(t) &\approx \sum_{k=0}^{v-1} W(k\delta t)[W((k+1)\delta t) - W(k\delta t)], \\ &= \frac{1}{2} \sum_{k=0}^{v-1} \left[(W((k+1)\delta t)^2 - W(k\delta t)^2) - (W((k+1)\delta t) - W(k\delta t))^2 \right]. \end{aligned}$$

Breaking this into two parts, we see that the first sum telescopes to give $W(\tau)^2$ (as $W(0) = 0$). On the other hand, from (6.7), we have

$$\lim_{v \rightarrow \infty} \mathbb{E} \sum_{k=0}^{v-1} [(W((k+1)\delta t) - W(k\delta t))^2] = \tau,$$

but an even stronger statement is possible. Since we are summing a large collection of random variables ΔW_k whose means are δt , the Central Limit Theorem tells us that, if we assume it to be well defined, the variance of the sum of squares from τ must tend to zero as a function of v . Thus we may understand the convergence in a somewhat stronger sense than convergence in expectation. We make this precise in the following proposition

Proposition 6.2 *Let $v\delta t = \tau$ then*

$$\text{l.i.m.}_{v \rightarrow \infty} \sum_{k=0}^{v-1} [(W((k+1)\delta t) - W(k\delta t))^2] = \tau,$$

where, for a sequence of random variables, A_v and a random variable B , we have

$$\text{l.i.m.}_{v \rightarrow \infty} A_v = B \Leftrightarrow \lim_{v \rightarrow \infty} \mathbb{E}(A_v - B)^2 = 0.$$

(This is referred to as convergence in the mean square sense.)

Proof With τ, v fixed, we have $\delta t = \tau/v$.

Let $\Delta W_{v,k} = W((k+1)\delta t) - W(k\delta t) = W((k+1)\tau/v) - W(k\tau/v)$ and observe that

$$\sum_{k=0}^{v-1} \Delta W_{v,k}^2 - \tau = \sum_{k=0}^{v-1} \left[\Delta W_{v,k}^2 - \frac{\tau}{v} \right].$$

Then

$$I_v \stackrel{\text{def}}{=} \mathbb{E} \left(\sum_{k=0}^{v-1} \Delta W_{v,k}^2 - \tau \right)^2 = \mathbb{E} \left(\sum_{k=0}^{v-1} \left[\Delta W_{v,k}^2 - \frac{\tau}{v} \right] \right)^2.$$

Terms of the form $Z_{v,k} \stackrel{\text{def}}{=} \Delta W_{v,k}^2 - \frac{\tau}{v}$ are independent and have mean zero. Therefore

$$\mathbb{E} \left(\sum_{k=0}^{v-1} Z_{v,k} \right)^2 = \mathbb{E} \sum_{k=0}^{v-1} Z_{v,k}^2 - 2\mathbb{E} \sum_{k \neq l} Z_{v,k} Z_{v,l} = \mathbb{E} \sum_{k=0}^{v-1} Z_{v,k}^2,$$

where the last equation follows from independence of the increments ($\mathbb{E}Z_k Z_l = 0$ if $k \neq l$).

Also observe that ΔW_k is a normally distributed random variable with the following properties

$$\mathbb{E}\Delta W_k = 0, \quad \mathbb{E}\Delta W_k^2 = \delta t = \tau/v, \quad \mathbb{E}\Delta W_k^4 = 3\delta t^2 = 3(\tau/v)^2.$$

Thus we have

$$\begin{aligned} I_v &= \mathbb{E} \sum_{k=0}^{v-1} (\Delta W_{v,k}^2 - \frac{\tau}{v})^2 \\ &= \sum_{k=0}^{v-1} \mathbb{E} \left(\Delta W_{v,k}^4 - 2\frac{\tau}{v} \Delta W_{v,k}^2 + \frac{\tau^2}{v^2} \right) \\ &= \sum_{k=0}^{v-1} \left(3\left(\frac{\tau}{v}\right)^2 - 2\left(\frac{\tau}{v}\right)^2 + \frac{\tau^2}{v^2} \right) = 2\frac{\tau^2}{v^2}v = 2\frac{\tau^2}{v}. \end{aligned}$$

Thus $I_v \rightarrow 0$ as $v \rightarrow 0$, which is the desired result. \square

The calculation implies that

$$\int_0^\tau W(t) dW(t) = \frac{1}{2} (W(\tau)^2 - \tau).$$

In contrast, the Stratonovich (midpoint) integral (denoted by $\int_0^\tau \circ dW(t)$) can be calculated as

$$\int_0^\tau W(t) \circ dW(t) = \text{l.i.m.}_{v \rightarrow \infty} \sum_{k=0}^{v-1} W(k\delta t + \delta t/2) [W((k+1)\delta t) - W(k\delta t)].$$

Writing

$$W(k\delta t + \delta t/2) = W\left(\frac{(k+1)\delta t + k\delta t}{2}\right) = \frac{1}{2} (W((k+1)\delta t) + W(k\delta t)) + \mathcal{O}(\sqrt{\delta t}),$$

allows us to evaluate the integral as

$$\int_0^\tau W(t) \circ dW(t) = \frac{1}{2} \text{l.i.m.}_{v \rightarrow \infty} \sum_{k=0}^{v-1} [W((k+1)\delta t)^2 - W(k\delta t)^2] = \frac{1}{2} W(\tau)^2.$$

Plainly this is different than the Itô version of the integral, but in the cases we consider it is possible to reformulate Stratonovich integrals as Itô integrals. In the remainder of this book we will adopt the Itô form of stochastic integration.

Defined by Itô integration, $Y(t) \stackrel{\text{def}}{=} \int_0^t g(s)dW(s)$ can be thought of as a random process. In the case that g indicated here is a deterministic function, $Y(t)$ is Gaussian in the sense that it is normally distributed for all time, as summarized in the following proposition.

Proposition 6.3 *Let g be a smooth deterministic function and $W(t)$ a Wiener process. The stochastic integral $Y(t) = \int_0^t g(s)dW(s)$ is, for all times $t \geq 0$, a normally distributed random variable such that*

$$\mathbb{E}(Y(t)) = 0,$$

$$\mathbb{E}(Y^2(t)) = \sigma^2(t) = \int_0^t g(s)^2 ds.$$

Proof See Exercise 2.

Finally, we observe that by calculating $\sigma^2(t_n)$ and generating random increments $R_n \sim \mathcal{N}(0, \sigma(t_n))$ we have a discrete representation of the continuous time stochastic process $Y(t)$, effectively an exact stroboscopic representation. Also it is natural to view the stochastic integral as the solution of the stochastic differential equation (SDE) with zero initial condition:

$$dY(t) = g(t)dW(t), \quad Y(0) = 0. \quad (6.8)$$

This notion of stochastic integration carries over to stochastic integration with respect to more general categories of stochastic processes. Importantly, with appropriate regularity we have the familiar relation from calculus:

$$\int_0^t dY(s) = Y(t) - Y(0).$$

6.3 Stochastic Differential Equations

In this section we briefly derive a more general stochastic differential equation as the limit of a biased random walk. The treatment here is intuitive, based on the concepts of limiting processes and stochastic integration introduced above. For a rigorous treatment of the material presented here, it is recommended to consult a reference such as the excellent book of Nelson [279] (which also contains a very lively historical discussion).

We introduce a pair of smooth functions $a(x, t)$ and $b(x, t)$, where a represents a drift tendency and b the average magnitude of the random jump. In the interval $[n\delta t, (n+1)\delta t]$, a step $\delta X_n = X_{n+1} - X_n$ of the random walk will be given by

$$\delta X_n = a(X_n, t_n) h + b(X_n, t_n) J_n \delta x, \quad (6.9)$$

where the random increment J_n was introduced in Sect. 6.2.1. Choose a positive t and sum (6.9) from $n = 0$ to $v-1$, where $v = \lfloor t/\delta t \rfloor$, obtaining

$$X_v - X_0 = \sum_{n=0}^{v-1} \delta X_n = \sum_{n=0}^{v-1} a(X_n, t_n) \delta t + \sum_{n=0}^{v-1} b(X_n, t_n) J_n \delta x. \quad (6.10)$$

Take the diffusion limit $\delta t \rightarrow 0$, $\delta x^2/\delta t \rightarrow 1$ with $v\delta t = t$ fixed, then we obtain, under the Itô convention,

$$X(t) - X(0) = \int_0^t a(X(s), s) ds + \int_0^t b(X(s), s) dW(s), \quad (6.11)$$

where X is obtained by a limiting process similar to that discussed above, and

$$\int_0^t a(X(s), s) ds \stackrel{\text{def}}{=} \lim_{\delta t \rightarrow 0} \sum_{n=0}^{v-1} a(X(n\delta t), n\delta t) \delta t, \quad (6.12)$$

$$\int_0^t b(X(s)) dW(s) \stackrel{\text{def}}{=} \text{l.i.m.}_{\delta t \rightarrow 0} \sum_{n=0}^{v-1} b(X(n\delta t), n\delta t) J_n \sqrt{\delta t}. \quad (6.13)$$

As $X(t) - X(0) = \int_0^t dX(s)$, we may view (6.11) as a relation between differentials:

$$dX(s) = a(X(s), s) ds + b(X(s), s) dW(s),$$

or, more simply

$$dX = a(X, t) dt + b(X, t) dW. \quad (6.14)$$

which is the general form of a scalar stochastic differential equation.

We mention in passing the extension to systems of SDEs. Let $\mathbf{a}(z, t)$ and $\mathbf{b}^{(i)}(z, t)$, $i = 1, 2, \dots, r$ be a set of $r+1$ vector fields in \mathbb{R}^m , and let W_1, W_2, \dots, W_r be a

collection of r independent Wiener processes, then we may write a system of SDEs in \mathbb{R}^m in the form

$$d\mathbf{Z} = \mathbf{a}(\mathbf{Z}, t)dt + \sum_{i=1}^r \mathbf{b}^{(i)}(\mathbf{Z}, t) dW_i. \quad (6.15)$$

alternatively, if \mathbf{B} is the matrix with columns $\mathbf{b}^{(1)}, \mathbf{b}^{(2)}, \dots, \mathbf{b}^{(r)}$, and \mathbf{W} represents the r -component vector of Wiener processes, then

$$d\mathbf{Z} = \mathbf{a}(\mathbf{Z}, t)dt + \mathbf{B}(\mathbf{Z}, t) d\mathbf{W}. \quad (6.16)$$

6.3.1 The Itô Formula

We shall derive, heuristically, a core piece of mathematical apparatus which permits much of the analysis of SDEs. Let $\phi(\cdot)$ be any continuously twice differentiable function and let $X_n \in \mathbb{R}$ represent the state of a biased random walk as considered in Sect. 6.3, i.e., with state $X_{n+1} = X_n + a(X_n, n\delta t)\delta t + b(X_n, n\delta t)J_n\delta x$. Let $\phi_n = \phi(X_n)$, then Taylor's theorem gives

$$\begin{aligned} \delta\phi &\stackrel{\text{def}}{=} \phi_{n+1} - \phi_n \\ &= \phi'(X_n)\delta X_n + \frac{1}{2}\phi''(X_n)\delta X_n^2 + o(\delta X_n^2) \\ &= \phi'(X_n)(a(X_n, n\delta t)\delta t + b(X_n, n\delta t)J_n\delta x) \\ &\quad + \frac{1}{2}\phi''(X_n)(a(X_n, n\delta t)\delta t + b(X_n, n\delta t)J_n\delta x)^2 + o(\delta X_n^2). \end{aligned}$$

Now we expand the 2nd order term and, working in the diffusion limit, recognize that $\delta x^2 \sim \delta t$, thus we have

$$\begin{aligned} \delta\phi &= \phi'(X_n)(a(X_n, n\delta t)\delta t + b(X_n, n\delta t)J_n\delta x) \\ &\quad + \frac{1}{2}\phi''(X_n)b(X_n, n\delta t)^2\delta t + \mathcal{O}(\delta t^{3/2}). \end{aligned}$$

Passing to the limit, this leads to the SDE:

$$d\phi(X) = \phi'(X)(a(X, t)dt + b(X, t)dW) + \frac{1}{2}\phi''(X)b(X, t)^2dt. \quad (6.17)$$

This is most often referred to as the *Itō formula*. In recognition of the earlier contributions of Doeblin, many authors now add the second name, and we will follow this convention, referring to (6.17) as the *Itō-Doeblin formula*.⁶

We also mention that the Itō-Doeblin formula can be easily generalized to functions of the form $\phi(x, t)$:

$$d\phi(X, t) = \phi_t(X, t) + \phi_x(X, t)(a(X, t)dt + b(X, t)dW) + \frac{1}{2}\phi_{xx}(X, t)b(X, t)^2dt. \quad (6.18)$$

6.3.2 Distributional Solution of the Ornstein-Uhlenbeck SDE

For now we will examine the special case of a scalar equation

$$dX = -\gamma Xdt + \sigma dW, \quad (6.19)$$

where $\gamma > 0$ and σ are constants. We term Eq. (6.19) the Ornstein-Uhlenbeck SDE.

We saw before that we could think of the simple SDE initial value problem (6.8) as having a solution defined by a certain random process. In the same way we would like to obtain, for the Ornstein-Uhlenbeck SDE (6.19), an explicit stochastic process which is in some sense equivalent to solving the SDE. Multiply both sides of (6.19) by the integrating factor $\exp(\gamma t)$, and observe that

$$d(\exp(\gamma t)X) = \exp(\gamma t)(dX + \gamma Xdt),$$

thus (6.19) becomes

$$d(\exp(\gamma t)X) = \sigma \exp(\gamma t)dW(t).$$

We then integrate both sides to obtain

$$\exp(\gamma t)X(t) = X(0) + \int_0^t \sigma \exp(\gamma s)dW(s).$$

Multiplying by $e^{-\gamma t}$ gives

$$X(t) = e^{-\gamma t}X(0) + \sigma e^{-\gamma t} \int_0^t \exp(\gamma s)dW(s).$$

⁶A convenient method for remembering it is to expand $d\phi(X) \stackrel{\text{def}}{=} \phi(X + dX) - \phi(X)$ in powers of dX up to the second order, then substitute for dX from the SDE (6.14) and finally set all higher powers and products of dt and dW to zero with the one exception $dW^2 = dt$.

Using Proposition 6.3, we know that for a Wiener process $W(t)$, $Y(t) \stackrel{\text{def}}{=} \int_0^t \exp(\gamma s) dW(s)$ is a Gaussian random variable with mean zero and variance

$$\text{Var}\{Y(t)\} = \int_0^t e^{2\gamma s} ds = \frac{e^{2\gamma t} - 1}{2\gamma}.$$

The solution with equivalent distribution is therefore

$$X(t) = e^{-\gamma t} X(0) + \sigma \sqrt{(2\gamma)^{-1}(1 - e^{-2\gamma t})} \hat{Y}(t).$$

where $\hat{Y}(t)$ should be interpreted as random process which at every time t evaluates to a normal random variable ($\hat{Y}(t) \sim N(0, 1)$). This is what we mean by the exact distributional solution of the Ornstein-Uhlenbeck SDE with prescribed initial value $X(0)$.

Let $\sigma = \sqrt{2\gamma k_B T m}$, then for large t the exponentials of the form $e^{-\gamma t}$ tend to zero, and we have

$$X(t) \approx \sqrt{k_B T m} \hat{Y}(t),$$

in which case $X(t)$ is drawn from the probability density

$$\rho_\infty(u) = \frac{1}{\sqrt{2\pi m k_B T}} \exp\left(-\frac{1}{k_B T} \frac{u^2}{2m}\right).$$

If we think of $X(t)$ as not the position, but actually the momentum, then the Ornstein-Uhlenbeck equation samples, in the long term, the Gibbs-Boltzmann distribution associated to a single particle in a thermal bath at temperature T . In recognition of this, from this point forward, we will replace X with p as the variable in the Ornstein-Uhlenbeck equation.⁷ For a system with N_c configurational variables we may write

$$dp_i = -\gamma p_i dt + \sqrt{2\gamma k_B T m_i} dW_i, \quad (6.20)$$

where $W_1(t), W_2(t), \dots, W_{N_c}(t)$ represent N_c independent Wiener processes, or, in vectorial notation, denoting $\mathbf{W} = [W_1, W_2, \dots, W_{N_c}]^T$, we have

$$dp = -\gamma p dt + \sqrt{2\gamma k_B T} M^{1/2} d\mathbf{W}. \quad (6.21)$$

⁷In so doing, we must in many cases give up the traditional notational convention of indicating solutions of SDEs by capital letters and the corresponding variables in the density function by the lower case equivalent. This however allows us to maintain better notational coherence with the earlier treatment of deterministic systems.

6.3.3 Models for Heat Baths and Langevin's Model for Brownian Motion

If the Ornstein-Uhlenbeck SDE models the momentum of particles undergoing collisions, it can be complemented by a corresponding differential equation for the position of the form

$$dq = m^{-1} pdt,$$

to provide a full description of the motion. This is the key idea in Langevin's model for Brownian motion [213].

Let us derive the Langevin dynamics model for the special case of a heavy particle (mass one) interacting with a large collection of light particles. We assume as in [138] that we are given a system of k coupled oscillators (a “heat bath”) in contact with a distinguished particle. The Hamiltonian is

$$H = \frac{P^2}{2} + \sum_{i=1}^k \frac{p_i^2}{2\mu_i} + U(Q) + \frac{1}{2k} \sum_{i=1}^k (q_i - Q)^2$$

where Q and P represent the position and momentum of the distinguished particle and $\{q_i, p_i\}$ are the positions and momenta of the particles of the bath, μ_i giving the mass of the i th light particle.

The equations of motion for the combined system are

$$\dot{Q} = P, \tag{6.22}$$

$$\dot{P} = -U'(Q) - k^{-1} \sum_{i=1}^k (Q - q_i), \tag{6.23}$$

where, for $i = 1, 2, \dots, k$,

$$\dot{q}_i = p_i / \mu_i, \tag{6.24}$$

$$\dot{p}_i = (Q - q_i) / k. \tag{6.25}$$

Because the system (6.24)–(6.25) is linear, we may solve it analytically for $\{q_i, p_i\}$; this yields:

$$q_i(t) = \cos(\Omega_i t) q_i(0) + \Omega_i^{-1} \sin(\Omega_i t) p_i(0) / \mu_i + k^{-1} \mu_i^{-1} \int_0^t \Omega_i^{-1} \sin(\Omega_i(t-s)) Q(s) ds, \tag{6.26}$$

where $\Omega_i = k^{-1/2} \mu_i^{-1/2}$ is the frequency of the i th oscillator. Integrating by parts, we have

$$\begin{aligned}\int_0^t \Omega_i \sin(\Omega_i(t-s)) Q(s) ds &= [\cos(\Omega_i(t-s)) Q(s)]_0^t - \int_0^t \cos(\Omega_i(t-s)) P(s) ds \\ &= Q(t) - \cos(\Omega_i t) Q(0) - \int_0^t \cos(\Omega_i(t-s)) P(s) ds.\end{aligned}$$

which leads to

$$\begin{aligned}q_i(t) - Q(t) &= \cos(\Omega_i t) q_i(0) + \Omega_i^{-1} \sin(\Omega_i t) p_i / \mu_i - \cos(\Omega_i t) Q(0) \\ &\quad - \int_0^t \cos(\Omega_i(t-s)) P(s) ds.\end{aligned}$$

Introducing this formula in (6.23), we obtain a reduced system

$$\dot{Q} = P, \tag{6.27}$$

$$\dot{P} = -U'(Q) - k^{-1} \sum_{i=1}^k (Q - q_i), \tag{6.28}$$

$$= -U'(Q) + f(t) - \int_0^t \psi(t-s) P(s) ds, \tag{6.29}$$

where we define

$$\begin{aligned}f(t) &= -k^{-1} \sum_{i=1}^k [\cos(\Omega_i t) q_i(0) + \Omega_i^{-1} \sin(\Omega_i t) p_i(0) / \mu_i - \cos(\Omega_i t) Q(0)], \\ \psi(t) &= k^{-1} \sum_{i=1}^k \cos(\Omega_i t).\end{aligned}$$

For large k and for many choices of the frequencies Ω_i and the initial conditions $\{q_i(0), p_i(0)\}$, function $f(t)$ will take on the character of a Wiener process; in fact the convergence can be shown in the weak sense. We may even take the initial conditions to be randomly distributed [13, 205]. The function $\psi(t)$ will typically exhibit an initial decay followed by rapid bounded fluctuation (see Fig. 6.4), with decay to zero in the limit of large k . Let $\{\Omega_i^{(k)} | i = 1, 2, \dots, k\}$ represent the frequencies used for a given k . We may make various proposals for the $\Omega_i^{(k)}$,

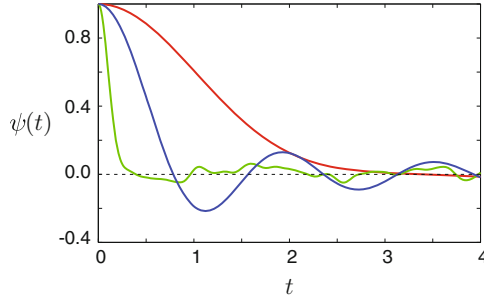


Fig. 6.4 The memory kernel ψ is shown for three different sets of frequencies Ω_i . Blue: $k = 400$, $\Omega_i = 0.01i$; red: $k = 1,000$, $\Omega_i \sim \mathcal{U}[0, 1]$; green: $k = 1,000$, $\Omega_i = 10\hat{\Omega}_i$, where $\hat{\Omega}_i \sim \mathcal{U}[0, 1]$

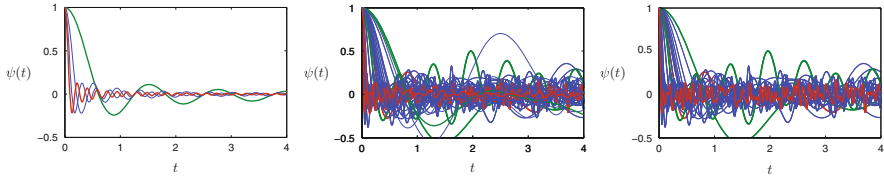


Fig. 6.5 The memory kernels are shown for various choices of $\Omega_i^{(k)}$. Left: $\Omega_i^{(k)} = i/\sqrt{k}$, $k = 5^2, 10^2, \dots, 35^2$; center: $\Omega_i = \sqrt{k}\hat{\Omega}_i$, $\hat{\Omega}_i \sim \mathcal{U}[0, 1]$, $k = 10, 20, \dots, 100$; right: $\Omega_i = k\hat{\Omega}_i$, $\hat{\Omega}_i \sim \mathcal{U}[0, 1]$, $k = 10, 20, \dots, 100$. In each case the red curve indicates the largest value of k considered, whereas green indicates the smallest value

for example choosing them to be equally spaced on $[0, k]$, uniformly (randomly) distributed on a fixed interval, or uniformly distributed in an interval of length \sqrt{k} . Different choices of sequences $\Omega_i^{(k)}$ will lead to different appearances of the kernel ψ , as shown in Fig. 6.5.

If sufficient high frequency components are present, then the mass of the memory kernel is typically found to be localized around 0; in such a situation of rapid decay it is found that one may replace the function ψ by a Dirac delta function scaled by a positive coefficient γ ; we say that the system is Markovian or memory-less in this situation and we replace the delay-differential equation (6.29) by the SDEs

$$dQ = Pdt, \quad (6.30)$$

$$dP = -U'(Q)dt + \sigma dW - \gamma Pdt, \quad (6.31)$$

where we have viewed the function $f(t)$ as being approximated by a Wiener increment. This system is referred to as Langevin dynamics. The details of the rigorous derivation of (6.30)–(6.31) are beyond the scope of this book; consult the following [13, 113, 138, 150, 185, 198, 205, 350, 402]. We will consider computations of *generalized Langevin dynamics* in Chap. 8. For the moment we

consider only the case of Wiener increments and delta-correlated (memory-less) processes.

Langevin's idea of including external random impacts in the equations of motion for a free particle can be extended to a system of particles. The equations of motion are, in vectorial form:

$$dq = M^{-1} pdt, \quad (6.32)$$

$$dp = -\nabla U(q)dt - \gamma pdt + \sqrt{2\gamma k_B T} M^{1/2} dW. \quad (6.33)$$

The physical interpretation is that we have a system of particles immersed in a fluid bath consisting of many particles which are much lighter (or give rise to weaker interactions) than those described by the potential U .

The coefficient γ , referred to alternatively as the *friction coefficient* or the *collision rate*, is a frequency and therefore has units of 1/time.

It is possible to further extend this model in a number of ways. In particular, a different friction coefficient γ can be used for each particle and these coefficients can even depend on spatial location, thus we might work with the following system:

$$dq = M^{-1} pdt, \quad (6.34)$$

$$dp = -\nabla U(q)dt - \Gamma(q)\Gamma(q)^T pdt + \sqrt{2k_B T} M^{1/2} \Gamma(q)dW, \quad (6.35)$$

where we use the matrix $\Gamma(q) \in \mathbb{R}^{N_c \times S}$ and a vector of S independent Wiener processes \hat{W} .

In the case of Langevin dynamics with different, variable friction coefficients for each particle, we have $S = N_c$ and

$$\Gamma = \text{diag}(\gamma_1(q), \gamma_1(q), \gamma_1(q), \gamma_2(q), \gamma_2(q), \dots, \gamma_N(q), \gamma_N(q), \gamma_N(q)).$$

Another application is *dissipative particle dynamics* [181], where typically $S = N_c(N_c - 1)/2$ and a random increment is applied for each pair interaction.

The Langevin dynamics equations have the Markov property in the sense that the state of the system at any future time has a dependency on the current state of the system, but not on the prior history.

Langevin dynamics can be regarded as a physical model where the parameter-functions encoded in $\Gamma(q)$ describe the instantaneous physical friction forces between the modelled particles and a simplified, anisotropic bath of particles. However, it should be noted that in many types of modelling, the physical nature of the interaction with the solvent bath is neglected and γ or $\Gamma(q)$ are simply viewed as artificial parameters which allow recovery of averages with respect to the canonical distribution.

6.3.4 Overdamped Limit of Langevin Dynamics

An interesting special case of Langevin dynamics is obtained by considering the large γ limit, often referred to as the “overdamped” limit. In cases where the friction constant is scaled by the inverse mass (so γ is replaced by γM^{-1} in (6.32)–(6.33)) such as in [233], this is instead known as the zero-mass limit. In this model the inertial dynamics is assumed to be dominated by collisional effects. Let $\mathbf{v} = \mathbf{M}^{-1}\mathbf{p}$ and assume that the acceleration is negligible, so that Langevin dynamics reduces to

$$d\mathbf{q} = \mathbf{v} dt, \quad 0 = -\nabla U(\mathbf{q})dt - \gamma \mathbf{M}\mathbf{v} dt + \sqrt{2\gamma k_B T} \mathbf{M}^{1/2} d\mathbf{W}.$$

The second equation can be solved for \mathbf{v} and we obtain the following SDE for \mathbf{q} :

$$d\mathbf{q} = -\gamma^{-1} \mathbf{M}^{-1} \nabla U(\mathbf{q}) dt + \sqrt{2k_B \gamma^{-1} T} \mathbf{M}^{-1/2} d\mathbf{W}. \quad (6.36)$$

This is also sometimes referred to as *Brownian dynamics* or Smoluchowski dynamics. The transition from Langevin to Brownian dynamics is typically referred to as the “Kramers to Smoluchowski limit.”

6.3.5 Properties of SDEs

In this section we introduce a few tools for studying the evolution of solutions for SDEs. Let X be a stochastic process satisfying the SDE (6.14), with suitable coefficients a, b independent of t , and let $\phi(\cdot)$ be any twice differentiable function. Then, taking the expectation of the Itô-Doeblin formula (6.17) we find

$$\begin{aligned} \mathbb{E}\{d\phi(X)\} &= \mathbb{E}\{\phi'(X)a(X)\}dt + \tfrac{1}{2}\mathbb{E}\{\phi''(X)b(X)^2\}dt \\ &= \mathbb{E}\{(\mathcal{L}\phi)(X)\}dt, \end{aligned} \quad (6.37)$$

where \mathcal{L} is a linear operator, called the *generator* of the stochastic process, defined by

$$\mathcal{L}\phi(x) = \left(a(x) \frac{d}{dx} + \tfrac{1}{2}b^2(x) \frac{d^2}{dx^2} \right) \phi(x). \quad (6.38)$$

The generator plays a role for SDEs which is similar to that of the Lie derivative in the context of deterministic systems.

6.3.6 The Fokker-Planck Equation

Consider now a collection of stochastic processes $X(t)$ that are the solutions of the SDE $dX = a(X)dt + b(X)dW$. If the initial conditions are drawn from a distribution with given density $\rho(x, 0)$ we would like to derive an equation for the corresponding density at time t , $\rho(x, t)$. We assume that ρ is C^∞ for all t and that the density tends to zero exponentially fast as $x \rightarrow \pm\infty$, whereas a and b are C^∞ functions which grow at most polynomially fast in these limits, that is, there are constants η_a, η_b such that

$$a(x) = O(|x|^{\eta_a}), \quad b(x) = O(|x|^{\eta_b}), \quad x \rightarrow \pm\infty.$$

This condition of polynomial growth of the coefficients is a common assumption in the analysis of SDEs. For future reference we define the space of functions which are C^∞ smooth and satisfy the polynomial growth restriction by C_p^∞ :

$$C_p^\infty = \{\phi \in C^\infty \mid \exists \eta \in \mathbb{N} : \phi(x) = \mathcal{O}(|x|^\eta), x \rightarrow \pm\infty\}.$$

For any $\phi \in C_p^\infty$, the expectation with respect to $\rho(x, t)$ is well defined and we have

$$\mathbb{E}\phi(X(t)) = \langle \phi, \rho \rangle = \int_{-\infty}^{+\infty} \phi(x)\rho(x, t)dx.$$

Taking the differential, we obtain an equation for $\mathbb{E}d\phi$ which must be equal to (6.37):

$$\int_{-\infty}^{+\infty} \phi(x) \frac{\partial \rho}{\partial t} dx = \int_{-\infty}^{+\infty} (\mathcal{L}\phi)(x)\rho(x, t)dx = \int_{-\infty}^{+\infty} (a(x)\phi' + \frac{1}{2}b^2(x)\phi''(x))\rho(x, t)dx.$$

Using the assumptions given above regarding the exponential rate of decay of the density, it is possible to recast the right hand side as an integral of a product with ϕ . First, we find

$$\begin{aligned} \int_{-\infty}^{+\infty} a(x)\phi'(x)\rho(x, t)dx &= [\phi(x)a(x)\rho(x, t)]|_{-\infty}^{+\infty} - \int_{-\infty}^{+\infty} \phi(x)(a(x)\rho(x, t))_x dx \\ &= - \int_{-\infty}^{+\infty} \phi(x)(a(x)\rho(x, t))_x dx. \end{aligned}$$

With two rounds of integration by parts on the term involving $b(x)$, we find, using the fact that the boundary terms vanish,

$$\int_{-\infty}^{+\infty} b^2(x) \phi''(x) \rho(x, t) dx = \int_{-\infty}^{+\infty} \phi(x) (b^2(x) \rho)_{xx}(x, t) dx.$$

Finally, putting these results together, we have

$$\int_{-\infty}^{+\infty} \phi(x) \left[\frac{\partial \rho}{\partial t} + \frac{\partial}{\partial x} (a(x) \rho(x, t)) - \frac{1}{2} \frac{\partial^2}{\partial x^2} (b^2(x) \rho) \right] dx = 0.$$

If this is to hold for all test functions ϕ , we must have

$$\frac{\partial \rho}{\partial t} = -\frac{\partial}{\partial x} (a(x) \rho) + \frac{1}{2} \frac{\partial^2}{\partial x^2} (b^2(x) \rho).$$

This partial differential equation is often called the Fokker-Planck equation. The great benefit of the Fokker-Planck equation is that it enables the macroscopic perspective on the solutions of an SDE.

The Fokker-Planck equation may be written in the compact form

$$\frac{\partial \rho}{\partial t} = \mathcal{L}^\dagger \rho,$$

where the operator appearing on the right hand side is the *adjoint* \mathcal{L}^\dagger of the generator of the stochastic process, satisfying the relation

$$\langle \mathcal{L}\phi, \rho \rangle = \langle \phi, \mathcal{L}^\dagger \rho \rangle.$$

In the case at hand the adjoint is

$$\mathcal{L}^\dagger \rho = -(a(x) \rho)_x + \frac{1}{2} (b^2(x) \rho)_{xx},$$

which we shall refer to as the Kolmogorov operator.

In case $b \equiv 0$, the SDE becomes an ordinary differential equation. Then the generator \mathcal{L} becomes simply the Lie derivative, and its adjoint is just the Liouvillian. Thus the framework developed here for SDEs is a proper generalization of what we have earlier seen in the deterministic case.

6.3.7 Fokker-Planck Equation for Systems of SDEs

We describe the generalization of the Itō-Doeblin formula and the Fokker-Planck equation to a system of SDEs. If ϕ is a scalar valued function of \mathbb{R}^m , and $\mathbf{Z}(t)$ is the solution of the SDE system

$$d\mathbf{Z} = \mathbf{a}(\mathbf{Z})dt + \mathbf{B} d\mathbf{W}, \quad (6.39)$$

where \mathbf{a} is a function in \mathbb{R}^m and \mathbf{B} is a constant matrix, then we have

$$d\phi(\mathbf{Z}(t)) = \nabla\phi \cdot [\mathbf{a}dt + \mathbf{B}d\mathbf{W}] + \frac{1}{2}d\mathbf{W}^T \mathbf{B}^T \phi'' \mathbf{B} d\mathbf{W}, \quad (6.40)$$

where ϕ'' is the Hessian matrix of ϕ , i.e. the matrix of second partial derivatives of ϕ with respect to pairs of the variables. In some applications $\mathbf{B} = \mathbf{B}(\mathbf{Z})$, in which case the SDE (6.39) is said to involve *multiplicative noise* (as oppose to the *additive* case we consider when \mathbf{B} is constant). For a discussion of the differences and applications of these types of noise, see [289, 324].

All components on the right hand side of (6.40) are evaluated at $\mathbf{Z}(t)$. Then using the shorthand rules $dW_i dW_j = dt \delta_{ij}$ (where δ_{ij} is one if $i = j$, zero otherwise), we have

$$d\phi(\mathbf{Z}(t)) = \nabla\phi \cdot [\mathbf{a}dt + \mathbf{B}d\mathbf{W}] + \frac{1}{2}\text{Tr}(\mathbf{B}^T \phi'' \mathbf{B}) dt, \quad (6.41)$$

where $\text{Tr}(\cdot)$ refers to the matrix trace, the sum of the diagonal elements of the given matrix.

In the multivariate case, the density is a function of the vector describing a state of the system \mathbf{z} and t , and is governed by the partial differential equation

$$\frac{\partial \rho}{\partial t} = -\nabla \cdot (\mathbf{a}(\mathbf{z})\rho(\mathbf{z})) + \frac{1}{2}\text{Tr}(\mathbf{B}^T \rho'' \mathbf{B}).$$

The second order “diffusion” term in this expression may be expanded as

$$\text{Tr}(\mathbf{B}^T \rho'' \mathbf{B}) = \sum_{i=1}^m \sum_{j=1}^m [\mathbf{B} \mathbf{B}^T]_{ij} \frac{\partial^2 \rho}{\partial z_i \partial z_j}.$$

6.3.8 Fokker-Planck Equation for Langevin Dynamics

In the special case of Langevin dynamics (6.32)–(6.33) for a system with N_c configuration variables, the density is a function of the vectors of positions \mathbf{q} , momenta \mathbf{p} , and time, and the formula for the Kolmogorov operator becomes

$$\mathcal{L}_{\text{LD}}^\dagger \rho = -\nabla_{\mathbf{q}} \cdot (\mathbf{M}^{-1} \mathbf{p} \rho) + \nabla_{\mathbf{p}} \cdot ([\nabla U(\mathbf{q}) + \gamma \mathbf{p}] \rho) + \gamma k_B T \Delta_M \rho, \quad (6.42)$$

where the mass-weighted Laplacian Δ_M is defined as

$$\Delta_M \stackrel{\text{def}}{=} \nabla \cdot (\mathbf{M} \nabla) = \sum_{i=1}^{N_c} m_i \frac{\partial^2}{\partial p_i^2}.$$

6.4 Ergodicity of Stochastic Differential Equations

The principal question that must be answered regarding an SDE model such as Langevin dynamics has to do with its *ergodic property*. Recall from the previous chapter that we had defined ergodicity with respect to the flow map of a Hamiltonian system with compact energy surfaces as the property that temporal averages taken along trajectories of the system almost surely yield spatial averages with respect to the microcanonical distribution (alternatively, every invariant set M at energy E has probability measure either zero or one). In the context of the Gibbs-Boltzmann ensemble at given positive temperature T , we think of the phase space as being unbounded, but assume that the distribution is normalizable due to properties of the energy function and the form of the distribution.

Instead of a deterministic system of ordinary differential equations, we now have a stochastic system. Given a set of points M_0 in the phase space, we consider the stochastic paths emanating from these points, with each point from the distribution viewed as an initial condition for the evolving SDE. At any time t we take a snapshot M_t of the resulting set of random variables. Even if M_0 is bounded, the evolving set of points would be expected to expand and fill in the phase space accessible at the temperature T ; eventually we hope that the points will be distributed in the entire phase space in accordance with the target measure (usually the Gibbs distribution $e^{-\beta H}$).

Equivalently we may study a single solution trajectory emanating from almost any initial point on M_0 , and ask that in the long-time limit the entirety of the phase space is covered according to the desired measure. The discussion we present here is necessarily condensed; we direct the motivated reader to [269] for a more complete discussion.

6.4.1 Irreducibility of Finite Markov Chains

The concept of ergodicity, and the method of analyzing it, can be understood using an analogy to a simpler finite model, a discrete Markov Chain.

A discrete Markov Chain is a stochastic process in which, at each step, a transition is made from the current state i to another j selected from a given probability distribution. In the case of a finite collection of states $\Sigma = \{1, 2, \dots, k\}$, we assume that the transition probabilities $\pi_{ij} \in [0, 1]$ are given and denote the state at time n by S_n . Thus we have

$$\Pr(S_{n+1} = j | S_n = i) = \pi_{ij},$$

where we denote by $\boldsymbol{\Pi} = (\pi_{ij}) \in \mathbb{R}^{k \times k}$ the matrix of transition probabilities, i.e. it is a matrix whose entries are all nonnegative and less than or equal to 1. The sum of the elements in row i gives the probability of being in *some* state at time $n + 1$ given that we were in state i at time n , thus it is one. The matrix $\boldsymbol{\Pi}$ is sometimes referred to as a *right stochastic matrix*.

A distribution on the state space is typically associated to a row vector $\psi = (\psi_1, \psi_2, \dots, \psi_k)$ with nonzero elements and which is normalized such that

$$\sum_{i=1}^k \psi_i = 1.$$

This might be viewed as defining the relative proportion, in a large collection of *walkers* (independent realizations of a stochastic evolution), that are found in each state. As the walkers make moves based on the transition probabilities, the distribution will vary. We may denote by $\psi_n = (\psi_{n,1}, \psi_{n,2}, \dots, \psi_{n,k})$ the distribution observed at step n of the iteration. The probability of being in state i at the $n + 1$ st iteration, is the sum over j of the probabilities of being in state j multiplied by the probability of transitioning from state j to state i , thus

$$\psi_{n+1} = \psi_n \boldsymbol{\Pi}.$$

This iteration can be viewed as analogous to dynamics. We may think of the evolution of the Markov chain as being realized through multiplication by the Markov matrix $\boldsymbol{\Pi}$. Let $\pi_{ij}^{(l)}$ represent the transition probability of being in state i at iteration l given that we were in state j at time 0, i.e. $\pi_{ij}^{(l)}$ is the (i,j) entry of the matrix $\boldsymbol{\Pi}^l$.

Two important properties of Markov chains are aperiodicity and communication. For each state of the chain, we define the number $d(i)$ to be the greatest common divisor of all integers l such that $\pi_{ii}^{(l)} > 0$ (if the probability of return to state i is zero, then we set $d(i) = 0$). If $d(i) = 1$, for all i then we say that the chain is *aperiodic*. States i and j are said to *communicate* if $\pi_{ij}^{(l_1)} > 0$ and $\pi_{ji}^{(l_2)} > 0$ for

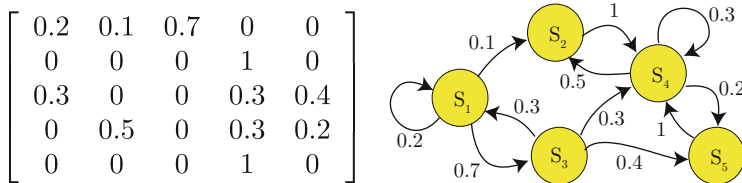


Fig. 6.6 A Markov matrix (left) and its graph representation (right). In this example, the Markov Chain is not irreducible

some integers l_1 and l_2 . This means that it is possible to reach j from i with positive probability and vice-versa.

A finite state space model is *irreducible* if every state is reachable from every other state in a finite “time”, where time in this context refers to the number of iterations of the chain. Equivalently, we say the model is irreducible if all states communicate.

A very useful representation of the Markov Chain transition matrix Π is by use of a weighted directed graph in which each node represents a state of the Markov Chain and the weights represent transition probabilities. Then one may understand irreducibility as expressing the connectedness⁸ of this graph (see Fig. 6.6).

An *invariant distribution* is a left eigenvector of Π , having only non-negative elements, and corresponding to the eigenvalue 1. That is, an invariant distribution ψ_* satisfies

$$\psi_* = \psi_* \Pi.$$

The fundamental result for Markov chains is the following: *If a given Markov chain is both irreducible and aperiodic, then it can be shown that there is a unique invariant distribution ψ_* such that*

$$\lim_{n \rightarrow \infty} \psi_n = \psi_*.$$

for arbitrary initial distribution ψ_0 . The convergence of an irreducible finite Markov chain to its stationary distribution can be understood through the properties of its eigenvalues by applying of the Perron-Frobenius theorem (see [269]).

⁸We say that a graph is *connected* if every node is linked to every other node by a sequence of contiguous edges. For a directed graph, we must have, for any pair of vertices A and B , paths which take us from A to B and vice-versa.

6.4.2 Ergodic Stochastic Differential Equations

Now consider an SDE system defined on the space $\mathcal{D} = \mathbb{T}^{k_1} \times \mathbb{R}^{k_2}$ for non-negative integers k_1 and k_2 :

$$d\mathbf{X} = \mathbf{b}_0(\mathbf{X})dt + \sum_{i=1}^r \mathbf{b}_i dW_i, \quad (6.43)$$

where \mathbf{b}_0 is C^∞ and the W_i are independent standard Wiener processes. In this book, we will only consider the analysis for the case of additive noise (i.e. the \mathbf{b}_i vectors multiplying a Wiener process are constant). The more complicated case of multiplicative noise (where all of the \mathbf{b}_i can vary) will not be needed here, as additive noise is sufficient to sample the canonical distribution.

Working in flat L^2 space, we have that the infinitesimal generator for (6.43) acting on a smooth test function $\phi(\mathbf{X})$ is

$$\mathcal{L}\phi = \mathbf{b}_0 \cdot \nabla \phi + \frac{1}{2} \text{Tr}(\mathbf{B}^T \phi'' \mathbf{B}),$$

where the columns of \mathbf{B} are $\mathbf{b}_1, \mathbf{b}_2, \dots, \mathbf{b}_r$. Taking the adjoint, the forward Kolmogorov or Fokker-Planck operator is \mathcal{L}^\dagger , acting on a density $\rho(\mathbf{X})$ as

$$\mathcal{L}^\dagger \rho = -\nabla \cdot (\mathbf{b}_0 \rho) + \frac{1}{2} \text{Tr}(\mathbf{B}^T \phi'' \mathbf{B}).$$

In the case of Langevin dynamics, the matrix \mathbf{B} is diagonal, simplifying the form of the operators by reducing the term involving second derivatives to a Laplacian.

We have seen that invariant distributions correspond in general to solutions of

$$\mathcal{L}^\dagger \rho_{\text{eq}} \equiv 0.$$

Solutions to this equation are of central importance to the probabilistic behavior of solutions to (6.43). Such solutions give distributions of points in phase space which will remain constant as solutions evolve in time. We may ask a number of questions related to these distributions:

- Is the solution ρ_{eq} unique, up to a constant scaling? (We can see that if ρ_{eq} is a solution, then so is $k \times \rho_{\text{eq}}$ for constant k .)
- If we start with an initial distribution ρ_0 which is different than ρ_{eq} , what sort of behavior do averages with respect to the evolving distribution $\rho(\mathbf{X}, t)$ exhibit? If they converge to a stationary average, at what rate? Does it matter if we start from a distribution “near to” (in a suitable sense) or “far away” from an invariant distribution?

The property of ergodicity combined with associated mixing properties similar to those mentioned in Chap. 5, provide a framework to give precise answers to some of these questions.

In the previous section we introduced the Fokker-Planck equation as a means of analyzing the evolution of the phase space density. If the system is ergodic and mixing, we expect that the phase space distribution is, ultimately, consistent with the Gibbs-Boltzmann ensemble in the sense that, for a C_0^∞ test function ϕ (smooth and compactly supported),

$$\lim_{t \rightarrow \infty} \int_{\mathcal{D}} \phi(\mathbf{q}, \mathbf{p}) \rho(\mathbf{q}, \mathbf{p}, t) d\omega = \int_{\mathcal{D}} \phi(\mathbf{q}, \mathbf{p}) \rho_\beta(\mathbf{q}, \mathbf{p}) d\omega,$$

regardless of the initial distribution.

There is a key difference between the concept of microcanonical ergodicity and canonical ergodicity. For deterministic dynamics, the distribution solves the Liouville equation

$$\frac{\partial \rho}{\partial t} = -\nabla \cdot (\mathbf{f}\rho), \quad \nabla = (\nabla_{\mathbf{q}}, \nabla_{\mathbf{p}}).$$

In the case of an SDE, the distribution may spread out over time. Even a single phase space point, which corresponds to a delta-function initial distribution, will instantly diffuse as the solution of the Fokker-Planck equation and, eventually, would cover the entire phase space. The incorporation of randomness has clearly changed the picture of the evolving phase space distribution in a fundamental way.

We have already seen a canonically ergodic SDE in a simplified setting in the example of the Ornstein-Uhlenbeck equation for a single degree of freedom (6.20), given an initial point distribution. The solution $p(t)$ to the Ornstein-Uhlenbeck equation, for any finite time t , is always normally distributed

$$\rho(p, t) = \exp\left(-\frac{(p - \mu(t))^2}{2\sigma(t)^2}\right), \quad (6.44)$$

where

$$\mu(t) = p_0 e^{-\gamma t}, \quad \sigma^2(t) = k_B T m (1 - e^{-2\gamma t}). \quad (6.45)$$

It is easy to see that the distribution converges to a unique invariant distribution (in this case a Gaussian with mean zero and variance $k_B T m$ as $t \rightarrow \infty$). Ergodicity is easily verified in the case of the Ornstein-Uhlenbeck equation, since we can find its exact distributional solution. However, we can still demonstrate ergodicity for more complex SDEs where it is extremely challenging (or impossible) to find a solution or even to give qualitative statements about the solution.

6.4.3 Ergodicity of Brownian Dynamics

Imagine a distribution $\rho_0(\mathbf{X})$ which we may take to be an initial macroscopic state of a stochastic differential equation system. This might be a smooth probability density such as a Gaussian, the indicator function ξ_D for a small disk D in the phase space, or, in the extreme case a Dirac delta distribution (indicating that all initial conditions are clustered at a single point in phase space). The density evolves according to the partial differential equation

$$\frac{\partial \rho}{\partial t} = \mathcal{L}^\dagger \rho(\mathbf{X}, t), \quad \rho(\mathbf{X}, 0) = \rho_0(\mathbf{X}),$$

so the solution can be written

$$\rho(\mathbf{z}, t) = \exp(t\mathcal{L}^\dagger) \rho_0(\mathbf{X}).$$

Under what conditions (and in what sense) can we say that the distribution obtained in this way converges to a known invariant distribution?

For example, let us return to Brownian dynamics (or overdamped Langevin dynamics) and set $\mathbf{M} = \mathbf{I}$ and $\gamma = 1$ in (6.36), giving an equation of motion

$$d\mathbf{q} = -\nabla U(\mathbf{q})dt + \sqrt{2k_B T} d\mathbf{W}. \quad (6.46)$$

Writing $\beta^{-1} = k_B T$ as usual, the generator of the stochastic process may be written as

$$\mathcal{L}f = -\nabla U^T \cdot \nabla f + \beta^{-1} \Delta f.$$

We demonstrate a very useful property of this operator.

Let $\bar{\rho}_\beta = \exp(-\beta U)$, and define the space of functions $C_0^2(\bar{\mu}_\beta)$ consisting of functions in C_0^2 on the configuration space $\Omega \subset \mathbb{R}^N$ together with the inner product

$$\langle f, g \rangle_\beta \stackrel{\text{def}}{=} \int_{\Omega} f(\mathbf{q})g(\mathbf{q})\bar{\mu}_\beta(d\omega_q) = \int_{\Omega} f(\mathbf{q})g(\mathbf{q})\bar{\rho}_\beta(\mathbf{q})d\omega_q,$$

where $d\omega_q = dq_1 dq_2 \dots dq_N$. Then \mathcal{L} is self-adjoint with respect to this inner product.

The proof is straightforward:

$$\begin{aligned} \langle f, \mathcal{L}g \rangle_\beta &= \int_{\Omega} f \left(-\nabla U^T \nabla g + \beta^{-1} \Delta g \right) \bar{\rho}_\beta d\omega_q \\ &= \int_{\Omega} f \left(-\nabla U^T \nabla g \right) \bar{\rho}_\beta d\omega_q + \beta^{-1} \int_{\Omega} f \Delta g \bar{\rho}_\beta d\omega_q. \end{aligned}$$

Integrating by parts in the second term we have

$$\begin{aligned}\beta^{-1} \int_{\Omega} f \Delta g \bar{\rho}_\beta d\omega_q &= -\beta^{-1} \int_{\Omega} \nabla g^T \nabla (f \bar{\rho}_\beta) d\omega_q \\ &= -\beta^{-1} \int_{\Omega} \nabla g^T [\nabla f \bar{\rho}_\beta - \beta \nabla U f \bar{\rho}_\beta] d\omega_q \\ &= -\beta^{-1} \int_{\Omega} \nabla g^T \nabla f \bar{\rho}_\beta d\omega_q + \int_{\Omega} f (\nabla g^T \nabla U) \bar{\rho}_\beta d\omega_q.\end{aligned}$$

Combining this with the first part of the inner product, we see that

$$\langle f, \mathcal{L}g \rangle_\beta = -\beta^{-1} \int_{\Omega} \nabla g^T \nabla f \bar{\rho}_\beta d\omega_q.$$

In this form we see that f and g appear symmetrically, so we may write

$$\langle f, \mathcal{L}g \rangle_\beta = \langle \mathcal{L}f, g \rangle_\beta,$$

hence, with respect to the weighted inner product, $\mathcal{L}^\dagger = \mathcal{L}$. (Note that the adjoint indicated here is quite different than the L^2 adjoint mentioned previously in connection with the Fokker-Planck operator.)

In addition to being self-adjoint, this operator (on the function space $C_0^2(\bar{\mu}_\beta)$) has other important properties. In particular, it has a *compact resolvent* [360]; this can be shown to imply that the spectrum consists only of a countable collection of eigenvalues, i.e. that the operator has a discrete spectrum. Moreover, from the calculation above,

$$\langle f, \mathcal{L}f \rangle = -\beta^{-1} \int_{\Omega} \|\nabla f\|^2 \bar{\rho}_\beta d\omega_q,$$

so that $\langle f, \mathcal{L}f \rangle \leq 0$ so the operator is negative definite and can only have non-positive eigenvalues. Many additional results are available for this case. A good summary of the state of the art is available in the forthcoming work of G. Pavliotis [298]. In particular, it is possible to show the properties of \mathcal{L} contained in Theorem 6.1.

Theorem 6.1 Define the generator of Brownian dynamics by

$$\mathcal{L}f \stackrel{\text{def}}{=} -\mathbf{M}^{-1} \nabla U^T \nabla f + \beta^{-1} \Delta_M f.$$

Suppose that U is smooth with periodic boundary conditions $\mathcal{Q} = \mathbb{T}^{N_c}$ (\mathbb{T}^{N_c} an N_c -dimensional torus). Then, with respect to the space $C_0^2(\mu_\beta)$ with inner product $\langle f, g \rangle_\beta$ as defined above, we have:

1. \mathcal{L} is self-adjoint, negative definite, with spectrum consisting of discrete eigenvalues on the half line $(-\infty, 0]$.
2. \mathcal{L} has a spectral gap, meaning that, with exception of the zero eigenvalue, the remainder of the spectrum satisfies $\sigma(\mathcal{L}) \subset (-\infty, -\alpha]$ for some $\alpha > 0$.
3. averages with respect to the evolving, time-dependent distribution converge exponentially rapidly to averages with respect to the invariant distribution, and, for any smooth, compactly supported test function ϕ , we have

$$|\bar{\phi}(t) - \text{Av}_\beta(\phi)| \leq K \|\phi\|_\beta e^{-\alpha t},$$

for some positive K and α , where recall $\bar{\phi}(t)$ denotes the time average of ϕ defined in (5.6).

Thus Brownian Dynamics is ergodic for the configurational Gibbs-Boltzmann distribution.

6.4.4 Ergodicity of Langevin Dynamics

The key feature of Brownian dynamics that makes it possible to verify the ergodic property is the fact that each variable of the system is directly in contact with an independent stochastic Wiener process. This ensures that at each point of phase space, all possible directions are sampled and the paths will have freedom to move in any direction. In Langevin dynamics, taking $\mathbf{M} = \mathbf{I}$ for simplicity,

$$\begin{aligned} d\mathbf{q} &= \mathbf{p} dt, \\ d\mathbf{p} &= -\nabla U(\mathbf{q}) dt - \gamma \mathbf{p} dt + \sqrt{2\gamma k_B T} d\mathbf{W}, \end{aligned} \tag{6.47}$$

as well as in a number of other important SDEs arising in molecular dynamics, the picture is less transparent. Stochastic noise is only introduced in some parts of the system, but it is not immediately clear that the stochastic character will be transferred through the internal dynamics of the system into all possible directions.

In these more complicated examples, we are able to demonstrate ergodicity without finding an explicit solution (as in the Ornstein-Uhlenbeck example) or study of the dynamics' generator (as in Brownian dynamics), given some assumptions on the behavior of solutions. We state (without proof) a powerful theorem on the ergodicity of degenerate stochastic diffusions, whose proof is essentially contained in [257, Theorem 2.5] (see also [44, 160, 161, 253, 266]). We denote by $\mathcal{B}_\delta(\mathbf{x})$ the open ball in \mathcal{D} centered on the point \mathbf{x} of radius δ , while $\mathcal{B}(\mathcal{D})$ is the Borel σ -algebra on \mathcal{D} (see Sect. 5.2.1).

Assumption 1 The Markov process generated by the SDE (6.43) satisfies, for some fixed compact set $C \in \mathcal{B}(\mathcal{D})$, the conditions:

- (i) For some $\mathbf{y} \in \text{int}(C)$, we have that for any $\delta > 0$ there is a $t_0 > 0$ such that

$$\Pr(\mathbf{X}(t_0) \in \mathcal{B}_\delta(\mathbf{y}) \mid \mathbf{X}(0) = \mathbf{X}_0) > 0, \quad \forall \mathbf{X}_0 \in C.$$

- (ii) For $t > 0$, the transition kernel possesses a density $\hat{\rho}(\mathbf{X}, \mathbf{z}, t)$ such that

$$\Pr(\mathbf{X}(t) \in A \mid \mathbf{X}(0) = \mathbf{X}_0) = \int_A \hat{\rho}(\mathbf{X}_0, \mathbf{z}, t) d\mathbf{z}, \quad \forall \mathbf{X}_0 \in C, A \in \mathcal{B}(\mathcal{D}) \cap \mathcal{B}(C),$$

and $\hat{\rho}(\mathbf{X}, \mathbf{z}, t)$ is jointly continuous in $C \times C \times [0, \infty)$.

It can be shown that this assumption is tantamount to the SDE satisfying a *minorization condition*. This condition is a particular case of the general concept of small sets, found in Markov literature for proving ergodicity. We can think of it as giving conditions on the regularity of the solution, in some small region C . The return to the set C is governed by the following assumption:

Assumption 2 There is a function $\phi : \mathcal{D} \rightarrow (0, \infty)$, with $\phi(\mathbf{X}) \rightarrow \infty$ as $|\mathbf{X}| \rightarrow \infty$ such that

$$\mathcal{L}\phi \leq -\alpha\phi + \delta$$

for positive constants α and δ , where \mathcal{L} is the generator of the stochastic process (6.43). The function ϕ is known as a Lyapunov function.

If these two assumptions hold, then we are able to state the following theorem [165]:

Theorem 6.2 (Geometric Ergodicity) *Let the solution to (6.43) be denoted $\mathbf{X}(t)$. If Assumption 1 and Assumption 2 are satisfied for*

$$C = \{\mathbf{X} \in \mathcal{D} \mid \phi(\mathbf{X}) \leq K_{\alpha, \delta}\},$$

where $K_{\alpha, \delta}$ is a particular positive value depending on α and δ , then

- (i) there exists a unique invariant measure ρ_* , with $\mathcal{L}^\dagger \rho_* = 0$, and
- (ii) there exist positive constants κ and λ such that for all suitable functions f with $|f| \leq \phi$,

$$|(e^{t\mathcal{L}} f)(\mathbf{X}_0) - \text{Av}(f)| \leq \kappa e^{-\lambda t} \phi(\mathbf{X}_0), \quad (6.48)$$

where $\text{Av}(f) = \int_{\mathcal{D}} f(\mathbf{z}) \rho_*(\mathbf{z}) d\mathbf{z}$ is the spatial average.

It is easily shown that both the Ornstein-Uhlenbeck equation and Brownian dynamics satisfy the assumptions and hence are both geometrically ergodic. We will show Langevin dynamics is geometrically ergodic by applying Theorem 6.2

with $\mathbf{X} = (\mathbf{q}, \mathbf{p})^T$ and demonstrating that the required assumptions hold for (6.47). It is reasonable to consider periodic boundary conditions for the position variable, so $\Omega = \mathcal{T}^N$ where \mathcal{T}^N is an N_c -dimensional torus. The use of periodic boundary conditions considerably simplifies the proofs, while also being more relevant to the practical realities of molecular dynamics simulation. The whole phase space is $\mathcal{D} = \mathcal{T}^N \times \mathbb{R}^{N_c}$.

We also consider the potential energy to be smooth (C^∞) with $U(\mathbf{q}) \rightarrow \infty$ as $|\mathbf{q}| \rightarrow \infty$. As we have a smooth potential on a bounded (position) domain, we have

$$1 < U_{\min} \leq U(\mathbf{q}) \leq U_{\max} < \infty, \quad \forall \mathbf{q} \in \Omega,$$

for some constants U_{\min} and U_{\max} .

For the Lyapunov condition (Assumption 2), we choose the Lyapunov function

$$\phi(\mathbf{q}, \mathbf{p}) = H^l(\mathbf{q}, \mathbf{p}) = \left(\frac{1}{2} \|\mathbf{p}\|^2 + U(\mathbf{q}) \right)^l,$$

for a fixed positive integer l . As the potential energy is bounded below by 1, it is clear that $\phi(\mathbf{q}, \mathbf{p}) \rightarrow \infty$ as $|(\mathbf{q}, \mathbf{p})| \rightarrow \infty$. Computing the generator of Langevin dynamics as

$$\mathcal{L}_{\text{LD}} f = \mathbf{p} \cdot \nabla_q f - \nabla U(\mathbf{q}) \cdot \nabla_p f - \gamma \mathbf{p} \cdot \nabla_p f + \gamma k_B T \Delta_p \phi,$$

we can see that

$$\mathbf{p} \cdot \nabla_q \phi - \nabla U(\mathbf{q}) \cdot \nabla_p \phi = \mathcal{L}_H \phi = 0,$$

where \mathcal{L}_H is the Lie derivative of our original Hamiltonian system (which preserves all functions of the Hamiltonian). Hence

$$\mathcal{L}_{\text{LD}} \phi = -\gamma \mathbf{p} \cdot \nabla_p \phi + \gamma k_B T \Delta_p \phi.$$

Using $\|\mathbf{p}\|^2 < 2H$, we compute derivatives to find

$$\begin{aligned} \mathbf{p} \cdot \nabla_p \phi &= l H^{l-1} \|\mathbf{p}\|^2 = 2l \phi - 2l H^{l-1} U(\mathbf{q}), \\ \Delta_p \phi &= l(l-1) H^{l-2} \|\mathbf{p}\|^2 + N_c l H^{l-1} \leq l(l+N_c-1) H^{l-1}. \end{aligned}$$

As H^l grows faster than H^{l-1} , for any fixed l we are able to find positive constants c and d such that

$$l(l+N_c-1) H^{l-1} \leq \frac{l}{2} H^l + c, \quad 2l H^{l-1} U(\mathbf{q}) < 2l H^{l-1} U_{\max} \leq \frac{l}{2} H^l + d.$$

giving

$$\begin{aligned}\mathcal{L}_{\text{LD}}\phi &\leq -2\gamma l\phi + 2\gamma lH^{l-1}U(\mathbf{q}) + \gamma l(l+N_c-1)H^{l-1}, \\ &\leq -\gamma l\phi + \gamma c + \gamma d, \\ &\leq -\alpha\phi + \delta,\end{aligned}$$

satisfying Assumption 2.

The purpose of using the l exponent in the Lyapunov function is to ensure that we can apply the theorem to a wide enough class of observables, as (6.48) is only valid for functions f with magnitude less than or equal to the Lyapunov function. As we have $\phi \geq U_{\min}^l$ and growing like $\|\mathbf{p}\|^{2l}$, we can choose l to be sufficiently large to bound a wide class of observables. However, for sufficiently fast-growing functions (such as exponentials) a different Lyapunov function would be required (if their averages do, in fact, converge).

We note that the condition of Assumption 1(ii) can be shown by demonstrating that *Hörmander's condition* holds over the entire space \mathcal{D} . This is a condition on the commutators or Lie brackets of vector fields.

The *Lie bracket* of a pair of vector fields $\mathbf{u}(z)$, $\mathbf{v}(z)$ is another vector field

$$[\mathbf{u}, \mathbf{v}] = \mathbf{v}'\mathbf{u} - \mathbf{u}'\mathbf{v},$$

where \mathbf{u}' is the Jacobian matrix of the vector field \mathbf{u} . In coordinates, if we let $\mathbf{w} = [\mathbf{u}, \mathbf{v}]$, then the coordinates of \mathbf{w} are

$$w_i = \sum_{j=1}^m \frac{\partial v_i}{\partial z_j} u_j - \frac{\partial u_i}{\partial z_j} v_j.$$

The Lie bracket is a bilinear and skew-symmetric operation:

- $[\alpha\mathbf{u} + \beta\mathbf{v}, \mathbf{w}] = \alpha[\mathbf{u}, \mathbf{w}] + \beta[\mathbf{v}, \mathbf{w}]$,
- $[\mathbf{u}, \mathbf{v}] = -[\mathbf{v}, \mathbf{u}]$ and $[\mathbf{u}, \mathbf{u}] = \mathbf{0}$.

Definition 6.1 (Hörmander's Condition) Let $\mathcal{U} \subset \mathbb{R}^m$ be open. The SDE (6.43) with C^∞ vector fields $\mathbf{b}_0, \mathbf{b}_1, \mathbf{b}_2, \dots, \mathbf{b}_r : \mathcal{U} \rightarrow \mathbb{R}^m$ are said to satisfy Hörmander's condition at $z \in \mathcal{U}$ if the vector space spanned by the collection of iterated Lie brackets

$$\mathbf{b}_0, \mathbf{b}_1, \dots, \mathbf{b}_r, [\mathbf{b}_0, \mathbf{b}_1], [\mathbf{b}_0, \mathbf{b}_2], \dots, [\mathbf{b}_{r-1}, \mathbf{b}_r], [\mathbf{b}_0, [\mathbf{b}_0, \mathbf{b}_1]] \dots$$

(evaluated at z) is \mathbb{R}^m .

Computing the iterated Lie brackets becomes, in many cases, an arduous task.

In the case of Langevin dynamics, we identify the vectors \mathbf{b}_i in (6.43) with the terms in (6.47). One puts Langevin dynamics into the correct form by using

$$\mathbf{b}_0 = \begin{bmatrix} \mathbf{p} \\ -\nabla U(\mathbf{q}) - \gamma \mathbf{p} \end{bmatrix}, \quad \mathbf{b}_i = \sigma \begin{bmatrix} \mathbf{0} \\ \mathbf{e}_i \end{bmatrix}, \quad i = 1, 2, \dots, N_c,$$

where \mathbf{e}_i is the i th Euclidean basis vector in \mathbb{R}^{N_c} and $\sigma = \sqrt{2\gamma k_B T}$ is constant. Now it is a straightforward matter of computing the commutators. For $i = 1, 2, \dots, N_c$, we have, using the fact that \mathbf{b}_i is a constant vector field and so its Jacobian matrix vanishes,

$$[\mathbf{b}_0, \mathbf{b}_i] = - \begin{bmatrix} \mathbf{0} & \mathbf{I} \\ -U''(\mathbf{q}) - \gamma \mathbf{I} & \mathbf{0} \end{bmatrix} \mathbf{b}_i = -\sigma \begin{bmatrix} \mathbf{e}_i \\ -\gamma \mathbf{e}_i \end{bmatrix},$$

where $U''(\mathbf{q})$ is the Hessian matrix of U . As these N_c vectors, taken together with the original \mathbf{b}_i , clearly provide a linearly independent set of $2N_c$ vectors, we have verified Hörmander's condition. Thus Assumption 1(ii) holds in the case of Langevin dynamics.

It remains to show that Assumption 1(i) is satisfied. We will in fact show a stronger result, given in the following lemma:

Lemma 6.1 *For all $t > 0$ and all open $C \subset \mathcal{D}$, we have that*

$$\Pr(\mathbf{X}(t) \in C | \mathbf{X}(0) = \mathbf{X}_0) > 0, \quad \forall \mathbf{X}_0 \in \mathcal{D},$$

where $\mathbf{X}(t) = (\mathbf{q}(t), \mathbf{p}(t))^T$ is a solution to Langevin dynamics (6.47).

Proof It is sufficient to show that the open ball of radius δ centered on a point $\mathbf{y} \in \mathcal{D}$, denoted $\mathcal{B}_\delta(\mathbf{y}) \subset \mathcal{D}$, has positive probability at any $t > 0$. To show this, the goal is to demonstrate that we have a positive probability of the realization of the noise process taking our initial condition inside the ball.

Consider the ODE

$$\frac{d^2\mathbf{q}}{dt^2} + \nabla U(\mathbf{q}) + \gamma \frac{d\mathbf{q}}{dt} = \sigma \frac{d\mathbf{R}}{dt}, \quad (6.49)$$

for some positive constants γ and σ . This is precisely Langevin dynamics (6.47), substituting a process $\mathbf{R}(t)$ in place of the Wiener process. Choose \mathbf{q} to be a C^∞ path such that for a given $t > 0$

$$(\mathbf{q}(0), \dot{\mathbf{q}}(0))^T = \mathbf{X}_0, \quad (\mathbf{q}(t), \dot{\mathbf{q}}(t))^T = \mathbf{y}.$$

Taking $\mathbf{R}(0) = 0$, we can obtain a C^∞ function $d\mathbf{R}/dt$ by substitution.

Using the results of [257, Lemma 3.4], we can deduce that for any $\delta > 0$, there exists a sufficiently small $\varepsilon > 0$ such that if a realization of the Wiener process \mathbf{W} remains close to our solution \mathbf{R}

$$\sup_{0 \leq s \leq t} \|\mathbf{W}(s) - \mathbf{R}(s)\| \leq \varepsilon, \quad (6.50)$$

then $\mathbf{X}(t) \in \mathcal{B}_\delta(\mathbf{y})$. That is, if the realized Wiener process stays within a tube of radius ε centered on our derived solution \mathbf{R} (for some sufficiently small ε), then our solution at time t is at most δ from the point \mathbf{y} .

The event (6.50) is shown in [349] to have positive probability for any $\varepsilon > 0$, and hence the required property is shown for any open set.

As Lemma 6.1 holds for all open subsets C , Assumption 1(i) holds as a corollary. Thus we have demonstrated that all of the necessary assumptions hold for Theorem 6.2. Hence Langevin dynamics is geometrically ergodic with respect to the canonical distribution

$$\rho_\beta(\mathbf{q}, \mathbf{p}) = \exp(-\beta H(\mathbf{q}, \mathbf{p})),$$

where it is easily checked that

$$\mathcal{L}_{\text{LD}}^\dagger \rho_\beta = 0.$$

Hence averages along solutions to (6.47) will converge to the spatial average with respect to ρ_β . Thus, Langevin dynamics is a useful tool for sampling the canonical distribution, as we may sample ρ_β by computing solutions to the SDE. This remains non-trivial, as the problem usually exists in a very high dimensional space (we may consider millions of particles) with complicated non-linear potential energy function $U(\mathbf{q})$. Many algorithms have been proposed for computing solutions to Langevin dynamics [46, 55, 62, 265, 311]. We shall compare the sampling accuracy of some of these schemes, and address strategies for the development of discretization methods for Langevin dynamics in the following chapter.

We may also investigate the properties of the operator \mathcal{L}_{LD} , just as we did for Brownian dynamics. However for Langevin dynamics, the lack of coupling between the noise process and all phase variables makes it relatively difficult to prove ergodicity. We denote by $\mathcal{H}^1(\mu)$ the space of functions $f(\mathbf{q}, \mathbf{p})$ defined on $\mathcal{D} = \mathbb{T}^{N_c} \times \mathbb{R}^{N_c}$ with bounded norm

$$\|f\|_{\mathcal{H}^1(\mu)}^2 \stackrel{\text{def}}{=} \|f\|_{L^2(\mu)}^2 + \|\nabla_{\mathbf{q}} f\|_{L^2(\mu)}^2 + \|\nabla_{\mathbf{p}} f\|_{L^2(\mu)}^2,$$

where

$$\|f\|_{L^2(\mu)}^2 = \int_{\mathcal{D}} f^2 \mu(d\omega),$$

and, for a vector function $w : \mathcal{D} \rightarrow \mathbb{R}^N$, we have

$$\|w\|_{L^2(\mu)}^2 = \sum_{i=1}^N \|w_i\|_{L^2(\mu)}^2.$$

With this in mind, we state a useful property that we will need in the next chapter in order to clarify results on the error in invariant measures.

Proposition 6.4 *Let U be C^∞ on the position domain $\mathcal{Q} = \mathbb{T}^N$ and suppose $g \in \mathcal{H}^1(\mu)$ satisfies*

$$\int_{\mathcal{D}} g d\mu_\beta = 0,$$

where μ_β is the canonical measure, then the Poisson equation

$$\mathcal{L}_{LD}^\dagger \varphi = g$$

has a solution $\varphi \in \mathcal{H}^1(\mu)$ which is unique up to addition of a constant multiple of the Gibbs density.

The condition is a consequence of the Fredholm Alternative which says that, for a linear operator \mathcal{A} with compact resolvent, we have one of the following two conditions:

- $\mathcal{A}\varphi = g$ has a solution.
- There is a function y with $\mathcal{A}^\dagger y = 0$ and $\langle y, g \rangle \neq 0$.

In our case, $\mathcal{A} = \mathcal{L}_{LD}^\dagger$. The only solutions of $\mathcal{L}_{LD}y = 0$ (conserved quantities of Langevin dynamics) are the constants. So the condition of the proposition eliminates the second alternative, leaving only the first.

If we have two solutions φ_1, φ_2 of $\mathcal{L}_{LD}\varphi = g$, then their difference w must be a solution of $\mathcal{L}_{LD}^\dagger w = 0$ and the only such solution is a constant multiple of the Gibbs density ρ_β .

More properties of the operator \mathcal{L}_{LD} are collected in [223].

6.4.5 Convergence of Averages

Given a collection of phase space points distributed according to the density $\rho_0(\mathbf{q}, \mathbf{p})$, we know that its evolution (under Langevin dynamics) after a time t will be described by

$$\rho(\mathbf{q}, \mathbf{p}, t) = e^{t\mathcal{L}_{LD}^\dagger} \rho_0(\mathbf{q}, \mathbf{p}).$$

More precisely this relation should be interpreted in the variational sense, so that we have, for any suitable test function ϕ , e.g. $\phi \in C^\infty$,

$$\int_{\mathcal{D}} \phi \rho(\mathbf{q}, \mathbf{p}, t) d\omega = \int_{\mathcal{D}} \phi e^{t\mathcal{L}_{LD}^\dagger} \rho_0(\mathbf{q}, \mathbf{p}) d\omega.$$

This is of course an inner product, and due to the properties of the inner product, we may interpret the right hand side as

$$\int_{\mathcal{D}} [e^{t\mathcal{L}_{LD}} \phi(\mathbf{q}, \mathbf{p})] \rho_0(\mathbf{q}, \mathbf{p}) d\omega,$$

which says that the average of a function ϕ with respect to the distribution at time t is equivalent to the average of the forward propagation of ϕ with respect to the initial distribution.

How rapidly an average converges will depend on the spectral properties of the operator as well as the choice of the initial distribution. For example, if we assume that $\lambda_1, \rho^{(1)}$ is some eigenvalue, eigenfunction pair with $\text{Re}(\lambda_1) < 0$ and take the initial distribution to be

$$\rho_0 = \rho_{\text{eq}} + \alpha \rho^{(1)},$$

for $\alpha \in \mathbb{R}$, then we have

$$\begin{aligned} \rho(\mathbf{q}, \mathbf{p}, t) &= e^{t\mathcal{L}_{LD}^\dagger} \rho_0 = e^{t\mathcal{L}_{LD}^\dagger} \rho_{\text{eq}} + \alpha e^{t\mathcal{L}_{LD}^\dagger} \rho^{(1)} \\ &= \rho_{\text{eq}} + \alpha e^{t\lambda_1} \rho^{(1)}. \end{aligned}$$

Since all the eigenvalues lie to the left of a vertical line in the left half plane, for any ϕ in C^∞ we have

$$\int_{\mathcal{D}} \phi \rho(\mathbf{q}, \mathbf{p}, t) d\omega = \text{Av}_\beta(\phi) + \alpha e^{t\lambda_1} \int_{\mathcal{D}} \phi \rho^{(1)} d\omega.$$

The latter integral is bounded since both ϕ and $\rho^{(1)}$ are in L^2 , and since $\text{Re}(\lambda_1) < 0$, we see that this converges exponentially to the desired average.

Exercises

1. Define $H = p^2/2 + \Omega^2 q^2/2$, and then compare the microcanonical and canonical covariances involving q and p :
 - a. $\text{Av}_{H=E}(p^2)$, $\text{Av}_\beta(p^2)$,
 - b. $\text{Av}_{H=E}(pq)$, $\text{Av}_\beta(pq)$,
 - c. $\text{Av}_{H=E}(q^2)$, $\text{Av}_\beta(q^2)$.
2. Prove Proposition 6.3 by writing

$$\int_0^\tau g(s)dW(s) = \sum_{i=0}^{v-1} g_i \Delta W_i,$$

where $g_i = g(t_i)$ and $\Delta W_i = W(s_{i+1}) - W(s_i)$, by using the independence of the Wiener increments.

3. Calculate the canonical partition function for $\exp(-\beta \mathbf{q}^T \mathbf{K} \mathbf{q}/2)$ for the case where $\mathbf{q} \in \Omega = \mathbb{R}^{N_c}$, where \mathbf{K} is a symmetric positive definite matrix.
4. Consider a variant of Langevin dynamics coupling the Ornstein-Uhlenbeck process to only one degree of freedom. Such equations of motion for a planar system with potential energy $U(x, y)$ are

$$\begin{aligned} dx &= p_x dt, \\ dy &= p_y dt, \\ dp_x &= -U_x(x, y)dt, \\ dp_y &= -U_y(x, y)dt - p_y dt + \sqrt{2k_B T} dW, \end{aligned}$$

where W is a standard Wiener process and U_x and U_y are the partial derivatives of $U(x, y)$ with respect to x and y respectively.

- a. Verify that the dynamics preserve the canonical distribution.
- b. Let $U(x, y) = (x + y)^2/2$ and verify that Hörmander's condition is satisfied by iterating Lie brackets (see Definition 6.1).
5. Recall that in (5.6) we defined the average of a function f at time t to be $\bar{f}(t)$. In the case of the harmonic oscillator ($U(q) = \Omega^2 q^2/2$) assuming the system is evolved using Brownian (overdamped) dynamics, find $\bar{f}_1(t)$ and $\bar{f}_2(t)$ where $f_1(q) = q$ and $f_2(q) = q^2$. That is, assume that q evolves according to the equation

$$dq = -\gamma^{-1} \Omega^2 q dt + \sqrt{2k_B T \gamma^{-1}} dW,$$

and recall that if \mathcal{L} is the generator of an SDE, then

$$\frac{d\bar{f}}{dt} = \mathbb{E}(\mathcal{L}f).$$

- 6. Let $g_1(q, p) = q^2$, $g_2(q, p) = qp$ and $g_3(q, p) = p^2$. Solve the time-dependent evolution of the covariances $\bar{g}_1(t)$, $\bar{g}_2(t)$ and $\bar{g}_3(t)$ in the case of the harmonic oscillator with unit mass ($H = p^2/2 + \Omega^2 q^2/2$), assuming the system is evolved using Langevin dynamics.
- 7. Let $U(x, y) = x^2 + y^2 + x^2y^2$. Find the value of the canonical average $\text{Av}_\beta(x^2 + y^2 + 2x^2y^2)$ and explain how this calculation is related to the configurational temperature (6.5).

Chapter 7

Numerical Methods for Stochastic Molecular Dynamics

In this chapter, we discuss principles for the design of algorithms for canonical sampling, based on the numerical discretization of stochastic dynamics models (such as Langevin dynamics) introduced in the previous chapter. Before we begin our discussion, let us consider the motivation for computing stationary averages using molecular dynamics.

One often views molecular sampling as exploration of the basins associated to local minima of the potential energy (or a free energy function, which would incorporate the effects of solvent degrees of freedom such as a bath of water). As a simplification, consider a system of N atoms interacting in a uniform pairwise potential energy function such as Lennard-Jones. It is estimated that the number of local minima of the potential is $\mathcal{O}(e^{N^2})$ [178], a spectacularly large number. Of course many of these will only be visited rarely, and the possibility of obtaining an average to a reasonable accuracy depends very much on the shape of the potential (e.g. the numbers of local minima accessible at a given temperature and the heights of the barriers between them), the sampling strategy, and even the particular observable being calculated. The large number of local minima, and the size of the sample space, make sampling a challenging problem, as methods such as Langevin dynamics must be run for a long time to generate a set of states which independently sample the various basins.

In fact, we might ask the question, “why use trajectories to calculate averages?” It seems that the task has little to do with the dynamics per se. We are simply computing the expectation of some function with respect to a given probability density, i.e. an integral on a large dimensional space. Although there may be stochastic differential equations available to us whose Fokker-Planck solutions are known to converge to the stationary distribution (for example Langevin dynamics), it is not obvious that computing trajectories provides the best way to sample it. Non-dynamical alternatives, such as Metropolis Monte-Carlo (see Appendix C), are available for the purpose and one might think that this is a more direct approach to the problem. In a Monte-Carlo method there is no direct way to calculate

dynamics information, but this may or may not be essential to the problem at hand: we often only wish to know the average of a given function $\phi(\mathbf{q})$ with respect the configurational density $\exp(-\beta U(\mathbf{q}))$, where U is the potential energy function of a molecular system. Nevertheless, Metropolis Monte-Carlo can encounter additional problems in the setting of molecular modelling. Where steep potentials (Lennard-Jones potentials, for example) and stiff bonds are present, Monte-Carlo methods may experience a high rejection rate. From another perspective, the “interesting region” for sampling a Gibbs distribution is an extremely small portion of the accessible phase space, since the measure of phase space is highly concentrated and localized by the inherent geometric constraints of the problem and/or steep potentials. As the dimensionality increases, the accessible phase space becomes thinner. A sampling algorithm must be guided from place to place in a large dimensional phase space riddled with steep barriers, and blind search typically leads to a lot of wasted effort. For this reason molecular dynamics, which benefits from acceleration information (the forces) to guide timestepping, and for which every step is accepted, is often superior to crude Monte-Carlo for molecular sampling. For a comparative discussion of Monte-Carlo and molecular dynamics methods, see [6, 278].

We hasten to add that there are many situations in which Monte-Carlo methods have the advantage. For example, we might have specific knowledge of a catalog of large scale structural “moves” that would allow our algorithm to scale energetic barriers without drastically biasing the sampling outcome. An example is when an assembly consisting of several component macromolecules is moved by rearranging the pieces, since it may take atomistic MD a very long time to make such moves. In those cases we would likely wish to make use of the system-specific knowledge that we have in order to accelerate the sampling. An alternative to assuming, *a priori*, a detailed book of moves, is to consider methods that adaptively construct good proposals, for example taking advantage of parallel computing methods. At the very least, one would expect that such methods need to take into consideration the local forces to avoid wasted steps. A practical way to do this is the Hybrid Monte-Carlo method mentioned in Appendix C.

Note that deterministic methods (e.g. Hamiltonian dynamics itself) can sometimes be used for molecular sampling, but without stochastic perturbation, such methods are not rigorously ergodic, since the Liouvillian operator does not possess a spectral gap and does not provide a unique stationary solution. The stochastic methods of this chapter are general purpose techniques that require little in the way of system-specific knowledge. They are workhorse methods which provide rigorous control of the canonical distribution. The challenge in using Langevin dynamics is to design maximally efficient methods that provide accurate averages for a wide range of observables using as large stepsizes as possible, and which converge as rapidly as possible. It is possible—even very easy—to build schemes that are wasteful, for example subject to unnecessarily stringent numerical stability barriers, and eliminating such mistakes is essential. This can be achieved by careful attention to the principles by which integrators are designed. Well designed stochastic differential equation approaches introduce dissipation without destroying

long term (invariant measure) conservation properties; in this way they can provide a rational and flexible framework for designing stable algorithms.

Once a stochastic molecular dynamics-based framework is developed it is possible to modify it or use it as a building block in order to enhance sampling efficiency. One can for example incorporate these methods into *kinetic Monte-Carlo*, other metropolized schemes, or various advanced “path sampling” techniques. Thus the design of good molecular SDE methods is the cornerstone of much of modern molecular modelling.

7.1 Bias

In this chapter, the focus is on sampling strategies based on approximating Langevin dynamics (6.32)–(6.33). As will be seen, these methods offer a great deal of flexibility and, most importantly, reliability and robustness in the approximation of the canonical measure. All standard methods based on discretizing SDEs introduce some stepsize-dependent error in computed averages, which we shall refer to as bias (related to the truncation error of the discretization scheme). This bias can be corrected for using certain ‘rebiasing’ algorithms, for example using a Metropolis (accept-reject) condition [44, 47], however there may be significant computational overhead in employing these schemes leading to inefficiency compared to standard MD, in spite of the introduced error.

An illustration of the sampling bias (i.e., due to discretization error) is shown in Fig. 7.1. As the stepsize is increased, the error in sampling is increased as well, limiting the effectiveness of numerical methods. This bias can be dramatically different for different numerical methods. As we shall show, with the right choice of numerical method it is often possible to substantially reduce this error, and it is also possible to calculate (under some assumptions) the perturbation introduced by the numerical method, and to correct for its presence.

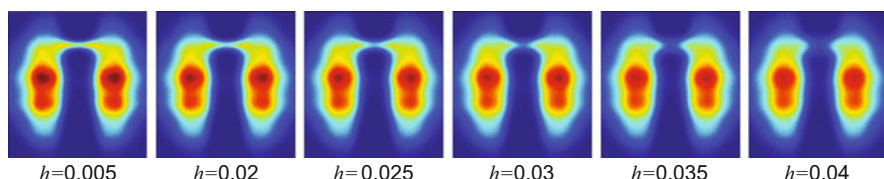


Fig. 7.1 We illustrate computed (canonical) distributions of $\mathbf{q} = (x, y)$ for a planar potential energy function with two distinct basins connected by a narrow transition corridor, where high/low intensity is colored red/blue respectively. Each distribution is computed through simulations using a different stepsize parameter—no other properties are changed between the simulations. The differences between the distributions are the result of discretization error. At simulations with a larger timestep we can see a qualitative change in the sampled landscape, with the bridge between the two regions disappearing. Figure reprinted with permission from [222]. Copyright 2013, AIP Publishing LLC

7.2 Error in Methods for Stochastic Differential Equations

We briefly present some standard material on the development of numerical schemes for SDEs. The interested reader is pointed to the standard textbooks [200, 270] for a more thorough discussion of foundational concepts. Let us begin with a discussion of the first order stochastic differential equation

$$dX = a(X)dt + b(X)dW,$$

where W defines a standard scalar Wiener process. The natural extension of the Euler method for SDEs like this one takes the form

$$X_{n+1} = X_n + ha(X_n) + b(X_n)\sqrt{h}R_n,$$

where R_n is a normal random variable with zero mean and unit variance. This method is referred to as the Euler-Maruyama method.

Note that from the definition of the SDE, we may write

$$X(t+h) = X(t) + \int_t^{t+h} a(X(s))ds + \int_t^{t+h} b(X(s))dW(s).$$

Just as in the deterministic case, we may build a numerical method by approximating these integrals over a small timestep h . However, when designing a numerical scheme it is important to keep in mind the goal of the discretization itself. For example, as we have considered Langevin dynamics as a tool for studying the canonical distribution, do we always need methods to give us good approximations of $X(t+h)$? If we seek to compute averages with respect to the canonical distribution, then the answer is no: we simply require that the average over the discretized trajectory is accurate.

The numerical analysis of stochastic differential equations is traditionally based on the concepts of *weak* and *strong* accuracy. Let a numerical method be given for solving an SDE in the form of a discrete stochastic process $X_{n+1} = \Phi(X_n, h)$ for $n = 0, 1, \dots, v-1$, where $v\tau = \tau$ is fixed. We denote the stochastic solution of the SDE by $X(t)$. In the case of strong accuracy, our measure of the global error is the quantity [200]

$$\text{Err}_{h,\tau;\alpha}^{\text{strong}} = \max_{n=0,1,2,\dots,v} [\mathbb{E} |X_n - X(nh)|^\alpha]^{1/\alpha}.$$

For $\alpha = 1$ this implies convergence of expectation. The more natural choice from the probabilistic point of view is $\alpha = 2$ (mean square convergence). Having settled on a choice of α , we say that a method has strong order r if $\text{Err}_{h,\tau}^{\text{strong}} < C(\tau)h^r$ for some coefficient $C(\tau)$ depending on the time interval.

The weak error is usually defined with reference to suitable test functions (observables) $\phi(x)$ by

$$\text{Err}_{h,\tau,\phi}^{\text{weak}} = \max_{n=0,1,2,\dots,v} |\mathbb{E}\phi(X_n) - \mathbb{E}\phi(X(nh))|,$$

and we say that a method has weak order r if $\text{Err}_{h,\tau,\phi}^{\text{weak}} < D(\tau)h^r$ for some $D(\tau)$, for all members of the chosen class of observables. It is easy to see that methods with high strong order give us high weak order too, but the converse is generally false.

As the focus of this chapter is on the computation of averages, the concept of weak order is more appropriate in evaluating methods.¹ Yet, even the weak order of convergence may not be suitable in molecular dynamics applications, or rather, we are interested in the very long term behavior of the weak error which is governed by the coefficient $D(\tau)$ as $\tau \rightarrow \infty$ [270, 356].

The standard approach to analyze the weak error would be based on computing a recurrence relation for $|\mathbb{E}\phi(X_n) - \mathbb{E}\phi(X(nh))|$ by use of the SDE and the methods of stochastic analysis. This approach mirrors the forward convergence analysis of ODE methods discussed in Chap. 2. It tends, however, to overestimate the magnitude of the quantity $D(\tau)$. In what follows, we show that, when the emphasis is on stationary averages, a more direct approach can be used to gain insight into the error based on an asymptotic expansion. In some cases, we are able to resolve explicitly the leading error term of computed averages in this long-time limit. The approach used here is analogous in many ways to the backward error analysis of deterministic problems presented in Chap. 3.

The *sampling error* is an additional error term that results from the finiteness of our trajectory: both in our inability to sample over an infinite time (for Langevin dynamics, we recover our averages only in the limit of $\tau \rightarrow \infty$) and our generation of only a finite number of points (averages are calculated from our discretized trajectory of v steps). In large, high-dimensional systems (such as many relevant biomolecular applications) often the computational resource required to sample long enough in time to recover good averages is not available—the challenge then can be viewed as an *exploration* problem. Obtaining a complete sampling of the phase space in a system with rare transitions is extremely difficult, and is the most important challenge in molecular simulation [401].

However, we emphasize in this chapter that the discretization error (or *perfect sampling bias*) is also a very important contribution to the overall error, and in some cases may dominate the sampling error (for example, in systems where local resolution of the measure is more important than the global search). This discretization bias cannot be removed by considering a longer simulation time, so in some sense it is akin to a modelling error. Indeed as computing power increases and new algorithms are utilized, it is likely that trajectory generation will always be

¹In practice all the methods presented here are convergent in the strong sense, but their strong convergence orders may be low, typically $r = 1/2$.

at the core of sampling in molecular dynamics. Hence we are motivated to find schemes that minimize this sampling bias introduced to the long-time averages, without significant increase to the method's computational cost.

Recall that for canonical sampling, the (stationary or invariant) average of an observable $\phi(\mathbf{q}, \mathbf{p})$ is given as

$$\text{Av}_\beta(\phi) = \int_{\mathcal{D}} \phi(\mathbf{q}, \mathbf{p}) \rho_\beta(\mathbf{q}, \mathbf{p}) d\omega, \quad (7.1)$$

where ρ_β is the canonical measure

$$\rho_\beta(\mathbf{q}, \mathbf{p}) = Z_{\text{can}}^{-1} \exp(-\beta H(\mathbf{q}, \mathbf{p})),$$

and Z_{can} is the canonical partition function

$$Z_{\text{can}}^{-1} = \int_{\mathcal{D}} \exp(-\beta H(\mathbf{q}, \mathbf{p})) d\omega,$$

ensuring the integral of ρ_β is unity. In this chapter, we will abbreviate the exact average of the observable ϕ to

$$\langle \phi \rangle \stackrel{\text{def}}{=} \text{Av}_\beta(\phi),$$

and write the observed average computed in experiment (using a discretization method with step size h) as $\langle \phi \rangle_h$. The error in the average of ϕ due to the perfect sampling bias can be evaluated as

$$\text{Error due to discretization} = |\langle \phi \rangle - \langle \phi \rangle_h|.$$

We assume that the observed value of $\langle \phi \rangle_h$ is corrupted as a result of our discretization, ignoring all other sources of error in our simulation. It is this sampling bias we would like to calculate (in order to correct our computed averages), or develop numerical sampling methods that naturally minimize this error.

In Fig. 7.2 we quantify the difference between the computed distribution of $q \in \mathbb{R}$ and the canonical distribution, for the one-dimensional double well potential $U(q) = (q^2 - 1)^2$, using Langevin dynamics with parameters $M = \gamma = \beta = 1$. The dynamics are discretized using a standard Langevin dynamics second-order algorithm taken from [62], where we sample the distribution of q along our discretized trajectory. Each step of the algorithm requires one force evaluation, so we may think of the vertical axis in Fig. 7.2 representing the total computational work.

If we were able to solve the Langevin dynamics SDE exactly, then as we evolve the system in time the distribution will converge towards the canonical distribution, however the effects of numerical discretization are apparent in the

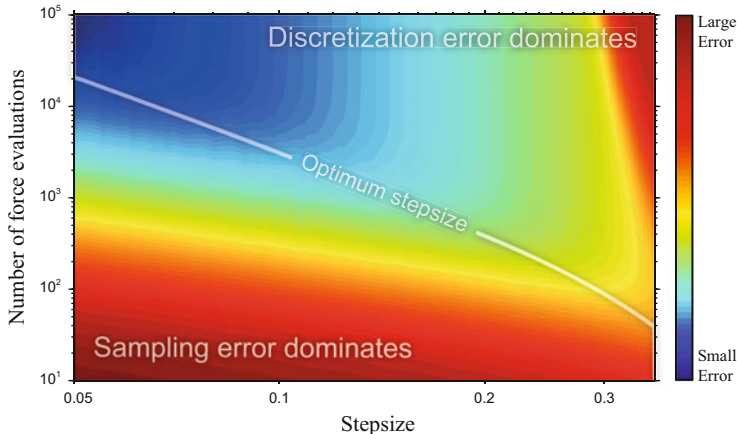


Fig. 7.2 We plot the error in the distribution of $q \in \mathbb{R}$ for $U(q) = (q^2 - 1)^2$. The error in the computed distribution is a function of both the number of force evaluations and the stepsize used, with the optimal choice of stepsize for a given number of force evaluations shown by the *white guideline*. Due to discretization bias, choosing the maximum stepsize is not always the best strategy

figure: while increasing the stepsize means we more rapidly converge with each step, the distribution that the discretization scheme converges to is incorrect. For small stepsizes, this error due to discretization may be negligible when compared to the sampling error, but we converge more slowly towards the final distribution. As the stepsize is increased, the discretization error may dominate the overall error in calculation.

7.3 Sampling Iterations

By way of illustration of what we mean by a numerical sampling method, consider the system of independent Ornstein-Uhlenbeck (OU) processes

$$dp = -\gamma p dt + \sqrt{2k_B T \gamma} M^{1/2} dW. \quad (7.2)$$

Following the argument of Sect. 6.3.2 in the previous chapter,

$$\begin{aligned} d[\exp(\gamma t)p] &= \gamma \exp(\gamma t)pd़t + \exp(\gamma t)[-pdt + \sqrt{2k_B T \gamma} M^{1/2} dW] \\ &= \exp(\gamma t) \sqrt{2k_B T \gamma} M^{1/2} dW. \end{aligned}$$

Integrating from t to $t + h$ and multiplying by $\exp(-\gamma t)$, we arrive at the solution

$$\mathbf{p}(t+h) = e^{-\gamma h} \mathbf{p}(t) + \sqrt{k_B T(1 - e^{-2\gamma h})} \mathbf{M}^{1/2} \mathbf{Z}, \quad (7.3)$$

where \mathbf{Z} is a vector of independent, standard normal random variables. Alternatively, we may write this as a discrete iteration in terms of a random map:

$$\mathbf{p}_{n+1} = e^{-\gamma h} \mathbf{p}_n + \sqrt{k_B T(1 - e^{-2\gamma h})} \mathbf{M}^{1/2} \mathbf{R}_n,$$

with normally distributed \mathbf{R} . For later purposes, we will think of this update as acting on both \mathbf{q} and \mathbf{p} , leaving \mathbf{q} unchanged, i.e.

$$(\mathbf{q}_{n+1}, \mathbf{p}_{n+1}) = (\mathbf{q}_n, e^{-\gamma h} \mathbf{p}_n + \sqrt{k_B T(1 - e^{-2\gamma h})} \mathbf{M}^{1/2} \mathbf{R}_n).$$

The Fokker-Planck operator for the OU system (7.2) can be computed directly as

$$\mathcal{L}_O^\dagger \phi(\mathbf{q}, \mathbf{p}) = \gamma \nabla_p \cdot (\mathbf{p} \phi) + \gamma k_B T \nabla_p \cdot \mathbf{M} \nabla_p \phi.$$

The Ornstein-Uhlenbeck process models the momentum of a Brownian particle, and in deriving it we thought of γ as being associated to the collisional frequency with the particles of the bath. Alternatively, if we ignore the physical origin of this parameter, we can think of γ as an arbitrary coefficient; the sampling of the invariant measure does not depend on this choice. Thus we have a family of *sampling iterations* for the Gaussian distribution, defined for different choices of γ .

7.3.1 Splitting Methods for Langevin Dynamics

We will now consider a family of iterations for molecular systems which are constructed from simple building blocks based on the splitting of an SDE, specifically Langevin dynamics:

$$\begin{aligned} d\mathbf{q} &= \mathbf{M}^{-1} \mathbf{p} dt, \\ d\mathbf{p} &= -\nabla U(\mathbf{q}) dt - \gamma \mathbf{p} dt + \sqrt{2\gamma k_B T} \mathbf{M}^{1/2} d\mathbf{W}. \end{aligned} \quad (7.4)$$

Just as in the deterministic setting (for Newton's equations of motion) we construct such splitting methods by way of an additive decomposition of the vector field, where the differential equations corresponding to any individual piece can be solved exactly. Methods are built from a sequence of updates corresponding to an exact solve of each piece. By "exact solve" we here mean the construction of a method of exactly sampling the distribution generated by the corresponding component. The

choice of splitting strategy (given by the definition of the splitting pieces) along with a prescribed sequence of updates defines a splitting method.

There are a great number of plausible splitting strategies for Langevin dynamics. For example we may split the equations into purely deterministic and stochastic parts, break the stochastic terms into dissipative and random components, or choose to decompose the vector field into N_c one-dimensional problems that can be solved to high-accuracy. For some potential energy functions, it may be beneficial to decompose the potential into many terms $U(\mathbf{q}) = U_1(\mathbf{q}) + U_2(\mathbf{q}) + \dots$, and use each term in a separate splitting piece in order to give a scheme improved stability or computational properties. In any case, it is not obvious *a priori* which splitting strategies will have more favorable sampling properties.

As propagating the Ornstein-Uhlenbeck process exactly will preserve the canonical distribution ρ_β , it is reasonable to assume that this is a good choice for one of the building blocks in a general splitting scheme. As the exact solution of the OU process is defined for any value of $\gamma \geq 0$, we may hope that our discretization scheme will be tolerant for extremely large frictions, although there is no guarantee that the resulting discretization remains consistent in the limiting case.

Other than the Ornstein-Uhlenbeck process, the remaining piece of the splitting corresponds to Newtonian constant-energy (microcanonical) Hamiltonian dynamics. Since Hamiltonian dynamics leaves invariant any function of the energy, its corresponding Fokker-Planck operator (in this case the Liouvillian, $\mathcal{L}_H^\dagger = -\mathcal{L}_H$) will preserve distributions that are functions of the Hamiltonian H . This implies in particular that it preserves ρ_β , which is proportional to $\exp(-\beta H)$. Thus the forward propagator associated to the Hamiltonian system automatically preserves the Gibbs distribution, and we have

$$e^{t\mathcal{L}_H^\dagger} \rho_\beta = \rho_\beta.$$

Formally, we could combine the flow map \mathcal{F}_h^H of Hamiltonian dynamics with an exact solve of the OU process to create a sampling iteration which preserves ρ_β , as we also have

$$e^{t\mathcal{L}_O^\dagger} \rho_\beta = \rho_\beta.$$

To make this practical in the general case, where the Hamiltonian system is not integrable (and we cannot explicitly compute its flow map), we need to be able to compute (or approximate) the maps involved.

This suggests to further split the Hamiltonian system, as we have done in deriving symplectic integrators in Chaps. 2 and 3.

We therefore consider dividing the Langevin system (7.4) into parts

$$d \begin{bmatrix} \mathbf{q} \\ \mathbf{p} \end{bmatrix} = \underbrace{\begin{bmatrix} \mathbf{M}^{-1} \mathbf{p} \\ \mathbf{0} \end{bmatrix}}_{\text{A}} dt + \underbrace{\begin{bmatrix} \mathbf{0} \\ -\nabla U(\mathbf{q}) \end{bmatrix}}_{\text{B}} dt + \underbrace{\begin{bmatrix} \mathbf{0} \\ -\gamma \mathbf{p} dt + \sigma \mathbf{M}^{1/2} d\mathbf{W} \end{bmatrix}}_{\text{O}}, \quad (7.5)$$

which we label A, B and O, where each of the three parts may be solved “exactly”, with individual updates given as

$$\begin{aligned}\mathcal{U}_h^A(\mathbf{q}, \mathbf{p}) &= (\mathbf{q} + h\mathbf{M}^{-1}\mathbf{p}, \mathbf{p}), \\ \mathcal{U}_h^B(\mathbf{q}, \mathbf{p}) &= (\mathbf{q}, \mathbf{p} - h\nabla U(\mathbf{q})), \\ \mathcal{U}_h^O(\mathbf{q}, \mathbf{p}) &= (\mathbf{q}, e^{-\gamma h}\mathbf{p} + \sqrt{k_B T(1 - e^{-2\gamma h})}\mathbf{M}^{1/2}\mathbf{R}),\end{aligned}$$

where \mathbf{R} is a vector of i.i.d. normal random numbers. For the deterministic pieces A and B, the updates correspond to their flow maps, while the update for the O piece corresponds to the solution derived in (7.3). The relevant forward propagators for each piece of the Hamiltonian part are computed through the adjoint of the Lie derivative as

$$\mathcal{L}_A^\dagger = -\mathbf{M}^{-1}\mathbf{p} \cdot \nabla_q, \quad \mathcal{L}_B^\dagger = \nabla U(\mathbf{q}) \cdot \nabla_p.$$

Using this splitting strategy, we can define a family of schemes by the desired sequence of updates, codified as a string using the alphabet “ABO”. For example, the method denoted $\llbracket \text{ABO} \rrbracket$ (acting from left to right) has a resulting update

$$\mathcal{U}_h^{\llbracket \text{ABO} \rrbracket} = \mathcal{U}_h^O \circ \mathcal{U}_h^B \circ \mathcal{U}_h^A.$$

This corresponds to using the adjoint symplectic Euler scheme to solve the Newtonian part of the Langevin dynamics SDE, followed by an exact OU solve. An alternative is to use velocity Verlet for the Hamiltonian part, resulting in a scheme denoted $\llbracket \text{BABO} \rrbracket$ with associated map

$$\mathcal{U}_h^{\llbracket \text{BABO} \rrbracket} = \mathcal{U}_h^O \circ \mathcal{U}_{h/2}^B \circ \mathcal{U}_h^A \circ \mathcal{U}_{h/2}^B.$$

Note that the presence of two B characters in the string results in halving the corresponding piece’s time step length. As we need the method to be consistent, we require that the each of the A, B and O pieces are propagated in time for a total time of h . As a result we use the convention that if a letter appears k times in a method’s string, then each individual update piece uses a timestep h/k . For example, the scheme denoted $\llbracket \text{OABOAOBAO} \rrbracket$ has an update

$$\mathcal{U}_h^{\llbracket \text{OABOAOBAO} \rrbracket} = \mathcal{U}_{h/4}^O \circ \mathcal{U}_{h/3}^A \circ \mathcal{U}_{h/2}^B \circ \mathcal{U}_{h/4}^O \circ \mathcal{U}_{h/3}^A \circ \mathcal{U}_{h/4}^O \circ \mathcal{U}_{h/2}^B \circ \mathcal{U}_{h/3}^A \circ \mathcal{U}_{h/4}^O,$$

where the random numbers used in each O update are independent. This scheme will require a total of $4N_c$ normal random numbers and two force evaluations per step (the force must be recomputed at the first B step following an A step; the number of force evaluations required is not directly related to the length of the string).

A class of methods like those considered above were discussed in [46] and given the general title of “Geometric” Langevin Algorithm (GLA). The idea of a GLA

method is to treat the Newtonian part of Langevin dynamics by a symplectic method, and follow this by an Ornstein-Uhlenbeck exact solve; this is just what is done in the schemes denoted $\llbracket \text{BABO} \rrbracket$ and $\llbracket \text{BAO} \rrbracket$. Thus we could give these two methods the alternate (and more descriptive) names Geometric Langevin (Velocity-Verlet) and Geometric Langevin (Position-Verlet) respectively.

Building on these schemes, the OU solves can instead be placed in the center of the step, or we may choose to have more than one OU solve distributed through the iteration. As it happens, some of these methods are of particular interest. We refer to the method obtained by inserting the OU solve in the middle of the Verlet method either by the strings $\llbracket \text{ABOBA} \rrbracket$ (Position-Verlet version) and $\llbracket \text{BAOAB} \rrbracket$ (Velocity-Verlet version) or by the more pronounceable names Symmetric Langevin Position-Verlet or Symmetric Langevin Velocity-Verlet, respectively.

For reference and to remove any ambiguity, we write out some of these algorithms below as single timestep maps (sample implementations in MATLAB are available at <http://www.MolecularDynamics.info>).

$\llbracket \text{ABAO} \rrbracket$

$$\begin{aligned}\mathbf{q}_{n+1/2} &= \mathbf{q}_n + (h/2)\mathbf{M}^{-1}\mathbf{p}_n, \\ \mathbf{p}_{n+1/2} &= \mathbf{p}_n - h\nabla U(\mathbf{q}_{n+1/2}), \\ \mathbf{q}_{n+1} &= \mathbf{q}_{n+1/2} + (h/2)\mathbf{M}^{-1}\mathbf{p}_{n+1/2}, \\ \mathbf{p}_{n+1} &= e^{-hy}\mathbf{p}_{n+1/2} + \xi_2\mathbf{M}^{1/2}\mathbf{R}_n,\end{aligned}$$

$\llbracket \text{ABOBA} \rrbracket$

$$\begin{aligned}\mathbf{q}_{n+1/2} &= \mathbf{q}_n + (h/2)\mathbf{M}^{-1}\mathbf{p}_n, \\ \mathbf{p}_{n+1/2} &= \mathbf{p}_n - (h/2)\nabla U(\mathbf{q}_{n+1/2}), \\ \hat{\mathbf{p}}_{n+1/2} &= e^{-hy}\mathbf{p}_{n+1/2} + \xi_2\mathbf{M}^{1/2}\mathbf{R}_n, \\ \mathbf{p}_{n+1} &= \hat{\mathbf{p}}_{n+1/2} - (h/2)\nabla U(\mathbf{q}_{n+1/2}), \\ \mathbf{q}_{n+1} &= \mathbf{q}_{n+1/2} + (h/2)\mathbf{M}^{-1}\mathbf{p}_{n+1},\end{aligned}$$

$\llbracket \text{OABAO} \rrbracket$

$$\begin{aligned}\mathbf{p}_{n+1/2} &= e^{-hy/2}\mathbf{p}_n + \xi_1\mathbf{M}^{1/2}\mathbf{R}_n, \\ \mathbf{q}_{n+1/2} &= \mathbf{q}_n + (h/2)\mathbf{M}^{-1}\mathbf{p}_{n+1/2}, \\ \hat{\mathbf{p}}_{n+1/2} &= \mathbf{p}_{n+1/2} - h\nabla U(\mathbf{q}_{n+1/2}), \\ \mathbf{q}_{n+1} &= \mathbf{q}_{n+1/2} + (h/2)\mathbf{M}^{-1}\hat{\mathbf{p}}_{n+1/2}, \\ \mathbf{p}_{n+1} &= e^{-hy/2}\hat{\mathbf{p}}_{n+1/2} + \xi_1\mathbf{M}^{1/2}\mathbf{R}_{n+1/2},\end{aligned}$$

$\llbracket \text{BABO} \rrbracket$

$$\begin{aligned}\mathbf{p}_{n+1/2} &= \mathbf{p}_n - (h/2)\nabla U(\mathbf{q}_n), \\ \mathbf{q}_{n+1} &= \mathbf{q}_n + h\mathbf{M}^{-1}\mathbf{p}_{n+1/2}, \\ \hat{\mathbf{p}}_{n+1/2} &= \mathbf{p}_{n+1/2} - (h/2)\nabla U(\mathbf{q}_{n+1}), \\ \mathbf{p}_{n+1} &= e^{-hy}\hat{\mathbf{p}}_{n+1/2} + \xi_2\mathbf{M}^{1/2}\mathbf{R}_n,\end{aligned}$$

$\llbracket \text{BAOAB} \rrbracket$

$$\begin{aligned}\mathbf{p}_{n+1/2} &= \mathbf{p}_n - (h/2)\nabla U(\mathbf{q}_n), \\ \mathbf{q}_{n+1/2} &= \mathbf{q}_n + (h/2)\mathbf{M}^{-1}\mathbf{p}_{n+1/2}, \\ \hat{\mathbf{p}}_{n+1/2} &= e^{-hy}\mathbf{p}_{n+1/2} + \xi_2\mathbf{M}^{1/2}\mathbf{R}_n, \\ \mathbf{q}_{n+1} &= \mathbf{q}_{n+1/2} + (h/2)\mathbf{M}^{-1}\hat{\mathbf{p}}_{n+1/2}, \\ \mathbf{p}_{n+1} &= \hat{\mathbf{p}}_{n+1/2} - (h/2)\nabla U(\mathbf{q}_{n+1}),\end{aligned}$$

$\llbracket \text{OBABO} \rrbracket$

$$\begin{aligned}\mathbf{p}_{n+1/2} &= e^{-hy/2}\mathbf{p}_n + \xi_1\mathbf{M}^{1/2}\mathbf{R}_n, \\ \hat{\mathbf{p}}_{n+1/2} &= \mathbf{p}_{n+1/2} - (h/2)\nabla U(\mathbf{q}_n), \\ \mathbf{q}_{n+1} &= \mathbf{q}_n + h\mathbf{M}^{-1}\hat{\mathbf{p}}_{n+1/2}, \\ \hat{\mathbf{p}}_{n+1} &= \hat{\mathbf{p}}_{n+1/2} - (h/2)\nabla U(\mathbf{q}_{n+1}), \\ \mathbf{p}_{n+1} &= e^{-hy/2}\hat{\mathbf{p}}_{n+1} + \xi_1\mathbf{M}^{1/2}\mathbf{R}_{n+1/2},\end{aligned}$$

where $\xi_j = [\text{k}_\text{B}T(1 - e^{-jy})]^{1/2}$, and $\mathbf{R}_n, \mathbf{R}_{n+1/2}$ are N_d vectors of standard independent $\mathcal{N}(0, 1)$ random variables, resampled at each step. Note that, as in the Velocity-Verlet method, the two apparent evaluations of the force $\mathbf{F} = -\nabla U$ in the methods labelled $\llbracket \text{BABO} \rrbracket$, $\llbracket \text{BAOAB} \rrbracket$ and $\llbracket \text{OBABO} \rrbracket$ actually require only a single evaluation at each timestep, since the second evaluation at one step may be reused at the first stage of the following step. Thus all of the above methods require only one force evaluation per timestep, and hence we can think of them having exactly the same computational cost as the evaluation of the force is the principle computational expense.

When iterated $n + 1$ times, we can see the scheme $\llbracket \text{OABA} \rrbracket$ produces a mapping of the form

$$\left(\mathcal{U}_h^{\llbracket \text{OABA} \rrbracket} \right)^{n+1} = \mathcal{U}_{h/2}^A \circ \mathcal{U}_{h/2}^B \circ \left(\mathcal{U}_h^{\llbracket \text{BAOAB} \rrbracket} \right)^n \circ \mathcal{U}_{h/2}^B \circ \mathcal{U}_{h/2}^A \circ \mathcal{U}_h^O,$$

therefore through a coordinate transformation the $\llbracket \text{OABA} \rrbracket$ method can be morphed into the $\llbracket \text{BAOAB} \rrbracket$ scheme. To put this another way, if we compute an iteration using $\llbracket \text{OABA} \rrbracket$ and simply evaluate it at different points within the step, we can recover the same results as the $\llbracket \text{BAOAB} \rrbracket$ method would provide. Another term to describe this relationship is to say that one method is *conjugate* to the other.

7.3.2 Other Langevin Integrators

We may use our alphabet of A, B and O splitting pieces to create a wide variety of methods other than those given in the previous section (some requiring multiple force evaluations). However, it is not obvious that there is any gain in increasing the complexity of the splitting scheme (in terms of the length of its codifying string). Some popular methods can be rewritten in terms of this splitting, for example the scheme considered in [62] is equivalent to $\llbracket \text{OBABO} \rrbracket$. Examples of methods based on this type of splitting were also proposed by De Fabritiis et al [96] and Thalmann and Farago [363], in the context of dissipative particle dynamics (see Chapter 8).

Other Langevin dynamics splitting schemes in common use utilize a different additive decomposition of the SDE vector field. For example, the Stochastic Position Verlet (SPV) method of [265] relies on the splitting strategy

$$d \begin{bmatrix} \mathbf{q} \\ \mathbf{p} \end{bmatrix} = \begin{bmatrix} \mathbf{M}^{-1} \mathbf{p} \\ \mathbf{0} \end{bmatrix} dt + \begin{bmatrix} \mathbf{0} \\ -\nabla U(\mathbf{q}) dt - \gamma \mathbf{p} dt + \sigma \mathbf{M}^{1/2} d\mathbf{W} \end{bmatrix}.$$

To solve the splitting piece including the stochastic $d\mathbf{W}$ term, we note that \mathbf{q} does not change through its integration, and hence we may treat $\mathbf{F} = -\nabla U$ as constant during this part of the step. The exact solution is hence given through the usual Ornstein-Uhlenbeck formula, where the scheme itself derives from a symmetric integration of the two parts:

Stochastic Position Verlet (SPV)

$$\begin{aligned} \mathbf{q}_{n+1/2} &= \mathbf{q}_n + (h/2) \mathbf{M}^{-1} \mathbf{p}_n \\ \mathbf{p}_{n+1} &= e^{-hy} \mathbf{p}_n - \eta \nabla U(\mathbf{q}_n) + \zeta \mathbf{M}^{1/2} \mathbf{R}_n \\ \mathbf{q}_{n+1} &= \mathbf{q}_{n+1/2} + (h/2) \mathbf{M}^{-1} \mathbf{p}_{n+1} \end{aligned}$$

where $\eta = (1 - e^{-hy})/\gamma$, $\zeta = [k_B T (1 - e^{-2\gamma h})]^{1/2}$. It is important to note that in the limit of infinite friction, we have $\eta \rightarrow 0$ independent of the timestep h . This suggests that this splitting strategy is unsuitable for large choices of the parameter γ as the

sampling will become inconsistent: the force will be dominated by the stochastic term, leaving the dynamics to evolve as a random walk.

Similar behavior is exhibited using the splitting strategy in (7.5), when interposing the *kick* term B between two O steps, such as in the schemes [[AOBOA]] or [[BOAOB]]. By avoiding “OBO” updates, we can derive schemes that are consistent even at infinite friction (the [[BAOAB]] and [[ABOBA]] schemes are examples of such methods).

The Brünger-Brooks-Karplus (BBK) Langevin integrator [55] is one of the most popular and widely-implemented schemes.

Brünger-Brooks-Karplus (BBK)

$$\begin{aligned}\mathbf{p}_{n+1/2} &= (1 - h\gamma/2)\mathbf{p}_n - (h/2)\nabla U(\mathbf{q}_n) + \frac{1}{2}\sqrt{2k_B T h \gamma} \mathbf{M}^{1/2} \mathbf{R}_n \\ \mathbf{q}_{n+1} &= \mathbf{q}_n + h\mathbf{M}^{-1} \mathbf{p}_{n+1/2} \\ \mathbf{p}_{n+1} &= [\mathbf{p}_{n+1/2} - (h/2)\nabla U(\mathbf{q}_{n+1}) + \frac{1}{2}\sqrt{2k_B T h \gamma} \mathbf{M}^{1/2} \mathbf{R}'_n]/(1 + h\gamma/2)\end{aligned}$$

Often \mathbf{R}' is chosen such that $\mathbf{R}'_n = \mathbf{R}_{n+1}$, so the random vector would be reused at the start of the following timestep, however there are many variants of this scheme that incorporate the redraw of random numbers differently. In other variants of BBK we take $\mathbf{R}'_n = \mathbf{R}_n$, reusing the random number within the step. We may also consider independent \mathbf{R}'_n and \mathbf{R}_n , however when using independent noise processes we must modify the algorithm as it will not sample canonically (see Exercise 1).

7.4 Error Results for Harmonic Problems

For general systems it can be very challenging to give a complete description of the weak error in averages computed from trajectories evolved through a Langevin dynamics discretization scheme. However, using a linear model problem significantly reduces the complexity, while using small dimensional test problems allows us to effectively annihilate sampling error in demonstrative numerical experiments.

As such, we return now to the harmonic oscillator, which as well as being the simplest molecular model is also one of the most relevant for molecular dynamics applications, as many issues of stability and timestep in molecular dynamics simulations arise due to harmonic potentials used to model covalent bonds (such as in crystalline solids and biomolecules). The canonical distributions of position and momentum are also of a simple form (Gaussians), making such oscillators particularly amenable to analysis.

Recall that the one-dimensional harmonic oscillator with spring constant Ω^2 has potential energy function $U(q) = \Omega^2 q^2/2$, with Hamiltonian

$$H(q, p) = \frac{p^2}{2m} + \frac{\Omega^2 q^2}{2}, \quad (7.6)$$

where $(q, p) \in \mathbb{R}^2$ represent a particle’s position and momentum, and $m > 0$ is the particle’s mass. In this setting, the canonical distribution ρ_β is the product of two

Gaussian distributions, where we have invariant (stationary) averages

$$\langle q \rangle = \langle p \rangle = 0,$$

and

$$\langle \Omega^2 q^2 \rangle = \langle p^2/m \rangle = k_B T, \quad \langle qp \rangle = 0.$$

We expect that the discretization schemes that we employ will introduce errors in the computed values of the invariant (long-time) averages. In the large-time limit, these averages will converge towards their invariant value, which we can find using the procedure outlined in [59].

For the harmonic oscillator, the force $-U'(q)$ will be linear, and therefore we would expect that any update step in an algorithm will be linear in the state variables q and p . Thus, denoting the iteration index as a subscript, we may explicitly write one iteration of a general numerical method for evolving the dynamics as

$$\begin{bmatrix} q_{n+1} \\ p_{n+1} \end{bmatrix} = \Psi \begin{bmatrix} q_n \\ p_n \end{bmatrix} + \mu_n, \quad (7.7)$$

where Ψ is a constant matrix that depends on the stepsize h , the friction coefficient γ , the particle mass m and the spring constant Ω . Additionally μ_n is a vector of stochastic processes. For example, in the BBK method we can compute directly from its update scheme that

$$\begin{aligned} \Psi^{\text{BBK}} &= \begin{bmatrix} 1 - \frac{h^2 \Omega^2}{2m} & \frac{h}{m} \left(1 - \frac{\gamma h}{2}\right) \\ \frac{h \Omega^2}{2m} \left(\frac{h^2 \Omega^2 - 4m}{2 + \gamma h}\right) & \frac{(2 - \gamma h)(2m - h^2 \Omega^2)}{2m(2 + \gamma h)} \end{bmatrix}, \\ \mu_n^{\text{BBK}} &= \begin{bmatrix} \sqrt{\frac{k_B T \gamma h^3}{2m}} R_n \\ \frac{\sqrt{2k_B T \gamma h m}}{2 + \gamma h} \left(\left(1 - \frac{h^2 \Omega^2}{2m}\right) R_n + R'_n\right) \end{bmatrix}. \end{aligned}$$

More generally, if we define the components of Ψ as ψ_{ij} and denote $\mu_n = [\mu_{n,1}, \mu_{n,2}]^T$ we can take products of the update equations defined by (7.7) to obtain

$$q_{n+1}^2 = \psi_{11}^2 q_n^2 + \psi_{12}^2 p_n^2 + \mu_{n,1}^2 + 2\psi_{11}\psi_{12}q_n p_n + 2\psi_{11}\mu_{n,1}q_n + 2\psi_{12}\mu_{n,1}p_n, \quad (7.8)$$

$$p_{n+1}^2 = \psi_{21}^2 q_n^2 + \psi_{22}^2 p_n^2 + \mu_{n,2}^2 + 2\psi_{21}\psi_{22}q_n p_n + 2\psi_{21}\mu_{n,2}q_n + 2\psi_{22}\mu_{n,2}p_n, \quad (7.9)$$

$$\begin{aligned} q_{n+1}p_{n+1} &= \psi_{11}\psi_{21}q_n^2 + \psi_{12}\psi_{22}p_n^2 + \mu_{n,1}\mu_{n,2} + (\psi_{11}\psi_{22} + \psi_{12}\psi_{21})q_n p_n \\ &\quad + (\psi_{11}\mu_{n,2} + \psi_{21}\mu_{n,1})q_n + (\psi_{22}\mu_{n,1} + \psi_{12}\mu_{n,2})p_n. \end{aligned} \quad (7.10)$$

Assuming that the discretization schemes preserve the ergodic property of Langevin dynamics, taking the expectation of these equations and considering the limit as n goes to infinity allows us to compute the invariant average of the schemes, and thus to evaluate the perfect sampling bias introduced by the discretization.

7.4.1 Invariant Averages for Schemes Using the A, B and O Splitting

The analysis of schemes using the splitting strategy coded with the A, B and O pieces is particularly simple, as we use a new random number for each stochastic update meaning that the random numbers and state variables are not correlated between steps. Hence we have

$$\mathbb{E}(\mu_{n,i} q_n) = \mathbb{E}(\mu_{n,i} p_n) = 0,$$

for any i and n . Thus, taking expectations of (7.8)–(7.10) for such schemes, and then considering the limit $n \rightarrow \infty$ we obtain a closed, linear system of equations

$$\begin{aligned}\langle q^2 \rangle_h &= \psi_{11}^2 \langle q^2 \rangle_h + \psi_{12}^2 \langle p^2 \rangle_h + 2\psi_{11}\psi_{12} \langle qp \rangle_h + \bar{\mu}_{11}, \\ \langle p^2 \rangle_h &= \psi_{21}^2 \langle q^2 \rangle_h + \psi_{22}^2 \langle p^2 \rangle_h + 2\psi_{21}\psi_{22} \langle qp \rangle_h + \bar{\mu}_{22}, \\ \langle qp \rangle_h &= \psi_{11}\psi_{21} \langle q^2 \rangle_h + \psi_{12}\psi_{22} \langle p^2 \rangle_h + (\psi_{11}\psi_{22} + \psi_{12}\psi_{21}) \langle qp \rangle_h + \bar{\mu}_{12},\end{aligned}\tag{7.11}$$

where we have constants

$$\bar{\mu}_{11} = \mathbb{E}(\mu_{n,1}^2), \quad \bar{\mu}_{12} = \mathbb{E}(\mu_{n,1}\mu_{n,2}), \quad \bar{\mu}_{22} = \mathbb{E}(\mu_{n,2}^2).$$

We can solve this linear system to find the invariant averages computed by the chosen discretization scheme for the harmonic oscillator with Hamiltonian (7.6).

Example 7.1 Consider the scheme coded $\llbracket \text{ABO} \rrbracket$, where

$$\begin{aligned}\llbracket \text{ABO} \rrbracket \\ \mathbf{q}_{n+1} &= \mathbf{q}_n + h\mathbf{M}^{-1}\mathbf{p}_n \\ \mathbf{p}_{n+1/2} &= \mathbf{p}_n - h\nabla U(\mathbf{q}_{n+1}) \\ \mathbf{p}_{n+1} &= e^{-h\gamma} \mathbf{p}_{n+1/2} + \zeta \mathbf{M}^{1/2} \mathbf{R}_n\end{aligned}$$

with $\zeta = [\kappa_B T (1 - e^{-2\gamma h})]^{1/2}$, and \mathbf{R}_n a vector of unit normal random numbers. We can write this update scheme succinctly as

$$\begin{aligned}\mathbf{q}_{n+1} &= \mathbf{q}_n + h\mathbf{M}^{-1}\mathbf{p}_n, \\ \mathbf{p}_{n+1} &= e^{-h\gamma}\mathbf{p}_n - he^{-h\gamma}\nabla U(\mathbf{q}_n + h\mathbf{M}^{-1}\mathbf{p}_n) + \zeta\mathbf{M}^{1/2}\mathbf{R}_n.\end{aligned}$$

In the case of the one-dimensional harmonic oscillator, we have $U'(q) = \Omega^2 q$, yielding the compact form of one iteration as

$$\begin{bmatrix} q_{n+1} \\ p_{n+1} \end{bmatrix} = \begin{bmatrix} 1 & h/m \\ -\Omega^2 h e^{-h\gamma} & (1 - \Omega^2 h^2/m)e^{-h\gamma} \end{bmatrix} \begin{bmatrix} q_n \\ p_n \end{bmatrix} + \begin{bmatrix} 0 \\ \zeta m^{1/2} \mathbf{R}_n \end{bmatrix}. \quad (7.12)$$

Taking expectations of (7.12) and then taking the limit as $n \rightarrow \infty$, we see immediately that

$$\langle q \rangle_h^{[\text{ABO}]} = \langle p \rangle_h^{[\text{ABO}]} = 0,$$

as $\mathbb{E}(\mathbf{R}_n) = 0$. Plugging the values for ψ_{ij} into (7.11), with

$$\bar{\mu}_{11} = \bar{\mu}_{12} = 0, \quad \bar{\mu}_{22} = m\xi^2,$$

we can solve to find the exact value of the method's stationary averages. For example, the relative increase in the variance of position is computed for the $[\text{ABO}]$ scheme as

$$\begin{aligned}\frac{\langle q^2 \rangle_h^{[\text{ABO}]} - \langle q^2 \rangle}{\langle q^2 \rangle} &= \frac{e^{h\gamma} m (1 + e^{-h\gamma})^2}{2m(1 + e^{-h\gamma}) - h^2 \Omega^2 e^{-h\gamma}} \\ &= 1 + \gamma h/2 + (\Omega^2 + \gamma^2 m)h^2/(4m) + \mathcal{O}(h^3).\end{aligned}$$

Hence we can see that the $[\text{ABO}]$ scheme gives a first-order error in the variance of q . For significantly small friction (relative to h), the leading order term will be dominated by the term at order h^2 , potentially giving us greater accuracy than we would expect from a first order scheme.

However, we see that the error grows exponentially as γ gets large. We can explain this by returning to the definition of the scheme, which has an O step (stochastic fluctuation) immediately preceding the only A step (drift), wiping out all force information for infinite friction. In practice, playing with the friction coefficient can affect the rate at which averages converge towards the invariant average.

From the work in Chap. 3, we may expect that performing the integration steps symmetrically (by using a Strang splitting) could provide desirable higher order behavior. Computing the coefficients in (7.11) for the each of the symmetric

Table 7.1 The expected long-time computed average using the given second-order Langevin dynamics discretization scheme

Scheme	$\langle q^2 \rangle_h / \langle q^2 \rangle$	$\langle p^2 \rangle_h / \langle p^2 \rangle$	$\langle qp \rangle$
[[ABOBA]]	1	$[1 - h^2 \Omega^2 / (4m)]^{-1}$	0
[[OBABO]]	$[1 - h^2 \Omega^2 / (4m)]^{-1}$	1	0
[[BAOAB]]	1	$1 - h^2 \Omega^2 / (4m)$	0
[[OABAO]]	$1 - h^2 \Omega^2 / (4m)$	1	0

schemes, we are able to compute the exact expected average by solving the linear equations. The results are summarized in Table 7.1, where we have not considered the [[AOBOA]] and [[BOAOB]] schemes due to their inconsistency at large friction (this does not preclude the analysis, but limits each those method's usefulness in simulation). Similar analysis can be conducted for more complicated composition schemes involving multiple force evaluations.

The mentioned splitting schemes give a second-order error in the computed averages, but surprisingly each gives an exact result for computed averages of either position or momentum. The exactness property is not born out of the symmetry of the method, but rather of the specific order of terms and choice of splitting “building blocks”. Even non-symmetric first-order schemes can exhibit similar qualities. For example, analysis shows that the schemes denoted [[AOAB]] or [[BAOA]] both exhibit a first order error in the covariance $\langle qp \rangle_h = \mathcal{O}(h)$, however they give exact results for both $\langle q^2 \rangle_h$ and $\langle p^2 \rangle_h$.

7.4.2 More General Schemes

We can conduct a similar analysis for any integrator that we can express in the form (7.7), simply by plugging in the relevant constants and solving a linear equation. The difficulty lies when random numbers are reused, leading to correlation between steps. This requires careful treatment to compute the expectation.

Example 7.2 Consider the variant of the BBK integrator that recycles the random number between steps:

Brünger-Brooks-Karplus with post-step re-use of random number (BBK*)

$$\begin{aligned} \mathbf{p}_{n+1/2} &= (1 - h\gamma/2)\mathbf{p}_n - (h/2)\nabla U(\mathbf{q}_n) + \frac{1}{2}\sqrt{2k_B T h \gamma} \mathbf{M}^{1/2} \mathbf{R}_n \\ \mathbf{q}_{n+1} &= \mathbf{q}_n + h\mathbf{M}^{-1} \mathbf{p}_{n+1/2} \\ \mathbf{p}_{n+1} &= [\mathbf{p}_{n+1/2} - (h/2)\nabla U(\mathbf{q}_{n+1}) + \frac{1}{2}\sqrt{2k_B T h \gamma} \mathbf{M}^{1/2} \mathbf{R}_{n+1}] / (1 + h\gamma/2), \end{aligned}$$

where \mathbf{R}_n is a vector of normal random numbers with zero mean and unit variance. In some systems, it can be computationally expensive to generate normal random numbers for each degree of freedom, hence algorithms may re-use the random

numbers between iterations to give a small computational saving. We can see that only one vector of random numbers is generated per iteration, with the new vector of random numbers being used in the following iteration. This gives some correlation between steps that complicates our analysis a little.

If we wish to find the perfect sampling bias in the case of the one-dimensional harmonic oscillator, we can apply this technique to find the invariant averages under this scheme. We have

$$\begin{aligned}\Psi^{\text{BBK}^*} &= \begin{bmatrix} 1 - \frac{h^2\Omega^2}{2m} & \frac{h}{m} \left(1 - \frac{\gamma h}{2}\right) \\ \frac{h\Omega^2}{2m} \left(\frac{h^2\Omega^2 - 4m}{2 + \gamma h}\right) & \frac{(2 - \gamma h)(2m - h^2\Omega^2)}{2m(2 + \gamma h)} \end{bmatrix}, \\ \mu_n^{\text{BBK}^*} &= \begin{bmatrix} \sqrt{\frac{k_B T \gamma h^3}{2m}} R_n \\ \frac{\sqrt{2k_B T \gamma h m}}{2 + \gamma h} \left(\left(1 - \frac{h^2\Omega^2}{2m}\right) R_n + R_{n+1} \right) \end{bmatrix} = \begin{bmatrix} \kappa_1 R_n \\ \kappa_2 R_n + \kappa_3 R_{n+1} \end{bmatrix},\end{aligned}$$

using the notation in (7.7). Taking expectations of the resulting equations, we can compute the values of the constants in (7.8)–(7.10) and solve to find the long-time averages. Care must be taken however, as unlike the schemes using the ABO splitting we must include some correlation between steps. Denoting the entries of Ψ^{BBK^*} by ψ_{ij} we have

$$\begin{aligned}\mathbb{E}(\mu_{n,2} p_n) &= \mathbb{E}((\kappa_2 R_n + \kappa_3 R_{n+1})(\psi_{21} q_{n-1} + \psi_{22} p_{n-1} + \kappa_2 R_{n-1} + \kappa_3 R_n)), \\ &= \kappa_2 \kappa_3.\end{aligned}$$

This additional quantity will slightly change the expectation of (7.9) compared to the standard BBK method, and hence the overall averages of the scheme. Additionally it is easily shown that

$$\mathbb{E}(\mu_{n,1} q_n) = \mathbb{E}(\mu_{n,2} q_n) = 0, \quad \mathbb{E}(\mu_{n,1} p_n) = \kappa_1 \kappa_3,$$

with

$$\mathbb{E}(\mu_{n,1}^2) = \kappa_1^2, \quad \mathbb{E}(\mu_{n,1} \mu_{n,2}) = \kappa_1 \kappa_2, \quad \mathbb{E}(\mu_{n,2}^2) = \kappa_2^2 + \kappa_3^2.$$

Thus taking expectations of (7.8)–(7.10) and substituting in the constants gives

$$\begin{aligned}\langle q^2 \rangle_h^{\text{BBK}^*} &= \psi_{11}^2 \langle q^2 \rangle_h^{\text{BBK}^*} + \psi_{12}^2 \langle p^2 \rangle_h^{\text{BBK}^*} + 2\psi_{11}\psi_{12} \langle qp \rangle_h^{\text{BBK}^*} + 2\psi_{12}\kappa_1 2\psi_{12}\kappa_1 \kappa_3 \\ &\quad + \kappa_1^2, \\ \langle p^2 \rangle_h^{\text{BBK}^*} &= \psi_{21}^2 \langle q^2 \rangle_h^{\text{BBK}^*} + \psi_{22}^2 \langle p^2 \rangle_h^{\text{BBK}^*} + 2\psi_{21}\psi_{22} \langle qp \rangle_h^{\text{BBK}^*} + 2\psi_{22}\kappa_2 2\psi_{22}\kappa_2 \kappa_3 \\ &\quad + \kappa_2^2 + \kappa_3^2,\end{aligned}$$

$$\begin{aligned}\langle qp \rangle_h^{\text{BBK}^*} &= \psi_{11}\psi_{21}\langle q^2 \rangle_h^{\text{BBK}^*} + \psi_{12}\psi_{22}\langle p^2 \rangle_h^{\text{BBK}^*} + (\psi_{11}\psi_{22} + \psi_{12}\psi_{21})\langle qp \rangle_h^{\text{BBK}^*} \\ &\quad + \kappa_1\kappa_2 + \psi_{12}\kappa_2\kappa_3 + \psi_{22}\kappa_1\kappa_3.\end{aligned}$$

Finally, solving the simultaneous equations gives the stationary observed averages as

$$\begin{aligned}\langle q^2 \rangle_h^{\text{BBK}^*} &= \frac{k_B T}{\Omega^2} \left(1 - \frac{\Omega^2 h^2}{4m}\right)^{-1}, \quad \langle p^2 \rangle_h^{\text{BBK}^*} = k_B T m \left(1 + \frac{\gamma h}{2}\right)^{-1}, \\ \langle qp \rangle_h^{\text{BBK}^*} &= 0.\end{aligned}$$

For more general methods requiring multiple correlated random numbers, a further history than just one step is required to evaluate the expectation correctly.

7.5 Errors in Configurational Quantities for the Perturbed Harmonic Oscillator

We can consider applying the analysis of Sect. 7.4 to a more complicated example, however in general for nonlinear systems we cannot adopt the same strategy by taking expectations of the update equations, as we do not end up with a closed system of linear equations to solve (the force term now involves terms of higher orders). However, if the nonlinear terms in the force are preceded by a small constant, we can truncate the equations to provide an approximation to the invariant behavior. We consider sampling canonically the Hamiltonian

$$H(q, p) = p^2/2 + q^2/2 + \varepsilon q^4/4, \quad (7.13)$$

using Langevin dynamics, where $q, p \in \mathbb{R}$, with a small nonlinearity parameter $\varepsilon > 0$. As the canonical momentum distribution is always Gaussian (and hence trivial to sample), we will be far more concerned with the behavior of the (more interesting) distribution of position. The system can be thought of as the harmonic oscillator with a small nonlinear perturbation term, so the canonical configurational distribution will remain “close” to a Gaussian in some sense (this potential energy function is equivalent to an unforced Duffing Oscillator with no damping). In the limit as $\varepsilon \rightarrow 0$, we would expect the averages to converge to the results of Table 7.1.

We consider estimating the value of $\langle q^2 \rangle_h$ by truncating the equations governing the evolution of the averages in powers of ε (to ensure closure of the resulting simultaneous equations). We examine the expected behavior of the average in the case of the four second-order schemes listed in Table 7.1, although we may conduct this analysis for any similar scheme.

We find that truncating the update equations to $\mathcal{O}(\varepsilon^3)$ is sufficient to explicitly resolve the leading order behavior of the error for these discretization schemes, and we give the differences between observed numerical averages and exact averages below:

$$\begin{aligned}\langle q^2 \rangle_h^{[\text{ABOBA}]} - \langle q^2 \rangle &= \frac{3h^2\varepsilon [48\varepsilon - 4 + 3\varepsilon^2(9\varepsilon - 1)]}{12\varepsilon^2 + 16} + \mathcal{O}(\varepsilon h^4 + \varepsilon^3 h^2), \\ \langle q^2 \rangle_h^{[\text{BAOAB}]} - \langle q^2 \rangle &= -\frac{9h^2\varepsilon^2}{6\varepsilon^2 + 8} - \frac{3h^4\varepsilon^2 [6\varepsilon^4 + 19\varepsilon^2 + 16]}{8(3\varepsilon^2 + 4)^2} + \mathcal{O}(\varepsilon^2 h^6 + \varepsilon^3 h^2), \\ \langle q^2 \rangle_h^{[\text{OBABO}]} - \langle q^2 \rangle &= h^2 \left(\frac{1}{4} + \frac{\varepsilon [144\varepsilon + 81\varepsilon^2 - 9\varepsilon^2 - 12]}{12\varepsilon^2 + 16} \right) + \mathcal{O}(h^4 + \varepsilon^3 h^2), \\ \langle q^2 \rangle_h^{[\text{OABAO}]} - \langle q^2 \rangle &= -h^2 \left(\frac{1}{4} + \frac{18\varepsilon^2}{12\varepsilon^2 + 16} \right) + \mathcal{O}(h^4 + \varepsilon^3 h^2).\end{aligned}\tag{7.14}$$

The behavior of the methods can thus be summarized as

$$\begin{aligned}|\langle q^2 \rangle_h^{[\text{ABOBA}]} - \langle q^2 \rangle| &= O(\varepsilon h^2), \\ |\langle q^2 \rangle_h^{[\text{BAOAB}]} - \langle q^2 \rangle| &= O\left(\frac{\varepsilon^2 h^2}{1 + \varepsilon^2} + \varepsilon^2 h^4\right), \\ |\langle q^2 \rangle_h^{[\text{OBABO}]} - \langle q^2 \rangle| &= O(h^2), \\ |\langle q^2 \rangle_h^{[\text{OABAO}]} - \langle q^2 \rangle| &= O(h^2).\end{aligned}\tag{7.15}$$

We would expect that both the $[\text{ABOBA}]$ and $[\text{BAOAB}]$ schemes would have a leading error term proportional to ε , given that it was shown in Table 7.1 that in the pure harmonic case (at $\varepsilon = 0$) these methods give perfect sampling. The twofold surprising result though, is that (a) the leading error of the $[\text{BAOAB}]$ scheme has behavior proportional to ε^2 , while (b) the leading order term of the $[\text{BAOAB}]$ scheme is annihilated for large ε .

It would seem that by ordering the A, B and O update terms favourably in an algorithm we are able to achieve significant sampling improvements on systems that are “nearly harmonic”, at no extra cost (in terms of force evaluations).

To illustrate this numerically, we use each of the four given second order methods to compute the absolute error in $\langle q^2 \rangle_h$ using the one dimensional perturbed harmonic oscillator with Hamiltonian given in (7.13) at a range of timesteps $h \in [0.1, 2]$ and nonlinearity parameters $\varepsilon \in [0.0001, 1]$. We choose $\beta = \gamma = 1$ for all experiments, and run the schemes using each parameter set for a fixed time window of length 10^8 . The results are shown in Fig. 7.3, and qualitatively agree with the results of (7.15).

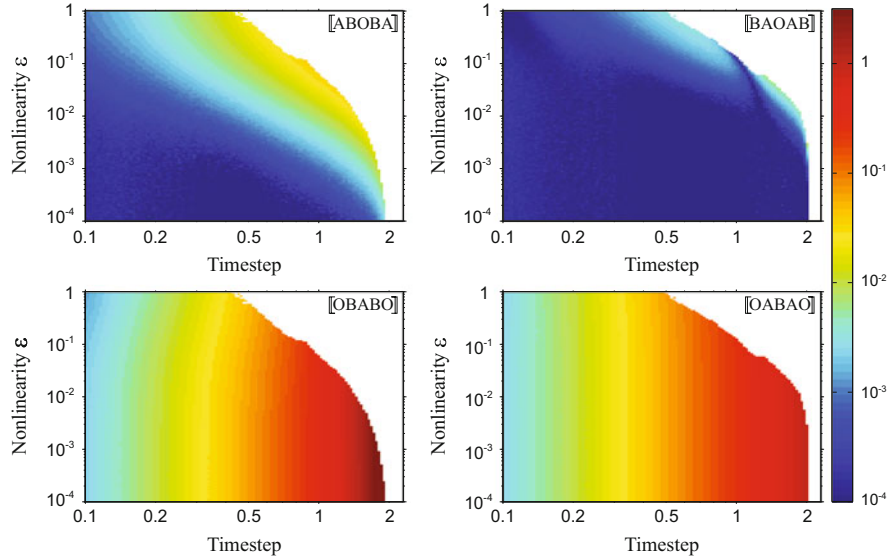


Fig. 7.3 Each pixel in the above grids marks the result of a numerical experiment using one of the four second order (in stepsize) symmetric Langevin discretization schemes. A pixel's color denotes the absolute error of $\langle q^2 \rangle_h$ from an experiment conducted at the given stepsize h (horizontal) and nonlinearity parameter ε (vertical) defining the potential energy in (7.13), with white pixels indicating instability. Experiments were taken over a sufficiently long time interval such that the observed errors are the result of discretization error, rather than sampling error

The $[\text{BAOAB}]$ scheme performs extremely well in this example, even in regimes of large ε and stepsize where our formal analysis is no longer valid. Though Table 7.1 demonstrates that both the $[\text{ABOBA}]$ and $[\text{BAOAB}]$ schemes give exact results at $\varepsilon = 0$, there remains qualitative difference between the two for positive ε , owing to the order ε^2 leading term in the latter scheme. If we are willing to accept an error of around 10^{-2} in our computed average, then in this example the $[\text{BAOAB}]$ scheme allows us to use a timestep considerably larger (even an order of magnitude larger at small ε) than the $[\text{OBABO}]$ or $[\text{OABAO}]$ schemes, for any value of ε tested.

7.6 An Exact Gibbs Sampling Method

The previous examples give some insight into the behavior of long-time averages for schemes applied to small models with simple oscillators, whereas in general for much larger systems with the full spectrum of molecular forces, it is much more difficult to offer concrete estimates on the efficacy of one method in comparison to another. Consider the splitting of Langevin dynamics into just two parts: the

deterministic Hamiltonian system taken first, followed by the Ornstein-Uhlenbeck equation for \mathbf{p} . The flows of each of these systems individually preserves the Gibbs distribution: denoting the Fokker-Planck operators associated to these flows by \mathcal{L}_H^\dagger and \mathcal{L}_O^\dagger we have

$$\mathcal{L}_H^\dagger \rho_\beta = 0, \quad \mathcal{L}_O^\dagger \rho_\beta = 0,$$

and hence

$$\exp(t\mathcal{L}_H^\dagger) \rho_\beta = \exp(t\mathcal{L}_O^\dagger) \rho_\beta = \rho_\beta.$$

We can consider the propagation of measure resulting from a numerical discretization defined by the composition of these two pieces. For a scheme $\llbracket \text{HO} \rrbracket$, we have the distribution first propagated under Hamiltonian dynamics, and then the momenta are evolved as the solution to the Ornstein-Uhlenbeck process, which clearly will preserve the Gibbs measure

$$\exp(h\mathcal{L}_O^\dagger) \left(\exp(h\mathcal{L}_H^\dagger) \rho_\beta \right) = \exp(h\mathcal{L}_O^\dagger) \rho_\beta = \rho_\beta.$$

The problem with this ‘‘method’’ is of course that it requires the exact flow map of the Hamiltonian system. However, this requirement can be relaxed. Given any divergence free vector field f , we have

$$-\nabla \cdot (f\rho) = -f \cdot \nabla \rho,$$

thus

$$\mathcal{L}_f^\dagger \rho = -\mathcal{L}_f \rho.$$

If \mathcal{L}_f preserves a first integral I , then \mathcal{L}_f preserves any distribution which is a function of I . It follows that any energy-preserving, divergence free vector field will always preserve the Gibbs distribution.

All symplectic methods preserve the volume, but for a system with no first integrals except the energy, it is known from a theorem of Ge and Marsden [400] that a symplectic method cannot preserve the system energy exactly (unless the symplectic method is itself a time-reparameterization of the exact solution). The options for volume preserving non-symplectic discretization methods that conserve energy exactly are limited (standard form schemes that rely on calculation of the vector field at a few points cannot achieve this [380]).

A class of methods that do provide the necessary features can be found in the work of Feng Kang [133], referred to as J-splitting by McLachlan and Quispel [261]. Let \mathbf{J} be the skew-symmetric canonical symplectic structure matrix. The idea is to consider a splitting of \mathbf{J} into a finite number K of skew-symmetric matrices \mathbf{J}_i , $i = 1, \dots, K$. This induces a splitting of the Hamiltonian vector field into K vector

fields $f_i = \mathbf{J}_i \nabla H$. Each of these vector fields preserves H and, because they are themselves Hamiltonian, their flows are also volume-preserving. Assuming each such vector field is exactly integrable, the system dynamics may be approximated by composing the flow maps for each vector field.

As an example of such a J -splitting, we may take $K = N_c$ with each \mathbf{J}_i to be defined by the components of the canonical symplectic structure matrix having to do with the i th position and momentum pair, thus the equations of motion for the i th vector field become

$$\dot{q}_i = \frac{p_i}{m_i}, \quad \dot{p}_i = -\frac{\partial U}{\partial q_i}(\bar{q}_1, \dots, \bar{q}_{i-1}, q_i, \bar{q}_{i+1}, \dots, \bar{q}_{N_c}),$$

where components with a bar over them are fixed during the calculation. This is, itself, a Hamiltonian system with a single degree of freedom q_i and the potential $\hat{U}_i(q_i)$ obtained by freezing all other components in the original potential function. Any such 1-dof Hamiltonian system is formally integrable (albeit in quadratures). Thus, if we are willing to solve a system using quadrature, we have a numerical method for the Hamiltonian system which preserves volume and energy. We solve each such dynamics from $i = 1$ to N_c , updating the values of each (q_i, p_i) in sequence (the temporally contiguous nature of the updates rules it out as a strategy for parallel computation).

Although this method can be applied to molecular systems, its implementation is challenging and it is not recommended for general computation. Some systems may have a structure amenable to exploitation via this splitting strategy, or it could potentially serve as a starting point in some special purpose methods. For another use of J -splitting in the setting of Metropolis correction of deterministic methods, see [48].

7.7 The Evolution of the Distribution Using a Numerical Method

In this section, we shall give an approach that allows the computation of the errors introduced by the discretization of Langevin dynamics for more general potential energy functions. The discretization schemes we shall consider will be those created by composition of the A, B and O splitting pieces described earlier in this chapter, but in principle we can apply this analysis to a wider class of SDE methods. We outline the basic approach for determining the leading order behavior of the discretization error introduced by our SDE integration scheme (see [221–223]), based on expansions due to Talay and Tubaro [357, 358].

In Chap. 3 we employed an asymptotic expansion of the conserved energy-like quantity of a numerical method in powers of the stepsize. By positing such an expansion we are able to calculate the term of any order directly, using a recursive approach. Given such an expansion of the Hamiltonian, we have a corresponding

expansion of the vector field, and therefore a similar expansion of the Liouvillian operator.

We begin by defining the generator $\hat{\mathcal{L}}$ associated to the propagation of averages under the numerical method for an SDE. We think of this generator as a perturbation of the exact Langevin dynamics generator \mathcal{L}_{LD} , or

$$\hat{\mathcal{L}} = \mathcal{L}_{\text{LD}} + h\mathcal{L}_1 + h^2\mathcal{L}_2 + h^3\mathcal{L}_3 + \mathcal{O}(h^4). \quad (7.16)$$

However, the operators involved are not equivalent to the operators that would arise from any stochastic differential equation (see [403]), so we must give up the direct analogy between the formal series and continuous SDE models (which is available in the deterministic setting). Nonetheless, it is possible to analyze the resulting operator expansion in a formal way.

We shall similarly consider the invariant (or native) distribution $\hat{\rho}$. We write this invariant distribution as a perturbation of the (target) canonical distribution

$$\hat{\rho} = \rho_\beta [1 + hf_1 + h^2f_2 + h^3f_3 + \mathcal{O}(h^4)], \quad (7.17)$$

with each *correction function* $f_k(\mathbf{q}, \mathbf{p})$ satisfying

$$\int_{\mathcal{D}} f_k(\mathbf{q}, \mathbf{p}) \rho_\beta(\mathbf{q}, \mathbf{p}) d\omega = 0,$$

ensuring a useful equivalence in the partition function

$$\int_{\mathcal{D}} \hat{\rho}(\mathbf{q}, \mathbf{p}) d\omega = \int_{\mathcal{D}} \rho_\beta(\mathbf{q}, \mathbf{p}) d\omega.$$

Our computed average is therefore

$$\langle \phi \rangle_h \stackrel{\text{def}}{=} \int_{\mathcal{D}} \phi(\mathbf{q}, \mathbf{p}) \hat{\rho}(\mathbf{q}, \mathbf{p}) d\omega.$$

The invariant distribution can, itself, be calculated by a formal expansion in powers of h , although in general this requires the solution of partial differential equations for the terms f_k . In some limiting cases it is possible to write down the solutions explicitly and to obtain, therefore, an understanding of the error induced in an average computed using a numerical method.

7.7.1 Expansion of the Operator $\hat{\mathcal{L}}$

Consider a Langevin splitting method using the A, B and O splitting pieces, where we compose exact solves of each of the vector fields in a prescribed sequence to define our discretization scheme. Because we solve each piece exactly, we are able to write down the action of each individual solve on the initial distribution in terms of the vector field's evolution operator (using the respective generators for each piece as in [99]), where

$$\begin{aligned}(e^{t\mathcal{L}_A}\phi)(\mathbf{q}, \mathbf{p}) &= \phi(\mathbf{q} + tM^{-1}\mathbf{p}, \mathbf{p}), \\ (e^{t\mathcal{L}_B}\phi)(\mathbf{q}, \mathbf{p}) &= \phi(\mathbf{q}, \mathbf{p} - t\nabla U(\mathbf{q})), \\ (e^{t\mathcal{L}_O}\phi)(\mathbf{q}, \mathbf{p}) &= \int_{\mathcal{P}} \phi\left(\mathbf{q}, e^{-\gamma t}\mathbf{p} + \zeta M^{1/2}\mathbf{x}\right) \frac{e^{-|\mathbf{x}|^2/2}}{(2\pi)^{N_c/2}} d\mathbf{x},\end{aligned}$$

where $\zeta = [k_B T (1 - e^{-2\gamma t})]^{1/2}$. The overall generator for an associated Langevin splitting method $\hat{\mathcal{L}}$ can be computed by composing each individual operator associated to the terms in the splitting. For example, for the method labelled by the string $\llbracket \text{ABAO} \rrbracket$, we have

$$\exp(h\hat{\mathcal{L}}_{\llbracket \text{ABAO} \rrbracket}) = \exp((h/2)\mathcal{L}_A) \exp(h\mathcal{L}_B) \exp((h/2)\mathcal{L}_A) \exp(h\mathcal{L}_O),$$

where importantly note the apparent reversal of the sequence of products, known as the *vertauschungssatz* (see the discussion in [164, Section III.5.1]), which is a consequence of the relation

$$\phi(\mathcal{U}_t^{f_1}(z)) = (e^{t\mathcal{L}_{f_1}}\phi)(z),$$

for some vector field f_1 with associated flow map $\mathcal{U}_t^{f_1}$ and generator \mathcal{L}_{f_1} , where the choice of $\phi(z) = \mathcal{U}_t^{f_2}(z) = (e^{t\mathcal{L}_{f_2}}\text{Id})(z)$ demonstrates this reversal.

We will find it more convenient to work with the adjoint of the perturbed generator, denoted $\hat{\mathcal{L}}^\dagger$, which we may compute as

$$\exp(h\hat{\mathcal{L}}_{\llbracket \text{ABAO} \rrbracket}^\dagger) = \exp(h\mathcal{L}_O^\dagger) \exp((h/2)\mathcal{L}_A^\dagger) \exp(h\mathcal{L}_B^\dagger) \exp((h/2)\mathcal{L}_A^\dagger).$$

Under the propagation of the numerical scheme (or the discretized dynamics), the Fokker-Planck equation gives us that the evolution of a density of points ρ is given by

$$\frac{\partial}{\partial t} \rho(z, t) = \hat{\mathcal{L}}^\dagger \rho,$$

with the important case of its invariant distribution satisfying the partial differential equation

$$\hat{\mathcal{L}}^\dagger \hat{\rho} = 0.$$

Our goal in the following section is to find $\hat{\mathcal{L}}^\dagger$ and solve the PDE for the distribution $\hat{\rho}$ by using our ansatz (7.17). The solution gives us the corrupted invariant distribution sampled by our numerical scheme, allowing us to correct our observed averages to achieve more accurate results. It also gives us a way of evaluating which schemes are best for sampling, by evaluating the error introduced by the discretization.

The terms of the perturbation expansion for $\hat{\mathcal{L}}^\dagger$ can be computed using the Baker-Campbell-Hausdorff (BCH) expansion already introduced in Chap. 3. Recall that for linear operators X and Y , we can write the composition of their exponentials as

$$\exp(hX) \exp(hY) = \exp(hZ),$$

where we have the expansion

$$Z = X + Y + \frac{h}{2}[X, Y] + \frac{h^2}{12}([X, [X, Y]] + [Y, [Y, X]]) + \mathcal{O}(h^3).$$

The notation $[X, Y] \stackrel{\text{def}}{=} XY - YX$ represents the commutator of the operators X and Y . By repeated application of the BCH formula, we can obtain such an expansion for any splitting-based method, however the terms grow in complexity at successive powers of h , requiring commutators of increasing length that make computation cumbersome. Additionally any careful mathematician should question the convergence of this sequence when computing $\hat{\mathcal{L}}$, as we deal only with formal series that offer no guidance on the boundedness of the resulting terms, which will involve high order derivatives in both \mathbf{q} and \mathbf{p} .

To offer some reassurance, let us define the evolution operator for our numerical method as

$$\mathcal{P}_t = e^{t\hat{\mathcal{L}}} = e^{t\mathcal{L}_1} e^{t\mathcal{L}_2} \dots e^{t\mathcal{L}_k},$$

where the numerical method has k -many stages with each \mathcal{L}_i proportional to one of \mathcal{L}_A , \mathcal{L}_B and \mathcal{L}_O . We can make use of Taylor's theorem to write the identity

$$\mathcal{P}_h = \mathcal{P}_0 + h \left. \frac{d\mathcal{P}_t}{dt} \right|_{t=0} + \dots + \frac{h^n}{n!} \left. \frac{d^n\mathcal{P}_t}{dt^n} \right|_{t=0} + \frac{h^{n+1}}{n!} \int_0^1 (1-\lambda)^n \left. \frac{d^{n+1}\mathcal{P}_t}{dt^{n+1}} \right|_{t=\lambda h} d\lambda,$$

for some finite truncation index $n \in \{1, 2, 3, \dots\}$. The remainder term at order h^{n+1} will involve the integration of finitely many derivatives of its argument. Hence for observables of sufficient smoothness with compact support, this remainder term will remain bounded (see [223]).

7.7.2 First Order Operator Expansion

As we consider schemes involving compositions of three splitting pieces, the minimum number of stages to our methods (in order for it to be consistent) will be three. The perturbed Fokker-Planck operator for a splitting method with three stages will be computed as

$$\exp(hS) = \exp(hZ) \exp(hY) \exp(hX), \quad (7.18)$$

where X, Y and Z are one of \mathcal{L}_A^\dagger , \mathcal{L}_B^\dagger and \mathcal{L}_O^\dagger . Let us work the first terms of this expansion out, retaining terms involving triple products only

$$\exp(hY) \exp(hX) = \exp\left(h\left((Y + X) + \frac{h}{2}[Y, X] + \frac{h^2}{12}([Y, Y, X] + [X, X, Y]) + \dots\right)\right),$$

where the notation $[A, B, C]$ is notation for $[A, [B, C]]$. Applying this formula one more time in (7.18), we find

$$\begin{aligned} S &= X + Y + Z + \frac{h}{2}[Y, X] + \frac{h^2}{12}([Y, [Y, X]] + [X, [X, Y]]) \\ &\quad + \frac{h}{2}\left[Z, Y + X + \frac{h}{2}[Y, X]\right] \\ &\quad + \frac{h^2}{12}([Z, [Z, Y + X]] - [Y + X, [Z, Y + X]]) + \dots \\ &= X + Y + Z + \frac{h}{2}([Z, Y] + [Z, X] + [Y, X]) + \frac{h^2}{4}[Z, Y, X] \\ &\quad + \frac{h^2}{12}([Y, Y, X] + [X, X, Y] + [Z, Z, Y] + [Z, Z, X] \\ &\quad + [Y + X, Y + X, Z]) + \dots \end{aligned}$$

In general the terms in this expansion will lead to complicated expansions. In the case of deterministic systems, the operators are always first order due to equality of mixed partials (the 2nd order derivatives are cancelled). Due to the second derivatives present in the \mathcal{L}_O^\dagger operator, derivatives of all orders will appear in the

expansion of the SDE method. The series expansion is therefore not particularly informative on its own, but only in relation to its action on some particular distribution.

A simple first order example of a Langevin dynamics integrator is the method obtained by composing one of the Symplectic Euler variants with an Ornstein-Uhlenbeck step. To get a feel for how the expansion goes, let us work out its terms for such a splitting scheme in the case of a one degree of freedom model with unit mass: $H = p^2/2 + U(q)$. To be explicit, let us say our numerical method first solves exactly the OU process, then evaluates the impulse due to the force $-U'(q)$ and lastly drifts in position space according to the momentum. This method is denoted in our notation as $\llbracket \text{OBA} \rrbracket$, where the evolution of measure in one step can be computed by writing

$$\exp(h\hat{\mathcal{L}}_{\llbracket \text{OBA} \rrbracket}^\dagger) = \exp(h\mathcal{L}_A^\dagger) \exp(h\mathcal{L}_B^\dagger) \exp(h\mathcal{L}_O^\dagger).$$

In this one dimensional example, we substitute

$$\begin{aligned} Z &= \mathcal{L}_A^\dagger = -p \frac{\partial}{\partial q}, & Y &= \mathcal{L}_B^\dagger = U'(q) \frac{\partial}{\partial p}, \\ X &= \mathcal{L}_O^\dagger = \gamma \left(\text{Id} + p \frac{\partial}{\partial p} \right) + \frac{\sigma^2}{2} \frac{\partial^2}{\partial p^2}, \end{aligned}$$

into (7.18), where $\sigma = \sqrt{2\gamma k_B T}$. This gives us an expansion for the Kolmogorov operator for our discretized map

$$\hat{\mathcal{L}}_{\llbracket \text{OBA} \rrbracket}^\dagger = S = \mathcal{L}_A^\dagger + \mathcal{L}_B^\dagger + \mathcal{L}_O^\dagger + \frac{h}{2} \left([\mathcal{L}_A^\dagger, \mathcal{L}_B^\dagger] + [\mathcal{L}_A^\dagger, \mathcal{L}_O^\dagger] + [\mathcal{L}_B^\dagger, \mathcal{L}_O^\dagger] \right) + \dots$$

It is clear that even writing out the $\mathcal{O}(h^2)$ terms considerably increases the complexity of the right hand side.

The commutators are best considered in relation to their action on a function (or rather, their action on a density) $\rho(q, p)$. For example, we may compute directly

$$\begin{aligned} [\mathcal{L}_A^\dagger, \mathcal{L}_B^\dagger]\rho &= -p \frac{\partial}{\partial q} \left(U'(q) \frac{\partial \rho}{\partial p} \right) - U'(q) \frac{\partial}{\partial p} \left(-p \frac{\partial \rho}{\partial q} \right) \\ &= -p(U'(q)\rho_p)_q + U'(q)(p\rho_q)_p, \\ &= -pU''(q)\rho_p - pU'(q)\rho_{pq} + U'(q)\rho_q + U'(q)p\rho_{qp}. \end{aligned}$$

As this is the commutator of two 1st order differential operators, the mixed partial term vanishes, leaving

$$[\mathcal{L}_A^\dagger, \mathcal{L}_B^\dagger]\rho = -pU''(q)\rho_p + U'(q)\rho_q.$$

Similar computations give

$$[\mathcal{L}_A^\dagger, \mathcal{L}_O^\dagger]\rho = \gamma p \rho_q + \sigma^2 \rho_{qp},$$

$$[\mathcal{L}_B^\dagger, \mathcal{L}_O^\dagger]\rho = \gamma U'(q) \rho_p.$$

To first order, the discretization map corresponding to scheme [OBA] alters the phase space density at each step as if it were solving the time dependent PDE

$$\rho_t = \hat{\mathcal{L}}^\dagger \rho,$$

where

$$\hat{\mathcal{L}}^\dagger \rho = \mathcal{L}_{LD}^\dagger \rho + \frac{h}{2} [-pU''(q)\rho_p + U'(q)\rho_q + \gamma p \rho_q + \sigma^2 \rho_{qp} + \gamma U'(q)\rho_p] + \mathcal{O}(h^2).$$

The validity of this sort of expansion, even for small h , should be considered carefully. Defining

$$\mathcal{L}_{LD}^\dagger = \mathcal{L}_A^\dagger + \mathcal{L}_B^\dagger + \mathcal{L}_O^\dagger$$

as the Kolmogorov operator for Langevin dynamics, the assumption of validity becomes more credible as we find that the operator \mathcal{L}_{LD}^\dagger has a compact resolvent and therefore a discrete spectrum, i.e. simple eigenvalues, as discussed in the previous chapter. It will have one zero eigenvalue corresponding to the invariant density ρ_β and all the remaining eigenvalues lie in the negative half plane. Of course it is not just this operator whose properties are important, but also all the other operators arising in the expansion, and bounding these in relation to \mathcal{L}_{LD}^\dagger is not a simple task (particularly for higher orders).

7.7.3 Perturbation Technique

Suppose we are able to derive a series expansion for $\hat{\mathcal{L}}^\dagger$ of the form

$$\hat{\mathcal{L}}^\dagger = \mathcal{L}_{LD}^\dagger + h\mathcal{L}_1^\dagger + h^2\mathcal{L}_2^\dagger + \mathcal{O}(h^3),$$

for some perturbation operators \mathcal{L}_i^\dagger . We assume that the invariant density has a similar expansion in powers of the stepsize, of the form given in (7.17). Inserting this ansatz into the stationary Fokker-Planck equation

$$\hat{\mathcal{L}}^\dagger \hat{\rho} = 0,$$

we obtain

$$\left(\mathcal{L}_{\text{LD}}^\dagger + h\mathcal{L}_1^\dagger + h^2\mathcal{L}_2^\dagger + \mathcal{O}(h^3) \right) (\rho_\beta[1 + hf_1 + h^2f_2 + \mathcal{O}(h^3)]) = 0.$$

Combining like powers, we have at zero'th order, the equation

$$\mathcal{L}_{\text{LD}}^\dagger \rho_\beta = 0,$$

which we know to hold since Langevin dynamics preserves the canonical ensemble. At first order we obtain

$$\mathcal{L}_{\text{LD}}^\dagger(\rho_\beta f_1) + \mathcal{L}_1^\dagger \rho_\beta = 0. \quad (7.19)$$

If \mathcal{L}_1^\dagger is known, we can calculate its action on ρ_β , giving an inhomogeneity for the above partial differential equation. It will be difficult to solve the perturbation equation (7.19) in general, although its linearity and the fact that $\mathcal{L}_{\text{LD}}^\dagger$ (with our assumptions) has a compact resolvent (and therefore a discrete spectrum) together imply that if the perturbation can be bounded, then it should be possible to solve for the correction function. We expect that this solution should be stable with respect to perturbation (and exponentially attracting). This also implies global existence (for all positive time) of the semigroup defining the solution of the time-dependent problem. We do not provide such a rigorous result here but simply plunge ahead, in the best tradition of applied mathematics, to obtain a perturbative expansion; verification of our results must therefore be obtained by numerical experiment, *a posteriori*.

The leading order errors can be computed in simulation by exploiting the specific form of our ansatz for the invariant measure associated to the discretized dynamics. For some observable $\vartheta(\mathbf{q}, \mathbf{p})$, we have that

$$\begin{aligned} \langle \vartheta \rangle_h &= \int_{\mathcal{D}} \vartheta(\mathbf{q}, \mathbf{p}) \hat{\rho}(\mathbf{q}, \mathbf{p}) d\omega, \\ &= \int_{\mathcal{D}} \vartheta(\mathbf{q}, \mathbf{p}) \rho_\beta(\mathbf{q}, \mathbf{p}) (1 + hf_1(\mathbf{q}, \mathbf{p}) + h^2f_2(\mathbf{q}, \mathbf{p}) + \dots) d\omega, \\ &= \int_{\mathcal{D}} \vartheta(\mathbf{q}, \mathbf{p}) \rho_\beta(\mathbf{q}, \mathbf{p}) d\omega + h \int_{\mathcal{D}} \vartheta(\mathbf{q}, \mathbf{p}) f_1(\mathbf{q}, \mathbf{p}) \rho_\beta(\mathbf{q}, \mathbf{p}) d\omega + \dots, \\ &= \langle \vartheta \rangle + h \langle \vartheta f_1 \rangle + h^2 \langle \vartheta f_2 \rangle + \dots \end{aligned}$$

Hence by obtaining the correction functions f_i , we are able to apply a modification to our computed expectation in order to recover the true canonical average.

7.8 First Order Schemes

Let us consider a scheme of the form $\llbracket XYZ \rrbracket$, where each letter in the string is distinct and corresponds to one of the A, B or O Langevin splitting pieces (giving six possible schemes). Given the simple structure of the scheme, we expect to recover a first order error in our invariant (long-time) averages. By composing the semigroup operators

$$\exp(h\mathcal{L}_{\llbracket XYZ \rrbracket}^\dagger) = \exp(h\mathcal{L}_Z^\dagger) \exp(h\mathcal{L}_Y^\dagger) \exp(h\mathcal{L}_X^\dagger),$$

and computing the terms in the BCH expansion, we have

$$\hat{\mathcal{L}}_{\llbracket XYZ \rrbracket}^\dagger = \mathcal{L}_{LD}^\dagger + h\mathcal{L}_{1,\llbracket XYZ \rrbracket}^\dagger + \mathcal{O}(h^2),$$

where

$$\mathcal{L}_{1,\llbracket XYZ \rrbracket}^\dagger = -\frac{1}{2} \left([\mathcal{L}_X^\dagger, \mathcal{L}_Y^\dagger] + [\mathcal{L}_X^\dagger, \mathcal{L}_Z^\dagger] + [\mathcal{L}_Y^\dagger, \mathcal{L}_Z^\dagger] \right). \quad (7.20)$$

The first order correction function for this scheme is then given by the particular solution to the PDE,

$$\mathcal{L}_{LD}^\dagger (f_{1,\llbracket XYZ \rrbracket} \rho_\beta) = -\mathcal{L}_{1,\llbracket XYZ \rrbracket}^\dagger \rho_\beta. \quad (7.21)$$

The general solution of (7.21) will consist of the sum of the homogeneous solution $f_{1,\llbracket XYZ \rrbracket}^{[HS]}(\mathbf{q}, \mathbf{p})$ and particular solution $f_{1,\llbracket XYZ \rrbracket}^{[PS]}(\mathbf{q}, \mathbf{p})$ in the usual way. However, since $\mathcal{L}_{LD}^\dagger \vartheta = 0$ has as its only solution $\vartheta \propto \rho_\beta$, the homogeneous solution of (7.21) is

$$f_{1,\llbracket XYZ \rrbracket}^{[HS]}(\mathbf{q}, \mathbf{p}) = c,$$

for some constant c . Our assumption that $\langle f_{1,\llbracket XYZ \rrbracket} \rangle = 0$ means that $c = -\langle f_{1,\llbracket XYZ \rrbracket}^{[PS]} \rangle$, and hence we only require a particular solution $f_{1,\llbracket XYZ \rrbracket}^{[PS]}(\mathbf{q}, \mathbf{p})$.

Thus for any first order scheme our line of attack will be to compute the perturbation operator \mathcal{L}_1^\dagger , plug it into the right hand side and solve the PDE to find the suitable correction function. It turns out that this is not so difficult at leading order, for simple first order schemes such as this. However at higher orders the complexity of the terms often limits our progress.

7.8.1 Computing the Correction Functions $f_1(\mathbf{q}, \mathbf{p})$

At this point we may plow ahead and compute the PDE for each corresponding scheme, but a more efficient route is offered by working with the structure of the inhomogeneity in (7.21). We may make use of the identity

$$\left([\mathcal{L}_O^\dagger, \mathcal{L}_A^\dagger] + [\mathcal{L}_O^\dagger, \mathcal{L}_B^\dagger]\right) \rho_\beta = \left([\mathcal{L}_O^\dagger, \mathcal{L}_A^\dagger + \mathcal{L}_B^\dagger]\right) \rho_\beta = 0,$$

as of course $\mathcal{L}_H^\dagger = \mathcal{L}_A^\dagger + \mathcal{L}_B^\dagger$ is the Liouvillian of our Hamiltonian system, which preserves any function of the energy. Thus, by the skew-symmetry of the commutator ($[P, Q] = -[Q, P]$) we can relate four of the six methods as

$$\mathcal{L}_{1, [\text{ABO}]}^\dagger \rho_\beta = \mathcal{L}_{1, [\text{OAB}]}^\dagger \rho_\beta = -\mathcal{L}_{1, [\text{OBA}]}^\dagger \rho_\beta = -\mathcal{L}_{1, [\text{BAO}]}^\dagger \rho_\beta = -\frac{1}{2} [\mathcal{L}_A^\dagger, \mathcal{L}_B^\dagger] \rho_\beta, \quad (7.22)$$

by virtue of (7.20). Hence the leading order correction functions of the schemes are related through

$$f_{1, [\text{ABO}]} = f_{1, [\text{OAB}]} = -f_{1, [\text{OBA}]} = -f_{1, [\text{BAO}]} . \quad (7.23)$$

The remaining two permutations of the possible $[\text{XYZ}]$ schemes have a similar relationship, with

$$\mathcal{L}_{1, [\text{AOB}]}^\dagger \rho_\beta = -\mathcal{L}_{1, [\text{BOA}]}^\dagger \rho_\beta = -\frac{1}{2} [\mathcal{L}_A^\dagger - \mathcal{L}_B^\dagger, \mathcal{L}_O^\dagger] \rho_\beta + \mathcal{L}_{1, [\text{ABO}]}^\dagger \rho_\beta. \quad (7.24)$$

This reduces our workload as we can find the leading order behavior for all six methods by computing the solution to two PDEs. This is not necessarily trivial, but it turns out that the structure of the equations is simple enough that we can find exact solutions. We work now to compute the right-hand side of the governing PDE given in (7.21).

In order to solve (7.21) for the $[\text{ABO}]$ scheme, we need to compute the right hand side of (7.22). First, note that if we define the function $g(\mathbf{q}, \mathbf{p})$ as

$$g(\mathbf{q}, \mathbf{p}) = \beta \mathbf{p}^T \mathbf{M}^{-1} \nabla U(\mathbf{q}),$$

then through simple computation we have

$$\mathcal{L}_A^\dagger \rho_\beta = -\mathcal{L}_B^\dagger \rho_\beta = g(\mathbf{q}, \mathbf{p}) \rho_\beta.$$

This is particularly useful as

$$\begin{aligned} [\mathcal{L}_A^\dagger, \mathcal{L}_B^\dagger] \rho_\beta &= (\mathcal{L}_A^\dagger \mathcal{L}_B^\dagger - \mathcal{L}_B^\dagger \mathcal{L}_A^\dagger) \rho_\beta = -(\mathcal{L}_A^\dagger + \mathcal{L}_B^\dagger)(g(\mathbf{q}, \mathbf{p}) \rho_\beta) \\ &= (\mathcal{L}_O^\dagger - \mathcal{L}_{LD}^\dagger)(g(\mathbf{q}, \mathbf{p}) \rho_\beta). \end{aligned}$$

Now notice that for a function $\psi(\mathbf{q})$ purely of position, we have

$$\mathcal{L}_{LD}^\dagger(\psi(\mathbf{q}) \rho_\beta) = -(\mathbf{p}^T \mathbf{M}^{-1} \nabla \psi(\mathbf{q})) \rho_\beta(\mathbf{q}, \mathbf{p}),$$

and hence we can compute

$$\begin{aligned} \mathcal{L}_O^\dagger(g(\mathbf{q}, \mathbf{p}) \rho_\beta) &= \gamma \rho_\beta(-p \cdot \nabla_p g(\mathbf{q}, \mathbf{p}) + \beta^{-1} \nabla_p \cdot \mathbf{M} \nabla_p g(\mathbf{q}, \mathbf{p})) \\ &= -\gamma g(\mathbf{q}, \mathbf{p}) \rho_\beta, \\ &= \gamma \beta \mathcal{L}_{LD}^\dagger(U(\mathbf{q}) \rho_\beta). \end{aligned}$$

This means that

$$\mathcal{L}_{I, [\text{ABO}]}^\dagger \rho_\beta = -\frac{1}{2} [\mathcal{L}_A^\dagger, \mathcal{L}_B^\dagger] \rho_\beta = -\frac{1}{2} \mathcal{L}_{LD}^\dagger([\gamma \beta U(\mathbf{q}) - g(\mathbf{q}, \mathbf{p})] \rho_\beta).$$

Hence, we can combine this equation with (7.21) to yield

$$\mathcal{L}_{LD}^\dagger f_{I, [\text{ABO}]} \rho_\beta = \frac{1}{2} \mathcal{L}_{LD}^\dagger([\gamma \beta U(\mathbf{q}) - g(\mathbf{q}, \mathbf{p})] \rho_\beta),$$

with the general solution

$$f_{I, [\text{ABO}]} = \frac{\beta}{2} (\gamma U(\mathbf{q}) - \mathbf{p}^T \mathbf{M}^{-1} \nabla U(\mathbf{q}) - c),$$

where $c = \gamma \langle U(\mathbf{q}) \rangle$ is a constant, chosen to ensure that the average of the correction function is zero. This solution gives the leading order correction for the three related schemes in (7.23).

For the final two schemes, we can compute the correction function through the use of (7.24). Our previous work has computed the second term on the right hand side already, so we are left with the initial term. However, its expression reduces quite easily, as

$$\begin{aligned} [\mathcal{L}_A^\dagger - \mathcal{L}_B^\dagger, \mathcal{L}_O^\dagger] \rho_\beta &= -\mathcal{L}_O^\dagger(\mathcal{L}_A^\dagger - \mathcal{L}_B^\dagger) \rho_\beta, \\ &= -2\mathcal{L}_O^\dagger(g(\mathbf{q}, \mathbf{p}) \rho_\beta), \\ &= -2\gamma \beta \mathcal{L}_{LD}^\dagger(U(\mathbf{q}) \rho_\beta). \end{aligned}$$

And hence we have

$$\mathcal{L}_{\text{LD}}^\dagger(f_{1,\llbracket \text{AOB} \rrbracket}\rho_\beta) = \mathcal{L}_{\text{LD}}^\dagger(f_{1,\llbracket \text{ABO} \rrbracket}\rho_\beta) - \gamma\beta\mathcal{L}_{\text{LD}}^\dagger(U(q)\rho_\beta),$$

giving the general solution

$$f_{1,\llbracket \text{AOB} \rrbracket} = -\frac{\beta}{2}(\gamma U(q) + \mathbf{p}^T \mathbf{M}^{-1} \nabla U(\mathbf{q}) - c),$$

for the same choice of c .

Hence using the symmetry in the commutators we are able to solve for the leading order corrections for each of the schemes of the form $\llbracket \text{XYZ} \rrbracket$. In summary, we find that

$$f_{1,\llbracket \text{ABO} \rrbracket}(\mathbf{q}, \mathbf{p}) = f_{1,\llbracket \text{OAB} \rrbracket}(\mathbf{q}, \mathbf{p}) = \frac{\beta}{2}(\gamma U(\mathbf{q}) - \mathbf{p}^T \mathbf{M}^{-1} \nabla U(\mathbf{q}) - c), \quad (7.25a)$$

$$f_{1,\llbracket \text{OBA} \rrbracket}(\mathbf{q}, \mathbf{p}) = f_{1,\llbracket \text{BAO} \rrbracket}(\mathbf{q}, \mathbf{p}) = -\frac{\beta}{2}(\gamma U(\mathbf{q}) - \mathbf{p}^T \mathbf{M}^{-1} \nabla U(\mathbf{q}) - c), \quad (7.25b)$$

$$f_{1,\llbracket \text{AOB} \rrbracket}(\mathbf{q}, \mathbf{p}) = -\frac{\beta}{2}(\gamma U(\mathbf{q}) + \mathbf{p}^T \mathbf{M}^{-1} \nabla U(\mathbf{q}) - c), \quad (7.25c)$$

$$f_{1,\llbracket \text{BOA} \rrbracket}(\mathbf{q}, \mathbf{p}) = \frac{\beta}{2}(\gamma U(\mathbf{q}) + \mathbf{p}^T \mathbf{M}^{-1} \nabla U(\mathbf{q}) - c), \quad (7.25d)$$

where the constant c is chosen to ensure each correction function has average 0, giving $c = \gamma \langle U(\mathbf{q}) \rangle$. If required, we may continue this procedure in order to find correction functions for higher orders, though the added complexity means that we cannot always solve to find an explicit solution.

The results of our analysis suggest that to leading order the error scales linearly with the reciprocal temperature β , but more importantly a non-constant term appears which is of order γ . As our correction is of the form $\langle \vartheta f_1 \rangle$ we can see that if $\vartheta = \vartheta_1(\mathbf{p})$ then this $\mathcal{O}(\gamma)$ term will not trouble us, as

$$\begin{aligned} \langle \vartheta_1(\mathbf{p}) f_1(\mathbf{q}, \mathbf{p}) \rangle &= \pm \frac{\beta}{2} \langle (\gamma U(\mathbf{q}) - c) \vartheta_1(\mathbf{p}) \pm \mathbf{p}^T \mathbf{M}^{-1} \nabla U(\mathbf{q}) \vartheta_1(\mathbf{p}) \rangle \\ &= \pm \frac{\beta}{2} \langle \mathbf{p}^T \mathbf{M}^{-1} \nabla U(\mathbf{q}) \vartheta_1(\mathbf{p}) \rangle, \end{aligned}$$

where the sign depends on the particular scheme used (which governs the form of f_1). Thus in the case of a function of pure momentum the order γ term does not

appear. However, if we instead set $\vartheta = \vartheta_2(\mathbf{q})$, then

$$\begin{aligned}\langle \vartheta_2(\mathbf{q}) f_1(\mathbf{q}, \mathbf{p}) \rangle &= \pm \frac{\beta}{2} \langle (\gamma U(\mathbf{q}) - c) \vartheta_2(\mathbf{q}) \pm \mathbf{p}^T \mathbf{M}^{-1} \nabla U(\mathbf{q}) \vartheta_2(\mathbf{q}) \rangle \\ &= \pm \frac{\gamma \beta}{2} \langle (U(\mathbf{q}) - \langle U(\mathbf{q}) \rangle) \vartheta_2(\mathbf{q}) \rangle,\end{aligned}$$

in which case our correction becomes $\mathcal{O}(\gamma)$. This is potentially disastrous if we choose the friction to be large (consider $\gamma \sim h^{-1}$), as the error introduced through discretization will dominate the true average to be sampled. Examining the algorithms themselves this is unsurprising, as although we have integrated the Ornstein-Uhlenbeck process exactly, when considering the limit of infinite friction in the $\llbracket XYZ \rrbracket$ schemes we obtain an inconsistent discretization. Hence these first-order schemes will be unsuitable for the integration of overdamped Langevin dynamics.

This is not always the case for first order schemes, however. For example the scheme denoted $\llbracket AOAB \rrbracket$ is consistent with the dynamics, and may be used for integrating the overdamped ($\gamma = \infty$) Langevin equation.

7.8.2 Numerical Experiment

Let us consider testing the computed first order corrections on a one dimensional example. Let $M = \beta = 1$ and define the biased double-well potential as

$$U(q) = (q^2 - 1)^2 + q/2.$$

We shall consider computing the average of a specific observable $\vartheta(q, p)$, and estimating the error due to discretization using the correction functions given in (7.25), where we choose the observable

$$\vartheta(q, p) = p^2 - qU'(q) + 2qp, \quad \langle \vartheta \rangle = 0.$$

The low dimensionality of the problem and the simplicity of the observable and potential energy function make resolving the perfect sampling bias to leading order an easy task, allowing us to give a good estimate (to order h^2) of the discretization error. In Fig. 7.4 we plot the results of $\langle \vartheta \rangle_h$ computed via numerical experiment, using each of the six first order schemes at either $\gamma = 1$ or $\gamma = 2$, and compare them to our first order prediction

$$\langle \vartheta \rangle_h \approx \langle \vartheta \rangle + h \langle f_1 \vartheta \rangle.$$

The numerical experiment at each timestep is averaged from 16 independent experiments, each running over a time interval of 10^8 . The results match our

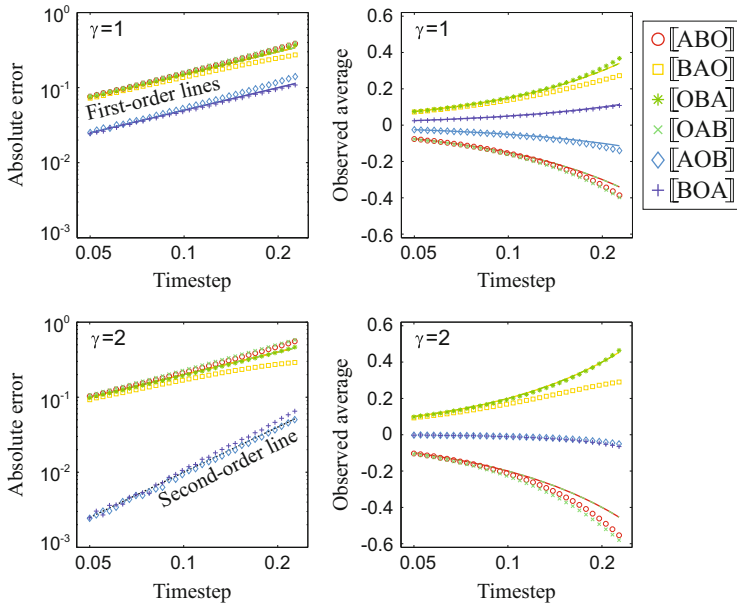


Fig. 7.4 We plot the absolute error in the computed value of $\langle \vartheta \rangle_h$ (left) and the observed value of $\langle \vartheta \rangle_h$ (right) as symbols, while our prediction computed using (7.25) is plotted as a solid line. For $\gamma = 1$ we find first order behavior (as expected), but for $\gamma = 2$ two methods exhibit higher order behavior. This is a special case for this observable that can be understood through our analysis

prediction extremely well, though at large stepsize there is evidence of higher order behavior $\mathcal{O}(h^2)$ having an effect on the computed average, evident by the divergence away from our prediction line.

The $[\text{AOB}]$ and $[\text{BOA}]$ schemes also demonstrate a surprising second order behavior for the experiments at $\gamma = 2$, that we would not necessarily expect. This is due to a felicitous choice of our observable, where the leading order correction can be shown to be zero. The fact that both of these schemes share this property is unsurprising, as $f_{1,[\text{AOB}]} = -f_{1,[\text{BOA}]}$, although for a general observable we would not expect second order averages for these methods. We could similarly construct special cases for other observables that would give higher order behavior for other schemes.

The first order correction term for the $[\text{BOA}]$ scheme is given by the formula

$$\begin{aligned} \langle \vartheta f_{1,[\text{BOA}]} \rangle &= \frac{\beta}{2} \int_{\mathcal{D}} (p^2 - qU'(q) + 2qp) (pU'(q) + \gamma U(q) - c) \rho_\beta d\omega, \\ &= \frac{1}{\beta} + \frac{\gamma}{2} \langle U \rangle - \frac{\gamma\beta}{2} \langle qUU' \rangle, \\ &= \frac{(2-\gamma)}{2\beta}. \end{aligned}$$

Hence for the critical value of $\gamma = 2$, the leading order correction will be zero, giving

$$\langle \vartheta \rangle_h^{[\text{BOA}]} = \langle \vartheta \rangle + \mathcal{O}(h^2).$$

This is exactly the behavior we see in Fig. 7.4.

7.9 Error Expansion for Symmetric Langevin Methods

Of particular interest for sampling the canonical distribution are symmetric Langevin methods. We believe these are likely to be the most useful class of methods for practitioners, as by symmetrizing the expansion the odd order terms in (7.16) vanish identically using the Jacobi identity in the BCH expansions. This implies that a symmetric scheme gives a second order error in computed averages. Many symmetric methods can be constructed that require only one evaluation of the force per iteration (effectively making them as inexpensive as a first order method).

In order to simplify the algebra, we will use $M = I$ throughout this section, which will not alter the major results and amounts to a linear change of variables. We shall consider general symmetric schemes of the form $[\text{XYZZYX}]$, and perform a similar analysis to the previous section. The terms appearing in the expansions will be significantly more complex than those encountered in first order methods. We make use of the following proposition for symmetric compositions:

Proposition 7.1 *Let \mathcal{L}_X^\dagger , \mathcal{L}_Y^\dagger and \mathcal{L}_Z^\dagger be general operators to which BCH can be applied, then defining*

$$e^{h\hat{\mathcal{L}}^\dagger} = e^{\frac{h}{2}\mathcal{L}_X^\dagger} e^{\frac{h}{2}\mathcal{L}_Y^\dagger} e^{h\mathcal{L}_Z^\dagger} e^{\frac{h}{2}\mathcal{L}_Y^\dagger} e^{\frac{h}{2}\mathcal{L}_X^\dagger}, \quad (7.26)$$

gives

$$\hat{\mathcal{L}}^\dagger = \mathcal{L}_0^\dagger + h^2 \mathcal{L}_2^\dagger + \mathcal{O}(h^4),$$

where

$$\begin{aligned} \mathcal{L}_0^\dagger &= \mathcal{L}_X^\dagger + \mathcal{L}_Y^\dagger + \mathcal{L}_Z^\dagger, \\ \mathcal{L}_2^\dagger &= \frac{1}{12} \left([\mathcal{L}_Z^\dagger, \mathcal{L}_Z^\dagger, \mathcal{L}_Y^\dagger] + [\mathcal{L}_Y^\dagger + \mathcal{L}_Z^\dagger, \mathcal{L}_Y^\dagger + \mathcal{L}_Z^\dagger, \mathcal{L}_X^\dagger] \right) \\ &\quad - \frac{1}{24} \left([\mathcal{L}_Y^\dagger, \mathcal{L}_Y^\dagger, \mathcal{L}_Z^\dagger] + [\mathcal{L}_X^\dagger, \mathcal{L}_X^\dagger, \mathcal{L}_Y^\dagger + \mathcal{L}_Z^\dagger] \right). \end{aligned}$$

For a scheme $\llbracket XYZYX \rrbracket$, we assume that each of the X , Y and Z characters in the string are distinct, and correspond to one of the A , B or O pieces of our splitting strategy. Thus we have $\mathcal{L}_0^\dagger = \mathcal{L}_{\text{LD}}^\dagger$.

Evidently, the scheme's associated Fokker-Planck operator $\hat{\mathcal{L}}^\dagger$ no longer has a leading order term that is linear in the stepsize, so it makes sense to revise our assumption on the form of the scheme's corresponding invariant measure, and replace it with a series with solely even order terms. If we suppose that the odd order correction functions are zero, then we are left with

$$\hat{\rho} = \rho_\beta(1 + h^2 f_2 + h^4 f_4 + \dots), \quad (7.27)$$

where each $\langle f_i \rangle = 0$ as usual. Thus the stationarity equation $\hat{\mathcal{L}}^\dagger \hat{\rho} = 0$ becomes

$$(\mathcal{L}_{\text{LD}}^\dagger + h^2 \mathcal{L}_2^\dagger + \dots)(\rho_\beta + h^2 \rho_\beta f_2 + \dots) = 0.$$

The equation is satisfied at zeroth order, and equating the second order terms we obtain

$$\mathcal{L}_{\text{LD}}^\dagger (\rho_\beta f_2) = -\mathcal{L}_2^\dagger \rho_\beta. \quad (7.28)$$

The procedure then follows just as in the case of the first order schemes. The form of the right-hand side $\mathcal{L}_2^\dagger \rho_\beta$ will be dependent on the choice of the update scheme, and can be computed using the BCH formula using Proposition 7.1. More complicated symmetric schemes involving more than five stages can be utilized, but these schemes may require more than one force evaluation per iteration, while increasing the complexity of the PDE to solve.

The condition on the existence of such a solution requires us to use the Fredholm alternative, which requires us to verify that the inhomogeneous term $\mathcal{L}_2^\dagger \rho_\beta$ integrates to zero.

7.9.1 Calculation of the Inhomogeneous Term

The computation of the right hand side in (7.28) is required in order to solve the corresponding partial differential equation and obtain the leading order correction function for our symmetric scheme $\llbracket XYZYX \rrbracket$. From the form of the \mathcal{L}_2^\dagger operator in Proposition 7.1, we can see that our life is made considerably easier if we initially consider methods $\llbracket OYZYO \rrbracket$, which substitutes

$$\mathcal{L}_X^\dagger = \mathcal{L}_O^\dagger, \quad \mathcal{L}_Y^\dagger + \mathcal{L}_Z^\dagger = \mathcal{L}_A^\dagger + \mathcal{L}_B^\dagger = \mathcal{L}_H^\dagger,$$

simplifying the computation to

$$\mathcal{L}_{2,\llbracket \text{OYZYO} \rrbracket}^\dagger \rho_\beta = \frac{1}{12} [\mathcal{L}_Z^\dagger, \mathcal{L}_Z^\dagger, \mathcal{L}_Y^\dagger] \rho_\beta - \frac{1}{24} [\mathcal{L}_Y^\dagger, \mathcal{L}_Y^\dagger, \mathcal{L}_Z^\dagger] \rho_\beta. \quad (7.29)$$

The inhomogeneity for the schemes $\llbracket \text{OABAO} \rrbracket$ and $\llbracket \text{OBABO} \rrbracket$ is hence a combination of the two commutator terms

$$\begin{aligned} [\mathcal{L}_A^\dagger, \mathcal{L}_A^\dagger, \mathcal{L}_B^\dagger] \rho_\beta &= (2\beta \mathbf{p}^T (\nabla^2 U) \nabla U - \nabla^3 U : \mathbf{p} \otimes \mathbf{p} \otimes \mathbf{p}) \rho_\beta, \\ [\mathcal{L}_B^\dagger, \mathcal{L}_B^\dagger, \mathcal{L}_A^\dagger] \rho_\beta &= -(2\beta \mathbf{p}^T (\nabla^2 U) \nabla U) \rho_\beta, \end{aligned}$$

giving overall equations to solve

$$\begin{aligned} \mathcal{L}_{LD}^\dagger (\rho_\beta f_{2,\llbracket \text{OABAO} \rrbracket}) &= -\mathcal{L}_{2,\llbracket \text{OABAO} \rrbracket}^\dagger \rho_\beta \\ &= \frac{\beta}{24} (6\mathbf{p}^T (\nabla^2 U) \nabla U - \nabla^3 U : \mathbf{p} \otimes \mathbf{p} \otimes \mathbf{p}) \rho_\beta, \\ \mathcal{L}_{LD}^\dagger (\rho_\beta f_{2,\llbracket \text{OBABO} \rrbracket}) &= -\mathcal{L}_{2,\llbracket \text{OBABO} \rrbracket}^\dagger \rho_\beta \\ &= \frac{\beta}{24} (2\nabla^3 U : \mathbf{p} \otimes \mathbf{p} \otimes \mathbf{p} - 6\mathbf{p}^T (\nabla^2 U) \nabla U) \rho_\beta. \end{aligned}$$

We can see immediately that the Fredholm alternative holds in both cases, as both equations have right-hand sides that are of odd order in p , and hence will average to 0.

If we instead consider schemes which use a central Ornstein-Uhlenbeck update, then the inhomogeneous term becomes significantly more complex, as we no longer have a significant number of cancellations in $\mathcal{L}_2^\dagger \rho_\beta$. Instead, we shall avoid computing the right-hand side for these schemes altogether, in favor of utilizing the following lemma [223]:

Lemma 7.1 Consider two numerical schemes with associated operators governing the evolution of measure \mathcal{ST} and \mathcal{TS} , with unique associated invariant distributions $\hat{\rho}_{ST}$ and $\hat{\rho}_{TS}$ respectively, such that

$$\mathcal{ST} \hat{\rho}_{ST} = \hat{\rho}_{ST}, \quad \mathcal{TS} \hat{\rho}_{TS} = \hat{\rho}_{TS}.$$

Under suitable ergodicity assumptions (such that in the long-time limit, all distributions converge to the invariant distribution), we have

$$\hat{\rho}_{ST} = \mathcal{S} \hat{\rho}_{TS}, \quad \text{and} \quad \hat{\rho}_{TS} = \mathcal{T} \hat{\rho}_{ST}.$$

Proof The proof is very simple, and follows almost directly from our ergodicity assumption. If we assume that

$$\lim_{n \rightarrow \infty} (\mathcal{ST})^n \rho = \hat{\rho}_{ST},$$

for any initial distribution ρ , then we have

$$\hat{\rho}_{ST} = \lim_{n \rightarrow \infty} (\mathcal{ST})^n \hat{\rho}_{ST} = \lim_{n \rightarrow \infty} \mathcal{S} (\mathcal{T}\mathcal{S})^{n-1} \mathcal{T} \hat{\rho}_{ST} = \mathcal{S} \hat{\rho}_{TS}.$$

A similar statement holds for $\hat{\rho}_{TS}$. \square

If we return to our scheme $\llbracket OYZYO \rrbracket$, which has a simple inhomogeneity, then we can relate its invariant distribution to invariant distributions of schemes with a central OU update by writing its evolution operator as

$$e^{h\hat{\mathcal{L}}_{\llbracket OYZYO \rrbracket}^\dagger} = \underbrace{e^{(h/2)\mathcal{L}_O^\dagger} e^{(h/2)\mathcal{L}_Y^\dagger} e^{(h/2)\mathcal{L}_Z^\dagger}}_{\mathcal{S}} \underbrace{e^{(h/2)\mathcal{L}_Z^\dagger} e^{(h/2)\mathcal{L}_Y^\dagger} e^{(h/2)\mathcal{L}_O^\dagger}}_{\mathcal{T}} = \mathcal{ST}.$$

By applying Lemma 7.1, we can equate the invariant distributions directly as

$$\hat{\rho}_{\llbracket ZYXYZ \rrbracket} = \exp((h/2)\mathcal{L}_Z^\dagger) \exp((h/2)\mathcal{L}_Y^\dagger) \exp((h/2)\mathcal{L}_O^\dagger) \hat{\rho}_{\llbracket OYZYO \rrbracket}.$$

Rewriting our ansatz (7.27) in place of the distributions, and expanding the exponential series gives

$$\begin{aligned} & \rho_\beta (1 + h^2 f_{2,\llbracket ZYXYZ \rrbracket} + \dots) \\ &= \left(\text{Id} + \frac{h}{2} \mathcal{L}_{\text{LD}}^\dagger + \frac{h^2}{4} \mathcal{L}_{1,\llbracket OYZ \rrbracket}^\dagger + \frac{h^2}{2} \mathcal{L}_{\text{LD}}^\dagger + \dots \right) (\rho_\beta (1 + h^2 f_{2,\llbracket OYZYO \rrbracket} + \dots)), \end{aligned}$$

and hence equating powers we have

$$f_{2,\llbracket ZYXYZ \rrbracket} \rho_\beta = f_{2,\llbracket OYZYO \rrbracket} \rho_\beta + \frac{1}{4} \mathcal{L}_{1,\llbracket OYZ \rrbracket}^\dagger \rho_\beta.$$

By virtue of (7.20), we have

$$\mathcal{L}_{1,\llbracket OAB \rrbracket}^\dagger \rho_\beta = \frac{1}{2} \mathcal{L}_H^\dagger (g \rho_\beta) \quad \mathcal{L}_{1,\llbracket OBA \rrbracket}^\dagger \rho_\beta = -\frac{1}{2} \mathcal{L}_H^\dagger (g \rho_\beta),$$

where recall $g(\mathbf{q}, \mathbf{p}) \rho_\beta = \mathcal{L}_A^\dagger \rho_\beta = \beta \mathbf{p}^T \mathbf{M}^{-1} \nabla U(\mathbf{q}) \rho_\beta$. Computing

$$\mathcal{L}_H^\dagger (g \rho_\beta) = \beta (|\nabla U(\mathbf{q})|^2 - \mathbf{p}^T \nabla^2 U(\mathbf{q}) \mathbf{p}) \rho_\beta,$$

the correction for the schemes with a central O update can be expressed as

$$f_{2,\llbracket \text{ABOBA} \rrbracket} = f_{2,\llbracket \text{OBABO} \rrbracket} - \frac{\beta}{8} (|\nabla U(\mathbf{q})|^2 - \mathbf{p}^T \nabla^2 U \mathbf{p}), \quad (7.30\text{a})$$

$$f_{2,\llbracket \text{BAOAB} \rrbracket} = f_{2,\llbracket \text{OABAO} \rrbracket} + \frac{\beta}{8} (|\nabla U(\mathbf{q})|^2 - \mathbf{p}^T \nabla^2 U \mathbf{p}). \quad (7.30\text{b})$$

Thus we need only compute the solutions to the simpler PDE (7.29), in order to relate the solutions of the conjugate schemes with centralized OU update. However, although this simplifies our task greatly, finding the general solution to (7.29) is still very challenging, and obtaining a closed form expression for the correction function is nontrivial.

7.9.2 Expansion in Powers of γ^{-1}

Although we do not give the general analytical solution to the partial differential equation of (7.28) for each of the four symmetric Langevin schemes we are considering, we can easily find a solution in an important limiting case: the high friction regime. We consider expanding f_2 into a series involving the reciprocal friction $\varepsilon = 1/\gamma$, and assume that for large friction our ansatz remains sensible. We will denote

$$f_2(\mathbf{q}, \mathbf{p}) = f_{2,0}(\mathbf{q}, \mathbf{p}) + \varepsilon f_{2,1}(\mathbf{q}, \mathbf{p}) + \varepsilon^2 f_{2,2}(\mathbf{q}, \mathbf{p}) + \dots \quad (7.31)$$

with each $\langle f_{2,i} \rangle = 0$. Dividing by the friction in (7.28) we obtain

$$\left(\bar{\mathcal{L}}_O^\dagger + \varepsilon \mathcal{L}_H^\dagger \right) (f_2 \rho_\beta) = -\varepsilon \mathcal{L}_2^\dagger \rho_\beta,$$

where $\bar{\mathcal{L}}_O^\dagger$ is independent of the friction

$$\bar{\mathcal{L}}_O^\dagger \vartheta = \varepsilon \mathcal{L}_O^\dagger \vartheta = \nabla_p \cdot (\mathbf{p} \vartheta) + \frac{1}{\beta} \Delta_p \vartheta.$$

From our earlier computation in (7.29), we can write

$$\mathcal{L}_{2,\llbracket \text{OABAO} \rrbracket}^\dagger \rho_\beta = w(\mathbf{q}, \mathbf{p}) \rho_\beta,$$

for $w(\mathbf{q}, \mathbf{p})$ independent of the friction

$$w(\mathbf{q}, \mathbf{p}) = -\frac{\beta}{24} (6\mathbf{p}^T (\nabla^2 U) \nabla U - \nabla^3 U : \mathbf{p} \otimes \mathbf{p} \otimes \mathbf{p}).$$

Hence we have

$$\left(\bar{\mathcal{L}}_O^\dagger + \varepsilon \mathcal{L}_H^\dagger \right) (\rho_\beta f_{2,0,[\text{OABAO}]}(\mathbf{q}, \mathbf{p}) + \varepsilon f_{2,1,[\text{OABAO}]}(\mathbf{q}, \mathbf{p}) + \dots) = -\varepsilon w(\mathbf{q}, \mathbf{p}) \rho_\beta,$$

and equating powers of the reciprocal friction ε gives us a sequence of equations to solve

$$\begin{aligned} \text{Order 1: } & \bar{\mathcal{L}}_O^\dagger (\rho_\beta f_{2,0,[\text{OABAO}]}) = 0, \\ \text{Order } \varepsilon: & \mathcal{L}_H^\dagger (\rho_\beta f_{2,0,[\text{OABAO}]}) + \bar{\mathcal{L}}_O^\dagger (\rho_\beta f_{2,1,[\text{OABAO}]}) = -w(\mathbf{q}, \mathbf{p}) \rho_\beta, \\ \text{Order } \varepsilon^2: & \mathcal{L}_H^\dagger (\rho_\beta f_{2,1,[\text{OABAO}]}) + \bar{\mathcal{L}}_O^\dagger (\rho_\beta f_{2,2,[\text{OABAO}]}) = 0, \\ \text{Order } \varepsilon^3: & \mathcal{L}_H^\dagger (\rho_\beta f_{2,2,[\text{OABAO}]}) + \bar{\mathcal{L}}_O^\dagger (\rho_\beta f_{2,3,[\text{OABAO}]}) = 0, \\ & \vdots \end{aligned}$$

The first equation at order one tells us that $f_{2,0,[\text{OABAO}]}(\mathbf{q}, \mathbf{p})$ must be a function of position only, as the kernel of $\bar{\mathcal{L}}_O^\dagger$ is the set of functions that are constant with respect to \mathbf{p} . Hence we shall denote

$$f_{2,0,[\text{OABAO}]}(\mathbf{q}, \mathbf{p}) = v(\mathbf{q}),$$

where our goal is now to explicitly find $v(\mathbf{q})$. Unfortunately, $v(\mathbf{q})$ is not explicitly determined at this point, we only know that it is a function of position only such that $\langle v \rangle = 0$. This function will be determined as we solve the higher order equations.

In order to determine $v(\mathbf{q})$, we will have to solve the next PDE at order ε ,

$$\bar{\mathcal{L}}_O^\dagger (\rho_\beta f_{2,1,[\text{OABAO}]}) + \mathcal{L}_H^\dagger (\rho_\beta f_{2,0,[\text{OABAO}]}) = -w(\mathbf{q}, \mathbf{p}) \rho_\beta, \quad (7.32)$$

where we will make use of the formulas

$$\begin{aligned} \bar{\mathcal{L}}_O^\dagger (\rho_\beta \nabla^3 U : \mathbf{p} \otimes \mathbf{p} \otimes \mathbf{p}) &= -3\rho_\beta \nabla^3 U : \mathbf{p} \otimes \mathbf{p} \otimes \mathbf{p} + \frac{6\rho_\beta}{\beta} \mathbf{p}^T \nabla_q \Delta_q U, \\ \bar{\mathcal{L}}_O^\dagger (\rho_\beta \mathbf{p}^T \nabla_q \Delta_q U) &= -\rho_\beta \mathbf{p}^T \nabla_q \Delta_q U, \\ \bar{\mathcal{L}}_O^\dagger (\rho_\beta \mathbf{p}^T (\nabla^2 U) \nabla U) &= -\rho_\beta \mathbf{p}^T (\nabla^2 U) \nabla U, \end{aligned}$$

to write

$$w(\mathbf{q}, \mathbf{p}) \rho_\beta = \frac{\beta}{24} \bar{\mathcal{L}}_O^\dagger \left(\left[6\mathbf{p}^T (\nabla^2 U) \nabla U - \frac{1}{3} \nabla^3 U : \mathbf{p} \otimes \mathbf{p} \otimes \mathbf{p} - \frac{2}{\beta} \mathbf{p}^T \nabla_q \Delta_q U \right] \rho_\beta \right). \quad (7.33)$$

Additionally, for $v(\mathbf{q})$ we have the identity

$$\mathcal{L}_H^\dagger (\rho_\beta v) = -\mathbf{p}^T \nabla v \rho_\beta = \bar{\mathcal{L}}_O^\dagger ([\mathbf{p}^T \nabla v + \mu(\mathbf{q})] \rho_\beta), \quad (7.34)$$

for some function of position $\mu(\mathbf{q})$. Plugging (7.33) and (7.34) into the PDE (7.32) gives

$$\begin{aligned}\bar{\mathcal{L}}_O^\dagger (\rho_\beta f_{2,1,\llbracket \text{OABAO} \rrbracket}) &= -w(\mathbf{q}, \mathbf{p})\rho_\beta - \mathcal{L}_H^\dagger (\rho_\beta v), \\ &= -\frac{\beta}{24} \left(\left[6\mathbf{p}^T (\nabla^2 U) \nabla U - \frac{1}{3} \nabla^3 U : \mathbf{p} \otimes \mathbf{p} \otimes \mathbf{p} \right. \right. \\ &\quad \left. \left. - \frac{2}{\beta} \mathbf{p}^T \nabla_q \Delta_q U \right] \rho_\beta \right) - \bar{\mathcal{L}}_O^\dagger ([\mathbf{p}^T \nabla v + \mu] \rho_\beta),\end{aligned}$$

and hence

$$\begin{aligned}f_{2,1,\llbracket \text{OABAO} \rrbracket} &= -\frac{\beta}{24} \left(6\mathbf{p}^T (\nabla^2 U) \nabla U - \frac{1}{3} \nabla^3 U : \mathbf{p} \otimes \mathbf{p} \otimes \mathbf{p} - \frac{2}{\beta} \mathbf{p}^T \nabla_q \Delta_q U \right) \\ &\quad - \mathbf{p}^T \nabla v - \mu.\end{aligned}$$

At this point, we might consider abandoning the prospect of determining the leading order correction altogether, as we now have two arbitrary functions of position $v(\mathbf{q})$ and $\mu(\mathbf{q})$ creeping into our solution. However, the form of $v(\mathbf{q})$ is determined by considering the next order PDE at ε^2 :

$$\bar{\mathcal{L}}_O^\dagger (\rho_\beta f_{2,2,\llbracket \text{OABAO} \rrbracket}) = -\mathcal{L}_H^\dagger (\rho_\beta f_{2,1,\llbracket \text{OABAO} \rrbracket}). \quad (7.35)$$

We are spared solving this equation by virtue of a solvability condition. Integrating the left hand side of (7.35) with respect to the momenta, we find

$$\int_{\mathcal{P}} \bar{\mathcal{L}}_O^\dagger (\rho_\beta f_{2,2,\llbracket \text{OABAO} \rrbracket}) d\omega_p = 0,$$

by simple computation. Hence we also require the average of the right-hand side of (7.35) to be zero with respect to the momentum, or

$$\int_{\mathcal{P}} \mathcal{L}_H^\dagger (\rho_\beta f_{2,1,\llbracket \text{OABAO} \rrbracket}) d\omega_p = \bar{\pi} \mathcal{L}_H^\dagger f_{2,1,\llbracket \text{OABAO} \rrbracket} = 0, \quad (7.36)$$

where $\bar{\pi}$ is the averaging operator

$$(\bar{\pi}f)(\mathbf{q}) = \int_{\mathcal{P}} f(\mathbf{q}, \mathbf{p}) \rho_\beta d\omega_p.$$

Hence by rewriting the correction function as

$$f_{2,1,\llbracket \text{OABAO} \rrbracket} = \frac{\beta}{24} \left(3\mathcal{L}_A^\dagger |\nabla U|^2 - \frac{1}{3} (\mathcal{L}_A^\dagger)^3 U - \frac{2}{\beta} \mathcal{L}_A^\dagger \Delta_q U \right) + \mathcal{L}_A^\dagger v - \mu,$$

we have

$$\bar{\pi} \mathcal{L}_H^\dagger f_{2,1,\llbracket \text{OABAO} \rrbracket} = \frac{\beta}{24} \left(3\mathcal{M} |\nabla U|^2 - \frac{1}{3} \mathcal{N} U - \frac{2}{\beta} \mathcal{M} \Delta_q U \right) + \mathcal{M} v,$$

where we abbreviate

$$\mathcal{M}\psi(\mathbf{q}) = \bar{\pi} \mathcal{L}_H^\dagger \mathcal{L}_A^\dagger \psi(\mathbf{q}) = \bar{\pi} \left((\mathcal{L}_A^\dagger)^2 + \mathcal{L}_B^\dagger \mathcal{L}_A^\dagger \right) \psi(\mathbf{q}) = \frac{1}{\beta} \Delta_q \psi(\mathbf{q}) - \nabla U \cdot \nabla_q \psi(\mathbf{q}),$$

$$\mathcal{N}\psi(\mathbf{q}) = \bar{\pi} \mathcal{L}_H^\dagger (\mathcal{L}_A^\dagger)^3 \psi(\mathbf{q}) = \bar{\pi} \left((\mathcal{L}_A^\dagger)^4 + \mathcal{L}_B^\dagger (\mathcal{L}_A^\dagger)^3 \right) \psi(\mathbf{q}) = \frac{3}{\beta} \mathcal{M} (\Delta_q \psi(\mathbf{q})).$$

Thus we have

$$\bar{\pi} \mathcal{L}_H^\dagger \rho_\beta f_{2,1,\llbracket \text{OABAO} \rrbracket} = \frac{\beta}{8} \mathcal{M} \left(|\nabla U|^2 - \frac{1}{\beta} \Delta_q U \right) + \mathcal{M} v,$$

and hence by (7.36) we finally obtain

$$v(\mathbf{q}) = \frac{1}{8} (\Delta_q U - \beta |\nabla U|^2),$$

where it is easily verified that $\langle v \rangle = 0$. This gives us our leading order solution

$$f_{2,0,\llbracket \text{OBABO} \rrbracket} = \frac{1}{8} (\Delta_q U - \beta |\nabla U|^2).$$

Applying the same procedure for the $\llbracket \text{OBABO} \rrbracket$ scheme yields

$$f_{2,0,\llbracket \text{OBABO} \rrbracket} = \frac{1}{8} (\beta |\nabla U|^2 - 2\Delta_q U + c),$$

where $c = \langle \Delta U \rangle$ is a constant chosen to ensure zero average. We can relate these schemes to their conjugate schemes with centralized OU update via Lemma 7.1 and Eq. (7.30), to give

$$f_{2,0,\llbracket \text{ABOBA} \rrbracket} = \frac{1}{8} (\beta \mathbf{p}^T \nabla^2 U(\mathbf{q}) \mathbf{p} - 2\Delta_q U + c),$$

$$f_{2,0,\llbracket \text{BAOAB} \rrbracket} = \frac{1}{8} (\Delta U - \beta \mathbf{p}^T \nabla^2 U(\mathbf{q}) \mathbf{p}).$$

Owing to our ansatz, we would expect that the computed average of some observable has behavior like

$$\langle \vartheta \rangle_h = \langle \vartheta \rangle + h^2 \langle \vartheta f_{2,0} \rangle + \mathcal{O}(\varepsilon h^2 + h^4).$$

At sufficiently small values of ε (and hence, large values of the friction coefficient γ) we would expect that the $\mathcal{O}(h^2)$ remainder will not be visible to us in our experiments, and we will be able to correct our average to $\mathcal{O}(h^4)$. The symmetric discretization schemes we have considered here will all be consistent in the overdamped ($\gamma \rightarrow \infty$) limit, and we would expect the correction function for the corresponding limiting schemes to be given by $f_{2,0}$.

7.9.3 Superconvergence of the [[BAOAB]] Scheme

In the regime of sufficiently large γ and small h , our doubly-asymptotic ansatz for the leading order correction to a function $\vartheta(q, p)$ is

$$\langle \vartheta \rangle = \langle \vartheta \rangle_h - h^2 \langle \vartheta f_{2,0} \rangle + O\left(\frac{h^2}{\gamma} + h^4\right), \quad (7.37)$$

where $f_{2,0}$ is method-dependent. The [[BAOAB]] scheme has leading order correction

$$f_{2,0,[[\text{BAOAB}]]}(\mathbf{q}, \mathbf{p}) = \frac{1}{8} (\Delta U - \beta \mathbf{p}^T \nabla^2 U(\mathbf{q}) \mathbf{p}),$$

which has the interesting property that its marginal average with respect to momentum is zero:

$$\bar{\pi} f_{2,0,[[\text{BAOAB}]]} = \int_{\mathcal{P}} f_{2,0,[[\text{BAOAB}]]}(\mathbf{q}, \mathbf{p}) \rho_\beta(\mathbf{q}, \mathbf{p}) d\omega_p = 0.$$

This is a very favorable quality for configurational sampling, where we consider averages of functions solely of position, as we can split up the integral such that

$$\begin{aligned} \langle \vartheta(\mathbf{q}) f_{2,0,[[\text{BAOAB}]]} \rangle &= \int_{\mathcal{D}} \vartheta(\mathbf{q}) f_{2,0,[[\text{BAOAB}]]} \rho_\beta d\omega, \\ &= \int_{\mathcal{Q}} \vartheta(\mathbf{q}) \int_{\mathcal{P}} f_{2,0,[[\text{BAOAB}]]} \rho_\beta d\omega_p d\omega_q, \\ &= 0. \end{aligned}$$

Thus we expect that the $\llbracket \text{BAOAB} \rrbracket$ scheme recovers $\mathcal{O}(h^4)$ configurational averages in the limit of infinite friction. This scheme requires no extra force evaluations, and this particular feature appears to simply be a serendipitous result of the form of the correction function.

This is a property common to no other Langevin splitting scheme that we are aware of. Though curiously its conjugate method, the $\llbracket \text{OABAO} \rrbracket$ scheme, has the property

$$\int_{\Omega} f_{2,0,\llbracket \text{OABAO} \rrbracket}(\mathbf{q}, \mathbf{p}) \rho_{\beta}(\mathbf{q}, \mathbf{p}) d\omega_q = 0,$$

implying that we obtain high-order averages for functions purely of the momenta in the limit of infinite friction. However, as the momenta are always Gaussian distributed in canonical sampling, we are far more interested in functions of position to high accuracy (and sampling $\exp(-\beta U(\mathbf{q}))$) rather than the Gaussian-distributed momenta).

It is important to note that this superconvergence property is only present in the limit of large time, i.e. this is an attribute of the invariant distribution of the discretization schemes $\hat{\rho}$. As such, there are no bonuses to the weak or strong order of the superconvergent schemes, though equally there is no added cost to using the methods.

All of the symmetric splitting schemes discussed are very easy to implement relative to other popular Langevin integrators, as many codes already implement the standard velocity Verlet $\llbracket \text{BAB} \rrbracket$ style integration. An exact Ornstein-Uhlenbeck solve can be added where it is required in the scheme in order to effectively integrate Langevin dynamics: then setting $\gamma = 0$ reduces the integrator to a standard Verlet scheme, integrating deterministic Newtonian dynamics.

7.10 The Limit Method

We now consider schemes in the limit $\gamma \rightarrow \infty$, where the exact solution of the vector OU process reduces to redrawing momenta from the canonical distribution, so $\mathbf{p}_{n+1} = \sqrt{k_B T M^{1/2}} \mathbf{R}$, where \mathbf{R} is a vector of i.i.d. normal random numbers. Alternatively, we could consider the limit of the particle mass going to 0, although this requires a reformulation of Langevin dynamics (7.4) so that the friction is proportional to the velocity instead of the momentum [233]. Whichever limit is taken, we would expect the ultimate result to be the same. (Here we have reintroduced the masses in order to present the method, since they may be useful scaling parameters in simulation.)

The first order schemes of the form $\llbracket \text{XYZ} \rrbracket$, as well as schemes such as $\llbracket \text{XOYOX} \rrbracket$ are not consistent in this overdamped limit: the errors in computed

observable averages diverge and we do not recover correct sampling in the limit of zero stepsize.

The symmetric schemes considered in the previous section are consistent however, each with their own limiting schemes corresponding to taking the limit of infinite friction in their update equations. As the momenta are continually redrawn from a normal distribution, we focus on the evolution of the configurations themselves. For the method denoted **[[OBABO]]**, we have the limiting scheme

$$\begin{aligned}\mathbf{p}_{n+1/2} &= \sqrt{k_B T} \mathbf{M}^{1/2} \mathbf{R}_n, \\ \hat{\mathbf{p}}_{n+1/2} &= \mathbf{p}_{n+1/2} - (h/2) \nabla U(\mathbf{q}_n), \\ \mathbf{q}_{n+1} &= \mathbf{q}_n + h \mathbf{M}^{-1} \hat{\mathbf{p}}_{n+1/2}, \\ \hat{\mathbf{p}}_{n+1} &= \hat{\mathbf{p}}_{n+1/2} - (h/2) \nabla U(\mathbf{q}_{n+1}), \\ \mathbf{p}_{n+1} &= \sqrt{k_B T} \mathbf{M}^{1/2} \mathbf{R}_{n+1/2},\end{aligned}$$

where \mathbf{R}_n and $\mathbf{R}_{n+1/2}$ are independent normal random vectors with mean zero and unit variance. It is clear that if our only desire is to make use of the position data \mathbf{q} , then the final two steps are redundant in this algorithm, as we update the momentum vector only to redraw it at the beginning of the next iteration. Any information about the initial momentum vector \mathbf{p}_n is unused in the scheme, making it simple to rewrite solely in terms of the position vector, giving us

$$\mathbf{q}_{n+1} = \mathbf{q}_n - \frac{h^2}{2} \mathbf{M}^{-1} \nabla U(\mathbf{q}_n) + h \sqrt{k_B T} \mathbf{M}^{-1/2} \mathbf{R}_n. \quad (7.38)$$

Denoting $\tau = h^2/2$, the update scheme (7.38) becomes the Euler-Maruyama scheme

$$\mathbf{q}_{n+1} = \mathbf{q}_n - \tau \mathbf{M}^{-1} \nabla U(\mathbf{q}_n) + \sqrt{2\tau k_B T} \mathbf{M}^{-1/2} \mathbf{R}_n, \quad (7.39)$$

which is known to give an error in long-time averages $\mathcal{O}(\tau) = \mathcal{O}(h^2)$, just as our analysis suggests.

If we instead consider the **[[BAOAB]]** scheme we find that unlike the **[[OBABO]]** scheme we no longer have redundant steps:

$$\begin{aligned}\mathbf{p}_{n+1/2} &= \mathbf{p}_n - (h/2) \nabla U(\mathbf{q}_n), \\ \mathbf{q}_{n+1/2} &= \mathbf{q}_n + (h/2) \mathbf{M}^{-1} \mathbf{p}_{n+1/2}, \\ \hat{\mathbf{p}}_{n+1/2} &= \sqrt{k_B T} \mathbf{M}^{1/2} \mathbf{R}_n, \\ \mathbf{q}_{n+1} &= \mathbf{q}_{n+1/2} + (h/2) \mathbf{M}^{-1} \hat{\mathbf{p}}_{n+1/2}, \\ \mathbf{p}_{n+1} &= \hat{\mathbf{p}}_{n+1/2} - (h/2) \nabla U(\mathbf{q}_{n+1}),\end{aligned}$$

where \mathbf{R}_n is an independent normal random vector with mean zero and unit variance. Expressing this as an update solely for the configurations, we obtain

$$\mathbf{q}_{n+1} = \mathbf{q}_n - \frac{h^2}{2} \mathbf{M}^{-1} \nabla U(\mathbf{q}_n) + \frac{h}{2} \sqrt{k_B T} \mathbf{M}^{-1/2} (\mathbf{R}_n + \mathbf{R}_{n-1}),$$

and substituting $\tau = h^2/2$ gives the BAOAB *Limit Method* (Leimkuhler-Matthews method) [221]

$$\mathbf{q}_{n+1} = \mathbf{q}_n - \tau \mathbf{M}^{-1} \nabla U(\mathbf{q}_n) + \sqrt{2\tau k_B T} \mathbf{M}^{-1/2} \left(\frac{\mathbf{R}_n + \mathbf{R}_{n-1}}{2} \right). \quad (7.40)$$

As we are in the overdamped regime, we would expect that this scheme should have an $\mathcal{O}(h^4) = \mathcal{O}(\tau^2)$ error in configurational averages, while inheriting the other properties of the [[BAOAB]] scheme for the harmonic and perturbed harmonic models considered in Sects. 7.4 and 7.5. Moreover, since we completely remove the second order term in the Langevin dynamics configurational density expansion, we expect to observe this behavior across all values of h and τ . This is quite a surprising result, given the qualitative similarity between Eqs. (7.39) and (7.40).

The benefit of (7.40) over the Euler-Maruyama scheme is that we can get second order accuracy in averages with only a single evaluation of the force at each timestep. However, our analysis presented here is only for the infinite time case. For averages computed in finite time, work in [224] has shown that (7.40) does indeed give a first order error, albeit one that vanishes exponentially fast in time as the simulation progresses. Hence for suitably long simulations, the observed error will be $\mathcal{O}(h^2)$.

We can think of the noise process in (7.40) as corresponding to a colored noise which has characteristics that directly depend on the stepsize, although the noise decorrelates in just a couple of timesteps. This is therefore no longer a Markov process, however it can be reformulated as such if one considers the appropriate extended space (or keeping the momenta \mathbf{p}_n).

7.11 Applying the Schemes to a Biomolecule

Numerical analysis of a scheme should always be supported (and informed by) thorough numerical testing. Often salient features of a discretization method can be missed because of a shallow scope of experimentation. Our goal will be to evaluate the efficacy of the numerical schemes for Langevin dynamics presented thus far. We shall look at the invariant (long-time) averages resulting from computations using the four symmetric Langevin integrators that we derived using our splitting, for which results for the harmonic oscillator are detailed in (7.15), and for which a more general error analysis was considered in Sect. 7.9.2. Additionally we will compare their results to the performance of the standard SPV and BBK schemes considered in Sect. 7.3.2.

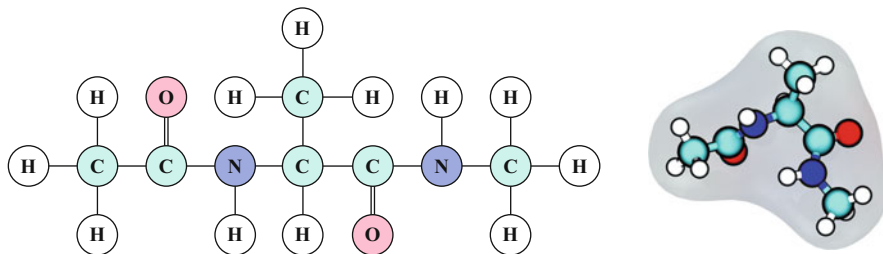


Fig. 7.5 The structure of the alanine dipeptide protein is shown (*left*) with a visualization of the molecule in simulation (*right*)

All of the methods we consider require one force evaluation per iteration, and we consider them as having the same computational cost. The performance of a scheme will be judged on the error we observe in configurational averages, obtained through the computation of Langevin dynamics trajectories. In molecular dynamics, we are very often interested in comparing accuracy of methods for the *largest* stepsizes for which averages can be stably computed.

Our experiments use a classic test case for molecular dynamics: the alanine dipeptide molecule (Fig. 7.5). This is a relatively small molecule, comprising 22 atoms with bonds modelled by a harmonic potential as well as angle bond and dihedral bending potentials to maintain its structure. Potential energy functions modelling the van der Waals and electronic forces are also present, making the model complicated enough to be interesting but simple enough to allow extensive simulation in a short time. The structural properties of the molecule give it two distinct orientations, described by its internal dihedral angles. More complicated molecules have a much greater number of native configurations to be sampled, so considering a molecule with only two major conformational states allows us to check that our algorithms promote barrier crossings at similar rates. As our goal will be to compare the discretization error introduced by a numerical scheme, we can run a large number of repeat simulations to drive down the sampling error.

We implement each of the methods in the NAMD-lite package [170, 302], and observe the effect of discretization error (if any) on computed averages. We initially consider the alanine dipeptide molecule in a vacuum, without boundary conditions, at $T = 300\text{ K}$ for a fixed time interval of 2.5 ns. The CHARMM22 forcefield [246] (giving parameters for the governing potential energy functions) is used to compute force interactions.

7.11.1 Choosing the Friction Parameter

One of the most important features of a numerical method for ergodic dynamics (such as Langevin dynamics) is its preservation of the theoretical global phase space

exploration rate. The spectral properties of the operator $\mathcal{L}_{\text{LD}}^\dagger$ guarantee that we will explore the entire phase space (ergodicity), while the relatively small perturbations to the operator induced by numerical discretization are hoped not to significantly alter the rate of search. Ultimately, pushing the timestep up is the only way to breach timescale gaps when computing trajectories, although this comes at the cost of corruption of the long-time averages.

The self-diffusion coefficient gives a metric quantifying the diffusion rate. It is often used as a way to compare the rate of phase space exploration between methods, and is typically calculated using the integral of the velocity auto-correlation function. However, in theory one can construct arbitrary methods to artificially scale the velocity auto-correlation function, hence giving inaccurate diffusion constants: the momentum sampled may not be the momentum we use to propagate the position with.

Indeed, calculating the temperature of the system from an average of kinetic energy by

$$N_d k_B T = \langle \mathbf{p}^T \mathbf{M}^{-1} \mathbf{p} \rangle, \quad (7.41)$$

gives a similar problem. Using Proposition 6.1 we may formulate many alternative functions whose averages are proportional to the system temperature [193, 211, 319]. Such observables are normally based on the periodic forces of the system in order to work in periodic boundary conditions; in the following experiments we shall use the configurational temperature

$$N_d k_B T = \langle \mathbf{q} \cdot \nabla U(\mathbf{q}) \rangle. \quad (7.42)$$

Were one able to solve the dynamics exactly, the kinetic and configurational temperatures would of course be equal. However, using a numerical method in the large-timestep regime we instead sample expectations with respect to the perturbed density $\hat{\rho}$, that may introduce discrepancies between configurational and kinetic temperatures. Often configuration-based temperature calculation is more useful and relevant for assessing the quality of configurational sampling methods.

In a similar way, the speed of exploration of the space should not be determined solely from functions of momentum. Far more reliable is to compute configurational quantities such as barrier crossing rates, passage times to reach some target region of phase space or the diffusion constant through an Einstein relation (which uses the position data).

The friction parameter is free in Langevin dynamics when it is used purely as a sampling method; we know that for any $\gamma > 0$ we will obtain states from an approximate canonical distribution, though it is unclear what value of γ we should choose in our simulation. From our analysis in Sect. 7.9.3, we have seen that the [[BAOAB]] scheme has a superconvergence property in the limit of large friction, giving us higher accuracy $\mathcal{O}(h^4)$ configurational averages. However, it is unclear what the scheme's behavior is in the middle-to-low friction limit, as we did not give

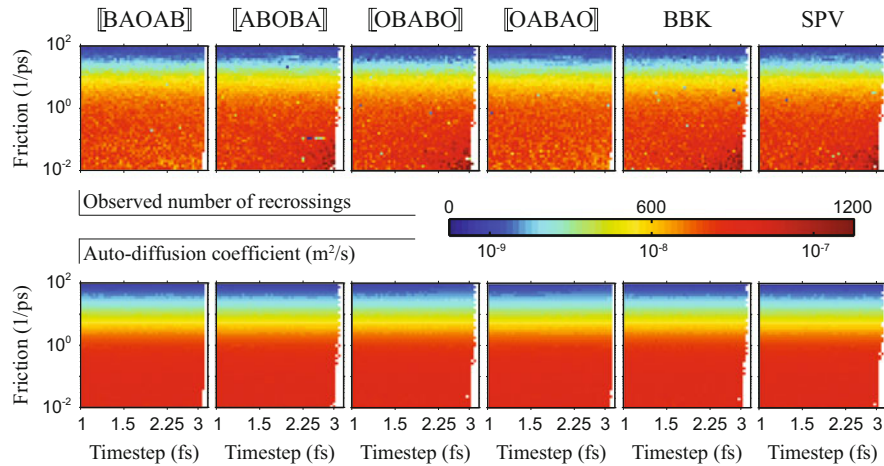


Fig. 7.6 Each pixel of the above grids gives the result of one experiment with the given friction and timestep parameters. We color the pixels according to the results from simulation of alanine dipeptide at 300 K in a vacuum for 2.5 ns, estimating the rate of traversal through the space by counting the number of changes in orientation (top set) as well as calculating the resulting diffusion coefficient (bottom set) for each experiment. It is clear that all of the schemes have similar behavior, with the rate of exploration substantially decreasing as the friction increases above 2/ps. Figure reprinted with permission from [222]. Copyright 2013, AIP Publishing LLC

explicit solutions for the correction functions that govern the leading order error behavior.

In order to examine the behavior of all of the schemes across a wide parameter set, we shall divide the (γ, h) parameter space into a 50×50 grid of points, using a logarithmic scale. We consider $\gamma \in [10^{-2}, 10^2]$ inverse picoseconds (1/ps) and $h \in [1, 3.2]$ femtoseconds (fs). For each gridpoint in parameterspace we run an experiment for the corresponding parameter set, which gives us a fair idea of the behavior of the methods as we vary these experimental parameters.

In order to examine the consequences of increasing the friction in our simulation, we estimate the rate of exploration through the phase space at each parameter set, plotted in Fig. 7.6. We color pixels of the grids by their corresponding exploration rate, quantifying this in two ways: we compute the diffusion coefficient by integrating the velocity autocorrelation function, as well as counting the number of times the alanine dipeptide molecule flips its orientation in experiment. White pixels in the grid indicate a method's instability, showing that in general there is a small stability threshold increase for the large-friction case.

From the results, it is clear that the large friction regime is not a practical choice for sampling large systems, as the rate of barrier crossings significantly diminishes. This is unfortunate for the [[BAOAB]] scheme, as we will likely not be able to take advantage of the superconvergence property in simulation, unless we wish to decrease our rate of exploration through the space.

7.11.2 Results for Configurational Sampling

We compute the relative error in several average quantities, for each experiment shown in Fig. 7.6. These computed errors are relative to a baseline solution, computed using the Stochastic Position Verlet scheme, at $\gamma = 1/\text{ps}$ and $h = 0.5 \text{ fs}$. The timestep for the baseline scheme is small enough that discretization effects will be negligible.

In Fig. 7.7 we plot grids giving the errors for the average total bond energy, and total potential energy of the molecule in each simulation. It is clear that, although sampling error is present, the dominant form of error for the BBK, [OBABO] and [OABAO] schemes is discretization error. If we use these schemes at large stepsizes, then on average the molecule accesses significantly higher energies than it should do at the given temperature. However, these schemes give excellent results for the average kinetic temperature (7.41), underlining the fact that one cannot infer the quality of sampling of position data using momentum data.

One salient feature of the results of Fig. 7.7, is that for the [BAOAB] scheme there is consistently less than a 1 % error in the computed configurational temperature (for moderate friction) across all step sizes, even the largest stable timesteps tested. The relative errors obtained were so small that no discernable trend (with step size) can be shown (due to the sampling error), whereas the other schemes tested show an error consistent with second-order discretization.

The similarity in results between the [ABOBA] and SPV schemes is unsurprising, as the SPV scheme effectively integrates a B+O splitting piece as its central step, whereas the [ABOBA] scheme performs a leapfrog integration of the B and O pieces. The difference between the two methods will depend on the choice of the friction, as for small γ we would expect similar behavior, but in the high friction regime SPV is no longer consistent. We do not increase the friction sufficiently in order to observe this difference in our experiment, and hence the two schemes exhibit very similar behavior.

7.11.2.1 Solvated Alanine Dipeptide

In order to provide a more realistic comparison to practical molecular dynamics simulation, we immerse the alanine dipeptide molecule in a sphere of flexible TIP3P water (10 \AA radius, total system contains 424 atoms, see Fig. 7.8) and equilibrate for 1 ns at 300 K to generate an initial configuration. Simulations were completed with each scheme considered in the unsolvated case, using a 10 \AA cutoff for the electrostatic and van der Waals potentials.

Given the significant increase in dimensionality of the system, we consider only measuring the effect of varying the stepsize on the computed averages. We choose a moderate value for the friction (we fix it at $1/\text{ps}$ in all simulations) which gave

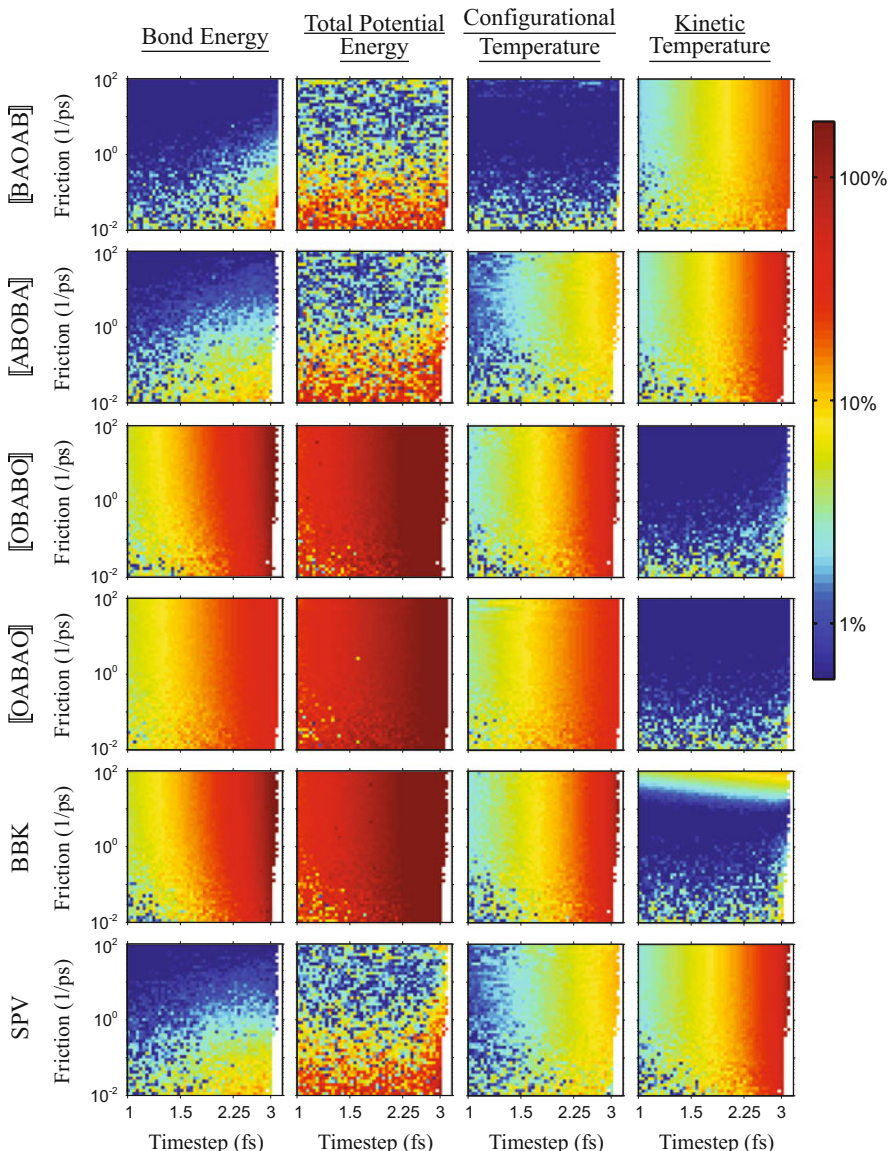


Fig. 7.7 Each pixel of the above grids gives the relative error in computed averages calculated in a vacuum simulation of alanine dipeptide at $T = 300\text{ K}$ for 2.5 ns , where trajectories were computed using one of the Langevin dynamics discretization schemes listed. Each experiment corresponds to a particular friction and timestep parameter set. Though sampling error is still evident, it is clear that discretization error causes many of the schemes significant problems at large stepsizes. Notably, despite not working in the high-friction regime, the $\llbracket \text{BAOAB} \rrbracket$ scheme demonstrates excellent results for configurational sampling. Figure reprinted with permission from [222]. Copyright 2013, AIP Publishing LLC

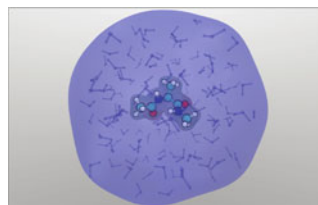


Fig. 7.8 Alanine dipeptide in solvent

reasonable results for all previous simulations in vacuum. We consider a range of timesteps, starting from $h = 1$ fs, with subsequent simulations increasing the step size by 5 %, until reaching a step size where all of the methods fail. This was found after 22 such increments in the timestep, giving a maximum stable step size of approximately 2.8 fs for this model. Note that this is a smaller maximum stepsize than we found in the vacuum case (where some schemes were stable at over 3 fs), due to the high frequency H-O bonds found in the water molecules.

Each simulation was run for 5 ns at 300 K using spherical (harmonically restrained) boundary conditions to maintain the shape of the droplet. The boundary conditions have no effect unless atoms stray out of the 10 Å droplet, at which point a harmonic force pulls them back in. These boundary conditions are considered gentle enough to not significantly alter the behavior of the schemes (the restraining energy was very small in all simulations). It should be noted that, in a realistic molecular dynamics simulation, periodic boundary conditions are implemented, requiring some special treatment of the force calculation to account (for example) for long ranged interactions from the periodic images. Using spherical boundary conditions instead provides a compromise between making the system complex enough to be interesting (and relevant), while keeping it simple enough to allow for highly resolved statistics.

We compute a histogram of the distribution of potential energy for each simulation, by dividing the interval $[-1,500, -1,000]$ (kcal/mol) into 150 bins and normalizing the resulting distribution. We compare the computed distributions with a baseline distribution computed using a SPV simulation at $h = 0.5$ fs. We plot all of the resulting histograms in Fig. 7.9, coloring the results according to the step size used to obtain them (increasing step size is marked from blue to red), overlaying the exact distribution in black.

The **[[ABOBA]]** and SPV schemes perform very well, with only a noticeable difference from the exact distribution as the step size approaches its stability limit. Some schemes, such as BBK or **[[OABAO]]** perform very poorly, with even the smallest step sizes tested giving a visible difference between the distributions. This indicates that the system is able to access much higher energy states than it would do in exact sampling. At the highest step sizes the exact and observed distributions have very little overlap, suggesting a complete failure to sample the system.

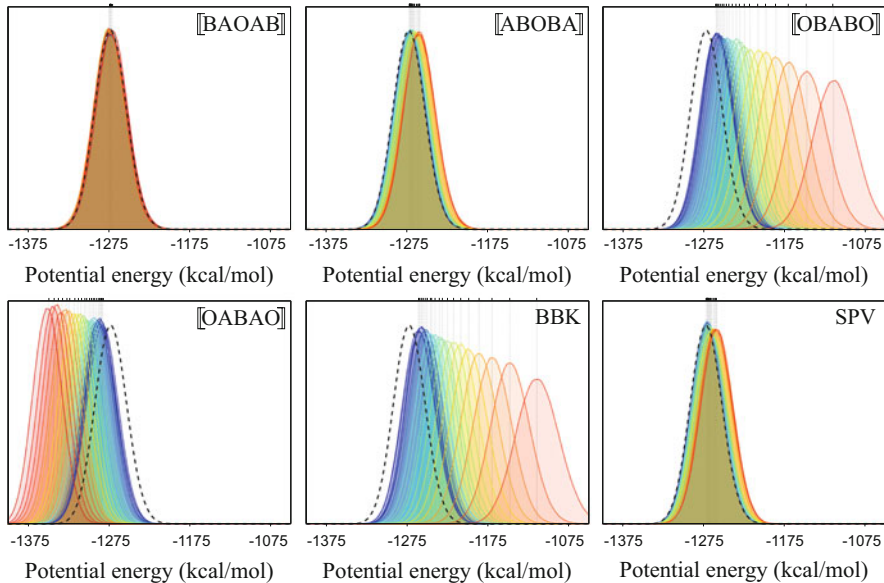


Fig. 7.9 Computed distributions of potential energy are overlaid for 22 experiments of solvated alanine dipeptide using the given discretization scheme. The distributions are colored by the stepsize used to generate them: from $h = 1\text{ fs}$ (blue) to $h = 2.8\text{ fs}$ (red), where the common black dashed distribution marks the baseline result

The distributions generated from trajectories computed using the [[BAOAB]] scheme deviate by only a very small amount, even at the highest step sizes tested. Comparing the energy breakdown, primarily the average bond and dihedral energy terms are responsible for the errors in average potential energy. From the results of the perturbed harmonic analysis in Eq. (7.15), the annihilation of the leading term in the error series (at order ε) appears to lead to the behavior of the [[BAOAB]] scheme. The parallel success of the [[ABOBA]] and SPV schemes (which share a similar update strategy, especially at small friction) support this observation, as such schemes also give excellent configurational sampling properties in (7.15).

In Fig. 7.10 we plot a more quantitative examination of the behavior of the Langevin dynamics scheme. Despite the presence of sampling error, it is clear that for configurational averages, in the large timestep regime, the [[BAOAB]] scheme outperforms the other schemes by a significant margin.

Noticeably the [[BAOAB]] scheme provides an order of magnitude improvement in the configurational temperature results at all step sizes tested. However, the results for its average kinetic temperature are rather poor, especially compared to its conjugate method [[OABAO]] produced from shuffling the terms around. This emphasizes the potentially misleading assumption of equivalence between the two

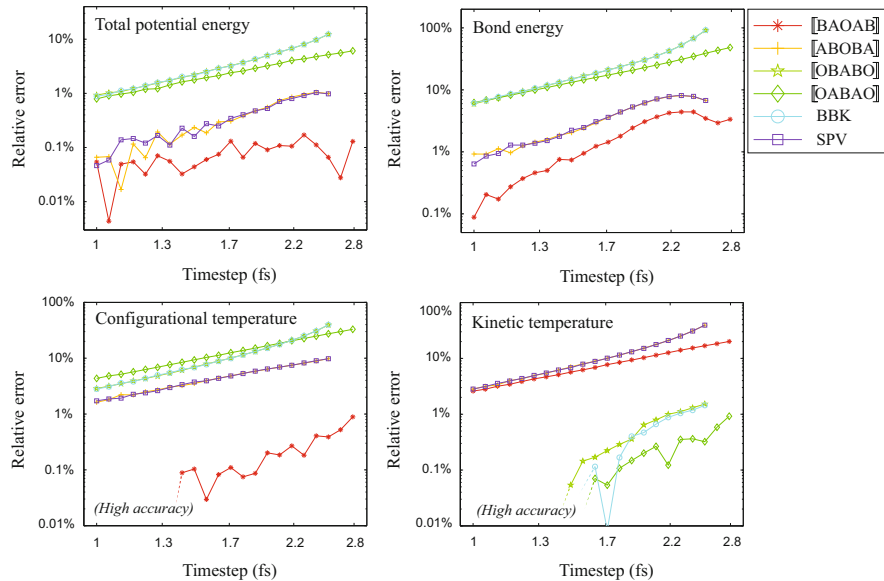


Fig. 7.10 We plot the relative error in computed averages for the a solvated alanine dipeptide model using $\gamma = 1/\text{ps}$ at 300 K, for various Langevin dynamics integrators

types of sampling: configurational sampling is of primary concern, and cannot be inferred from the sampling of momenta.

The success of the $\llbracket \text{BAOAB} \rrbracket$ scheme, even at modest friction, suggests that large improvements could be made to any methods that use Langevin dynamics as a tool for trajectory generation. Improving a method's efficiency (e.g. allowing the use of a larger basic timestep in simulation) thus has a knock-on effect on the efficiency of all the methods that rely on such trajectories. Improvements of just a few percentages in efficiency could merit a minor change in software implementation, the analysis we present here suggests a dramatic difference among various methods, in particular for problems which are dominated by harmonic components (e.g fully flexible atomistic systems).

The contribution of error coming from the restraining boundary condition energy was extremely small, suggesting that the properties of the bulk water in the model are responsible for the differences in efficiency seen here. Hence we would expect the observed corruption of averages to be generalizable to any simulations involving other boundary conditions, or other simulations involving water. Note that we would not expect similar results had we looked at the momentum distribution, but instead this behavior is unique to configurational sampling.

7.12 Constrained Langevin Dynamics

We may use a splitting approach to develop discretization algorithms for other forms of dynamics. In Chap. 4, we included holonomic constraints to the ODEs defining constant-energy Hamiltonian dynamics, as a way to increase the stability of our algorithms and increase the usable timestep. We can add constraints to the Langevin dynamics SDEs similarly as

$$dq = M^{-1}p dt, \quad (7.43)$$

$$dp = -\nabla U(q)dt - \gamma p dt + \sqrt{2\gamma k_B T M} dW - g'(q)^T \lambda dt, \quad (7.44)$$

$$\mathbf{0} = g(q), \quad (7.45)$$

where the vector of l constraints is given by $g : \mathbb{R}^{N_c} \rightarrow \mathbb{R}^l$ and λ is an l -dimensional vector of Lagrange multipliers. W is a vector of standard Wiener processes, with the usual friction parameter $\gamma > 0$. As in the constant energy dynamics, permissible phase points lie in the co-tangent bundle defined by the constraint and hidden constraint

$$g(q) = \mathbf{0}, \quad g'(q)M^{-1}p = \mathbf{0},$$

while in the infinite time limit, we have that solution trajectories of constrained Langevin (7.43)–(7.45) sample $\tilde{\rho}_\beta$ ergodically, such that

$$\lim_{T \rightarrow \infty} \frac{1}{T} \int_0^T \phi(q(t), p(t)) dt = \int_{\mathcal{D}} \phi(q, p) \tilde{\rho}_\beta d\omega,$$

where $\tilde{\rho}_\beta$ is the normalized constrained canonical distribution

$$\tilde{\rho}_\beta = Z^{-1} \exp(-\beta H(q, p)) \delta[g(q)] \delta[g'(q)M^{-1}p],$$

for normalizing constant Z and where $\delta[z] := \prod_i \delta[z_i]$ for a vector z . The goal is now to find solutions to the constrained dynamics, in order to sample the target distribution.

One approach for algorithms is simply to evolve unconstrained Langevin dynamics using any algorithm of choice, then follow each step by a step of the SHAKE algorithm (see Chapter 4 or [322]) to pull the system back on to the manifold satisfying the holonomic constraints.

We could instead consider splitting the dynamics up and performing the integration using a splitting method. Such a splitting strategy is considered in [232] where one uses

$$\begin{bmatrix} \mathbf{d}\mathbf{q} \\ \mathbf{dp} \\ \mathbf{0} \end{bmatrix} = \underbrace{\begin{bmatrix} \mathbf{M}^{-1}\mathbf{p}dt \\ -\nabla U(\mathbf{q})dt - \mathbf{g}'(\mathbf{q})^T \boldsymbol{\lambda} dt \\ \mathbf{g}(\mathbf{q}) \end{bmatrix}}_{H_c} + \underbrace{\begin{bmatrix} \mathbf{0} \\ -\gamma \mathbf{p}dt + \sqrt{2\gamma k_B T} \mathbf{M}^{-1} \mathbf{W} - \mathbf{g}'(\mathbf{q})^T \boldsymbol{\lambda} dt \\ \mathbf{g}(\mathbf{q}) \end{bmatrix}}_{O_c},$$

splitting the dynamics into two pieces: the constrained Hamiltonian (NVE) equations, and a constrained Ornstein-Uhlenbeck piece.

We solve these two pieces symmetrically, where the constrained Hamiltonian part is solved over a step h , in between two solves of the Ornstein-Uhlenbeck SDE with stepsize $h/2$. The SHAKE (or RATTLE) algorithm can be used to solve the constrained Hamiltonian part to a high degree of accuracy, while solving the Ornstein-Uhlenbeck piece along the manifold amounts to finding the solution of a linear system. We observe the constraint in both solutions, so that the computed points lie in the co-tangent bundle of the constraint manifold. Instead of solving the Ornstein-Uhlenbeck exactly, we discretize using a midpoint Euler scheme, yielding the following scheme:

Midpoint Euler - Verlet - Midpoint Euler (see [232])

$$\begin{aligned} \text{Solve } & \left\{ \begin{array}{l} \mathbf{p}_{n+1/4} = \mathbf{p}_n - \frac{h\gamma}{4}(\mathbf{p}_n + \mathbf{p}_{n+1/4}) + \sqrt{h\gamma k_B T} \mathbf{R}_n - \mathbf{g}'(\mathbf{q}_n)^T \boldsymbol{\lambda}_{n+1/4} \\ \text{Such that } \mathbf{g}'(\mathbf{q}_n) \mathbf{M}^{-1} \mathbf{p}_{n+1/4} = \mathbf{0} \end{array} \right. \\ \text{Solve } & \left\{ \begin{array}{l} \mathbf{p}_{n+1/2} = \mathbf{p}_{n+1/4} - \frac{h}{2} \nabla U(\mathbf{q}_n) - \mathbf{g}'(\mathbf{q}_n)^T \boldsymbol{\lambda}_{n+1/2} \\ \mathbf{q}_{n+1} = \mathbf{q}_n + h \mathbf{M}^{-1} \mathbf{p}_{n+1/2} \end{array} \right. \\ \text{Solve } & \left\{ \begin{array}{l} \mathbf{p}_{n+3/4} = \mathbf{p}_{n+1/2} - \frac{h}{2} \nabla U(\mathbf{q}_{n+1}) - \mathbf{g}'(\mathbf{q}_{n+1})^T \boldsymbol{\lambda}_{n+3/4} \\ \text{Such that } \mathbf{g}'(\mathbf{q}_{n+1}) \mathbf{M}^{-1} \mathbf{p}_{n+3/4} = \mathbf{0} \text{ and } \mathbf{g}(\mathbf{q}_{n+1}) = \mathbf{0}. \end{array} \right. \\ & \left. \begin{array}{l} \mathbf{p}_{n+1} = \mathbf{p}_{n+3/4} - \frac{h\gamma}{4}(\mathbf{p}_{n+3/4} + \mathbf{p}_{n+1}) + \sqrt{h\gamma k_B T} \mathbf{R}_{n+1/2} - \mathbf{g}'(\mathbf{q}_{n+1})^T \boldsymbol{\lambda}_{n+1} \\ \text{Such that } \mathbf{g}'(\mathbf{q}_{n+1}) \mathbf{M}^{-1} \mathbf{p}_{n+1} = \mathbf{0} \end{array} \right. \end{aligned}$$

The vectors \mathbf{R}_n and $\mathbf{R}_{n+1/2}$ are vectors of $\mathcal{N}(0, 1)$ i.i.d. random numbers, with $\gamma \geq 0$ the usual Langevin dynamics friction parameter. Setting $\gamma = 0$ reduces the scheme to the usual RATTLE scheme for solving holonomically constrained Hamiltonian equations of motion, whereas if γ is chosen large then this will be expected to cause instability in the scheme, as we are not solving the OU process exactly. The

Lagrange multiplier $\lambda_{n+1/4}$ (and likewise λ_{n+1}) can be obtained by solving the linear system

$$\mathbf{g}'(\mathbf{q}_n) \mathbf{M}^{-1} \left[\left(1 - \frac{h\gamma}{4} \right) \mathbf{p}_n + \sqrt{h\gamma k_B T M} \mathbf{R}_n - \mathbf{g}'(\mathbf{q}_n)^T \boldsymbol{\lambda}_{n+1/4} \right] = \mathbf{0},$$

which is easily computed once the \mathbf{R}_n vector is evaluated in the step, and gives us a stability criterion

$$\gamma h < 4. \quad (7.46)$$

A similar calculation and linear solve is needed to compute $\lambda_{n+3/4}$ in order to maintain the hidden constraint for $\mathbf{p}_{n+3/4}$, whereas the Lagrange multiplier $\lambda_{n+1/2}$ is responsible for ensuring that $\mathbf{g}(\mathbf{q}_{n+1}) = \mathbf{0}$, and is typically found using an implicit solve.

There are many other ways we could choose to combine traditional molecular dynamics discretization schemes with constrained solvers such as variants of the SHAKE algorithm (see, for example [81, 383, 396]). The following section presents an alternative based upon the work on splitting methods in this chapter so far.

7.12.1 A “Geodesic Integrator”

We may consider alternative splittings of the dynamics in order to build a library of available schemes, just as we did in the unconstrained case in Sect. 7.3.1. Solving the constrained OU part exactly would alleviate the condition (7.46), while we may hope to reduce discretization error in the spirit of the success of the [[BAOAB]] scheme in Sect. 7.9.3. The natural splitting template to consider would be to again split into potential and kinetic energies, with the constrained Ornstein-Uhlenbeck piece:

$$\begin{bmatrix} d\mathbf{q} \\ d\mathbf{p} \\ \mathbf{0} \end{bmatrix} = \underbrace{\begin{bmatrix} \mathbf{M}^{-1} \mathbf{p} dt \\ -\mathbf{g}'(\mathbf{q})^T \boldsymbol{\lambda} dt \\ \mathbf{g}(\mathbf{q}) \end{bmatrix}}_{A_c} + \underbrace{\begin{bmatrix} \mathbf{0} \\ -\nabla U(\mathbf{q}) dt - \mathbf{g}'(\mathbf{q})^T \boldsymbol{\lambda} dt \\ \mathbf{g}(\mathbf{q}) \end{bmatrix}}_{B_c} \\ + \underbrace{\begin{bmatrix} \mathbf{0} \\ -\gamma \mathbf{p} dt + \sqrt{2\gamma k_B T M} d\mathbf{W} - \mathbf{g}'(\mathbf{q})^T \boldsymbol{\lambda} dt \\ \mathbf{g}(\mathbf{q}) \end{bmatrix}}_{O_c}.$$

Observe that the holonomic constraint (as well as the hidden constraint) is maintained in each part, changing the usual A piece into a *geodesic drift* along the

manifold defined by $\mathbf{g}(\mathbf{q}) = 0$. We will denote schemes using this splitting in a similar fashion to the unconstrained case, but precede the schemes with “c-” to label the constrained form (for example c-[[BAOAB]] rather than the more cumbersome notation [[B_cA_cO_cA_cB_c]])]. Such a constrained scheme would be:

c-[[BAOAB]]

$$\begin{aligned} \text{Solve } & \left\{ \begin{array}{l} \mathbf{p}_{n+1/5} = \mathbf{p}_n - \frac{\hbar}{2} \nabla U(\mathbf{q}_n) - \mathbf{g}'(\mathbf{q}_n)^T \boldsymbol{\lambda}_{n+1/3} \\ \text{Such that } \mathbf{g}'(\mathbf{q}_n) \mathbf{M}^{-1} \mathbf{p}_{n+1/5} = \mathbf{0} \end{array} \right. \end{aligned}$$

Solve the geodesic flow A_c for $h/2$, and map $[\mathbf{q}_n, \mathbf{p}_{n+1/5}] \rightarrow [\mathbf{q}_{n+1/2}, \mathbf{p}_{n+2/5}]$

$$\begin{aligned} \text{Solve } & \left\{ \begin{array}{l} \mathbf{p}_{n+3/5} = e^{-\gamma h} \mathbf{p}_{n+2/5} + \sqrt{(1 - e^{-2\gamma h}) k_B T} \mathbf{R}_n - \mathbf{g}'(\mathbf{q}_{n+1/2})^T \boldsymbol{\lambda}_{n+2/3} \\ \text{Such that } \mathbf{g}'(\mathbf{q}_{n+1/2}) \mathbf{M}^{-1} \mathbf{p}_{n+3/5} = \mathbf{0} \end{array} \right. \end{aligned}$$

Solve the geodesic flow A_c for $h/2$, and map $[\mathbf{q}_{n+1/2}, \mathbf{p}_{n+3/5}] \rightarrow [\mathbf{q}_{n+1}, \mathbf{p}_{n+4/5}]$

$$\begin{aligned} \text{Solve } & \left\{ \begin{array}{l} \mathbf{p}_{n+1} = \mathbf{p}_{n+4/5} - \frac{\hbar}{2} \nabla U(\mathbf{q}_{n+1}) - \mathbf{g}'(\mathbf{q}_{n+1})^T \boldsymbol{\lambda}_{n+1} \\ \text{Such that } \mathbf{g}'(\mathbf{q}_{n+1}) \mathbf{M}^{-1} \mathbf{p}_{n+1} = \mathbf{0}, \end{array} \right. \end{aligned}$$

where \mathbf{R}_n is a vector of i.i.d $\mathcal{N}(0, 1)$ random numbers and the Lagrange multipliers $\boldsymbol{\lambda}$, ensuring that the hidden constraint is satisfied, can be computed through a linear solve. We do not necessarily need to solve the geodesic flow exactly in practice, though for the purposes of analysis we shall assume we do. If we are considering a second order scheme, then solving the A_c piece to at least second order would be sufficient to preserve the overall order of the scheme, although a scheme may have potentially better accuracy and stability properties if a higher order solve is used.

In practice, we can solve the A_c piece using any constraint algorithm for constant energy dynamics (see Sect. 4.3.6) and substituting zero force. A more accurate solution is obtained for the geodesic drift by either using a number of small steps to integrate over the total time, or composing steps in a certain order to obtain a higher order solution (see Sect. 3.3.3). Relative to the force calculation, solving the geodesic drift step (even to high accuracy) can, in typical molecular systems, be considered computationally cheap. Given these splitting pieces, one may write down constrained equivalents of any of the schemes described in Sect. 7.3.1.

We then ask how to analyze such schemes using the algebraic machinery developed throughout this chapter. As we solve each vector field on the constraint manifold, it is natural to consider the associated Lie derivatives on these manifolds and solve the corresponding Fokker-Planck equation for the discretization to find an invariant distribution, just as we did in the unconstrained case. This is a complicated programme and we do not develop this in detail here.

To compare the performance of the various schemes we perform a numerical experiment to quantify the discretization error caused by the schemes. We implement the c-[[BAOAB]] and c-[[OBABO]] schemes into the NAMD-lite [170, 302] package and consider 233 TIP3P water molecules in a periodic box with dimensions $20 \times 20 \times 20$ Angstroms at 300 K. We constrain the angles and bond lengths of each molecule so that the only forces felt are due to the van der Waals and electronic interactions, parameterized by the CHARMM22 forcefield [246] with an 8-Angstrom cutoff. The system was simulated for a fixed total time of 3ns, after a

In the equilibration period. Full electrostatics were computed using the native NAMD MGRID force routines, while the corresponding geodesic drift step (the ‘A’ step) was computed using the built-in SETTLE algorithm [274]. We would not expect any differences from using a RATTLE-style algorithm to compute the drift instead.

We would expect the c-[[OBABO]] scheme to give very similar results to the ‘Midpoint Euler - Verlet - Midpoint Euler’ (MEVME) algorithm in [232], as both schemes follow the same symmetric update form: ‘fluctuate-kick-drift-kick-fluctuate’. However, as the ‘fluctuate’ step (Ornstein-Uhlenbeck process) is solved exactly in the c-[[OBABO]] scheme, at large friction values γ we would expect that the MEVME scheme would give inferior sampling while being constrained by the stability condition (7.46). There is an additional subtle difference in that we do not solve a geodesic drift in the MEVME scheme, but adjust the momentum in the preceding kick step to remain on the constraint manifold. While it is difficult to quantify what difference this would make to the overall results, modifying a scheme to include a geodesic solve should never reduce the accuracy of the scheme. Hence we would expect the c-[[OBABO]] method to give equivalent, if not superior, sampling to MEVME.

As in the unconstrained experiment reported in Fig. 7.10, we compute the averages of kinetic and potential energy functions, averaged over five independent runs, at friction parameters 0.2/ps and 5/ps, using ten different stepsizes with the lowest 2.5 fs and increasing by 17 % up to 10.3 fs (note that this range of stepsizes is much increased from the unconstrained tests). Computed averages are compared to baseline results averaged over five runs using the c-[[BAOAB]] scheme with stepsize $h = 1\text{ fs}$ and $\gamma = 1/\text{ps}$.

In Fig. 7.11 we plot the computed averages of potential and kinetic energies using either the c-[[OBABO]] scheme, or the c-[[BAOAB]] scheme. Surprisingly for such a short experiment, we are able to resolve the second order behavior of either potential or kinetic energy for each method due to the dominance in discretization error. The results also mirror the flexible case: the c-[[BAOAB]] scheme gives a strong second order result for kinetic energy, while the c-[[OBABO]] scheme is second order for the potential energy. However, as expected we are unable to resolve the higher order behavior due possibly to the presence of statistical noise, and can only show a dramatic difference between the methods in terms of the evident error. Due to the poor resolution, it is difficult to see clear differences in the results as we change the Langevin dynamics friction parameter γ , although it is evident in the c-[[BAOAB]] case that increasing friction offers a small increase in stepsize. The only significant difference was noted at the largest stepsize tested, where the c-[[BAOAB]] scheme performed markedly better at larger friction.

It is clear that the c-[[BAOAB]] scheme gives a superior calculation of the average of potential energy (the computed distributions are plotted in Fig. 7.12), with an apparent order of magnitude improvement in the error compared to c-[[OBABO]]. Additionally it allows for a significant improvement in stability between the two

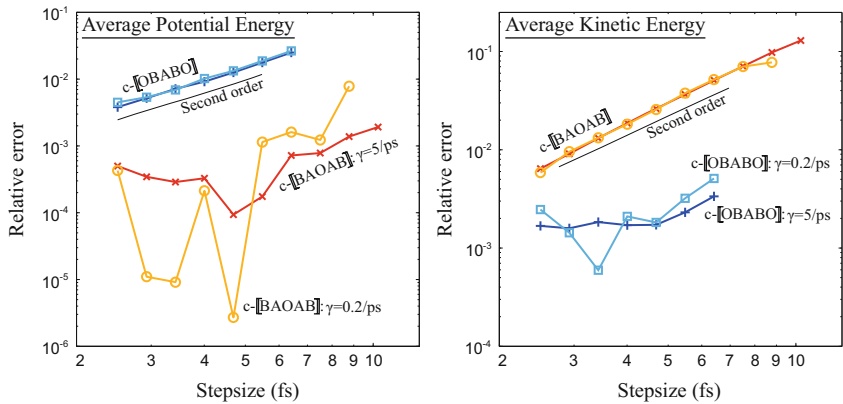


Fig. 7.11 The error in the computed average kinetic and potential energies for a box of 233 rigid water molecules is compared for the two schemes using varying stepsizes. The c-[OBABO] scheme clearly provides superior averages of the kinetic energy, while the c-[BAOAB] scheme gives considerably improved results for the average potential energy

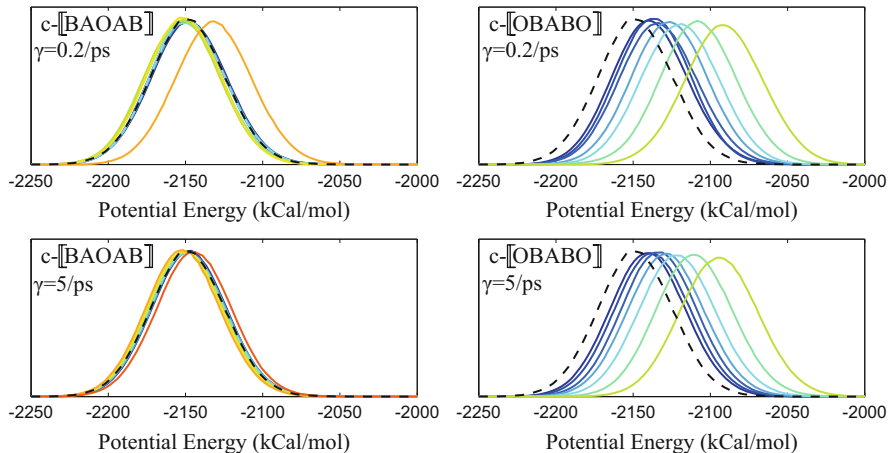


Fig. 7.12 We plot the normalized potential energy distributions for simulations of water using the schemes (c-[BAOAB] left, c-[OBABO] right) and friction parameters ($\gamma = 0.2/\text{ps}$ top, $\gamma = 5/\text{ps}$ bottom) with distributions colored by increasing step size (2.5 fs in blue to 10.3 fs in red) with successive lines indicating a 17% increase in the step size. The baseline distribution is plotted as a black dashed line

schemes; the c-[OBABO] scheme became unstable around $h = 7$ fs, while we were able to increase the timestep for the c-[BAOAB] to beyond $h = 9$ fs without obvious repercussions.

7.13 Multiple Timestepping

Recall the r-RESPA multiple timestepping scheme introduced in Sect. 4.2, designed to propagate systems which have a fast highly oscillatory motion, as well as a slower long-ranged force term. Splitting the potential energy function into fast and slow components in the deterministic setting provided only a small gain in the stability threshold, as we encountered linear resonance phenomena at step sizes that were integer multiples of half a period. In systems where the timescale gap is very large, the r-RESPA scheme does not give significant improvement, with the stability threshold scaling identically to the Symplectic Euler method.

Our hope would be that using Langevin dynamics to add stochasticity would disrupt resonance effects and permit larger usable timesteps. While some considerable efficiency improvements have been demonstrated using multiple timestepping methods for Langevin dynamics with constraints [118], we shall investigate the simpler fast/slow splitting demonstrated in previous chapters.

We consider propagating a system with Hamiltonian

$$H(q, p) = p^2/2 + U(q), \quad U(q) = U_F(q) + U_S(q),$$

where $q, p \in \mathbb{R}$ and U_S and U_F denote the slow and fast components of the potential energy respectively. For the purposes of analysis, we shall model these with harmonic potentials, with

$$U_S(q) = q^2/2, \quad U_F(q) = \Omega^2 q^2/2, \tag{7.47}$$

where $\Omega \gg 1$. The question we shall be interested in is whether using Langevin dynamics with a multiple timestepping algorithm gives us any extra stability compared to the deterministic case. Let us consider splitting the dynamics into

$$\begin{bmatrix} dq \\ dp \end{bmatrix} = \underbrace{\begin{bmatrix} p dt \\ -\Omega^2 q dt - \gamma p dt + \sqrt{2\gamma/\beta} dW \end{bmatrix}}_{\text{Fast}} + \underbrace{\begin{bmatrix} 0 \\ -q dt \end{bmatrix}}_{\text{Slow}}, \tag{7.48}$$

and proceed as in the case of the r-RESPA scheme. As before, we consider the case where we are able to solve the fast part exactly (in practice we use several small timesteps as the fast parts are considered computationally ‘‘cheap’’). Writing

$$\mathbf{F} = \begin{bmatrix} 0 & 1 \\ -\Omega^2 & -\gamma \end{bmatrix},$$

we can write down the solution to the fast dynamics as

$$\begin{bmatrix} q(t) \\ p(t) \end{bmatrix} = \exp(\mathbf{F}t) \begin{bmatrix} q(0) \\ p(0) \end{bmatrix} + \mathbf{B}_t \mathbf{R},$$

where \mathbf{R} is a column vector of two i.i.d. random normal numbers distributed as $\mathcal{N}(0, 1)$, and

$$\mathbf{B}_t \mathbf{B}_t^T = \frac{2\gamma}{\beta} \int_0^t \exp(\mathbf{F}(t-s)) \begin{bmatrix} 0 & 0 \\ 0 & 1 \end{bmatrix} \exp(\mathbf{F}^T(t-s)) ds.$$

The solution to the slow part of our splitting is just

$$\begin{bmatrix} q(t) \\ p(t) \end{bmatrix} = \begin{bmatrix} 1 & 0 \\ -t & 1 \end{bmatrix} \begin{bmatrix} q(0) \\ p(0) \end{bmatrix}.$$

Thus for a method taking one step of the fast system followed by a step of the slow system, using fixed step size $h > 0$, we can write the update scheme for $\mathbf{z} = [q, p]^T$ as

$$\mathbf{z}_{n+1} = \mathbf{X}\mathbf{z}_n + \mathbf{Y}\mathbf{R}_n,$$

for

$$\mathbf{X} = \begin{bmatrix} 1 & 0 \\ -h & 1 \end{bmatrix} \exp(h\mathbf{F}), \quad \mathbf{Y} = \begin{bmatrix} 1 & 0 \\ -h & 1 \end{bmatrix} \mathbf{B}_h.$$

The stability of the method therefore depends solely on the spectral radius of the matrix \mathbf{X} . Denoting $\eta = \sqrt{\gamma^2 - 4\Omega^2}$, then we compute

$$\det(\mathbf{X}) = e^{-\gamma h}, \quad \text{tr}(\mathbf{X}) = \frac{\eta - h}{\eta} e^{(\eta - \gamma)h/2} + \frac{\eta + h}{\eta} e^{(-\eta - \gamma)h/2},$$

giving a stability condition

$$\left| \frac{\eta - h}{\eta} e^{(\eta - \gamma)h/2} + \frac{\eta + h}{\eta} e^{(-\eta - \gamma)h/2} \right| \leq 1 + e^{-\gamma h}.$$

Multiplying by $e^{\gamma h/2}$ gives

$$\left| \cosh\left(\frac{\eta h}{2}\right) + \frac{h}{\eta} \sinh\left(-\frac{\eta h}{2}\right) \right| \leq \cosh\left(\frac{\gamma h}{2}\right),$$

which reduces to the deterministic stability condition as expected in the limit $\gamma = 0$. For $\gamma > 0$, we can simplify to

$$\left| \cosh\left(\frac{\eta h}{2} - \operatorname{atanh}\left(\frac{h}{\eta}\right)\right) \sqrt{1 - \frac{h^2}{\eta^2}} \right| \leq \cosh\left(\frac{\gamma h}{2}\right).$$

We consider the case with $\gamma \ll \Omega$, allowing us to write $\eta = i\hat{\eta}$ for $\hat{\eta} \in \mathbb{R}$, and

$$\left| \cos\left(\frac{\hat{\eta}h}{2} - \operatorname{atanh}\left(\frac{h}{\hat{\eta}}\right)\right) \sqrt{1 + \frac{h^2}{\hat{\eta}^2}} \right| \leq \cosh\left(\frac{\gamma h}{2}\right).$$

The term on the left hand side of the inequality is oscillatory in h , while the term on the right hand side uniformly grows with step size. This implies that for any suitable $\gamma > 0$, we can find small pocket regions of the step size where the left hand side is sufficiently minimized in order to give stability. However, just as in the deterministic case, these island stability regions are difficult to predict the location of in a more general system.

The oscillatory cosine term is bounded between ± 1 , implying that we have stability for all step sizes provided the condition

$$\sqrt{1 + \frac{h^2}{\hat{\eta}^2}} \leq \cosh\left(\frac{\gamma h}{2}\right), \quad (7.49)$$

holds. We expect there to exist stability regions for smaller values of the friction where this condition is violated, but these will be interposed between unstable regions coming from the oscillatory term. We have guaranteed stability where (7.49) holds, which we can simplify to

$$\frac{h}{\sqrt{4\Omega^2 - \gamma^2}} \leq \sinh\left(\frac{\gamma h}{2}\right).$$

For a fixed value of the friction, if we increase the step size the right hand side will grow exponentially compared to the linear growth on the left hand side, so it would seem that for large h we actually need a smaller friction in order to be stable. Hence the minimum required friction for stability can be found by considering the case of small timestep. This gives a bound

$$\frac{1}{\sqrt{4\Omega^2 - \gamma^2}} \leq \frac{\gamma}{2},$$

which gives a stability condition for all step sizes h as long as

$$\gamma \geq \Omega \sqrt{2 - 2\sqrt{1 - \Omega^{-4}}} \geq \sqrt{2}/\Omega.$$

Therefore we expect that the minimum friction value required for stability for all timesteps $h > 0$, scales with the value of inverse Ω . Unlike the deterministic case, we are able to remove linear resonance effects with a sufficiently large friction term.

We illustrate this numerically in Fig. 7.13, by applying the splitting scheme (7.48) using various timesteps and frictions. Each gridpoint marks an independent simula-

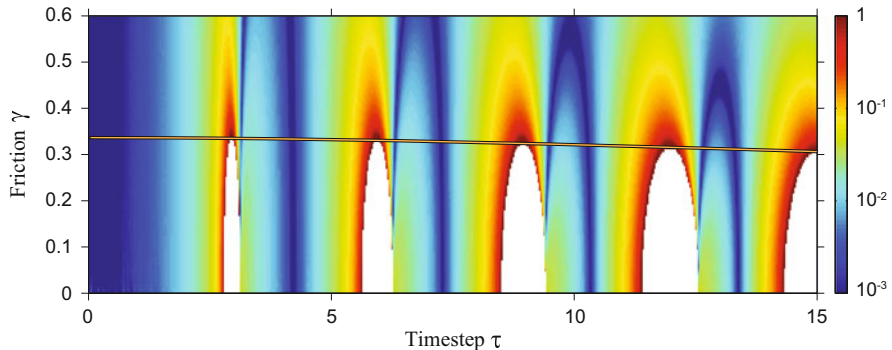


Fig. 7.13 We consider the stability of a multiple timestepping scheme incorporating Langevin dynamics, with potential energy function (7.47) choosing $\Omega = 3$. Each pixel represents a simulation undertaken with parameters (τ, γ) , for $\tau = \Omega h$. The color of a pixel indicating the absolute error in $\langle q^2 \rangle_h$ where white pixels indicate instability of the method. The plotted line gives the boundary to the region where (7.49) is satisfied

tion of 10^8 steps using $\Omega = 3$ with the given values of γ and τ (where $\tau = \Omega h$). The plotted line marks the boundary of the region where (7.49) is satisfied, which matches the experimental stability limit. For small friction, the stability limit occurs at $\tau = \pi$, which is commensurate with the deterministic case ($\gamma = 0$) presented in Chap. 4.

The island regions of instability vanish as expected for large values of friction, while choosing $\gamma = \sqrt{2}/\Omega \approx 0.471$ in this example is plainly sufficient to give stability for all visible step sizes.

It is important to emphasize the tremendous complexity of molecular dynamics in relation to the simple model scenario presented here. In [22, 29], multiple timestepping was used effectively to treat large scale systems where the force splitting is defined in the context of particle-mesh Ewald long-ranged force computations. We also point out that where additional constraints are present, the prospects for multiple timestepping may be significantly better, as, in the previously mentioned work [118] and in Sect. 8.6 of the next chapter, where isokinetic constraints are used to stabilize the system.

Exercises

1. If we use $\mathbf{R}'_n = \mathbf{R}_{n+1}$ in the BBK scheme, then we arrive at the BBK* scheme encountered in Example 7.2. Compute the value of $\langle q^2 \rangle_h$ for the variants of the BBK scheme where $H = p^2/2 + q^2/2$ with the choices of

- a. $\mathbf{R}'_n = \mathbf{R}_n$,
- b. $\mathbf{R}'_n = \mathbf{R}_{n-1}$,
- c. $\mathbf{R}'_n = \mathbf{R}_{n+1/2}$, (here \mathbf{R}'_n and \mathbf{R}_n will be independent).

When choosing the two noises to be independent, the BBK scheme will produce an error independent of stepsize h . Modifying the given noise processes in (c) such that $\mathbb{E}\mathbf{R}_{n+1/2}^2 = \mathbb{E}\mathbf{R}_n^2 = \lambda$, find a $\lambda > 0$ that recovers canonical sampling when h is small.

2. Consider the Stochastic Position Verlet (SPV) splitting method defined in Sect. 7.3.2.
 - a. For the one dimensional harmonic oscillator, find the values of $\langle q^2 \rangle_h$, $\langle p^2 \rangle_h$ and $\langle qp \rangle_h$ when using the SPV scheme.
 - b. Find the leading order error in $\langle q^2 \rangle_h$ for the perturbed harmonic oscillator with potential energy function $U(q) = q^2/2 + \varepsilon q^4/4$.
3. We were able to use Lemma 7.1 to relate the schemes with central OU update to those with OU updates at the ends, however we could have continued to solve the original PDEs instead.
 - a. Compute $\mathcal{L}_{2,\llbracket\text{ABOBA}\rrbracket}^\dagger \rho_\beta$ and $\mathcal{L}_{2,\llbracket\text{BAOAB}\rrbracket}^\dagger \rho_\beta$.
 - b. Verify that the Fredholm alternative is satisfied.
4. Consider the GLA schemes of the form $\llbracket\text{OXYX}\rrbracket$, making the ansatz that the invariant distribution is

$$\hat{\rho} = \rho_\beta(1 + hf_{1,\llbracket\text{OXYX}\rrbracket} + h^2f_{2,\llbracket\text{OXYX}\rrbracket} + h^3f_{3,\llbracket\text{OXYX}\rrbracket} + \dots).$$

- a. Verify that $f_{1,\llbracket\text{OABA}\rrbracket} = f_{1,\llbracket\text{OBAB}\rrbracket} = 0$.
- b. Using the results of Lemma 7.1, find $f_{2,\llbracket\text{OABA}\rrbracket}$ and $f_{2,\llbracket\text{OBAB}\rrbracket}$ in terms of $f_{2,\llbracket\text{OABAO}\rrbracket}$ and $f_{2,\llbracket\text{OABAO}\rrbracket}$.
- c. Find the third order correction $f_{3,\llbracket\text{OABA}\rrbracket}$ and $f_{3,\llbracket\text{OBAB}\rrbracket}$ in terms of $f_{2,\llbracket\text{OABAO}\rrbracket}$ and $f_{2,\llbracket\text{OABAO}\rrbracket}$.
5. Write out the limiting schemes for the $\llbracket\text{OAB}\rrbracket$ and $\llbracket\text{OBA}\rrbracket$ methods and verify that they are inconsistent with the dynamics by comparing them to the Euler-Maruyama scheme.
6. Consider the Langevin dynamics splitting strategy

$$d \begin{bmatrix} q \\ p \end{bmatrix} = \underbrace{\begin{bmatrix} M^{-1}p \\ \mathbf{0} \end{bmatrix}}_A dt + \underbrace{\begin{bmatrix} \mathbf{0} \\ -\nabla U \end{bmatrix}}_B dt + \underbrace{\begin{bmatrix} \mathbf{0} \\ -\gamma p \end{bmatrix}}_C dt + \underbrace{\begin{bmatrix} \mathbf{0} \\ \sqrt{2\gamma k_B T} M^{1/2} \end{bmatrix}}_D dW.$$

- a. Find \mathcal{L}_C^\dagger and \mathcal{L}_D^\dagger .
- b. Write down the scheme corresponding to $\llbracket\text{ABCD}\rrbracket$, and compute $\mathcal{L}_{\llbracket\text{ABCD}\rrbracket}^\dagger$ to first order for q and $p \in \mathbb{R}$.
- c. Using your answer to (b.), compute the first order correction function for the method $\llbracket\text{ABCD}\rrbracket$ by considering the solution to $\mathcal{L}_{\llbracket\text{ABCD}\rrbracket}^\dagger \rho = 0$.
- d. What behavior do you expect in the limit of large friction γ ?

- 7. [Computer Investigation]** Consider canonically sampling the planar system with Hamiltonian

$$H(x, y, p_x, p_y) = p_x^2/2 + p_y^2/2 + (x^2 - 1)^2/4 + (y^2 - 1)^2/4 + xy,$$

at inverse temperature $\beta = 1$.

- a. Verify that $\langle x^2 + y^2 \rangle \approx 3.043$, by either using a discretization scheme with small discretization parameter, or using a high-accuracy numerical solver (e.g. MAPLE or Mathematica).
- b. Use the Euler-Maruyama scheme (7.39) to compute $\langle x^2 + y^2 \rangle_\tau$ for several values of the stepsize $\tau \in (0, 0.2]$.
- c. Run the same experiment as part (b) using the (7.40) instead. Compare the errors in the computed averages for both schemes, as well as the overall stability of the methods.
- d. In the limit $\gamma \rightarrow \infty$, the $\llbracket\text{OBABO}\rrbracket$ scheme converges to Euler-Maruyama, while the $\llbracket\text{BAOAB}\rrbracket$ scheme converges to the scheme (7.40). Implement $\llbracket\text{OBABO}\rrbracket$ and $\llbracket\text{OBABO}\rrbracket$ in your language of choice and investigate their behavior in this limit (i.e. repeat parts (b) and (c) for fixed small, medium and large values of γ).

Chapter 8

Extended Variable Methods

In the previous chapter we described numerical methods for solving the equations of Langevin dynamics, a system of stochastic differential equations that sample the canonical ensemble. The methods allow us to compute averages of the form

$$\text{Av}_\beta(\phi(\mathbf{q}, \mathbf{p})) = \frac{\int_{\mathcal{D}} \phi(\mathbf{q}, \mathbf{p}) \rho_\beta(\mathbf{q}, \mathbf{p}) d\omega}{\int_{\mathcal{D}} \rho_\beta(\mathbf{q}, \mathbf{p}) d\omega},$$

where $\rho_\beta = \exp(-\beta H)$, and H is the system Hamiltonian. In this chapter we extend the range of systems that can be used to accomplish this task using methods based on the incorporation of auxiliary variables. We also consider schemes for sampling alternative thermodynamic ensembles, for example those defined by constant number of atoms N , pressure P and temperature T . In some of the methods, based on purely deterministic models, the ergodic property may be compromised, so an important issue is to design schemes that restore this. We will focus on methods that introduce random processes in direct contact with the auxiliary variables.

Besides canonical or configurational sampling, another common purpose of molecular simulation is the calculation of a dynamical (time-dependent) quantity such as the rearrangement of a molecular group over time or a diffusion rate. The only dynamical calculations that make sense in the context of molecular modelling, where trajectories are chaotic, are those that involve some sort of average. We consider this average in a thermodynamic sense and assume that the calculation can be formulated as the determination of the canonically weighted correlation between two quantities evaluated at different times, for example

$$C_\beta(\tau) = \frac{\int_{\mathcal{D}} \mathbf{A}(\mathbf{z}) \cdot \mathbf{B}(\mathcal{F}_\tau^H(\mathbf{z})) \rho_\beta d\omega}{\int_{\mathcal{D}} \mathbf{A}(\mathbf{z}) \cdot \mathbf{B}(\mathbf{z}) \rho_\beta d\omega}.$$

\mathcal{F}_t^H represents the flow map of Hamiltonian dynamics. Thus $C(0) = 1$. At large τ , if the system is “mixing,” and loses memory of its starting point, hence

$$\text{Av}_\beta [\mathbf{A}(\mathbf{z}) \cdot \mathbf{B}(\mathcal{F}_\tau^H(\mathbf{z}))] \approx \text{Av}_\beta [\mathbf{A}(\mathbf{z})] \cdot \text{Av}_\beta [\mathbf{B}(\mathbf{z})]$$

is approximately independent of τ . Thus the correlation should approximately vanish at large time, provided the scalar product of the average of \mathbf{A} and the average \mathbf{B} vanishes. Computing an autocorrelation function $C_\beta(\tau)$ normally involves performing a stationary thermodynamic calculation in which the observable itself depends on a Hamiltonian dynamics calculation.

There is no reason for taking the averages solely with respect to ρ_β . We could in effect assume any prior distribution for the initial conditions. Our choice of Gibbs statistics in defining autocorrelation is made for purely practical reasons—it simplifies the study of the problem by allowing us to bring to bear the common techniques of thermodynamic sampling. In some cases, the Gibbs weight is ignored and the calculation is performed as an average two point correlation along a single trajectory. In some cases this calculation is performed using a single thermostatted molecular dynamics trajectory. Such a calculation is only justified when the thermostat is “weakly coupled” to the physical system. In this setup, the key to accurately computing averaged dynamics of molecular systems is to use thermostat techniques that minimally perturb the physical dynamics. We will briefly discuss how this may be achieved while maintaining the ergodic property.

8.1 Dynamics-Based Thermostat Techniques

Deterministic trajectories can sometimes be used to sample the canonical measure. A very simple technique of this type is Hamiltonian dynamics itself.

Let a Hamiltonian $H(\mathbf{q}, \mathbf{p})$ be given and let \mathcal{L} be its Liouvillian

$$\mathcal{L} = \nabla_{\mathbf{p}} H \cdot \nabla_{\mathbf{q}} - \nabla_{\mathbf{q}} H \cdot \nabla_{\mathbf{p}}.$$

Recall from Chap. 5 that, as the dynamics automatically preserves functions of H , the Liouvillian satisfies $\mathcal{L}\varphi(H) = 0$. We also know that for Hamiltonian dynamics \mathcal{L} is skew-adjoint, i.e., $\mathcal{L}^\dagger = -\mathcal{L}$ which implies that $\mathcal{L}^\dagger\psi(H) = 0$. Hence any density which is a function of H will be preserved, and this includes the canonical one $\psi(H) = \exp(-\beta H)$.

If we select a set of points at random from the canonical distribution, then initiate trajectories of Hamiltonian dynamics from each of these points, the points will remain Gibbs-distributed over time. If the paths themselves are ergodic on the surfaces of constant energy $H = E$ then the collection of paths may provide a usable sampling of the canonical distribution. Such a sampling technique relies on having the means of choosing initial points from the canonical distribution; as this is the

purpose of the sampling strategy itself, the method of sampling by Hamiltonian trajectories seems less than robust.

Alternative families of methods exist which are based on extending the phase space of the system in such a way as to (a) disturb the conserved quantity $H = E$, while (b) nonetheless preserving the phase space distribution. In general these methods involve introducing additional variables $\xi = (\xi_1, \xi_2, \dots, \xi_k)$ and additional equations of motion to drive them. The combined system is carefully designed to preserve an extended invariant distribution

$$\tilde{\rho}(\mathbf{q}, \mathbf{p}, \boldsymbol{\xi}) = \rho_\beta(\mathbf{q}, \mathbf{p}) \times \hat{\rho}(\boldsymbol{\xi}), \quad (8.1)$$

where the auxiliary density $\hat{\rho}$ has a simple form (typically, a multivariate Gaussian). Then it follows that

$$\int \int \int g(\mathbf{q}, \mathbf{p}) \tilde{\rho}(\mathbf{q}, \mathbf{p}, \boldsymbol{\xi}) d\omega_q d\omega_p d^k \boldsymbol{\xi} \propto \int \int g(\mathbf{q}, \mathbf{p}) \rho_\beta(\mathbf{q}, \mathbf{p}) d\omega_q d\omega_p.$$

Assuming ergodicity of the coupled system it is then possible to calculate averages with respect to the Gibbs-Boltzmann measure by direct averaging along trajectories of the extended system.

The assumption of ergodicity is a major one (just as difficult to demonstrate as would be the corresponding assumption for a Hamiltonian system); indeed it is likely that it fails generically, and there are certainly known cases where thermodynamic averages computed using deterministic thermostats are incorrect. However, deterministic methods are nonetheless often used in molecular simulation, suggesting that, for the systems involved, averages can be recovered with sufficient accuracy starting from most points of phase space.

8.1.1 Nosé Dynamics: A Deterministic Thermostat

The simplest scheme of this type is the Nosé-Hoover method [182, 284–286]. There is just one auxiliary variable ξ and the extended system takes the form

$$\frac{d\mathbf{q}}{dt} = \mathbf{M}^{-1}\mathbf{p}, \quad (8.2)$$

$$\frac{d\mathbf{p}}{dt} = -\nabla U(\mathbf{q}) - \xi \mathbf{p}, \quad (8.3)$$

$$\mu \frac{d\xi}{dt} = \mathbf{p}^T \mathbf{M}^{-1} \mathbf{p} - N_d \beta^{-1}. \quad (8.4)$$

We have deliberately written N_d . The number of degrees of freedom in the last equation must be used so that the equation is in balance at thermal equilibrium.

The equation for the variable ξ represents a negative feedback loop which acts to control the value of ξ (and hence to regulate the kinetic energy). When the temperature of the system, measured as the average kinetic energy per degree of freedom, is high compared to the “target temperature” β^{-1} , the control equation will insure that ξ increases, eventually becoming positive. This will damp (cool) the physical variables; eventually the kinetic energy will fall below the target value, and ξ will become negative. By fluctuating in this way, ξ typically maintains the time-averaged kinetic energy of the system at very near $N_d\beta^{-1}/2$.

The parameter μ_0 is arbitrary and can be used to improve the performance of the method in practical calculations.

This method preserves an extended measure with density of the form

$$\tilde{\rho}(\mathbf{q}, \mathbf{p}, \xi) = \rho_\beta(\mathbf{q}, \mathbf{p}) \times e^{-\beta\mu\xi^2/2}. \quad (8.5)$$

That is, one can show that $\mathcal{L}_f^\dagger \tilde{\rho} = 0$, where f is the full vector field associated to the Nosé-Hoover system.

Observe that we can split f into two parts: $f = f_1 + f_2$, where

$$f_1 = \begin{bmatrix} \mathbf{M}^{-1}\mathbf{p} \\ -\nabla U(\mathbf{q}) \\ 0 \end{bmatrix}, \quad f_2 = \begin{bmatrix} 0 \\ -\xi\mathbf{p} \\ \mu^{-1}(\mathbf{p}^T \mathbf{M}^{-1} \mathbf{p} - N_d \beta^{-1}) \end{bmatrix}.$$

The Liouvillian¹ follows a similar decomposition:

$$\mathcal{L}_f^\dagger = \mathcal{L}_{f_1}^\dagger + \mathcal{L}_{f_2}^\dagger.$$

Since the first part (which is simply Hamiltonian dynamics) preserves the extended Gibbs measure $\tilde{\rho}$, it is evidently enough to show that the system

$$\frac{d\mathbf{p}}{dt} = -\xi\mathbf{p}, \quad (8.6)$$

$$\mu \frac{d\xi}{dt} = \mathbf{p}^T \mathbf{M}^{-1} \mathbf{p} - N_d \beta^{-1}, \quad (8.7)$$

preserves $\tilde{\rho}$ as well. The Liouvillian $\mathcal{L}_{f_2}^\dagger$ associated to this system is defined by

$$\mathcal{L}_{f_2}^\dagger \phi = \nabla_{\mathbf{p}} \cdot (\xi \mathbf{p} \phi) - \frac{\partial}{\partial \xi} (\mu^{-1} [\mathbf{p}^T \mathbf{M}^{-1} \mathbf{p} - N_d \beta^{-1}] \phi).$$

It is left as an exercise to demonstrate that, with this definition and (8.5), $\mathcal{L}_{f_2}^\dagger \tilde{\rho}_\beta = 0$.

¹Technically, “Liouville’s equation” refers to the continuity equation in the setting of a volume preserving flow. Here we use the term “Liouvillian” to refer to the operator whose action on a density gives the right hand side of the general continuity equation.

Let a further dynamical variable s be defined by

$$\frac{ds}{dt} = \xi.$$

The extended Nosé-Hoover system then has a conserved quantity (see Exercise 2):

$$I_{\text{NH}}(\mathbf{q}, \mathbf{p}, \xi, s) = H(\mathbf{q}, \mathbf{p}) + \frac{\mu \xi^2}{2} + N_d \beta^{-1} \ln s. \quad (8.8)$$

This integral can be used to monitor the performance of numerical methods.

8.1.2 Numerical Methods for Extended System Thermostats

We next describe some numerical procedures (based on the concept of splitting introduced in Chaps. 2 and 3) which are appropriate for thermostats based on the incorporation of auxiliary variables.

Nosé-Hoover dynamics is not a Hamiltonian system, despite the presence of the mentioned first integral. It is, however, time-reversible: changing the sign of \mathbf{p} and ξ simultaneously in the equations of motion is equivalent to reversing the arrow of time $t \rightarrow -t$. For this reason, time-reversible numerical methods are often proposed for Nosé-Hoover. A typical integrator is described below.

To simplify the notation and to use a format that might more closely match what would be implemented in software, we write the algorithm for a single timestep of the method in which positions, momenta and auxiliary variables are updated *in situ*.

Nosé-Hoover Timestep Map

$$\begin{aligned} \mathbf{q} &:= \mathbf{q} + (h/2)\mathbf{M}^{-1}\mathbf{p} \\ \mathbf{p} &:= e^{-h\xi/2}\mathbf{p} - c(h/2, \xi)\nabla U(\mathbf{q}) \\ \xi &:= \xi + h\mu^{-1} [\mathbf{p}^T \mathbf{M}^{-1} \mathbf{p} - N_d k_B T] \\ \mathbf{p} &:= e^{-h\xi/2}\mathbf{p} - c(h/2, \xi)\nabla U(\mathbf{q}) \\ \mathbf{q} &:= \mathbf{q} + (h/2)\mathbf{M}^{-1}\mathbf{p} \end{aligned}$$

Here we have solved successively, the first, second and third equations, sequentially, and then in reverse order to make a symmetric (and second order) integrator. The auxiliary function involved $c(t, \xi) = \frac{1-e^{-t\xi}}{\xi}$ is easily evaluated from a few terms of its Maclaurin series expansion

$$c(t, \xi) = t - t^2 \xi / 2 + \dots$$

It is easy to verify that this method is time-reversible. If we write the timestep map as $(\mathbf{q}, \mathbf{p}, \xi) \mapsto \mathcal{G}_h(\mathbf{q}, \mathbf{p}, \xi)$, then we may check that

$$\mathbf{R} \circ \mathcal{G}_h \circ \mathbf{R} = \mathcal{G}_h^{-1}, \quad \mathbf{R}(\mathbf{q}, \mathbf{p}, \xi) = (\mathbf{q}, -\mathbf{p}, -\xi).$$

8.1.2.1 Nosé-Poincaré Dynamics: A Symplectic Approach

As we have seen in earlier chapters, there is a strong foundation for using symplectic integrators, for example the existence of perturbative backward error expansions which are relatively easily calculated, it is desirable to work within this class. On the other hand, as we have mentioned, Nosé-Hoover dynamics is not a Hamiltonian system. The Nosé-Poincaré method resolves this issue by providing a Hamiltonian-based extension of the physical system whose projected trajectories are actually equivalent to Nosé-Hoover trajectories, in the absence of numerical errors. This extended Hamiltonian system can then be discretized using a symplectic method.

Nosé's original proposal involved using the dynamics of the Hamiltonian

$$H_N = \frac{1}{2s^2} \tilde{\mathbf{p}}^T \mathbf{M}^{-1} \tilde{\mathbf{p}} + \frac{\pi^2}{2\mu} + U(\mathbf{q}) + (N_d + 1)k_B T \ln s$$

to define an extension which can be used for canonical sampling. The dynamics for constant Nosé extended energy, when reduced to the $(\mathbf{q}, \mathbf{p} = \tilde{\mathbf{p}}/s)$ plane will preserve the canonical measure ρ_β . However, the scaling of kinetic energy induces a time transformation, which is inconvenient for molecular modelling purposes. The Nosé-Poincaré method introduces an explicit unraveling of the time transformation. One works with the modified Nosé-Poincaré (NP) Hamiltonian [41, 102]:

$$H_{NP} = s[H_N - E_N] = s \left[\frac{1}{2s^2} \tilde{\mathbf{p}}^T \mathbf{M}^{-1} \tilde{\mathbf{p}} + \frac{\pi^2}{2\mu} + U(\mathbf{q}) + N_d k_B T \ln s - E_N \right], \quad (8.9)$$

where E_N is a constant equal to the initial Nosé energy of the system. Trajectories of this system unfold on a timescale which is in some sense commensurate with that of Hamiltonian dynamics. The NP Hamiltonian system can be treated with symplectic integrators, conferring a possible stability advantage. Symplectic integrators for this system are compared in [41].

The equations of motion associated to (8.9) are

$$\frac{d}{dt} \mathbf{q} = \mathbf{M}^{-1} \tilde{\mathbf{p}}/s, \quad (8.10)$$

$$\frac{d}{dt} \tilde{\mathbf{p}} = s\mathbf{F}, \quad (8.11)$$

$$\frac{d}{dt} s = sp_s/\mu, \quad (8.12)$$

$$\frac{d}{dt} p_s = \frac{\tilde{\mathbf{p}}^T \mathbf{M}^{-1} \tilde{\mathbf{p}}}{s^2} - N_d k_B T - \Delta H_N, \quad (8.13)$$

where $\Delta H_N = H_N - H_N^0$ (H_N^0 represents the value of the Nosé Hamiltonian at the initial point).

The relation between (8.10)–(8.13) and (8.2)–(8.4) becomes evident through the substitution $\mathbf{p} = \tilde{\mathbf{p}}/s$ and $\xi = p_s/\mu$. Then (8.10)–(8.11) are seen to be the same as the corresponding equations in the Nosé-Hoover method, and the final pair of equations become

$$\begin{aligned}\frac{d}{dt}s &= s\xi, \\ \frac{d}{dt}\xi &= \frac{1}{\mu}(\mathbf{p}^T \mathbf{M}^{-1} \mathbf{p} - N_d k_B T - \Delta H_N).\end{aligned}$$

The only difference between the last equation and (8.4) lies in the perturbation $\mu^{-1}\Delta H_N$, which is zero along the exact solution. Under discretization, however, we do not expect ΔH_N to vanish, so trajectories obtained from Nosé-Poincaré and Nosé-Hoover will differ considerably over long time simulations.

A benefit of respecting the symplectic structure lies in the prospect of using backward error analysis to analyze the behavior of the method. As shown in [40] it is possible to work out the terms of the perturbative expansion of the Nosé-Poincaré Hamiltonian, i.e. to calculate the expansion

$$\tilde{H}_h = H_{NP} + h^2 H_{[2]} + \mathcal{O}(h^4)$$

for a second order, symmetric, symplectic numerical method. Then one may determine the effective distribution associated to the symplectic discretization method by “integrating out” the microcanonical density with respect to the auxiliary variable and its conjugate momentum. One obtains in this way

$$\tilde{\rho}(\mathbf{q}, \mathbf{p}) = \rho_\beta(\mathbf{q}, \mathbf{p})\xi(\mathbf{q}, \mathbf{p}, h) + \mathcal{O}(h^4).$$

An explicit formula for ξ is given in [40] for several symplectic methods. During simulation, one may calculate the factor ξ and use this quantity to adjust averages. For example, if we wish to calculate the average of a function $g(\mathbf{q}, \mathbf{p})$, we may perform the calculation using v steps of the Nosé-Poincaré method with the given symplectic, time-reversible, second order integrator, calculate g_n and ζ_n at each timestep, and approximate the canonical average from

$$\langle g \rangle = \frac{1}{v+1} \sum_{n=0}^v g_n \zeta_n^{-1} + \mathcal{O}(h^4).$$

For further details, refer to [40]. Technically, a similar calculation can be carried out for the Nosé-Hoover formulation, but the calculations are more involved.

A good symplectic integrator for Nosé-Poincaré has been given by Nosé [287]. For further discussion and numerical experiments using this idea, see [94] (which also considers stochastic methods).

8.2 More General Deterministic Thermostats

We have now seen that it is possible to construct stochastic differential equations that preserve the Gibbs distribution or to design deterministic perturbations of Hamiltonian dynamics, in an extended phase space, that do the same thing. The latter class of methods are not rigorously ergodic, but the dynamics based thermostating technique adds a great deal of flexibility. For example it is easy to control the ensemble using dynamic perturbations introduced only in some special phase space directions. In this section, we show how to design distributional controls which blend deterministic dynamics with restricted stochastic perturbations, with, in some cases, provable ergodicity. We will present the methods of this section in some generality.

Let a system be provided with Hamiltonian (energy) function $H = H(z)$, $z \in \mathbb{R}^m$, and microcanonical dynamics

$$\dot{z} = J\nabla H, \quad (8.14)$$

where J is skew symmetric. In principle, J need not be constant, as long as it satisfies certain constraints, but as the extra generality is not needed for our current purposes, we restrict the case J constant. We describe dynamical and stochastic-dynamical techniques for computing averages with respect to a smooth density, for simplicity the Gibbsian one, $\rho_\beta \propto \exp(-\beta H)$.

We first consider methods that are based on perturbation of the conservative system (8.14), i.e.

$$\dot{z} = J\nabla H + \Phi(\xi, z), \quad (8.15)$$

where $\xi \in \mathbb{R}^m$ is controlled by the dynamical system

$$\frac{d\xi}{dt} = g(\xi, z).$$

8.2.1 Continuity Equation

Given a deterministic thermostating method, the density will evolve under the continuity equation,

$$\frac{\partial \rho}{\partial t} = -\nabla_z \cdot [\rho(J\nabla_z H + \Phi)] - \nabla_\xi \cdot (\rho g(\xi, z)) =: \mathcal{L}^\dagger \rho.$$

We have, using product rule,

$$\mathcal{L}^\dagger \rho = -(\nabla_z \rho) \cdot (J\nabla_z H + \Phi) - \rho \nabla_z \cdot (J\nabla_z H + \Phi) - (\nabla_\xi \rho) \cdot g - \rho \nabla_\xi \cdot g.$$

We divide this into four parts: $\mathcal{L}^\dagger \rho = W_1 + W_2 + W_3 + W_4$, where

$$\begin{aligned} W_1 &= -(\nabla_z \rho) \cdot (\mathbf{J} \nabla_z H + \boldsymbol{\Phi}), & W_2 &= -\rho \nabla_z \cdot (\mathbf{J} \nabla_z H + \boldsymbol{\Phi}), \\ W_3 &= -(\nabla_\xi \rho) \cdot \mathbf{g}, & W_4 &= -\rho \nabla_\xi \cdot \mathbf{g}. \end{aligned}$$

We seek perturbations of Hamiltonian dynamics with separable equilibria, i.e., such that $\rho = \rho_\beta(H(z))\hat{\rho}(\xi)$ is a stationary solution.

Taking this as an ansatz, the first term can be simplified as follows:

$$\begin{aligned} W_1 &= -\hat{\rho}(\xi)\rho'_\beta(H)\nabla_z H \cdot (\mathbf{J} \nabla_z H + \boldsymbol{\Phi}) \\ &= \beta\hat{\rho}(\xi)\rho_\beta(H)\nabla_z H \cdot \boldsymbol{\Phi} = \beta\rho\nabla_z H \cdot \boldsymbol{\Phi} \end{aligned}$$

as \mathbf{J} is skew-symmetric.

Using the volume preservation of Hamiltonian systems, the second term satisfies

$$W_2 = -\rho \nabla_z \cdot (\mathbf{J} \nabla_z H + \boldsymbol{\Phi}) = -\rho \nabla_z \cdot \boldsymbol{\Phi},$$

hence

$$W_1 + W_2 = -\rho[\nabla_z - \beta\nabla_z H] \cdot \boldsymbol{\Phi}.$$

There are many possibilities for the distribution of ξ , of course, but we will assume this is Gaussian for simplicity: $\hat{\rho}(\xi) = \exp(-\beta \sum_{i=1}^m \mu_i \xi_i^2 / 2) = \exp(-\beta \xi^T \boldsymbol{\mu}^{-1} \xi / 2)$ to get

$$W_3 = -(\nabla_\xi \rho) \cdot \mathbf{g}(\xi, z) = \beta\rho\xi^T \boldsymbol{\mu}^{-1} \mathbf{g}.$$

Finally, for an equilibrium solution we must have $W_1 + W_2 + W_3 + W_4 = 0$, so

$$-\left[\nabla_z - \beta\nabla_z H\right] \cdot \boldsymbol{\Phi} + \beta\xi^T \boldsymbol{\mu}^{-1} \mathbf{g} - \nabla_\xi \cdot \mathbf{g} = 0.$$

This equation is the fundamental one for deterministic thermostats.

Example 8.1 To recover Nosé-Hoover, assume an even dimensional phase space, $\mathbf{z} = (\mathbf{q}, \mathbf{p})$, N_d degrees of freedom, and $\xi \in \mathbb{R}$,

$$\boldsymbol{\Phi} = -\xi \begin{bmatrix} \mathbf{0} \\ \mathbf{p} \end{bmatrix}, \quad g(z) = \mu^{-1}(\mathbf{p} \cdot \nabla_p H - N_d k_B T).$$

Example 8.2 Slightly more generally, let

$$\boldsymbol{\Phi} = \xi \mathbf{G}(\mathbf{z}), \quad g(\xi, \mathbf{z}) = g(\mathbf{z}) = \mu^{-1}[\nabla_z H - k_B T \nabla_z] \cdot \mathbf{G}(\mathbf{z}).$$

This is a slightly generalized form of the technique suggested by Bulgac and Kusnezov [58].

Assuming ρ goes to zero sufficiently rapidly at infinity, we have

$$\int \nabla_z \cdot \mathbf{G}(z) \rho d\omega = - \int (\nabla_z \rho) \cdot \mathbf{G}(z) d\omega = \beta \int \nabla_z H \cdot \mathbf{G}(z) \rho d\omega,$$

using integration by parts, therefore, since $\beta^{-1} = k_B T$,

$$T = k_B^{-1} \frac{\langle \nabla_z H \cdot \mathbf{G} \rangle}{\langle \nabla \cdot \mathbf{G} \rangle},$$

which gives formulas for temperature in terms of phase space averages (compare Chap. 6, Proposition 6.1).

Suppose we let K be a scalar valued function of position, and set

$$\mathbf{G}(z) = \begin{bmatrix} \nabla_q K(\mathbf{q}) \\ \mathbf{0} \end{bmatrix}$$

then we arrive at

$$g(z) = \mu^{-1} [\nabla_q U - k_B T \nabla_q] \cdot \nabla_q K(\mathbf{q}).$$

This is an example of a “configurational thermostat” [193, 211, 319].

A useful fact about thermostats is the following:

Proposition 8.1 (Thermostats are Additive) *Suppose we are given two thermostats,*

$$\dot{z} = J \nabla H + \Phi_1(\xi, z), \quad \dot{\xi} = g_1(\xi, z),$$

with stationary density $\hat{\rho}_1(\xi)\rho_\beta$, and another

$$\dot{z} = J \nabla H + \Phi_2(\eta, z), \quad \dot{\eta} = g_2(\eta, z),$$

with stationary density $\hat{\rho}_2(\eta)\rho_\beta$, then

$$\begin{aligned} \dot{z} &= J \nabla H + \Phi_1(\xi, z) + \Phi_2(\eta, z), \\ \dot{\xi} &= g_1(\xi, z), \\ \dot{\eta} &= g_2(\eta, z) \end{aligned}$$

is another thermostat and has stationary density $\tilde{\rho} = \hat{\rho}_1(\xi)\hat{\rho}_2(\eta)\rho_\beta$.

The proof is an immediate consequence of the linearity of the divergence operator, since the Liouville operator is constructed from this.

8.2.2 Nosé-Hoover Chains

Let us employ the additivity property to derive “Nosé-Hoover Chains” [251], a popular deterministic thermostat designed to give a more thorough sampling of the phase space than the standard Nosé-Hoover method.

The equations of Nosé-Hoover Chains may be written [251]

$$\dot{\mathbf{q}} = \mathbf{M}^{-1}\mathbf{p}, \quad (8.16)$$

$$\dot{\mathbf{p}} = -\nabla U(\mathbf{q}) - \xi_1 \mathbf{p}, \quad (8.17)$$

$$\mu_1 \dot{\xi}_1 = \mathbf{p}^T \mathbf{M}^{-1} \mathbf{p} - N_d k_B T - \mu_1 \xi_2 \xi_1, \quad (8.18)$$

$$\mu_2 \dot{\xi}_2 = \mu_1 \xi_1^2 - k_B T - \mu_2 \xi_2 \xi_3, \quad (8.19)$$

$$\mu_3 \dot{\xi}_3 = \mu_2 \xi_2^2 - k_B T - \mu_3 \xi_3 \xi_4, \quad (8.20)$$

⋮

$$\mu_k \dot{\xi}_k = \mu_{k-1} \xi_{k-1}^2 - k_B T. \quad (8.21)$$

By creating a more substantial bath of oscillators, each of which is forced to have the target kinetic energy, the physical system may more closely approximate the canonical distribution.

To see that this is a thermostat, note the equations (8.16)–(8.21) can be split into the following pieces:

$$\begin{bmatrix} \dot{\mathbf{q}} \\ \dot{\mathbf{p}} \\ \mu_1 \dot{\xi}_1 \\ \mu_2 \dot{\xi}_2 \\ \vdots \\ \mu_{k-1} \dot{\xi}_{k-1} \\ \mu_k \dot{\xi}_k \end{bmatrix} = \begin{bmatrix} \mathbf{M}^{-1} \mathbf{p} \\ -\nabla U(\mathbf{q}) - \xi_1 \mathbf{p} \\ \mathbf{p}^T \mathbf{M}^{-1} \mathbf{p} - N_d k_B T \\ 0 \\ \vdots \\ 0 \\ 0 \end{bmatrix} + \begin{bmatrix} \mathbf{0} \\ \mathbf{0} \\ -\mu_1 \xi_1 \xi_2 \\ \mu_1 \xi_1^2 - k_B T \\ \vdots \\ 0 \\ 0 \end{bmatrix} + \dots + \begin{bmatrix} \mathbf{0} \\ \mathbf{0} \\ 0 \\ 0 \\ \vdots \\ -\mu_{k-1} \xi_{k-1} \xi_k \\ \mu_{k-1} \xi_{k-1}^2 - k_B T \end{bmatrix}.$$

The first piece of the system corresponds to Nosé-Hoover, which we already know preserves $\rho_\beta \exp(-\beta \mu_1 \xi_1^2 / 2)$. By examination, the distribution $\exp(-\beta \mu_1 \xi_1^2 / 2) \exp(-\beta \mu_2 \xi_2^2 / 2)$ is preserved by the second piece, the next piece preserves

$\exp(-\beta\mu_2\xi_2^2/2)\exp(-\beta\mu_3\xi_3^2/2)$ and so on. Thus the full system preserves the combined distribution

$$\tilde{\rho} = \rho_\beta \exp\left(-\beta \sum_{i=1}^k \mu_i \xi_i^2 / 2\right).$$

Of course this is only a demonstration that the dynamics is compatible with $\tilde{\rho}$; there may be other invariant distributions.

Numerical treatment of the Nosé-Hoover Chain system can be performed by splitting, just as in Newtonian and Langevin dynamics. Various related methods and comparisons may be found in [65, 192, 230, 253].

8.2.3 Lack of Ergodicity of Deterministic Thermostats

Deterministic methods like the ones in the previous subsection are sometimes used for sampling calculations, however, our and others' experience is that these methods are not always ergodic.

In the case of Nosé-Hoover, this problem was known to both of the inventors and has been observed by many authors (see e.g. [251] and [180]). More recently, it has been studied analytically [218]. Some confusion arises from the fact that the practical ergodic properties (and other properties) in Nosé-Hoover simulations are sensitive to the particular system under study and the values of parameters. For example it is known that in the case of simple liquids and gases, Nosé-Hoover does (at least under some conditions) enable reliable calculation of thermodynamical quantities [77], whereas in other systems results are poor and cannot be rectified by adjustment of parameters. In general, the control of temperature requires that the thermostat couples tightly to the physical variables, which generally calls for a small thermal mass, but this may be at odds with efficiency reduction (it may lead to a need to use smaller timesteps to resolve the motion of the auxiliary variable).

Ergodicity is less well known as a potential problem for methods involving thermostating chains. Figure 8.1 shows a projection of a torus in phase space found numerically for a chain-thermostatted harmonic oscillator. As the number of auxiliary chain variables increases, we observe that the tori become increasingly thin but wind in a complicated way through the phase space. Even for initial conditions trapped within one of the tori, crude sampling may be possible, provided that the torus itself is of sufficient size, but the presence of such tori will impose a finite accuracy limit on the averages that can be obtained.

The reliable use of deterministic thermostats is system dependent—it is essential that there be mechanisms within the underlying physical dynamics model that promote energetic exchange among the degrees of freedom.

Numerical methods for Nosé-Hoover chains are easily constructed by splitting of the equations of motion.

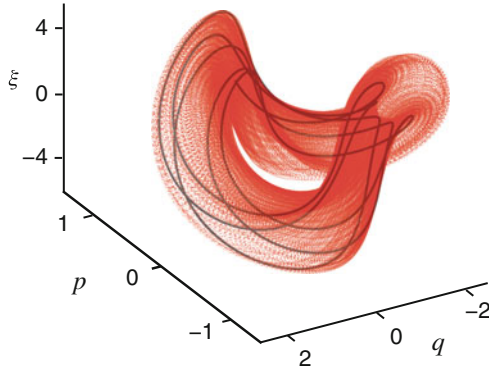


Fig. 8.1 Trajectories of the Nosé-Hoover Chain system may be trapped forever in restricted regions of phase space. Here a torus is shown in a projection of the full extended phase space for the harmonic oscillator with a length two thermostatted chain. (Equations of motion: $\dot{q} = p; \dot{p} = -q - \xi_1 p; \dot{\xi}_1 = (p^2 - 1)/\mu_1 - \xi_1 \xi_2; \dot{\xi}_2 = (\mu_1 \xi_1^2 - 1)/\mu_2$, with $\mu_1 = 0.2$, and $\mu_2 = 1$)

It should also be mentioned that the “measure-preserving” thermostating methods discussed in [373] refer rather to the underlying measure of the phase space and not the thermodynamic equilibrium distribution; those methods are deterministic and, like Nosé-Hoover based schemes, will exhibit thermodynamic errors due to both lack of ergodicity and discretization error, in addition to sampling errors.

8.3 Metropolis-Based Stochastic Sampling

One approach to providing ergodicity to deterministic systems is to introduce random fluctuations via a Monte-Carlo technique [268]. Several Monte-Carlo methods are described in Appendix C. Randomized steps are taken and then an accept-reject mechanism is introduced in order to ensure that the steps are consistent with the canonical distribution. It is possible to combine the Metropolis-Hastings concept with timestepping procedures in a variety of ways, which are often subsumed under the title “Monte-Carlo Markov Chain methods”, these include

- *Metropolis correction.* The *Hybrid Monte-Carlo* (HMC) method combines constant energy molecular dynamics (deterministic timestepping) with stochastic perturbation. A great advantage of HMC methods is that, under certain circumstances, they are not only ergodic, but also *exact* in the sense that the provide results that are unbiased, whereas a native timestepping method generally introduces some bias due to the finite timestep. The HMC approach can be used in combination with, for example the Nosé-Hoover method to provide rigorous sampling. Hybrid Monte-Carlo methods are likely to be most effective when used with an underlying deterministic method that has a high sampling bias, since

otherwise there is little clear advantage and a potentially significant price to be paid, since HMC methods only work by rejecting steps. For reading on Hybrid Monte Carlo methods, the reader should consult [110, 188] and other references mentioned in Appendix C.

- *Kinetic Monte-Carlo (KMC) methods* are a broad family of multiscale sampling methods which use a local sampling mechanism to explore basins while invoking an Arrhenius law to estimate the rates or timescales for transitions between basins (we can think of basins as neighborhoods of potential energy minima). The Arrhenius law relates the rate constant k associated to a particular state-to-state transition to the exponential of the activation energy” which is defined as the difference ΔE between the energy at a local minimum and that at the energy barrier between the states

$$k \sim A e^{-\Delta E/k_B T}$$

In a KMC method, it is typically assumed that various possible state-to-state transitions from a given state are well modelled by the Arrhenius law and then molecular dynamics is used to calculate the prefactor A and energy difference ΔE in order to understand the timescales and relative probabilities of different rare events. A Markov state model can be developed to help understand the global dynamics and simplify the model as a whole. For references on many interesting approaches to this important topic, the reader is referred to [36, 42, 137, 149, 391].

- *Andersen Thermostat*. Of particular interest is the simple and useful *Andersen thermostat* [11]. This method works by selecting atoms at random and randomly perturbing their momenta in a way consistent with prescribed thermodynamic conditions. It has been rigorously proven to sample the canonical distribution [114].

8.4 Ergodic Stochastic-Dynamic Thermostats

In this section, we consider the combination of stochastic perturbation with a deterministic thermostat. Methods constructed in this way can be ergodic for the canonical distribution while also providing flexibility in way equilibrium is achieved. We distinguish in (6.16) between multiplicative noise, where $\mathbf{B} = \mathbf{B}(z)$ varies with z and additive noise, where \mathbf{B} is constant. In our treatment of this topic we will only consider additive noise. The presence of multiplicative noise may complicate discretization. As we shall see, the reliance on additive noise improves the performance of discretization schemes.

To give this some specificity for molecular dynamics, we write the stochastic dynamical model as

$$dq = M^{-1} p dt, \quad (8.22)$$

$$dp = -\nabla U(q)dt - \Phi(\xi, z) - \Gamma p dt + \sqrt{2k_B T} M^{1/2} \Gamma^{1/2} dW, \quad (8.23)$$

$$d\xi = g(\xi, q, p)dt - \hat{\Gamma} \xi dt + \sqrt{2k_B T} \hat{M}^{1/2} \hat{\Gamma}^{1/2} d\hat{W}. \quad (8.24)$$

Here $\Gamma, \hat{\Gamma}$ are symmetric, square matrices of appropriate dimension, W is a vector of N Wiener processes, and \hat{W} is a vector of m Wiener processes, all independent of each other. We assume that the deterministic thermostat represented by the Φ and g terms preserves the extended distribution $\hat{\rho}(\xi)\rho_\beta$, where $\hat{\rho}(\xi) = \exp(-\beta \xi^T \hat{M}^{-1} \xi / 2)$. The matrix \hat{M} is symmetric and positive definite; one could take it to be diagonal.

The additivity property of thermostats mentioned above holds also for stochastic thermostats, since the Fokker-Planck equation is constructed from linear operations on the vector fields involved, thus it is enough to require that the newly introduced terms satisfy appropriate fluctuation-dissipation relationships so that they are compatible with the extended Gibbs distribution of the deterministic part. That is, we require

$$dp = -\Gamma p dt + \sqrt{2k_B T} M^{1/2} \Gamma^{1/2} dW$$

to preserve the distribution with density $\bar{\rho} = \exp(-\beta p^T M^{-1} p / 2)$, and

$$d\xi = -\hat{\Gamma} \xi dt + \sqrt{2k_B T} \hat{M}^{1/2} \hat{\Gamma}^{1/2} d\hat{W}$$

to preserve $\hat{\rho}$. These two problems are essentially the same. Considering the former, the stationary Fokker-Planck equation reads

$$\underbrace{\nabla_p \cdot (\Gamma p \bar{\rho})}_{\text{drift}} + \underbrace{\beta^{-1} \text{Tr} \left(\Gamma^{1/2} M^{1/2} \nabla_p^2 \bar{\rho} M^{1/2} \Gamma^{1/2} \right)}_{\text{diffusion}} = 0.$$

The drift term here equates to

$$\text{Tr}(\Gamma) \bar{\rho} + (-\beta) p^T \Gamma M^{-1} p \bar{\rho}.$$

For the diffusion term, we calculate

$$\nabla \bar{\rho} = -\beta \bar{\rho} M^{-1} p,$$

thus

$$\nabla^2 \bar{\rho} = \bar{\rho} [\beta^2 M^{-1} p p^T M^{-1} - \beta M^{-1}],$$

so the diffusion term is

$$\beta^{-1} \text{Tr} \left(\boldsymbol{\Gamma}^{1/2} \mathbf{M}^{1/2} [\beta \mathbf{M}^{-1} \mathbf{p} \mathbf{p}^T \mathbf{M}^{-1} - \mathbf{M}^{-1}] \mathbf{M}^{1/2} \boldsymbol{\Gamma}^{1/2} \right) \bar{\rho} = -\text{drift},$$

where we have used the cyclic property of the trace (and the symmetry of $\boldsymbol{\Gamma}$) to reduce the expression. The validity of the term involving ξ is easily verified by a similar argument.

Thus we know that the Gibbs distribution will be invariant. It remains to prove that the SDE (8.22)–(8.24) is ergodic. Certainly this would be expected in the case where a full Langevin dynamics contribution is present ($\boldsymbol{\Gamma}$ positive definite), but as we shall see next there are cases where noise only contacts the auxiliary degrees of freedom but the system is nonetheless ergodic.

We state here a useful observation that allows to simplify the commutator calculations in the case of an SDE of the following type:

$$dz = \mathbf{F}(z)dt + \xi \mathbf{G}(z)dt, \quad (8.25)$$

$$d\xi = g(z)dt - \gamma \xi dt + \sigma dW, \quad (8.26)$$

where $z \in \mathbb{R}^m$, $\mathbf{F}, \mathbf{G} : \mathbb{R}^m \rightarrow \mathbb{R}^m$.

Proposition 8.2 *If the Lie algebra generated by \mathbf{F} and \mathbf{G} in (8.25) spans \mathbb{R}^m , then the Hörmander condition holds for the system (8.25)–(8.26).*

Proof First observe that the premise holds if and only if the Lie algebra of the vectors in \mathbb{R}^{m+1} defined by

$$\tilde{\mathbf{F}} = \begin{bmatrix} \mathbf{F} \\ 0 \end{bmatrix}, \quad \tilde{\mathbf{G}} = \begin{bmatrix} \mathbf{G} \\ 0 \end{bmatrix},$$

together with e_{m+1} spans \mathbb{R}^{m+1} . Thus the problem is to show that we can generate $\tilde{\mathbf{F}}$ and $\tilde{\mathbf{G}}$ from the vector fields that define (8.25)–(8.26), which are

$$\mathbf{b}_0 = \begin{bmatrix} \mathbf{F} + \xi \mathbf{G} \\ g - \gamma \xi \end{bmatrix}, \quad \mathbf{b}_1 = \begin{bmatrix} \mathbf{0} \\ \sigma \end{bmatrix}.$$

Computing the commutator gives

$$\mathbf{c} = [\mathbf{b}_0, \mathbf{b}_1] = \begin{bmatrix} -\sigma \mathbf{G} \\ \sigma \gamma \end{bmatrix},$$

hence

$$\tilde{\mathbf{G}} = \frac{-1}{\sigma} [\mathbf{c} - \gamma \mathbf{b}_1].$$

This means that we have built one of our two vectors. The second follows as a linear combination of the others:

$$\tilde{\mathbf{F}} = \mathbf{b}_0 - \xi \tilde{\mathbf{G}} - (g - \gamma \xi) \sigma^{-1} \mathbf{b}_1.$$

□

The fact that the Hörmander condition holds is, as we know from Chap. 6, only part of the story. However based on known results for Langevin dynamics, we conjecture that ergodicity will hold if (i) the Hörmander condition holds, (ii) U is sufficiently smooth, and (iii) the configurational phase space is compact, e.g. periodic boundary conditions are employed. However we stress that each possible method will ultimately need to be carefully and systematically checked to verify the ergodic properties.

8.4.1 Nosé-Hoover-Langevin: An Ergodic Weakly Coupled Thermostat

The Nosé-Hoover-Langevin (NHL) method is based on a simple idea: replace the “chain” in the Nosé-Hoover Chain, whose sole purpose is to maintain a Gaussian distribution in the auxiliary variable, by a stochastic Langevin-type thermostat. The method was first proposed in [323]. The proof of ergodicity (more precisely the confirmation of the Hörmander condition), for a problem with harmonic internal interactions, was given in [226] and we roughly follow the treatment from this paper.

The Nosé-Hoover-Langevin equations are

$$dq = M^{-1} p dt, \quad (8.27)$$

$$dp = -\nabla U(q) dt - \xi p dt, \quad (8.28)$$

$$d\xi = \mu^{-1} [p^T M^{-1} p - N_d k_B T] dt - \gamma \xi dt + \sqrt{2k_B T \gamma \mu^{-1}} dW, \quad (8.29)$$

where $(q, p) \in \mathcal{D}$ with $\xi \in \mathbb{R}$. Let us emphasize that the principal features of this thermostat: (1) it is essentially Nosé-Hoover plus a perturbation, (2) it incorporates a single Wiener process, (3) it has two free parameters γ and μ .

Let us first demonstrate that the Nosé-Hoover-Langevin method, is, in fact, a thermostat. We observe that we have already shown that the Nosé-Hoover method preserves the extended canonical distribution $\rho_\beta \exp(-\beta \mu \xi^2 / 2)$. Therefore, by the additivity property, all that is needed is to show that the additional part

$$d\xi = -\gamma \xi dt + \sqrt{2k_B T \gamma \mu^{-1}} dW$$

preserves $\hat{\rho}(\xi) = \exp(-\beta\mu\xi^2/2)$. However, this is obvious from our earlier investigations of Ornstein-Uhlenbeck equations.

In order to show that this thermostat is ergodic, we need to demonstrate that the assumptions presented in Sect. 6.4.4 are valid. Assumption 1(ii) requires us to verify that a Hörmander condition (see Definition 6.1) holds for the Nosé-Hoover-Langevin system. Because of the complexity of the high order commutators, we will work here with the assumption of a quadratic potential in the physical model. In some sense this is the most difficult case for a thermostat, but paradoxically, the assumption facilitates the mathematical analysis. We will assume throughout the following that $N_d = N_c$, i.e. that there are no constraints in the system. Our potential will therefore be assumed to be

$$U(\mathbf{q}) = \frac{1}{2}\mathbf{q}^T \mathbf{A} \mathbf{q},$$

for \mathbf{A} a symmetric, positive definite $N_c \times N_c$ matrix, with

$$\nabla U(\mathbf{q}) = \mathbf{A} \mathbf{q}.$$

We will further assume $\mathbf{M} = \mathbf{I}$. If this is not the case, then one may introduce the rescaling $\tilde{\mathbf{q}} = \mathbf{M}^{-1/2} \mathbf{q}$, $\tilde{\mathbf{p}} = \mathbf{M}^{1/2} \mathbf{p}$ in order to rewrite the system in a form that does not involve \mathbf{M} . Thus the system under study is

$$d\mathbf{q} = \mathbf{p} dt, \tag{8.30}$$

$$d\mathbf{p} = -\mathbf{A} \mathbf{q} dt - \xi \mathbf{p} dt, \tag{8.31}$$

$$d\xi = \mu^{-1} [\|\mathbf{p}\|^2 - N_d k_B T] dt - \gamma \xi dt + \sigma dW. \tag{8.32}$$

Let $\mathbf{u}_1, \mathbf{u}_2, \dots, \mathbf{u}_{N_c}$ be the eigenvectors of \mathbf{A} with $\lambda_1, \dots, \lambda_{N_c}$ the corresponding eigenvalues. Observe that if $\mathbf{q}_0 \cdot \mathbf{u}_k = \mathbf{p}_0 \cdot \mathbf{u}_k = 0$, then, using (8.30)–(8.31), we have at this point

$$\mathbf{u}_k \cdot \mathbf{p} = 0, \quad \mathbf{u}_k \cdot [-\mathbf{A} \mathbf{q} - \xi \mathbf{p}] = -\lambda_k \mathbf{u}_k \cdot \mathbf{q} = 0,$$

which implies that $V_k = \{(\mathbf{q}, \mathbf{p}) | \mathbf{u}_k \cdot \mathbf{q} = 0, \mathbf{u}_k \cdot \mathbf{p} = 0\}$ is an invariant submanifold. Therefore we must require that $\mathbf{u}_k \cdot \mathbf{q}$ and $\mathbf{u}_k \cdot \mathbf{p}$ do not simultaneously vanish, that is, $(\mathbf{q}, \mathbf{p}) \in \mathcal{D} = \mathbb{R}^{2N_c} \setminus \bigcup_{k=1}^{N_c} V_k$.

Theorem 8.1 *If \mathbf{A} is symmetric positive definite and has distinct eigenvalues, then (8.30)–(8.32) satisfies the Hörmander condition on $\mathcal{D} \times \mathbb{R}$.*

Proof Observe that Nosé-Hoover-Langevin dynamics is a special case of the system (8.25)–(8.26). Applying the proposition in our case, the problem is to show that the Lie algebra generated by

$$\mathbf{F} = \begin{bmatrix} \mathbf{p} \\ -\mathbf{A}\mathbf{q} \end{bmatrix}, \quad \mathbf{G} = \begin{bmatrix} \mathbf{0} \\ \mathbf{p} \end{bmatrix},$$

spans \mathbb{R}^{2N_c} . We shall write $S\{\mathbf{F}, \mathbf{G}\}$ for the Lie algebra generated by \mathbf{F} and \mathbf{G} .

Next we note:

Lemma 8.1 For $k = 1, 2, \dots$,

$$\mathbf{C}_k = \begin{bmatrix} \mathbf{A}^{k-1}\mathbf{p} \\ \mathbf{A}^k\mathbf{q} \end{bmatrix} \in S\{\mathbf{F}, \mathbf{G}\},$$

and

$$\mathbf{D}_k = \begin{bmatrix} \mathbf{A}^k\mathbf{q} \\ -\mathbf{A}^k\mathbf{p} \end{bmatrix} \in S\{\mathbf{F}, \mathbf{G}\}.$$

The proof of this is straightforward by induction on k . (See exercises.)

The conclusion of the proof of the theorem is based on the following proposition:

Proposition 8.3 Assume \mathbf{A} to be a symmetric positive definite matrix with distinct eigenvalues, and let $\mathbf{C}_k, \mathbf{D}_k$ be defined as in Lemma 8.1, then the $2N_c$ vectors $\mathbf{C}_1, \mathbf{D}_1, \mathbf{C}_2, \mathbf{D}_2, \dots, \mathbf{C}_{N_c}, \mathbf{D}_{N_c}$ form a linearly independent set on \mathcal{D} .

Proof \mathbf{A} , being symmetric positive definite is unitarily similar to a diagonal matrix Λ , so $\mathbf{A} = \mathbf{U}\Lambda\mathbf{U}^T$. Define $\hat{\mathbf{p}} = \mathbf{U}^T\mathbf{p}, \hat{\mathbf{q}} = \mathbf{U}^T\mathbf{q}$. The domain \mathcal{D} is defined by the condition that \hat{p}_i and \hat{q}_i are not simultaneously zero.

With the change of variables, the problem is to show that $\hat{\mathbf{C}}_1, \hat{\mathbf{D}}_1, \dots, \hat{\mathbf{C}}_{N_c}, \hat{\mathbf{D}}_{N_c}$ are linearly independent, where

$$\hat{\mathbf{C}}_k = \begin{bmatrix} \Lambda^{k-1}\hat{\mathbf{p}} \\ \Lambda^k\hat{\mathbf{q}} \end{bmatrix}, \quad \hat{\mathbf{D}}_k = \begin{bmatrix} \Lambda^k\hat{\mathbf{q}} \\ -\Lambda^k\hat{\mathbf{p}} \end{bmatrix}.$$

Suppose the vectors are linearly dependent, then there exist coefficients $\alpha_0, \alpha_1, \dots, \alpha_{N_c-1}$ and $\beta_0, \beta_1, \dots, \beta_{N_c-1}$ not all zero such that:

$$\sum_{j=1}^{N_c} \alpha_j \hat{\mathbf{C}}_j + \sum_{j=1}^{N_c} \beta_j \hat{\mathbf{D}}_j = 0.$$

Define polynomials $\pi(x) = \sum_{j=0}^{N_c-1} \alpha_j x^j$, $\sigma(x) = \sum_{j=0}^{N_c-1} \beta_j x^j$, then, for each j , we have

$$\pi(\lambda_j)\hat{q}_j + \lambda_j\sigma(\lambda_j)\hat{p}_j = 0, \quad \lambda_j\pi(\lambda_j)\hat{p}_j - \lambda_j\sigma(\lambda_j)\hat{q}_j = 0,$$

multiplying the first equation by \hat{q}_j and the second by \hat{p}_j and adding, we obtain

$$[\hat{q}_j^2 + \lambda_j\hat{p}_j^2]\pi(\lambda_j) = 0.$$

The first factor is nonzero by the condition of being in \mathcal{D} and the positive definiteness of \mathbf{A} , thus we must have $\pi(\lambda_j) = 0$ for all N_c distinct λ_j . But as π has degree $N_c - 1$, this is a contradiction. Thus the collection must be linearly independent.

Demonstrating the Hörmander condition is sufficient for Assumption 1(ii) in Sect. 6.4.4. Assumption 1(i) can be verified by proving that solutions are able to access an open set around any point $y \in \mathcal{D} \times \mathbb{R}$. We omit the proof of Assumption 1(i) for Nosé-Hoover-Langevin dynamics as it follows the same structure as the proof of Lemma 6.1 for Langevin dynamics. The details of the proof can be found in [283], with examples for more general SDEs given in [256, 257].

The final requirement for geometric ergodicity (specified in Assumption 2 in Sect. 6.4.4) requires a function $\phi : \mathcal{D} \times \mathbb{R} \rightarrow (0, \infty)$ such that

$$\mathcal{L}\phi \leq -\alpha\phi + \delta,$$

for positive constants α and δ and where \mathcal{L} is the generator of the stochastic process. Such a function is called a Lyapunov function.

The generator for Nosé-Hoover-Langevin dynamics (8.27)–(8.29), acting on a suitable test function $f(\mathbf{q}, \mathbf{p}, \xi)$ is

$$\begin{aligned} \mathcal{L}_{\text{NHL}}f &= \mathbf{M}^{-1}\mathbf{p} \cdot \nabla_{\mathbf{q}}f - \nabla U(\mathbf{q}) \cdot \nabla_{\mathbf{p}}f - \xi\mathbf{p} \cdot \nabla_p + \mu^{-1} [\mathbf{p}^T \mathbf{M}^{-1} \mathbf{p} - N_d k_B T] \frac{\partial f}{\partial \xi} \\ &\quad - \gamma\xi \frac{\partial f}{\partial \xi} + k_B T \gamma \mu^{-1} \frac{\partial^2 f}{\partial \xi^2}. \end{aligned}$$

If we consider $\mathbf{M} = \mathbf{I}$ for simplicity, a Lyapunov function is given in [283] as

$$\phi(\mathbf{q}, \mathbf{p}, \xi) = \frac{1}{2}\|\mathbf{p}\|^2 + U(\mathbf{q}) + \frac{\mu}{2}(\xi - a)^2,$$

where a is a constant. As our potential is smooth, it is reasonable to make the assumption that

$$1 < U_{\min} \leq U(\mathbf{q}) \leq U_{\max} < \infty, \quad \forall \mathbf{q} \in \mathcal{Q},$$

for some constants U_{\min} and U_{\max} . Hence ϕ is strictly positive over the entire space, and we can compute that

$$\begin{aligned}\mathcal{L}_{\text{NHL}}\phi &= \mathbf{p} \cdot \nabla U(\mathbf{q}) - \nabla U(\mathbf{q}) \cdot \mathbf{p} - \xi \|\mathbf{p}\|^2 + [\|\mathbf{p}\|^2 - N_d k_B T] (\xi - a) \\ &\quad - \gamma \mu \xi (\xi - a) + k_B T \gamma, \\ &\leq -a \|\mathbf{p}\|^2 - \gamma \mu \xi^2 + (a \gamma \mu - N_d k_B T) \xi + a N_d k_B T + k_B T \gamma.\end{aligned}$$

Choosing a so that $a \gamma \mu - N_d k_B T = 0$, we obtain

$$\mathcal{L}_{\text{NHL}}\phi = -a \|\mathbf{p}\|^2 - \gamma \mu \xi^2 - \gamma \mu a^2 + \gamma \mu a^2 + a N_d k_B T + k_B T \gamma.$$

Using $-\xi^2 - a^2 \leq -(\xi - a)^2/2$ gives

$$\mathcal{L}_{\text{NHL}}\phi \leq -2a \frac{1}{2} \|\mathbf{p}\|^2 - \gamma \mu \frac{1}{2} (\xi - a)^2 + \gamma \mu a^2 + a N_d k_B T + k_B T \gamma.$$

Now choosing

$$\alpha = \min(2a, \gamma \mu),$$

we have

$$\begin{aligned}\mathcal{L}_{\text{NHL}}\phi &\leq -\alpha \phi + \alpha U(\mathbf{q}) + \gamma \mu a^2 + a N_d k_B T + k_B T \gamma, \\ &\leq -\alpha \phi + \delta,\end{aligned}$$

for constants α and δ as required, where

$$\delta = \alpha U_{\max} + \gamma \mu a^2 + a N_d k_B T + k_B T \gamma.$$

This gives the necessary Lyapunov condition for the Nosé-Hoover-Langevin equations, and hence the dynamics are geometrically ergodic. Solution trajectories will sample the extended canonical distribution, and it remains to compute solutions using an appropriate discretization scheme.

8.4.2 Numerical Integration of the Nosé-Hoover-Langevin Equations

Many older schemes for Nosé-Hoover and Langevin dynamics make use of computational shortcuts to (for example) reduce the number of computed random values per iteration, reduce the data storage needed for an algorithm or replace functions that are costly to evaluate (e.g. exponential or trigonometric functions)

by an approximate series expansion. In modern computer architectures, the number of force evaluations is responsible for the overwhelming majority of the time spent per iteration.

We can apply the splitting approach considered in Chap. 7 to integrate equations (8.27)–(8.29). One suitable choice of algorithm that we shall use in the following subsection is

$$\begin{aligned}\mathbf{p}_{n+1/2} &= \mathbf{p}_n - (h/2)\nabla U(\mathbf{q}_n), \\ \mathbf{q}_{n+1/2} &= \mathbf{q}_n + (h/2)\mathbf{M}^{-1}\mathbf{p}_{n+1/2}, \\ \xi_{n+1/2} &= \xi_n + (h/2)\mu^{-1} \left[\mathbf{p}_{n+1/2}^T \mathbf{M}^{-1} \mathbf{p}_{n+1/2} - N_d k_B T \right], \\ \tilde{\mathbf{p}}_{n+1/2} &= e^{-(h/2)\xi_{n+1/2}} \mathbf{p}_{n+1/2}, \\ \hat{\xi}_{n+1/2} &= e^{-\gamma h} \xi_{n+1/2} + \zeta R_n, \\ \hat{\mathbf{p}}_{n+1/2} &= e^{-(h/2)\hat{\xi}_{n+1/2}} \tilde{\mathbf{p}}_{n+1/2}, \\ \xi_{n+1} &= \hat{\xi}_{n+1/2} + (h/2)\mu^{-1} \left[\hat{\mathbf{p}}_{n+1/2}^T \mathbf{M}^{-1} \hat{\mathbf{p}}_{n+1/2} - N_d k_B T \right], \\ \mathbf{q}_{n+1} &= \mathbf{q}_{n+1/2} + (h/2)\mathbf{M}^{-1}\hat{\mathbf{p}}_{n+1/2}, \\ \mathbf{p}_{n+1} &= \hat{\mathbf{p}}_{n+1/2} - (h/2)\nabla U(\mathbf{q}_{n+1}),\end{aligned}$$

where $\zeta = \sqrt{k_B T \mu^{-1} (1 - \exp(-2\gamma h))}$ and R_n is a normal random number with unit variance and zero mean.

This numerical method requires only one evaluation of the force per timestep. It also reduces to a Nosé-Hoover integrator when $\gamma = 0$, and as it solves the Ornstein-Uhlenbeck process exactly, it is stable under the large (or infinite) limit of friction.

8.4.3 Numerical Comparison of Dynamics

We shall compare the long-time averages evaluated by computing solution trajectories for Nosé-Hoover, Langevin and Nosé-Hoover-Langevin dynamics. We will look at the impact that the choice of dynamics (and associated parameters) has on the rate of convergence of averages in time, as well as the perturbation introduced into dynamical quantities (such as autocorrelation functions).

The test model we shall use to study this problem will be a Lennard-Jones liquid. We place $N = 125$ atoms with unit mass in a 3D periodic box with total potential energy given by

$$U(\mathbf{q}) = \sum_{i=1}^N \sum_{j=i+1}^N \varphi_{\text{LJ}}(r_{ij}),$$

where

$$r_{ij} = \|\mathbf{q}_i - \mathbf{q}_j\|, \quad \varphi_{\text{LJ}}(r) = r^{-12} - r^{-6}.$$

The particles' positions are initialized on a $5 \times 5 \times 5$ grid, with equidistant grid spacing $2^{1/6}$: the minimum of the Lennard-Jones potential $\varphi_{\text{LJ}}(r)$. We will sample canonically at reciprocal temperature $\beta = 10$, with a force cutoff chosen equal to the side length of the periodic box. The size of the box defines the particle density of the simulation and hence the phase of matter that we shall study. After some experimentation, a cubic box with side length 7 was found to give conditions for a liquid state.

In order to compare the rate of convergence of averages, we initialize 625 identical (and independent) copies of our system, and propagate each forward in time. The values of the instantaneous kinetic and potential energy for the system are averaged over all of the systems at each time. In all simulations, we use a timestep of $h = 0.005$. Specific cases considered are: Nosé-Hoover with μ ranging from 0.02 to 20, and Nosé-Hoover-Langevin with that range of μ and $\gamma = 0.5$ or $\gamma = 5$. We also include simulations using Langevin dynamics with values of γ ranging from 0.01 to 10. In Fig. 8.2 we plot the convergence of the average kinetic energy of the system towards its equilibrium average, while Fig. 8.3 illustrates the convergence of the average potential energy as a function of time. The equilibrium average is known exactly for the kinetic energy, whereas the equilibrium average for the potential energy was computed to high accuracy by averaging over several long trajectories.

The results show residual oscillations of average kinetic energy in Nosé-Hoover that may be indicative of long term correlations—the method is, as we know, not ergodic. Decreasing μ increases the frequency of oscillations observed, which can present problems for numerical integration of the dynamics (i.e. a small stepsize may be needed), which would introduce inefficiency. It is also known from a dynamical systems analysis that Nosé dynamics is not ergodic in the large μ limit [217]; as μ is increased, the thermalizing auxiliary variable is increasingly decoupled from the physical variables, so that thermal control is impaired; in practice, for large μ in Nosé-Hoover, one may observe long period oscillations in system temperature.

For the Nosé-Hoover-Langevin method, we observe that, while small values of μ increase the high frequency oscillations observed in the kinetic energy, the rate of convergence is essentially determined by γ and the average kinetic energy indeed converges in the timescale of these simulations. The presence of the stochastic

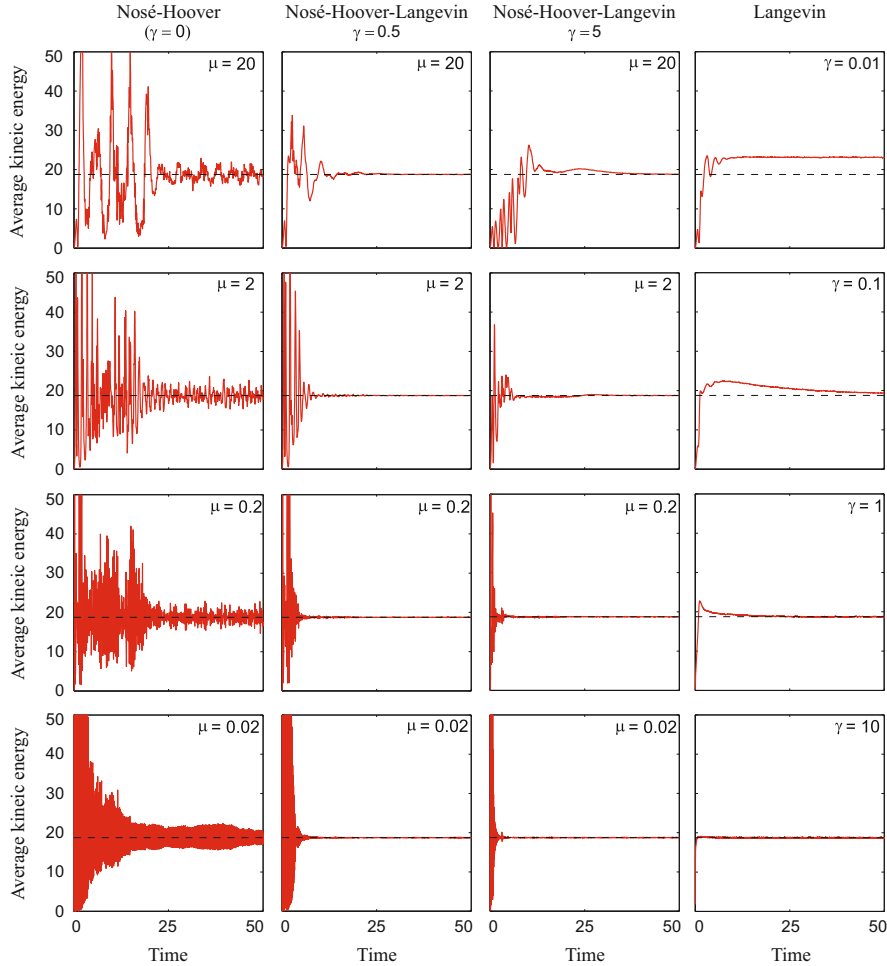


Fig. 8.2 We plot the evolution of the average of kinetic energy in time for several choices of the thermostat. We vary the parameters used for the dynamics to illustrate the effect on the convergence of averages. The averages will converge to the dashed line in the large-time limit

terms ensure that the residual oscillatory behavior of the Nosé-Hoover dynamics is damped, removing any long-lived oscillations.

Finally, we see that Langevin dynamics shows that the rate of convergence of the kinetic energy is highly dependent on the choice of friction γ . At the smallest friction value considered the convergence is very poor, taking a significant time to properly thermalize. Larger friction results in rapid convergence of the momentum towards equilibrium.

Results for the convergence of potential energy are shown in Fig. 8.3 are entirely consistent with the results for kinetic energy. One subtle observation to note is that

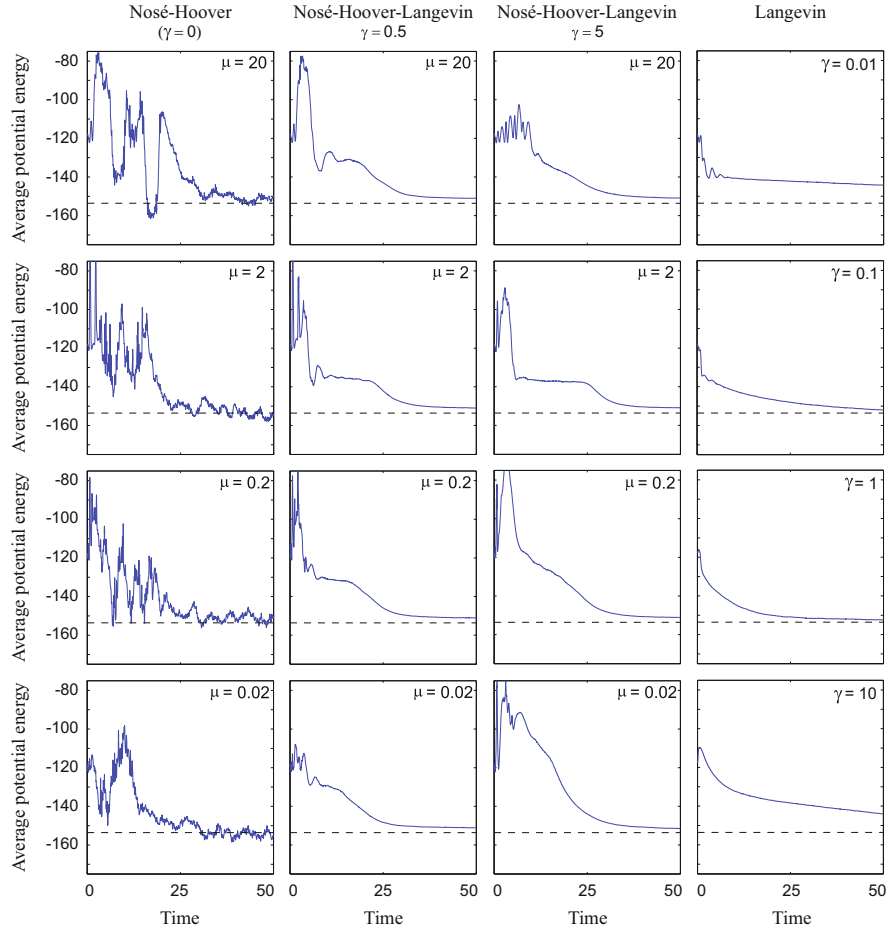


Fig. 8.3 The evolution of the average of potential energy as a function of time is plotted, using different choices of the friction parameter γ and the coupling parameter μ in different thermostats. The long-time average of the simulation is shown as the *dashed line*

in the case of Langevin dynamics, the fastest convergence of the average of potential energy occurs between the minimum and maximum values tested. At large values of γ the convergence is impaired due to the reduction in the diffusion rate (compare Fig. 7.6). This would suggest the existence of some optimum value of the friction to ensure rapid convergence of configurational averages (which would likely depend on the observable).

Very important differences emerge if we attempt to use the stochastic integrators to compute dynamics, e.g. a time-correlation function. Velocity auto-correlation functions are shown in Fig. 8.4 for various choices of the parameters.

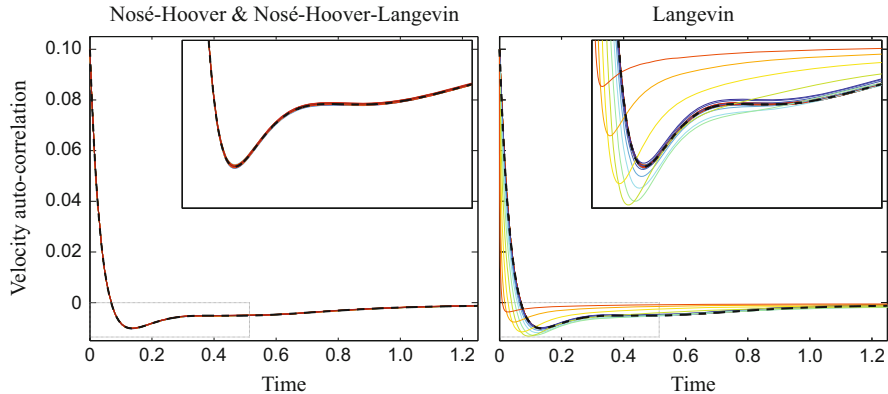


Fig. 8.4 The computed velocity auto-correlation functions are plotted for Nosé-Hoover and Nosé-Hoover-Langevin dynamics (*left*), where we overlay plots from simulations using all possible parameter sets where $\gamma \in \{0, 0.05, 0.5, 5, 50\}$ and $\mu \in \{20, 2, 0.2, 0.02\}$. We additionally plot the same result for Langevin dynamics (*right*), overlaying curves for $\gamma \in \{0.05, 0.1, 0.2, \dots, 51.2\}$, where high to low friction is plotted from *red* to *blue* respectively. The salient qualitative features of the results remain qualitatively unchanged when using different values of the parameters for the Nosé-Hoover thermostats (see *inset*) whereas the Langevin thermostat has a much harsher effect on the dynamics, with significant differences as the friction is increased

It may seem that the difference between Nosé-Hoover-Langevin and Langevin dynamics is a technical one that essentially hinges on choice of parameters. Both methods are ergodic and it may appear that by simply choosing a small value of friction in Langevin dynamics, we can match the behavior of Nosé-Hoover-Langevin to any desired accuracy. However, this is most definitely not the case, as a careful analysis of Figs. 8.3 and 8.4 reveals. If an accurate velocity autocorrelation function is required, then the friction parameter in Langevin dynamics needs to be chosen very small (much less than $\gamma = 0.1$), see Fig. 8.4. But if the friction is chosen in this way, the convergence to canonical equilibrium is drastically impaired (Figs. 8.2 and 8.3). By contrast it is relatively easy to find parameter choices for Nosé-Hoover-Langevin which provide quite rapid convergence of canonical averages while preserving the accuracy of autocorrelation functions.

The convergence to equilibrium for Nosé-Hoover-Langevin is difficult to calculate analytically. The only existing analysis is that of [225] which restricts consideration to the convergence of the kinetic energy. It turns out that one may obtain a nonlinear system in terms of the following two variables:

$$\bar{\theta}(t) = \int_{\mathcal{D} \times \mathbb{R}} 2K\rho(\mathbf{q}, \mathbf{p}, \xi, t) d\omega d\xi,$$

where K is the kinetic energy, and the mean auxiliary variable $\bar{\xi}$

$$\bar{\xi}(t) = \int_{\mathcal{D} \times \mathbb{R}} \xi \rho(\mathbf{q}, \mathbf{p}, \xi, t) d\omega d\xi.$$

ρ that appears here is the normalized pre-equilibrium density which evolves according to the Fokker-Planck equation of the extended Nosé-Hoover-Langevin system.

It is then possible to perform a local stability analysis to characterize the convergence to equilibrium of $\bar{\theta}$ and $\bar{\xi}$ to the equilibrium $(N_d k_B T, 0)$. Although the analysis makes certain stringent assumptions they are verified in [225] for a Lennard-Jones molecular system.

8.4.4 Velocity Rescaling

An alternative stochastic-dynamical method for thermostating molecular dynamics is the stochastic velocity rescaling method proposed by Bussi and collaborators [60, 63] and somewhat generalized in [225]. The equations are (for the case $\mathbf{M} = \mathbf{I}$, considered for simplicity):

$$\begin{aligned} d\mathbf{q} &= \mathbf{p} dt \\ d\mathbf{p} &= -\nabla U(\mathbf{q}) dt - \Psi(K) \mathbf{p} dt + \sqrt{2k_B T \Phi(K)} \mathbf{p} dW, \end{aligned}$$

where $W(t)$ is a single Wiener process, Φ is an arbitrary smooth positive function and Ψ is defined by

$$\Psi(K) \stackrel{\text{def}}{=} (2K - (1 + N_d)k_B T)\Phi(K) - 2k_B T K \frac{d\Phi}{dK}.$$

With these definitions, the method preserves the canonical probability density ρ_β . We do not prove the ergodicity of the method here, but expect that it would follow by an analysis similar to that given above for Nosé-Hoover-Langevin.

The original proposal of Bussi et al. had

$$\Phi(K) = \frac{\gamma_{\text{VR}}}{2K}, \quad \text{so that} \quad \Psi(K) = (1 - (N_d - 1)k_B T/2K) \gamma_{\text{VR}},$$

where γ_{VR} is a positive constant.

For the more general case, the required conditions on Φ are as follows:

$K\Phi(K)$ is bounded as $K \rightarrow 0$, $\Phi(K)$ grows at most polynomially as $K \rightarrow \infty$.

8.4.5 The Efficiency of a Thermostat and “Gentle” Thermostats

To understand the reason for this fundamental, qualitative difference between Nosé-Hoover-Langevin and Langevin dynamics, and to compare it with Velocity Rescaling, one may study a quantity that relates the rate of convergence to equilibrium to the rate of growth of the error in the autocorrelation function. In [225], this precise quantity is introduced and termed the *efficiency* of the thermostat:

$$\text{efficiency} = \frac{\text{rate of convergence to equilibrium}}{\text{rate of growth of perturbation of dynamics}}.$$

The rate of convergence to equilibrium is quite difficult to calculate in general, as it would typically relate to the spectral gap of the diffusion. In light of the observations of Fig. 8.3, one may choose to estimate this in terms of the rate of convergence of the average kinetic energy to the target temperature.

The rate of accumulation of error due to the thermostat is also difficult to quantify analytically, since it requires calculation of the error in an autocorrelation function over a time interval which may not be short compared to the simulation stepsize, particularly for slow-relaxing systems. Again, an estimate is obtainable by considering the rate of error accumulation at short times (obtained by Taylor expansion of the exact and approximate autocorrelation functions). The result of these two estimates is then an analytical estimate for the efficiency that relates various schemes for various values of the parameters involved.

An interesting observation is that, while for both Langevin dynamics and Velocity Rescaling the error accumulation is linear in time, the same is not true for Nosé-Hoover-Langevin: the error in NHL increases initially in proportion to t^2 ; the instantaneous diffusion rate is inherited from the system to which it is applied. This means that, while NHL cannot be used to model imposed target diffusion rates, its influence on dynamics within the setting of molecular dynamics thermostating is also very slight: it is a *gentle* thermostat. The Velocity Rescaling method is also gentle in another sense: the rate of growth of error is small. Estimating the efficiency for both Langevin and Velocity Rescaling is similar—we find the ratio of the estimated rate of convergence of kinetic energy to the estimated rate of linear error growth in the velocity autocorrelation function. For Nosé-Hoover-Langevin, which has quadratic-in-time error growth, we determine the characteristic time until convergence (the reciprocal of the exponential rate of convergence) and from this determine how much perturbation accumulates in the velocity autocorrelation function.

In Table 8.1 we show the comparison of the relevant estimates of the above quantities, including the efficiency, for different choices of thermostat.

Table 8.1 Estimated rates of convergence, perturbation growth, and efficiency for different methods

Thermostat	Convergence rate	Error (to lowest order in t)	Efficiency
Langevin	γ	γt	≈ 1
Velocity Rescaling	$4 \frac{\text{Av}_\beta \{K^2 \Phi(K)\}}{TN_d k_B}$	$\frac{2}{N_d} \text{Av}_\beta \{K \Phi(K)\} t$	$O(N_d)$
VR with $\Phi(K) = \frac{\gamma_{\text{VR}}}{2K}$	γ_{VR}	$\frac{\gamma_{\text{VR}}}{N_d} t$	$\approx N_d$
NHL	$\sqrt{\frac{N_d k_B T}{\mu}}$ (at critical damping)	$\frac{k_B T}{2\mu} t^2$	$\approx 2N_d$

8.5 Non-Newtonian Dynamics-Based Iterations for Molecular Sampling

Given that we can decompose the stochastic dynamics into deterministic part and stochastic process, and approximately or exactly solve the parts, it is common to iterate the maps for each building block sequentially in such a way that the calculation approximates the dynamics of the system. This is, very likely, an unnecessary restriction on the sampling strategy. The crucial things that effect the ultimate success of the method are that the parts themselves preserve the measure (or approximately so), the stages are volume preserving, and that the stochastic processes are sufficiently strongly coupled so that the overall iteration is ergodic.

There is essentially no need to use maps based on Newtonian deterministic dynamics. There are many alternative dynamics models which leave invariant the canonical measure, going well beyond those considered so far. To illustrate this with one intriguing example, we explore here the stochastic dynamical system in $2N_c + 1$ variables defined by

$$d\mathbf{q} = \xi M^{-1} \mathbf{p} dt, \quad (8.33)$$

$$d\mathbf{p} = -\gamma \mathbf{p} dt + \sigma M^{1/2} d\mathbf{W}, \quad (8.34)$$

$$d\xi = -[(M^{-1} \mathbf{p}) \cdot \nabla U(\mathbf{q})/\mu + \gamma' \xi] dt + \sigma' dZ, \quad (8.35)$$

where \mathbf{W} is a vector of N_c Wiener processes, Z is a scalar Wiener process and $\sigma = \sqrt{2k_B T \gamma}$, and $\sigma' = \sqrt{2k_B T \gamma' / \mu}$ this system preserves the augmented distribution with density

$$\tilde{\rho}(\mathbf{q}, \mathbf{p}, \xi) = e^{-\beta(p^T M^{-1} p / 2 + U(\mathbf{q}) + \mu \xi^2 / 2)}.$$

For this system, it is possible to show that the Hörmander condition holds. Setting all parameters to 1 and taking $M = I$ (without loss of generality in this demonstration) we write our SDE in the form $d\varphi = D + \sum_{i=1}^{N_c+1} Y_i dW_i$, where φ is the vector of all phase variables, $Y_i = \mathbf{e}_{N_c+i}$, for $i = 1, \dots, N_c + 1$, is the $i + N_c$ th basis function in

\mathbb{R}^{2N_c+1} , the W_i are independent Wiener processes, and D is the “deterministic part:”

$$D = \begin{bmatrix} \xi p \\ -p \\ -p \cdot \nabla U - \xi \end{bmatrix}.$$

Then we calculate directly

$$D' = [D, Y_{N_c+1}] = \begin{bmatrix} p \\ 0 \\ 1 \end{bmatrix},$$

and from this we see that $[D', Y_i] = e_i$ for $i = 1, 2, \dots, N_c$. Thus all the basis vectors of \mathbb{R}^{2N_c+1} are found in the Lie algebra of the components of the Hörmander decomposition; as we know, this is the key step in the proof of ergodicity. Thus the method (8.33)–(8.35) is an alternative for molecular sampling dynamics, even though it is not based on a Newtonian model. Leaving the stochastic term off the final equation (i.e. in ξ) is easily shown to destroy the ergodicity property (the Hörmander condition is then violated).

Now consider the splitting into deterministic and OU parts. The deterministic part

$$\dot{q} = \xi M^{-1} p, \quad \dot{p} = 0, \quad \dot{\xi} = -(M^{-1} p) \cdot \nabla U(q)/\mu, \quad (8.36)$$

preserves volume and the function $U(q) + \mu \xi^2/2$ and hence also the distribution with density $\tilde{\rho}_A(q, \xi) = e^{-\beta(U(q)+\mu\xi^2/2)}$. By the same token the OU processes collectively preserve $\tilde{\rho}_B(p, \xi) = e^{-\beta(p^T M^{-1} p/2 + \mu \xi^2/2)}$. In combination the full dynamics preserves the extended canonical measure. If we iterate the two parts (assuming the deterministic part is solved exactly) the distribution will converge to the exact canonical distribution, due to especially to incorporation of $N_c + 1$ noise processes.

The OU process defining the fluctuations in p is completely decoupled from q and ξ , so it is perhaps most natural to think of the iteration as a random walk on the reduced space (q, ξ) where the directions are generated by an auxiliary OU process. Then the algorithm proceeds as follows: (1) choose a random direction p using the OU process, and (2) sample the reduced (stochastic) dynamics for (q, ξ) in the direction p . We refer to this procedure as *stochastic line sampling* (SLS), for the following reason. With p fixed in step (2), the motion of q is confined to the straight line: $q = q_0 + \eta M^{-1} p$, where η is a scalar function of time. Inserting this coordinate change in (8.36) we see that the equations reduce to $\dot{\eta} = \xi$, $\dot{\xi} = -\partial/\partial \eta U(q_0 + \eta M^{-1} p)$. This is a one-degree of freedom system and hence is theoretically exactly solvable in quadratures, although the complexity of the force will render this impractical in calculations, and, as mentioned above, an additional stochastic process must be incorporated to drive ξ .

The deterministic part may however be approximated in various ways. We may solve it by splitting into two (volume preserving) parts, integrating first $\dot{\mathbf{q}} = \xi \mathbf{M}^{-1} \mathbf{p}$, where ξ and \mathbf{p} are fixed (thus a drift along a given direction), followed by solving $\dot{\xi} = -(\mathbf{M}^{-1} \mathbf{p}) \cdot \nabla U/\mu$, which is a similar drift in the auxiliary variable. Composing these drifts successively in a leapfrog approach, we arrive at the deterministic sequence:

$$\begin{aligned}\xi_{n+1/2} &= \xi_n - (h/2)(\mathbf{M}^{-1} \mathbf{p}) \cdot \nabla U(\mathbf{q}_n)/\mu, \\ \mathbf{q}_{n+1} &= \mathbf{q}_n + h\xi_{n+1/2} \mathbf{M}^{-1} \mathbf{p}, \\ \xi_{n+1} &= \xi_{n+1/2} - (h/2)(\mathbf{M}^{-1} \mathbf{p}) \cdot \nabla U(\mathbf{q}_{n+1})/\mu.\end{aligned}$$

Coupling this to the stochastic evolution computed from solving the OU parts in both ξ and \mathbf{p} yields an alternative to Langevin dynamics that is 2nd order accurate in its steady state distribution and long term averages. Let us refer to this as the stochastic line sampling with leapfrog method.

Going a step further we may again obtain methods which exactly preserve the canonical measure based on canonical coordinate splitting, resulting in systems of the form

$$\dot{q}_i = \xi m_i^{-1} p_i, \quad \dot{\xi} = -p_i U_{q_i}/(\mu m_i).$$

Up to time-rescaling by p_i , these are in fact the same types of systems as we encountered previously in our treatment of J-splitting of the Hamiltonian system. If desired, an r th order area-preserving approximation of the q_i, p_i dynamics could be substituted. This method results in paths that differ slightly from the linear path in the direction $\mathbf{M}^{-1} \mathbf{p}$. In simulations we found that this method, which we term “stochastic line sampling with coordinate splitting,” was more stable than the leapfrog version when implemented using a further leapfrog splitting in each coordinate plane. However, we emphasize that both methods are highly experimental and are presented here as illustrations of the flexibility available in constructing methods to sample the canonical distribution—they have not yet been shown to be beneficial for molecular sampling applications.

We compare the trajectories and invariant distributions of the non-Newtonian line sampling thermostat (8.33)–(8.35) with three Newtonian-based thermostats: Langevin dynamics (7.4), Nosé-Hoover (8.2)–(8.4) and Nosé-Hoover-Langevin (8.27)–(8.29) dynamics. We seek to canonically sample a one-dimensional system with double-well potential energy function given as

$$U(q) = (q^2 - 1)^2.$$

Choosing all arbitrary system parameters to be one (i.e. setting $\beta = M = \gamma = \gamma' = \mu = 1$ for the methods), we select initial conditions $q(0) = p(0) = 1$ and $\xi(0) = 0.5$ with a timestep parameter $\delta t = 0.01$ sufficiently small to eliminate the possibility of numerical errors warping the results.

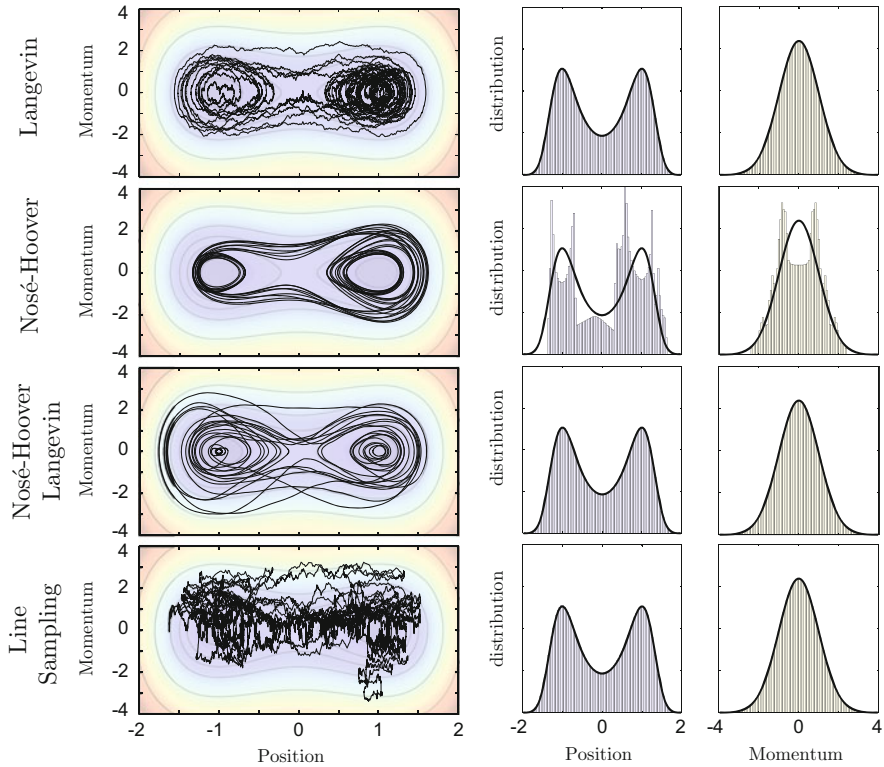


Fig. 8.5 We show sample trajectories (left) and long-time distributions (right) for a number of thermostatted dynamics. A lack of ergodicity in the case of the deterministic Nosé-Hoover thermostat prevents sampling ergodically, when compared to the exact distributions in **bold**

In Fig. 8.5 we give a realization of a trajectory computed using each dynamics, in the (q, p) plane. The Nosé-Hoover and Nosé-Hoover Langevin trajectories are significantly smoother than the others, indicating that these offer much more gentle thermostat techniques to reduce the perturbation to the dynamics. However, the Nosé-Hoover thermostat remains stuck in a periodic cycle preventing exploration of the space. This behavior persisted using other initial conditions and parameter values, indicating that it is symptomatic of a lack of ergodicity in the system.

By contrast, it is clear that the non-Newtonian thermostat explores the space in a very different way to the Newtonian-based thermostats. It is possible that this different type of exploration of the phase space could be advantageous in certain models (for example the linear stability threshold for step size may be different), however exploiting this difference may involve tuning the three parameters γ , γ' and μ , making it more difficult to work with than Langevin dynamics.

We also plot a histogram of the distributions of the position and momentum in Fig. 8.5, computed from a single trajectory of 10^9 discrete points. Overlaying

the exact expected result ρ_β , we can see the three stochastic methods perform excellently, whereas the results from using the Nosé-Hoover thermostat reveal extremely poor sampling as a result of the trajectory being trapped.

We would expect that using Nosé-Hoover Chains (8.16)–(8.21) may provide deterministic, ergodic sampling, by using a sufficiently long chain of artificial variables and correctly chosen mass parameters μ_i . However, the choice of these parameter values may prove crucial to the ergodicity of the dynamics. Therefore, we suggest that for equilibrium canonical sampling it is far more efficient to use a stochastic thermostat, in comparison to the ergodicity issues and additional parameter tuning required in the case of deterministic thermostats.

8.6 Isokinetic Methods and Integration with Very Large Timestep

In the last chapter we examined various numerical methods for Langevin dynamics, observing very substantial differences in the accuracy obtainable for configurational sampling using different schemes. In this section, we discuss methods that accelerate sampling using a more radical approach, namely modification of the ensemble to incorporate isokinetic constraints. We again assume in what follows that $N_c = N_d$, so there are no constraints acting on the system (other than the isokinetic constraint we are going to impose).

The starting point here is the Gaussian isokinetic thermostat [124]. This type of constraint can be introduced into Newtonian dynamics $\dot{\mathbf{q}} = \mathbf{M}^{-1}\mathbf{p}$, $\dot{\mathbf{p}} = \mathbf{F}(\mathbf{q})$ by adding a Lagrange multiplier, i.e. changing the equations of motion to

$$\begin{aligned}\dot{\mathbf{q}} &= \mathbf{M}^{-1}\mathbf{p}, \\ \dot{\mathbf{p}} &= \mathbf{F}(\mathbf{q}) - \xi\mathbf{p}, \\ K_0 &= K(\mathbf{p}) \stackrel{\text{def}}{=} \mathbf{p}^T \mathbf{M}^{-1} \mathbf{p}.\end{aligned}$$

By differentiating the constraint and introducing the second equation, we obtain an equation for ξ :

$$0 = \mathbf{p}^T \mathbf{M}^{-1} \dot{\mathbf{p}} = \mathbf{p}^T \mathbf{M}^{-1} [\mathbf{F}(\mathbf{q}) - \xi\mathbf{p}].$$

This yields

$$\xi = \frac{\mathbf{p}^T \mathbf{M}^{-1} \mathbf{F}(\mathbf{q})}{\mathbf{p}^T \mathbf{M}^{-1} \mathbf{p}}.$$

Simply substitute this expression into the differential equations to obtain the unconstrained equations

$$\dot{\mathbf{q}} = \mathbf{M}^{-1}\mathbf{p}, \quad (8.37)$$

$$\dot{\mathbf{p}} = \mathbf{F}(\mathbf{q}) - \frac{\mathbf{p}^T \mathbf{M}^{-1} \mathbf{F}(\mathbf{q})}{\mathbf{p}^T \mathbf{M}^{-1} \mathbf{p}} \mathbf{p}. \quad (8.38)$$

These equations preserve $\mathbf{p}^T \mathbf{M}^{-1} \mathbf{p} = \text{constant}$. (Note: It is tempting to replace the denominator in this expression by K_0 , the value of kinetic energy, but this is not recommended since it then destroys the first integral.) The system (8.37)–(8.38) can be rewritten in the alternative form

$$\begin{aligned}\dot{\mathbf{q}} &= \mathbf{M}^{-1}\mathbf{p}, \\ \dot{\mathbf{p}} &= [\mathbf{I} - \mathcal{H}] \mathbf{F}(\mathbf{q}),\end{aligned}$$

where $\mathcal{H} = \mathbf{p}(\mathbf{p}^T \mathbf{M}^{-1} \mathbf{p})^{-1} \mathbf{p}^T \mathbf{M}^{-1}$ is a *projector* matrix which is idempotent: $\mathcal{H}^2 = \mathcal{H}$. The invariant subspace associated to this projector is $\text{span}(\mathbf{p})$:

$$\mathcal{H}\mathbf{p} = \mathbf{p}.$$

Isokinetic dynamics has nonvanishing divergence, which requires a special treatment to elucidate its statistical mechanical properties [338, 376]. In order to find a stationary solution, one substitutes

$$\rho(\mathbf{q}, \mathbf{p}) = e^{-w(\mathbf{q}, \mathbf{p})} \Phi(K(\mathbf{p})), \quad (8.39)$$

(with Φ a nonvanishing function of K) into the continuity equation for the isokinetic system, the function w being at this point unknown. Then one obtains, with \mathbf{f}_{iso} denoting the vector field in (8.37)–(8.38), that

$$\begin{aligned}0 &= \nabla \cdot (\rho \mathbf{f}_{\text{iso}}) = (\nabla \rho) \cdot \mathbf{f}_{\text{iso}} + \rho(\nabla \cdot \mathbf{f}_{\text{iso}}) \\ &= (-\nabla w \rho + \rho \frac{\Phi'(K)}{\Phi(K)} \nabla K) \cdot \mathbf{f}_{\text{iso}} + \rho(\nabla \cdot \mathbf{f}_{\text{iso}}).\end{aligned}$$

Using the isokinetic property, the term involving K drops out. One next calculates the divergence of the isokinetic vector field and finds that (see Exercise 5)

$$\nabla \cdot \mathbf{f}_{\text{iso}} = (N_c - 1) \frac{\mathbf{p}^T \mathbf{M}^{-1} \mathbf{F}}{\mathbf{p}^T \mathbf{M}^{-1} \mathbf{p}}.$$

Thus the condition to have a stationary state of the form (8.39) is that

$$\nabla w \cdot \mathbf{f}_{\text{iso}} = (N_c - 1) \frac{\mathbf{p}^T \mathbf{M}^{-1} \mathbf{F}}{\mathbf{p}^T \mathbf{M}^{-1} \mathbf{p}}.$$

A solution of this equation for w is easily found, it is

$$w = (N_c - 1) \frac{U(\mathbf{q})}{K(\mathbf{p})}.$$

The invariant probability density, which is associated to a surface of constant kinetic energy, can be written as a generalized function using the Dirac notation:

$$\rho(\mathbf{q}, \mathbf{p}) = Z^{-1} e^{-(N_c - 1)U(\mathbf{q})/K(\mathbf{p})} \delta[K(\mathbf{p}) - K_0].$$

If we work on the surface of constant kinetic energy $K(\mathbf{p}) = K_0 \stackrel{\text{def}}{=} \beta^{-1}(N_c - 1)$, the invariant density is of the form

$$\rho \propto \bar{\rho}_\beta \delta[K(\mathbf{p}) - k_B T(N_c - 1)]$$

which demonstrates that the isokinetic method, with this choice for the total kinetic energy, leaves invariant the configurational Gibbs distribution. Ergodicity has not been demonstrated, so it is not possible to conclude that the invariant distribution is unique; as we have seen before, the incorporation of stochastic terms can allow the formulation of strong statements regarding the ergodicity and mixing properties.

8.6.1 A Stochastic, Isokinetic Method for Gibbs Sampling

Minary et al. [271, 272] studied the isokinetic method as a means to control the instability in multiple timestepping due to resonance. They suggested that each physical degree of freedom be coupled to its own NHC thermostat through an isokinetic constraint in a “massive” thermostating approach. These massive thermostats introduced some complexity (each degree of freedom had an associated Nosé-Hoover chain system as well as the constraint); obtaining an accurate solution for this large system is involving. A potentially more serious problem is that, although Nosé-Hoover chains and the isokinetic method may in some cases appear to be “practically ergodic,” no proof of ergodicity exists. A recent article (by one of us, together with Margul and Tuckerman [220]) addressed these problems by replacing the Nosé-Hoover chains with stochastic terms (of Ornstein-Uhlenbeck type).

We first demonstrate the idea of [220] by considering the following SDE with a single degree of freedom:

$$dq = pdt, \quad (8.40)$$

$$dp = [F(q) - \lambda p] dt, \quad (8.41)$$

$$d\xi_1 = -\lambda \xi_1 dt - \xi_2 \dot{\xi}_1 dt, \quad (8.42)$$

$$d\xi_2 = \mu_2^{-1}(\mu_1 \xi_1^2 - k_B T) dt - \gamma \xi_2 dt + \sigma dW, \quad (8.43)$$

where ξ_1 and ξ_2 are auxiliary variables, $\sigma = \sqrt{2\gamma/\beta\mu_2}$, γ is the friction constant, μ_1 and μ_2 are coupling coefficients, and λ is a Lagrange multiplier which is chosen to maintain the isokinetic relation involving p and ξ_1 :

$$p^2 + \frac{1}{2}\mu_1 \xi_1^2 = k_B T. \quad (8.44)$$

We calculate the multiplier by differentiating the constraint to obtain

$$2p\dot{p} + \mu_1 \xi_1 \dot{\xi}_1 = 0$$

or, using the differential equations,

$$2(pF(q) - \lambda p^2) + \mu_1 \xi_1 (-\lambda \xi_1 dt - \xi_2 \dot{\xi}_1) = 0,$$

thus

$$\lambda = \frac{pF(q) - \mu_1 \xi_1^2 \xi_2 / 2}{p^2 + \mu_1 \xi_1^2 / 2}.$$

Upon reintroduction of this expression in (8.40)–(8.43) this allows us to write a closed-form SDE system for q, p, ξ_1, ξ_2 .

We follow an analogous procedure to that used to study the distribution in the case of the standard isokinetic system, for the moment *ignoring the stochastic terms*. This requires us to solve the equation

$$\nabla w \cdot f = \text{div}(f),$$

where now f is the vector field in (8.40)–(8.43) where we take $\gamma = 0$. The divergence is

$$\text{div}(f) = -\frac{d}{dp}(\lambda p) - \frac{d}{d\xi_1}(\lambda \xi_1) - \xi_2.$$

Let $\eta_1 = pF - \mu_1 \xi_1^2 \xi_2 / 2$, $\eta_2 = p^2 + \mu_1 \xi_1^2 / 2$, so $\lambda = \eta_1 / \eta_2$, then calculate

$$\begin{aligned}\frac{d}{dp} \lambda &= (\eta_2 F - 2\eta_1 p) / \eta_2^2, \\ \frac{d}{d\xi_1} \lambda &= (-\mu_1 \xi_1 \xi_2 \eta_2 - \mu_1 \xi_1 \eta_1) / \eta_2^2,\end{aligned}$$

to see that

$$\begin{aligned}p \frac{d\lambda}{dp} + \xi_1 \frac{d\lambda}{d\xi_1} &= \frac{(pF - \mu_1 \xi_1^2 \xi_2) \eta_2 - (2p^2 + \mu_1 \xi_1^2) \eta_1}{\eta_2^2} \\ &= 2 \left[-\frac{pF}{2\eta_2} + \lambda - \lambda \right] = -\frac{pF}{\eta_2},\end{aligned}$$

hence

$$\begin{aligned}\text{div}(\mathbf{f}) &= \frac{pF}{\eta_2} - 2\lambda - \xi_2 \\ &= \frac{pF - 2(pF - \mu_1 \xi_1^2 \xi_2 / 2)}{p^2 + \mu_1 \xi_1^2 / 2} - \xi_2 \\ &= \frac{-pF + \mu_1 \xi_1^2 \xi_2}{p^2 + \mu_1 \xi_1^2 / 2} - \xi_2.\end{aligned}$$

We find that a solution of the equation $\nabla w \cdot \mathbf{f} = \text{div}(\mathbf{f})$ is then given by

$$w = \frac{U + \frac{1}{2} \xi_2^2}{p^2 + \frac{1}{2} \mu_1 \xi_1^2}.$$

Integrating over the isokinetic surface $p^2 + \frac{1}{2} \mu_1 \xi_1^2 = \beta^{-1}$, and with respect to the variable ξ_2 , yields the Gibbs configurational density.

The exciting prospect here is that we now have a new variable ξ_2 which has, in equilibrium, a Gaussian distribution. The Ornstein-Uhlenbeck terms are therefore compatible with this extended distribution and can be incorporated (as in Nosé-Hoover-Langevin) to provide ergodicity and control of the convergence to equilibrium.

8.6.2 Ergodicity

Following the discussion in [220], let us show ergodicity for the stochastic isokinetic harmonic oscillator:

$$\begin{aligned} dq &= pdt \\ dp &= [-q - \lambda p]dt \\ d\xi_1 &= [-\lambda \xi_1 - \xi_2 \dot{\xi}_1]dt \\ d\xi_2 &= [\dot{\xi}_1^2 - k_B T - \gamma \xi_2]dt + \sigma dW \end{aligned} \quad (8.45)$$

with $\lambda = \frac{-qp - \xi_2 \dot{\xi}_1^2/2}{p^2 + \dot{\xi}_1^2/2}$ and $\sigma = \sqrt{2\gamma k_B T}$. We have taken the coupling coefficients μ_1, μ_2 both one for simplicity as their particular values (as long as nonzero) have no bearing on the ergodic property.

The constraint, $p^2 + \dot{\xi}_1^2/2 = \text{const}$, defines a three-dimensional manifold \mathcal{M} , a generalized cylinder. $\xi_1 = 0$ is an invariant manifold of the isokinetic equations, with solutions therefore confined for all time to one or the other half-space ($\xi_1 < 0$ or $\xi_1 > 0$). It is enough to sample one or the other of the two half spaces. To show that the solutions do so, we need to demonstrate that an appropriate Hörmander condition holds. Define f and g as the vector fields

$$f = p\partial_q - (q + \lambda p)\partial_p - (\lambda \xi_1 + \xi_2 \dot{\xi}_1)\partial_{\xi_1} + [(\dot{\xi}_1^2 - k_B T) - \gamma \xi_2]\partial_{\xi_2}, \quad (8.46)$$

and

$$g = \sigma \partial_{\xi_2}. \quad (8.47)$$

We will show that the dimension of the ideal spanned by the iterated commutators of the vector fields f and g is three, i.e. that it spans the tangent space to \mathcal{M} at any point. For this purpose, we use the collection of vectors

$$f, g, [f, g], [f, [f, g]], [f, [f, [f, g]]].$$

We will see that these provide a basis at every point excluding the one-dimensional set defined by the union \mathcal{M}_0 of the two lines ℓ_+, ℓ_- defined by

$$q = 0, \quad p = 0, \quad \xi_1 = \pm \sqrt{2\mu_1^{-1}k_B T},$$

and arbitrary ξ_2 . [Note: the choice $\xi_1 = \pm \sqrt{2\mu_1^{-1}k_B T}$ is made so that the isokinetic constraint is satisfied. In [220] this value was incorrectly defined.] The vectors f and g are linearly independent except on \mathcal{M}_0 .

The proof requires calculation of the vector fields

$$\mathbf{u}_0 = \boldsymbol{\Pi}f, \quad \mathbf{u}_1 = \boldsymbol{\Pi}[f, g], \quad \mathbf{u}_2 = \boldsymbol{\Pi}[f, [f, g]], \quad \mathbf{u}_3 = \boldsymbol{\Pi}[f, [f, [f, g]]],$$

where $\boldsymbol{\Pi}$ is the projector onto the first three components. Because $g = \sigma e_4$, it is enough to show that any pair from among these four vectors are linearly independent, except possibly on \mathcal{M}_0 . Note that projection can only be performed after the full calculation of the relevant commutator. Because the commutators quickly become quite messy, we used a symbolic computing package to assist in these calculations.

The first two vectors are:

$$\mathbf{u}_0 = p\partial_q - (q + \lambda p)\partial_p - (\lambda\xi_1 + \xi_1\xi_2)\partial_{\xi_1}, \quad (8.48)$$

and

$$\mathbf{u}_1 = \sigma p \frac{\partial \lambda}{\partial \xi_2} \partial_p + \xi_1 \left(1 + \frac{\partial \lambda}{\partial \xi_2} \right) \partial_{\xi_1}. \quad (8.49)$$

After expanding the derivatives of λ we have

$$\mathbf{u}_1 = p\partial_q + \xi_1^2 \left(\frac{-q + p\xi_2}{D} \right) \partial_p - 2\xi_1 p \left(\frac{-q + p\xi_2}{D} \right) \partial_{\xi_1}, \quad (8.50)$$

and

$$\mathbf{u}_2 = -\sigma(\xi_1^2 p/D)\partial_p + (2\sigma\xi_1 p^2/D)\partial_{\xi_1}, \quad (8.51)$$

where $D = 2p^2 + \xi_1^2$.

If $q \neq 0$ and $p \neq 0$, then clearly \mathbf{u}_1 and \mathbf{u}_2 are linearly independent. However, if $p = 0$ then $\mathbf{u}_2 = 0$. We proceed to compute the commutator $[f, [f, g]]$. Projecting to the first three components results in

$$\mathbf{u}_2 = \sigma \left(\frac{\xi_1^2 p}{D} \right) \partial_q - \sigma \left(\frac{2\gamma p^3 + \gamma \xi_1^2 p - \xi_1^2 q}{D^2} \right) \partial_p + 2\sigma \xi_1 p \left(\frac{2\gamma p^3 + \gamma \xi_1^2 p - \xi_1^2 q}{D^2} \right) \partial_{\xi_1}. \quad (8.52)$$

Again, we substitute $p = 0$ and find that

$$\mathbf{u}_2|_{p=0} = (\sigma \xi_1^2 q / D^2) \partial_p. \quad (8.53)$$

Unfortunately, this is parallel to \mathbf{u}_1 (for $p = 0$), and hence yet one more commutator is required in this case.

We calculate $[f, [f, [f, g]]]$ and project onto the space spanned by the first three components to find

$$\begin{aligned} \mathbf{u}_3 = \sigma & \left(\frac{2\gamma p^3 - 4p^3\xi_2 + 4p^2q + \xi_1^2 p \xi_2 + \gamma \xi_1^2 p - 2\xi_1^2 q}{D^2} \right) \partial_q \\ & - \sigma \xi_1^2 \left(\frac{\eta}{D^3} \right) \partial_p + 2\sigma \xi_1 p \left(\frac{\eta}{D^3} \right) \partial_{\xi_1}. \end{aligned} \quad (8.54)$$

with

$$\begin{aligned} \eta = & 4p^5\gamma^2 - 8p^5\xi_1^2 - 4\xi_1^2 p^3 + 4p^3\gamma^2\xi_1^2 - 4p^3\xi_1^4 \\ & - 2\gamma\xi_1^2 p^2 q + 4p^2 q \xi_2 \xi_1^2 - 4\xi_1^2 q^2 p - 2\xi_1^4 p + p\gamma^2\xi_1^4 - q\gamma\xi_1^4 + \xi_1^4 \xi_2 q. \end{aligned} \quad (8.55)$$

Along $p = 0$, \mathbf{u}_3 becomes

$$\begin{aligned} \mathbf{u}_3|_{p=0} = & -2\sigma q \partial_q - \sigma \left(\frac{-q\gamma\xi_1^4 + \xi_1^4 \xi_2 q}{\xi_1^4} \right) \partial_p \\ = & -2\sigma q \partial_q - \sigma q(-\gamma + \xi_2) \partial_p. \end{aligned} \quad (8.56)$$

Together with \mathbf{u}_0 we obtain a linearly independent set as long as $q \neq 0$.

If $p = 0$ and $q = 0$ then we are on \mathcal{M}_0 . If $p \neq 0$ then \mathbf{u}_2 and \mathbf{u}_0 are linearly independent. If $q \neq 0$ then \mathbf{u}_3 and \mathbf{u}_0 are linearly independent. From these we establish that the Hörmander condition holds everywhere except on a space of co-dimension 2 (that is except on the one-dimensional set \mathcal{M}_0).

In this case, it is possible to complete the proof by introducing a Lyapunov function ϕ to demonstrate the necessary contractivity in the ξ_2 direction. The generator of this system is

$$\mathcal{L}_{\text{isok}} = p \frac{\partial}{\partial q} + \left[F - (p^2/\Lambda)F \right] \frac{\partial}{\partial p} - \frac{p\xi_1 F}{\Lambda} \frac{\partial}{\partial \xi_1} + \mathcal{L}_N + \mathcal{L}_O$$

with $\Lambda = p^2 + \xi_1^2/2$,

$$\mathcal{L}_N = \frac{1}{2} \frac{\xi_1^2 \xi_2 p}{\Lambda} \frac{\partial}{\partial p} + \frac{1}{2} \frac{\xi_1^3 \xi_2}{\Lambda} \frac{\partial}{\partial \xi_1} - \xi_2 \xi_1 \frac{\partial}{\partial \xi_1} + [\xi_1^2 - \beta^{-1}] \frac{\partial}{\partial \xi_2},$$

and

$$\mathcal{L}_O = -\gamma \xi_2 \frac{\partial}{\partial \xi_2} + \frac{\sigma^2}{2} \frac{\partial^2}{\partial \xi_2^2}.$$

Let us apply the operator $\mathcal{L}_{\text{isok}}$ to $\phi \stackrel{\text{def}}{=} \xi_2^2/2$. As this is only a function of ξ_2 , many terms vanish and we are left with

$$\mathcal{L}_{\text{isok}}\phi = \mathcal{L}_N\phi + \mathcal{L}_O\phi,$$

$$\mathcal{L}_N\phi = [\xi_1^2 - \beta^{-1}]\xi_2,$$

and

$$\mathcal{L}_O\phi = -\gamma\xi_2^2 + \frac{\sigma^2}{2}.$$

Because ξ_1 is uniformly bounded due to the isokinetic constraint, we have

$$\mathcal{L}_{\text{isok}}\phi \leq -\gamma\xi_2^2 + K\xi_2 + \frac{\sigma^2}{2}.$$

For $|\xi_2|$ sufficiently large this term is negative. This contractivity, together with assumptions of boundedness of configurations (the use of periodic boundary conditions) and the isokinetic constraints on p and ξ_1 , as well as the existence of a candidate measure which is positive on open sets, will ultimately ensure the ergodicity of the system, relying on arguments similar to those in [256, 257].

8.6.3 Multiple Timestepping Using the Stochastic Isokinetic Formulation

The numerical integration of the equations of the stochastic isokinetic system can be performed using splitting, in a style that should by now be familiar, with the proviso that the isokinetic condition itself should be satisfied exactly (i.e. to rounding error).

Molecular sampling using Langevin dynamics and other methods involves integration over the infinite cylinder $\mathbb{T}^N \times \mathbb{R}^N$. The power of the isokinetic method is that it allows us to reformulate the configurational sampling problem as integration on a compact manifold. The fact that we also slightly extend the domain by introducing auxiliary variables is more than offset by the stabilizing effect of the isokinetic constraints. One approach would be to introduce an isokinetic constraint on the entire system, but in practice it is found that no great crime is committed in configurational sampling by constraining each degree of freedom (together with associated auxiliary variables).

To develop a multiple timestepping method, we begin by supposing that the potential energy function and therefore the force can be decomposed into fast and slow terms, thus $U(\mathbf{q}) = U_S(\mathbf{q}) + U_F(\mathbf{q})$ and the force acting on the j th degree of freedom is $F_j = F_j^S + F_j^F$. Because the SIN(R) method is based on a non-Hamiltonian formulation, we do not obtain a symplectic integrator (in the absence

of stochastic perturbation). Unlike for r-RESPA, the splitting needs to be performed at the level of the differential equations. We suppress the index of the degree of freedom, takes its mass to be one for simplicity of presentation, and write the equations of motion for the variables associated to a single physical degree of freedom in the form

$$\begin{aligned} dq &= pdt, \\ dp &= Fdt - \left(\frac{p(F^F + F^S) - \frac{1}{2}\mu_1\xi_1^2\xi_2}{\Lambda} \right) pdt, \\ d\xi_1 &= - \left(\frac{p(F^F + F^S) - \frac{1}{2}\mu_1\xi_1^2\xi_2}{\Lambda} \right) \xi_1 dt - \xi_2 \xi_1 dt, \\ d\xi_2 &= \mu_2^{-1}(\mu_1\xi_1^2 - \beta^{-1})dt - \gamma\xi_2 dt + \sigma dW, \end{aligned}$$

where $\Lambda = p^2 + \frac{1}{2}\mu_1\xi_1^2$. $\Lambda = \beta^{-1}$ is constant of motion.

Because of the form of the coupling, we observe that this vector field can be additively decomposed based on the various terms in the stochastic isokinetic equations, including the fast-slow splitting of the forces, into the following generators:

Kinetic part:

$$\mathcal{L}_K = p \frac{\partial}{\partial q},$$

isokinetic Fast force:

$$\mathcal{L}_F = [F^F - (p^2/\Lambda)F^F] \frac{\partial}{\partial p} - \frac{p\xi_1 F^F}{\Lambda} \frac{\partial}{\partial \xi_1},$$

isokinetic Slow force:

$$\mathcal{L}_S = [F^S - (p^2/\Lambda)F^S] \frac{\partial}{\partial p} - \frac{p\xi_1 F^S}{\Lambda} \frac{\partial}{\partial \xi_1},$$

isokinetic Nosé terms:

$$\mathcal{L}_N = \frac{1}{2} \frac{\mu_1 \xi_1^2 \xi_2 p}{\Lambda} \frac{\partial}{\partial p} + \frac{1}{2} \frac{\mu_1 \xi_1^3 \xi_2}{\Lambda} \frac{\partial}{\partial \xi_1} - \xi_2 \xi_1 \frac{\partial}{\partial \xi_1} + \mu_2^{-1} [\mu_1 \xi_1^2 - \beta^{-1}] \frac{\partial}{\partial \xi_2},$$

Ornstein-Uhlenbeck term:

$$\mathcal{L}_O = -\gamma \xi_2 \frac{\partial}{\partial \xi_2} + \frac{\sigma^2}{2} \frac{\partial^2}{\partial \xi_2^2}.$$

It is straightforward to show that each of the terms of the corresponding vector field splitting preserves the first integral $\Lambda = \text{constant}$. For example

$$\begin{aligned}\mathcal{L}_F\Lambda &= [F^F - (p^2/\Lambda)F^F] \frac{\partial\Lambda}{\partial p} - \frac{p\xi_1 F^F}{\Lambda} \frac{\partial\Lambda}{\partial\xi_1} \\ &= [F^F - (p^2/\Lambda)F^F](2p) - \frac{p\xi_1 F^F}{\Lambda}(\mu_1\xi_1) \\ &= pF^F[2 - \Lambda^{-1}(2p^2 + \mu_1\xi_1^2)] \\ &= 2pF^F[1 - \Lambda^{-1}\Lambda] = 0.\end{aligned}$$

The proof for the other terms is similar.

The given decomposition can be used to construct a variety of algorithms, for example the following which we term the Stochastic Isokinetic Nosé-Hoover RESPA algorithm.

SIN(R) Algorithm

Propagate p, ξ_1, ξ_2 by $\exp[(h/2)\mathcal{L}_N]$.

Propagate p, ξ_1 by $\exp[(\tilde{h}/2)\mathcal{L}_F + (h/2)\mathcal{L}_S]$, $(\tilde{h} = h/r)$.

Propagate q by $\exp[\tilde{h}\mathcal{L}_K]$.

Propagate ξ_2 by $\exp[\tilde{h}\mathcal{L}_O]$.

Propagate p, ξ_1 by $\exp[(\tilde{h}/2)\mathcal{L}_F]$.

Repeat $r - 2$ times:

Propagate p, ξ_1 by $\exp[(\tilde{h}/2)\mathcal{L}_F]$.

Propagate q by $\exp[(\tilde{h}/2)\mathcal{L}_K]$.

Propagate ξ_2 by $\exp[(\tilde{h})\mathcal{L}_O]$.

Propagate q by $\exp[(\tilde{h}/2)\mathcal{L}_K]$.

Propagate p, ξ_1 by $\exp[(\tilde{h}/2)\mathcal{L}_F]$.

Propagate p, ξ_1 by $\exp[(\tilde{h}/2)\mathcal{L}_F]$.

Propagate ξ_2 by $\exp[\tilde{h}\mathcal{L}_O]$.

Propagate q by $\exp[\tilde{h}\mathcal{L}_K]$.

Propagate p, ξ_1 by $\exp[(\tilde{h}/2)\mathcal{L}_F + (h/2)\mathcal{L}_S]$.

Propagate p, ξ_1, ξ_2 by $\exp[(h/2)\mathcal{L}_N]$.

We stress that the implementation of this method is in fact quite straightforward, despite its apparent complexity. The following details regarding the implementation are discussed in [220]:

- For the integration of the Nosé terms, it is recommended to use a further splitting:

$$\mathcal{L}_N = \mathcal{L}_N^{(1)} + \mathcal{L}_N^{(2)},$$

where

$$\mathcal{L}_N^{(1)} = \frac{1}{2} \frac{\mu_1 \xi_1^2 \xi_2 p}{\Lambda} \frac{\partial}{\partial p} + \frac{1}{2} \frac{\mu_1 \xi_1^3 \xi_2}{\Lambda} \frac{\partial}{\partial \xi_1} - \xi_2 \xi_1 \frac{\partial}{\partial \xi_1},$$

and

$$\mathcal{L}_N^{(2)} = \mu_2^{-1} [\mu_1 \xi_1^2 - \beta^{-1}] \frac{\partial}{\partial \xi_2}.$$

Moreover a Yoshida/Suzuki type higher order decomposition is used to obtain more accuracy in this component.

- The term $\exp[h\mathcal{L}_F]$ (like similar terms) is completely integrable. Note that in general this reduces to solving

$$\begin{aligned}\dot{p} &= F - p^2 F / \Lambda, \\ \dot{\xi}_1 &= p \xi_1 F / \Lambda,\end{aligned}$$

with F a constant.

The solution in a timestep h is

$$\begin{aligned}p(h) &= \frac{p(0) + (F/m)s(h)}{\dot{s}(h)}, \\ \xi_1(h) &= \frac{\xi_1(0)}{\dot{s}(h)},\end{aligned}$$

where

$$s(t) = b^{-1/2} \sinh(t\sqrt{b}) + \frac{a}{b} (\cosh(t\sqrt{b}) - 1)$$

with $a = Fp(0)/\Lambda$ and $b = F^2/\Lambda$, $\Lambda = \beta^{-1}$.

Care must be taken in the evaluation of s and \dot{s} for a, b close to zero.

Note that other decompositions are possible [220].

8.6.4 Numerical Example

Let us briefly summarize the numerical experiments of [220] using the SIN(R) method to simulate a system of 512 flexible water molecules using a fully flexible molecular model [294] and the smooth particle-mesh Ewald method (SPME) [123] (see Appendix A) to compute electrostatic forces. Initial simulations were conducted without a fast-slow force decomposition to demonstrate the effectiveness of the method as a thermostating scheme. This technique was shown to allow accurate computation of the OH, HH and OO radial distribution functions when suitably small timesteps were used.

As explained in Chap. 4, the resonances in multiple timestepping restrict the size of the large (outer) stepsize usable in simulation. In the case of fully flexible water the maximum outer stepsize that can be used for stable RESPA simulation is typically found to be less than 5 fs [245, 329]. A multiple timestepping method for the SPME method can be based on the decomposition

$$U_{\text{Total}} = U_{\text{bonds}} + U_{\text{s.r.}} + U_{\text{l.r.}}$$

where U_{bonds} includes length and angle bonds, $U_{\text{s.r.}}$ includes all other short-ranged components, and $U_{\text{l.r.}}$ incorporates both the “reciprocal space part” from Particle Mesh Ewald summation (normally calculated using 3D FFT) as well as longer-ranged screened Coulombic pair terms within the simulation cell. Then a nested multiple timestepping hierarchy can be used with stepsizes h_{inner} , h_{mid} and h_{outer} , each larger stepsize being an integer multiple of the next smaller. There is no difficulty with adapting the SIN(R) scheme (which was presented for a two-level setup) to this multi-level hierarchical timestepping framework.

The article [220] provides more detail of the SPME parameters and a detailed analysis of the numerical performance. We merely mention here that with $h_{\text{inner}} = 0.5$ fs and $h_{\text{mid}} = 3$ fs, it was possible to use outer stepsizes of up to 99 fs for stable integration and accurate resolution of all three radial distribution functions, with no evidence of resonances. The short-range cutoff in the reported simulations was around 8 Å. High efficiency improvements would be anticipated in simulations with a large simulation cell. These methods could be valuable in more complex applications, including systems with mixed quantum and classical simulation domains, and in the setting of high performance computing architectures, e.g. GPU systems.

8.7 Generalized Langevin Dynamics

We have already encountered Generalized Langevin dynamics in Chap. 6, where it appeared as an intermediate stage in the derivation of Langevin dynamics. In some cases, the properties of the heat bath and the resulting memory kernel are important

and have to be modelled as part of the simulation process. Our presentation of this topic follows that of [19] and earlier works [69, 85, 204, 276] which treat the non-Markovian Generalized Langevin equation as a Markov system in an extended phase space.

The equations of Generalized Langevin dynamics are normally written in the form

$$dq = M^{-1}p dt, \quad (8.57)$$

$$dp = -\nabla U(q)dt - \int_0^t \Gamma(t-s)p(s)ds dt + dB, \quad (8.58)$$

subject to initial conditions $q(0) = q_0, p(0) = p_0$. Here $\Gamma(t) = (\gamma_{ij}(t))$ is a $N_c \times N_c$ matrix-valued function of t which we refer to as the “memory kernel”. The term

$$F_d = - \int_0^t \Gamma(t-s)p(s)ds dt$$

represents a drag force acting on the system due to the interaction with the particles of the bath. dB is the increment of the colored-noise (non-Gaussian) stochastic process. Often this increment is treated formally as an impulse $R(t)dt$, where R is referred to as a “random force,” which calls to mind the origin of the stochastic term as the model for interaction with a large (but finite) heat bath. We use this language for consistency with the literature. The driving forces are correlated in a way that is described by the fluctuation-dissipation theorem [202, 402]. This states that at temperature T the components of the random forces satisfy

$$\langle R_i(t+s)R_j(t) \rangle = k_B T \gamma_{ij}(s) \delta_{ij}, \quad s \geq 0. \quad (8.59)$$

Here, δ_{ij} is the Kronecker delta, and k_B is Boltzmann’s constant.

Numerical methods for treating (8.57)–(8.58) include calculation of the drag force F_d which requires a convolution of the momenta with $\Gamma(t)$ and therefore storage of some portion of the time-history of p . Typically we will compute a discrete sequence of p_0, p_1, \dots , and so it will be necessary to store a collection of, say $\ell > 0$, previous momentum vectors. This may be somewhat demanding in a large scale simulation setting. Moreover, computing R requires the generation of a sequence of random numbers with prescribed correlation, as specified in Eq. (8.59). Both these issues may be addressed sensibly using the technique of Prony series and an extended variable representation

In the remainder of this discussion, for the purpose of simplified presentation, we confine ourselves to the simple case of a scalar memory kernel, writing

$$\Gamma(t) = \gamma(t)I.$$

For systems in which the memory kernel decays fairly rapidly, it is not unreasonable to consider its approximation by a linear combination of exponential functions, a so-called *Prony series*:

$$\gamma(t) = \sum_{k=1}^{k_{\max}} \frac{c_k}{\tau_k} \exp\left[-\frac{t}{\tau_k}\right], \quad t \geq 0. \quad (8.60)$$

The properties of the system in the limit $\tau_k \rightarrow 0$ are studied in [293].

The use of this representation for the memory kernel allows us to replace the history-dependent equations (8.57)–(8.58) by a Markovian system in a larger dimensional space, by introducing k additional degrees of freedom per physical degree of freedom. This method obviously increases storage requirements, and, in large systems, it may be significant. However, the evolution of these additional variables is elementary and the overall computational cost low.

8.7.1 Using an Extended Variable Representation

We introduce a set of extended variables whose evolution is described by standard Brownian motions using Ornstein-Uhlenbeck (OU) processes. For this treatment, let the particle positions and momenta be enumerated as (q_i, p_i) , $i = 1, \dots, N_c$ and define the extended variable, $\eta_{i,k}(t)$, associated with the k th term in the Prony series in interaction with the i th physical variable by

$$\eta_{i,k}(t) = - \int_0^t \frac{c_k}{\tau_k} \exp\left[-\frac{(t-s)}{\tau_k}\right] p_i(s) ds. \quad (8.61)$$

Equations (8.57)–(8.58) can then be rewritten in the form

$$dq_i = m_i^{-1} p_i dt \quad (8.62)$$

$$dp_i = F_i dt + \sum_{k=1}^{k_{\max}} \eta_{i,k} dt + R_i dt. \quad (8.63)$$

We note that $\eta_{i,k}$ is the solution of an ODE of the form

$$d\eta_{i,k} = -\frac{1}{\tau_k} \eta_{i,k}(t) dt - \frac{c_k}{\tau_k} p_i dt. \quad (8.64)$$

We have thus resolved the convolution integral.

To calculate the random forces associated to the k th term of the expansion, we note that these can be viewed as the solution of a linear SDE, specifically

$$dR_{i,k} = -\frac{1}{\tau_k} R_{i,k}(t) dt + \frac{1}{\tau_k} \sqrt{2k_B T c_k} dW_{i,k}(t) \quad (8.65)$$

where $W_{i,k}$ is a standard Wiener process. The random force is seen to be defined as the solution of an Ornstein-Uhlenbeck process induced by the Prony representation. It is easily shown that $R_{i,k}(t)$ has zero mean and autocorrelation defined by

$$\langle R_{i,k}(t+s) R_{i,k}(t) \rangle = k_B T \frac{c_k}{\tau_k} \exp\left[-\frac{1}{\tau_k} s\right], \quad s \geq 0 \quad (8.66)$$

The total random force is then obtained by summation

$$R_i = \sum_{k=1}^{k_{\max}} R_{i,k}. \quad (8.67)$$

Observe that both random and drag forces are incorporated via summation of the components $\eta_{i,k}$ and $R_{i,k}$ defined by linear equations, respectively the ODE (8.64) and SDE (8.65). It is therefore possible to replace these components by their sum

$$\sigma_{i,k} = \eta_{i,k} + R_{i,k}$$

which may be evolved by a single SDE. The equations therefore become

$$dq_i = m_i^{-1} p_i dt, \quad (8.68)$$

$$dp_i = F_i dt + \sum_{k=1}^{k_{\max}} \sigma_{i,k} dt, \quad (8.69)$$

$$d\sigma_{i,k} = -\frac{1}{\tau_k} \sigma_{i,k} dt - \frac{c_k}{\tau_k} p_i dt + \frac{1}{\tau_k} \sqrt{2k_B T c_k} dW_{i,k}. \quad (8.70)$$

The relation between the Prony series representation and Langevin dynamics can be seen in an informal sense by multiplying the equation for $\sigma_{i,k}$ equation by τ_k , and considering $\tau_k \rightarrow 0$, giving

$$\sigma_{i,k} dt = -c_k p_i dt + \sqrt{2k_B T c_k} dW_{i,k},$$

which results in

$$dp_i = F_i dt - \left(\sum_{k=1}^{k_{\max}} c_k \right) p_i dt + \sqrt{2k_B T} \sum_{k=1}^{\ell} \sqrt{c_k} dW_{i,k}.$$

Observing that the sum of ℓ independent Gaussian random variables of variance c_k is a Gaussian random variable with variance $\sum_{k=1}^{\ell} c_k$, we see that this is in the form of Langevin dynamics

$$dp_i = F_i dt - \hat{\gamma} p_i dt + \sqrt{2k_B T \hat{\gamma}} dW_{i,k},$$

with

$$\hat{\gamma} = \sum_{k=1}^{N_k} c_k.$$

(For the formal treatment of this limit refer to [293].)

For numerical integration, the system (8.68)–(8.70) can be handled via splitting. A natural family of methods based on Verlet is the following [19]:

Generalized Langevin Dynamics Method

$$\begin{aligned} \mathbf{p}_{n+1/2} &:= \mathbf{p}_n + \frac{h}{2} \mathbf{F}(\mathbf{q}_n) + \frac{h}{2} \sum_{k=1}^{k_{\max}} \boldsymbol{\sigma}_{n,k}, \\ \mathbf{q}_{n+1} &:= \mathbf{q}_n + h \mathbf{M}^{-1} \mathbf{p}_{n+1/2}, \\ \boldsymbol{\sigma}_{n+1,k} &:= \theta_k \boldsymbol{\sigma}_{n,k} - (1 - \theta_k) c_k \mathbf{p}_{n+1/2} + \alpha_k \sqrt{2k_B T c_k} \mathbf{Z}_k^n, \\ \mathbf{p}_{n+1} &:= \mathbf{p}_{n+1/2} + \frac{h}{2} \mathbf{F}(\mathbf{q}_{n+1}) + \frac{h}{2} \sum_{k=1}^{k_{\max}} \boldsymbol{\sigma}_{n+1,k}, \end{aligned}$$

where $\boldsymbol{\sigma}_{n,k}$ is a N_c -dimensional vector, and the components of the N_c -dimensional vectors $\mathbf{Z}_{n,k}$ are independent standard normal random variables.

The real-valued coefficients θ_k and α_k which must satisfy, for consistency, the equations

$$\theta_k = 1 - \frac{h}{\tau_k} + \mathcal{O}(h^2), \quad \alpha_k = \frac{\sqrt{h}}{\tau_k} + \mathcal{O}(h).$$

An argument is given in [19] that α_k and θ_k should be taken as

$$\theta_k = \exp(-h/\tau_k), \quad \alpha_k = \sqrt{\frac{(1 - \theta_k)^2}{h}},$$

since, for this choice, the Langevin limit is preserved. Alternative methods are possible. For many comparisons and numerical experiments, refer to [19].

8.8 Constant Temperature and Pressure Molecular Dynamics

The isobaric, isothermal or NPT ensemble models a system in contact with a heat bath (temperature T) and a “pressure reservoir” maintained at pressure P . The pressure is defined by the formula

$$P = - \left[\frac{\partial E}{\partial V} \right]_{S,N}$$

where E is the energy, V is volume, S is entropy. The notation $[\dots]_{x,y}$ means that the indicated partial derivatives should be taken with respect to constant values of the indicated variables.

An isothermal-isobaric system exchanges energy with the bath in such a way as to maintain the constant temperature; at the same time the volume fluctuates to control the pressure. The state of the system can be expressed in terms of particle positions and momenta as well as the volume V , i.e. we think of the probability density as a function of q, p and V .

Let N, V, E be the number of atoms, volume and energy, respectively, of the system of interest, and N_2, V_2, E_2 be the corresponding quantities describing the bath system; we have $N + N_2 = \tilde{N}, V + V_2 = \tilde{V}, E + E_2 = \tilde{E}$ all constant. We view the entropy as a function of the other variables and expand in a Taylor series in both volume and energy:

$$S(N_2, V_2, E_2) = S(\tilde{N} - N, \tilde{V} - V, \tilde{E} - E) \approx S(N_2, \tilde{V}, \tilde{E}) - \frac{\partial S}{\partial E} E - \frac{\partial S}{\partial V} V.$$

Bear in mind that here E and V are small relative perturbations of the total energy and volume. The quantity $\frac{\partial S}{\partial E}$ is the reciprocal temperature.

To calculate $\frac{\partial S}{\partial V}$ we may use *Maxwell's thermodynamic relation* [372]:

$$\left[\frac{\partial S}{\partial E} \right]_{V,N} \left[\frac{\partial E}{\partial V} \right]_{S,N} \left[\frac{\partial V}{\partial S} \right]_{E,N} = -1.$$

Since $\left[\frac{\partial S}{\partial E} \right]_{V,N}$ is T^{-1} and $\left[\frac{\partial E}{\partial V} \right]_{S,N}$ is $-P$, we obtain

$$\left[\frac{\partial S}{\partial V} \right]_{E,N} = \frac{1}{\left[\frac{\partial V}{\partial S} \right]_{E,N}} = P/T.$$

This results in the formula

$$S(N_2, V_2, E_2) \approx \text{constant} - \frac{E + PV}{T},$$

which leads to the probability density

$$\rho_{\text{NPT}} = Z_{\text{NPT}}^{-1} e^{-\beta(H+PV)},$$

where H is the Hamiltonian, and $\beta^{-1} = k_B T$.

The NPT model may be viewed as corresponding to a thermostatted system which incorporates a “piston” controlling the overall volume of the system to be consistent with the target pressure. During simulation, the volume must be free to change; whereas the methods presented so far retain a fixed volume. In NVE or NVT simulation, the volume enters in two ways into the molecular simulation method: (i) as a modification of the potential (allowing for periodic replicas) and (ii) in the mechanism by which atoms are mapped from one boundary to the other of the rectangular domain, simulating motion on a torus. It is not obvious how to generalize these to the NPT setting where V is a dynamical variable.

The method of Andersen [11] (“Andersen’s piston”) is to control the volume by reparamaterizing the coordinates to lie in a cubic box with unit side. Assuming the system occupies a cubic domain, say, $[-L/2, L/2] \times [-L/2, L/2] \times [-L/2, L/2]$, where $L = V^{1/3}$, we may write, for each three-dimensional atomic coordinate vector \mathbf{q}_i

$$\mathbf{q}_i = V^{1/3} \bar{\mathbf{q}}_i, \quad (8.71)$$

where $\bar{\mathbf{q}}_i$ is confined to the unit-side cube. Then we have

$$\dot{\mathbf{q}}_i = \frac{1}{3} V^{-2/3} \dot{V} \bar{\mathbf{q}}_i + V^{1/3} \frac{d}{dt} \bar{\mathbf{q}}_i.$$

The kinetic energy of the atomic system may be written

$$K = \sum_{i=1}^N m_i \frac{\|\dot{\mathbf{q}}_i\|^2}{2}.$$

After coordinate transformation this becomes

$$\begin{aligned} \bar{K} &= \sum_{i=1}^N \frac{m_i}{2} \left\| \frac{1}{3} V^{-2/3} \dot{V} \bar{\mathbf{q}}_i + V^{1/3} \frac{d}{dt} \bar{\mathbf{q}}_i \right\|^2 \\ &= \sum_{i=1}^N \frac{m_i}{2} \left[\frac{1}{9} V^{-4/3} \dot{V}^2 \|\bar{\mathbf{q}}_i\|^2 + \frac{2}{3} V^{-1/3} \dot{V} \bar{\mathbf{q}}_i \cdot \dot{\bar{\mathbf{q}}}_i + V^{2/3} \|\dot{\bar{\mathbf{q}}}_i\|^2 \right], \end{aligned}$$

thus the momentum vector conjugate to $\bar{\mathbf{q}}_i$ becomes

$$\bar{\mathbf{p}}_i = \frac{\partial \bar{K}}{\partial \dot{\bar{\mathbf{q}}}_i}$$

$$= m_i \left[\frac{1}{3} V^{-1/3} \dot{V} \bar{\mathbf{q}}_i + V^{2/3} \dot{\bar{\mathbf{q}}}_i \right],$$

from which, we observe

$$\bar{\mathbf{p}}_i = m_i V^{1/3} \dot{\bar{\mathbf{q}}}_i. \quad (8.72)$$

There is still the question of how to adjust the volume in simulation. The idea of Andersen was to view the volume V as a dynamical quantity on equal footing with the coordinates of the system by viewing PV as the potential energy term and introducing an artificial kinetic energy term of the form $\mu_V \dot{V}^2$. The barostat mass μ_V becomes a free parameter, analogous to the thermal mass used in Nosé dynamics. An extended Hamiltonian may then be written by introducing a momentum variable p_V conjugate to V :

$$\hat{H}(\bar{\mathbf{q}}, \bar{\mathbf{p}}, V, p_V) = \sum_{i=1}^N \frac{\|\bar{\mathbf{p}}_i\|^2}{2m_i V^{2/3}} + \bar{U}(\bar{\mathbf{q}}; V) + \frac{p_V^2}{2\mu_V} + PV, \quad (8.73)$$

where we have written $\bar{U}(\bar{\mathbf{q}}; V) = U(V^{1/3} \bar{\mathbf{q}})$.

In the extended space, we then observe that

$$\rho_{\text{NPT}} = \sqrt{\frac{\beta}{2\pi\mu_V}} \int e^{-\beta\hat{H}(\bar{\mathbf{q}}, \bar{\mathbf{p}}, V, p_V)} dp_V,$$

from the definitions (8.71) and (8.72).

There are several ways to proceed. Andersen suggested to use a Monte-Carlo method to control the temperature during simulation. This approach has the advantage of simplicity, but only allows the determination of configurational averages. If dynamical information is required (e.g. an autocorrelation function or a diffusion coefficient), some sort of dynamics-based scheme is needed. The progress in developing formulations and numerical methods can be charted in [11, 32, 128, 183, 199, 248, 252, 288, 373].

Deterministic methods can be used based on Nosé-Hoover to control the temperature. A problem with methods of this type that one sometimes encounters “ringing” or “breathing” depending on the tuning of various parameters.

Stochastic-dynamical thermostats greatly improve control of the convergence to equilibrium. We have already seen several methods of this type, specifically the Langevin dynamics method and the Nosé-Hoover-Langevin method. These schemes may be applied in conjunction with the Andersen Hamiltonian \hat{H} . The extended system approach outlined here was developed in collaboration with R. Elber and M. Di Pierro; it is close in spirit to the method of Klein [199], but incorporates stochastic terms as in Nosé-Hoover-Langevin in the equations defining the auxiliary variables to ensure ergodicity.

8.8.1 Equations of Motion for the NHL Piston

In the framework of [199], rewriting the equations of motion for the physical variables q and p , the dynamics takes the form

$$\begin{aligned}\dot{\mathbf{q}} &= \mathbf{M}^{-1}\mathbf{p} + \eta\mathbf{q}, \\ \dot{\mathbf{p}} &= -\nabla U(\mathbf{q}) - \eta\mathbf{p} - \xi\mathbf{p}, \\ \dot{V} &= \eta V,\end{aligned}$$

with auxiliary variables η and ξ governed by additional dynamical equations of motion

$$\begin{aligned}\dot{\xi} &= h_T \stackrel{\text{def}}{=} (\mathbf{p}^T \mathbf{M}^{-1} \mathbf{p} - N_d k_B T) / \mu_T, \\ \dot{\eta} &= h_P \stackrel{\text{def}}{=} (V \Pi(\mathbf{q}, \mathbf{p}, V) - PV + k_B T) / \mu_P,\end{aligned}$$

where

$$\Pi(\mathbf{q}, \mathbf{p}, V) \stackrel{\text{def}}{=} \frac{1}{V} \left(\mathbf{p}^T \mathbf{M}^{-1} \mathbf{p} - \mathbf{q} \cdot \nabla U(\mathbf{q}) - V \frac{\partial}{\partial V} U(\mathbf{q}) \right),$$

is the expression for the pressure.

Now let us examine the distribution conserved by the dynamics. First, we observe

$$\rho_1 = \varphi_1(\mathbf{p}^T \mathbf{M}^{-1} \mathbf{p} / 2 + U(\mathbf{q})) \times \psi(V, \xi, \eta)$$

is stationary for the Liouvillian operator for the vector field $(\mathbf{p}, -\nabla U, 0, 0, 0)$.

The function ψ can be chosen as any smooth function that integrates out with respect to V, ξ, η over $[0, \infty] \times \mathbb{R} \times \mathbb{R}$. We already know from our discussion of Nosé-Hoover that $\dot{\mathbf{p}} = -\xi\mathbf{p}$; $\dot{\xi} = (\mathbf{p}^T \mathbf{M}^{-1} \mathbf{p} - N_d k_B T) / \mu_T$ will have as stationary states functions of the form

$$\rho_2 = \exp(-\beta[\mathbf{p}^T \mathbf{M}^{-1} \mathbf{p} + \mu_T \xi^2 / 2]) \psi_2(\mathbf{q}, \eta, V).$$

Finally the remaining terms $\dot{\mathbf{q}} = \eta\mathbf{q}$, $\dot{\mathbf{p}} = -\eta\mathbf{p}$, $\dot{V} = \eta V$, $\dot{\eta} = (V \Pi(\mathbf{q}, \mathbf{p}, V) - PV + k_B T) / \mu_P$ give rise to the Liouvillian

$$\mathcal{L}^\dagger \rho = -\eta \nabla_{\mathbf{q}} \cdot (\mathbf{q} \rho) + \eta \nabla_{\mathbf{p}} \cdot (\mathbf{p} \rho) - \eta \frac{\partial}{\partial V} (V \rho) - \frac{\partial}{\partial \eta} [\rho (V \Pi(\mathbf{q}, \mathbf{p}, V) - PV + k_B T) / \mu_P].$$

If ρ has the form $\rho = \exp(-\beta\mu_P\eta^2/2) \times \psi(\mathbf{q}, \mathbf{p}, V, \xi)$ then eliminate η , reducing $\mathcal{L}^\dagger\rho = 0$ to

$$-\nabla_{\mathbf{q}} \cdot (\mathbf{q}\psi) + \nabla_{\mathbf{p}} \cdot (\mathbf{p}\psi) - \frac{\partial}{\partial V}(V\psi) + \beta(V\Pi(\mathbf{q}, \mathbf{p}, V) - PV + k_B T)\psi = 0.$$

This results in

$$-\mathbf{q} \cdot \nabla_{\mathbf{q}}\psi + \mathbf{p} \cdot \nabla_{\mathbf{p}}\psi - \psi - V\frac{\partial\psi}{\partial V} + (\beta V\Pi(\mathbf{q}, \mathbf{p}, V) - \beta PV + 1)\psi = 0. \quad (8.74)$$

A solution (the desired one) is given by

$$\psi \propto \exp(-\beta(H + PV)),$$

where substituting into (8.74) gives

$$\begin{aligned} & \left[\beta\mathbf{q} \cdot \nabla U(\mathbf{q}) - \beta\mathbf{p} \cdot \mathbf{M}^{-1}\mathbf{p} - 1 + \beta V\frac{\partial U}{\partial V} \right. \\ & \left. + \beta PV + (\beta V\Pi(\mathbf{q}, \mathbf{p}, V) - \beta PV + 1) \right] \psi = 0, \end{aligned}$$

which is quickly checked to be true, and hence the dynamics preserves $\rho = \exp(-\beta\mu_P\eta^2/2) \times \psi$.

It is difficult to see how there could be other solutions ψ , but we know from the Nosé-Hoover case that this must be possible. We improve the robustness of the method by introducing Ornstein-Uhlenbeck type stochastic processes in the two auxiliary variables ξ and η , yielding the system

$$\dot{\mathbf{q}} = \mathbf{M}^{-1}\mathbf{p} + \eta\mathbf{q}, \quad (8.75)$$

$$\dot{\mathbf{p}} = \mathbf{F}(\mathbf{q}) - \eta\mathbf{p} - \xi\mathbf{p}, \quad (8.76)$$

$$\dot{V} = \eta V, \quad (8.77)$$

$$d\xi = [h_T - \gamma_T\xi] dt + \sqrt{2k_B T \gamma_T / \mu_T} dW_T, \quad (8.78)$$

$$d\eta = [h_P - \gamma_P\eta] dt + \sqrt{2k_B T \gamma_P / \mu_P} dW_P, \quad (8.79)$$

where $\gamma_T, \gamma_P \geq 0$ are two parameters governing the strength of the noise.

8.8.2 Discretization of the NHL Piston

Observations in Chap. 7 and our experience with the Nosé-Hoover-Langevin method lead us to propose splitting methods to separate the Ornstein-Uhlenbeck processes

and solve the latter exactly. It is not technically necessary to require symmetry of the way that stochastic and deterministic terms are interleaved if the only purpose is equilibrium sampling, although symmetry is required within any splitting method used for the deterministic part in order to gain even order (in our case an $\mathcal{O}(h^2)$ error) in short time approximation and in the accuracy of computed thermodynamic quantities.

In the case of (8.75)–(8.79) this suggests

$$\begin{aligned}\xi &:= \xi + (\Delta t/2)h_T, & \eta &:= \eta + (\Delta t/2)h_P, \\ \mathbf{p} &:= e^{-(\xi+\eta)\Delta t/2} \mathbf{p} + \psi(-\xi - \eta, \Delta t/2) \mathbf{F}(\mathbf{q}), \\ \mathbf{q} &:= e^{\eta\Delta t} \mathbf{q} + \psi(\eta, \Delta t) \mathbf{M}^{-1} \mathbf{p}, \\ \mathbf{p} &:= e^{-(\xi+\eta)\Delta t/2} \mathbf{p} + \psi(-\xi - \eta, \Delta t/2) \mathbf{F}(\mathbf{q}), \\ V &:= e^{\eta\Delta t} V, \\ h_T &:= h_T(\mathbf{p}), & h_P &:= h_P(\mathbf{q}, \mathbf{p}, V), \\ \xi &:= \xi + (\Delta t/2)h_T, & \eta &:= \eta + (\Delta t/2)h_P, \\ \xi &:= e^{-\gamma_T \Delta t} \xi + \sqrt{\beta^{-1}(1 - e^{-2\gamma_T \Delta t})/\mu_T} R_\xi, \\ \eta &:= e^{-\gamma_P \Delta t} \eta + \sqrt{\beta^{-1}(1 - e^{-2\gamma_P \Delta t})/\mu_P} R_\eta,\end{aligned}$$

where

$$\psi(\alpha, t) \stackrel{\text{def}}{=} \begin{cases} \frac{e^{\alpha t} - 1}{\alpha} & \alpha \neq 0 \\ t & \alpha = 0 \end{cases},$$

and R_ξ , R_η are two scalar i.i.d. $\mathcal{N}(0, 1)$ random numbers. Periodic boundary conditions are enforced whenever \mathbf{q} or V is updated, to ensure that the system remains inside the cube with side length $V^{1/3}$.

We perform an experiment with the given discretization for 64 atoms in a 3D periodic box using a pairwise Lennard-Jones potential. We set $P = 0.5$, $k_B T = 0.1$ and $\mu_P = \mu_T = 5$, with all particle masses set to one and $h = 0.001$. As plotted in Fig. 8.6, we initialize the particles in a cubic formation within a $5 \times 5 \times 5$ periodic box (so $V(0) = 125$). As we run the simulation, V decreases and the pressure is increased.

We set $\gamma_T = \gamma_P = \gamma$ and compare simulations using three values of γ . Choosing $\gamma = 0$ removes any stochastic terms from the simulation, reducing the dynamics to a similar form to the Nosé-Hoover thermostat. The distribution of the pressure Π , plotted in Fig. 8.7 (centered on the target pressure P), is well sampled under all three choices of the friction γ . However, as in the NVT experiment in Fig. 8.2, without any stochastic terms in the equations of motion the system exhibits a pronounced

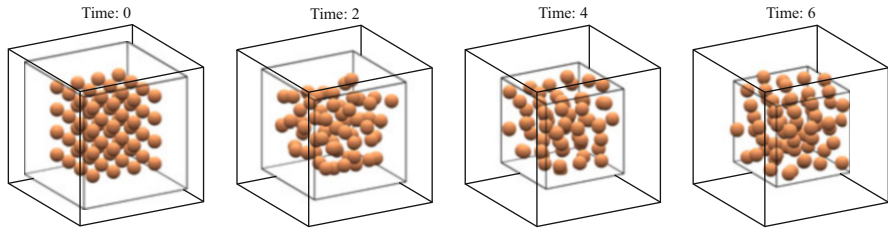


Fig. 8.6 We simulate 64 atoms at constant pressure in 3D using a Lennard-Jones interaction between them. The volume V of the simulation box (marked with *black lines*) shrinks and stabilizes in size as the simulation evolves in time. Periodic boundary conditions with respect to this simulation box are enforced throughout the simulation

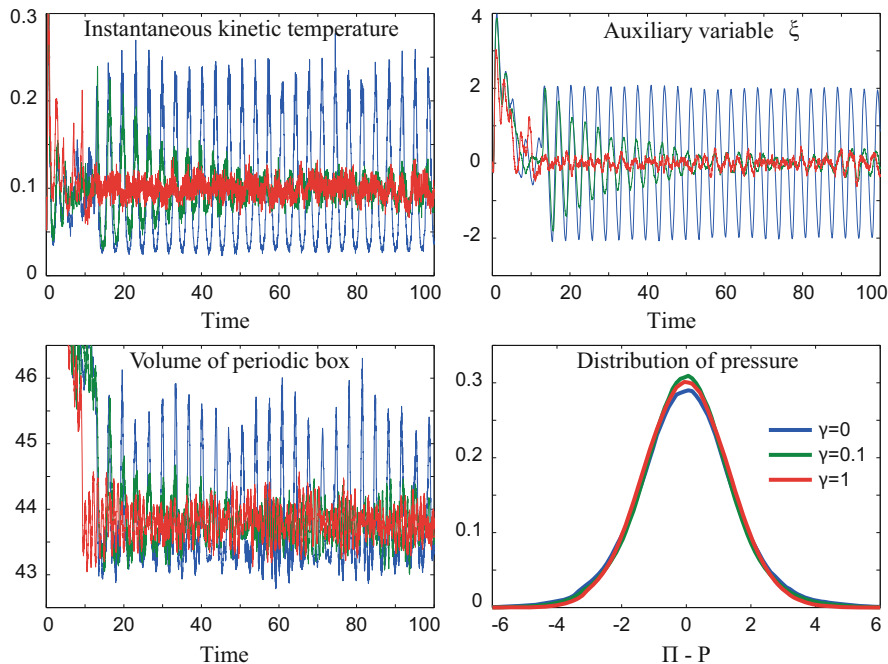


Fig. 8.7 We plot the results of an NPT simulation of 64 atoms of Lennard-Jonesium using the given discretization where $\gamma_T = \gamma_P = \gamma$, with γ set to zero (blue), $\gamma = 0.1$ (green) or $\gamma = 1$ (red). Although the distribution of instantaneous pressure Π (centered on the target pressure P) looks similar for all three cases, we can see that without any stochasticity the simulation exhibits artificial periodic fluctuations in the temperature and volume

oscillation in its kinetic energy (and in the extended variable ξ that regulates the kinetic energy), with the temperature fluctuating between double and half of its target. The volume also periodically fluctuates when $\gamma = 0$, giving rise to the

“breathing” mode. We would expect these fluctuations to be especially long-lived in the case of large values of μ . Decreasing the values of μ will increase the frequency of the oscillations; if the frequency of the periodic motion is too high then the overall stability of the simulation will become threatened (a smaller timestep h may be required).

Choosing $\gamma = 0.1$ or $\gamma = 1$ removes this artificial oscillatory behavior, with the larger choice of γ giving faster dissipation of the periodic oscillation. Figure 8.7 demonstrates that when setting $\gamma = 1$ the temperature and volume rapidly stabilize and give small, random fluctuations compared to the non-stochastic case. For some alternatives and more in-depth discussion of constant temperature and pressure strategies, including numerical experiments, refer to [128, 194, 199, 238, 252].

8.8.3 Anisotropic Simulation Cell: The Method of Parrinello and Rahman

Not all molecules are naturally simulated in a cubic unit cell and indeed the system may undergo dramatic changes of shape during simulation. Parrinello and Rahman [296] explained how to extend the method of Andersen to allow for a system confined to a cell with dimensions that are allowed to vary during simulation. Three vectors \mathbf{a} , \mathbf{b} and \mathbf{c} define the sides of the simulation cell. Let \mathbf{h} be the 3×3 matrix with these vectors as columns, then its volume is $V = \det(\mathbf{h}) = \mathbf{a} \cdot (\mathbf{b} \times \mathbf{c})$, where \mathbf{a} , \mathbf{b} , \mathbf{c} and \mathbf{h} are viewed as time-dependent variables.

Any position vector may be decomposed into coordinates defined by the matrix \mathbf{h} , thus

$$\mathbf{q}_i = \mathbf{h}\bar{\mathbf{q}}_i = \xi_i\mathbf{a} + \eta_i\mathbf{b} + \zeta_i\mathbf{c}, \quad 0 \leq \xi_i, \eta_i, \zeta_i \leq 1.$$

Introducing the metric tensor $\mathbf{G} = \mathbf{h}^T \mathbf{h}$, the Lagrangian describing the system then becomes

$$L = \frac{1}{2} \sum_{i=1}^N m_i \dot{\bar{\mathbf{q}}}_i^T \mathbf{G} \dot{\bar{\mathbf{q}}}_i - \bar{U}(\bar{\mathbf{q}}) + \frac{1}{2} \mu \text{Tr}(\dot{\mathbf{h}}^T \dot{\mathbf{h}}) - PV,$$

where μ is an artificial “mass” parameter which can be adjusted to alter the tightness of the coupling of the barostat to the physical variables.

This system can then be coupled to a thermostat as in the Andersen or Hoover formulation [266].

The method works well as long as there are internal molecular structures that prevent a degeneracy (one cell dimension collapsing) as might happen, for example, if the scheme were applied to a simple liquid such as Lennard-Jonesium.

8.9 Momentum-Conserving Thermostats and the Dissipative Particle Dynamics (DPD) Method

In many applications, it is important to preserve the total momentum while calculating canonical thermodynamic averages, i.e. one works in an ensemble that is restricted by the additional momentum constraint. Momentum conservation plays a key role in capturing long-ranged hydrodynamic interactions in coarse-grained models of complex fluids [8]. Standard Langevin and Nosé dynamics methods fail to preserve the momentum. This is quite obvious in the case of Langevin dynamics. In Nosé dynamics we have the following differential equation for the momenta:

$$\frac{dp}{dt} = -\nabla U(\mathbf{q}) - \xi p.$$

Assuming central forces, we have $\sum_{i=1}^N \nabla_{q_i} U = \mathbf{0}$, thus we obtain the following equation for the total momentum vector \mathbf{p}_{tot} :

$$\sum_{i=1}^N \frac{dp_i}{dt} = \frac{d\mathbf{p}_{\text{tot}}}{dt} = -\xi \mathbf{p}_{\text{tot}}.$$

If the total momentum is chosen to be zero, then it will formally remain zero along trajectories (see [78, 254] for a discussion on the affect this has on canonical sampling). However, in practice, a small numerical artifact may be introduced. Moreover, under numerical discretization, bias due to finite stepsize may be present allowing a build up of total momentum in long simulations.

An interesting potential consequence of the lack of momentum conservation is the so-called “flying ice cube” problem [172], whereby the system acquires a large total momentum but the internal momenta due to interactions among the particles becomes small.

It is desirable to construct formulations and numerical methods which exactly (i.e. up to rounding error) preserve the total momentum from step to step. One obvious approach to this problem is to simply project the momenta onto the linear momentum constraint at the end of each step (or after some number of steps). Such a projection introduces potential issues in terms of convergence order and would certainly complicate the analyses presented thus far in this book. Moreover, the optimal choice of projection is unclear and it is easy to define poor schemes (for example, modifying always the momentum of just the first particle in order to balance all the remaining components) which are likely to introduce artifacts (bias) in simulation. For this reason, there is interest in “building in” momentum conservation into the equations of motion (and indeed the integrator). Ideally this should be done in a localized and homogeneous way so that momentum is not transferred by a nonphysical mechanism between distant particles.

One of the most popular scheme of this type is the technique of dissipative particle dynamics (DPD) which was introduced in 1992 by Hoogerbrugge and Koelman [181]. DPD groups several fluid molecules and treats these as a single particle (which may be thought of as a lump of fluid). The particles of a DPD system interact through a short-ranged “soft” pairwise (distance-based) potential energy function. The use of such a soft potential increases the usable timestep, thus the benefit of using DPD as opposed to MD is felt both in reduction of system dimension and increase in the timestep and thus the accessible time interval in simulation [156]. DPD can be viewed as a Langevin dynamics in which configuration dependence is present in both dissipative and stochastic perturbations. We will consider numerical methods for DPD in this section; for discussion of coarse-graining applications of DPD, see for example [39, 88, 330].

The equations of DPD are a little more complicated than standard MD. It is therefore important to design accurate and efficient methods tailored to their special form. Most numerical methods for DPD simulation exhibit substantial statistical bias. Some methods have been developed to reduce the per timestep efficiency but at a price in terms of the conservation properties. The only way that the errors are tamed in some ad hoc schemes is by reducing the timestep size excessively (well below the stability threshold), but this may destroy the practical value of those methods.

In this section we present numerical methods based on splitting for DPD and for another stochastic momentum-conserving method, the pairwise Nosé-Hoover-Langevin (PNHL) method.

8.9.1 Formulation of DPD

We describe here the formulation of dissipative particle dynamics due to Español and Warren [122].

Let the N particles be described in the usual way by positions \mathbf{q}_i and momenta \mathbf{p}_i . We assume their masses to be m_i for $i = 1, \dots, N$. The DPD equations of motion are of the form

$$\frac{d\mathbf{q}_i}{dt} = \frac{\mathbf{p}_i}{m_i}, \quad \frac{d\mathbf{p}_i}{dt} = \mathbf{F}_i, \quad (8.80)$$

where \mathbf{F}_i is the total interparticle force acting on particle i due to the presence of the other particles. The force is composed of three pairwise contributions

$$\mathbf{F}_i = \sum_{j \neq i} (\mathbf{F}_{ij}^C + \mathbf{F}_{ij}^D + \mathbf{F}_{ij}^R), \quad (8.81)$$

where \mathbf{F}_{ij}^C , \mathbf{F}_{ij}^D and \mathbf{F}_{ij}^R represent conservative, dissipative and random forces, acting on particle i due to the j -th particle, respectively.

Many choices are possible for the conservative force field [219, 244, 342]. In case the DPD equations are used simply to control the momentum (and not as a coarse-graining device), any empirical molecular force field may be used. When DPD is used for coarse-graining, it is common to adopt a simplified pair potential, namely

$$\mathbf{F}_{ij}^C = \begin{cases} \alpha \left(1 - \frac{r_{ij}}{r_c} \right) \hat{\mathbf{q}}_{ij}, & r_{ij} < r_c; \\ 0, & r_{ij} \geq r_c, \end{cases} \quad (8.82)$$

where r_{ij} is the interparticle distance, $\hat{\mathbf{q}}_{ij} = r_{ij}^{-1}(\mathbf{q}_i - \mathbf{q}_j)$, parameters α define the strength of the repulsion of particles i and j , and r_c is the cutoff radius. The use of a cutoff is important for efficiency reasons—in a large system, only the particles interacting at close range will generate nonzero forces of interaction so the force calculation may be substantially reduced. Both α and r_c could be allowed to be different for different particle pairs, although they are most often taken to be homogeneous. The pair potential corresponding to the force is

$$\varphi_{\text{DPD}}(r) = \begin{cases} \frac{\alpha r_c}{2} \left(1 - \frac{r}{r_c} \right)^2, & r < r_c; \\ 0, & r \geq r_c. \end{cases} \quad (8.83)$$

so that the conservative potential energy is:

$$U_{\text{DPD}} = \sum_{i < j} \varphi_{\text{DPD}}(r_{ij}), \quad r_{ij} = \|\mathbf{q}_i - \mathbf{q}_j\|. \quad (8.84)$$

The choice of dissipative and random forces is made so as to maintain a prescribed temperature. The typical formulas used for this purpose are

$$\mathbf{F}_{ij}^D = -\gamma \omega^D(r_{ij}) (\hat{\mathbf{q}}_{ij} \cdot \mathbf{v}_{ij}) \hat{\mathbf{q}}_{ij}, \quad (8.85)$$

$$\mathbf{F}_{ij}^R = \sigma \omega^R(r_{ij}) \theta_{ij} \hat{\mathbf{q}}_{ij}, \quad (8.86)$$

where γ and σ parameterize the forces (again, they could be taken to be different for different pairs), and ω^D and ω^R are configuration-dependent weight functions that typically incorporate a cut-off similar to that used in the conservative force, e.g. one may take

$$\omega^R(r) = \begin{cases} 1 - \frac{r}{r_c}, & r < r_c; \\ 0, & r \geq r_c, \end{cases} \quad (8.87)$$

where r_c is the same cutoff used in the conservative force. The relative velocities are denoted by $\mathbf{v}_{ij} = \mathbf{p}_i/m_i - \mathbf{p}_j/m_j$, and θ_{ij} is a symmetric ($\theta_{ij} = \theta_{ji}$) Gaussian

white-noise term with the following stochastic property

$$\langle \theta_{ij}(t) \rangle = 0, \quad \langle \theta_{ij}(t)\theta_{kl}(t') \rangle = (\delta_{ik}\delta_{jl} + \delta_{il}\delta_{jk})\delta(t - t'), \quad (8.88)$$

and are independent for each pair of interacting particles at each time step. Invariance of the canonical distribution under these equations of motion follows if

$$\omega^D(r_{ij}) = [\omega^R(r_{ij})]^2, \quad \sigma^2 = 2\gamma k_B T, \quad (8.89)$$

where k_B is the Boltzmann constant and T the equilibrium temperature. Note that the “canonical distribution” in the case of the DPD system or other momentum-conserving thermostat should have a density which is reduced to the leaves of constant total momentum, i.e.

$$\hat{\rho}_\beta \stackrel{\text{def}}{=} Z^{-1} e^{-\beta H(q,p)} \times \delta \left[\sum_{i=1}^N p_{i,x} - \pi_x \right] \delta \left[\sum_{i=1}^N p_{i,y} - \pi_y \right] \delta \left[\sum_{i=1}^N p_{i,z} - \pi_z \right]$$

where $\boldsymbol{\pi} = (\pi_x, \pi_y, \pi_z)$ is the total momentum vector.

The conservation of the total momentum is a direct result of the symmetric form of the various forces, thus DPD may be viewed as an isotropic Galilean-invariant thermostat which preserves hydrodynamics [8]. The ergodicity of DPD (i.e. that $\hat{\rho}_\beta$ is the unique measure sampled by the dynamics) has only been demonstrated in the case of a high density of particles in one dimension [334].

The DPD system may be viewed as a special case of the generalized Langevin dynamics with equations

$$\begin{aligned} dq &= M^{-1} pdt, \\ dp &= -\nabla U(q)dt - \Delta(q)pdt + \Sigma(q)dW, \end{aligned} \quad (8.90)$$

where the potential U is given in (8.84), and the damping matrix Δ and stochastic multiplier matrix Σ are related by

$$\Delta = \frac{M^{-1}}{2k_B T} \Sigma \Sigma^T.$$

In the next subsection we describe the numerical treatment of the DPD system. We then take up the alternative scheme, the pairwise Nosé-Hoover-Langevin (PNHL) method, of [228] which also conserves momentum exactly. Other alternatives to the DPD system include the Peters thermostat [299], the Lowe-Andersen method [241], and the Nosé-Hoover-Lowe-Andersen thermostat [347]. We do not discuss these schemes here, but note that they are compared to DPD and some of the other schemes introduced below in [228].

8.9.2 Numerical Treatment of the DPD System

In comparing the DPD system to standard molecular dynamics, a key feature is the “soft” nature of the repulsive potential U_{DPD} defined by (8.84). The lack of any sort of stiff harmonic component or steep repulsive potentials such as those present in typical molecular models means that the stepsize is not dominated by the stability restriction, but rather by accuracy requirements. That is, DPD simulations may be stable for stepsizes which lead to very large errors in thermodynamic averages.

Many efforts have been made to develop accurate integration schemes for the DPD system. With few exceptions, the methods used are variants of the velocity-Verlet integrator, owing to its long history in MD. Some early integration schemes are to be found in the papers of Groot and Warren [157], Gibson et al. [148], and Besold et al. [34, 385]. The latter work describes the so-called DPD-Velocity Verlet (DPD-VV) method. Unfortunately [34, 385], all of these methods exhibit significant simulation errors for large stepsize. Much of the error can be seen as the result of requiring an explicit treatment of the dissipative terms, for reasons of computational efficiency. More accurate schemes are possible by using implicit (or semi-implicit) methods such the self-consistent leap-frog integrator (see [34, 295]). However, these methods are typically much slower than the simpler, explicit methods [73, 281], the consequence being that the simpler DPD-VV is most often used (with a relatively small timestep). Further alternatives to the DPD-VV method include a scheme of den Otter and Clarke [101], splitting methods (Shardlow [333], De Fabritiis et al. [96] and Thalmann and Farago [363]), and multiple time step schemes of Jakobsen et al. [191].

8.9.2.1 DPD Velocity-Verlet

With integration stepsize h , the DPD-VV method may be written as

$$\mathbf{p}_{n+1/2} = \mathbf{p}_n + \frac{h}{2} \mathbf{F}^C(\mathbf{q}_n) + \frac{h}{2} \mathbf{F}^D(\mathbf{q}_n, \mathbf{p}_n) + \frac{\sqrt{h}}{2} \mathbf{F}^R(\mathbf{q}_n), \quad (8.91)$$

$$\mathbf{q}_{n+1} = \mathbf{q}_n + h \mathbf{M}^{-1} \mathbf{p}_{n+1/2}, \quad (8.92)$$

$$\mathbf{p}_{n+1} = \mathbf{p}_{n+1/2} + \frac{h}{2} \mathbf{F}^C(\mathbf{q}_{n+1}) + \frac{h}{2} \mathbf{F}^D(\mathbf{q}_{n+1}, \mathbf{p}_{n+1/2}) + \frac{\sqrt{h}}{2} \mathbf{F}^R(\mathbf{q}_{n+1}). \quad (8.93)$$

In this scheme, the conservative forces are recalculated once per timestep (the conservative force computed may be re-used at the following timestep). The dissipative force must be computed twice, and the new random force used in (8.93) should also be used in the subsequent step. This scheme is not symmetric for

deterministic systems and would be expected to be only first order accurate. It could be made symmetric by a simple change, for example replacing \mathbf{p}_n in the force computation at the first step by $\mathbf{p}_{n+1/2}$, but these changes would make the method implicit.

8.9.2.2 Shardlow's Splitting Method

Shardlow [333] proposed splitting methods for DPD based on dividing the force field of the DPD system into its separate (conservative+dissipative+random) parts. Several integrators are then derived based on approximating the various terms. In the most popular and efficient variant, the scheme of Brünger, Brooks and Karplus (BBK) [55] is used to solve the dissipative+stochastic terms, with standard velocity Verlet applied to the conservative part.

We first separate the system of stochastic differential equations for DPD (8.90) into three pieces, which we label as A, B and O:

$$d \begin{bmatrix} \mathbf{q}_i \\ \mathbf{p}_i \end{bmatrix} = \underbrace{\begin{bmatrix} m_i^{-1} \mathbf{p}_i \\ \mathbf{0} \end{bmatrix}}_{\text{A}} dt + \underbrace{\begin{bmatrix} \mathbf{0} \\ \mathbf{F}_i^C \end{bmatrix}}_{\text{B}} dt + \underbrace{\begin{bmatrix} \mathbf{0} \\ \mathbf{F}_i^D dt + \sigma \mathbf{R}_i \end{bmatrix}}_{\text{O}}, \quad (8.94)$$

where $\mathbf{R}_i = \sum_{j \neq i} \omega^R(r_{ij}) \hat{\mathbf{q}}_{ij} dW_{ij}$, for standard i.i.d. Wiener processes $W_{ij}(t)$, such that $dW_{ij} = dW_{ji}$. The generators for each part of the SDE may be written out as follows:

$$\mathcal{L}_A = \sum_i \frac{\mathbf{p}_i}{m_i} \cdot \nabla_{\mathbf{q}_i}, \quad (8.95)$$

$$\mathcal{L}_B = \sum_i \mathbf{F}_i^C \cdot \nabla_{\mathbf{p}_i} = - \sum_i \nabla_{\mathbf{q}_i} U(\mathbf{q}) \cdot \nabla_{\mathbf{p}_i}, \quad (8.96)$$

$$\mathcal{L}_O = \sum_i \sum_{j \neq i} \left(-\gamma \omega^D(r_{ij}) (\hat{\mathbf{q}}_{ij} \cdot \mathbf{v}_{ij}) + \frac{\sigma^2}{2} [\omega^R(r_{ij})]^2 \hat{\mathbf{q}}_{ij} \cdot \left[\nabla_{\mathbf{p}_i} - \nabla_{\mathbf{p}_j} \right] \right) \hat{\mathbf{q}}_{ij} \cdot \nabla_{\mathbf{p}_i}. \quad (8.97)$$

Thus, the generator for the DPD system can be written as

$$\mathcal{L}_{DPD} = \mathcal{L}_A + \mathcal{L}_B + \mathcal{L}_O, \quad (8.98)$$

and the flow map may be written in the standard shorthand as

$$\mathcal{F}_t = e^{t\mathcal{L}_{DPD}}.$$

Approximations of \mathcal{F}_t can be constructed as for Langevin dynamics.

As an example, the phase space propagation of Shardlow's method [333], may be written as

$$\exp(h\hat{\mathcal{L}}_{DPD-S}) = \exp(h\mathcal{L}_O) \exp\left(\frac{h}{2}\mathcal{L}_B\right) \exp(h\mathcal{L}_A) \exp\left(\frac{h}{2}\mathcal{L}_B\right), \quad (8.99)$$

where h is the stepsize and, as usual, $\exp(h\mathcal{L}_f)$ represents the phase space propagator associated to the corresponding vector field f . In practice, Shardlow's method is typically implemented by further reducing the vector field O into interacting pairs:

$$\exp(h\hat{\mathcal{L}}_O) = \exp(h\mathcal{L}_{O_{N-1,N}}) \cdots \exp(h\mathcal{L}_{O_{1,3}}) \exp(h\mathcal{L}_{O_{1,2}}),$$

with the operators associated to each interacting pair defined as

$$\mathcal{L}_{O_{ij}} = \left(-\gamma\omega^D(r_{ij})(\hat{\mathbf{q}}_{ij} \cdot \mathbf{v}_{ij}) + \frac{\sigma^2}{2}[\omega^R(r_{ij})]^2 \hat{\mathbf{q}}_{ij} \cdot \left[\nabla_{\mathbf{p}_i} - \nabla_{\mathbf{p}_j} \right] \right) \hat{\mathbf{q}}_{ij} \cdot \nabla_{\mathbf{p}_i}. \quad (8.100)$$

Each interacting pair thus preserves the invariant distribution $\hat{\rho}_\beta$.

8.9.2.3 DPD Trotter Scheme

In the stochastic DPD-Trotter scheme, the standard DPD system (8.90) is split into two parts, which are labelled "A" and "S" as indicated below

$$d\begin{bmatrix} \mathbf{q}_i \\ \mathbf{p}_i \end{bmatrix} = \underbrace{\begin{bmatrix} m_i^{-1} \mathbf{p}_i \\ \mathbf{0} \end{bmatrix}}_A dt + \underbrace{\begin{bmatrix} \mathbf{0} \\ \mathbf{F}_i^C dt + \mathbf{F}_i^D dt + \sigma \mathbf{R}_i \end{bmatrix}}_S. \quad (8.101)$$

The corresponding operator of part A is exactly the same as in Shardlow's method, while the operator of part S is actually the sum of the operators of B and O defined above

$$\mathcal{L}_S = \mathcal{L}_B + \mathcal{L}_O. \quad (8.102)$$

As in Shardlow's method, the vector field S is typically split into exactly solvable interacting pairs. Subtracting $d\mathbf{v}_j$ from $d\mathbf{v}_i$ and multiplying $\hat{\mathbf{q}}_{ij}$ on both sides gives

$$m_{ij} dv_{ij} = F_{ij}^C(r_{ij})dt - \gamma\omega^D(r_{ij})v_{ij}dt + \sigma\omega^R(r_{ij})dW_{ij}, \quad (8.103)$$

where $m_{ij} = m_i m_j / (m_i + m_j)$ is the “reduced mass”, $v_{ij} = \hat{\mathbf{q}}_{ij} \cdot \mathbf{v}_{ij}$ and $F_{ij}^C(r_{ij})$ is the magnitude of the conservative force (8.82). This equation is an Ornstein-Uhlenbeck process with the exact (in the sense of distributions) solution [200]

$$v_{ij}(t) = \frac{F_{ij}^C}{\tau m_{ij}} + e^{-\tau t} \left(v_{ij}(0) - \frac{F_{ij}^C}{\tau m_{ij}} \right) + \sqrt{\frac{k_B T (1 - e^{-2\tau t})}{m_{ij}}} R_{ij}(t), \quad (8.104)$$

for $i < j$ with $\tau = \gamma \omega^D / m_{ij}$, where $v_{ij}(0)$ are the initial relative velocities and $R_{ij}(t)$ are normally distributed variables with zero mean and unit variance. Thus the incremental velocities are given by

$$v_{ij} = v_{ij}(t) - v_{ij}(0) = \left(v_{ij}(0) - \frac{F_{ij}^C}{\tau m_{ij}} \right) (e^{-\tau t} - 1) + \sqrt{\frac{k_B T (1 - e^{-2\tau t})}{m_{ij}}} R_{ij}(t). \quad (8.105)$$

The momenta are then obtained from

$$\mathbf{p}_i^{n+1} = \mathbf{p}_i^n + m_{ij} v_{ij} \hat{\mathbf{q}}_{ij}^n, \quad (8.106)$$

$$\mathbf{p}_j^{n+1} = \mathbf{p}_j^n - m_{ij} v_{ij} \hat{\mathbf{q}}_{ij}^n, \quad (8.107)$$

thus defining the propagator $e^{h\hat{\mathcal{L}}_{S_{i,j}}}$ for each particle pair. The DPD-Trotter propagator is then

$$\exp\left(h\hat{\mathcal{L}}_{\text{DPD-Trotter}}\right) = \exp\left(\frac{h}{2}\mathcal{L}_S\right) \exp(h\mathcal{L}_A) \exp\left(\frac{h}{2}\mathcal{L}_S\right),$$

where the momentum part is defined by

$$\exp\left(\frac{h}{2}\hat{\mathcal{L}}_S\right) = \exp\left(\frac{h}{2}\mathcal{L}_{S_{N-1,N}}\right) \cdots \exp\left(\frac{h}{2}\mathcal{L}_{S_{1,3}}\right) \exp\left(\frac{h}{2}\mathcal{L}_{S_{1,2}}\right).$$

8.9.3 Extended Variable Momentum-Conserving Thermostats: Pairwise Nosé-Hoover/Nosé-Hoover-Langevin Methods

Because of the form of the force laws, the number of interaction terms (and computational cost) involved in the three force terms in DPD are roughly balanced. In this setting the computational time needed to generate the independent random number streams can be significant (depending on the particle density and cutoff radius), particularly in very large systems solved in parallel where communication between cells can require a significant amount of time [1, 301]. For this reason, Allen and Schmid [8] proposed a Nosé-Hoover type thermostating scheme in

which the stochastic terms are eliminated and replaced by a kinetic energy control law based only on relative velocities of interacting pairs. We refer to this as the pairwise Nosé-Hoover (PNH) thermostat; it is designed to conserve the momentum and is also Galilean-invariant. This method is particularly useful in nonequilibrium molecular dynamics (NEMD) applications where the total momentum needs to be preserved under thermostating [342].

The equations of motion of the PNH thermostat (for particle i) is given by

$$\begin{aligned} d\mathbf{q}_i &= m_i^{-1} \mathbf{p}_i dt, \\ d\mathbf{p}_i &= \mathbf{F}_i^C(\mathbf{q}) dt + \xi \tilde{\mathbf{F}}_i^D dt, \\ d\xi &= G(\mathbf{q}, \mathbf{p}) dt, \end{aligned} \quad (8.108)$$

where ξ is a dynamical variable, the dissipative/driving coupling term is defined as

$$\tilde{\mathbf{F}}_i^D = \sum_{j=1}^N \tilde{\mathbf{F}}_{ij}^D, \quad \tilde{\mathbf{F}}_{ij}^D = -\omega^D(r_{ij})(\hat{\mathbf{q}}_{ij} \cdot \mathbf{v}_{ij})\hat{\mathbf{q}}_{ij},$$

(i.e. $\gamma = 1$ in the dissipative term for DPD), and $G(\mathbf{q}, \mathbf{p})$ is the instantaneous accumulated deviation of the kinetic temperature away from the target temperature [8]

$$G(\mathbf{q}, \mathbf{p}) = \mu^{-1} \sum_i \sum_{j>i} \omega^D(r_{ij}) \left[(\mathbf{v}_{ij} \cdot \hat{\mathbf{q}}_{ij})^2 - k_B T / m_{ij} \right], \quad (8.109)$$

where μ is a coupling parameter which is referred to as the “thermal mass”. The invariant distribution is defined in the $(\mathbf{q}, \mathbf{p}, \xi)$ extended space, with density

$$\hat{\rho}_\beta(\mathbf{q}, \mathbf{p}, \xi) = \hat{Z}^{-1} \exp(-\beta H(\mathbf{q}, \mathbf{p})) \exp(-\beta \mu \xi^2 / 2), \quad (8.110)$$

where \hat{Z} is a suitable normalizing coefficient so that the density integrates to one over the entire accessible space (subject, as usual, to the conservation of momentum constraint).

A nonsymmetric integration algorithm was applied in the original paper [8] to solve the system.

8.9.4 Pairwise Nosé-Hoover-Langevin Thermostat

To improve ergodicity, it is intuitive to employ the same stochastic device used in the Nosé-Hoover-Langevin method, namely linear (OU-type) stochastic terms introduced in the equation for the auxiliary variable ξ . If the OU process is properly tuned the extended canonical distribution with density $\hat{\rho}_\beta$ will still be preserved.

The pairwise-NHL (PNHL) system takes the form

$$\begin{aligned} d\mathbf{q}_i &= m_i^{-1} \mathbf{p}_i dt, \\ d\mathbf{p}_i &= \mathbf{F}_i^C(\mathbf{q}) dt + \xi \tilde{\mathbf{F}}_i^D dt, \\ d\xi &= G(\mathbf{q}, \mathbf{p}) dt - \tilde{\gamma} \xi dt + \tilde{\sigma} dW, \end{aligned} \quad (8.111)$$

where all notation is as for PNH and the coefficients $\tilde{\gamma}$ and $\tilde{\sigma}$ are chosen to preserve the target temperature

$$\tilde{\sigma}^2 = 2\tilde{\gamma}k_B T/\mu, \quad (8.112)$$

and $W = W(t)$ is a standard Wiener process.

Splitting methods for the pairwise-NHL (PNHL) system (including those given here) are taken up in [228]. The PNHL system can be divided into five parts such that each piece can be solved exactly, in the sense of distributions:

$$\begin{aligned} d \begin{bmatrix} \mathbf{q}_i \\ \mathbf{p}_i \\ \xi \end{bmatrix} &= \underbrace{\begin{bmatrix} m_i^{-1} \mathbf{p}_i \\ \mathbf{0} \\ 0 \end{bmatrix}}_{\text{A}} dt + \underbrace{\begin{bmatrix} \mathbf{0} \\ \mathbf{F}_i^C \\ 0 \end{bmatrix}}_{\text{B}} dt + \underbrace{\begin{bmatrix} \mathbf{0} \\ +\xi \tilde{\mathbf{F}}_i^D \\ 0 \end{bmatrix}}_{\text{C}} dt \\ &\quad + \underbrace{\begin{bmatrix} \mathbf{0} \\ \mathbf{0} \\ G \end{bmatrix}}_{\text{D}} dt + \underbrace{\begin{bmatrix} \mathbf{0} \\ \mathbf{0} \\ -\tilde{\gamma} \xi dt + \tilde{\sigma} dW \end{bmatrix}}_{\text{O}}. \end{aligned} \quad (8.113)$$

Note that the operators corresponding to parts A and B are exactly the same as defined in (8.95) and (8.96), respectively. The operators corresponding to the other terms in the vector field are

$$\begin{aligned} \mathcal{L}_C &= \xi \sum_i \tilde{\mathbf{F}}_i^D(\mathbf{q}, \mathbf{p}) \cdot \nabla_{\mathbf{p}_i}, \\ \mathcal{L}_D &= G(\mathbf{q}, \mathbf{p}) \frac{\partial}{\partial \xi}, \\ \mathcal{L}_O &= -\tilde{\gamma} \xi \frac{\partial}{\partial \xi} + \frac{\tilde{\sigma}^2}{2} \frac{\partial^2}{\partial \xi^2}. \end{aligned}$$

Note that the generator \mathcal{L}_O now only affect the auxiliary variable (as in NHL). The generator for the PNHL system is then defined by

$$\mathcal{L}_{\text{PNHL}} = \mathcal{L}_A + \mathcal{L}_B + \mathcal{L}_C + \mathcal{L}_D + \mathcal{L}_O. \quad (8.114)$$

We could split this system in a number of ways. Each of these maps $\exp(t\mathcal{L}_*)$ may be integrated in the weak sense. Two examples of integrators are the PNHL-S and PNHL-N schemes defined in [228] as

$$e^{h\hat{\mathcal{L}}_{\text{PNHL-S}}} = e^{\frac{h}{2}\mathcal{L}_A} e^{\frac{h}{2}\mathcal{L}_B} e^{\frac{h}{2}\mathcal{L}_C} e^{\frac{h}{2}\mathcal{L}_D} e^{h\mathcal{L}_O} e^{\frac{h}{2}\mathcal{L}_D} e^{\frac{h}{2}\mathcal{L}_C} e^{\frac{h}{2}\mathcal{L}_B} e^{\frac{h}{2}\mathcal{L}_A},$$

and

$$e^{h\hat{\mathcal{L}}_{\text{PNHL-N}}} = e^{\frac{h}{2}\mathcal{L}_A} e^{\frac{h}{2}\mathcal{L}_B} e^{\frac{h}{2}\mathcal{L}_C} e^{\frac{h}{2}\mathcal{L}_D} e^{h\mathcal{L}_O} e^{\frac{h}{2}\mathcal{L}_D} e^{\frac{h}{2}\mathcal{L}_C} e^{\frac{h}{2}\mathcal{L}_A} e^{\frac{h}{2}\mathcal{L}_B}.$$

Traditionally, and elsewhere in this book, we have found symmetric compositions to have superior performance. This is normally due to the fact that they deliver even order of accuracy. In the case of PNHL-S, the supposed advantage would be compounded by the fact that, as in the Verlet and [BAOAB] methods, the forces need only be computed once per timestep. However, rather surprisingly, and for reasons that are as yet unclear, it turns out that the most advantageous technique from the point of view of accuracy with respect to the invariant measure has been observed to be the *nonsymmetric* integration strategy PNHL-N. This method also shows, for a variety of observables, 2nd order approximation of averages. It also allows the use of a much larger integration timestep in practice—so large that it is still more efficient for DPD-like simulations when the extra force calculation is taken into account!

8.10 Numerical Experiments

We investigate a simple test system of 18 unit-mass particles in a 2D periodic 3×3 box using the typical soft DPD potential given in (8.83), with a cutoff radius of 1.0 and $\alpha = 25$. In our simulations the temperature was fixed at $T = 1$.

We implement the Nosé-Hoover-Langevin and Langevin dynamics schemes, as well as the momentum-conserving PNHL thermostat, and plot the normalized momentum distributions and time evolution of total momentum for the methods in Fig. 8.8. Additionally we compare against the method of Berendsen [32], which modifies Netwon's equations of motion to incorporate a relaxation process for the total system temperature, representing the exchange of energy from the coupling of the external bath. If the instantaneous temperature at time t is $T(t)$, with target temperature T , then using the Berendsen device we have

$$\dot{T}(t) = \gamma_T(T - T(t)),$$

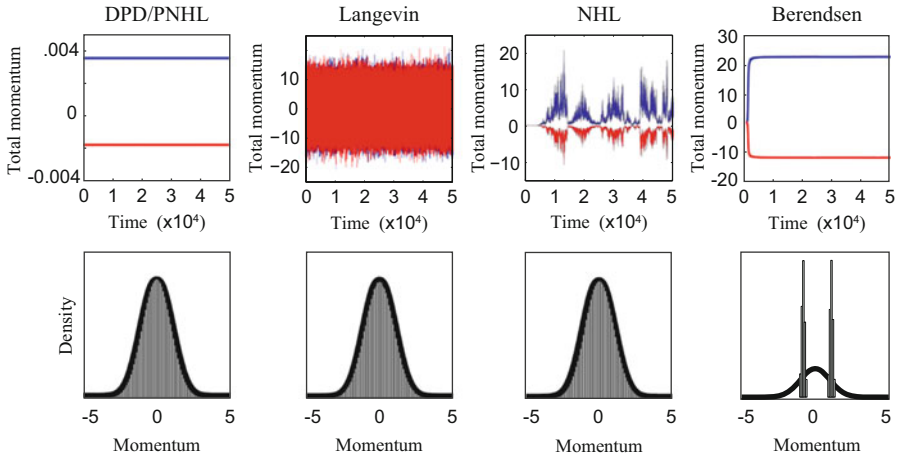


Fig. 8.8 We compare the time evolution of the system’s total momentum in the x and y components (top row, marked blue and red respectively), and momentum distributions (bottom row) for various methods. In the lower row of figures, the dark, solid curve represents the exact normal density, while the superimposed histograms are constructed from the simulation data. From left to right: the PNHL-N thermostat, Langevin dynamics, Nosé-Hoover-Langevin (NHL) dynamics and the Berendsen device. The same initial conditions were used with small values of total momenta. The Berendsen device shows a rapid and systematic increase in the momenta, NHL and Langevin exhibit different behavior, obtaining large fluctuating values, whereas the PNHL-N thermostat preserves the total momenta exactly. Standard DPD results are identical to those of PNHL in this respect

for some decay constant $\gamma_T > 0$. The dynamics will not necessarily sample canonically, but the method will ensure that the average temperature is well-controlled (and is hence sometimes useful for equilibration purposes). We implement the version of the scheme given in [186], which completes a step of the velocity Verlet scheme followed by a scaling of the momenta:

$$\mathbf{p} \leftarrow \sqrt{1 + \gamma_T h \left(\frac{N_d k_B T}{\|\mathbf{p}\|^2} - 1 \right)} \mathbf{p},$$

for the given timestep h .

We use parameters $\gamma = 4.5$, $\mu = 1$ and $\gamma_T = 1$ for the integrators, with a small stepsize of $h = 0.05$ (making any qualitative sampling errors unlikely). We started the simulations with very small net momenta ($\ell_x = 0.0035$, $\ell_y \approx -0.0019$) and observed a dramatic increase in magnitude of both components when using the simple (deterministic) Berendsen scheme. If the system is ergodic in Euclidean

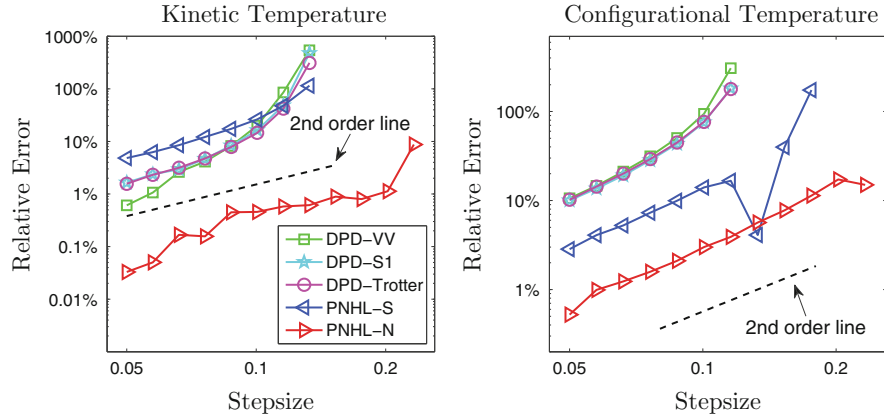


Fig. 8.9 Log-log plot of the relative error in kinetic temperature (*left*) and configurational temperature (*right*) against stepsize by using various numerical methods. The system was simulated for 1,000 reduced time units but only a trajectory's tail of time length 800 was used to calculate the static quantity to make sure the system was well equilibrated. The stepsizes tested began at $h = 0.05$ and were increased incrementally by 15 % until all methods either were above 100 % relative error or became unstable

space, the total momenta are sums of normally distributed random variables with mean zero and so the total momenta too, should have normal distributions with mean zero. Since Langevin dynamics does not respect the momentum constraint, the normal distribution is obtained. By contrast, the momentum vector is preserved exactly using the PNHL method. The NHL scheme performs somewhat oddly. In the Nosé-Hoover-Langevin method, the total momentum fluctuates but remains positive or negative if respective initial conditions are positive or negative (see the exercises at the end of the chapter). This behavior does not however contradict its mentioned ergodic properties (one needs to pay close attention to the assumptions being placed on the system in the proof of the ergodicity).

We also briefly compare DPD and PNHL methods. In Fig. 8.9 we show the kinetic and configurational temperature errors as functions of the stepsize. The results show the advantage of using the PNHL in terms of providing a more accurate sampling for given stepsize; the result is especially important since the PNHL methods are also more efficient in practice. In Fig. 8.10 the velocity autocorrelation functions are contrasted for different values of the friction coefficient. This graph shows that for small values of γ the DPD and PNHL methods perform similarly, whereas at large friction the DPD decay of correlation is substantially more rapid than that for PNHL. For some additional discussion on these points, see [228].

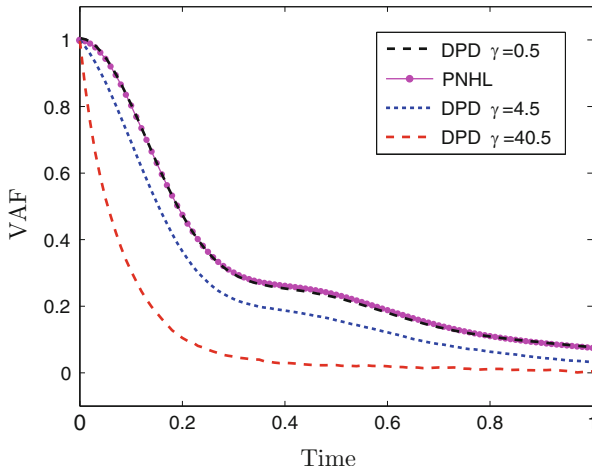


Fig. 8.10 Comparisons of velocity autocorrelation function (VAF) of various numerical methods by using very small stepsize $h = 0.01$. Standard DPD methods with three different values of friction coefficient were calculated by using DPD-S1 method to compare with other methods. 100 different runs were averaged to reduce the sampling errors after the system was well equilibrated

Exercises

1. Show that $\tilde{\rho}$ defined by (8.5) is conserved by the Nosé-Hoover equations of motion.
2. Show that (8.8) is a first integral of the extended Nosé-Hoover system:

$$\begin{aligned}\frac{dq}{dt} &= M^{-1}p, \\ \frac{dp}{dt} &= -\nabla U(q) - \xi p, \\ \mu \frac{d\xi}{dt} &= p^T M^{-1} p - N_d \beta^{-1}, \\ \frac{ds}{dt} &= \xi s.\end{aligned}$$

3. Nosé proposed the following Hamiltonian

$$H_N = \frac{1}{2s^2} \tilde{p}^T M^{-1} \tilde{p} + \frac{\pi^2}{2\mu} + U(q) + (N_d + 1)k_B T \ln s.$$

- a. Write out the equations of motion corresponding to H_N (treating \tilde{p} as the canonical momentum vector corresponding to q , and π as the canonical momentum corresponding to s).

b. Introduce the change of variables

$$\mathbf{p} = s^{-1}\tilde{\mathbf{p}}.$$

Show that the equations resulting from this transformation are

$$\dot{\mathbf{q}} = s^{-1}\mathbf{M}^{-1}\mathbf{p}, \quad \dot{s} = \pi/\mu,$$

$$\dot{\mathbf{p}} = -s^{-1}\nabla U - \frac{\dot{s}}{s}\mathbf{p}, \quad \dot{\pi} = \frac{2K}{s} - \frac{N_d k_B T}{s},$$

where K is the kinetic energy, $K = \mathbf{p}^T \mathbf{M}^{-1} \mathbf{p} / 2$.

c. Apply the time-rescaling $dt = s d\tau$ and then introduce $\xi \equiv \dot{s} = \pi/\mu$ to obtain the Nosé-Hoover equations of motion (8.2)–(8.4)

4. Show that the system (8.6)–(8.7) preserves distributions with densities of the form

$$\rho(\mathbf{q}, \mathbf{p}, \xi) = \varphi(\mathbf{q}) \times \exp(-\beta \mathbf{p}^T \mathbf{M}^{-1} \mathbf{p} / 2) \times \exp(-\beta \mu \xi^2 / 2),$$

where φ is an arbitrary L_2 function.

- 5 **Isokinetic Thermostat.** Let \mathbf{f}_{iso} be the vector field of the isokinetic system (8.37)–(8.38). Calculate the divergence to show that

$$\nabla \cdot \mathbf{f}_{\text{iso}} = (N_c - 1) \frac{\mathbf{p}^T \mathbf{M}^{-1} \mathbf{F}}{\mathbf{p}^T \mathbf{M}^{-1} \mathbf{p}}.$$

- 6 **“Massive” Nosé-Hoover Thermostats.** Attach a Nosé-Hoover thermostat to each degree of freedom. That is, consider a method where, for each $i = 1, 2, \dots, N_c$ we have

$$\begin{aligned} \dot{q}_i &= m_i^{-1} p_i, \\ \dot{p}_i &= -\partial U / \partial q_i - \xi_i p_i, \\ \mu_i \dot{\xi}_i &= p_i^2 / m_i - k_B T. \end{aligned}$$

Under what circumstances is this a proper thermostat (i.e. under what circumstances does the dynamics preserve the canonical ensemble)?

7. Prove Lemma 8.1.

- 8 **Force Perturbation Thermostat.** Let the potential in an N_c -degree of freedom system be decomposed as $U = U_1 + U_2$. Show that the following is a thermostat

$$d\mathbf{q} = \mathbf{M}^{-1} \mathbf{p} dt,$$

$$d\mathbf{p} = -\nabla U_1(\mathbf{q}) dt - \beta \xi^2 \nabla U_2(\mathbf{q}) dt,$$

$$d\xi = -[\beta \mathbf{p}^T \mathbf{M}^{-1} \nabla U(\mathbf{q}) + \gamma] \xi dt + \sqrt{2k_B T \gamma} dW.$$

9 Projective Thermostat. Consider the following method for thermostating $H(\mathbf{q}, \mathbf{p}) = \|\mathbf{p}\|^2/2 + U(\mathbf{q})$ ($\mathbf{q}, \mathbf{p} \in \mathbb{R}^{N_c}$):

$$d\mathbf{q} = \mathbf{p} dt, \quad (8.115)$$

$$d\mathbf{p} = -\nabla U(\mathbf{q})dt - \xi \mathbf{R}(\mathbf{q})\mathbf{p} dt, \quad (8.116)$$

$$d\xi = \mathbf{p}^T \mathbf{R}(\mathbf{q})\mathbf{p} dt - \theta \text{tr}(\mathbf{R}(\mathbf{q}))dt, \quad (8.117)$$

where

$$\mathbf{R}(\mathbf{q}) = \frac{1}{\|\boldsymbol{\alpha}(\mathbf{q})\|^2} \boldsymbol{\alpha}(\mathbf{q}) \boldsymbol{\alpha}(\mathbf{q})^T$$

is a symmetric projector matrix onto the direction $\boldsymbol{\alpha}(\mathbf{q})$. Show that this method preserves the canonical distribution. [Observe that in the Fokker-Planck equation for this method, derivatives with respect to \mathbf{q} are only applied for the first equations, thus the task is identical to showing the result for constant \mathbf{R} .]

- 10.** Show that when the Nosé-Hoover or Nosé-Hoover-Langevin method is used, any individual component of the total momentum vector $\sum_j \mathbf{p}_j$ remains positive for all time, if initialized from a positive value (similarly negative momenta stay negative). When is this property maintained under discretization? Discuss this fact in relation to the proof given for ergodicity of the Nosé-Hoover-Langevin thermostat in Sect. 8.4.1.

Appendix A

Force Computation

The computation of forces may be exceedingly costly depending on the size of the system and the types of potentials involved and strongly affect the overall efficiency of a large scale molecular dynamics simulation. For modest sized systems it is usually just a matter of careful coding to produce a reliable force field routine. For a pair potential φ which is a function of the separation between atoms i and j , the forces are accumulated as follows:

$$\begin{aligned} r &:= \|\mathbf{q}_i - \mathbf{q}_j\| \\ \Delta &:= \frac{\varphi'(r)}{r}(\mathbf{q}_j - \mathbf{q}_i) \\ \mathbf{F}_i &:= \mathbf{F}_i + \Delta \\ \mathbf{F}_j &:= \mathbf{F}_j - \Delta. \end{aligned}$$

Very often, for larger systems with many short-ranged interactions, mechanisms are used to eliminate wasted computation. For example, a Verlet *neighbor list* [140, 307, 387] is sometimes employed. In this case, a list of neighbor atoms is maintained and adjusted from timestep to timestep. The list identifies the labels of atoms which are likely to be sufficiently close (e.g. within 3σ , where σ is the parameter in the Lennard-Jones potential which defines the distance unit for the molecular model) to a given atom so that the force between them is non-negligible. At the end of the timestep (or every l timesteps) the lists must be updated based on the positions and velocities of the atoms to reflect new potential neighbors. Normally the lists include all atoms within the collision radius, as well as those which could enter the collision radius within l timesteps. Theoretically, within a large system, almost any energy could accumulate in a single particle which would suggest that extraordinary ballistic motions could arise, but in practice the individual particle momenta would be expected to be consistent with the Boltzmann distribution which falls off rapidly for large p .

In recent years, Verlet lists have often been supplanted by (or combined with) the Linked Cell List method [7]. For discussion of these techniques, see [86, 173, 303, 307]. See also [49, 50, 203, 335, 341] for work on fast parallel computation of molecular forces.

A.1 Accumulation of Long-Ranged Forces

When periodic boundary conditions are used, it is not possible to neglect far-field interactions via long-ranged potentials due to electrostatics, thus periodic boundary conditions must be extended to include replica systems at distance $\pm L, \pm 2L, \dots$. The total energy is, up to a constant scaling,

$$U(\mathbf{q}) = \sum_{\mathbf{n}} \sum_{i=1}^{N-1} \sum_{j=i+1}^N \frac{Q_i Q_j}{\|\mathbf{q}_i - \mathbf{q}_j + L\mathbf{n}\|}$$

where \mathbf{n} is a multi-index with three integer components corresponding the three spatial directions. The Coulombic summation is only *conditionally convergent* in \mathbb{R}^3 , meaning that its result depends on the way in which the terms are accumulated. We can see why this is the case in three-dimensions by considering a spherical shell around a given particle at distance r . The potential energies are proportional to $1/r$ but the number of terms is proportional to r^2 . Thus, if there are no cancellations, the sum cannot converge and absolute convergence refers precisely to the situation where the signs do not matter. We can only resolve this by considering electrically neutral systems (which ensures adequate cancellation) and also by describing the way in which the sum is computed. Even when this is resolved through some convention, the sum converges slowly.

A variety of methods are available for computing electrostatic energies (and forces), including the Fast Multipole Method [38], the Particle-Particle-Particle-Mesh Method [179], and methods based on the technique of Ewald Summation [125, 367]; we only discuss a particular variant of the latter approach here and not in detail.

A.2 Particle Mesh Ewald (PME)

The starting point these methods is an additive decomposition of the pair potential into two terms

$$\varphi_{\text{Coulomb}}(r) = \varphi_{\text{s.r.}}(r) + \varphi_{\text{l.r.}}(r),$$

where s.r. and l.r. refer to “short-ranged” and “long-ranged” respectively, obtained using a suitable decomposition. The precise way in which this is done is not too critical from a theoretical point of view, but can have dramatic impact on the efficiency of the method. With this in mind, we separate the total energy into sums of short-ranged and long-range contributions, the latter including the terms due to interactions of distant copies of the simulation cell. The total potential energy thus can be written

$$U = U_{\text{s.r.}} + U_{\text{l.r.}}$$

The short-ranged part is calculated in the normal manner by direct summation of force contributions. The long-ranged part includes components that can be calculated by a discrete convolution on an interpolating grid, using a 3D Fast Fourier Transform (FFT). When implemented as described in [123], the method can be shown to have asymptotic complexity ($\mathcal{O}(N \log N)$).

For further reading on force calculation issues the reader is advised to consult [24, 38, 89, 90, 109, 123, 134, 154, 173, 367].

An entirely different approach to the treatment of electrostatic interactions is to eliminate them entirely in favor of implicit solvation techniques [28, 315] which either solve the Poisson-Boltzmann equation [144, 337] or employ the Generalized Born [291] model of excluded volumes.

Appendix B

Concepts from Probability

A general probability space is defined by a triple $(\Omega, \mathcal{F}, \Pr)$ where Ω is the sample space of all possible *outcomes*, \mathcal{F} is a collection of sets of outcomes referred to as *events*, and \Pr is a probability function which assigns real values between 0 and 1 to the events of \mathcal{F} .

Discrete random variables are characterized by a discrete probability density which defines the probability associated with some set of states, that is if we have a random variable X which can take on states $i = 1, 2, \dots$, the non-negative density may be viewed as a sequence $\mathbf{f} = \{f_i\}$ which is assumed to be summable with $\sum_{i=1}^{\infty} f_i = 1$. Then the probability that the random variable lies in a given subset of the natural numbers is just the sum of the corresponding density values:

$$\Pr(X \in S \subset \mathbb{N}) = \sum_{i \in S} f_i.$$

If X has discrete density \mathbf{f} we write $X \sim \mathbf{f}$. The cumulative distribution $\mathbf{F} = \{F_i\}$ associated to a random variable with density \mathbf{f} is just defined by the partial sums $F_n = \sum_{i \leq n} f_i$. Thus $0 \leq F_n \leq 1, \forall n$ and $F_n = \Pr(X \leq n)$.

In the continuous case, we suppose the sample space is the Euclidean space \mathbb{R}^m , and assume there is a (normalized) probability measure $d\mu$ defined by the density ρ which is a non-negative function. In this case the standard event space \mathcal{F} is then typically taken to be the *Borel* σ -algebra of subsets of \mathbb{R}^m which includes open balls and countable unions, countable intersections or relative complements of open balls in \mathbb{R}^m . The measure of the set can be defined by Lebesgue integration

$$\Pr(S) \equiv \Pr(X \in S \subset \mathbb{R}) = \int_S d\mu(x) = \int_S \rho(x) dx,$$

and we have the properties

$$\rho(x) \geq 0, \quad \Pr(\mathbb{R}) = \int_{\mathbb{R}} \rho(x)dx = 1,$$

and, for any two measurable sets \mathcal{A} and \mathcal{B} ,

$$\Pr(\mathcal{A} \cup \mathcal{B}) = \Pr(\mathcal{A}) + \Pr(\mathcal{B}) - \Pr(\mathcal{A} \cap \mathcal{B}).$$

Given two random variables, X and Y , we define their joint probability distribution in terms of a joint density $f(x, y)$ thus

$$\Pr(X \in \mathcal{A}, Y \in \mathcal{B}) = \int_{\mathcal{A}} \int_{\mathcal{B}} f(x, y)dxdy,$$

with a similar concept for larger collections.

The *conditional probability* $\Pr(\mathcal{A}|\mathcal{B})$ is the probability of event \mathcal{A} , given event \mathcal{B} . It is defined by

$$\Pr(\mathcal{A}|\mathcal{B}) := \frac{\Pr(\mathcal{A} \cap \mathcal{B})}{\Pr(\mathcal{B})}, \quad \Pr(\mathcal{B}) \neq 0.$$

Events \mathcal{A} and \mathcal{B} are said to be (*statistically*) *independent* if $\Pr(\mathcal{A}|\mathcal{B}) = \Pr(\mathcal{A})$. In other words, \mathcal{A} and \mathcal{B} are independent if

$$\Pr(\mathcal{A} \cap \mathcal{B}) = \Pr(\mathcal{A})\Pr(\mathcal{B}).$$

The *expectation* or *mean* of a random variable is the average value over the whole distribution. For a discrete random variable with density f_i and state space S , we have, denoting expectation by the symbol \mathbb{E} ,

$$\mathbb{E}X = \sum_{i \in S} X_i f_i.$$

It is common to write \bar{X} for $\mathbb{E}X$.

In the case of a continuous random variable, we have, if the state space is S and ρ is the density,

$$\mathbb{E}X \equiv \int_S x\rho(x)dx.$$

It is common to denote the mean of a random variable by μ .

In a similar way we may compute the expectation of any function of the random variable as a sum or integral over states. For example, the variance is defined for a discrete random variable by

$$\text{Var}(X) = \mathbb{E}(X - \mathbb{E}X)^2 = \sum_{i \in S} (X_i - \bar{X})^2 f_i,$$

with a similar formula for the continuous case. The standard deviation is the square root of the variance. It is common to denote the standard deviation by σ and the variance by σ^2 .

An important example of a random variable is the *normal* or *Gaussian* distribution with density

$$\rho_{\text{normal}}(x) = \frac{1}{\sigma \sqrt{2\pi}} e^{-\frac{(x-\mu)^2}{2\sigma^2}}.$$

where μ is the mean and σ^2 the variance.

The expectation of a certain random variable X given some condition, such as another random variable Y being in set \mathcal{A} , is referred to as a conditional expectation and is denoted $\mathbb{E}(X|Y \in \mathcal{A})$. If X and Y are independent random variables, their joint probability density is a product $f(x, y) = g(x)h(y)$ and the conditional expectation of X is therefore independent of any event pertaining to Y , $\mathbb{E}(X|Y \in \mathcal{A}) \equiv \mathbb{E}(X)$.

One of the fundamental results in probability is the Central Limit Theorem which concerns an infinite collection of mutually independent, identically distributed random variables. The basic observation is that if we have some random variables drawn from some particular distribution we may define a new random variable by averaging. The average will not have the same distribution as those of the collection, but it will have a well defined density. The Central Limit Theorem effectively describes the limiting density obtained by averaging over an infinite collection. Remarkably, independent of the density of a particular member of the collection, this averaged random variable will ultimately be Gaussian with mean and variance specified by the mean and variance associated to the members of the collection.

Theorem B.1 (Central Limit Theorem) *Let X_1, X_2, \dots be a collection of independent, identically distributed random variables with $\mathbb{E}(X_i) = \mu$ and $\text{Var}(X_i) = \sigma^2 > 0$. Define*

$$S_n = \frac{X_1 + X_2 + \dots + X_n}{n},$$

which can be viewed as the average of the random variables. Then the distribution of $(S_n - \mu)\sqrt{n}$ converges to a normal distribution with mean zero and standard deviation σ^2 .

The notion of convergence in distribution in the Central Limit Theorem is that of pointwise convergence of the probability distribution function defined by

$F(x) = \int_{-\infty}^x f(x)dx$. When a sequence of random variables converges in the sense of distributions to another random variable, we indicate this by the symbol $\widehat{\lim}$, thus the Central Limit Theorem states that

$$\widehat{\lim}_{n \rightarrow \infty} \sqrt{n}\sigma^{-1} \left(\frac{1}{n} \sum_{i=1}^n X_n - \mu \right) = X \sim \mathcal{N}(0, 1).$$

The notion of a *stochastic process* is central to Chaps. 6–8. A stochastic process is a family of random variables generated by a rule

$$t \mapsto X(t)$$

where t is taken from some index set and X is a random variable on a given probability space. For a discrete, finite state-space model we replace t with $n \in 0, 1, 2, \dots$, the random variable can only take on one of a finite number of discrete values, say $1, 2, \dots, J$ and we think of the state at time n as being defined in terms of the history of the process by some appropriate probability law. In this book we are primarily interested in *Markov processes* for which the law takes the form

$$\Pr(X(n) = k | X(n-1) = j) = \pi_{jk} \in [0, 1].$$

In the case of a Markov process with state space a subset of \mathbb{R} , and with \mathcal{F} the associated Borel σ -algebra, and with a continuous index variable $t \in \mathbb{R}_+$, the transition probabilities are defined instead for sets $\mathcal{A} \in \mathcal{F}$:

$$P(\mathcal{A}, x_0, t) = \Pr(X(t) \in \mathcal{A} | X(0) = x_0).$$

In many cases we may assume the existence of a density $\pi(x_0, z, t)$ such that the transition probability is given by Lebesgue integration:

$$P(\mathcal{A}, x_0, t) = \int_{\mathcal{A}} \pi(x_0, z, t) dz.$$

In the case of a discrete time Markov chain with a continuous state space, we may simply suppress the variable t in the above formulas, and write

$$P(\mathcal{A}, x_0) = \int_{\mathcal{A}} \pi(x_0, z) dz.$$

In a discrete Markov chain, we have a sequence X_0, X_1, \dots of random variables, with densities $\rho_i(x)$, $i = 0, 1, 2, \dots$. These are related by the equation

$$\rho_n(x) = \int_{\mathcal{D}} \pi(y, x) \rho_{n-1}(y) dy.$$

Appendix C

Monte-Carlo Markov Chains

In this section, we outline a broad family of Monte-Carlo methods which are useful in molecular modelling. The reader is suggested to consult references on this subject such as [269, 312] for a more comprehensive treatment, such as the details of proofs of ergodicity.

The first use of the Monte-Carlo method in a form similar to that used today was by Ulam, von Neumann and Metropolis. The goal is to calculate the expectation of some observable $g(X)$ of a random variable X (assumed to be defined by a complicated process) having a given probability density $f(x)$. By definition

$$\mathbb{E}[g(X)] = \int_{\mathcal{D}} g(x)f(x)dx.$$

Let $X_i, i = 1, 2, \dots$ be a discrete process and define

$$S_n(g) = \frac{1}{n} \sum_{i=1}^n g(X_i)$$

this is sometimes referred to as the *Monte-Carlo estimator* of $\mathbb{E}[g(X)]$. Using the Central Limit Theorem it is easy to see that if each of the iterates X_i has the same distribution as X , and both mean $\mathbb{E}[g(X)]$ and variance σ^2 of $g(x)$ are defined then

$$\widehat{\lim}_{n \rightarrow \infty} \sqrt{n}\sigma^{-1} (S_n(g) - \mathbb{E}[g(X)]) = Y \sim \mathcal{N}(0, 1).$$

In particular $S_n(g)$ will tend to the desired expectation.

If we have some means of generating a random process X_i for which the iterates have the same distribution as X (or a sufficiently close approximation) we can use this method to compute an estimate of the expectation $\mathbb{E}[g(X)]$.

In the Monte-Carlo Markov Chain algorithm one assumes that one is given a density ρ defined on domain \mathcal{D} with respect to which the average of an observable

$$\mathbb{E}[g(X)] = \int_{\mathcal{D}} g(x)\rho(x)dx$$

is to be computed, and then one constructs a sequence of iterates X_i as a discrete-time Markov Chain such that the transition probability density $\pi(x, y)$ satisfies

$$\int_{\mathcal{D}} \pi(x, y)\rho(x)dx = \rho(y).$$

This means that the Markov chain preserves the density ρ as an invariant distribution.

Under certain circumstances it can be shown that in the limit of large number of iterations of the process, the random variable X_n tends to X (in distribution). Thus the Monte-Carlo Markov Chain method can be used to generate sets of independent realizations of the random variable which can be used to calculate an expectation. In practice, one prefers to use a long sequence of the iterates from a single starting value. The efficacy (specifically the ergodicity and rate of convergence) of the Monte-Carlo Markov-Chain method depends on the choice of the transition density.

Let ρ be the distribution which we seek to sample. Let $\pi(x, y)$ be the transition density of a Markov chain such that

$$\Pr(X_{k+1} \in \mathcal{A} | X_k = y) = \int_{\mathcal{A}} \pi(x, y)dy.$$

Also define $\pi^n(x, y)$ as the time- n transition density,

$$\pi^n(x, y) = \int \int \cdots \int \pi(x, z_{n-1})\pi(z_{n-1}, z_{n-2}) \cdots \pi(z_1, y)dz_1 dz_2 \dots dz_{n-1}.$$

A set of assumptions can be used to ensure that the chain will correctly sample the distribution $\rho(x)$:

Reversibility $\rho(x)\pi(x, y) = \rho(y)\pi(y, x)$. (This is also referred to as *detailed balance*.)

Irreducibility For all x, y , there exists a time n such that $\pi^n(x, y) > 0$.

Aperiodicity For all x , $\gcd\{n | \pi^n(x, x) > 0\} = 1$, where \gcd is the greatest common divisor.

Let us note that detailed balance implies that

$$\int_{\mathcal{D}} \rho(x)\pi(x, y)dx = \rho(y) \int_{\mathcal{D}} \pi(y, x)dx = \rho(y),$$

and thus, in this case, ρ will be invariant under the process.

The *Metropolis-Hastings* Monte-Carlo algorithm is a type of Monte-Carlo Markov-Chain scheme in which a computable (but not necessarily rigorously ergodic) proposal step (taken from a “prior” distribution) is corrected by means of an elementary test in order to provide exact sampling of the target distribution. Let the prior distribution be represented by a density $\bar{\pi}(x, y)$. We assume the prior to be easily sampled and select \bar{X}_{k+1} given the current state X_k using the probability distribution defined by

$$\Pr(\bar{X}_{k+1} \in \mathcal{A} | X_k = y) = \int_{\mathcal{A}} \bar{\pi}(x, y) dy.$$

The proposal distribution is *not* assumed to satisfy *detailed balance*, i.e.

$$\rho(x)\bar{\pi}(x, y) \neq \rho(y)\bar{\pi}(y, x).$$

However, if we define

$$\alpha(x, y) = \min \left\{ 1, \frac{\bar{\pi}(y, x)\rho(y)}{\bar{\pi}(x, y)\rho(x)} \right\}, \quad (\text{C.1})$$

which is termed the *acceptance coefficient* or the *acceptance rate*, then

$$\rho(x)\alpha(x, y)\bar{\pi}(x, y) = \rho(y)\alpha(y, x)\bar{\pi}(y, x).$$

In other words we have constructed a new transition density $\pi(x, y) = \alpha(x, y)\bar{\pi}(x, y)$, and, consequently, a new iterative procedure, in such a way that detailed balance is restored.

The Metropolis-Hastings algorithm can be written as:

Metropolis-Hastings Monte-Carlo Algorithm

repeat for $k = 0, 1, 2, \dots$

 Given X_k , make a trial move ($X_k \rightarrow Y_{k+1}$) using a given prior distribution with density $\bar{\pi}(x, y)$

 Draw a uniformly distributed random variable $u \sim \mathcal{U}(0, 1)$.

 Compute the acceptance coefficient $\alpha = \alpha(X_k, Y_{k+1})$ using (C.1).

if $u < \alpha$

 Accept the step: $X_{k+1} := Y_{k+1}$.

else

 Reject the step: $X_{k+1} := X_k$.

until sampling complete

We now consider several variants of this basic approach.

C.1 Metropolis Monte-Carlo

In the traditional method, the goal is to sample some given distribution with smooth density $\rho(x)$. Only the interatomic potential is evaluated at each step. The choice of the proposal distribution is open but is assumed to be symmetric, meaning that $\bar{\pi}(x, y) = \bar{\pi}(y, x)$. Therefore

$$\begin{aligned}\alpha(x, y) &= \min \left\{ 1, \frac{\bar{\pi}(y, x)\rho(y)}{\bar{\pi}(x, y)\rho(x)} \right\} \\ &= \min \{1, \rho(y)/\rho(x)\}\end{aligned}$$

A typical choice for the proposal is

$$\pi(x, y) = \sigma^{-1} \mathbf{1}_{[-\sigma/2, \sigma/2]}(y - x),$$

i.e., $y - x$ has a uniform distribution on the interval $[-\sigma/2, \sigma/2]$. Alternatively, we may choose normally distributed perturbations

$$\pi(x, y) = \frac{1}{\sqrt{2\pi}\sigma} e^{-(y-x)^2/2\sigma^2}.$$

In either case, the determination of the optimal value of σ , which parameterizes the mean step-length, is nontrivial. If σ is chosen very small, the acceptance rate will be high, but progress toward sampling the Gibbs measure will be slow. If σ is chosen very large, then the spatial moves are large, but many of these are likely to be rejected.

This method is easily extended to the multivariate case, for example where $\rho = \bar{\rho}_\beta(\mathbf{q}) = \exp(-\beta U(\mathbf{q}))$.

C.2 Metropolis Correction of Numerical Methods

In these methods, we choose the proposal using a timestep of a numerical method for an appropriate system, with the accept/reject condition chosen to give exact sampling of the target distribution. The usual setting for molecular dynamics is sampling the Gibbs-Boltzmann distribution $\exp(-\beta H(\mathbf{q}, \mathbf{p}))$.

There are many variants of this scheme. For example the Metropolis-Adjusted Langevin Algorithm (MALA) [313] uses a proposal defined by a step of a numerical method applied to Langevin (or overdamped Langevin) dynamics. Under certain circumstances, the resulting Markov Chain can be shown to be exponentially convergent to the target distribution (“geometrically ergodic”). Because the proposal is generated by a numerical method, it is possible, for large timestep, for this to exhibit pathological properties, in which case the exponential convergence may be

lost. Modifications of the basic scheme presented in [313] address this issue by truncation of the proposal distribution. Much subsequent work has focused on the design of MALA-type methods with the aim of obtaining optimal convergence to equilibrium.

In [43, 47, 48] the corrections are applied to a deterministic or stochastic molecular dynamics method with the goal of improving numerical stability at large timestep and/or enhancing phase space exploration. A practical overview of these methods, with a molecular dynamics test example, may be found in [43].

A fundamental issue for these schemes is that, for efficiency purposes, the acceptance ratio must be kept sufficiently high. At fixed stepsize, the acceptance ratio will tend to deteriorate with increasing system size [43], so smaller stepsizes are generally needed for large systems in practice. By contrast the straightforward, uncorrected discretization methods accept every step; this leads to error due to numerical bias in proportion to a power of the stepsize.

When certain methods are used (see Chap. 7 for examples) the error due to bias in molecular dynamics can be well controlled, in which case the benefits of a Metropolis-Hastings correction may be modest. Metropolis-Hastings correction in MD, as described in the algorithms mentioned above, is likely to be most helpful in situations where very high accuracy is needed, or where, for some practical reasons, the underlying basic integrator is a low-accuracy (in the sense of invariant measure) integration method. Moreover, the Monte-Carlo framework tends to impose a strong perturbation on dynamics, so that temporal correlations can no longer be recovered from the sampling paths. Technically, this is also the case for Langevin dynamics itself, but as discussed in Chap. 8, the perturbation of dynamics is controlled by the friction parameter γ (and even better methods for weak perturbation of dynamics are described in Chap. 8, based on extended systems).

C.3 Hybrid Monte-Carlo Methods

As an intermediate between deterministic integration and Monte-Carlo, one may consider *Hybrid Monte-Carlo (HMC) methods* [110, 278]. These schemes use, for the proposal distribution, a moderate length path obtained from deterministic molecular dynamics (usually computed by the Verlet method). Thus, at each step of an HMC scheme, we obtain $s + 1$ timesteps

$$\left\{ \mathcal{G}_h^j \begin{bmatrix} \mathbf{q}_k \\ \mathbf{p}_k \end{bmatrix} \mid j = 0, 1, 2, \dots, s \right\}$$

which approximate the local Hamiltonian evolution. It is important that the underlying scheme \mathcal{G}_h is time-reversible and volume preserving in the case of deterministic dynamics.

As explained in Gardiner [142], it is necessary, upon rejection of a step, to incorporate a change of sign of the momentum (a “momentum flip” [2]). The

acceptance criterion is based on the change in energy along the computed path. That is, we evaluate the energy difference

$$\Delta H = H\left(\begin{bmatrix} \mathbf{q}_k \\ \mathbf{p}_k \end{bmatrix}\right) - H\left(\begin{bmatrix} \mathbf{q}_k \\ \mathbf{p}_k \end{bmatrix}\right)$$

and accept the step if either $\Delta H < 0$ or else if $\Delta H > 0$ but

$$\exp(-\beta\Delta H) > u \sim \mathcal{U}(0, 1).$$

If the step is rejected, we set $\mathbf{q}_{k+1} := \mathbf{q}_k$, $\mathbf{p}_{k+1} := -\mathbf{p}_k$ and continue.

Note that when a symplectic integration method is used, we have, from the discussion in Chap. 3, a perturbed energy function and, moreover, from Theorem 3.1, the error in energy H is $\mathcal{O}(h^r)$, nonetheless the perturbations are large for a large stepsize h . In the *Shadow Hybrid Monte-Carlo (SHMC) method* [2, 3, 188], the accept-reject test is based on the modified Hamiltonian \tilde{H}_h (see Chap. 3), derived from the Baker-Campbell-Hausdorff expansion. SHMC can improve efficiency by decreasing the rejection rate.

References

1. Afshar, Y., Schmid, F., Pishevar, A., Worley, S.: Exploiting seeding of random number generators for efficient domain decomposition parallelization of dissipative particle dynamics. *Comput. Phys. Commun.* **184**(4), 1119–1128 (2013). doi:[10.1016/j.cpc.2012.12.003](https://doi.org/10.1016/j.cpc.2012.12.003)
2. Akhmatkaya, E., Bou-Rabee, N., Reich, S.: A comparison of generalized hybrid Monte Carlo methods with and without momentum flip. *J. Comput. Phys.* **228**, 2256–2265 (2009). doi:[10.1016/j.jcp.2008.12.014](https://doi.org/10.1016/j.jcp.2008.12.014)
3. Akhmatkaya, E., Reich, S.: New hybrid Monte Carlo methods for efficient sampling: from physics to biology and statistics. *Prog. J. Nucl. Sci. Technol.* **2**, 447–462 (2011)
4. Alder, B., Wainwright, T.: Phase transition for a hard sphere system. *J. Chem. Phys.* **27**, 1208–1209 (1957). doi:[10.1063/1.1743957](https://doi.org/10.1063/1.1743957)
5. Alder, B., Wainwright, T.: Studies in molecular dynamics. I. General method. *J. Chem. Phys.* **31**, 459–466 (1959). doi:[10.1063/1.1730376](https://doi.org/10.1063/1.1730376)
6. Allen, M., Quigley, D.: Some comments on Monte Carlo and molecular dynamics methods. *Mol. Phys.* **111**, 3442–3447 (2013). doi:[10.1080/00268976.2013.817623](https://doi.org/10.1080/00268976.2013.817623)
7. Allen, M., Tildesley, D.: Computer Simulation of Liquids. Oxford University Press, Oxford (1989). ISBN:978-0198556459
8. Allen, M.P., Schmid, F.: A thermostat for molecular dynamics of complex fluids. *Mol. Simul.* **33**(1–2), 21–26 (2007). doi:[10.1080/08927020601052856](https://doi.org/10.1080/08927020601052856)
9. Allinger, N.L., Chen, K., Lii, J.H.: An improved force field (MM4) for saturated hydrocarbons. *J. Comput. Chem.* **17**(5–6), 642–668 (1996). doi:[10.1002/\(SICI\)1096-987X\(199604\)17:5<642::AID-JCC6>3.0.CO;2-U](https://doi.org/10.1002/(SICI)1096-987X(199604)17:5<642::AID-JCC6>3.0.CO;2-U)
10. Allinger, N.L., Yuh, Y.H., Lii, J.H.: Molecular mechanics. the MM3 force field for hydrocarbons 1. *J. Am. Chem. Soc.* **111**(23), 8551–8566 (1989). doi:[10.1021/ja00205a001](https://doi.org/10.1021/ja00205a001)
11. Andersen, H.: Molecular dynamics simulations at constant pressure and/or temperature. *J. Chem. Phys.* **72**, 2384–2393 (1980). doi:[10.1063/1.439486](https://doi.org/10.1063/1.439486)
12. Andersen, H.: Rattle: a “velocity” version of the shake algorithm for molecular dynamics calculations. *J. Comput. Phys.* **52**, 24–34 (1983). doi:[10.1016/0021-9991\(83\)90014-1](https://doi.org/10.1016/0021-9991(83)90014-1)
13. Ariel, G., Vanden-Eijnden, E.: A strong limit theorem in the Kac-Zwanzig model. *Nonlinearity* **22**, 145–162 (2009). doi:[10.1088/0951-7715/22/1/008](https://doi.org/10.1088/0951-7715/22/1/008)
14. Arizumi, N., Bond, S.: On the estimation and correction of discretization error in molecular dynamics averages. *Appl. Numer. Math.* **62**, 1938–1953 (2012). doi:[10.1016/j.apnum.2012.08.005](https://doi.org/10.1016/j.apnum.2012.08.005)
15. Arnold, V.: Mathematical Methods of Classical Mechanics, 2nd edn. Springer, New York (1989). ISBN:978-3540968900

16. Arnold, V.: Ordinary Differential Equations, 2nd edn. Springer, New York (1992). ISBN:978-0262510189
17. Ascher, U., Reich, S.: The midpoint scheme and variants for Hamiltonian systems: advantages and pitfalls. *SIAM J. Numer. Anal.* **21**, 1045–1065 (1999). doi:[10.1137/S106482597316059](https://doi.org/10.1137/S106482597316059)
18. Ash, R., Basic Probability Theory, Dover Publications Inc. (2008), ISBN:978-0-486-46628-6
19. Baczewski, A., Bond, S.: Numerical integration of the extended variable generalized Langevin equation with a positive Prony representable memory kernel. *J. Chem. Phys.* **139** (2013). doi:[10.1063/1.4815917](https://doi.org/10.1063/1.4815917)
20. Bae, D.S., Haug, E.: A recursive formulation for constrained mechanical system dynamics: part I: open loop systems. *Mech. Struct. Mach.* **15**, 359–382 (1987). doi:[10.1080/08905458708905124](https://doi.org/10.1080/08905458708905124)
21. Bakhturin, Y.A.: Campbell-Hausdorff formula. In: Encyclopedia of Mathematics. Springer, New York (2001). ISBN:978-1556080104
22. Barash, D., Yang, L., Qian, X., Schlick, T.: Inherent speedup limitations in multiple time step/particle mesh Ewald algorithms. *J. Comput. Chem.* **24**, 77–88 (2003). doi:[10.1002/jcc.10196](https://doi.org/10.1002/jcc.10196)
23. Barducci, A., Bonomi, M., Parrinello, M.: Metadynamics. *Wiley Interdiscip. Rev.* **1**(5), 826–843 (2011). doi:[10.1002/wcms.31](https://doi.org/10.1002/wcms.31)
24. Barnes, J., Hut, P.: A hierarchical $O(N \log N)$ force-calculation algorithm. *Nature* **324**, 446–449 (1986). doi:[10.1006/jcph.2002.7026](https://doi.org/10.1006/jcph.2002.7026)
25. Barth, E., Kuczera, K., Leimkuhler, B., Skeel, R.: Algorithms for constrained molecular dynamics. *J. Comput. Chem.* **16**, 1192–1209 (1995). doi:[10.1002/jcc.540161003](https://doi.org/10.1002/jcc.540161003)
26. Bartle, R.: The Elements of Integration and Lebesgue Measure. Classica library. Wiley, New York (1955). ISBN:978-0471042228
27. Bartók, A., Payne, M., Kondor, R., Csányi, G.: Gaussian approximation potentials: the accuracy of quantum mechanics, without the electrons. *Phys. Rev. Lett.* **104**, 136,403 (2010). doi:[10.1103/PhysRevLett.104.136403](https://doi.org/10.1103/PhysRevLett.104.136403)
28. Bashford, D., Karplus, M.: pKa's of ionizable groups in proteins: atomic detail from a continuum electrostatic model. *Biochemistry* **29**, 10,219–10,225 (1990). doi:[10.1021/bi00496a010](https://doi.org/10.1021/bi00496a010)
29. Batcho, P.F., Case, D., Schlick, T.: Optimized particle-mesh Ewald/multiple-time step integration for molecular dynamics simulations. *J. Chem. Phys.* **115**, 4003–4018 (2001). doi:[10.1063/1.1389854](https://doi.org/10.1063/1.1389854)
30. Beeman, D.: Some multistep methods for use in molecular dynamics calculations. *J. Comput. Phys.* **20**, 130–139 (1976). doi:[10.1016/0021-9991\(76\)90059-0](https://doi.org/10.1016/0021-9991(76)90059-0)
31. Benettin, G., Giorgilli, A.: On the Hamiltonian interpolation of near to the identity symplectic mappings with application to symplectic integration algorithms. *J. Stat. Phys.* **74**, 1117–1143 (1994). doi:[10.1007/BF02188219](https://doi.org/10.1007/BF02188219)
32. Berendsen, H., Postma, J., van Gunsteren, W., DiNola, A., Haak, J.: Molecular dynamics with coupling to an external bath. *J. Chem. Phys.* **81**, 3684–3690 (1984). doi:[10.1063/1.448118](https://doi.org/10.1063/1.448118)
33. Berendsen, H., van der Spoel, D., Vandrunen, R.: GROMACS—a message-passing parallel molecular-dynamics implementation. *Comput. Phys. Commun.* **91**, 43–56 (1995). doi:[10.1016/0010-4655\(95\)00042-E](https://doi.org/10.1016/0010-4655(95)00042-E)
34. Besold, G., Vattulainen, I., Karttunen, M., Polson, J.M.: Towards better integrators for dissipative particle dynamics simulations. *Phys. Rev. E* **62**(6), R7611 (2000). doi:[10.1103/PhysRevE.62.R7611](https://doi.org/10.1103/PhysRevE.62.R7611)
35. Biesiadecki, J., Skeel, R.: Dangers of multiple time step methods. *J. Comput. Phys.* **109**(2), 318–328 (1993). doi:[10.1006/jcph.1993.1220](https://doi.org/10.1006/jcph.1993.1220)
36. Binder, K., Heermann, D.: Monte Carlo Simulation in Statistical Physics. Springer, New York (2010)
37. Blanes, S., Casas, F., Murua, A.: Splitting and composition methods in the numerical integration. *Bol. Soc. Esp. Mat. Apl.* **45**, 89–145 (2008)
38. Board, J., Schulten, K.: The fast multipole algorithm. *Comput. Sci. Eng.* **2**, 76–79 (2000). doi:[10.1109/5992.814662](https://doi.org/10.1109/5992.814662)

39. Boek, E., Coveney, P., Lekkerkerker, H., van der Schoot, P.: Simulating the rheology of dense colloidal suspensions using dissipative particle dynamics. *Phys. Rev. E* **55**(3), 3124 (1997). doi:[10.1103/PhysRevE.55.3124](https://doi.org/10.1103/PhysRevE.55.3124)
40. Bond, S., Leimkuhler, B.: Molecular dynamics and the accuracy of numerically computed averages. *Acta Numerica* **16**, 1–65 (2007). doi:[10.1017/S0962492906280012](https://doi.org/10.1017/S0962492906280012)
41. Bond, S., Leimkuhler, B., Laird, B.: The Nosé-Poincaré method for constant temperature molecular dynamics. *J. Comput. Phys.* **151**, 114–134 (1999). doi:[10.1006/jcph.1998.6171](https://doi.org/10.1006/jcph.1998.6171)
42. Bortz, A., Kalos, M., Lebowitz, J.: A new algorithm for Monte Carlo simulation of Ising spin systems. *J. Comput. Phys.* **17**, 10–18 (1975). doi:[10.1016/0021-9991\(75\)90060-1](https://doi.org/10.1016/0021-9991(75)90060-1)
43. Bou-Rabee, N.: On Metropolis integrators for molecular dynamics (2014). doi:[10.3390/e16010138](https://doi.org/10.3390/e16010138)
44. Bou-Rabee, N.: Time integrators for molecular dynamics. *Entropy* **16**(1), 138–162 (2014). doi:[10.3390/e16010138](https://doi.org/10.3390/e16010138)
45. Bou-Rabee, N., Owhadi, H.: Ergodicity of Langevin processes with degenerate diffusion in momentums. *Int. J. Pure Appl. Math.* **45**, 475–490 (2008)
46. Bou-Rabee, N., Owhadi, H.: Long-run accuracy of variational integrators in the stochastic context. *SIAM J. Numer. Anal.* **48**, 278–297 (2010). doi:[10.1137/090758842](https://doi.org/10.1137/090758842)
47. Bou-Rabee, N., Vanden-Eijnden, E.: Pathwise accuracy and ergodicity of metropolized integrators for SDEs. *Commun. Pure Appl. Math.* **63**, 655–696 (2010). doi:[10.1002/cpa.20306](https://doi.org/10.1002/cpa.20306)
48. Bou-Rabee, N., Vanden-Eijnden, E.: A patch that imparts unconditional stability to explicit integrators for Langevin-like equations. *J. Comput. Phys.* **231**, 2565–2580 (2012). doi:[10.1016/j.jcp.2011.12.007](https://doi.org/10.1016/j.jcp.2011.12.007)
49. Bowers, K., Dror, R., Shaw, D.: The midpoint method for parallelization of particle simulations. *J. Chem. Phys.* **124**, 184,109 (2006). doi:[10.1063/1.2191489](https://doi.org/10.1063/1.2191489)
50. Bowers, K., Dror, R., Shaw, D.: Zonal methods for the parallel execution of range-limited n-body simulations. *J. Comput. Phys.* **221**, 303–329 (2007). doi:[10.1016/j.jcp.2006.06.014](https://doi.org/10.1016/j.jcp.2006.06.014)
51. Boyce, W., Diprima, R.C.: Elementary Differential Equations, 9th edn. Wiley, New York (2008). ISBN:978-0470039403
52. Brauer, F., Nohel, J.: The Qualitative Theory of Ordinary Differential Equations: An Introduction. Dover Books on Mathematics Series. Dover, New York (1989)
53. Brooks, B.R., Bruccoleri, R.E., Olafson, B.D., States, D.J., Swaminathan, S., Karplus, M.: CHARMM: a program for macromolecular energy, minimization, and dynamics calculations. *J. Comput. Chem.* **4**(2), 187–217 (1983). doi:[10.1002/jcc.540040211](https://doi.org/10.1002/jcc.540040211)
54. Brooks III, C., Karplus, M., Pettitt, B.: Proteins: A Theoretical Perspective of Dynamics, Structure and Thermodynamics. Advances in Chemical Physics, vol. 71. Wiley, New York (1988). ISBN:ISBN 0-471-62801-8
55. Brünger, A., Brooks III, C., Karplus, M.: Stochastic boundary conditions for molecular dynamics simulations of ST2 water. *Chem. Phys. Lett.* **105**, 495–500 (1984). doi:[10.1016/0009-2614\(84\)80098-6](https://doi.org/10.1016/0009-2614(84)80098-6)
56. Buckingham, R.A.: The classical equation of state of gaseous helium, neon and argon. *Proc. R. Soc. Lond.* **168**, 264–283 (1938). doi:[10.1098/rspa.1938.0173](https://doi.org/10.1098/rspa.1938.0173)
57. Bühler, O.: A Brief Introduction to Classical, Statistical and Quantum Mechanics. Courant Lecture Notes. AMS, Providence (2006). ISBN:978-0821842324
58. Bulgac, A., Kusnezov, D.: Canonical ensemble averages from pseudomicrocanonical dynamics. *Phys. Rev. A* **42**, R5045–R5048 (1990). doi:[10.1103/PhysRevA.42.5045](https://doi.org/10.1103/PhysRevA.42.5045)
59. Burrage, K., Lythe, G.: Accurate stationary densities with partitioned numerical methods for stochastic differential equations. *SIAM J. Numer. Anal.* **47**, 1601–1618 (2009). doi:[10.1137/060677148](https://doi.org/10.1137/060677148)
60. Bussi, G., Donadio, D., Parrinello, M.: Canonical sampling through velocity rescaling. *J. Chem. Phys.* **126**(1), 014,101 (2007). doi:[10.1063/1.2408420](https://doi.org/10.1063/1.2408420)
61. Bussi, G., Laio, A., Parrinello, M.: Equilibrium free energies from nonequilibrium metadynamics. *Phys. Rev. Lett.* **96**, 090,601 (2006). doi:[10.1103/PhysRevLett.96.090601](https://doi.org/10.1103/PhysRevLett.96.090601)
62. Bussi, G., Parrinello, M.: Accurate sampling using Langevin dynamics. *Phys. Rev. E* **75**, 056,707 (2007). doi:[10.1103/PhysRevE.75.056707](https://doi.org/10.1103/PhysRevE.75.056707)

63. Bussi, G., Parrinello, M.: Stochastic thermostats: comparison of local and global schemes. *Comput. Phys. Commun.* **179**, 26–29 (2008). doi:[10.1016/j.cpc.2008.01.006](https://doi.org/10.1016/j.cpc.2008.01.006)
64. Cancès, E., Castella, F., Chartier, P., Faou, E., Le Bris, C., Legoll, F., Turinici, G.: Long-time averaging for integrable Hamiltonian dynamics. *Numer. Math.* **100**(2), 211–232 (2005). doi:[10.1007/s00211-005-0599-0](https://doi.org/10.1007/s00211-005-0599-0)
65. Cancès, E., Legoll, F., Stoltz, G.: Theoretical and numerical comparison of sampling methods for molecular dynamics. *Math. Model. Numer. Anal.* **41**(2), 351–390 (2007). doi:[10.1051/m2an:2007014](https://doi.org/10.1051/m2an:2007014)
66. Candy, J., Rozmus, W.: A symplectic integration algorithm for separable Hamiltonian functions. *J. Comput. Phys.* **92**(1), 230–256 (1991). doi:[10.1016/0021-9991\(91\)90299-Z](https://doi.org/10.1016/0021-9991(91)90299-Z)
67. Carter, E., Ciccotti, G., Hynes, J.T., Kapral, R.: Constrained reaction coordinate dynamics for the simulation of rare events. *Chem. Phys. Lett.* **156**(5), 472–477 (1989). doi:[10.1016/S0009-2614\(89\)87314-2](https://doi.org/10.1016/S0009-2614(89)87314-2)
68. Celledoni, E., Fasso, F., Säfström, N., Zanna, A.: The exact computation of the free rigid body motion and its use in splitting methods. *SIAM J. Sci. Comput.* **30**(4), 2084–2112 (2008). doi:[10.1137/070704393](https://doi.org/10.1137/070704393)
69. Ceriotti, M., Bussi, G., Parrinello, M.: Langevin equation with colored noise for constant-temperature molecular dynamics simulations. *Phys. Rev. Lett.* **102**, 020,601 (2009). doi:[10.1103/PhysRevLett.102.020601](https://doi.org/10.1103/PhysRevLett.102.020601)
70. Chandler, D.: Introduction to Modern Statistical Mechanics. Oxford University Press, New York (1987)
71. Channell, P.: Symplectic integration algorithms. Tech. Rep. AT-6:ATN 83–9, Los Alamos National Laboratory (1983)
72. Channell, P., Scovel, C.: Symplectic integration of Hamiltonian systems. *Nonlinearity* **3**(2), 231 (1990). doi:[10.1088/0951-7715/3/2/001](https://doi.org/10.1088/0951-7715/3/2/001)
73. Chaudhri, A., Lukes, J.R.: Velocity and stress autocorrelation decay in isothermal dissipative particle dynamics. *Phys. Rev. E* **81**(2), 026,707 (2010). doi:[10.1103/PhysRevE.81.026707](https://doi.org/10.1103/PhysRevE.81.026707)
74. Chawla, M.: On the order and attainable intervals of periodicity of explicit nystrom methods for $y'' = f(t,y)$. *SIAM J. Numer. Anal.* **22**, 127–131 (1985). doi:[10.1137/0722009](https://doi.org/10.1137/0722009)
75. Chen, P.H., Avchachov, K., Nordlund, K., Pussi, K.: Molecular dynamics simulation of radiation damage in cacd6 quasicrystal cubic approximant up to 10 keV. *J. Chem. Phys.* **138**(234505) (2013). doi:[10.1063/1.4811183](https://doi.org/10.1063/1.4811183)
76. Chipot, C., Hénin, J.: Exploring the free-energy landscape of a short peptide using an average force. *J. Chem. Phys.* **123**(24) (2005). doi:[10.1063/1.2138694](https://doi.org/10.1063/1.2138694)
77. Cho, K., Joannopoulos, J.: Ergodicity and dynamical properties of constant-temperature molecular dynamics. *Phys. Rev. A* **45**, 7089–7097 (1992). doi:[10.1103/PhysRevA.45.7089](https://doi.org/10.1103/PhysRevA.45.7089)
78. Cho, K., Joannopoulos, J., Kleinman, L.: Constant-temperature molecular dynamics with momentum conservation. *Phys. Rev. E* **47**(5), 3145–3151 (1993). doi:[10.1103/physreve.47.3145](https://doi.org/10.1103/physreve.47.3145)
79. Ciccotti, G., Ferrario, M.: Rare events by constrained molecular dynamics. *J. Mol. Liq.* **89**(1–3), 1–18 (2000). doi:[10.1016/S0167-7322\(00\)90001-1](https://doi.org/10.1016/S0167-7322(00)90001-1)
80. Ciccotti, G., Ferrario, M., Ryckaert, J.P.: Molecular dynamics of rigid systems in Cartesian coordinates: a general formulation. *Mol. Phys.* **47**(6), 1253–1264 (1982). doi:[10.1080/00268978200100942](https://doi.org/10.1080/00268978200100942)
81. Ciccotti, G., Kalibaeva, G.: Deterministic and stochastic algorithms for mechanical systems under constraints. *Philos. Trans. R. Soc. Lond. Series A* **362**, 1583–1594 (2004). doi:[10.1098/rsta.2004.1400](https://doi.org/10.1098/rsta.2004.1400)
82. Ciccotti, G., Kapral, R.: Molecular dynamics: an account of its evolution. In: Theory and Applications of Computational Chemistry: The First Forty Years. Elsevier, Amsterdam (2005)
83. Ciccotti, G., Kapral, R., Vanden-Eijnden, E.: Blue moon sampling, vectorial reaction coordinates, and unbiased constrained dynamics. *ChemPhysChem* **6**(9), 1809–1814 (2005). doi:[10.1002/cphc.200400669](https://doi.org/10.1002/cphc.200400669)
84. Ciccotti, G., Ryckaert, J.: Molecular dynamics simulation of rigid molecules. *Comput. Phys. Rep.* **4**, 346–392 (1986). doi:[10.1016/0167-7977\(86\)90022-5](https://doi.org/10.1016/0167-7977(86)90022-5)

85. Ciccotti, G., Ryckaert, J.P.: On the derivation of the generalized Langevin equation for interacting Brownian particles. *J. Stat. Phys.* **26**(1), 73–82 (1981). doi:[10.1007/BF01106787](https://doi.org/10.1007/BF01106787)
86. Clark, T., McCammon, J., Scott, L.: Parallel molecular dynamics. In: Proceedings of the Fifth SIAM Conference on Parallel Processing for Scientific Computing, pp. 338–344. Society for Industrial and Applied Mathematics, Philadelphia (1992)
87. Corbera, M., Llibre, J., Pérez-Chavela, E.: Equilibrium points and central configurations for the Lennard-Jones 2- and 3-body problems. *Celest. Mech. Astron.* **89**, 235–266 (2004). doi:[10.1023/B:CELE.0000038600.74660.34](https://doi.org/10.1023/B:CELE.0000038600.74660.34)
88. Coveney, P.V., Novik, K.E.: Computer simulations of domain growth and phase separation in two-dimensional binary immiscible fluids using dissipative particle dynamics. *Phys. Rev. E* **54**(5), 5134 (1996). doi:[10.1103/PhysRevE.54.5134](https://doi.org/10.1103/PhysRevE.54.5134)
89. Darden, T., Perera, L., Li, L., Pedersen, L.: New tricks for modelers from the crystallography toolkit: the particle mesh Ewald algorithm and its use in nucleic acid simulations. *Structure* **7**, R55–R60 (1999). doi:[10.1016/S0969-2126\(99\)80033-1](https://doi.org/10.1016/S0969-2126(99)80033-1)
90. Darden, T., York, D., Pedersen, L.: Particle mesh Ewald: an $N \cdot \log(N)$ method for Ewald sums in large systems. *J. Chem. Phys.* **98**, 10,089–10,092 (1993). doi:[10.1063/1.464397](https://doi.org/10.1063/1.464397)
91. Darve, E., Pohorille, A.: Calculating free energies using average force. *J. Chem. Phys.* **115**(20), 9169–9183 (2001). doi:[10.1063/1.1410978](https://doi.org/10.1063/1.1410978)
92. Darve, E., Rodríguez-Gómez, D., Pohorille, A.: Adaptive biasing force method for scalar and vector free energy calculations. *J. Chem. Phys.* **128**(14) (2008). doi:[10.1063/1.2829861](https://doi.org/10.1063/1.2829861)
93. Darve, E., Wilson, M.A., Pohorille, A.: Calculating free energies using a scaled-force molecular dynamics algorithm. *Mol. Simul.* **28**(1–2), 113–144 (2002). doi:[10.1080/08927020211975](https://doi.org/10.1080/08927020211975)
94. Davidchack, R.: Discretization errors in molecular dynamics simulations with deterministic and stochastic thermostats. *J. Comput. Phys.* **229**, 9323–9346 (2010). doi:[10.1016/j.jcp.2010.09.004](https://doi.org/10.1016/j.jcp.2010.09.004)
95. Daw, M., Foiles, S., Baskes, M.: The embedded-atom method: a review of theory and applications. *Mater. Sci. Eng. Rep.* **9**, 251–310 (1993). doi:[10.1016/0920-2307\(93\)90001-U](https://doi.org/10.1016/0920-2307(93)90001-U)
96. De Fabritiis, G., Serrano, M., Españo, P., Coveney, P.: Efficient numerical integrators for stochastic models. *Physica A* **361**(2), 429–440 (2006). doi:[10.1016/j.physa.2005.06.090](https://doi.org/10.1016/j.physa.2005.06.090)
97. de la Llave, R.: A Tutorial on KAM Theory. American Mathematical Society, Providence (2003). ISBN:978-0821835326
98. de Vogelaere, R.: Methods of integration which preserve the contact transformation property of the Hamiltonian equations. Tech. Rep. 4, Department of Mathematics, University of Notre Dame (1956)
99. Debussche, A., Faou, E.: Weak backward error analysis for SDEs. *SIAM J. Numer. Anal.* **50**(3), 1735–1752 (2012). doi:[10.1137/110831544](https://doi.org/10.1137/110831544)
100. DeKock, R.: Chemical Structure. University Science Books, Sausalito, CA (1989)
101. Den Otter, W., Clarke, J.: A new algorithm for dissipative particle dynamics. *Europhys. Lett.* **53**(4), 426 (2001)
102. Dettmann, C.P., Morriss, G.P.: Hamiltonian reformulation and pairing of Lyapunov exponents for Nosé-Hoover dynamics. *Phys. Rev. E* **55**, 3693–3696 (1997). doi:[10.1103/PhysRevE.55.3693](https://doi.org/10.1103/PhysRevE.55.3693)
103. Devaney, R.: Dynamics of simple maps. *Proc. Symp. Appl. Math.* **39**, 1–24 (1989). ISBN:978-0821801376
104. Dickson, B., Legoll, F., Lelièvre, T., Stoltz, G., Fleurat-Lessard, P.: Free energy calculations: An efficient adaptive biasing potential method. *J. Phys. Chem. B* **114**(17), 5823–5830 (2010). doi:[10.1021/jp100926h](https://doi.org/10.1021/jp100926h)
105. Dieci, L., Van Vleck, E.: Software for Lyapunov exponent calculation. http://www.math.ku.edu/~evanvleck/software_les.html. Accessed 14 May 2013
106. Dirac, P.: Quantum mechanics of many-electron systems. *Proc. R. Soc. Lond. Series A* **123**, 714–733 (1929). doi:[10.1098/rspa.1929.0094](https://doi.org/10.1098/rspa.1929.0094)
107. Donev, A., Garcia, A.L., Alder, B.J.: Stochastic event-driven molecular dynamics. *J. Comput. Phys.* **227**, 2644–2665 (2008). doi:[10.1016/j.jcp.2007.11.010](https://doi.org/10.1016/j.jcp.2007.11.010)

108. Donev, A., Torquato, S., Stillinger, F.: Neighbor list collision-driven molecular dynamics simulation for nonspherical hard particles. I. Algorithmic details. *J. Comput. Phys.* **202**, 737–764 (2005). doi:[10.1016/j.jcp.2004.08.014](https://doi.org/10.1016/j.jcp.2004.08.014)
109. Duan, Z., Krasny, R.: Treecode algorithms for computing nonbonded particle interactions. In: Schlick, T., Gan, H.H. (eds.) *Computational Methods for Macromolecules: Challenges and Applications, Proceedings of the 3rd International Workshop on Algorithms for Macromolecular Modeling*, New York. Lecture Notes in Computational Science and Engineering, vol. 24, pp. 359–380. Springer, New York (2002)
110. Duane, S., Kennedy, A., Pendleton, B., Duncan, R.: Hybrid Monte Carlo. *Phys. Lett. B* **195**, 216–222 (1987). doi:[10.1016/0370-2693\(87\)91197-X](https://doi.org/10.1016/0370-2693(87)91197-X)
111. van Duin, A., Dasgupta, S., Lorant, F., Goddard, W.: Reaxff: a reactive force field for hydrocarbons. *J. Phys. Chem. A* **105**, 9396–9409 (2001). doi:[10.1021/jp004368u](https://doi.org/10.1021/jp004368u)
112. Dullweber, A., Leimkuhler, B., McLachlan, R.: Symplectic splitting methods for rigid body molecular dynamics. *J. Chem. Phys.* **107**, 5840–5851 (1997). doi:[10.1063/1.474310](https://doi.org/10.1063/1.474310)
113. Dürr, D., Goldstein, S., Lebowitz, J.: A mechanical model of Brownian motion. *Commun. Math. Phys.* **78**(4), 507–530 (1980). doi:[10.1007/BF02046762](https://doi.org/10.1007/BF02046762)
114. E, W., Li, D.: The Andersen thermostat in molecular dynamics. *Commun. Pure Appl. Math.* **61**, 96–136 (2008). doi:[10.1002/cpa.20198](https://doi.org/10.1002/cpa.20198)
115. E, W., Ren, W., Vanden-Eijnden, E.: String method for the study of rare events. *Phys. Rev. B* **66**, 052,301 (2002). doi:[10.1103/PhysRevB.66.052301](https://doi.org/10.1103/PhysRevB.66.052301)
116. E, W., Ren, W., Vanden-Eijnden, E.: Finite temperature string method for the study of rare events. *J. Phys. Chem. B* **109**(14), 6688–6693 (2005). doi:[10.1021/jp0455430](https://doi.org/10.1021/jp0455430)
117. E, W., Ren, W., Vanden-Eijnden, E.: Simplified and improved string method for computing the minimum energy paths in barrier-crossing events. *J. Chem. Phys.* **126**(16) (2007). doi:[10.1063/1.2720838](https://doi.org/10.1063/1.2720838)
118. Eastman, P., Doniach, S.: Multiple time step diffusive Langevin dynamics for proteins. *Proteins* **30**, 215–227 (1998). doi:[10.1002/\(SICI\)1097-0134\(19980215\)30:3<215::AID-PROT1>3.0.CO;2-J](https://doi.org/10.1002/(SICI)1097-0134(19980215)30:3<215::AID-PROT1>3.0.CO;2-J)
119. Edberg, R., Evans, D., Morriss, G.: Constrained molecular dynamics: simulations of liquid alkanes with a new algorithm. *J. Chem. Phys.* **84**, 6933–6939 (1986). doi:[10.1063/1.450613](https://doi.org/10.1063/1.450613)
120. Ehlich, R., Campbell, E., Knospe, O., Schmidt, R.: Collisional dynamics of c60 with noble-gas-atoms studied by molecular dynamics with empirical two- and three-body forces. *Zeitschrift für Physik D* **28**, 153–161 (1993). doi:[10.1007/BF01436983](https://doi.org/10.1007/BF01436983)
121. Engle, R., Skeel, R., Drees, M.: Monitoring energy drift with shadow Hamiltonians. *J. Comput. Phys.* **206**, 432–452 (2005). doi:[10.1016/j.jcp.2004.12.009](https://doi.org/10.1016/j.jcp.2004.12.009)
122. Españoł, P., Warren, P.: Statistical mechanics of dissipative particle dynamics. *Europhys. Lett.* **30**(4), 191 (1995). doi:[10.1209/0295-5075/30/4/001](https://doi.org/10.1209/0295-5075/30/4/001)
123. Essmann, U., Perera, L., Berkowitz, M., Darden, T., Lee, H., Pedersen, L.: A smooth particle mesh Ewald method. *J. Chem. Phys.* **103**, 8577–8593 (1995). doi:[10.1063/1.470117](https://doi.org/10.1063/1.470117)
124. Evans, D., Morriss, G.: *Statistical Mechanics of Non-equilibrium Liquids*. Academic Press, London (1990)
125. Ewald, P.: Die berechnung optischer und elektrostatischer gitterpotentiale. *Ann. Phys.* **369**, 253–287 (1921). doi:[10.1002/andp.19213690304](https://doi.org/10.1002/andp.19213690304)
126. Faou, E., Lelièvre, T.: Conservative stochastic differential equations: Mathematical and numerical analysis. *Math. Comput.* **78**(268), 2047–2074 (2009). doi:[10.1090/S0025-5718-09-02220-0](https://doi.org/10.1090/S0025-5718-09-02220-0)
127. Farrés, A., Laskar, J., Blanes, S., Casas, F., Makazaga, J., Murua, A.: High precision symplectic integrators for the solar system. *Celest. Mech. Dyn. Astron.* **116**, 141–174 (2013). doi:[10.1007/s10569-013-9479-6](https://doi.org/10.1007/s10569-013-9479-6)
128. Feller, S., Zhang, Y., Pastor, R., Brooks, B.: Constant pressure molecular dynamics simulation: the Langevin piston method. *J. Chem. Phys.* **103**, 4613–4622 (1995). doi:[10.1063/1.470648](https://doi.org/10.1063/1.470648)
129. Feng, K.: On difference schemes and symplectic geometry. In: *Proceedings of the 1984 Beijing Symposium on Differential Geometry and Differential Equations*, pp. 42–58. Science Press, Beijing (1985)

130. Feng, K.: Difference schemes for Hamiltonian formalism and symplectic geometry. *J. Comput. Math.* **4**, 279–289 (1986)
131. Feng, K.: Symplectic geometry and numerical methods in fluid dynamics. In: Zhuang, F., Zhu, Y. (eds.) Tenth International Conference on Numerical Methods in Fluid Dynamics. Lecture Notes in Physics, vol. 264, pp. 1–7. Springer, Berlin/Heidelberg (1986). doi:[10.1007/BFb0041762](https://doi.org/10.1007/BFb0041762). ISBN:978-3-540-17172-0
132. Feng, K., Qin, M.: Hamiltonian algorithms for Hamiltonian systems and a comparative numerical study. *Comput. Phys. Commun.* pp. 173–187 (1991). doi:[10.1016/0010-4655\(91\)90170-P](https://doi.org/10.1016/0010-4655(91)90170-P)
133. Feng, K., Shang, Z.: Volume-preserving algorithms for source-free dynamical systems. *Numer. Math.* **71**, 451–463 (1995). doi:[10.1007/s002110050153](https://doi.org/10.1007/s002110050153)
134. Fennell, C., Gezelter, J.: Is the Ewald summation still necessary? Pairwise alternatives to the accepted standard for long-range electrostatics. *J. Chem. Phys.* **124**(234104) (2006). doi:[10.1063/1.2206581](https://doi.org/10.1063/1.2206581)
135. Ferrario, M., Fionino, A., Cicotti, G.: Long-time tails in two-dimensional fluids by molecular dynamics. *Physica A* **240**, 268–276 (1997). doi:[10.1016/S0378-4371\(97\)00150-7](https://doi.org/10.1016/S0378-4371(97)00150-7)
136. Fetecau, R.C., Marsden, J.E., Ortiz, M., West, M.: Nonsmooth Lagrangian mechanics and variational collision integrators. *SIAM J. Appl. Dyn. Sys.* **2**, 381–416 (2003). doi:[10.1137/S111111102406038](https://doi.org/10.1137/S111111102406038)
137. Fichtthorn, K., Weinberg, W.: Theoretical foundations of dynamical Monte Carlo simulations. *J. Chem. Phys.* **95**, 1090–1096 (1991). doi:[10.1063/1.461138](https://doi.org/10.1063/1.461138)
138. Ford, G., Kac, M., Mazur, P.: Statistical mechanics of assemblies of coupled oscillators. *J. Math. Phys.* **6**, 504–515 (1965). doi:[10.1063/1.1704304](https://doi.org/10.1063/1.1704304)
139. Forest, E., Ruth, R.: Fourth-order symplectic integration. *Physica D* **43**, 105–117 (1990). doi:[10.1016/0167-2789\(90\)90019-L](https://doi.org/10.1016/0167-2789(90)90019-L)
140. Frenkel, D., Smit, B.: Understanding Molecular Simulation: From Algorithms to Applications, 2nd edn. Oxford University Press, Oxford (2001). ISBN:978-0122673511
141. García-Archilla, B., Sanz-Serna, J.M., Skeel, R.: Long-time-step methods for oscillatory differential equations. *SIAM J. Sci. Comput.* **20**, 930–963 (1998). doi:[10.1137/S1064827596313851](https://doi.org/10.1137/S1064827596313851)
142. Gardiner, C.: Handbook of stochastic methods for physics, chemistry, and the natural sciences, 3rd edn. Springer, New York (2004). ISBN:9783540156079
143. Gay, J., Berne, B.: Modification of the overlap potential to mimic a linear site–site potential. *J. Chem. Phys.* **74**(6), 3316–3319 (1981). doi:[10.1063/1.441483](https://doi.org/10.1063/1.441483)
144. Geng, W., Krasny, R.: A treecode-accelerated boundary integral Poisson-Boltzmann solver for solvated biomolecules. *J. Comput. Phys.* **247**, 62–78 (2013). doi:[10.1016/j.jcp.2013.03.056](https://doi.org/10.1016/j.jcp.2013.03.056)
145. Germann, T., Kadau, K.: Trillion-atom molecular dynamics becomes a reality. *Int. J. Modern Phys. C* **19**, 1315–1319 (2008). doi:[10.1142/S0129183108012911](https://doi.org/10.1142/S0129183108012911)
146. Giardina, C., Kurchan, J., Lecomte, V., Tailleur, J.: Simulating rare events in dynamical processes. *J. Stat. Phys.* **145**(4), 787–811 (2011). doi:[10.1007/s10955-011-0350-4](https://doi.org/10.1007/s10955-011-0350-4)
147. Gibbs, J.: Elementary principles in statistical mechanics. C. Scribner, New York (1902). <http://archive.org/details/elementaryprinci00gibbrich>
148. Gibson, J., Chen, K., Chynoweth, S.: The equilibrium of a velocity-Verlet type algorithm for DPD with finite time steps. *Int. J. Modern Phys. C* **10**(01), 241–261 (1999). doi:[10.1142/S0129183199000176](https://doi.org/10.1142/S0129183199000176)
149. Gillespie, D.: A general method for numerically simulating the stochastic time evolution of coupled chemical reactions. *J. Comput. Phys.* **22**, 403–434 (1976). doi:[10.1016/0021-9991\(76\)90041-3](https://doi.org/10.1016/0021-9991(76)90041-3)
150. Givon, D., Kupferman, R., Stuart, A.: Extracting macroscopic dynamics: model problems and algorithms. *Nonlinearity* **17**(6), R55 (2004)
151. Goldstein, H., Poole, C., Safko, J.: Classical Mechanics, 3rd edn. Addison Wesley, San Francisco (2002). ISBN:978-0201657029

152. Gonzalez, O., Simo, J.: On the stability of symplectic and energy-momentum algorithms for non-linear Hamiltonian systems with symmetry. *Comput. Methods Appl. Mech. Eng.* **134**, 197–222 (1995). doi:[10.1016/0045-7825\(96\)01009-2](https://doi.org/10.1016/0045-7825(96)01009-2)
153. Gray, S.K., Noid, D.W., Sumpter, B.G.: Symplectic integrators for large scale molecular dynamics simulations: a comparison of several explicit methods. *J. Chem. Phys.* **101**, 4062–4072 (1994). doi:[10.1063/1.467523](https://doi.org/10.1063/1.467523)
154. Greengard, L.: Fast algorithms for classical physics. *Science* **265**, 909–914 (1994). doi:[10.1126/science.265.5174.909](https://doi.org/10.1126/science.265.5174.909)
155. Griebel, M., Knapek, S., Zumbusch, G.: Numerical simulation in molecular dynamics. In: *Numerics, Algorithms, Parallelization. Texts in Computational Science and Engineering*, vol. 5. Springer, New York (2007)
156. Groot, R.D.: Applications of dissipative particle dynamics. In: *Novel Methods in Soft Matter Simulations*, pp. 5–38. Springer, New York (2004). doi:[10.1007/978-3-540-39895-0_1](https://doi.org/10.1007/978-3-540-39895-0_1)
157. Groot, R.D., Warren, P.B.: Dissipative particle dynamics: bridging the gap between atomistic and mesoscopic simulation. *J. Chem. Phys.* **107**, 4423 (1997). doi:[10.1063/1.474784](https://doi.org/10.1063/1.474784)
158. Grubmüller, H., Heller, H., Windemuth, A., Schulten, K.: Generalized Verlet algorithm for efficient molecular dynamics simulations with long-range interactions. *Mol. Simul.* **6**, 121–142 (1991). doi:[10.1080/08927029108022142](https://doi.org/10.1080/08927029108022142)
159. Haile, J.: *Molecular Dynamics Simulation: Elementary Methods*. Wiley, New York (1997). ISBN:978-0471184393
160. Hairer, M.: A probabilistic argument for the controllability of conservative systems. <http://arxiv.org/pdf/math-ph/0506064.pdf> (2008). Unpublished
161. Hairer, M.: Convergence of Markov processes. The canonical distribution and stochastic differential equations (2010). Unpublished
162. Hairer, E.: Lecture notes on geometric numerical integration (2010). http://www.unige.ch/~hairer/poly_geoint/week3.pdf
163. Hairer, E., Lubich, C.: The lifespan of backward error analysis for numerical integrators. *Numer. Math.* **76**, 441–462 (1997). doi:[10.1007/s002110050271](https://doi.org/10.1007/s002110050271)
164. Hairer, E., Lubich, C., Wanner, G.: *Geometric Numerical Integration: Structure-Preserving Algorithms for Ordinary Differential Equations*, Springer Series in Computational Mathematics, vol. 31. Springer, New York (2006). ISBN:978-3-540-30666-5
165. Hairer, M., Mattingly, J.C.: Yet Another Look at Harris' Ergodic Theorem for Markov Chains. In: Dalang, R., Dozzi, M. and Russo, F. (eds) *Seminar on Stochastic Analysis, Random Fields and Applications VI*. Springer Basel **63**, 109–117 (2011). doi:[10.1007/978-3-0348-0021-1_7](https://doi.org/10.1007/978-3-0348-0021-1_7) ISBN:978-3034800204
166. Hairer, E., McLachlan, R., Skeel, R.D.: On energy conservation of the simplified Takahashi-Imada method. *Math. Model. Numer. Anal.* **43**, 631–644 (2009). doi:[10.1051/m2an/2009019](https://doi.org/10.1051/m2an/2009019)
167. Hairer, E., Nørsett, S., Wanner, G.: *Solving Ordinary Differential Equations I: Nonstiff Problems*, 2nd edn. Springer (2009). ISBN:978-3642051630
168. Hansen, J.P., McDonald, I.R.: *Theory of Simple Liquids*, 2nd edn. Academic, New York (1986)
169. Hansson, T., Oostenbrink, C., van Gunsteren, W.: Molecular dynamics simulations. *Curr. Opin. Struct. Biol.* **12**(2), 190–196 (2002). doi:[10.1016/S0959-440X\(02\)00308-1](https://doi.org/10.1016/S0959-440X(02)00308-1)
170. Hardy, D.: NAMD-Lite. University of Illinois at Urbana-Champaign, <http://www.ks.uiuc.edu/Development/MDTools/namdlite/> (2007)
171. Hartmann, C.: Model reduction in classical molecular dynamics. Ph.D. thesis, Fachbereich Mathematik und Informatik, Freie Universität Berlin (2007)
172. Harvey, S.C., Tan, R.K.Z., Cheatham, T.E.: The flying ice cube: velocity rescaling in molecular dynamics leads to violation of energy equipartition. *J. Comput. Chem.* **19**(7), 726–740 (1998). doi:[10.1002/\(SICI\)1096-987X\(199805\)19:7<726::AID-JCC4>3.0.CO;2-S](https://doi.org/10.1002/(SICI)1096-987X(199805)19:7<726::AID-JCC4>3.0.CO;2-S)
173. Heinz, N., Huenenberger, P.: A fast pairlist-construction algorithm for molecular simulations under periodic boundary conditions. *J. Comput. Chem.* **25**, 1474–1486 (2004). doi:[10.1002/jcc.20071](https://doi.org/10.1002/jcc.20071)

174. Hénon, M.: Numerical exploration of Hamiltonian systems. In: Iooss, G. (ed.) *Chaotic Behaviour of Deterministic Systems*, pp. 53–170. Elsevier Science Ltd., New York (1983) ISBN:978-0444865427
175. Hess, B., Bekker, H., Berendsen, H., Fraaije, J.: LINCS: A linear constraint solver for molecular simulations. *J. Comput. Chem.* **18**, 1463–1472 (1997). doi:[10.1002/\(SICI\)1096-987X\(199709\)18:12<1463::AID-JCC4>3.0.CO;2-H](https://doi.org/10.1002/(SICI)1096-987X(199709)18:12<1463::AID-JCC4>3.0.CO;2-H)
176. Heyes, D.M.: Molecular dynamics simulations of restricted primitive model 1:1 electrolytes. *Chem. Phys.* **69**, 155–163 (1982). doi:[10.1016/0301-0104\(82\)88142-1](https://doi.org/10.1016/0301-0104(82)88142-1)
177. Hirsch, M., Smale, S., Devaney, R.: *Differential Equations, Dynamical Systems and an Introduction to Chaos*, 3rd edn. Academic, New York (2012). ISBN:978-0123820105
178. Hoare, M.: Structure and dynamics of simple microclusters. *Adv. Chem. Phys.* **40**, 49–135 (1979). doi:[10.1002/9780470142592.ch2](https://doi.org/10.1002/9780470142592.ch2)
179. Hockney, R., Eastwood, J.: *Computer Simulation Using Particles*. Taylor and Francis, Bristol (1988). ISBN:978-0852743928
180. Holian, B., Voter, A., Ravelo, R.: Thermostatted molecular dynamics: how to avoid the Toda demon hidden in Nosé-Hoover dynamics. *Phys. Rev. E* **52**, 2338–2347 (1995). doi:[10.1103/PhysRevE.52.2338](https://doi.org/10.1103/PhysRevE.52.2338)
181. Hoogerbrugge, P., Koelman, J.: Simulating microscopic hydrodynamic phenomena with dissipative particle dynamics. *Europhys. Lett.* **19**, 155 (1992). doi:[10.1209/0295-5075/19/3/001](https://doi.org/10.1209/0295-5075/19/3/001)
182. Hoover, W.: Canonical dynamics: equilibrium phase-space distributions. *Phys. Rev. A* **31**, 1695–1697 (1985). doi:[10.1103/PhysRevA.31.1695](https://doi.org/10.1103/PhysRevA.31.1695)
183. Hoover, W.: Constant-pressure equations of motion. *Phys. Rev. A* **34**, 2499–2500 (1986). doi:[10.1103/PhysRevA.34.2499](https://doi.org/10.1103/PhysRevA.34.2499)
184. Hounoungbo, Y., Laird, B., Leimkuhler, B.: A molecular dynamics algorithm for mixed hard-core/continuous potentials. *Mol. Phys.* **98**, 309–316 (2000). doi:[10.1080/00268970009483294](https://doi.org/10.1080/00268970009483294)
185. Huisingsa, W., Schütte, C., Stuart, A.: Extracting macroscopic stochastic dynamics: model problems. *Commun. Pure Appl. Math.* **56**, 234 (2003). doi:[10.1002/cpa.10057](https://doi.org/10.1002/cpa.10057)
186. Hünenberger, P.H.: Thermostat algorithms for molecular dynamics simulations. In: *Advanced Computer Simulation*, pp. 105–149. Springer, New York (2005). doi:[10.1007/b99427](https://doi.org/10.1007/b99427)
187. Isgro, T.A., Sotomayor, M., Cruz-Chu, E.: Case study: water and ice. <http://www.ks.uiuc.edu/Training/CaseStudies/pdfs/water-1.pdf>. Accessed 14 Oct 2014
188. Izaguirre, J., Hampton, S.: Shadow hybrid Monte Carlo: an efficient propagator in phase space of macromolecules. *J. Comput. Phys.* **200**(2), 581–604 (2004). doi:[10.1016/j.jcp.2004.04.016](https://doi.org/10.1016/j.jcp.2004.04.016)
189. Izaguirre, J., Reich, S., Skeel, R.: Longer timesteps for molecular dynamics. *J. Chem. Phys.* **110**, 9853–9865 (1999). doi:[10.1063/1.478995](https://doi.org/10.1063/1.478995)
190. Jain, A., Vaidehi, N., Rodriguez, G.: A fast recursive algorithm for molecular dynamics simulation. *J. Comput. Phys.* **106**, 258–268 (1993). doi:[10.1016/S0021-9991\(83\)71106-X](https://doi.org/10.1016/S0021-9991(83)71106-X)
191. Jakobsen, A.F., Besold, G., Mouritsen, O.G.: Multiple time step update schemes for dissipative particle dynamics. *J. Chem. Phys.* **124**, 094,104 (2006). doi:[10.1063/1.2167645](https://doi.org/10.1063/1.2167645)
192. Jang, S., Voth, G.: Simple reversible molecular dynamics algorithms for Nosé-Hoover chain dynamics. *J. Chem. Phys.* **107**(22), 9514–9526 (1997). doi:[10.1063/1.475247](https://doi.org/10.1063/1.475247)
193. Jepps, O., Ayton, G., Evans, D.: Microscopic expressions for the thermodynamic temperature. *Phys. Rev. E* **62**, 4757–4763 (2000). doi:[10.1103/PhysRevE.62.4757](https://doi.org/10.1103/PhysRevE.62.4757)
194. Kalibaeva, G., Ferrario, M., Ciccotti, G.: Constant pressure-constant temperature molecular dynamics: a correct constrained NPT ensemble using the molecular virial. *Mol. Phys.* **101**, 765 (2003). doi:[10.1080/0026897021000044025](https://doi.org/10.1080/0026897021000044025)
195. Kaur, N., Gupta, S., Dharamvir, K., Jindal, V.: The formation of dimerized molecules of C60 and their solids. *Carbon* **46**, 349–358 (2008). doi:[10.1016/j.carbon.2007.12.001](https://doi.org/10.1016/j.carbon.2007.12.001)
196. Khalilullin, R., Eshet, H., Kühne, T., Behler, J., Parrinello, M.: Nucleation mechanism for the direct graphite-to-diamond phase transition. *Nat. Mater.* **10**, 693–697 (2011). doi:[10.1038/nmat3078](https://doi.org/10.1038/nmat3078)

197. Khinchin, A.: Mathematical Foundations of Statistical Mechanics. Dover, New York (1949). ISBN:978-0486138732
198. Kim, S.: Brownian motion in assemblies of coupled harmonic oscillators. *J. Math. Phys.* **15**, 578 (1974). doi:[10.1063/1.1666687](https://doi.org/10.1063/1.1666687)
199. Klein, P.: Pressure and temperature control in molecular dynamics simulation: a unitary approach in discrete time. *Model. Simul. Mater. Sci. Eng.* **6**, 405–422 (1998). doi:[10.1088/0955-0393/6/4/009](https://doi.org/10.1088/0955-0393/6/4/009)
200. Kloeden, P., Platen, E.: Numerical Solution of Stochastic Differential Equations. Applications of Mathematics. Springer, New York (1992). ISBN:978-3540540625
201. Kol, A., Laird, B., Leimkuhler, B.: A symplectic method for rigid-body molecular simulation. *J. Chem. Phys.* **107**, 2580–2588 (1997). doi:[10.1063/1.474596](https://doi.org/10.1063/1.474596)
202. Kubo, R.: The fluctuation-dissipation theorem. *Rep. Prog. Phys.* **29**, 255–284 (1966). doi:[10.1088/0034-4885/29/1/306](https://doi.org/10.1088/0034-4885/29/1/306)
203. Kunaseth, M., Kalia, R., Nakano, A., Nomura, K., Vashishta, P.: A scalable parallel algorithm for dynamic range-limited n-tuple computation in many-body molecular dynamics simulation. In: Proceedings of SC13: International Conference for High Performance Computing, Networking, Storage and Analysis, SC '13, pp. 71:1–71:12. Association of Computing Machinery, New York (2013). doi:[10.1145/2503210.2503235](https://doi.org/10.1145/2503210.2503235)
204. Kupferman, R.: Fractional kinetics in Kac-Zwanzig heat bath models. *J. Stat. Phys.* **114**, 291–326 (2004). doi:[10.1023/B:JOSS.0000003113.22621.f0](https://doi.org/10.1023/B:JOSS.0000003113.22621.f0)
205. Kupferman, R., Stuart, A., Terry, J., Tupper, P.: Long term behavior of large mechanical systems with random initial data. *Stochastics Dyn.* **2**, 533 (2002). doi:[10.1142/S0219493702000571](https://doi.org/10.1142/S0219493702000571)
206. Kuptsov, L.: Brachistochrone. In: Encyclopedia of Mathematics. Springer, New York (2001). ISBN:978-1-556080104
207. Laio, A., Gervasio, F.L.: Metadynamics: a method to simulate rare events and reconstruct the free energy in biophysics, chemistry and material science. *Rep. Prog. Phys.* **71**(12), 126,601 (2008). doi:[10.1088/0034-4885/71/12/126601](https://doi.org/10.1088/0034-4885/71/12/126601)
208. Laio, A., Parrinello, M.: Escaping free-energy minima. *Proc. Natl. Acad. Sci.* **99**(20), 12,562–12,566 (2002). doi:[10.1073/pnas.202427399](https://doi.org/10.1073/pnas.202427399)
209. Lamb, J.: Area-preserving dynamics that is not reversible. *Phys. A* **228** (1996). doi:[10.1016/0378-4371\(95\)00430-0](https://doi.org/10.1016/0378-4371(95)00430-0)
210. Lanczos, C.: The Variational Principles of Mechanics. Dover Books on Physics. Dover, New York (1986)
211. Landau, L.D., and Lifshitz, E.M., *Statistical Physics (Volume 5, Course of Theoretical Physics)*, Third Edition, Butterworth-Heinemann (1980), ISBN: 978-0-750-63372-7.
212. Landau, L., Lifshitz, E.: Course in Theoretical Physics, Vol I: Mechanics. Pergamon, Oxford (1976). ISBN:978-0750628969
213. Langevin, P.: Sur la théorie de mouvement brownien. *C.R. Acad. Sci. Paris* **146**, 530–533 (1908)
214. Lasagni, F.M.: Canonical runge-kutta methods. *Zeitschrift für Angewandte Mathematik und Physik* **39**, 952–953 (1988). doi:[10.1007/BF00945133](https://doi.org/10.1007/BF00945133)
215. Leach, A.R.: Molecular Modelling: Principles and Applications. Pearson Education. Prentice Hall, London (2001)
216. Lebovitz, N.: Ordinary Differential Equations. Brooks/Cole, Pacific Grove, CA (1999). ISBN:978-0534365523
217. Legoll, F., Luskin, M., Moeckel, R.: Non-ergodicity of the Nosé-Hoover thermostatted harmonic oscillator. *Arch. Ration. Mech. Anal.* **184**, 449–463 (2007). doi:[10.1007/s00205-006-0029-1](https://doi.org/10.1007/s00205-006-0029-1)
218. Legoll, F., Luskin, M., Moeckel, R.: Non-ergodicity of Nosé-Hoover dynamics. *Nonlinearity* **22**, 1673–1694 (2009). doi:[10.1088/0951-7715/22/7/011](https://doi.org/10.1088/0951-7715/22/7/011)
219. Lei, H., Caswell, B., Karniadakis, G.E.: Direct construction of mesoscopic models from microscopic simulations. *Phys. Rev. E* **81**(2) (2010). doi:[10.1103/physreve.81.026704](https://doi.org/10.1103/physreve.81.026704)

220. Leimkuhler, B., Margul, D., Tuckerman, M.: Stochastic, resonance-free multiple time-step algorithm for molecular dynamics with very large time steps. *Mol. Phys.* **111**, 3579–3594 (2013). doi:[10.1080/00268976.2013.844369](https://doi.org/10.1080/00268976.2013.844369)
221. Leimkuhler, B., Matthews, C.: Rational construction of stochastic numerical methods for molecular sampling. *Appl. Math. Res. Express* **1**, 4–56 (2013). doi:[10.1093/amrx/abs010](https://doi.org/10.1093/amrx/abs010)
222. Leimkuhler, B., Matthews, C.: Robust and efficient configurational molecular sampling via Langevin dynamics. *J. Chem. Phys.* **138**, 174,102 (2013). doi:[10.1063/1.4802990](https://doi.org/10.1063/1.4802990)
223. Leimkuhler, B., Matthews, C. and Stoltz G.: The computation of averages from equilibrium and nonequilibrium Langevin molecular dynamics. *IMA J Numer Anal* (2015). doi:[10.1093/imanum/dru056](https://doi.org/10.1093/imanum/dru056)
224. Leimkuhler, B., Matthews, C., Tretyakov, M.V.: On the long-time integration of stochastic gradient systems. *Proc. R. Soc. A* **470**(2170) (2014). doi:[10.1098/rspa.2014.0120](https://doi.org/10.1098/rspa.2014.0120)
225. Leimkuhler, B., Noorizadeh, E., Penrose, O.: Comparing the efficiencies of stochastic isothermal molecular dynamics methods. *J. Stat. Phys.* **143**, 921–942 (2011). doi:[10.1007/s10955-011-0210-2](https://doi.org/10.1007/s10955-011-0210-2)
226. Leimkuhler, B., Noorizadeh, E., Theil, F.: A gentle stochastic thermostat for molecular dynamics. *J. Stat. Phys.* **135**, 261–277 (2009). doi:[10.1007/s10955-009-9734-0](https://doi.org/10.1007/s10955-009-9734-0)
227. Leimkuhler, B., Reich, S.: *Simulating Hamiltonian Dynamics*. Cambridge University Press, Cambridge (2005). doi:[10.1017/CBO9780511614118](https://doi.org/10.1017/CBO9780511614118). ISBN:978-0521772907
228. Leimkuhler, B., Shang, X.: On the numerical treatment of dissipative particle dynamics and related systems. *J. Comput. Phys.* **280**, 72–95 (2015). doi:[10.1016/j.jcp.2014.09.008](https://doi.org/10.1016/j.jcp.2014.09.008)
229. Leimkuhler, B., Skeel, R.: Symplectic numerical integrators in constrained Hamiltonian systems. *J. Comput. Phys.* **112**, 117–125 (1994). doi:[10.1006/jcph.1994.1085](https://doi.org/10.1006/jcph.1994.1085)
230. Leimkuhler, B., Sweet, C.: A Hamiltonian formulation for recursive multiple thermostats in a common timescale. *SIAM J. Appl. Dyn. Syst.* **4**, 187–216 (2005). doi:[10.1137/040606090](https://doi.org/10.1137/040606090)
231. Lelièvre, T., Rousset, M., Stoltz, G.: Long-time convergence of an adaptive biasing force method. *Nonlinearity* **21**(6) (2008). doi:[10.1088/0951-7715/21/6/001](https://doi.org/10.1088/0951-7715/21/6/001)
232. Lelièvre, T., Rousset, M., Stoltz, G.: Langevin dynamics with constraints and computation of free energy differences. *Math. Comput.* **81**, 2071 (2012). doi:[10.1090/S0025-5718-2012-02594-4](https://doi.org/10.1090/S0025-5718-2012-02594-4)
233. Lelièvre, T., Stoltz, G., Rousset, M.: *Free Energy Computations: A Mathematical Perspective*. World Scientific, Singapore (2010)
234. LeSar, R.: *Introduction to Computational Materials Science*. Cambridge University Press, Cambridge (2013). ISBN:9780521845878
235. Leyendecker, S., Hartmann, C., Koch, M.: Variational collision integrator for polymer chains. *J. Comput. Phys.* **231**, 3896–3911 (2012). doi:[10.1016/j.jcp.2012.01.017](https://doi.org/10.1016/j.jcp.2012.01.017)
236. Lindahl, E., Hess, B., van der Spoel, D.: GROMACS 3.0: a package for molecular simulation and trajectory analysis. *J. Mol. Model.* **7**, 306–317 (2001). doi:[10.1007/s008940100045](https://doi.org/10.1007/s008940100045). <http://www.gromacs.org>
237. Lippert, R., Bowers, K., Dror, R., Eastwood, M., Gregersen, B., Klepeis, J., Kolossvary, I., Shaw, D.: A common, avoidable source of error in molecular dynamics integrators. *J. Chem. Phys.* **126**, 046,101–1 (2007). doi:[10.1063/1.2431176](https://doi.org/10.1063/1.2431176)
238. Lippert, R., Predescu, C., Ierardi, D., Mackenzie, K., Eastwood, M., Dror, R., Shaw, D.: Accurate and efficient integration for molecular dynamics simulations at constant temperature and pressure. *J. Chem. Phys.* **139**, 164,106 (2013). doi:[10.1063/1.4825247](https://doi.org/10.1063/1.4825247)
239. López-Marcos, M., Sanz-Serna, J., Skeel, R.: Explicit symplectic integrators using hessian–vector products. *SIAM J. Sci. Comput.* **18**, 223–238 (1997). doi:[10.1137/S1064827595288085](https://doi.org/10.1137/S1064827595288085)
240. Lopreore, C., Wyatt, R.: Quantum wave packet dynamics with trajectories. *Phys. Rev. Lett.* **82**, 5190–5193 (1999). doi:[10.1103/PhysRevLett.82.5190](https://doi.org/10.1103/PhysRevLett.82.5190)
241. Lowe, C.: An alternative approach to dissipative particle dynamics. *Europhys. Lett.* **47**(2), 145 (1999). doi:[10.1209/epl/i1999-00365-x](https://doi.org/10.1209/epl/i1999-00365-x)

242. Lupo, J.A., Wang, Z., McKenney, A.M., Pachter, R., Mattson, W.: A large scale molecular dynamics simulation code using the fast multipole algorithm (FMD): performance and application. *J. Mol. Graph. Model.* **21**(2), 89–99 (2002). doi:[10.1016/S1093-3263\(02\)00125-0](https://doi.org/10.1016/S1093-3263(02)00125-0)
243. Luskin, M., Ortner, C.: Atomistic-to-continuum-coupling. *Acta Numerica* (2013). doi:[10.1017/S0962492913000068](https://doi.org/10.1017/S0962492913000068)
244. Lyubartsev, A., Laaksonen, A.: Calculation of effective interaction potentials from radial distribution functions: a reverse Monte Carlo approach. *Phys. Rev. E* **52**(4), 3730–3737 (1995). doi:[10.1103/physreve.52.3730](https://doi.org/10.1103/physreve.52.3730)
245. Ma, Q., Izaguirre, J., Skeel, R.: Verlet-I/r-RESPA/Impulse is limited by nonlinear instabilities. *SIAM J. Sci. Comput.* **24**, 1951–1973 (2003). doi:[10.1137/S1064827501399833](https://doi.org/10.1137/S1064827501399833)
246. MacKerell Jr., A., Brooks III, C., Nilsson, L., Roux, B., Won, Y., Karplus, M.: CHARMM: The Energy Function and Its Parameterization with an Overview of the Program. *The Encyclopedia of Computational Chemistry*, vol. 1, pp. 271–277. Wiley, Chichester (1998). <http://www.charmm.org>
247. Mandziuk, M., Schlick, T.: Resonance in the dynamics of chemical systems simulated by the implicit midpoint scheme. *Chem. Phys. Lett.* **237**, 525–535 (1995). doi:[10.1016/0009-2614\(95\)00316-V](https://doi.org/10.1016/0009-2614(95)00316-V)
248. Marry, V., Ciccotti, G.: Trotter derived algorithms for molecular dynamics with constraints: velocity Verlet revisited. *J. Comput. Phys.* **222**, 428–440 (2007). doi:[10.1016/j.jcp.2006.07.033](https://doi.org/10.1016/j.jcp.2006.07.033)
249. Marsden, J., Ratiu, T.: *Mechanics and Symmetry*, 2nd edn. Springer, New York (1998). ISBN:978-0387986432
250. Martin, M.G., Siepmann, J.I.: Transferable potentials for phase equilibria. I. united-atom description of n-alkanes. *J. Phys. Chem. B* **102**(14), 2569–2577 (1998). doi:[10.1021/jp972543+](https://doi.org/10.1021/jp972543+)
251. Martyna, G., Klein, M., Tuckerman, M.: Nosé-Hoover chains: the canonical ensemble via continuous dynamics. *J. Chem. Phys.* **97**, 2635–2643 (1992). doi:[10.1063/1.463940](https://doi.org/10.1063/1.463940)
252. Martyna, G., Tobias, D., Klein, M.: Constant-pressure molecular dynamics algorithms. *J. Chem. Phys.* **101**, 4177–4189 (1994). doi:[10.1063/1.467468](https://doi.org/10.1063/1.467468)
253. Martyna, G., Tuckerman, M., Tobias, D., Klein, M.: Explicit reversible integrators for extended systems dynamics. *Mol. Phys.* **87**(5), 1117–1157 (1996). doi:[10.1080/00268979600100761](https://doi.org/10.1080/00268979600100761)
254. Martyna, G.J.: Remarks on “constant-temperature molecular dynamics with momentum conservation”. *Phys. Rev. E* **50**, 3234–3236 (1994). doi:[10.1103/PhysRevE.50.3234](https://doi.org/10.1103/PhysRevE.50.3234)
255. Mathiowetz, A., Jain, A., Karasawa, N., III, W.G.: Protein simulations using techniques suitable for very large systems: the cell multipole method for nonbond interactions and the Newton-Euler inverse mass operator method for internal coordinate dynamics. *Proteins* **20**, 227–247 (1994). doi:[10.1002/prot.340200304](https://doi.org/10.1002/prot.340200304)
256. Mattingly, J., Stuart, A.: Geometric ergodicity of some hypo-elliptic diffusions for particle motions. *Markov Process. Relat. Fields* **8**, 199–214 (2002)
257. Mattingly, J., Stuart, A., Higham, D.: Ergodicity for SDEs and approximations: locally Lipschitz vector fields and degenerate noise. *Stochastic Process. Appl.* **101**, 185–232 (2002). doi:[10.1016/S0304-4149\(02\)00150-3](https://doi.org/10.1016/S0304-4149(02)00150-3)
258. McLachlan, R.: Explicit Lie-Poisson integration and the Euler equations. *Phys. Rev. Lett.* **71**, 3043–3046 (1993). doi:[10.1103/PhysRevLett.71.3043](https://doi.org/10.1103/PhysRevLett.71.3043)
259. McLachlan, R.: Composition methods in the presence of small parameters. *BIT Numer. Math.* **35**, 258–268 (1995). doi:[10.1007/BF01737165](https://doi.org/10.1007/BF01737165)
260. McLachlan, R.: On the numerical integration of ordinary differential equations by symmetric composition methods. *SIAM J. Sci. Comput.* **16**, 151–168 (1995). doi:[10.1137/0916010](https://doi.org/10.1137/0916010)
261. McLachlan, R., Quispel, G.: Geometric integration of conservative polynomial ODEs. *Appl. Numer. Math.* **45**, 411–418 (2003). doi:[10.1016/S0168-9274\(03\)00022-9](https://doi.org/10.1016/S0168-9274(03)00022-9)
262. McLachlan, R., Quispel, G.R.W.: Splitting methods. *Acta Numerica* **11**, 341–434 (2002)

263. McNeil, W.J., Madden, W.G.: A new method for the molecular dynamics simulation of hard core molecules. *J. Chem. Phys.* **76**(12), 6221–6226 (1982). doi:[10.1063/1.443025](https://doi.org/10.1063/1.443025)
264. McQuarrie, D.A.: Statistical Mechanics. Harper and Row, New York (1976)
265. Melchionna, S.: Design of quasisymplectic propagators for Langevin dynamics. *J. Chem. Phys.* **127**(4), 044108 (2007). doi:[10.1063/1.2753496](https://doi.org/10.1063/1.2753496)
266. Melchionna, S., Ciccotti, G., Holian, B.: Hoover NPT dynamics for systems varying in shape and size. *Mol. Phys.* **78**(3), 533–544 (1993). doi:[10.1080/00268979300100371](https://doi.org/10.1080/00268979300100371)
267. Menyuk, C.: Some properties of the discrete Hamiltonian method. *Physica D* **11**, 109–129 (1984). doi:[10.1016/0167-2789\(84\)90438-X](https://doi.org/10.1016/0167-2789(84)90438-X)
268. Metropolis, N., Rosenbluth, A., Rosenbluth, M., Teller, A., Teller, E.: Equation of state calculations by fast computing machines. *J. Chem. Phys.* **21**, 1087–1091 (1953). doi:[10.1063/1.1699114](https://doi.org/10.1063/1.1699114)
269. Meyn, S., Tweedie, R.: Markov Chains and Stochastic Stability. Cambridge Mathematical Library, 2nd edn. Cambridge University Press, Cambridge (2009). ISBN:9781139477970
270. Milstein, G., Tretyakov, M.: Stochastic Numerics for Mathematical Physics. Springer, New York (2004). doi:[10.1007/978-3-662-10063-9](https://doi.org/10.1007/978-3-662-10063-9)
271. Minary, P., Martyna, G.J., Tuckerman, M.E.: Algorithms and novel applications based on the isokinetic ensemble. i. Biophysical and path integral molecular dynamics. *J. Chem. Phys.* **118**, 2510 (2003). doi:[10.1063/1.1534582](https://doi.org/10.1063/1.1534582)
272. Minary, P., Tuckerman, M.E., Martyna, G.J.: Long time molecular dynamics for enhanced conformational sampling in biomolecular systems. *Phys. Rev. Lett.* **93**, 150,201 (2004). doi:[10.1103/PhysRevLett.93.150201](https://doi.org/10.1103/PhysRevLett.93.150201)
273. Mirsky, L.: An Introduction to Linear Algebra. Dover Books on Mathematics Series. Dover, New York (1990)
274. Miyamoto, S., Kollman, P.: Settle: An analytical version of the SHAKE and RATTLE algorithm for rigid water models. *J. Comput. Chem.* **13**, 952–962 (1992). doi:[10.1002/jcc.540130805](https://doi.org/10.1002/jcc.540130805)
275. Moler, C., Van Loan, C.: Nineteen dubious ways to compute the exponential of a matrix, twenty-five years later. *SIAM Rev.* **45**(1), 3–49 (2003). doi:[10.1137/S00361445024180](https://doi.org/10.1137/S00361445024180)
276. Mori, H.: Transport, collective motion, and Brownian motion. *Progress Theor. Phys.* **33**, 423–455 (1965). doi:[10.1143/PTP.33.423](https://doi.org/10.1143/PTP.33.423)
277. Murua, A., Sanz-Serna, J.: Order conditions for numerical integrators obtained by composing simpler integrators. *Philos. Trans. R. Soc. Lond. A* **357**, 1079–1100 (1999). doi:[10.1098/rsta.1999.0365](https://doi.org/10.1098/rsta.1999.0365)
278. Neal, R.: MCMC using Hamiltonian dynamics. In: Handbook of Markov Chain Monte Carlo, pp. 113–162. Chapman and Hall, Boca Raton (2011)
279. Nelson, E.: Dynamical Theories of Brownian Motion, 2nd edn. Princeton University Press, Princeton (2001). <https://web.math.princeton.edu/~nelson/books/bmotion.pdf>
280. Newmark, N.: A method of computation for structural dynamics. *J. Eng. Mech. ASCE* **85**, 67–94 (1959)
281. Nikunen, P., Karttunen, M., Vattulainen, I.: How would you integrate the equations of motion in dissipative particle dynamics simulations? *Comput. Phys. Commun.* **153**(3), 407–423 (2003). doi:[10.1016/S0010-4655\(03\)00202-9](https://doi.org/10.1016/S0010-4655(03)00202-9)
282. Noé, F., Schütte, C., Vandenh-Eijnden, E., Reich, L., T.Weikl: Constructing the equilibrium ensemble of folding pathways from short off-equilibrium simulations. *Proc. Natl. Acad. Sci.* **106**, 19,011–19,016 (2009). doi:[10.1073/pnas.0905466106](https://doi.org/10.1073/pnas.0905466106)
283. Noorizadeh, E.: Highly degenerate diffusions for sampling molecular systems. Ph.D. thesis, University of Edinburgh (2009)
284. Nosé, S.: A molecular dynamics method for simulations in the canonical ensemble. *Mol. Phys.* **52**(2), 255–268 (1984). doi:[10.1080/00268978400101201](https://doi.org/10.1080/00268978400101201)
285. Nosé, S.: A unified formulation of the constant temperature molecular dynamics methods. *J. Chem. Phys.* **81**, 511–519 (1984). doi:[10.1063/1.447334](https://doi.org/10.1063/1.447334)
286. Nosé, S.: Constant temperature molecular dynamics methods. *Prog. Theor. Phys. Supp.* **103**, 1–46 (1991). doi:[10.1143/PTPS.103.1](https://doi.org/10.1143/PTPS.103.1)

287. Nosé, S.: An improved symplectic integrator for Nosé-Poincaré thermostat. *J. Phys. Soc. Jpn.* **70**, 75–77 (2001). doi:[10.1143/JPSJ.70.75](https://doi.org/10.1143/JPSJ.70.75)
288. Nosé, S., Klein, M.: Constant pressure molecular dynamics for molecular systems. *Mol. Phys.* **50**, 1055–1076 (1983). doi:[10.1080/00268978300102851](https://doi.org/10.1080/00268978300102851)
289. Øksendal, B.: *Stochastic Differential Equations: An Introduction with Applications*. Hochschultext/Universitext. Springer, New York (2003). ISBN:978-3540047582
290. Okunbor, D., Skeel, R.: Explicit canonical methods for Hamiltonian systems. *Math. Comput.* **59**, 439–455 (1992). doi:[10.1090/S0025-5718-1992-1136225-3](https://doi.org/10.1090/S0025-5718-1992-1136225-3)
291. Onufriev, A., Bashford, D., Case, D.A.: Modification of the Generalized Born model suitable for macromolecules. *J. Phys. Chem. B* **104**, 3712–3720 (2000). doi:[10.1021/jp994072s](https://doi.org/10.1021/jp994072s)
292. Ortega, J., Rheinboldt, W.: *Iterative Solution of Nonlinear Equations in Several Variables*. SIAM, Philadelphia (1970). ISBN:978-0898714616
293. Otto, M., Pavliotis, G.: Asymptotic analysis for the generalized Langevin equation. *Nonlinearity* **24**, 1629–1653 (2011). doi:[10.1088/0951-7715/24/5/013](https://doi.org/10.1088/0951-7715/24/5/013)
294. Paesani, F., Zhang, W., Case, D., Cheatham, T., Voth, G.: An accurate and simple quantum model for liquid water. *J. Chem. Phys.* **125**, 184,507 (2006). doi:[10.1063/1.2386157](https://doi.org/10.1063/1.2386157)
295. Pagonabarraga, I., Hagen, M., Frenkel, D.: Self-consistent dissipative particle dynamics algorithm. *Europhys. Lett.* **42**(4), 377 (1998). doi:[10.1209/epl/i1998-00258-6](https://doi.org/10.1209/epl/i1998-00258-6)
296. Parrinello, M., Rahman, A.: Polymorphic transitions in single crystals: A new molecular dynamics method. *J. Appl. Phys.* **52**, 7182–7190 (1981). doi:[10.1063/1.328693](https://doi.org/10.1063/1.328693)
297. Pathria, R.: *Statistical Mechanics*, 2nd edn. Butterworth-Heinemann, Oxford (1996). ISBN:978-0750624695
298. Pavliotis, G.A.: *Stochastic Processes and Applications*. Springer, New York (2014), ISBN 978-1-4939-1323-7
299. Peters, E.: Elimination of time step effects in DPD. *Europhys. Lett.* **66**(3), 311 (2004). doi:[10.1209/epl/i2004-10010-4](https://doi.org/10.1209/epl/i2004-10010-4)
300. Pettifor, D., Oleinik, I.: Analytic bond-order potentials beyond Tersoff-Brenner. i. Theory. *Phys. Rev. B* **59**, 8487–8499 (1999). doi:[10.1103/PhysRevB.59.8487](https://doi.org/10.1103/PhysRevB.59.8487)
301. Phillips, C.L., Anderson, J.A., Glotzer, S.C.: Pseudo-random number generation for Brownian dynamics and dissipative particle dynamics simulations on GPU devices. *J. Comput. Phys.* **230**(19), 7191–7201 (2011). doi:[10.1016/j.jcp.2011.05.021](https://doi.org/10.1016/j.jcp.2011.05.021)
302. Phillips, J., Braun, R., Wang, W., Gumbart, J., Tajkhorshid, E., Villa, E., Chipot, C., Skeel, R., Kalé, L., Schulten, K.: Scalable molecular dynamics with NAMD. *J. Comput. Chem.* **26**(16), 1781–1802 (2005). doi:[10.1002/jcc.20289](https://doi.org/10.1002/jcc.20289). <http://www.ks.uiuc.edu/Research/namd/>
303. Plimpton, S.: Fast parallel algorithms for short-range molecular dynamics. *J. Comput. Phys.* **117**(1), 1–19 (1995). doi:[10.1006/jcph.1995.1039](https://doi.org/10.1006/jcph.1995.1039). <http://lammps.sandia.gov>
304. Poincaré, H.: *Science et Méthode*. Flammarion, Paris (1908)
305. Price, S.L.: *Toward More Accurate Model Intermolecular Potentials for Organic Molecules*, pp. 225–289. Wiley, New York (2007). doi:[10.1002/9780470125915.ch4](https://doi.org/10.1002/9780470125915.ch4)
306. Rahman, A.: Correlations in the motion of atoms in liquid argon. *Phys. Rev.* **136**, A405–A411 (1964). doi:[10.1103/PhysRev.136.A405](https://doi.org/10.1103/PhysRev.136.A405)
307. Rapaport, D.: *The Art of Molecular Dynamics Simulation*. Cambridge University Press, Cambridge (2004). ISBN:978-0521825689
308. Reich, S.: Enhancing energy conserving methods. *BIT* **36**, 122–134 (1996). doi:[10.1007/BF01740549](https://doi.org/10.1007/BF01740549)
309. Reich, S.: On higher-order semi-explicit symplectic partitioned Runge-Kutta methods for constrained Hamiltonian systems. *Numer. Math.* **76**, 231–247 (1997). doi:[10.1007/s002110050261](https://doi.org/10.1007/s002110050261)
310. Reich, S.: Backward error analysis for numerical integrators. *SIAM J. Numer. Anal.* **36**, 1549–1570 (1999). doi:[10.1137/S0036142997329797](https://doi.org/10.1137/S0036142997329797)
311. Ricci, A., Ciccotti, G.: Algorithms for Brownian dynamics. *Mol. Phys.* **101**(12), 1927–1931 (2003). doi:[10.1080/0026897031000108113](https://doi.org/10.1080/0026897031000108113)
312. Robert, C., Casella, G.: *Monte Carlo Statistical Methods*, 2nd edn. Springer, New York (2005)

313. Roberts, G., Tweedie, R.: Exponential convergence of Langevin distributions and their discrete approximations. *Bernoulli* **2**, 341–363 (1996). doi:[10.2307/3318418](https://doi.org/10.2307/3318418)
314. Rogers, L., Williams, D.: *Diffusions, Markov Processes, and Martingales*, 2nd edn. Cambridge University Press, Cambridge (2000). ISBN:978-0521775946
315. Roux, B., Simonson, T.: Implicit solvent models. *Biophys. Chem.* **78**, 1–20 (1999). doi:[10.1016/S0301-4622\(98\)00226-9](https://doi.org/10.1016/S0301-4622(98)00226-9)
316. Rowlands, G.: A numerical algorithm for Hamiltonian systems. *J. Comput. Phys.* **97**, 235–239 (1991). doi:[10.1016/0021-9991\(91\)90046-N](https://doi.org/10.1016/0021-9991(91)90046-N)
317. Rudin, W.: *Principles of Mathematical Analysis*. International Series in Pure and Applied Mathematics, 3rd edn. McGraw-Hill International, New York (1976). ISBN:978-0070856134
318. Ruelle, D.: *Chance and Chaos*. Princeton University Press, Princeton, NJ (1993). ISBN:978-0691021003
319. Rugh, H.: Dynamical approach to temperature. *Phys. Rev. Lett.* **78**, 772–774 (1997). doi:[10.1103/PhysRevLett.78.772](https://doi.org/10.1103/PhysRevLett.78.772)
320. Ruth, R.: A canonical integration technique. *IEEE Trans. Nucl. Sci.* **30**, 2669–2671 (1983). doi:[10.1109/TNS.1983.4332919](https://doi.org/10.1109/TNS.1983.4332919)
321. Ryckaert, J., Bellemans, A.: Molecular dynamics of liquid n-butane near its boiling point. *Chem. Phys. Lett.* **30**, 123–125 (1975). doi:[10.1016/0009-2614\(75\)85513-8](https://doi.org/10.1016/0009-2614(75)85513-8)
322. Ryckaert, J., Ciccotti, G., Berendsen, H.: Numerical integration of the Cartesian equations of motion of a system with constraints: molecular dynamics of n-alkanes. *J. Comput. Phys.* **23**, 327–341 (1977). doi:[10.1016/0021-9991\(77\)90098-5](https://doi.org/10.1016/0021-9991(77)90098-5)
323. Samoletov, A.A., Dettmann, C.P., Chaplain, M.A.J.: Thermostats for “slow” configurational modes. *J. Stat. Phys.* **128**, 1321–1336 (2007). doi:[10.1007/s10955-007-9365-2](https://doi.org/10.1007/s10955-007-9365-2)
324. Sancho, J., SanMiguel, M., Katz, S., Gunton, J.: Analytical and numerical studies of multiplicative noise. *Phys. Rev. A* **26**, 1589–1609 (1982). doi:[10.1103/PhysRevA.26.1589](https://doi.org/10.1103/PhysRevA.26.1589)
325. Sanz-Serna, J.: Runge-Kutta schemes for Hamiltonian systems. *BIT* **28**, 877–883 (1988). doi:[10.1007/BF01954907](https://doi.org/10.1007/BF01954907)
326. Sanz-Serna, J., Calvo, M.: *Numerical Hamiltonian Problems*. Applied Mathematics and Mathematical Computation. Chapman & Hall, London (1994). ISBN:9780412542909
327. Schlick, T.: Molecular dynamics-based approaches for enhanced sampling of long-time, large-scale conformational changes in biomolecules. *F1000 Biology Reports* pp. 1–51 (2009). doi:[10.3410/B1-51](https://doi.org/10.3410/B1-51)
328. Schlick, T.: *Molecular Modeling and Simulation: An Interdisciplinary Guide* (Interdisciplinary Applied Mathematics), 2nd edn. Springer, New York (2010). ISBN:978-1441963505
329. Schlick, T., Mandziuk, M., Skeel, R., Srinivas, K.: Nonlinear resonance artifacts in molecular dynamics simulations. *J. Comput. Phys.* **140**, 1–29 (1998). doi:[10.1006/jcph.1998.5879](https://doi.org/10.1006/jcph.1998.5879)
330. Schlijper, A., Hoogerbrugge, P., Manke, C.: Computer simulation of dilute polymer solutions with the dissipative particle dynamics method. *J. Rheol.* **39**, 567 (1995). doi:[10.1122/1.550713](https://doi.org/10.1122/1.550713)
331. Schofield, P.: Computer simulation studies of the liquid state. *Comput. Phys. Commun.* **5**, 17–23 (1973). doi:[10.1016/0010-4655\(73\)90004-0](https://doi.org/10.1016/0010-4655(73)90004-0)
332. Schütte, C., Huisings, W.: Biomolecular conformations can be identified as metastable sets of molecular dynamics. In: Ciarlet, P.G. (ed.) *Handbook of Numerical Analysis. Computational Chemistry* (C. Lebris, Guest Editor), vol. 10. Elsevier, New York (2003)
333. Shardlow, T.: Splitting for dissipative particle dynamics. *SIAM J. Sci. Comput.* **24**(4), 1267–1282 (2003). doi:[10.1137/S1064827501392879](https://doi.org/10.1137/S1064827501392879)
334. Shardlow, T., Yan, Y.: Geometric ergodicity for dissipative particle dynamics. *Stochastics Dyn.* **6**(01), 123–154 (2006). doi:[10.1142/S0219493706001670](https://doi.org/10.1142/S0219493706001670)
335. Shaw, D.: A fast, scalable method for the parallel evaluation of distance-limited pairwise particle interactions. *J. Comput. Chem.* **26**, 1318–1328 (2005). doi:[10.1002/jcc.20267](https://doi.org/10.1002/jcc.20267)
336. Sigurgeirsson, H., Stuart, A., Wan, W.L.: Algorithms for particle-field simulations with collisions. *J. Comput. Phys.* **172**, 766–807 (2001). doi:[10.1006/jcph.2001.6858](https://doi.org/10.1006/jcph.2001.6858)
337. Sitkoff, D., Sharp, K., Honig, B.: Accurate calculation of hydration free energies using macroscopic solvent models. *J. Phys. Chem.* **98**, 1978–1988 (1994). doi:[10.1021/j100058a043](https://doi.org/10.1021/j100058a043)

338. Skeel, R.: What makes molecular dynamics work? *SIAM J. Sci. Comput.* **31**, 1363–1378 (2009). doi:[10.1137/070683660](https://doi.org/10.1137/070683660)
339. Skeel, R., Srinivas, K.: Nonlinear stability analysis of area-preserving integrators. *SIAM J. Numer. Anal.* **38**, 129–148 (2000). doi:[10.1137/S0036142998349527](https://doi.org/10.1137/S0036142998349527)
340. Smit, B., Karaborni, S., Siepmann, J.: Computer simulations of vapor-liquid phase equilibria of n-alkanes. *J. Chem. Phys.* **102**, 2126–2141 (1995). doi:[10.1063/1.469563](https://doi.org/10.1063/1.469563)
341. Snir, M.: A note on n-body computations with cutoffs. *Theory Comput. Syst.* **37**(2), 295–318 (2004). doi:[10.1007/s00224-003-1071-0](https://doi.org/10.1007/s00224-003-1071-0)
342. Sodemann, T., Dünweg, B., Kremer, K.: Dissipative particle dynamics: a useful thermostat for equilibrium and nonequilibrium molecular dynamics simulations. *Phys. Rev. E* **68**(4), 046,702 (2003). doi:[10.1103/PhysRevE.68.046702](https://doi.org/10.1103/PhysRevE.68.046702)
343. Sprott, J.: *Chaos and Time-Series Analysis*. Oxford University Press, Oxford (2003). ISBN:978-0198508397
344. Stillinger, F., Weber, T.: Computer simulation of local order in condensed phases of silicon. *Phys. Rev. B* **31**, 5262–5271 (1985). doi:[10.1103/PhysRevB.31.5262](https://doi.org/10.1103/PhysRevB.31.5262)
345. Stockmayer, W.H.: Second virial coefficients of polar gas mixtures. *J. Chem. Phys.* **9**, 863–870 (1941). doi:[10.1063/1.1750858](https://doi.org/10.1063/1.1750858)
346. Stoddard, S.D., Ford, J.: Numerical experiments on the stochastic behavior of a Lennard-Jones gas system. *Phys. Rev. A* **8**, 1504–1512 (1973). doi:[10.1103/PhysRevA.8.1504](https://doi.org/10.1103/PhysRevA.8.1504)
347. Stoyanov, S.D., Groot, R.D.: From molecular dynamics to hydrodynamics: a novel Galilean invariant thermostat. *J. Chem. Phys.* **122**, 114,112 (2005). doi:[10.1063/1.1870892](https://doi.org/10.1063/1.1870892)
348. Stratton, R., Holmgren, S., Chandler, D.: Constrained impulsive molecular dynamics. *Mol. Phys.* **42**(5), 1233–1243 (1981). doi:[10.1080/00268978100100921](https://doi.org/10.1080/00268978100100921)
349. Stroock, D.: *Lectures on Topics in Stochastic Differential Equations*. Tata Institute of Fundamental Research, Bombay. Springer, Berlin (1982)
350. Stuart, A., Warren, J.: Analysis and experiments for a computational model of a heat bath. *J. Stat. Phys.* **97**, 687 (1999). doi:[10.1023/A:1004667325896](https://doi.org/10.1023/A:1004667325896)
351. Su, J.: An electron force field for simulating large scale excited electron dynamics (2007). Ph.D. Thesis, California Institute of Technology
352. Suh, S.H., Mier-y-Teran, L., White, H.S., Davis, H.T.: Molecular dynamics study of the primitive model of 1–3 electrolyte solutions. *Chem. Phys.* **142**, 203–211 (1990). doi:[10.1016/0301-0104\(90\)89081-Z](https://doi.org/10.1016/0301-0104(90)89081-Z)
353. Suris, Y.: Some properties of methods for the numerical integration of systems of the form $\ddot{x} = f(x)$. *USSR Comput. Math. Math. Phys.* **27**, 149–156 (1987). doi:[10.1016/0041-5553\(87\)90061-9](https://doi.org/10.1016/0041-5553(87)90061-9)
354. Suzuki, M.: Fractal decomposition of exponential operators with applications to many-body theories and monte carlo simulations. *Phys. Lett. A* **146**, 319–323 (1990). doi:[10.1016/0375-9601\(90\)90962-N](https://doi.org/10.1016/0375-9601(90)90962-N)
355. Takahashi, M., Imada, M.: Monte Carlo calculation of quantum systems. ii. higher order correction. *J. Phys. Soc. Jpn.* **53**, 3765–3769 (1984). doi:[10.1143/JPSJ.53.3765](https://doi.org/10.1143/JPSJ.53.3765)
356. Talay, D.: Simulation and Numerical Analysis of Stochastic Differential Systems: A Review. *Rapports de recherche. Institut National de Recherche en Informatique et en Automatique* (1990)
357. Talay, D.: Stochastic Hamiltonian dissipative systems: exponential convergence to the invariant measure, and discretization by the implicit Euler scheme. *Markov Process. Relat. Fields* **8**, 163–198 (2002)
358. Talay, D., Tubaro, L.: Expansion of the global error for numerical schemes solving stochastic differential equations. *Stoch. Anal. Appl.* **8**, 483–509 (1990). doi:[10.1080/07362999008809220](https://doi.org/10.1080/07362999008809220)
359. Tang, Y.F.: Formal energy of a symplectic scheme for Hamiltonian systems and its applications (I). *Comput. Math. Appl.* **27**, 31–39 (1994). doi:[10.1016/0898-1221\(94\)90083-3](https://doi.org/10.1016/0898-1221(94)90083-3)
360. Taylor, M.: *Partial Differential Equations I: Basic Theory*. Applied Functional Analysis: Applications to Mathematical Physics. U.S. Government Printing Office, Washington, DC (1996)

361. Tersoff, J.: New empirical approach for the structure and energy of covalent systems. *Phys. Rev. B* **37**, 6991–7000 (1988). doi:[10.1103/PhysRevB.37.6991](https://doi.org/10.1103/PhysRevB.37.6991)
362. Teschl, G.: Ordinary Differential Equations and Dynamical Systems. Graduate Studies in Mathematics, vol. 140. American Mathematical Society, Providence (2012). ISBN:978-0821883280
363. Thalmann, F., Farago, J.: Trotter derivation of algorithms for Brownian and dissipative particle dynamics. *J. Chem. Phys.* **127**, 124,109 (2007). doi:[10.1063/1.2764481](https://doi.org/10.1063/1.2764481)
364. Tien, C., Lienhard, J.: Statistical Thermodynamics, revised edition. Hemisphere, Washington, DC (1979)
365. Todorov, I., Smith, W.: DL_Poly 4 user manual (v. 4.05.1). Tech. rep., STFC Daresbury Laboratory (2013).
366. Tolman, R.: The Principles of Statistical Mechanics. Dover, New York (2003). ISBN:978-0486638966
367. Toukmaji, A., J.A. Board, J.: Ewald summation techniques in perspective: a survey. *Comput. Phys. Commun.* **95**, 73–92 (1996). doi:[10.1016/0010-4655\(96\)00016-1](https://doi.org/10.1016/0010-4655(96)00016-1)
368. Touma, J., Wisdom, J.: Lie-Poisson integrators for rigid body dynamics in the solar system. *Astron. J.* **107**, 1189–1202 (1994). doi:[10.1086/116931](https://doi.org/10.1086/116931)
369. Toxvaerd, S.: Hamiltonians for discrete dynamics. *Phys. Rev. E* **50**, 2271–2274 (1994). doi:[10.1103/PhysRevE.50.2271](https://doi.org/10.1103/PhysRevE.50.2271)
370. Trotter, H.F.: On the product of semi-groups of operators. *Proc. Am. Math. Soc.* **10**(4), 545–551 (1959). doi:[10.1090/S0002-9939-1959-0108732-6](https://doi.org/10.1090/S0002-9939-1959-0108732-6)
371. Tsige, M., Curro, J.G., Grest, G.S., McCoy, J.D.: Molecular dynamics simulations and integral equation theory of alkane chains: comparison of explicit and united atom models. *Macromolecules* **36**(6), 2158–2164 (2003). doi:[10.1021/ma0212543](https://doi.org/10.1021/ma0212543)
372. Tuckerman, M.: Statistical Mechanics: Theory and Molecular Simulation. Oxford Graduate Texts. Oxford University Press, Oxford (2010). ISBN:978-0198525264
373. Tuckerman, M., Alejandre, J., López-Rendón, R., Jochim, A., Martyna, G.: A Liouville-operator derived measure-preserving integrator for molecular dynamics simulations in the isothermal-isobaric ensemble. *J. Phys. A* **39**, 5629–5651 (2006). doi:[10.1088/0305-4470/39/19/S18](https://doi.org/10.1088/0305-4470/39/19/S18)
374. Tuckerman, M., Berne, B.: Molecular dynamics in systems with multiple time scales: systems with stiff and soft degrees of freedom and with short and long range forces. *J. Chem. Phys.* **95**, 8362–8365 (1991). doi:[10.1063/1.461263](https://doi.org/10.1063/1.461263)
375. Tuckerman, M., Berne, B., Martyna, G.: Molecular dynamics algorithm for multiple time scales: systems with long range forces. *J. Chem. Phys.* **94**, 6811–6815 (1991). doi:[10.1063/1.460259](https://doi.org/10.1063/1.460259)
376. Tuckerman, M., Liu, Y., Ciccotti, G., Martyna, G.J.: Non-Hamiltonian molecular dynamics: generalizing Hamiltonian phase space principles to non-Hamiltonian systems. *J. Chem. Phys.* **115**, 1678–1702 (2001). doi:[10.1063/1.1378321](https://doi.org/10.1063/1.1378321)
377. Tuckerman, M., Martyna, G., Berne, B.: Molecular dynamics algorithm for condensed systems with multiple time scales. *J. Chem. Phys.* **93**, 1287–1292 (1990). doi:[10.1063/1.459140](https://doi.org/10.1063/1.459140)
378. Tully, J., Preston, R.: Trajectory surface hopping approach to nonadiabatic molecular collisions: the reaction of H^+ with D_2 . *J. Chem. Phys.* **55**, 562–572 (1971). doi:[10.1063/1.1675788](https://doi.org/10.1063/1.1675788)
379. Tupper, P.: Ergodicity and the numerical simulation of Hamiltonian systems. *SIAM J. Appl. Dyn. Syst.* **4**, 563–587 (2005). doi:[10.1137/040603802](https://doi.org/10.1137/040603802)
380. Tupper, P.: A non-existence result for Hamiltonian integrators (2006). <http://arxiv.org/abs/math/0607641>
381. Tupper, P.: The relation between approximation in distribution and shadowing in molecular dynamics. *SIAM J. Appl. Dyn. Syst.* **8**, 734–755 (2009). doi:[10.1137/08072526X](https://doi.org/10.1137/08072526X)
382. van Zon, R., Omelyan, I., Schofield, J.: Efficient algorithms for rigid body integration using optimized splitting methods and exact free rotational motion. *J. Chem. Phys.* **128**(136102) (2008). doi:[10.1063/1.2889937](https://doi.org/10.1063/1.2889937)

383. Vanden-Eijnden, E., Ciccotti, G.: Second-order integrators for Langevin equations with holonomic constraints. *Chem. Phys. Lett.* **429**, 310–316 (2006). doi:[10.1016/j.cplett.2006.07.086](https://doi.org/10.1016/j.cplett.2006.07.086)
384. Vanden-Eijnden, E., Venturoli, M.: Revisiting the finite temperature string method for the calculation of reaction tubes and free energies. *J. Chem. Phys.* **130**(19) (2009). doi:[10.1063/1.3130083](https://doi.org/10.1063/1.3130083)
385. Vattulainen, I., Karttunen, M., Besold, G., Polson, J.M.: Integration schemes for dissipative particle dynamics simulations: from softly interacting systems towards hybrid models. *J. Chem. Phys.* **116**, 3967 (2002). doi:[10.1063/1.1450554](https://doi.org/10.1063/1.1450554)
386. Verhulst, F.: Nonlinear Differential Equations and Dynamical Systems, 2nd edn. Universitext. Springer, New York (2013). ISBN:978-3540609346
387. Verlet, L.: Computer “experiments” on classical fluids. i. Thermodynamical properties of Lennard-Jones molecules. *Phys. Rev.* **159**, 98–103 (1967). doi:[10.1103/PhysRev.159.98](https://doi.org/10.1103/PhysRev.159.98)
388. Vesely, F.: N-particle dynamics of polarizable Stockmayer-type molecules. *J. Comput. Phys.* **24**, 361–371 (1977). doi:[10.1016/0021-9991\(77\)90028-6](https://doi.org/10.1016/0021-9991(77)90028-6)
389. Volkov, A., Shiga, T., Nicholson, D., Shiomi, J., Zhitilei, L.: Effect of bending buckling of carbon nanotubes on thermal conductivity of carbon nanotube materials. *J. Appl. Phys.* **111**, 053,501 (2012). doi:[10.1063/1.3687943](https://doi.org/10.1063/1.3687943)
390. Voskoboinikov, R.: Molecular dynamics simulations of radiation damage in D_{0.19} Ti₃Al intermetallic compound. *Nucl. Instrum. Methods Phys. Res. Sect. B* **307**, 25–28 (2013). doi:[10.1016/j.nimb.2012.12.079](https://doi.org/10.1016/j.nimb.2012.12.079)
391. Voter, A.: An introduction to the kinetic Monte Carlo method. In: Radiation Effects in Solids, pp. 1–23. Springer/NATO Publishing Unit, Dordrecht (2007). doi:[10.1007/978-1-4020-5295-8_1](https://doi.org/10.1007/978-1-4020-5295-8_1)
392. Weinbach, Y., Elber, R.: Revisiting and parallelizing SHAKE. *J. Comput. Phys.* **209**, 193–206 (2005). doi:[10.1016/j.jcp.2005.03.015](https://doi.org/10.1016/j.jcp.2005.03.015)
393. Weiner, S., Kollman, P., Case, D., Singh, U., Alagona, G., Jr., S.P., Weiner, P.: A new force field for the molecular mechanical simulation of nucleic acids and proteins. *J. Am. Chem. Soc.* **106**, 765–784 (1984). doi:[10.1021/ja00315a051](https://doi.org/10.1021/ja00315a051). <http://ambermd.org>
394. Weiner, S.J., Kollman, P.A., Case, D.A., Singh, U.C., Ghio, C., Alagona, G., Profeta, S., Weiner, P.: A new force field for molecular mechanical simulation of nucleic acids and proteins. *J. Am. Chem. Soc.* **106**(3), 765–784 (1984). doi:[10.1021/ja00315a051](https://doi.org/10.1021/ja00315a051)
395. West, M., Kane, C., Marsden, J., Ortiz, M.: Variational integrators, the newmark scheme, and dissipative systems. In: Proceedings of the International Conference on Differential Equations, pp. 1009–1011. World Scientific, Singapore (2000). ISBN:978-9810243593
396. White, T., Ciccotti, G., Hansen, J.P.: Brownian dynamics with constraints. *Mol. Phys.* **99**(24), 2023–2036 (2001). doi:[10.1080/00268970110090854](https://doi.org/10.1080/00268970110090854)
397. Wisdom, J., Holman, M., Touma, J.: Symplectic correctors. In: Integrational Algorithms and Classical Mechanics. American Mathematical Society, Providence (1996). ISBN:978-0821802595
398. Yoshida, H.: Construction of higher order symplectic integrators. *Phys. Lett. A* **150**, 262–268 (1990). doi:[10.1016/0375-9601\(90\)90092-3](https://doi.org/10.1016/0375-9601(90)90092-3)
399. Zhao, G., Perilla, J., Yufenyuy, E., X. Meng, B.C., Ning, J., Ahn, J., Gronenborn, A., Schulten, K., Aiken, C., Zhang, P.: Mature HIV-1 capsid structure by cryo-electron microscopy and all-atom molecular dynamics. *Nature* **497**, 643–646 (2013). doi:[10.1038/nature12162](https://doi.org/10.1038/nature12162)
400. Zhong, G., Marsden, J.E.: Lie-Poisson Hamilton-Jacobi theory and Lie-Poisson integrators. *Phys. Lett. A* **133**, 134–139 (1988). doi:[10.1016/0375-9601\(88\)90773-6](https://doi.org/10.1016/0375-9601(88)90773-6)
401. Zuckerman, D.M.: Equilibrium sampling in biomolecular simulations. *Ann. Rev. Biophys.* **40**(1), 41–62 (2011). doi:[10.1146/annurev-biophys-042910-155255](https://doi.org/10.1146/annurev-biophys-042910-155255)
402. Zwanzig, R.: Nonlinear generalized Langevin equations. *J. Stat. Phys.* **9**, 215–220 (1973). doi:[10.1007/BF01008729](https://doi.org/10.1007/BF01008729)
403. Zygalakis, K.: On the existence and the applications of modified equations for stochastic differential equations. *SIAM J. Sci. Comput.* **33**, 102–130 (2011). doi:[10.1137/090762336](https://doi.org/10.1137/090762336)

Index

- Acceptance rate (of a Markov Chain), 415
Accuracy, 58, 66
Action functional, 60
derivation of Verlet method using, 63
Additive property of thermostats, 338, 343
Adjoint method, 81, 82, 96
Adjoint operator, 186
Affine invariance, 130, 138
Affine invariant, 138
Alanine dipeptide, 11, 12, 308, 309
Alkane, 15
Andersen piston, 379, 380
Andersen thermostat, 342
Angle bond, 13, 47
Angular momentum, 42, 47, 49, 71
conservation of, 39, 49
for a rigid body, 171
Angular velocity
in body reference frame, 169
spatial, 169
Anisotropic oscillator, 42, 70, 201
Aperiodicity, 414
Area preservation, 76
Argon, 22, 35
Asymptotic expansion, 285
of the approximate Fokker-Planck operator,
284
of modified Hamiltonian, 100
Attractive force, 10
Autocorrelation function, 203, 204, 310
Average, 184, 195, 197, 261, 329
convergence of, 257
Averaging, 194
for chaotic trajectories, 196
Backward error analysis, 97, 100, 103, 106,
114, 116, 118, 265
Backward Euler method, 86
Baker-Campbell-Hausdorff, 106, 285, 286
Barostat, 381
BBK*, 279
Bcc lattice, 35
BCH formula, 106, 285, 286, 298
Bead-on-wire problem, 175
Berendsen, 396
Bias, 266, 275
in numerical discretization, 263, 266,
320
2-body problem, 47
Bond, 8, 9, 47, 141
angle, 13
constraint, 150
Bond order potential, 14
Borel sigma algebra, 407
Born-Oppenheimer approximation, 5, 6
Brachistochrone problem, 176
Brownian dynamics, 225, 236
Brownian motion, 268
Brünger-Brooks-Karplus (BBK), 273, 274,
277, 308, 313
Buckingham potential, 10, 16
Buckminsterfullerene, 14
Bulgac-Kusnezov thermostat, 338
Butane, 15
Canonical average, 220
Canonical ensemble, 211, 213, 219, 239, 274,
331, 344

- Canonical partition function, 266
 Canonical sampling, 261
 Carbon nanotubule, 14
 Central forces, 49, 71
 Central Limit Theorem, 227, 409, 413
 Chaotic system, 41, 179
 CHARMM, 165, 312
 CHARMM22, 165, 309, 321
 Classical mechanics, 5
 Commutator, 286
 Composition method, 84, 85, 103, 163, 173
 for Langevin dynamics, 277
 Conditional expectation, 409
 Conditional probability, 408, 409
 Configurational sampling, 305, 312
 Configurational temperature, 260, 310, 338
 Configurational thermostat, 338
 Confining potential, 33
 Confining property, 26
 Conjugate method, 88, 96
 stochastic, 272
 Conservation law, 72
 Conservation of energy, 19, 26, 282
 Conservation of momentum, 34
 Conserved quantity
 and discretization methods, 71
 Consistency (of a numerical method), 67
 Constant pressure, 379, 380
 Constrained dynamics, 87, 149–151, 153, 154, 159
 Constraint manifold, 152
 Constraints, 144, 317
 Continuity equation, 185, 336
 Convergence, 55, 66, 68, 71
 in sense of distribution, 410
 Coordinate frame, 168
 Correction function, 284
 Co-tangent bundle, 152
 Coulomb potential, 12, 404
 screened, 12
 Covalent bond, 273
 Cut-off of potential energy, 12, 35
 Cyclic trace formula, 344
- Degree of freedom, 18
 Delta-distribution, 191
 Density, 179, 180, 182
 continuous, 407
 discrete, 407
 Detailed balance, 414
 Differential, 76
 Diffusion, 243
 constant, 311
- limit, 226
 Dihedral potential, 13
 Dipolar liquid, 169
 Dipole model, 47, 48
 Discrete spectrum, 250, 251
 Discrete trajectory, 56
 Discretization, 54
 Dissipative particle dynamics, 239, 386
 Distance potentials, 38
 Distribution, 188
 Divergence free, 210
 Divergence theorem, 184
 DLM algorithm for rigid body molecular dynamics, 173
 Double pendulum, 200
 Double well potential, 196
 Duffing Oscillator, 279
 Dynamical averages, 203, 204
- Embedded atom potential, 14
 Empirical force field, 6
 Energy
 conservation, 26, 70, 74, 97, 119, 120, 122, 132
 drift, 119, 120, 122, 132
 error, 58, 69, 70
 function, 18–20
 projection, 125
 surface, 196, 198
 Energy conserving method, 122, 124, 125
 Energy-volume method, 282
 Equations of motion, 6
 Equilibrium
 point, 31, 37, 49
 solution, 189
 statistical, 203, 213
 Ergodicity, 42, 196–198, 202, 210, 244, 247–249, 251, 254
 lack of for deterministic thermostats, 340
 and Nosé-Hoover chains, 340
 of the trimer, 207
- Error
 in numerical solution of SDE, 264
 for perturbed harmonic oscillator, 280
 in sampling, 266
- Error analysis
 for Langevin applied to harmonic oscillator, 273
- Error growth, 55
 Error in averages, 279
 Euler equations, 171, 172, 177
 Euler-Lagrange equations, 151
 Euler-Maruyama, 264, 328

- Euler's method, 54–56, 58, 75, 82, 96, 97, 119, 139
accuracy of, 57
- Event space, 407
- Ewald summation, 373, 404
- Exact averages, 277
- Existence-uniqueness theorem, 25
- Expansion of operator, 284
- Expectation of a random variable, 408
- Exponential series, 103
- Fast multipole method, 404
- Fcc lattice, 35, 36, 50
- Fermi-Pasta-Ulam problem, 175
- First integral, 70, 118, 123
and discretization methods, 71
- First order method
for Langevin dynamics, 288
- Flow map, 26, 54, 100, 101, 269
approximation of, 54
relation to solution operator, 181
- Fokker-Planck equation, 241, 244, 248, 261, 285, 343
- Fokker-Planck operator, 268, 282
- Force computation, 403
- Force perturbation thermostat, 400
- 1-form, 76
- 2-form, 76–78
conservation of, 78
- Fredholm alternative, 257, 299
- Free rigid body, 171, 177
- Friction coefficient, 310
- Function space, 182
- Gaussian distribution, 409
- Gaussian isokinetic thermostat, 361
- Gaussian random variable, 235
- Gauss-Legendre Runge-Kutta method, 90
- Gauss-Newton iteration, 157
- Gauss-Seidel-Newton iteration, 159
- Gay-Berne potential, 17
- Generalized Bulgac-Kusnezov thermostat, 337
- Generalized function, 188
- Generalized Langevin dynamics method, 377
- Generalized Langevin equation, 374, 375
- Generator, 240
Brownian dynamics, 250
- Geodesic flow, 164
- Geodesic integrator, 319
- Geometric integration, 71, 72, 98
- Geometric Langevin Algorithm (GLA), 271, 273, 276
- Gibbs-Boltzmann measure, 331
- Gibbs distribution, 244, 251, 269
- Global error, 55, 56, 58
- H_2^+ molecule
potential for, 8
- H_2 potential, 8
- Hamiltonian, 26, 32
- Hamiltonian formulation, 25
- Hamiltonian system, 23, 26, 172
- Hamilton's principle, 61
- Harmonic oscillator, 19, 20, 26, 99, 137, 139, 141, 142, 209, 273, 274, 276
error in averages for various methods, 276
Langevin dynamics applied to, 275
microcanonical distribution for, 193
perturbed, 280
- Harmonic potentials, 273
- Hartman-Grobman theorem, 32
- Hcp lattice, 36
- Hessian matrix, 33, 61, 93
- Hexagonal lattice, 35
- Higher order method, 59, 109
- High friction limit, 305
- Hilbert space, 183
- HMC method, 262, 342, 417
- Holonomic constraint, 150, 317
- Homeomorphism, 88
- Hörmander condition, 254, 344, 358
- Hybrid Monte-Carlo method, 262, 342, 417
- Hydrodynamic preservation, 386
- Hydrogen bond, 10
- Hypoelliptic operator, 358
- Implicit Euler method, 144
- Implicit method, 86, 142, 144
- Implicit midpoint method, 96, 142, 175
- Implicit solvation, 405
- Independence (statistical), 408
- Initial value problem, 53
- Inner product space, 183
- Invariant distribution, 190, 246, 331
and backward error analysis, 206
convergence to, 249
of a discretization method, 306
of a numerical method, 206, 208
perturbed, 289
uniqueness of, 254
- Invariant measure, 191
- Invariant set, 197
- Irreducibility, 245, 246, 414
- Isobaric, isothermal ensemble, 379

- Isokinetic method, 361
 Itô formula, 233, 234, 240, 243
 Itô integral, 228
- Jacobi identity, 104, 137
 Jacobian matrix, 44, 59, 75, 76
 Joint probability density, 408
 J-splitting, 282
- KAM (Kolmogorov-Arnold-Moser) theory, 132, 201
 Kinetic energy, 22, 312, 332
 Kinetic Monte-Carlo, 263, 342
 Kolmogorov equation, 242, 247
 Kolmogorov operator, 242, 244, 247
- L^2 space, 183
 Lagrange multipliers, 152, 317
 Lagrangian, 23, 60
 - formulation, 25
 - function, 22
 Langevin dynamics, 236, 240, 251, 260, 261, 269, 272, 277, 282, 344
 - numerical comparison, 308
 Langevin dynamics discretization scheme
 - $[\![\text{ABAO}]\!]$, 271, 285
 - $[\![\text{ABO}]\!]$, 270, 275, 276
 - $[\![\text{ABOBA}]\!]$, 271, 277, 312
 - $[\![\text{AOBOA}]\!]$, 273, 277
 - $[\![\text{BABO}]\!]$, 270
 - $[\![\text{BAOAB}]\!]$, 271, 277, 305, 312, 328
 - $[\![\text{BOAOB}]\!]$, 277
 Brünger-Brooks-Karplus (BBK), 273, 274, 277, 308, 313
 Notation, 270
 - $[\![\text{OABAO}]\!]$, 271, 277, 312
 - $[\![\text{OBABO}]\!]$, 271, 272, 277, 328
 Stochastic Position Verlet (SPV), 272, 273, 308, 313
- Lattice structures, 33
 Lattice vibrations, 36
 Leapfrog, 60
 Lebesgue integral, 182, 183
 Lebesgue integration, 410
 Legendre transformation, 24
 Length bond, 9
 Lennard-Jones 7 atom system, 118
 Lennard-Jonesium, 351, 385
 Lennard-Jones potential, 10, 11, 21, 35, 38, 39, 48, 219
 Lennard-Jones trimer, 38, 39, 56, 69
- Lie algebra, 344
 Lie bracket, 254
 Lie derivative, 100, 102, 105, 209, 242
 Limit method, 306, 328
 Linearization, 31
 Linear stability analysis, 146
 Linear system, 27, 37
 Linked cell list method, 404
 Liouville equation, 180, 184–186, 199
 Liouville’s theorem, 72–74, 95
 Liouvillian, 262, 332
 Lipschitz condition, 66, 68
 Local error, 67, 68
 London dispersion, 10
 Lyapunov exponent, 44–46
- Macroscopic perspective, 179, 212
 Macrostate, 180
 Markov chain, 245, 246, 410
 Markov process, 227, 410
 Markov property, 227
 Massive Nosé-Hoover thermostat, 400
 Matrix exponential, 46, 101
 Mean of a random variable, 408
 Measurable set, 183, 194
 Metropolis-Adjusted Langevin Algorithm (MALA), 417
 Metropolis correction
 - of molecular dynamics, 417
 - of numerical methods, 416
 Metropolis-Hastings Monte-Carlo method, 415
 Metropolis Monte-Carlo method, 261, 416
 Microcanonical distribution, 187, 193–195
 Microcanonical ensemble, 213
 Microcanonical ergodicity, 197
 Microcanonical measure, 191
 Microcanonical partition function, 193
 Microscopic dynamics, 179
 Minimum image convention, 35
 Modified Hamiltonian, 98, 106
 Mollified impulse method (MOLLY), 148, 149
 Momentum, 19
 Momentum conservation, 19, 34, 123
 - under thermostating, 386
 Momentum flip, 417
 Monte-Carlo, 261, 380
 - compared to molecular dynamics, 262
 Monte-Carlo estimator, 413
 Monte-Carlo Markov Chain, 414
 Monte-Carlo method, 413
 Morse potential, 8, 94
 MTS, 149
 Multiderivative method, 92

- Multiple timestepping, 4, 144, 145, 147–149, 323
Multistep methods, 93
- NAMD, 165, 309, 321
NAMD-lite, 309, 321
N-body problem, 18
Neighbor list, 403
Newmark method, 92
Newtonian dynamics, 6
Newton iteration, 144, 157, 158
Newton's equations, 18
Newton's method, 86
NHL thermostat, 401
Nonlinear resonance, 148
Non-Newtonian dynamics, 357
Normal distribution, 409
Normal modes, 37
Normal random variable, 409
Nosé-Hoover Chain, 339
Nosé-Hoover-Langevin, 345, 350, 380
numerical experiment, 351
Nosé-Hoover method, 331–333, 380, 399
first integral for, 333, 399
lack of ergodicity of, 351
Nosé-Poincaré method, 334
NPT ensemble, 379, 380
Numerical stochastic differential equation, 264
NVT ensemble, 218
- Observable, 195
One-step method, 54
Operator expansion, 285
Order of accuracy, 55, 66, 67
Ornstein-Uhlenbeck equation, 234, 248, 267–269, 282, 295
Orthogonality constraint, 171
OU process, 269
Overdamped Langevin dynamics, 240, 305, 308
- Particle-mesh Ewald summation, 373, 404
Partitioned Runge-Kutta method, 90, 140, 141
Pauli exclusion principle, 10
Pauli repulsion, 10
Pendulum, 49, 210
Perfect sampling bias, 266, 275
Periodic boundary conditions, 33–35, 214, 220, 223
in constant pressure simulation, 379
Perturbed harmonic oscillator, 280
- Phase space, 25
Poisson-Boltzmann equation, 405
Poisson bracket, 100, 102, 104
Polarization, 14
Potential cut-off, 50
Potential energy function, 5–8, 22
Pressure, 379, 381
Principle of least action, 60
Probability density, 182, 408
Probability measure, 180, 182
Probability theory, 407
Processed method, 88, 93
Projection method, 124
Projective thermostat, 401
Propagator, 182
Propagator of measure, 186
Proposal distribution, 415
Pull-back, 77
- Quantum mechanics, 5
- Random variable
continuous, 407
discrete, 407
Random walk, 225, 231
RATTLE, 161–163, 171, 176
Repulsive force, 10
Reservoir, 212
Resonance, 146, 147
RESPA, 4, 145
Reversibility, 414
Rigid body
constrained formulation, 171
Rigid body dynamics, 166, 170
using SHAKE or RATTLE, 171
Rigid body water, 167
Rotational kinetic energy, 168
Rotation matrix, 167, 170
Rowlands' method, 92
R-RESPA, 175
Runge-Kutta method, 82, 89, 94, 97, 120, 175
affine invariantness of, 138
projected, 125
symplectic, 89
- Sampling, 261, 331
bias, 266, 275, 279
efficiency of, 262
error, 266
- Schrödinger equation, 5, 6

- Second order methods, 60
 Langevin dynamics, 297
- Secular drift, 120
 Secular growth, 70
 Self-adjoint operator, 249
 Shadow Hamiltonian, 106, 114, 116, 118
 Shadow Hybrid Monte-Carlo method (SHMC), 418
- SHAKE, 87, 149, 161–163, 171
 Shear transformation, 138
 Short-ranged potential, 35
 Skew-adjoint operator, 187
 Smoluchowski limit, 240
 Solution operator, 180, 181
 Solvent, 14, 312
 Space filling curve, 202
 Spatial angular velocity, 169
 Spatial average, 184
 Spectral gap, 251, 262
 Splitting method, 82, 85, 96, 100, 103, 145, 173, 209, 269, 270, 340
 affine invariantness of, 138
 efficiency of, 271
 Langevin dynamics, 268, 270, 271, 273, 277, 288
- Stability, 67, 137, 142
 of a numerical method, 139, 140
 region, 141
 threshold, 142
 of Verlet, 141
- Stationary average, 274
 Statistical mechanics, 53, 179
 canonical, 211
- Steady state, 189, 213
 Stepsize, 54, 139
 choice of, 55
 threshold, 142
- Stiff-oscillatory system, 139
 Stillinger-Weber potential, 14
 Stochastic differential equation (SDE), 231, 232, 247, 249, 264
 Stochastic dynamics, 261
 Stochastic integration, 228
 Stochastic isokinetic method, 363
 Stochastic line sampling, 359
 Stochastic Position Verlet (SPV), 272, 273, 308, 313
 Stochastic process, 225, 245
 Stochastics, 212
 Stockmayer liquid, 48
 Strang splitting, 108, 277
 Stratonovich integral, 228, 230
 Störmer-Verlet, 60
 Strong accuracy of numerical method, 264
- Strong local minimum, 32
 Superconvergence, 305, 306, 311
 Support of a function, 183
 Suzuki-Yoshida methods, 109
 Symmetric Langevin methods, 301
 Symmetric method, 82, 162
 Symmetry, 82
 Symplectic corrector, 89
 Symplectic Euler method, 80, 82, 84, 96, 140, 175
 backward error analysis, 106
 constrained version, 156, 159
- Symplectic form, 76, 77
 Symplectic integrator, 80, 82, 97, 100
 Symplectic map, 72, 78, 79
 constrained dynamics, 156
 group property of, 79
 Symplectic method, 72, 76, 92, 127, 334
 Symplectic property, 76, 154
 Symplectic Runge-Kutta method
 condition for, 89
- Symplectic structure with constraints, 153
- Takahashi-Imada method, 92, 93, 112
 Simplified variant, 138
- Target temperature, 332
 Taylor series method, 59
 Temperature, 220, 221, 223, 244
 configurational, 222, 310
- Tersoff potential, 14
 Test function, 188, 189
 Thermodynamic average, 220
 Thermodynamic limit, 212
 Thermodynamic parameter, 212
 Thermodynamics, 212
 Thermostat, 329, 330, 342, 345, 350, 357
 deterministic vs stochastic, 359, 361
- Time correlation function, 329
 Time-reversal symmetry, 128, 130, 162
 associated eigenvalue structure, 131
 of molecular dynamics, 128
- Time-reversibility, 128
 TIP4P, 166, 167
 Topological conjugacy, 32
 Topologically transitive, 41
 Torsion, 15
 Trajectory averages, 261
 Transient, 213
 Transition density, 414
 Transition probability, 245, 410
 Trimer, 38, 56
 TU Lemma, 299

- Underlying ordinary differential equation, 153
Unit cell, 36
- Vacuum, 14
Van der Waals, 10
Variable stepsize, 55
Variance, 409
Variational equations, 44, 45, 50, 73, 79
Velocity autocorrelation function, 204, 311
Velocity Verlet, 64, 165
Verlet list, 403
Verlet method, 60, 64–66, 68, 86, 88, 91, 97, 122, 141
 - backward error analysis, 107
 - for constraints, 161
 - order of accuracy of, 67
 - position Verlet, 107
- symplecticness of, 85
velocity Verlet, 107
Vertauschungssatz, 285
Volume preservation, 72, 74, 128, 210
 - of Hamiltonian flow maps, 78
- Water model, 5, 14, 165
Weak error in numerical SDEs, 265
Weak sense, 190
Wedge product, 76, 155
Wiener increment, 233
Wiener measure, 228
Wiener process, 226
- Yoshida methods, 109
Yukawa potential, 12